Investigation of the Synthesis of Transition Metal Complexes Featuring Bulky Allyl Ligands

By

Henry Pearce DeGroot

Thesis

Submitted to the Faculty of the
Graduate School of Vanderbilt University
in partial fulfillment of the requirements
for the degree of

MASTER OF SCIENCE
in
Chemistry

May 10th, 2024

Nashville, Tennessee

Timothy P. Hanusa, Ph.D.
Nathan D. Schley, Ph.D.

In memory of Dean Pearce, whose footsteps in life I so often hope to follow

Acknowledgements:

Financial support provided by the Vanderbilt University Graduate School, the Vanderbilt University Chemistry Department, and the National Science Foundation (CHE-1665327, CHE-2155144) is gratefully acknowledged.

First and foremost, I must express overwhelming gratitude to my advisor, Dr. Tim Hanusa, who has been ceaselessly kind, encouraging, and genuinely excited to share his passion for fundamental chemistry. That his door might be open any given night at 10 PM to have a chat about whatever chemistry was happening was a constant source of comfort. He was constantly kind, engaged, and willing to offer me much more grace than I could reasonably have asked for. But more so than anything else, the thing I most appreciated was that, no matter what was going on or what kind of predicament I found myself in, I could reliably go to his office, have a talk, and feel much better afterwards. I truly cannot thank him enough.

I must also thank my committee members, Drs. Nathan Schley, Janet Macdonald, and Greg Walker, who have been forced to gather in a room and listen to me talk for far, far too long by this point. Their time and expertise were valuable, and I am cognizant of how fortunate I am to have received so much of it. Special thanks must be given to Dr. Schley both for his recruiting efforts, without which I would likely have never come to Nashville, and his exceedingly generous diffractometry services. That he continued to offer his time after what felt like my first thirty samples failed was an unreasonably selfless act, but one I was very thankful to receive. I also gratefully acknowledge the crystallographic work of Dr. Bill Brennessel, who worked diligently on some horrendous samples, and managed to be highly positive and supportive in the process. I must also recognize Dr. Walker, who stepped in to serve on this committee on extremely short notice, and without whom I would have been entirely out of luck.

My time in the lab would have been nearly as pleasant had I not been so lucky to have an exceedingly pleasant collection of co-workers. To Dr. Ross Koby, thank you for taking me under your wing when I first joined the lab and for being so thorough with record keeping and SOP compiling. You really are an excellent chemist and most of the best laboratory practices I know, I learned from you. To Isaiah Speight, thank you for all the camaraderie throughout the years. Your outgoing, genuinely friendly aura was a substantial contributor to my joining the lab, even though, and I mean this sincerely, your slide titles are a menace to civilized society. To Kev Jung, thank you for your dedication to the work, even when absolutely nothing ended up working, and for your relentlessly cheerful disposition. I have kept the hoe you gifted me and guard it jealously. To Dillon Button-Jennings, I am grateful that the lab is being left in such capable hands; you already know more about pump maintenance than I ever managed to learn, so I don't have any worries about the future. I sincerely hope you continue to text me every once in a while with a new crystal structure or interesting reaction. To Dr. Lauren Wenger, thank you very much for your patience and

willingness to share your weird NMRs; discussing them over and over was a treat. I am truly thankful that we became friends, and without our conversations, these last couple years would have been quite dreary indeed. I hope that the Indiana homeland has nothing but good things in store for you. To my undergraduate mentors who guided me to the start of this journey, Drs. Gary Gray, Jackie Nikles, Ethan Cagle, Timothy Tosch, and David French, thank you very much.

To my friends in the department, I thank you all very much for continuing to invite me to things even as I when I worked the most absurd of schedules. To Xavier Streety, I am not sure why you decided to stop at my desk one day instead of heading past to Lauren's, but it meaningfully improved my at-work experience when you did. Bucks in Six. To Sophie Click, thank you for sharing your ever infectious energy and long lunchtime commiserations. To Chris Sharp, you are absolutely right, I was a scheduling nightmare, but it is largely thanks to your perseverance that I had a social life at all, and I thank you very much for your efforts. I also must admit that your restaurant recommendations were unimpeachable. I very much look forward to visiting and wanted to let you know that I thought the first couple episodes of Death Parade were pretty alright. To Velia Garcia, I am glad to have had a friend which whom I could share so much of the Graduate School experience. Please let me know at least a week in advance when you plan to come down and visit.

I must also give thanks to all those in my personal life who made all of this possible. To Sandhya Krishna, thank you for picking up so much of the slack in my absence. To Cathy Esensoy, who helped hold so many things together during tough times. To Ian and Mariah Till, I couldn't ask for better friends to forget my troubles with. To Vishal Shroff, thank you for always providing a mind with which to meld. To Zach Koenig, thank you for everything, and I simply cannot wait to make up for lost time. To my dearest family, Pam, Scott, and George, whose constant and steady support made so many parts of this journey possible in the first place and without whose efforts I would have lived a much less pleasant life these past years. And of course, I must thank my wife, Dr. Alinea Esensoy, whose contributions are simply too numerous to begin to express here.

Table of Contents

Figure List

Table List

List of Commonly Used Abbreviations

Ar^{Me6} = C_6H_3-2,6-(C_6H_2-2,4,6-$(CH_3)_3)_2$

bpy = 2,2′-bipyridine

Cp = cyclopentadienide, $C_5H_5^-$

Cp* = η^5-C_5H_4Me

18-crown-6 = 1,4,7,10,13,16-hexaoxacyclooctadecane

crypt-2.2.2 = 1,7,13,16,21,24-hexaoxa-1,10-di-azabicyclo[8.8.8]hexacosane

dppe = 1,2-bis(diphenylphosphino)ethane, $Ph_2PCH_2CH_2PPh_2$

dppm = bis(diphenylphosphino)methane, $Ph_2PCH_2PPh_2$

en = Ethylenediamine, $H_2NCH_2CH_2NH_2$

EXAFS = Extended X-Ray Absorption Fine Structure

H_2bpmb = 1,2-bis(pyridine-2-carboxamido)benzene

PPN = Bis(triphenylphosphine)iminium cation, $[(Ph_3P)_2N]^+$

pyz = Pyrazine (1,4-diazabenzene)

Tp′ = Hydridotris(3,5-dimethylpyrazolyl)borate

XAS = X-ray Absorption Spectroscopy

NMR = Nuclear Magnetic Resonance spectroscopy

COSY = Correlation NMR Spectroscopy

HSQC = Heteronuclear Spin Quantum Coherence

TMS- = Trimethylsilyl-; -$Si(CH_3)_3$

*t*Bu- = *Tert*-butyl-; -$C(CH_3)_3$

THF = Tetrahydrofuran

DMSO = Dimethylsulfoxide

IMes = 1,3-Dimesitylimidazol-2-ylidene

Eq. = Molar equivalents

M_n = Number average of molecular weight (of a polymer)

M_w = Weighted average of molecular weight (of a polymer)

COD = 1,5-cyclooctadiene

AcAc, acac = Acetlyacetonate

diglyme = 1-Methoxy-2-(2-methoxyethoxy)ethane

Note: Abbreviations referring to solvent molecules (ex. THF, COD etc.) are written in lower case when used in the formula of a solvate compound.

Introduction

In.1 Organometallic chemistry: definitions and brief historical context

Organometallic chemistry is the discipline that focuses on the synthesis and study of compounds containing carbon-metal bonds. To define some common terms, molecular metal compounds are often called "complexes." Complexes are composed of a metal atom or ion, often referred to as a "center," chemically bonded, or "coordinated," to some number of surrounding chemical entities. These groups are called "ligands;" ligands are generally referred to as distinct, independent units, even when part of a larger molecule. For example, the following molecule would be referred to as [(dimethyl)(diethylamine)(triphenylphosphine)platinum(II)].

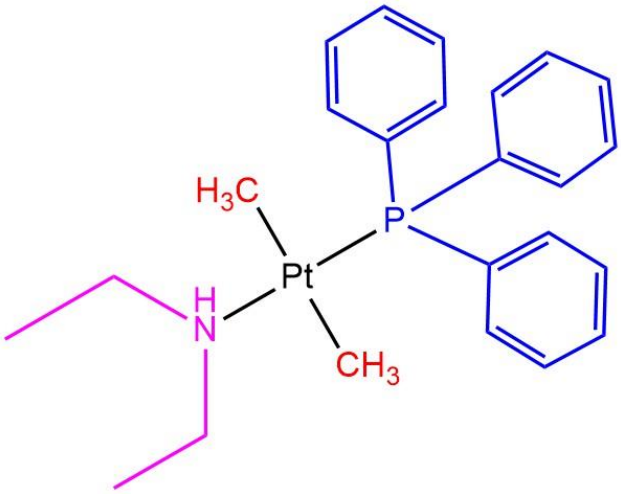

Figure In.1: Structure of a simple organoplatinum complex with color coded ligands.

Organometallic compounds are of great academic and practical importance, most notably due to their relevance to efficient catalytic processes. As such, a great deal of research is dedicated to advancing fundamental understanding of and synthetic methodology for organometallic compounds. Given the vibrant state of the modern field, one forgets that the recognition of organometallic chemistry as a distinct discipline was a fairly recent development.

The field truly began to resemble its modern form in the mid-twentieth century, spurred by the study of complexes with delocalized organic ligands. The exceptional stability of complexes such as ferrocene led to a revolution in the understanding of the structure, bonding, and reactivity of organometallic compounds, culminating in Geoffrey Wilkinson and E. O. Fischer receiving the 1973 Nobel Prize in Chemistry for their work on metallocenes.[1–3] While cyclopentadienide is the most ubiquitous of these early organic ligands, its smaller relative, the allyl ligand also played a prominent role in progressing the collective understanding of organometallic bonding, molecular dynamics, and potential applications.[4–6]

In.2 The allyl ligand

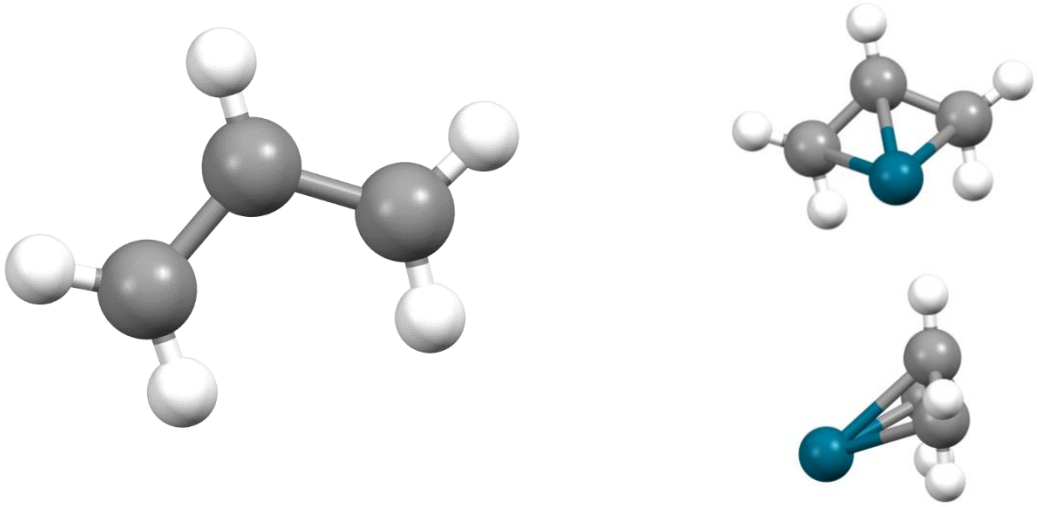

Figure In.2: Left) Simple model of the parent allyl ligand, $C_3H_5^-$ Right) Model of the η^3-binding mode most commonly seen in transition metal complexes. The allyl is planar, as expected for an ideal π-delocalized anion.

The allyl ligand ($C_3H_5^-$ = A) is the most basic of the π-delocalized organic ions, being composed of only three carbons. In the anionic form, it contains 4 π-electrons spread across its three carbon atoms backbone. As such, the most common binding mode is η^3, in which all three carbons participate equally in the carbon metal bonding. However, a notable feature of allyls is their ability to slip to a monodentate η^1-form, becoming highly compact and opening coordination sites on a metal center.

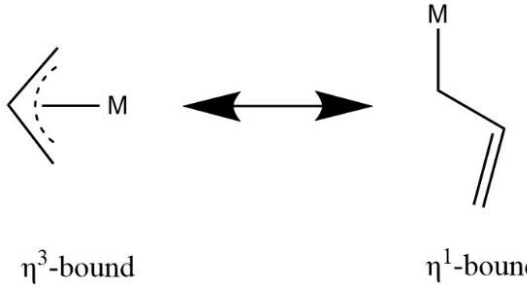

Figure In.3: Diagram of allyl "slippage," and important contributor to the diverse reactivity of allylmetal compounds

In.3 Substituted allyl ligands and the value of bulk

While its compact size and diverse bonding modes give the allyl ligand a number of desirable properties, they also create a recurring problem in the study of allylmetal complexes – instability. Allyl

complexes can decompose via a number of accessible mechanisms,[7,8] most notably reductive elimination from a metal center. Indeed, looking at the simple homoleptic complexes of the transition metals included in a 1966 review, most of them are too unstable to be handled at room temperature.[8] One common strategy to address stability issues in organometallic complexes is the use of bulky ligands.[9–11] Indeed, this has been applied with great success to the allyl ligand. The A′ ligand, shown below, has allowed chemists to access allyl complexes of 38 different elements. Nickel complexes in particular offer a compelling example of this steric stabilization. The homoleptic complex of the parent allyl ignites in air, and spontaneously decomposes below room temperature.[5] [NiA′$_2$], on the other hand, can be dissolved in hexanes and layered above water for hours before decomposing.[12]

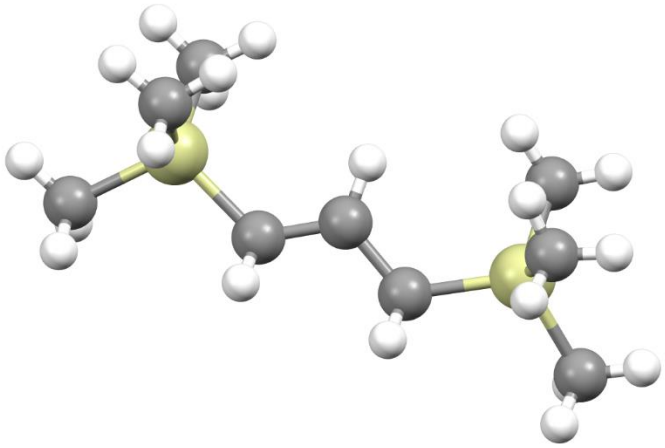

Figure In.4: Model of 1,3-bis(trimethylsilyl)allyl, an archetypal bulky allyl ligand.

In.4 Group 10 metals

The group 10 metals (nickel, palladium, and platinum) lie near the rightmost edge of the transition metal series. Like other metals in this section of the periodic table, these metals were first notable due to their general resistance towards oxidation. While the inertness of platinum metal may have long been the most notable chemical property of the group 10 metals, in recent years the spotlight has indisputably shifted onto palladium, due to its exceptional ability to catalyze organic transformations.[13] However, with palladium's increasingly recognized utility comes increased demand. This is troubling, as palladium is particularly rare in the earth's crust.[14]

Nickel offers a potentially compelling alternative to palladium, as it shares palladium's electron configuration, yet is much more common and inexpensive. While much work has been done exploring the catalytic potential of nickel, the high demand for base metal catalysts makes further development necessary. Even outside of direct comparisons with palladium, the organic chemistry of nickel is particularly interesting. As it lies to the far right of the first row of transition metals, it can be considered as an

intermediate metal between the electropositive early transition metals and the more electronegative noble metals, able to undergo reactions characteristic of both sets.

In.5 Group 10 metal allyls

Due to their shared column of the periodic table, it is unsurprising that the group 10 metals bond to allyl ligands in similar ways. For all three metals, the most common oxidation state is +II, corresponding to a d^8-electron configuration. As such, allyl complexes of these metals most commonly display square planar geometries. As the allyl group takes up two, necessarily adjacent coordination sites, there is a limited number of ways to complete the coordination sphere; while there are exceptions, the majority of compounds do so in one of the three ways shown below in Figure In.4.

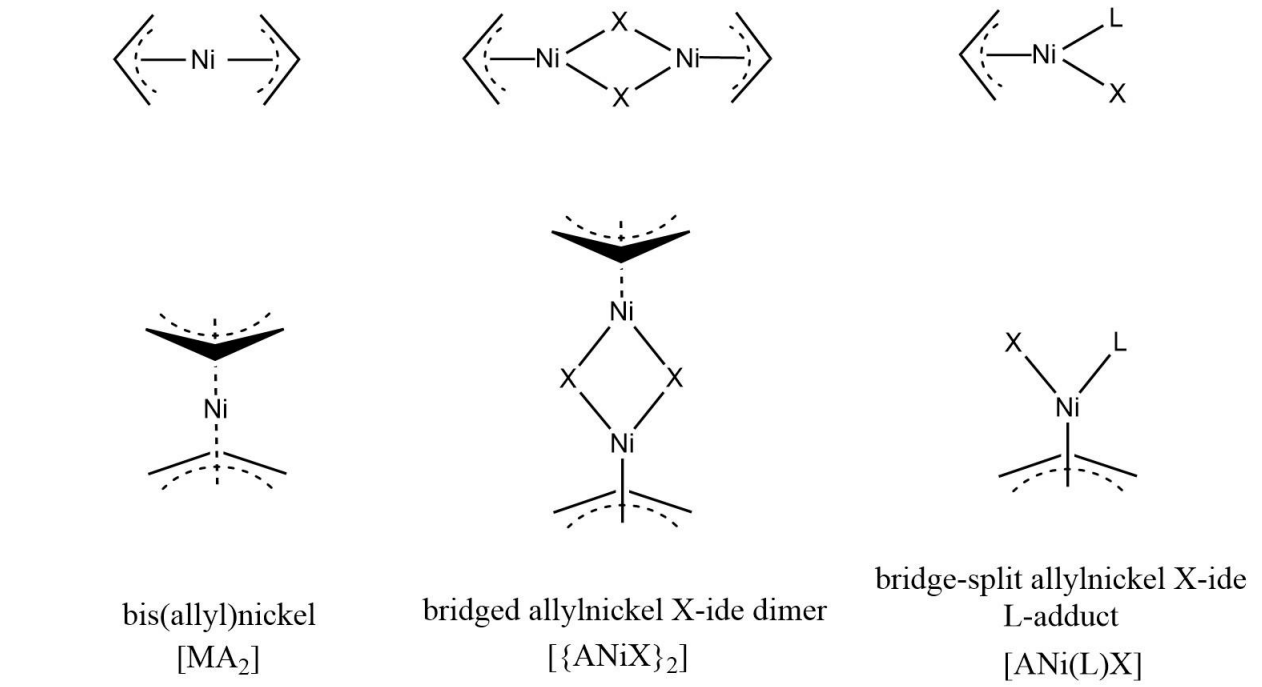

Figure In.5: 2- and 3-dimensional representations of the three most common structural motifs in allyl-nickel compounds, along with common ways to refer to them. X refers to a monodentate anionic ligand, while L refers to a monodentate neutral ligand. Nickel is used here as an example, but the same motifs are commonly observed for palladium and platinum.

Most of the allyl complexes that will be discussed in this work fall into one of the three above categories, so certain consistently observed stereochemical relationships will be introduced here. The terminology used in the literature for these relationships varies greatly; indeed, all three pairs of terms discussed below have been used to describe the single relationship depicted in Figure In.5B. In this work, I attempted to adopt terminology that is clear and intuitive, yet still broad enough to effectively describe the surprisingly complex stereochemical space generated by these compounds.

The three-carbon allyl backbone is inherently directional, forming a triangle that can point in one direction or the other. In any complex that contains two allyl groups, the triangles of the two allyl groups can be pointing in the same direction (eclipsed) or opposite directions (staggered). Groups bound to the terminal allyl carbons can either point in the same direction as the three-carbon triangle, called *syn*, or in the opposite direction, termed *anti*. This is not a trivial distinction; *syn* and *anti* substituents show meaningful differences in their structural and spectroscopic properties.

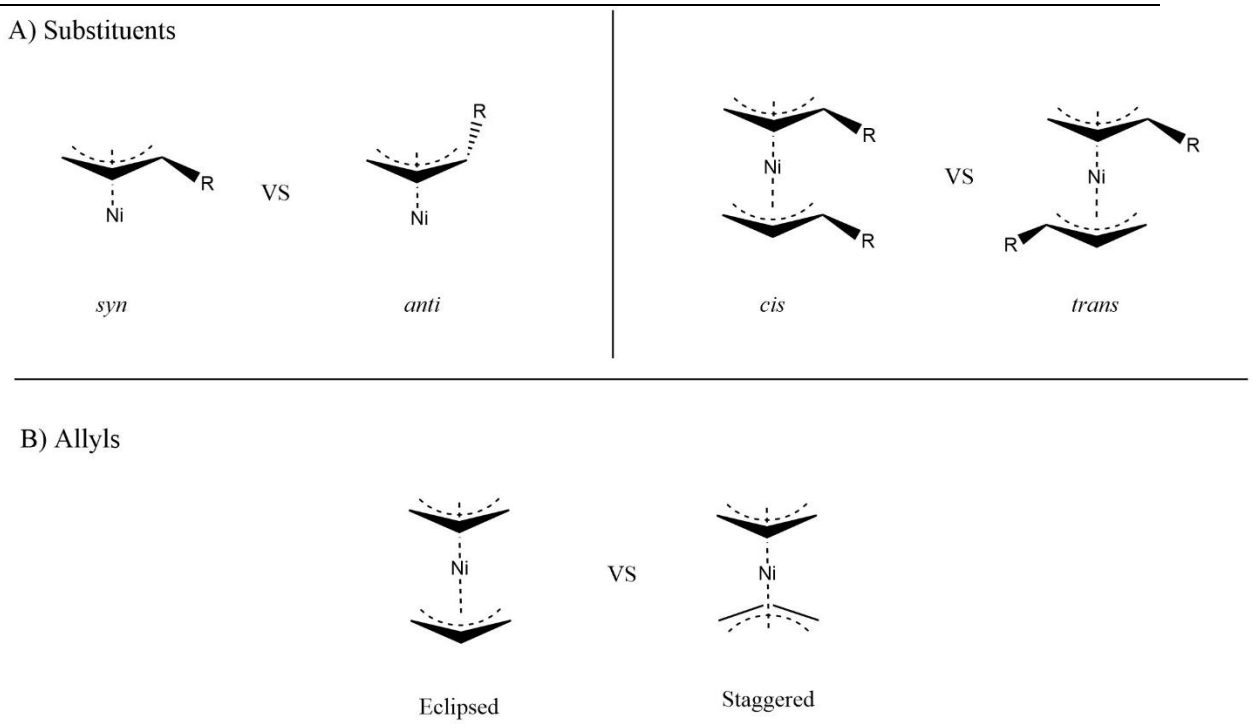

Figure In.6: Definitions of commonly invoked stereochemical relationships seen in allylnickel complexes. A) Configurations for each terminal allyl substituent or for a pair of terminal substituents B) A relationship defined by the relative orientation of two separate allyl backbones.

Finally, if two substituted allyls are present at the same metal center, the substituted carbons can lie on the same side of molecule or on opposite sides of the molecule. These "sides" can be formally defined by a plane running through the metal center and both center allyl carbons. This formalism is also used in the common case of disubstituted bis(allyl) complexes with different substituents on the 1 and 3 carbons. If both copies of a substituent lie on the same side of the molecule, it is considered *cis*.

In.6 References:

(1) Fischer, E. O.; Pfab, W. Cyclopentadien-Metallkomplexe Ein Neuer Typ Metallorganischer Verbindungen. *Z. Naturforsch. - Sect. B* **1952**, *7* (7), 377–379. https://doi.org/10.1515/znb-1952-0701.

(2) Wilkinson, G. Ferrocene. *Org. Synth.* **1956**, *36* (September), 31.

https://doi.org/10.15227/orgsyn.089.0274.

(3) Wilkinson, G.; Rosenblum, M.; Whiting, M. C.; Woodward, R. B. THE STRUCTURE OF IRON BIS-CYCLOPENTADIENYL. *J. Am. Chem. Soc.* **1952**, *74* (8), 2125–2126.

(4) Fischer, E. O.; Burger, G. Uber Ein Dimeres Pi-Allyl-Nickel-Brornid. *Z. Naturforsch.* **1961**, *16 b*, 77–78.

(5) Wilke, G.; Bogdanovic, B. Bis-Pi-Allyl-Nickel. *Angew. Chem.* **1961**, *73* (23), 756. https://doi.org/https://doi.org/10.1002/ange.19610732306.

(6) Jolly, P. W.; Wilke, G. π-Allyl Nickel Complexes. In *The Organic Chemistry of Nickel*; Academic, 1974; pp 329–401. https://doi.org/10.1016/b978-0-12-388401-5.50012-9.

(7) Henc, B.; Jolly, P. W.; Salz, R.; Stobbe, S.; Wilke, G.; Benn, R.; Mynott, R.; Seevogel, K.; Goddard, R.; Krüger, C. Transition Metal Allyls III The (η^3-Allyl)2M Complexes of Nickel, Palladium and Platinum: Structural Considerations. *J. Organomet. Chem.* **1980**, *191* (2), 449–475. https://doi.org/10.1016/s0022-328x(00)81073-6.

(8) Wilke, G.; Bogdanović, B.; Hardt, P.; Heimbach, P.; Keim, W.; Kröner, M.; Oberkirch, W.; Tanaka, K.; Steinrücke, E.; Walter, D.; Zimmermann, H. Allyl-Transition Metal Systems. *Angew. Chem. Int. Ed. Engl.* **1966**, *5* (2), 151–164. https://doi.org/10.1002/anie.196601511.

(9) Power, P. P. Some Highlights from the Development and Use of Bulky Monodentate Ligands. *J. Organomet. Chem.* **2004**, *689* (24 SPEC. ISS.), 3904–3919. https://doi.org/10.1016/j.jorganchem.2004.06.010.

(10) Poater, A.; Bahri-Laleh, N.; Cavallo, L. Rationalizing Current Strategies to Protect N-Heterocyclic Carbene-Based Ruthenium Catalysts Active in Olefin Metathesis from C-H (de)Activation. *Chem. Commun.* **2011**, *47* (23), 6674–6676. https://doi.org/10.1039/c1cc11594d.

(11) Chmely, S. C.; Hanusa, T. P. Complexes with Sterically Bulky Allyl Ligands: Insights into Structure and Bonding. *Eur. J. Inorg. Chem.* **2010**, No. 9, 1321–1337. https://doi.org/10.1002/ejic.200900813.

(12) Quisenberry, K. T.; Smith, J. D.; Voehler, M.; Stec, D. F.; Hanusa, T. P.; Brennessel, W. W. Trimethylsilylated Allyl Complexes of Nickel. The Stabilized Bis(π-Allyl)Nickel Complex [H3-1,3-$(SiMe_3)_2C_3H_3]_2$Ni and Its Mono(π-Allyl)NiX (X = Br, I) Derivatives. *J. Am. Chem. Soc.* **2005**, *127* (12), 4376–4387. https://doi.org/10.1021/ja044308s.

(13) Seechurn, C. C. C. J.; Kitching, M. O.; Colacot, T. J.; Snieckus, V. Palladium-Catalyzed Cross-Coupling A Historical Contextual Perspective to the 2010 Nobel Prize. *Angew. Chem. - Int. Ed.* **2012**, *51*, 5062–5085.

(14) Helmi, A.; Gallucci, F.; Van Sint Annaland, M. Resource Scarcity in Palladium Membrane Applications for Carbon Capture in Integrated Gasification Combined Cycle Units. *Int. J. Hydrogen Energy* **2014**, *39* (20), 10498–10506. https://doi.org/10.1016/j.ijhydene.2014.05.009.

Chapter 1: Transition Metal Cyanide Complexes

The contents of this chapter were modified from its original publication as "Cyanide Complexes of the Transition Metals" in Encyclopedia of Inorganic and Bioinorganic Chemistry, 2020, R. A. Scott (Ed.) and has been reproduced with the permission of the publisher and my co-author, Timothy Hanusa.

Abstract

Cyano metal complexes contain one or more bound cyanide ligands, CN^-, and constitute one of the largest and longest-known classes of compounds in inorganic chemistry. Like carbon monoxide, the cyanide ion can function as a π-acid ligand, but because of its negative charge, the cyanide ion can also form strong sigma bonds. This bifunctional behavior allows CN^- to stabilize both high and low oxidation states of metals. The cyanide ion can bind to metals in both terminal and bridging (M–C≡N–M′) modes; bridges are present in Prussian Blue and many other polymeric metal cyanides and are most commonly linear. Framework solids with high degrees of void space can be formed with bridging cyanide ligands. Cyano metal complexes undergo a variety of oxidation-reduction reactions but, owing to the strong sigma-donor properties of CN^-, only a few ligands are capable of directly replacing metal-bound cyanide. For most substitution reactions, photochemically-induced dissociation of one or more of the CN^- ligands is required. Cyano complexes are used as pigments and dyes, and are being increasingly employed as electroactive, zeolitic, and chemical sensing materials.

1.1 Introduction

The cyanide ion, CN^-, is one of the most common and longest-known ligands in coordination chemistry. The first coordination compound to be intentionally synthesized was the cyano metal complex Prussian Blue, $[Fe_4\{Fe(CN)_6\}_3]$, made by the Berlin dye maker Johann Diesbach and the alchemist Johann Dippel in the first decade of the 18th century, likely around 1706.[1] Much of our understanding of classic coordination chemistry can be attributed to research on cyano metal complexes.

Cyanide complexes are often compared to metal carbonyls, and both cyanide and carbon monoxide, CO, can function as π-acid ligands. Unlike CO, the cyanide ion possesses a negative charge, and can form very strong σ-bonds with metal ions. This characteristic, along with other behavior such as the formation of a hydracid (HCN) and a dimer (cyanogen, $(CN)_2$), is reminiscent of halogen ligands; the cyanide ion has accordingly been described as a *pseudo*-halide. Cyano metal complexes in fact display some similarities to metal halide complexes, which has often led them to be classified. However, with very few exceptions, all

cyanide complexes display metal-carbon interactions, the defining characteristic of organometallic compounds, so they are also sometimes included in this grouping. Comprehensive coverage of early cyano metal chemistry can be found in the classic monograph by Sharpe;[2] more recent, specialized reviews are available.[3–7]

1.2 The Cyanide Ion

1.2.1 Properties of the Cyanide Ion

The cyanide ion is isoelectronic with CO, N_2 and NO^+, and is modeled in the Lewis sense as a nitrogen triply bonded to carbon, with each atom having a lone pair of electrons ($[:C{\equiv}N:]^-$). The carbon-nitrogen triple bond distance is 1.17 Å in the free cyanide ion; the fundamental vibrational frequency of the C≡N bond (aqueous solution) is 2080 cm^{-1}. The effective crystallographic radius of CN^-, as determined in cubic alkali metal cyanides, is 1.92 Å; this value is intermediate between those of chloride and bromide. As expected from electronegativity considerations, calculations have indicated that the negative charge of the cyanide ion is predominantly on the N atom.[8] As a step above the Lewis picture, a basic molecular orbital analysis yields the electron configuration $(1\sigma)^2(2\sigma)^2(3\sigma)^2(4\sigma)^2(1\pi)^4(5\sigma)^2$. This treatment is distinct from the Lewis model in that no non-bonding lone pairs are present in the MO configuration; instead, the weakly antibonding 5σ orbital shows substantial density around both atoms. The slight polarization of this antibonding orbital towards the less electronegative carbon is the cause of the cyanide ion's preference towards C-M rather than N-M binding. The simpler Lewis model is generally sufficient to describe the reactivity of the cyanide anion, but more complex interactions, such as those involving the vibrational frequencies of cyanide complexes, require MO-based rationalizations.

1.2.2 Cyanide Ion as a Ligand

When the cyanide ion binds to metal atoms through the lone pair of electrons on the carbon atom, the resulting M–CN σ-bond is one the strongest metal-ligand bonds known. The σ-donor capacity of CN^- allows it to stabilize transition metals with high oxidation numbers. However, the cyanide ion also can function as a π-acid ligand (Figure 1.1), by accepting electron density from a filled metal d-orbital into an empty antibonding orbital of the carbon-nitrogen bond. This allows CN^- to stabilize transition metals with low oxidation numbers as well; hence cyano complexes can often be formed for several different oxidation states of a given metal. It should be stressed, however, that owing to the repulsive effect of its negative charge, the π-bonding capability of CN^- is considerably less than that of either CO or NO^+.

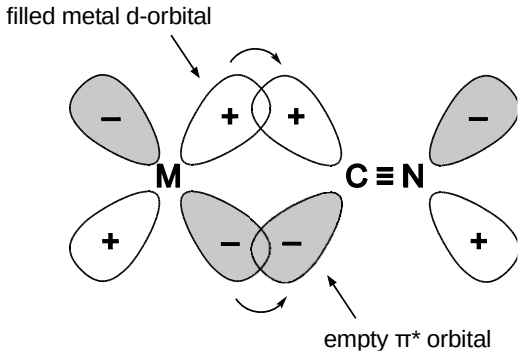

Figure 1.1: 1π-Backbonding in the metal–cyanide bond

The bonding properties of CN^- make it a very strong-field ligand, one of the highest in the spectrochemical series. The strong-field character of CN^- is exemplified by its ability to form a low-spin octahedral Fe^{II} complex, $[Fe(CN)_6]^{4-}$, and in its stabilization of a d^7, square-planar Co^{II} complex, $(PPN)_2[Co(CN)]_4$.[9] The cyanide ion also exhibits a strong *trans* effect and a large nephelauxetic effect, indicative of the high degree of covalency often displayed by metal-cyanide bonds.

1.2.3 Binding Modes

Monodentate cyanide ligands most often bind to metal centers through the carbon atom as in (I) (Figure 1.2). Monodentate isocyano linkages (II) were originally confined to a few gas-phase species, but solid state examples now known as well, such as the trigonal pyramidal $[U(NC)\{N(SiMe_3)_2\}_3]$ (**1**).[10] Cyanide also can act as a bridging, bidentate ligand through binding of the lone pair of electrons on the nitrogen atom to another metal center. Usually, the cyanide ion bridges two metals in a linear fashion (III); this type of bridging cyanide is present in Prussian Blue and several other polymeric metal cyanides. Other CN^- bridging modes, although much less common, are known. Cyanide is capable of acting as a σ-π bridging ligand, as in (V). In complexes of this type, e.g., (**2**), the bridging bond is formed by metal coordination to the π-bond of the cyanide.[11] Cyanide also can bond to metals with a single-atom bridging structure analogous to that seen in metal carbonyls, (VI) and (VII). In $\{[Cu^{II}(en)_2]_2[Cu^{I}_2(CN)_6]\}[Cu^{II}(en)_2]_2[Cu^{I}(CN)_3]_2$ (**3**),[12] the carbon atoms of the cyanides bridge two Cu atoms, whereas in $Ru_3(CO)_{10}[\mu\text{-NC–Mn}(CO)_2Cp]_2$ (**4**), the nitrogen atoms are bridging.[13]

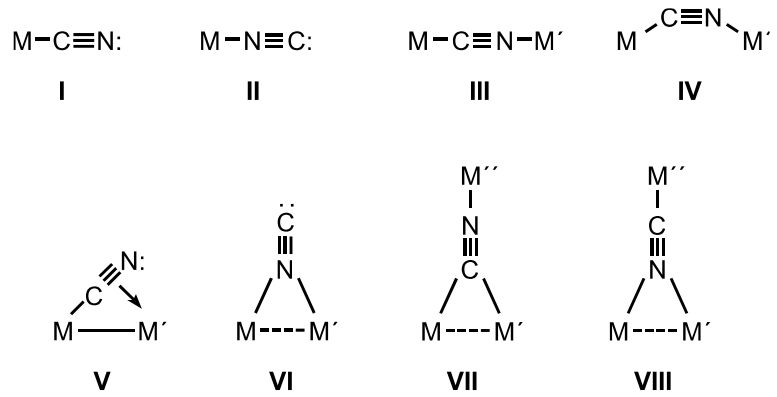

Figure 1.2: Metal–ligand binding modes found in cyanide complexes

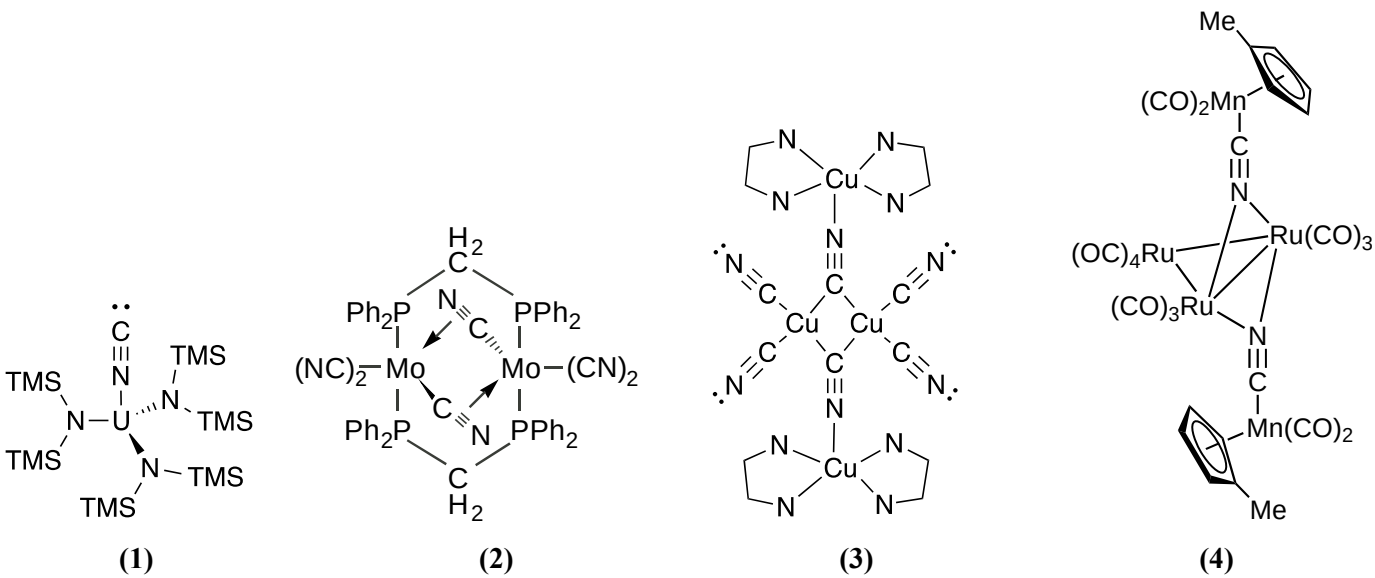

1.3 Synthesis

1.3.1 Cyanide Substitution

Cyano metal complexes are commonly formed by the addition of an excess of cyanide ion (usually as an alkali metal salt) to a transition metal complex in water or a polar organic solvent (equation 1.1).[2] The completely cyanide-substituted metal complex is usually isolated from these reactions, although one or more steps in the reaction may be relatively slow. In certain cases, cyanide substitution is not complete, resulting in partially substituted cyano metal complexes; an example is the addition of CN^- to Pt^{II} alkyl compounds, from which $[PtR(CN)_3]^{2-}$ species are isolated.[14] Heterometallic cyanoaurate complexes such as

$KCo[Au(CN)_2]_3$, $KNi[Au(CN)_2]_3$, and $Cu(H_2O)_2[Au(CN)_2]_2$ have been prepared by grinding stoichiometric amounts of $K[Au(CN)_2]$ and transition metal(II) chlorides for ca. 30 minutes.[15] The solution reactions are much slower, and 4 days are required for the formation of $KNi[Au(CN)_2]_3$ in water from the same reagents.

$$ML_n^{x+} + CN^- \text{ (excess)} \xrightarrow{H_2O} [M(CN)_m]^{x-} + nL \quad (1.1)$$

External oxidizing or reducing reagents are often used during CN^- substitution reactions to change the oxidation state of the metal in the cyano complex. Cyanide itself can act as a reducing agent in these reactions, as it is easily oxidized to cyanogen, $(CN)_2$, or cyanate, CNO^-.[2] Liquid ammonia is used as a solvent for the synthesis of hydrolytically unstable cyano complexes, such as those of Ti^{III} and the f-block metals,[16] or to provide added solubility in the synthesis of Ag^I and Au^I cyanides.[17] In the case of the square planar $[Pt(CN)_4]^{2-}$ complexes, partial oxidation with halogens produces the one-dimensional conducting salts $[Pt(CN)_4]X_{0.3}\bullet 3H_2O$.[18]

1.3.2 Oxidative Addition

Cyano metal complexes can be formed by the oxidative addition of cyanogen to a transition metal complex.[19] The oxidative addition of $(CN)_2$ usually requires a low valent, electron-rich metal center such as Ni^0, Pt^0 or Rh^I; this leads to *trans* dicyanide complexes, unless steric crowding at the metal center enforces a *cis* geometry on the incoming cyanide ligands. Owing to the synthetic utility of the -CN functional group, recent years have seen substantial development in E-CN bond activations. Oxidative addition of E-CN (E = H, Si, B, Ge, Sn, S, Br, and O) bonds to transition metal centers has been proposed as an important step in various catalyzed cyanation reactions (e.g., equation 1.2).[19]

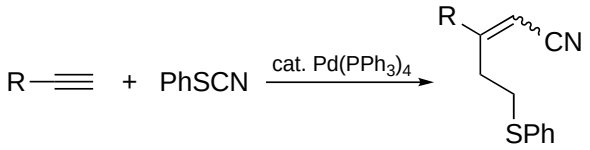

(1.2)

1.3.3 Indirect Synthesis of the Cyanide Ligand

There are cases in which a cyanide ligand is generated during a reaction to give a cyano metal complex. The addition of PMe_3 to an alkylruthenium nitrosyl complex results in a Ru-bound cyanide formed from the NO^+ and methyl ligands (equation 1.3).[20] Pyrazine and nitric acid are found to react in the presence of CuO to give a polymeric Cu^I cyanide complex; the coordinated cyanide is evidently generated by acid catalyzed decomposition of the pyrazine (equation 1.4).[21] The reductive cleavage of the nitrogen-alkyl bond in isocyanide ligands, –C≡NR, is another indirect route to cyano metal complexes. The iron^0 complex $(PMe_3)_2Fe(CNBu^t)_3$ reacts upon mild heating to yield isobutylene and $(PMe_3)_2(CNBu^t)_2FeH(CN)$ in quantitative yield, in which N-C bond cleavage is followed by C-H bond activation.[22] Directly analogous

reactivity has also been demonstrated by main group metals; the germanium isocyanide adduct $(Ar^{Me6})_2GeCNBu^t$ reacts with excess isocyanide under mild heating and vacuum to yield the corresponding diarylgermanium cyanide hydride compound (equation 1.5).[23]

$$(C_5Me_5)Ru(NO)(CH_3)_2 + 2\,PMe_3 \xrightarrow[C_6H_6]{150\ ^\circ C} (C_5Me_5)Ru(PMe_3)_2CN + CH_4 + H_2O \quad (1.3)$$

$$CuO + pyz + HNO_3 \xrightarrow[2\ days]{200\ ^\circ C} Cu(CN)(pyz) + Cu(NO_2)_2(pyz) \quad (1.4)$$

$$Ge(Ar^{Me6})_2 + CNBu^t \longrightarrow (Ar^{Me6})_2GeCNBu^t \longrightarrow (Ar^{Me6})_2Ge(H)(CN) \quad (1.5)$$

Carbon atom transfer from the carbene bis(diisopropylamino)cyclopropenylidene (BAC) to the Fe^{IV} nitride complex $PhB(^iPr_2Im)_3Fe{\equiv}N$ generates $PhB(^iPr_2Im)_3Fe(CN)(N_2)(BAC)$ along with the alkyne $^iPr_2N–C{\equiv}C–N^iPr_2$.[24] The yellow cyano complex from this four-electron reaction is in equilibrium with the blue N_2-free analogue.

1.4 Reactions

1.4.1 Electrochemistry

Cyano metal complexes undergo a variety of oxidation-reduction reactions. One of the most studied is the fast self-exchange reaction of the $[Fe(CN)_4]^{3/4-}$ anions, and information from this research was instrumental in establishing the outer-sphere mechanism for transition metal oxidation-reduction reactions. The nature of the solvent has a pronounced effect on the oxidation of $[Fe(CN)_6]^{4-}$; its rate of oxidation by O_2 is dramatically enhanced in electron-donor solvents. Conversely, the reduction of $[Et_4N]_3[Fe(CN)_4]$ becomes much more favorable on increasing the electron acceptor properties of the solvent.[25] Cyano metal complexes also can undergo inner sphere redox reactions. A classic illustration of the ligand interaction involved in such reactions is provided by the cyanide-bridged bimetallic complex $[(NC)_5Co^{III}(\mu\text{-}NC)Fe^{II}(CN)_5]^{6-}$, which can be isolated from the redox reaction of $[Co^{II}(CN)_5]^{3-}$ and $[Fe^{III}(CN)_6]^{3-}$.

In certain cases, a bound cyanide ligand can participate in an oxidation-reduction reaction. For example, the electroreduction of the complex *trans*-$[Mo(CN)Cl(dppe)_2]$ in the presence of phenol reduces the cyanide ligand to the simplest aminocarbyne ligand, $\equiv CNH_2$, and gives *trans*-$[(Mo{\equiv}CNH_2)Cl(dppe)_2]$. The reduction of the cyanide is reversible, as oxidation of the aminocarbyne complex regenerates *trans*-$[Mo(CN)Cl(dppe)_2]$.[26] The trigonal bipyramidal (triphosphinosilyl)iron cyanide complex in Figure 1.3 can also be converted into an aminocarbyne complex, but additionally is capable of an alternative reduction pathway. Specifically, when exposed to an excess of strong reducing agent and strong acid, the complex reacts to yield ammonia and methane in moderate yield; isotope labeling confirms that the nitrogen in the ammonia is derived from the cyanide *N*-atom.[27]

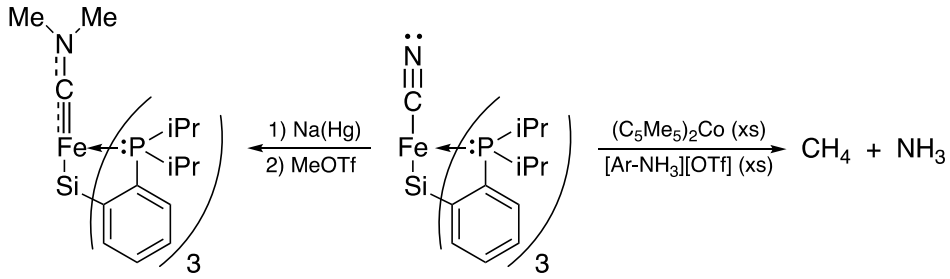

Figure 1.3: Synthesis of the neutral dialkylaminocarbyne complex [SiP^{iPr}_3]Fe($CNMe_2$), and reductive protonolysis of [SiP^{iPr}_3]Fe(CN) to form methane and ammonia.

1.4.2 Substitution of Coordinated Cyanide

Owing to the strong σ-donor properties of CN^-, only a few ligands are capable of directly replacing metal-bound cyanide: these include strong π-acids such as CO or NO^+, or aromatic N-donor chelating ligands such as 2,2′-bipyridine or 1,10-phenanthroline.[2] For most substitution reactions of cyano metal complexes, photochemically induced dissociation of one or more of the CN^- ligands is needed. A substituted cyanide complex obtained in this manner is $[Cr(CN)_5(NH_3)]^{2-}$, synthesized from the irradiation of $[Cr(CN)_6]^{3-}$ in methanol, followed by addition of ammonia (Figure 1.4).[28] In some cases, photolysis can be replaced by transmetallation, as is the case for the substitution of a cyanide for EDTA from the hexacyanoferrate ion in the presence of Hg^{2+}, though UV irradiation is still needed if catalytic reactivity is desired.[29] Although they do not generally affect the absorption spectra of cyano metal complexes, the second sphere coordination of polyammonium macrocyclic ligands can markedly suppress photochemically induced substitution reactions. This is exemplified in the decreased quantum yield of 0.10 mol/einstein for the photosolvation of the supramolecular polyammonium complex of $[Co(CN)_6]^{3-}$ (**5**), compared to quantum yield of 0.30 for free $[Co(CN)_6]^{3-}$.[30] Hydrogen bonding interactions with the cyanide ligands prevent their dissociation upon irradiation.

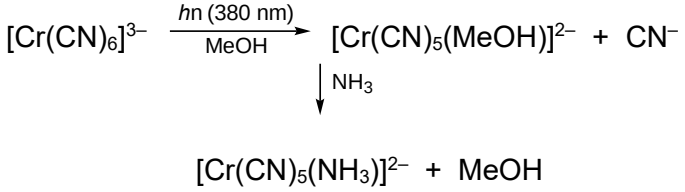

Figure 1.4: Photochemically induced CN^- substitution reaction

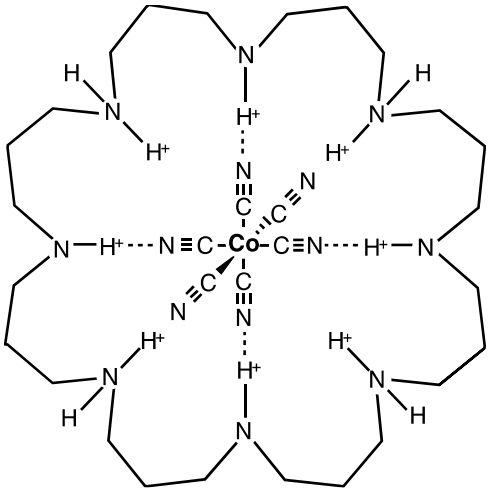

(5)

Protonation of a cyanide ligand also can lead to enhanced rates of cyanide substitution, since this weakens the M–CN σ-bond. This is especially true for *trans*-substituted cyano complexes, where the strong *trans* effect of the cyanide ligands renders them more susceptible to protonation than in *cis* cyano complexes. As a result, *trans*-$[Cr(NH_3)_4(CN)_2]^+$, for example, undergoes a substitution reaction in acidic solution to give *trans*-$[Cr(NH_3)_4(H_2O)_2]^{3+}$ at a rate approximately 1000 times that of *cis*-$[Cr(H_2O)_4(CN)_2]^+$.[31]

1.4.3 Addition to Coordinated Cyanide

The lone pair of electrons on the nitrogen atom of bound cyanide can react with Lewis acids to form adducts of the type M–C≡N:→L. Often strong Lewis acids such as BF_3 or $B(C_6F_5)_3$ are used to generate complexes of this type (equation 1.6),[32,33] although weaker Lewis acids, such as Me_3SnCl, also can form cyanide adducts (equation 1.7).[34] The binding of sterically bulky Lewis acids such as triphenylborane to coordinated cyanide ligands has been used to introduce asymmetric steric pressures, leading to increased regioselectivity in the transition metal catalyzed hydrocyanation reaction of alkenes.

$$Tp'(CO)(CN)W(PhC{\equiv}CMe) + BF_3{\bullet}Et_2O \xrightarrow{CH_2Cl_2} Tp'(CO)(CN{\bullet}BF_3)W(PhC{\equiv}CMe) + Et_2O \quad (1.6)$$

$$3\ Me_3SnCl(aq) + K_3[Cu(CN)_4](aq) + pyz \rightarrow [(Me_3SnNC)Fe(CN)(pyz)]_n \quad (1.7)$$

Addition of an electrophile to metal-bound cyanides will often form an isocyanide ligand, –C≡N–R. For example, the compound $[Fe\{P(OMe)_3\}(NO)_2(\eta^3\text{-}C_3H_4R)]$, which is a source of the allyl cation $(\eta^3\text{-}C_3H_4R)^+$,

reacts with *trans*-[Mn(CN)(CO)(dppm)$_2$] to alkylate the cyanide, giving an allyl isocyanide ligand (equation 1.8).[3] Rhenium chalcogenide clusters of the form $[Re_6Q_8(CN)_6]^{4-}$ (Q = S, Se, Te) can be alkylated with an excess of methyl triflate or trimethyloxonium tetrafluoroborate to yield the corresponding permethylated cation $[Re_6Q_8(CNCH_3)_6]^{2+}$.[35] Mixtures of silver and potassium cyanide have been used to generate isocyanides from alkyl bromides, implicating Ag(CN)(CNR) as a likely intermediate.[36] The tungsten alkyne complexes Tp′(CO)(CN)W(RC≡CR′) (R = H, Ph; R′= H, ^{n}Bu, Ph, Me) react with triflic acid or methyl triflate to form the corresponding hydrogen or methyl isocyanide complexes [Tp′(CO)(CN(H,Me))W(RC≡CR′)][O_3SCF_3] (equation 1.9).[32] Fluoroboric acid is exceptional in this regard, as the same tungsten complexes react with HBF_4 in CH_2Cl_2 solution to produce BF_3 adducts (equation 1.10), rather than the anticipated hydrogen isocyanide complexes.

$$\textit{trans}\text{-[Mn(CN)(CO)(dppm)}_2\text{]} + \text{[Fe\{P(OMe)}_3\text{\}(NO)}_2(\eta^3\text{-C}_3\text{H}_4\text{R)][PF}_6\text{]} \xrightarrow{\text{THF}} \textit{trans}\text{-[Mn(CO)(CNCH}_2\text{CH=CHR)(dppm)}_2\text{][PF}_6\text{]•thf} \quad (1.8)$$

$$\text{Tp′(CO)(CN)W(RC≡CR′)} \xrightarrow[\text{CH}_2\text{Cl}_2]{\text{[Me][O}_3\text{SCF}_3\text{]}} \text{[Tp′(CO)(CNMe)W(RC≡CR′)][O}_3\text{SCF}_3\text{]} \quad (1.9)$$

$$\text{Tp′(CO)(CN)W(RC≡CR′)} \xrightarrow[\text{CH}_2\text{Cl}_2]{\text{HBF}_4\text{, 0 °C}} \text{[Tp′(CO)(CNBF}_3\text{)W(RC≡CR′)][O}_3\text{SCF}_3\text{]} \quad (1.10)$$

1.5 Physical Methods of Characterization

1.5.1 Vibrational Spectroscopy

The characteristic absorption band in the vibrational spectroscopy of cyano metal complexes is the C≡N bond stretch, which occurs in the frequency range of approximately 1950 to 2250 cm^{-1}. Most other bands, notably the M–C bond stretch, occur at much lower wavenumbers (<600 cm^{-1}). Variations in the frequency of the C≡N bond stretching band have been used to probe the extent of metal–cyanide π-bonding; increased M–CN π-bonding decreases the strength of the C≡N bond, and therefore decreases ν(CN). For example, the C≡N stretching vibration in $[Fe(CN)_6]^{3-}$ occurs at 2135 cm^{-1}, whereas in $[Fe(CN)_6]^{4-}$ the same band is at 2098 cm^{-1}, indicative of stronger metal-cyanide π-bonding in the latter complex, with its more electron-rich metal center. Similarly, the increase in ν(CN) observed upon increasing the oxidation state of the metal (and thus decreasing the number of d electrons) has been attributed to a decrease in metal-cyanide π-bonding. It should be noted, however, that the shifts in ν(CN) due to varying degrees of π-bonding in cyano metal complexes are much smaller than the analogous shifts seen in metal carbonyls, since metal-cyanide π-bonding is weaker. Indeed, density functional theory calculations have suggested that the

effective positive charge of the metal center may be a more influential factor on ν (CN) frequencies than π-orbital considerations.[37]

In a molecular orbital analysis, the CN^- lone pairs reside in a C–N antibonding orbital, and it is to be expected that involvement of the nitrogen end of the cyanide anion in bonding will increase the strength of the carbon-nitrogen bond, which is manifested in an increase in ν(CN) for bridging cyanides. This is illustrated by the binding of BF_3 to the cyanide in Tp′(CO)(CN)W(PhC≡CMe) (equation 1.9), which shifts the C≡N bond stretching frequency from 2110 to 2185 cm^{-1}.[32] This is supported by computational work on the related HCN molecule, in which binding of the nitrogen to a Lewis acid leads to an increase in stretching frequency. It is worth noting, though, that owing to the polarization of the C–N antibonding orbital toward carbon, binding through nitrogen has less of an impact on the stretching frequency than binding through carbon, and large frequency shifts upon nitrogen binding are only seen with very strong Lewis acids.[38]

1.5.2 Diffraction Methods

X-ray diffraction has proven to be an invaluable tool for the determination of the solid-state structures of cyano metal complexes. Accurate data on bond distances and angles obtained from X-ray structural determinations have provided information on the bonding in cyano complexes, although interactions in the solid state can complicate interpretation of bond lengths. For example, the finding that in the solid state the Fe–C bond is shorter in the Fe^{II} complex $Cs_2Mg[Fe(CN)_6]$ (1.90 Å) than in the isomorphous Fe^{III} complex $Cs_2Li[Fe(CN)_6]$ (1.93 Å) was taken as evidence of stronger metal-cyanide π-bonding in the $[Fe^{II}(CN)_6]^{4-}$ ion.[2] However, the ferricyanide and ferrocyanide ions have been studied in solution with EXAFS spectroscopy, and the Fe–C bond distance is found to increase by 0.03 Å on electroreduction of Fe^{III} to Fe^{II}.[39]

High precision charge-density X-ray diffraction and spin-polarized neutron diffraction experiments on $Cs_2K[Fe(CN)_6]$ were used to determine quantitatively the electron orbital populations of the Fe–CN bonds.[40] As coordination frameworks including metal-cyanide complexes have grown in prominence, so too has the use of powder X-ray diffraction in place of single-crystal methods. Powder X-ray patterns are able to give substantial structural detail, which is invaluable for difficult to crystallize compounds.[41,42]

A common problem encountered in X-ray structural studies of oligomeric cyano metal compounds is the inability to distinguish between the carbon and nitrogen atoms in linearly bridging cyanide ligands. This problem stems from the similar electron densities and metal bond distances for both the carbon and nitrogen atoms in a bridging cyanide ligand, although in certain cases the symmetry of the lattice forces the cyanide to be crystallographically disordered over both bridging configurations.

1.5.3 NMR Spectroscopy

NMR spectroscopy (^{13}C and ^{15}N) is routinely used in the characterization of cyano metal complexes. The free CN^- ion exhibits a ^{13}C NMR shift of δ 166.2, but the ^{13}C NMR shift in complexes is almost always upfield of this value, and the ^{15}N shift is correspondingly downfield. Information on the rates of reactions for cyano metal complexes can be obtained from NMR studies. The self-exchange rates for electron transfer in the $[Fe(CN)_6]^{3-/4}$, $[Ru(CN)_6]^{3-/4-}$, $[Os(CN)_6]^{3-/4-}$ and $[W(CN)_8]^{3-/4-}$ couples have been determined with ^{13}C or ^{15}N NMR line-broadening techniques, but cation-catalyzed pathways dominate the observed rate constants. Experiments using sequestered K^+ (by either 18-crown-6 or crypt-2.2.2) found an exchange constant for $[Fe(CN)_6]^{3-/4-}$ of 2.4 x 10^2 L mol^{-1} s^{-1} (25 °C, ionic strength 0.2 mol L^{-1}); this is two orders of magnitude less than a frequently quoted value of 1.9 x 10^4 L mol^{-1} s^{-1}.[43]

When bound to strongly coupled metal centers, observation of satellite peaks in ^{13}C or ^{15}N NMR spectra can indicate the connectivity of the ligand, even when an X-ray structure is ambiguous.[44] NMR measurements on the metal nucleus in cyanide complexes also can yield useful information. For example, variable temperature ^{95}Mo NMR studies indicate that the $[Mo(CN)_8]^{4-}$ ion, which exhibits several different geometries in the solid state, is dodecahedral in aqueous solution.[45] Substantial progress has been made in NMR analysis of paramagnetic materials, and in fact the broadened spectral window displayed by these compounds can sometimes be beneficial. For example, solid state ^{113}Cd NMR studies of compounds of the form $[Cd_3\{Fe/Co(CN)_6\}_2]\cdot 15H_2O$ were able to determine the structure of lattice vacancies, which had been ambiguous under X-ray analysis.[46]

1.5.4 Other Methods

The energies of d-d electronic and metal-to-ligand charge transfer transitions that occur in transition metal cyanide complexes can be determined by electronic spectroscopy; this technique has also been used to measure reaction rates and to detect intermediates in reactions. Mössbauer spectroscopy has been used to establish the relative contribution of Fe–L σ and π-bonding in a series of $[Fe(CN)_5L]^{n-}$ complexes, and can be used in iron-containing complexes to ascertain the spin and oxidation state of the iron.[47,48] XAS spectroscopies have also come to play an important role in the electronic characterization of metal-cyanide coordination polymers.[49] The use of liquid secondary-ion mass spectrometry has been used to study the preferential solvation of the CN^- ligands during electron- and proton-transfers in the substituted cyano-ruthenium complex, *cis*-$[Ru(CN)_2(bpy)_2]$.[50]

1.6 Structures

1.6.1 Monomeric Cyano Metal Complexes

In most instances, rationalization of the geometries exhibited by monomeric cyano metal complexes is straightforward. All known six-coordinate metal cyanide complexes have the expected octahedral geometry. Cyano metal complexes with the d^{10} metal centers Au^{I} and Ag^{I} are two-coordinate, i.e. $[Au(CN)_2]^-$ and $[Ag(CN)_2]^-$, and have linear geometries. Four-coordinate cyano complexes are either tetrahedral, when the metal center has a d^{10} configuration, or square-planar in complexes containing d^8 ions such as Ni^{2+}, Pd^{2+}, and Pt^{2+}. Often the individual square-planar tetracyano metal ions stack so that the metal ions form one-dimensional infinite chains with metal-metal interactions; this is especially well-studied for the tetracyanoplatinate anion $[Pt(CN)_4]^{2-}$ and its derivatives. These chains can be straight, helical or zig-zag in shape, and can possess uniform or staggered (short-long) intermolecular metal-metal distances. Partially oxidized tetracyanoplatinate chains, such as those found in the series of Krogmann salts (e.g., $Rb_2[Pt(CN)_4]Cl_{0.3}•3H_2O$ (**6**)), are examples of one-dimensional metallic conductors.[18]

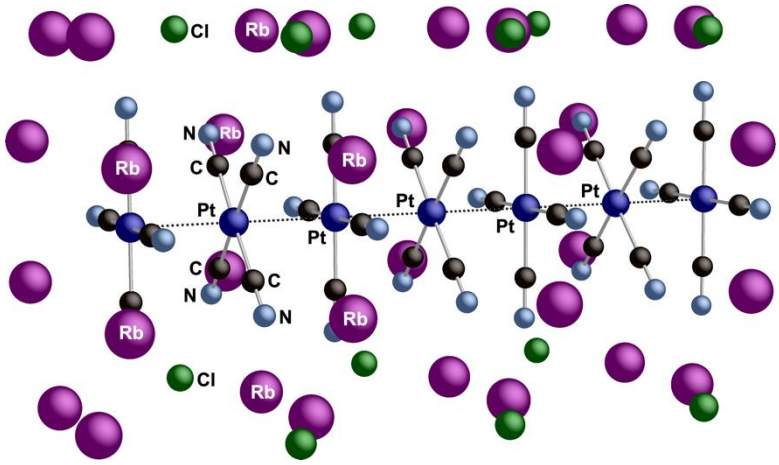

(**6**)

For certain coordination numbers, the structures of cyano metal complexes show a surprising degree of variability. For example, the complex $[Cr(en)_3][Ni(CN)_5]•1.5H_2O$ contains both square pyramidal and trigonal bipyramidal $[Ni(CN)_5]^{3-}$ ions, and desolvation of the compound converts all the anions to the square pyramidal geometry.[51] The $[Mo(CN)_8]^{3-}$ and $[Mo(CN)_8]^{4-}$ anions have variable geometries in the solid state depending on the specific counterion present. The structure of the anions ranges from dodecahedral in $K_4[Mo(CN)_8]•2H_2O$, to square antiprismatic in $Na_3[Mo(CN)_8]•4H_2O$, to approximately bicapped trigonal prismatic in $Cs_3[Mo(CN)_8]•2H_2O$.[52]

1.6.2 Bridging Cyano Metal Complexes.

One of the most distinctive features of the cyanide ligand is its ability to form a bridging M–CN–M′ bond between two metal centers. Consequently, the cyanide ion has been increasingly used as a bridging ligand in the synthesis of discrete, molecular bi- and trimetallic mixed valence compounds. A nine-membered ring is present in the trimeric compound $[Cp_2Ti(\mu\text{-}CN)]_3$ (**7**),[53] and an unusual cyclic cluster, $[(CO)Pd(\mu\text{-}CN)Mn(Cp')(CO)_2]_4$ (**8**), was obtained by the reaction of the "cyanometallate ligand" $[(CpMe)Mn(CO)_2(CN)]^-$ with a tetrameric palladium acetate cluster.[54]

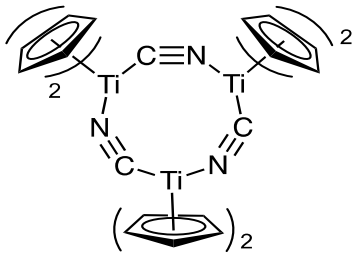

(7)

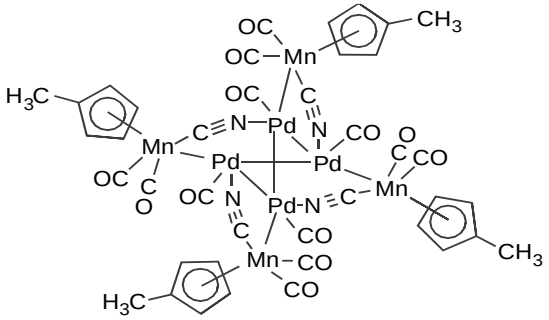

(8)

In some instances, the presence of templating ions strongly affects the nature of cage structures formed by bridging CN^- ligands. For example, reaction of $[Mo(Mes)(CO)_3]$ with $(Et_4N)CN$ in a 1:1 ratio generates $(Et_4N)_3[Mo_4(\mu\text{-}CN)_4(CO)_{12}(MeCN)_4]$, which contains a square 12-membered ring;[55] with excess cyanide in the presence of lithium or sodium as templating ions, the tetrahedral cyanometallates $(Et_4N)_5[(Li,Na)\{Mo_4(\mu\text{-}CN)_6(CO)_{12}\}]$ are formed (**9**).[56] Furthermore, addition of Cs^+ will convert the tetrahedral species into the cesium analogue of the less strained, trigonal prismatic cage $(Et_4N)_8[K[Mo_6(\mu\text{-}CN)_9(CO)_{18}]$. The same trigonal prismatic cage (**10**) will be formed if K^+ ion is used instead of Li^+ or Na^+ in the original reaction.[55] A box-like aggregate forms from $[(C_5Me_5)Rh(CN)_3]^-$ and $[Mo(Mes)(CO)_3]$ in the presence of K^+ or Cs^+ (**11**).

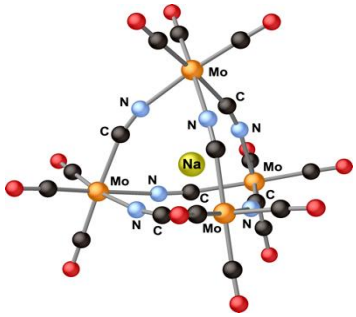

(9)

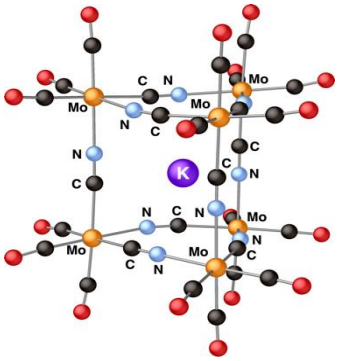

(10)

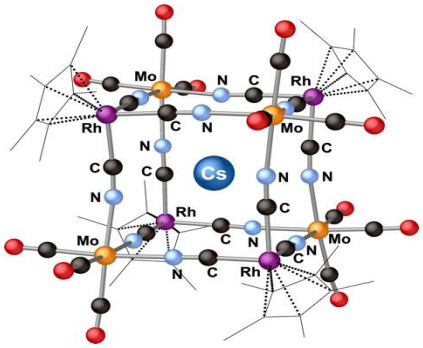

(11)

Many other large aggregates are known, such as $[Mn^{II}\{Mn^{II}(MeOH)_3\}_8(\mu\text{-}CN)_{30}\{Mo(V)(CN)_3\}_6]\bullet 5MeOH\bullet 2H_2O$ (**12**), in which six Mo(V) ions surround a central Mn^{II} ion, and the faces of the octahedron are capped by eight additional Mn^{II} ions, producing an approximate rhombododecahedron.[57] The molecule has 51 unpaired electrons, and ferromagnetic coupling leads to an $S = {}^{51}/_2$ ground state. The bimetallic $[\{Mn(salen)\}_6\{Fe(bpmb)(CN)_2\}_6]\cdot 7H_2O$ (**13**) forms a macrocyclic structure from simple precursors, while its corresponding linear polymeric analogue is not observed.[58]

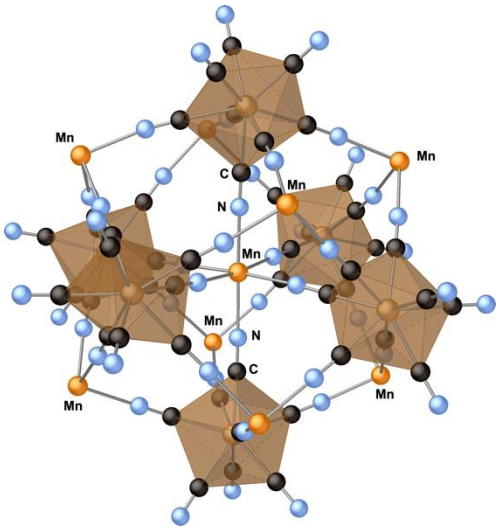

(12)

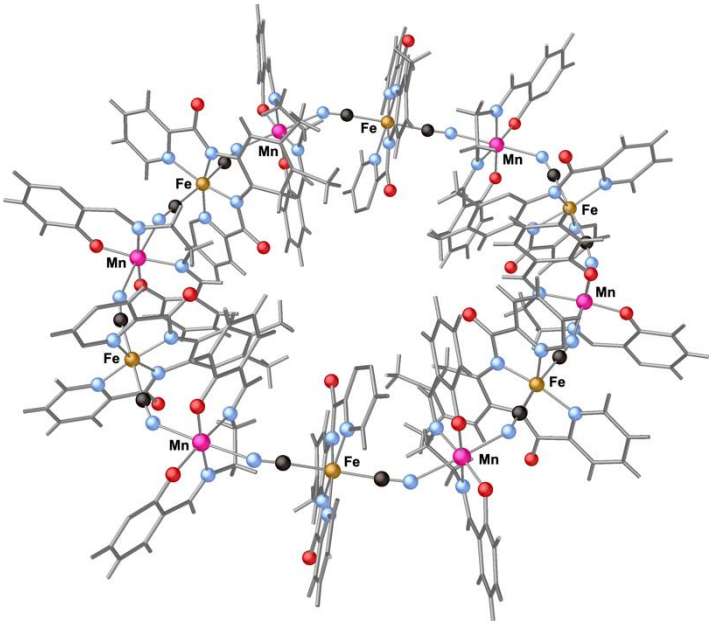

(13)

Unlike the discrete molecular complexes described above, many compounds with bridging cyanide ligands are three-dimensional coordination polymers. The classic example of this type of compound is Prussian Blue, $[Fe_4\{Fe(CN)_6\}_3]\bullet xH_2O$ (**14**), whose intense color arises from an intervalence transfer

transition from low-spin Fe^{2+} to high-spin Fe^{3+} at 680 nm. Although long in dispute because of various amounts of water and/or potassium ions in different samples (potassium ions are present in "soluble" Prussian Blue, which is actually a colloidal dispersion), the generally accepted structure has a cubic face-centered lattice with CN^- ligands on the edges of the cube bridging the iron cations. The iron centers have octahedral geometries with the Fe^{2+} ions ligated by six C-bonded cyanides and the Fe^{3+} ions by six N-bonded cyanides.[59] To achieve the 4:3 ratio of the iron atoms, one-fourth of the $[Fe(CN)_6]^{4-}$ groups are absent from the lattice; the vacancies left by the cyanide ligands are occupied by coordinated water molecules.

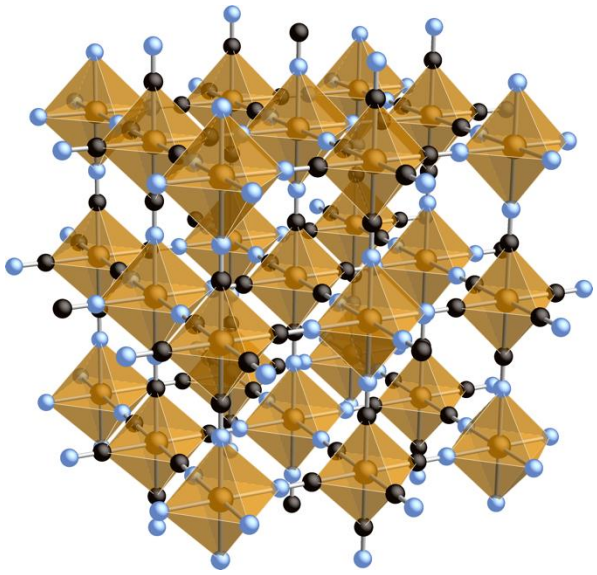

(14)

Many other transition metals also form hexacyanometallate coordination polymers; heterometallic species can also be easily accessed by addition of a coordinatively unsaturated metal ion to a source of cyanometallate ions. Both of these classes of compounds tend to have structures directly analogous to Prussian Blue, with cubic repeating units of octahedrally coordinated metal centers. The size and free volume of these cubic units can be varied by modifying the metals used, allowing for tunable porosity. This architectural regularity can be broken, however, by incorporating a chelating organic ligand in addition to cyanide. These heteroleptic species also form cyanide-bridged coordination polymers but restricted to two or even just one dimension. With appropriate consideration of metal valency and choice of ancillary ligand, a high degree of control of atomic scale architecture can be achieved.[60–62]

A wide variety of other structural types are known for polymeric cyano complexes, some with high

degrees of void space (>50%). These range from "expanded" Prussian blues, in which octahedral $[Fe(CN)_6]^{4-}$ units are replaced with larger aggregates such as $[Re_6Se_8(CN)_6]^{4-}$ (**15**),[63] to the interpenetrating diamond-like frameworks of $[Cd(CN)_2]_n$, to the PtS-related structure of $[NMe_4][CuPt(CN)_4]$, which has large hexagonal and square channels.[64] Often the structures of polymeric cyano complexes can be related to the structures of silicates and zeolites.[41] Cyano metal complexes also form an immense variety of clathrates, examples being the so-called Hofmann-type clathrates $M(NH_3)_2M'(CN)_4 \bullet (guest)_2$ (M = Mn, Fe, Co, Ni, Cu, Zn, Cd; M′= Ni, Pd, Pt; guest = C_4H_5N, C_4H_4S, C_6H_6, $C_6H_5NH_2$), and "mineralomimetic" compounds with a β-cristobalite $Cd(CN)_2$ framework; the latter can be crystallized with a variety of hydrocarbon, chlorocarbon, and chlorofluorocarbon molecules in their structural cavities.[65]

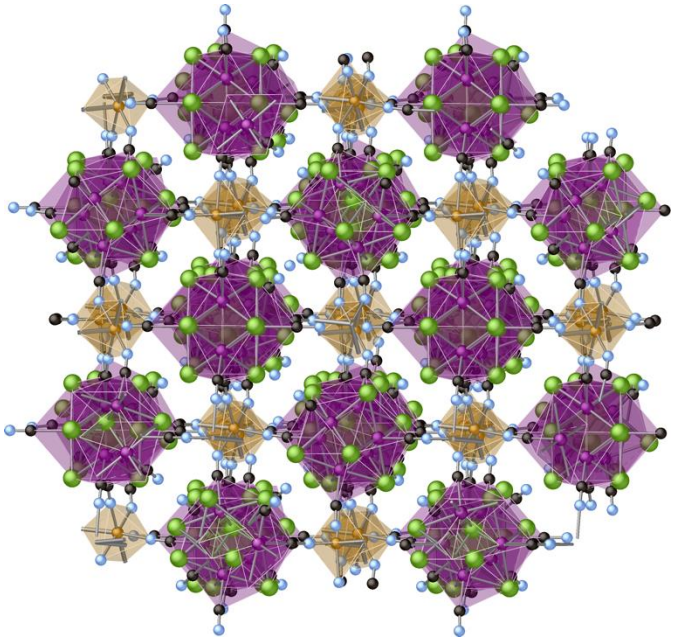

(15)

An important feature of cyanometallate coordination polymers is their structural stability. These compounds are generally stable in solvents, including acidic aqueous solution, and are often stable to 150 °C and above. The structural persistence of this class of compounds is well illustrated by heterobimetallic cyanometallate species; these are frequently formed as hydrates, in which the coordination sphere of the non-cyanated metal is saturated by solvent molecules. However, the water molecules can be thermally removed without substantially changing the structure of the coordination polymer. For the copper ferricyanide compound $Cu_2[Fe(CN)_6]_2 \bullet 10H_2O$, for example, dehydration merely induced a 3% reduction in the unit cell volume.[41] Indeed, this unsaturation of the coordination sphere of a metal ion with limited rearrangement is an important factor in the adsorptive abilities of these materials.[66]

1.7 Applications

Historically, the major application of cyano metal complexes was centered on Prussian Blue and its use as a pigment in the painting, printing and dying industries. Since the 1970s, however, organic pigments such as phthalocyanine blue have supplanted Prussian Blue for some of these purposes. Prussian blue has been used as an oral drug to increase fecal excretion of cesium and thallium and has been used to remediate nuclear wastes containing ^{137}Cs. Prussian Blue has been deposited in thin films on chemically modified electrodes. Such electrodes have been used for ion detection and promoting electrocatalytic reactions.

Expansion of the field of cyanometallate coordination frameworks has led to a parallel expansion in potential applications. Many of these applications make use of the unique porosity of these materials. For example, transition metal nitroprussides, $M_x[Fe(NO)(CN)_5]_y$, are promising materials for reversible hydrogen storage,[67] while $[Fe(pyz)Pt(CN)_4]$ is able to capture CO_2 very effectively with limited structural degradation over many adsorption/desorption cycles.[68] The architecture can also be designed for efficient capture of ions in pores. This has led to interest in cyanometallate materials as detectors of hazardous waste.[62,69] The ability to reversibly capture small cations has also spurred research into next generation batteries with lower manufacturing costs and greater energy density than lithium-ion technology.[70–72]

As noted above, the synthetic utility of the nitrile functional group has led to increased development of various cyanation reactions. Cyanation provides a convenient 1-carbon synthon that can be later converted into other terminal nitrogen functionalities. These reactions are often transition metal catalyzed, and mechanistic studies frequently suggest that oxidative addition of an organic cyanide to a low oxidation state metal is involved. These transition metal–cyanide intermediate complexes are sometimes isolated and characterized; such is the case for the nickel $(C_6HF_4)(PCy_3)_2Ni(CNBPh_3)$ (**16**), which was implicated in the catalytic conversion of alkynes to 1-cyano-2-polyfluoroarylalkenes; the binding of a Lewis acid like BPh_3 appears to be important in facilitating the initial C-CN bond cleavage.[73] Recent developments in methodology using more diverse cyanide sources have also allowed for the concurrent installation of multiple functionalities.[19]

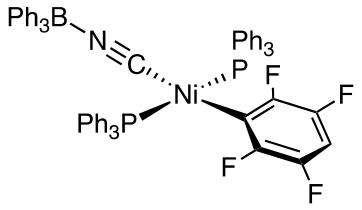

(16)

As previously noted, the ability of the cyanide ligand to bridge between multiple metal centers gives rise to a diverse and tunable set of architectures. Furthermore, given its Lewis acid-base amphiphilicity, electronic or magnetic energy can be passed from one metal center to another through cyanide bridges. As

such, heterometallic cyanide-bridged species are of major importance in the development of multiferroics, photomagnets, and molecular switches.[74–77] Of particular interest is their use in single chain magnets. The excellent bridging ability of the cyanide ligand allows for access to 1-D materials that have the high degree of magnetic anisotropy that is desired for such materials.[78] In the cyanide-bridged Co^{II}/W^{V} complex (**17**), distortion of the coordination environment of one of the cobalt atoms (Co′) in the repeating unit creates an asymmetric magnetic environment, leading to very strong single chain magnetic behavior.[79]

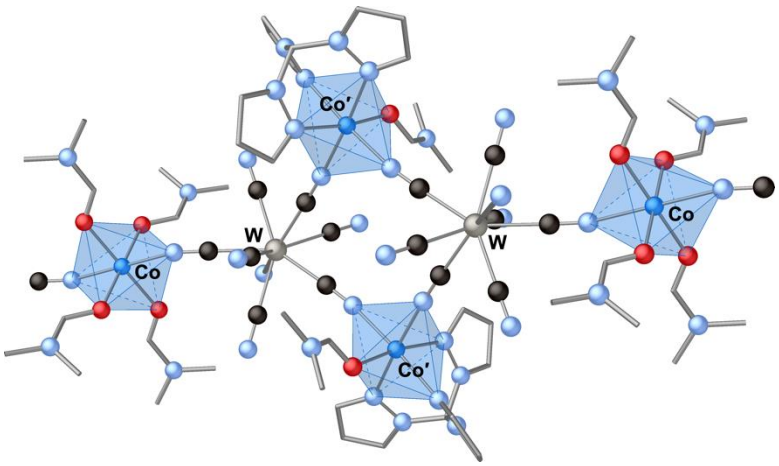

(17)

Photoinduced electron transfer has been described in "antenna-sensitizer" molecules, such as $[\{Ru(bpy)_2(CN)_2\}_2\text{-}Ru(bpyCOO)_2]^{2-}$, in which peripheral substituents absorb light energy and transfer it to a central component (**18**).[80] Such molecules serve as sensitizers for TiO_2 in photovoltaic cells. Similarly, cyanide ligands have been used to bridge sensitizing transition metals to highly luminescent lanthanide chromophores; the π-acidic cyanide allows for effective energy transfer from the transition metal to the lanthanide, avoiding forbidden f-f transitions. These complexes are relevant to emerging imaging and display technologies.[81]

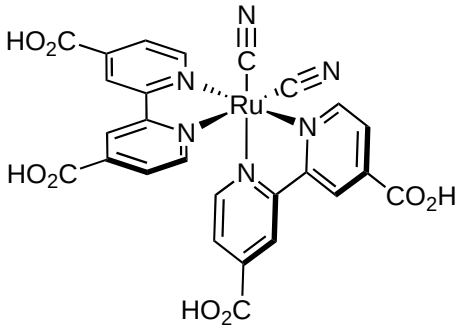

(**18**)

The ability of some porous cyanide complexes to serve as hosts for organic molecules has been noted above. Platinum compounds containing alternating anions ($[Pt(CN)_4]^{2-}$) and cations ($[Pt(CNR)_4]^{2+}$; R = *i*Pr, *c*-$C_{12}H_{23}$, *p*-$(C_2H_5)C_6H_4$) have been developed that undergo striking color changes on absorption of volatile organic compounds, and are being examined as chemical sensing agents.[82] The same is true of the mechanochemically prepared blue $Co[Au(CN)_2]_2$ complex, which exhibits reversible vapochromic response when exposed to water, ammonia, and a range of organic solvents.[15] A set of iridium-rhenium and iridium-lanthanide complexes have also demonstrated slight color changes in solvents of differing donor ability, and even more striking shifts upon exposure to barium or zinc ions.[83]

1.8 References:

(1) Kraft, A. On the Discovery and History of Prussian Blue. *Bull. Hist. Chem.* **2008**, *32* (2), 61–67.

(2) Sharpe, A. G. *The Chemistry of Cyano Complexes of the Transition Metals*; Academic: London, 1976.

(3) Fehlhammer, W. P.; Fritz, M. Emergence of a CNH and Cyano Complex Based Organometallic Chemistry. *Chem. Rev.* **1993**, *93* (3), 1243–1280. https://doi.org/10.1021/cr00019a016.

(4) Sieklucka, B. Reactivity and Photoreactivity of Cyanocomplexes of the Transition Metals. *Prog. React. Kinet. Mech.* **1999**, *24* (3), 165–221. https://doi.org/10.3184/007967499103165085.

(5) Shatruk, M.; Avendano, C.; Dunbar, K. P. Cyanide-Bridged Complexes of the Transition Metals: A Molecular Magnetism Perspective. In *Progr. Inorg. Chem.*; Karlin, K. D., Ed.; 2009; pp 155–334. https://doi.org/10.1002/9780470440124.ch3.

(6) Pike, R. D. Structure and Bonding in Copper(I) Carbonyl and Cyanide Complexes. *Organometallics* **2012**, *31* (22), 7647–7660. https://doi.org/10.1021/om3004459.

(7) Alexandrov, E. V.; Virovets, A. V.; Blatov, V. A.; Peresypkina, E. V. Topological Motifs in Cyanometallates: From Building Units to Three-Periodic Frameworks. *Chem. Rev.* **2015**, *115* (22), 12286–12319. https://doi.org/10.1021/acs.chemrev.5b00320.

(8) Von Ragué Schleyer, P.; Sawaryn, A.; Reed, A. E.; Hobza, P. The Remarkable Structure of Lithium Cyanide/Isocyanide. *J. Comput. Chem.* **1986**, *7* (5), 666–672. https://doi.org/10.1002/jcc.540070509.

(9) Carter, S. J.; Foxman, B. M.; Stuhl, L. S. Cobalt(II) Cyanides in Aprotic Media: Effect of Varying Counterion and Solvent. *Inorg. Chem.* **1986**, *25* (16), 2888–2894. https://doi.org/10.1021/ic00236a046.

(10) Hervé, A.; Bouzidi, Y.; Berthet, J. C.; Belkhiri, L.; Thuéry, P.; Boucekkine, A.; Ephritikhine, M. UIII-CN versus UIV-NC Coordination in Tris(Silylamide) Complexes. *Inorg. Chem.* **2015**, *54* (5), 2474–2490. https://doi.org/10.1021/acs.inorgchem.5b00034.

(11) Szalay, P. S.; Dunbar, K. R. A New Family of Dimolybdenum Compounds with Cyanide and Phosphine Ligands. *Inorg. Chem. Commun.* **2000**, *3* (2), 49–51. https://doi.org/10.1016/S1387-7003(99)00183-5.

(12) Weiss, R.; Jansen, G.; Boese, R.; Epple, M. Crystal Structure and Thermochemical Reactivity of an Unusual Copper Complex That Contains Copper in Four Different Coordination Geometries. *Dalton Trans.* **2006**, *6* (15), 1831–1835. https://doi.org/10.1039/b514540f.

(13) Oswald, B.; Powell, A. K.; Rashwan, F.; Heinze, J.; Vahrenkamp, H. Redoxchemie, Zweikernkomplexe Und Ru3-Clusterderivate Des "Liganden" $[Cp(CO)_2Mn\text{-}CN]^-$. *Chem. Ber.* **1990**, *123* (2), 243–250. https://doi.org/https://doi.org/10.1002/cber.19901230204.

(14) Hung, A. Y. C.; Woolcock, J. C.; Rettig, M. F.; Wing, R. M. Cyanide Exchange of the Methyltricyanoplatinate(II) Dianion: Temporal Resolution of Cis and Trans Cyanide Exchange. *Inorg. Chem.* **1992**, *31* (5), 810–812. https://doi.org/10.1021/ic00031a023.

(15) Jobbágy, C.; Tunyogi, T.; Pálinkás, G.; Deák, A. A Versatile Solvent-Free Mechanochemical Route to the Synthesis of Heterometallic Dicyanoaurate-Based Coordination Polymers. *Inorg. Chem.* **2011**, *50* (15), 7301–7308. https://doi.org/10.1021/ic200893n.

(16) Golub, A. M.; Kohler, H.; Skopenko, V. V. *Chemistry of Pseudohalides*; Elsevier: Berlin, 1986.

(17) Gans, P.; Gill, J. B.; Johnson, L. H. Spectrochemistry of Solutions. Part 19. Complexation of Gold(I) by Cyanide in Liquid Ammonia: An Infrared and Raman Spectroscopic Study. *J. Chem. Soc. Dalt. Trans.* **1987**, No. 3, 673–675. https://doi.org/10.1039/DT9870000673.

(18) Hendon, C. H.; Walsh, A.; Akiyama, N.; Konno, Y.; Kajiwara, T.; Ito, T.; Kitagawa, H.; Sakai, K. One-Dimensional Magnus-Type Platinum Double Salts. *Nat. Commun.* **2016**, *7* (May). https://doi.org/10.1038/ncomms11950.

(19) Wang, R.; Falck, J. R. Transition Metals Catalyzed Element-Cyano Bonds Activation. *Catal. Rev.* **2014**, *56* (3), 1–7. https://doi.org/10.1038/jid.2014.371.

(20) Chang, J.; Seidler, M. D.; Bergman, R. G. Synthesis of Alkylruthenium Nitrosyl Complexes. Migratory Insertion to Coordinated Nitric Oxide and the Mechanism of the Conversion of the Resultant Nitrosoalkyl Compounds to Oximate, Carboxamide, and Cyano Compounds. *J. Am. Chem. Soc.* **1989**, *111* (9), 3258–3271. https://doi.org/https://doi.org/10.1021/ja00191a024.

(21) Kuhlman, R.; Schimek, G. L.; Kolis, J. W. Inorganic-Organic Composites from Solvothermal Routes: Extended Structures of $[CuX(Pyrazine)]\infty$ (X=CN, Cl, CF_3CO_2), and $Cu(NO_2)_2(Pyz)$. *Polyhedron* **1999**, *18* (10), 1379–1387. https://doi.org/10.1016/S0277-5387(98)00425-2.

(22) Tennent, C. L.; Jones, W. D. Kinetics and Mechanism of Dealkylation of Coordinated Isocyanide in $Fe(PMe_3)_2(t\text{-}BuNC)_3$. *Can. J. Chem.* **2005**, *83* (6–7), 626–633. https://doi.org/10.1139/v05-023.

(23) Brown, Z. D.; Vasko, P.; Fettinger, J. C.; Tuononen, H. M.; Power, P. P. A Germanium Isocyanide

Complex Featuring (n → Π*) Back-Bonding and Its Conversion to a Hydride/Cyanide Product via C-H Bond Activation under Mild Conditions. *J. Am. Chem. Soc.* **2012**, *134* (9), 4045–4048. https://doi.org/10.1021/ja211874u.

(24) Martinez, J. L.; Lin, H. J.; Lee, W. T.; Pink, M.; Chen, C. H.; Gao, X.; Dickie, D. A.; Smith, J. M. Cyanide Ligand Assembly by Carbon Atom Transfer to an Iron Nitride. *J. Am. Chem. Soc.* **2017**, *139* (40), 14037–14040. https://doi.org/10.1021/jacs.7b08704.

(25) Baraldo, L. M.; Forlano, P.; Parise, A. R.; Slep, L. D.; Olabe, J. A. Advances in the Coordination Chemistry of $[M(CN)_5L]^{n-}$ Ions (M = Fe, Ru, Os). *Coord. Chem. Rev.* **2001**, *219–221*, 881–921. https://doi.org/10.1016/S0010-8545(01)00383-6.

(26) Michelin, R. A.; Pombeiro, A. J. L.; Guedes Da Silva, M. F. *Aminocarbene Complexes Derived from Nucleophilic Addition to Isocyanide Ligands*; 2001; Vol. 218. https://doi.org/10.1016/S0010-8545(01)80004-7.

(27) Rittle, J.; Peters, J. C. Proton-Coupled Reduction of an Iron Cyanide Complex to Methane and Ammonia. *Angew. Chem. - Int. Ed.* **2016**, *55* (40), 12262–12265. https://doi.org/10.1002/anie.201606366.

(28) Zinato, E.; Riccieri, P. Pentacyanochromate(III) Complexes: Ground-and Excited-State Chemistry. *Coord. Chem. Rev.* **2001**, *211* (1), 5–24. https://doi.org/10.1016/s0010-8545(00)00290-3.

(29) Siddiqi, K. S.; Khan, A. A. P.; Mohd, A.; Bano, S. Spectroscopic and Substitution Kinetic Studies of Hexacyanoferrate(II) Complexes by EDTA Catalysed with Mercury(II). *E-Journal Chem.* **2009**, *6* (SUPPL. 1), 103–111. https://doi.org/10.1155/2009/696809.

(30) Pina, F.; Parola, A. J. Photochemistry of Supramolecular Species Involving Anionic Coordination Compounds and Polyammonium Macrocyclic Receptors. *Coord. Chem. Rev.* **1999**, *185–186*, 149–165. https://doi.org/10.1016/s0010-8545(98)00265-3.

(31) Zinato, E. Chromium (III) Cyano-Am(m)ine Complexes. *Coord. Chem. Rev.* **1994**, *129*, 195–245.

(32) Frohnapfel, D. S.; Reinartz, S.; White, P. S.; Templeton, J. L. Electrophilic Addition to Cyanide Ligands in Tungsten(II) Four-Electron-Donor Alkyne Complexes. *Organometallics* **1998**, *17* (17), 3759–3769. https://doi.org/10.1021/om980127l.

(33) Chan, K. C.; Cheng, S. C.; Lo, L. T. L.; Yiu, S. M.; Ko, C. C. Luminescent Charge-Neutral Copper(I) Phenanthroline Complexes with Isocyanoborate Ligand. *Eur. J. Inorg. Chem.* **2018**, No. 7, 897–903. https://doi.org/10.1002/ejic.201701205.

(34) Etaiw, S. E. din H.; Marie, H.; Shalaby, E. M.; Farag, R. S.; Elsharqawy, F. A. Sensing and Photocatalytic Properties of Nanosized Cu(I)CN Organotin Supramolecular Coordination Polymer Based on Pyrazine. *Appl. Organomet. Chem.* **2019**, *33* (9), 1–14. https://doi.org/10.1002/aoc.5114.

(35) Mikhaylov, M. A.; Mironova, A. D.; Brylev, K. A.; Sukhikh, T. S.; Eltsov, I. V; Stass, D. V;

Gushchin, A. L.; Kitamura, N.; Sokolov, M. N. Functionalization of $[Re_6Q_8(CN)_6]^{4-}$ Clusters by Methylation of Cyanide Ligands. *New J. Chem.* **2019**, *8* (43), 16338–16348. https://doi.org/10.1039/c9nj02971k.

(36) Kaim, L. El; Grimaud, L.; Schlitz, A. "Isocyanide-Free" Ugi Reactions. *Org. Biomol. Chem.* **2009**, *7*, 3024–3026. https://doi.org/10.1039/b908541f.

(37) Kettle, S. F. A.; Aschero, G. L.; Diana, E.; Rossetti, R.; Stanghellini, P. L. The Vibrational Spectra of the Cyanide Ligand Revisited: Terminal Cyanides. *Inorg. Chem.* **2006**, *45* (13), 4928–4937. https://doi.org/10.1021/ic0514041.

(38) Millar, L. J.; Ford, T. A. Ab Initio Investigations of Some Molecular Complexes Containing Hydrogen Cyanide : Hydrogen-Bonded or Donor – Acceptor ? *J. Mol. Struct.* **2005**, 195–205. https://doi.org/10.1016/j.molstruc.2004.10.123.

(39) Sharpe, L. R.; Heineman, W. R.; Elder, R. C. EXAFS Spectroelectrochemistry. *Chem. Rev.* **1990**, *90* (5), 705–722. https://doi.org/https://doi.org/10.1021/cr00103a002.

(40) Day, P.; Delfs, C. D.; Figgis, B. N.; Reynolds, P. A.; Tasset, F. Polarized Neutron Diffraction from $Cs_2KFe(CN)_6$. *Mol. Phys.* **1993**, *78* (4), 769–780. https://doi.org/https://doi.org/10.1080/00268979300100521.

(41) Balmaseda, J.; Reguera, E.; Rodríguez-Hernández, J.; Reguera, L.; Autie, M. Behavior of Transition Metals Ferricyanides as Microporous Materials. *Microporous Mesoporous Mater.* **2006**, *96* (1–3), 222–236. https://doi.org/10.1016/j.micromeso.2006.06.039.

(42) Kato, K.; Tanaka, H. Visualizing Charge Densities and Electrostatic Potentials in Materials by Synchrotron X-Ray Powder Diffraction. *Advances in Physics: X*. Taylor & Francis 2016, pp 55–80. https://doi.org/10.1080/23746149.2016.1142830.

(43) Zahl, A.; Van Eldik, R.; Swaddle, T. W. Cation-Independent Electron Transfer between Ferricyanide and Ferrocyanide Ions in Aqueous Solution. *Inorg. Chem.* **2002**, *41* (4), 757–764. https://doi.org/10.1021/ic010957i.

(44) Aguiar, P. M.; Katz, M. J.; Leznoff, D. B.; Kroeker, S. Natural Abundance ^{13}C and ^{15}N Solid-State NMR Analysis of Paramagnetic Transition-Metal Cyanide Coordination Polymers. *Phys. Chem. Chem. Phys.* **2009**, *11*, 6925–6934. https://doi.org/10.1039/b914008p.

(45) Brownlee, R. T. C.; Shehan, B. P.; Wedd, A. G. Applications of ^{95}Mo NMR Spectroscopy. 1. ^{95}Mo and ^{14}N Relaxation Time Measurements Confirming That $[Mo(CN)_8]^{4-}$ Is Dodecahedral in Aqueous Solution. *Inorg. Chem.* **1987**, *26* (8), 2022–2024. https://doi.org/https://doi.org/10.1021/ic00260a003.

(46) Flambard, A.; Kohler, F. H.; Lescouezec, R. Revisiting Prussian Blue Analogues with Solid-State MAS NMR Spectroscopy : Spin Density and Local Structure In. *Angew. Chem. Int. Ed.* **2009**, *48*,

1673–1676. https://doi.org/10.1002/anie.200805415.

(47) Borges, S. da S. S.; Coelho, A. L.; Moreira, I. S. Spectroscopic and Substitution Kinetic Studies of Pentacyanoferrate(II) Complexes with Sulphur Heterocyclic Ligands. *Polyhedron* **1994**, *13* (6–7), 1015–1022. https://doi.org/10.1016/S0277-5387(00)83025-9.

(48) Mikolasek, M.; Félix, G.; Molnár, G.; Terki, F.; Nicolazzi, W.; Bousseksou, A. Role of Surface Vibrational Properties on Cooperative Phenomena in Spin-Crossover Nanomaterials. *Phys. Rev. B - Condens. Matter Mater. Phys.* **2014**, *90* (7), 1–8. https://doi.org/10.1103/PhysRevB.90.075402.

(49) Cano, A.; Lartundo-Rojas, L.; Shchukarev, A.; Reguera, E. Contribution to the Coordination Chemistry of Transition Metal Nitroprussides: A Cryo-XPS Study. *New J. Chem.* **2019**, *43* (12), 4835–4848. https://doi.org/10.1039/c9nj00141g.

(50) Tanaka, M.; Miki, E. The Importance of Preferential Solvation of the CN Ligands in Electron- and Proton- Trnasfers Observed for Cis-$[Ru(CN)_2(Bpy)_2]$ Under Ion Bombardment. *J. Am. Soc. forMass Spectrom.* **2002**, *13*, 1209–1217.

(51) Terzis, A.; Raymond, K. N.; Spiro, T. G. On the Structure of $[Ni(CN)_5]^{3-}$. Raman, Infrared, and X-Ray Crystallographic Evidence. *Inorg. Chem.* **1970**, *9* (11), 2415–2420. https://doi.org/https://doi.org/10.1021/ic50093a006.

(52) Basson, S. S.; Leipoldt, J. G.; Bok, L. D. C.; van Vollenhoven, J. S.; Cilliers, P. J. The Structure of Tricaesium Octacyanomolybdate(V) Dihydrate, $Cs_3Mo(CN)_8 \cdot 2H_2O$ - a New Stereochemical Configuration for $[M(CN)_8]^{n-}$ Ions. *Acta Crystallogr. Sect. B* **1980**, *B36*, 1765–1768. https://doi.org/https://doi.org/10.1107/S0567740880007194.

(53) Ruhmann, M.; Spannenberg, A.; Villinger, A.; Schulz, A.; Beweries, T. Reactions of Titanocene with Triazines and Dicyandiamide: Formation of Novel Di- and Trinuclear Metallacyclic Complexes. *Z. Anorg. Allg. Chem.* **2013**, *639* (10), 1717–1721. https://doi.org/10.1002/zaac.201300226.

(54) Braunstein, P.; Oswald, B.; Tiripicchio, A.; Camellini, M. T. Novel Bonding Mode for a Cyanometalate Ligand: Synthesis and Crystal Structure of the Mn_4Pd_4 Cluster $[(OC)Pd(\mu\text{-}NC)Mn(\eta\text{-}C_5H_4Me)(CO)_2]_4$ Containing an Orthogonal Arrangement of Helical Units. *Angew. Chem. - Int. Ed.* **1990**, *29* (10), 1140–1143. https://doi.org/https://doi.org/10.1002/anie.199011401.

(55) Contakes, S. M.; Rauchfuss, T. B. $\{K\subset[Mo_6(\mu\text{-}CN)_9(CO)_{18}]\}^{8-}$: A Trigonal-Prismatic Cyanometalate Cage. *Angew. Chem. - Int. Ed.* **2000**, *39* (11), 1984–1986. https://doi.org/https://doi.org/10.1002/1521-3773(20000602)39:11%3C1984::AID-ANIE1984%3E3.0.CO;2-M.

(56) Contakes, S. M.; Rauchfuss, T. B. Alkali Metal-Templated Assembly of the Tetrahedral Cyanometallate Cages $[M\subset Mo_4(\mu\text{-}CN)_6(CO)_{12}]^{5-}$(M = Li, Na). *Chem. Commun.* **2001**, *4* (6), 553–

554. https://doi.org/10.1039/b010192n.

(57) Larionova, J.; Gross, M.; Pilkington, M.; Andres, H.; Stoekli-Evans, H.; Gudel, H. U.; Decurtins, S. High-Spin Molecules: A Novel Cyano-Bridged Mn(II)9Mo(V)6 Molecular Cluster with a S=51/2 Ground State and Ferromagnetic Intercluster Ordering at Low Temperatures. *Angew. Chem. - Int. Ed.* **2000**, *39* (9), 1605–1609. https://doi.org/https://doi.org/10.1002/(SICI)1521-3773(20000502)39:9%3C1605::AID-ANIE1605%3E3.0.CO;2-5.

(58) Ni, Z. H.; Kou, H. Z.; Zhang, L. F.; Ge, C.; Cui, A. L.; Wang, R. J.; Li, Y.; Sato, O. $[MnIII(Salen)]_6[FeIII(Bpmb)(CN)_2]_6 \cdot 7H_2O$: A Cyanide-Bridged Nanosized Molecular Wheel. *Angew. Chem. - Int. Ed.* **2005**, *44* (47), 7742–7745. https://doi.org/10.1002/anie.200502699.

(59) Dunbar, K. R.; Heintz, R. A. Chemistry of Transition Metal Cyanide Compounds: Modern Perspectives. In *Progr. Inorg. Chem., Volume 45*; Karlin, K. D., Ed.; John Wiley and Sons, 1996; pp 283–391. https://doi.org/https://doi.org/10.1002/9780470166468.ch4.

(60) Li, Y. H.; He, W. R.; Ding, X. H.; Wang, S.; Cui, L. F.; Huang, W. Cyanide-Bridged Assemblies Constructed from Capped Tetracyanometalate Building Blocks $[M\ A(Ligand)(CN)_4]^{1-/2-}$ (M A=Fe or Cr). *Coord. Chem. Rev.* **2012**, *256* (23–24), 2795–2815. https://doi.org/10.1016/j.ccr.2012.09.014.

(61) Jassal, V.; Shanker, U.; Shankar, S. Synthesis, Characterization and Applications of Nano-Structured Metal Hexacyanoferrates: A Review. *J. Environ. Anal. Chem.* **2015**, *2* (2). https://doi.org/10.4172/2380-2391.1000128.

(62) Wang, S.; Ding, X. H.; Li, Y. H.; Huang, W. Dicyanometalate Chemistry: A Type of Versatile Building Block for the Construction of Cyanide-Bridged Molecular Architectures. *Coord. Chem. Rev.* **2012**, *256* (3–4), 439–464. https://doi.org/10.1016/j.ccr.2011.10.029.

(63) Bennett, M. V.; Beauvais, L. G.; Shores, M. P.; Long, J. R. Expanded Prussian Blue Analogues Incorporating $[Re_6Se_8(CN)_6]^{3-/4-}$ Clusters: Adjusting Porosity via Charge Balance. *J. Am. Chem. Soc.* **2001**, *123* (33), 8022–8032. https://doi.org/10.1021/ja0110473.

(64) O'Keeffe, M.; Eddaoudi, M.; Li, H.; Reineke, T.; Yaghi, O. M. Frameworks for Extended Solids: Geometrical Design Principles. *J. Solid State Chem.* **2000**, *152* (1), 3–20. https://doi.org/10.1006/jssc.2000.8723.

(65) Iwamoto, T.; Nishikiori, S. I.; Kitazawa, T.; Yuge, H. Mineralomimetic Chemistry as a Modern Aspect of Co-Ordination Chemistry. *J. Chem. Soc. - Dalton Trans.* **1997**, No. 22, 4127–4136. https://doi.org/10.1039/a702539d.

(66) Roque, J.; Reguera, E.; Balmaseda, J.; Rodríguez-Hernández, J.; Reguera, L.; del Castillo, L. F. Porous Hexacyanocobaltates(III): Role of the Metal on the Framework Properties. *Microporous Mesoporous Mater.* **2007**, *103* (1–3), 57–71. https://doi.org/10.1016/j.micromeso.2007.01.030.

(67) Reguera, L.; Balmaseda, J.; Krap, C. P.; Reguera, E. Hydrogen Storage in Porous Transition Metals Nitroprussides. *J. Phys. Chem. C* **2008**, *112* (28), 10490–10501. https://doi.org/10.1021/jp801955p.

(68) Alvarado-alvarado, D.; Gonza, J. H.; Flores, J. G.; Raziel, J. A.; Chastanet, G.; Gonza, E.; Aguilar-pliego, J.; Islas-ja, A.; Gonidec, M.; Ibarra, I. A.; Lara-garc, H. A.; Alca, B. Water Adsorption Properties of Fe(Pz)[Pt(CN)$_4$] and the Capture of CO_2 and CO. *Organometallics* **2019**. https://doi.org/10.1021/acs.organomet.9b00711.

(69) Noroozifar, M.; Khorasani-Motlagh, M.; Taheri, A. Determination of Cyanide in Wastewaters Using Modified Glassy Carbon Electrode with Immobilized Silver Hexacyanoferrate Nanoparticles on Multiwall Carbon Nanotube. *J. Hazard. Mater.* **2011**, *185* (1), 255–261. https://doi.org/10.1016/j.jhazmat.2010.09.026.

(70) Piernas-Munoz, M. J.; Castillo-Martinez, E.; Bondarchuk, O.; Armand, M.; Rojo, T. Higher Voltage Plateau Cubic Prussian White for Na-Ion Batteries. *J. Power Sources* **2016**, *324*, 766–773. https://doi.org/10.1016/j.jpowsour.2016.05.050.

(71) Chae, M. S.; Hyoung, J.; Jang, M.; Lee, H.; Hong, S. Potassium Nickel Hexacyanoferrate as a High-Voltage Cathode Material for Nonaqueous Magnesium-Ion Batteries. *J. Power Sources* **2017**, *363*, 269–276. https://doi.org/10.1016/j.jpowsour.2017.07.094.

(72) Targholi, E.; Mousavi-Khoshdel, S. M.; Rahmanifara, M.; Yahya, M. Z. A. Cu- and Fe-Hexacyanoferrate as Cathode Materials for Potassium Ion Battery : A First-Principles Study. *Chem. Phys. Lett.* **2017**, *687*, 244–249. https://doi.org/10.1016/j.cplett.2017.09.029.

(73) Minami, Y.; Yoshiyasu, H.; Nakao, Y.; Hiyama, T. Highly Chemoselective Carbon-Carbon σ-Bond Activation: Nickel/Lewis Acid Catalyzed Polyfluoroarylcyanation of Alkynes. *Angew. Chem. - Int. Ed.* **2013**, *52* (3), 883–887. https://doi.org/10.1002/anie.201207880.

(74) Ohkoshi, S. I.; Tokoro, H.; Matsuda, T.; Takahashi, H.; Irie, H.; Hashimoto, K. Coexistence of Ferroelectricity and Ferromagnetism in a Rubidium Manganese Hexacyanoferrate. *Angew. Chem. - Int. Ed.* **2007**, *46* (18), 3238–3241. https://doi.org/10.1002/anie.200604452.

(75) Nihei, M.; Ui, M.; Yokota, M.; Han, L.; Maeda, A.; Kishida, H.; Okamoto, H.; Oshio, H. Two-Step Spin Conversion in a Cyanide-Bridged Ferrous Square. *Angew. Chem. - Int. Ed.* **2005**, *44* (40), 6484–6487. https://doi.org/10.1002/anie.200502216.

(76) Dei, A. Photomagnetic Effects in Polycyanometallate Compounds: An Intriguing Future Chemically Based Technology? *Angew. Chem. - Int. Ed.* **2005**, *44* (8), 1160–1163. https://doi.org/10.1002/anie.200461413.

(77) Mitsumoto, K.; Oshiro, E.; Nishikawa, H.; Shiga, T.; Yamamura, Y.; Saito, K.; Oshio, H. Cyanide-Bridged [Fe_8M_6] Clusters Displaying Single-Molecule Magnetism (M=Ni) and Electron-Transfer-Coupled Spin Transitions (M=Co). *Chem. Eur. J.* **2011**, *17* (35), 9612–9618.

https://doi.org/10.1002/chem.201101404.

(78) Wei, R. M.; Cao, F.; Li, J.; Yang, L.; Han, Y.; Zhang, X. L.; Zhang, Z.; Wang, X. Y.; Song, Y. Single-Chain Magnets Based on Octacyanotungstate with the Highest Energy Barriers for Cyanide Compounds. *Sci. Rep.* **2016**, *6* (April), 1–8. https://doi.org/10.1038/srep24372.

(79) Zhang, Y. Z.; Dolinar, B. S.; Liu, S.; Brown, A. J.; Zhang, X.; Wang, Z. X.; Dunbar, K. R. Enforcing Ising-like Magnetic Anisotropy: Via Trigonal Distortion in the Design of a W(V)-Co(II) Cyanide Single-Chain Magnet. *Chem. Sci.* **2018**, *9* (1), 119–124. https://doi.org/10.1039/c7sc02925j.

(80) Kent, C. A.; Liu, D.; Ma, L.; Papanikolas, J. M.; Meyer, T. J.; Lin, W. Light Harvesting in Microscale Metal-Organic Frameworks by Energy Migration and Interfacial Electron Transfer Quenching. *J. Am. Chem. Soc.* **2011**, *133*, 12940–12943. https://doi.org/https://doi.org/10.1021/ja204214t.

(81) Ward, M. D. Transition-Metal Sensitised near-Infrared Luminescence from Lanthanides in d-f Heteronuclear Arrays. *Coord. Chem. Rev.* **2007**, *251* (13-14 SPEC. ISS.), 1663–1677. https://doi.org/10.1016/j.ccr.2006.10.005.

(82) Grate, J. W.; Moore, L. K.; Janzen, D. E.; Veltkamp, D. J.; Kaganove, S.; Drew, S. M.; Mann, K. R. Steplike Response Behavior of a New Vapochromic Platinum Complex Observed with Simultaneous Acoustic Wave Sensor and Optical Reflectance Measurements. *Chem. Mater.* **2002**, *14* (3), 1058–1066. https://doi.org/10.1021/cm0104506.

(83) Ali, N. M.; MacLeod, V. L.; Jennison, P.; Sazanovich, I. V.; Hunter, C. A.; Weinstein, J. A.; Ward, M. D. Luminescent Cyanometallates Based on Phenylpyridine-Ir(Iii) Units: Solvatochromism, Metallochromism, and Energy-Transfer in Ir/Ln and Ir/Re Complexes. *Dalton Trans.* **2012**, *41* (8), 2408–2419. https://doi.org/10.1039/c1dt11328c.

Chapter 2: Mechanochemical Investigation of Solvent and Structural Factors on the Outcome of Salt Metathesis Reactions

Section 2.1 of this chapter was modified from its original publication as "Solvate-Assisted Grinding: Metal Solvates as Solvent Sources in Mechanochemically Driven Organometallic Reactions" in Organometallics, 2021, and has been reproduced with the permission of the publisher and my co-author, Timothy Hanusa.

Abstract

Solvent effects in synthetic chemistry can be analyzed in various ways, but a perhaps counterintuitive approach is to remove the solvent entirely from the reaction environment. Mechanochemical initiation (grinding or milling of solid reagents) can then be used to replace the mixing and energy that would be supplied by a solvent. The effect of complete solvent elimination can be unpredictable, however, and even partial removal, as found in the realm of liquid-assisted grinding (LAG), can alter reaction outcomes profoundly. Reduced quantities of solvents can also be present in the form of solvates. Although their use has been classified under the category of neat grinding, "solvate-assisted grinding" (SAG) might be a more descriptive term, as the outcome of such reactions can differ from both LAG and neat grinding. This study examines the mechanochemically driven synthesis of the bis(allyl)metal complexes [MA′$_2$] (M = Cr, Fe, Co, Ni; A′ = 1,3-(SiMe$_3$)$_2$C$_3$H$_3$) via halide metathesis. Particular emphasis is given to the nickel system, whose synthesis from nickel halide solvates is compared with the same reaction using the anhydrous metal halide and various quantities of solvent. The reactions employing solvate-assisted grinding yield the nickel allyl complex the most efficiently, suggesting that the intimate interaction of coordinated solvents with the metal centers is an important variable in determining the outcome of the metathesis reactions. Although developed in the context of mechanochemically driven reactions, these results have implications for solution-based synthesis as well, where the use of solvated reagents can strongly affect outcomes. Further study on the nickel system using a broader selection of solvated and unsolvated nickel(II) sources has yielded preliminary insight into the origins of this effect, suggesting generally that nickel precursors containing easily displaced ligands are effective participants in salt metathesis reactions.

2.1 Investigation of the Role of Solvent in Mechanochemical Salt Metathesis Reactions

2.1.1 Introduction

How does one disentangle the myriad roles of solvents in synthetic chemistry, given that everything from dispersing the heat of exothermic processes to affecting reaction rates and yields can be in play?[1–3] An established approach to addressing this complex question involves exchanging one solvent for another with different chemical or physical properties (e.g., basicity or hydrogen bonding capability), and then analyzing changes in the yields or identities of products. Although perhaps counterintuitive, completely omitting the solvent from a reaction and then observing the outcome can also provide insights into solvent-reagent interactions. The mixing and energy input that accompanies solvent use can be replaced with mechanochemical activation, by the grinding or milling of the dry reagents.[4–9] Not surprisingly, such omission frequently—although not always—changes the products or their yields, and in possibly dramatic ways. In particular, the high concentration of reagents and the often far-from-equilibrium conditions that exist during solid-state reactions can lead to the preferential formation of kinetic products that do not reflect the stoichiometric ratios of the starting reagents.[10–12] Given the potential insights that could be gained from the mechanochemical approach, however, there remains a critical need to accurately understand, predict, and control the effects of solvent removal or restriction during synthetic reactions.

Halide metathesis is one of the most versatile synthetic methods for the production of transition metal organometallic complexes, with proven utility for a broad range of metals and ligands.[13] These reactions are most commonly done using binary metal halide salts, MX_n, but in cases where these are not sufficiently reactive, a solvated metal halide, $M(L)_mX_n$, can be substituted as a more reactive precursor. The increased reactivity of solvated precursors has been attributed to their increased solubility, as in the case of the formation of nickelocene, but this has not been a well-studied conclusion.[14]

A bridge between traditional solution-based chemistry and the solid-state alternative is the use of liquid-assisted grinding (LAG; also known as 'solvent-drop grinding'[15] or 'kneading'[16]). In a reaction conducted under LAG conditions, a small amount of liquid is introduced into the mechanochemical environment, which can have substantial effects on the outcome.[17–19] The field has developed enough that there are multiple variations on the technique, such as ILAG (the use of room temperature ionic liquids as the additive)[20] and POLAG (polymer additives),[21] and the method has been included in several reviews.[22–25]

Under conventionally defined LAG conditions, the solubility of reagents in the added solvent is no longer an important consideration—as such, the solvent has been described as functioning essentially as a catalyst.[26,27] Thus a commonly used descriptor of the LAG environment is the 'η' scale, defined as a simple volume/mass ratio (specifically, η is the μL solvent added per mg of total reagents).[26] A completely solvent-free reaction has $\eta = 0$, and empirical study has suggested that distinct LAG reactivity occurs in the range

η ≈ 0–1 (Figure 2.1). It should be noted that these cutoffs are approximate and defined in the context of scales commonly used in mechanochemical research. As an illustration of the boundaries of this system, the preparation of ferrocene ([$FeCp_2$]) at gram scale was performed at an η value of 1. [$FeCl_2$] (1.00 g) and [NaCp] (1.39 g) powders, which represent the appropriate 1 : 2 molar ratio, were combined with 2.4 mL of THF; the resulting material was a noticeably wet paste (See Appendix 2 for a photograph of the mixture.) Given its definition, the η scale is independent of a solvent's identity (and hence core properties such as polarity, basicity, or hydrogen bonding ability) and the relative molar masses of the solvent and reagents. The operation of LAG in organometallic systems is particularly complex, as direct solvent involvement in the coordination sphere of a metal can produce a variety of reaction outcomes, whether by generating weak interactions that are easily replaced with other substrates (so-called 'virtual' or 'latent' sites)[28,29] or by more direct changes, such as oxidative addition.[30–32] Despite such issues, the η parameter has found use as a descriptor in organometallic reactions.[33–39]

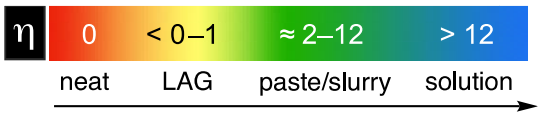

Figure 2.1: The conventional η scale for mechanochemical reactions (μL liquid added/mg of total reagents). Distinctive liquid-assisted grinding (LAG) is proposed to occur in the region immediately above solvent-free conditions (η = 0) and before the formation of paste-like mixtures (η ≈ 2).

Even as LAG conditions lie between dry reactions and those conducted in solution, the line between dry and LAG environments is blurred with the use of solvated reagents. Because such compounds introduce molecules of solvent into reactions in a solid form,[40,41] their use has been considered a type of dry grinding,[41] and so outside the realm of LAG (and η). Nevertheless, hydrates and their organic equivalents, solvates, can display complicated behavior when it comes to providing solvent molecules, and the outcome of reactions may not be the same as when free liquid is added to the anhydrous species.[41]

The use of metal solvates as the sole source of solvent molecules has not been a systematically explored option in organometallic mechanochemistry, and even when solvates are employed as the metal source in solution-based reactions, it is rare to find much methodical study of their effects.[42,43] The topic is one of potentially enormous scope, and could not be given even superficially adequate coverage within the confines of a single manuscript. To narrow the focus to a tractable level, we elected to study the formation of the known polymerization initiators[44] [MA'_2] ([A′] = [1,3-$(SiMe_3)_2C_3H_3$]$^-$; M = Cr, Fe, Co, Ni)[45,46] (Figure 2.2), primarily under reduced-solvent mechanochemical conditions, either using LAG or solvated

metal salts, with some solution-based reactions added for context. Such results could help address the question of whether the use of solvates as reagents deserves its own category of mechanochemical reaction type, and could make a contribution to our understanding of the function of solvated reagents in solution-based reactions. Throughout this study, effective η values for solvated metal precursors will be reported. In order to avoid "double-counting" the initially bound solvent in both the volume of solvent and mass of solid terms, the following formula (eq. 2.1) is used

$$\eta = \frac{\frac{\text{x mol(solvent)} \bullet \text{MM}}{\text{density(solvent)}}}{\text{mass}([MX_2]) + \text{mass}(K[A'])}, \qquad (2.1)$$

where MM is the molar mass of the solvent and mass[MX_2] is the mass of the unsolvated metal halide.

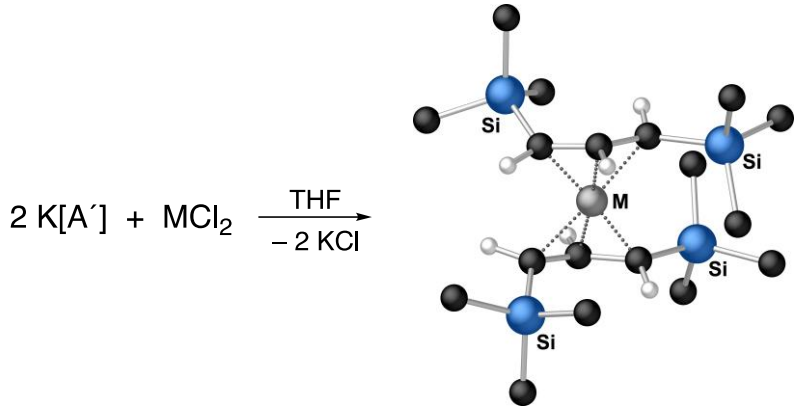

Figure 2.2: Formation of [MA'_2] complexes via halide metathesis; in solution the solvent is commonly THF. The geometric conformation with staggered allyl ligands (as shown) is crystallographically confirmed for Cr, Fe, Co, and Ni. A structure with eclipsed allyl ligands is also known for M = Ni.

2.1.2 Results.

2.1.2.1 Initial solution phase investigation

Previous work has shown that the metathetical reaction of Cr, Fe, and Co dichlorides with [KA´] in THF produces the corresponding bis(allyl) complexes in very good to excellent yields (all ≥ 75%).[44,47,48] As such, there would be little incentive to investigate other compounds of these metals for the sole purpose of improving yields of the complexes in solution. In sharp contrast, however, [KA´] reacts with the anhydrous, and virtually insoluble, nickel halides ([$NiCl_2$], [$NiBr_2$], or [NiI_2]) in THF via a redox reaction pathway. Evidently oxidation of the $[A']^-$ anion to the corresponding radical $[A']^\bullet$ occurs, followed by its homocoupling to produce the coupled ligand product 1,3,4,6-tetrakis(trimethylsilyl)hexa-1,5-diene ({A´}$_2$); the desired [NiA'_2] appears in no more than trace yields, if that.[49] Switching to the chelated halide

[Ni(dme)Br_2] in THF instead leads to the metathesis pathway proceeding efficiently, allowing for the isolation of [NiA′$_2$] in 72% yield. The intriguing change in reaction outcome induced by the use of a metal halide solvate suggested that the nickel system could provide a useful testing ground for evaluating the effects of solvates.

In an initial study, the sparingly soluble THF solvate [Ni(thf)$_{1.5}Cl_2$][50] was allowed to react in THF with [KA′], and the outcome compared to that with unsolvated [$NiCl_2$] (See Appendix 2, Table A2.1, entries 1,2). The yield of [NiA′$_2$] detectably increases with [Ni(thf)$_{1.5}Cl_2$] (from 2 to 10%), and the complex:hexadiene ratio falls somewhat (from 1:19 to 1:7), suggesting slightly greater activity for the solvate. The same reaction with [Ni(thf)$_{1.5}Cl_2$] in diethyl ether, in which the adduct has only trace solubility, results in the same yield as with unsolvated [$NiCl_2$], but with even more production of {A′}$_2$ (Table A2.1, entry 3). Remarkably, however, if the solvate precursor is changed to the highly THF-insoluble pyridine solvate [Ni(pyr)$_4Cl_2$],[51] [NiA′$_2$] is produced in 91% yield without any trace of {A′}$_2$ (Table A2.1, entry 4). Clearly solubility alone does not correlate with the reactivity of the solvates. In order to study these effects decoupled from the influence of bulk solubility, further studies were focused on reactions performed under mechanochemical conditions.

2.1.2.2 Dry grinding and use of THF (LAG conditions) with [MCl_2]

Considering the uncertain importance that metal halide solubility has on the synthesis of [MA′$_2$], the dry grinding of [KA′] with MCl_2 (M = Cr, Fe, Co, Ni) was examined. The bis(allyl)metal complexes are in fact obtained, but always in a mixture with {A′}$_2$, and the yield of [MA′$_2$] is never greater than 12% (Figure 2.3; exact quantities are given in Table 2.1, entries 1, 5, 9, 13).

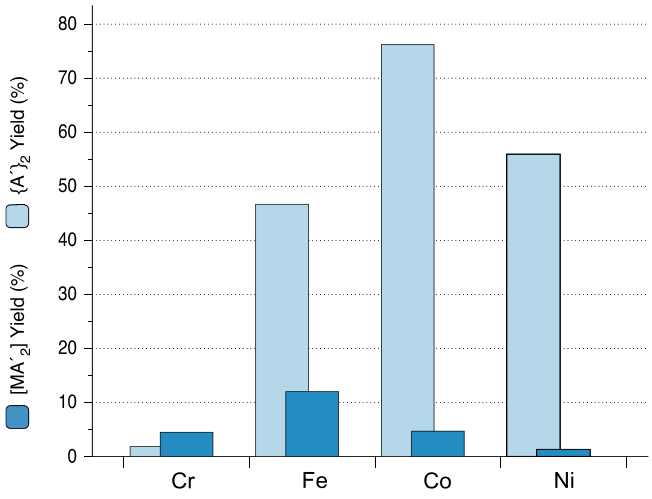

Figure 2.3: Outcomes of 10 min. dry grinds between 2 eq. of [KA´] and [MCl_2]. The dimerized ligand $\{A´\}_2$ is always the major product except in the case of Cr, for which the yield of [$CrA´_2$] does not exceed 5%.

The proportion of the complex to the hexadiene decreases on moving from chromium to nickel, with the hexadiene as the predominant product for all but the chromium system. This behavior tracks with the increasing reduction potential along the series,[52] becoming progressively easier to reduce the metal and oxidize the allyl anion.

The reactions were then repeated under LAG conditions ($\eta \approx 0.7–1.5$) by introducing a small amount of THF into the grinding jars before 10-minute grinds at 600 RPM. In all cases, addition of THF increased the proportion of complex to the hexadiene formed (Figure 2.4; Table 2.1, entries 1/2, 5/6, 9/10, 13/14). Doubling the molar equivalents of THF from 5 to 10 generally improved the yield of the [$MA´_2$] complexes, and in the case of chromium, by as much as 70%. This effect becomes less pronounced moving across the row, such that no increase is observed in the case of nickel (Table 2.1, entries 2/3, 6/7, 10/11, 14/15). For comparison, the reactions were also performed in solution for all the metals under uniform conditions, which confirmed the good yields for the three earlier metals, and again highlighted the poor outcome with nickel. (It should be noted that the reactions referred to as taking place in "solution" might be more accurately termed as "in a slurry", owing to the limited solubility of the metal halide salts in the solvents.) In any case, large excesses (>> 10 eq.) of the solvent were always present, and the reactions were well outside the LAG regime ($\eta > 100$).)

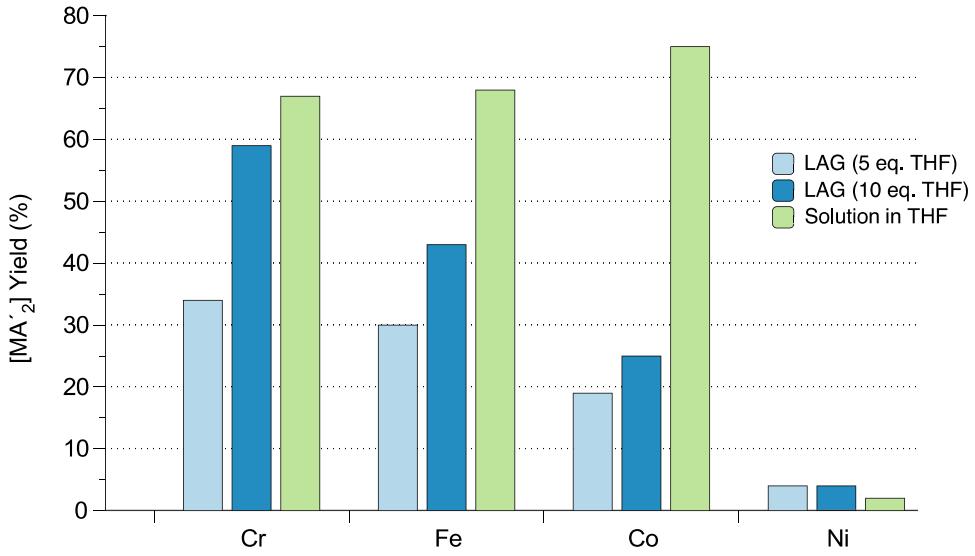

Figure 2.4: Yields of [MA´$_2$] from the reaction between [KA´], [MCl_2], and THF.

As yields from the nickel halide systems varied from no better than near-trace ([$NiCl_2$] in THF, or dry grind with [$NiCl_2$]) to 91% ([$Ni(pyr_4)_4Cl_2$] in Et_2O), there was a large reaction space in which to examine the details of LAG/solvate effects. Consequently, continued study focused on nickel precursors, specifically the metal halides and their solvates.

Table 2.1: Reaction outcomes from mixing [KA´], [MCl_2], and THF

No.	Condition	Metal halide	Time	Eq. THF[a]	η	[$MA´_2$] yield[c] (%)	{$A´_2$} yield[c] (%)
1	Dry grind	[$CrCl_2$]	10 min	0	0	5	2
2	LAG		10 min	5	0.75	34	9
3			10 min	10	1.47	59	9
4	Solution		1 day	>>10	>100	67	1
5	Dry grind	[$FeCl_2$]	10 min	0	0	12	47
6	LAG		10 min	5	0.78	30	25
7			10 min	10	1.48	43	16
8	Solution		1 day	>>10	>100	68	10
9	Dry grind	[$CoCl_2$]	10 min	0	0	5	76
10	LAG		10 min	5	0.75	19	41
11			10 min	10	1.49	25	45
12	Solution		1 day	>>10	>100	75	7
13	Dry grind	[$NiCl_2$]	10 min	0	0	1	56
14	LAG		10 min	5	0.73	4	55
15			10 min	10	1.44	4	68
16	Solution		1 day	>>10	>100	2	37

[a]Molar equivalents relative to [MCl_2]; [b]determined by protonolysis of the product mixture followed by ^{1}H NMR (M = Cr, Fe, Co) or ^{1}H NMR of the product mixture (M = Ni); [c]determined by assigning the isolated mass between the two products according to their ^{1}H NMR ratios.

2.1.2.3 Use of other nickel halides and THF solvates

The effect of the identity of halide counterion in the nickel chemistry was investigated. [$NiBr_2$] and [NiI_2] were already known to be ineffective in generating [NiA′$_2$] in solution reactions,[49] and the same was also found to be true under mechanochemical conditions (Table A2.2). Used either as a dry grind with [KA′] or under LAG conditions, the other halides produced only trace or near-trace quantities ($\lesssim$ 5%) of the allyl complex, and the hexadiene was consistently generated in high yield. The nickel chloride THF adduct [$Ni(thf)_{1.5}Cl_2$][50] was also examined as a halide source (Table A2.2, entry 7). Although [NiA′$_2$] was identified in a very low but easily detectable yield of 5%, {A′}$_2$ was still the overwhelmingly favored product by a ratio of 14:1. The behavior of the [$Ni(thf)_{1.5}Cl_2$] adduct was slightly bettered by the [$Ni_3(thf)_5Br_6$] adduct,[53] giving a yield of 9% and with far less production of the hexadiene compared with the unsolvated [$NiBr_2$] ({A′}$_2$: [NiA′$_2$] ratios of 4:1 and 44:1, respectively) (Table A2.2, entries 5,8).

2.1.2.4 Use of metal dimethoxyethane solvates as the solvent source

Even though the [$Ni(thf)_{1.5}Cl_2$] or [$Ni_3(thf)_5Br_6$] solvates were not synthetically promising nickel sources, the dimethoxyethane solvate [$Ni(dme)Br_2$] had been effective in the synthesis of [NiA′$_2$] in THF solution, and so its reactivity and that of its chloride analogue were examined under several conditions. The "solution-based" interaction of [$NiBr_2$] with [KA′] in DME (as noted above, more of a slurry, owing to the near insolubility of anhydrous [$NiBr_2$] in DME) generated a complex mixture in which [NiA′$_2$] could be identified, but in only negligible yield (1%, Table A2.3, entry 4). Introduction of liquid DME under LAG conditions (5 eq.) produced the same trace yield with $NiBr_2$ (Table A2.3, entry 1). Grinding the solvates [$Ni(dme)Br_2$] and [$Ni(dme)Cl_2$] with [KA′] produced essentially the same results, with near-trace production of [NiA′$_2$] (3–4%; Table A2.2, entries 2, 3).

Before abandoning further study of the DME adducts, an additional experiment was performed in which [$Ni(dme)Br_2$] was the nickel source and THF was the LAG solvent. Even before grinding, exposure of [$Ni(dme)Br_2$] to THF caused a color shift from a salmon pink to lavender, indicating the onset of a reaction. Upon grinding for 10 minutes at 600 RPM, the allyl complex was found in a dramatically improved 52% yield, with a 2:1 ratio of [NiA′$_2$] to {A′}$_2$ (eq 2.2).

$$2\,[KA'] + [Ni(dme)Br_2] \xrightarrow[\substack{\text{LAG with THF}\\ (h = 0.6)}]{} [NiA'_2] + 2\,KBr + \{A'\}_2 \qquad (2.2)$$

(52%)

The increase in reactivity prompted a separate investigation of the interaction of THF with bulk [$Ni(dme)Br_2$]. Adding excess THF to solid [$Ni(dme)Br_2$] generates a lavender solution from which red

crystals can be obtained; these crystals were identified with X-ray crystallography as the known solvate $[Ni_3(thf)_5Br_6]$.[53] However, the behavior of $[Ni(dme)Br_2]$ in a large excess of THF could be distinct from its reactivity in the small amount of THF present under LAG conditions, and in fact the behavior of the lavender solid produced from the addition of LAG quantities of THF does not match that of the red $[Ni_3(thf)_5Br_6]$. As noted above (Section 2.1.2.3), dry grinding of isolated $[Ni_3(thf)_5Br_6]$ with [KA′] yields $\{A'\}_2$ as the major product and the allyl complex in only 9% yield (Table A2.2, entry 8), so it appears that the presence of DME has an important auxiliary effect in the synthesis.

2.1.2.5 The dihydrate $[Ni(H_2O)_2Cl_2]$ as the nickel source

As part of the survey of the nickel solvates, nickel chloride dihydrate $[Ni(H_2O)_2Cl_2]$ was also included. The dihydrate is the usual endpoint of heating the hexahydrate.[54] Although the hexahydrate has been used to prepare a variety of nickel coordination complexes[55–60] and even some organometallic complexes as water-sensitive as $[Ni(cod)_2]$,[61] use of the dihydrate in synthesizing coordination complexes species is rarer,[62–65] and to the best of our knowledge, has not previously been reported for organometallic species. In fact, the dihydrate was found to display reactivity similar to that of the anhydrous salt. As with anhydrous $[NiCl_2]$, $[Ni(H_2O)_2Cl_2]$ appeared as an unpromising precursor to $[NiA'_2]$, and grinding either by itself, or with THF, DME, Et_2O, or benzene under LAG conditions ($\eta \approx 0.7–0.9$) never produced more than trace amounts of $[NiA'_2]$, but always large yields of the hexadiene (Table A2.4, entries 1–5).

2.1.2.6 Impact of pyridine on reactivity

The pronounced effect on $[NiA'_2]$ yield from the use of the pyridine solvate $[Ni(py)_4Cl_2]$ in diethyl ether solution (Section (a)) prompted further investigation of the general nickel chloride/pyridine system. As a start, a 10 min grind at 600 RPM between [KA′] and $[Ni(pyr)_4Cl_2]$ was found to produce $[NiA'_2]$ cleanly in 69% yield, with no evidence of $\{A'\}_2$ formation (Table 2.2, entry 5). The consistently effective reactivity of $[Ni(pyr)_4Cl_2]$ under both solution and solvent-free conditions raised the broader question of just how the form and quantity in which pyridine is introduced into the $[NiCl_2]$ + [KA′] reaction affects the outcome.

The reaction of unsolvated nickel chloride and [KA′] was then studied in pyridine solution, where obviously a large excess of pyridine was present. Unlike the reactions previously studied, this yielded a dark brown viscous oil. ^{1}H NMR analysis of a hexane extract of the dried oil showed the presence of $[NiA'_2]$ and the absence of $\{A'\}_2$. However, the complex was only a minor component of a highly complex mixture of species, not all of which could be identified, and the amount of $[NiA'_2]$ itself could not be quantified (Figure A2.1). A related outcome was found when $[Ni(H_2O)_2Cl_2]$ was used as the nickel source, and bulk pyridine was the solvent. After 48 hours, the mixture was evaporated, leaving a dark brown residue. The ^{1}H

NMR spectrum was somewhat cleaner than that from anhydrous [$NiCl_2$], and now both [NiA'_2] and {A'}$_2$ in a ratio of 15:1 could be identified, with a net yield of [NiA'_2] of 14% (Table 2.2, entry 2). Clearly, pyridine as a bulk solvent was less promising for [NiA'_2] yield than when it was introduced in the form of the solvate.

Under LAG conditions, unsolvated [$NiCl_2$] and 5 eq. of pyridine ($\eta = 0.70$) generated both [NiA'_2] and {A')$_2$ in about 30% yield (Table 2.2, entry 3). In contrast, [$Ni(H_2O)_2Cl_2$] under the same LAG conditions produced [NiA'_2] in 46% yield, without any trace of the hexadiene (Table 2, entry 1). It is possible that the water released from the [$Ni(H_2O)_2Cl_2$] hydrate degrades other sensitive products, resulting in a cleaner spectrum, or that it shuts down a redox pathway. Taking the [$NiCl_2$]/[$Ni(H_2O)_2Cl_2$] LAG data together, the dihydrate exhibits somewhat greater reactivity and selectivity as a nickel source with pyridine compared to the behavior of the anhydrous chloride.

The curious difference in reactivity between [$NiCl_2$]/[$Ni(H_2O)_2Cl_2$] under LAG conditions led us to directly examine the interactions between pyridine and the two nickel halide sources (without [KA']). A 10-minute grind of [$NiCl_2$] with 5 eq. of pyridine generated a grey powder, which PXRD analysis indicates is a mixture of compounds, primarily [$Ni(pyr)_4Cl_2$] and [$Ni(pyr)_2Cl_2$][66] (Figure A2.2). On the other hand, applying the same conditions (5 eq. pyridine, 10 min grinding) converted the yellow [$Ni(H_2O)_2Cl_2$] into a bright blue power, revealed from PXRD data as essentially pure [$Ni(pyr)_4Cl_2$] (Figure A2.3). Grinding of the isolated [$Ni(pyr)_4Cl_2$] for 20 min did not yield any evidence for decomposition. The high metathesis reactivity and ease of formation of the tetrakis(pyridine) complex further underscores its importance in the formation of [NiA'_2].

Table 2.2: Reaction outcomes of grinding [KA´], $[Ni(H_2O)_2Cl_2]$/$NiCl_2$, and pyridine (or adduct)

No.	Condition	Nickel source	Time	Eq. pyridine	η (or eq.)	[NiA´$_2$] yield (%)	[NiA´$_2$] : {A´}$_2$
1	LAG	$[Ni(H_2O)_2Cl_2]$	10 min	6.4	0.70	46	no {A´}$_2$
2	Solution	$[Ni(H_2O)_2Cl_2]$	48 h	>>10	>100	14	15:1
3	LAG	$[NiCl_2]$	10 min	5	0.70	29	0.9:1
4	Solution	$[NiCl_2]$	48 h	>>10	>100	*a*	no {A´}$_2$
5	Adduct grind	$[Ni(pyr)_4Cl_2]$	10 min	4	0.55	69	no {A´}$_2$

[a]Complex mixture of products prevented quantification of [NiA´$_2$].

The results with the nickel halides suggested that reaction of the isolated pyridine adduct of a metal chloride might be effective with other metals. As a preliminary test of this, a 10 min grind of [KA´] with the monomeric $[Fe(pyr)_4Cl_2]$ complex[67] was conducted. This precursor generated [FeA´$_2$] in 61% yield and in a 22:1 ratio with the hexadiene. These represent nearly the same yield of complex as the THF solution reaction with $[FeCl_2]$ (Table 2.1, entry 8) but with much greater selectivity for the complex (i.e., the complex:hexadiene ratio is 7:1 from solution).

2.1.2.7 Structure of meso-(1,3,4,6-tetrakis(trimethylsilyl)hexa-1,5-diene)

Previous study of {A´}$_2$ generated in solution found it in two diastereomeric forms of C_i (*meso*) and C_2 (*rac*) symmetry.[49] One form was always in excess, with an average ratio of 1.7:1, although this varied somewhat with the preparation. The compound was crystalline, but it yielded a severely disordered single crystal X-ray structure. The space group (monoclinic *C*2) was compatible with an enantiomeric mixture of the C_2-symmetric forms, but the low quality of the structure could not rule out the co-crystallization of C_i and C_2 forms.

Considerable amounts of {A´}$_2$ were produced during the course of the mechanochemical experiments, including some in highly crystalline form. An investigation of these crystals indicates that the hexa-1,5-diene crystallized in a different space group ($P2_1/c$) from the previously obtained crystals, and comprised a single diastereomer, the *meso* form (Figure 2.5). The inversion symmetry is only approximate, and is not crystallographically imposed. The structure is largely as would be expected; the central C3–C4 bond, at 1.558(4) Å, although slightly long for a single bond, is shorter than the comparable distance found in [(^{t}BuMe$_2$Si)CH(CH=CHSiMe$_2{}^t$Bu)]$_2$ (1.571(4) Å), for example, which was ascribed to steric crowding

between the bulky alkylsilyl groups.[68] It is unclear why the mechanochemical preparation yielded higher quality crystals of exclusively the *meso* form, as the ratio of diastereomers did not deviate significantly from the solution phase results as determined with ^{1}H NMR.

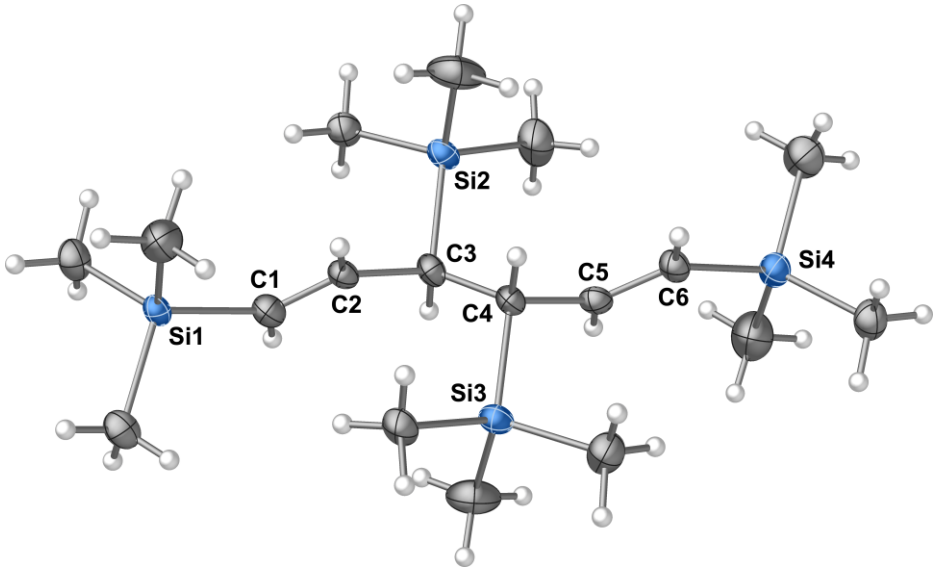

Figure 2.5: Thermal ellipsoid plot (50% level) of the structure of *meso*-{A´}$_2$; hydrogen atoms are given arbitrary radii. Selected bond distances (Å) and angles (°): C1–C2, 1.330(4); C2–C3, 1.496(3); C3–C4, 1.558(4); C4–C5, 1.500(3); C5–C6, 1.332(4); C1–C2–C3, 127.9(3), C2–C3–C4, 112.3(2), C3–C4–C5, 111.6(2), C4–C5–C6, 127.6(3).

The structures and relative energy of the *meso* and *rac* forms were evaluated with DFT calculations at the B3PW91-D3BJ/def2TZVP level (illustrations available in Appendix 2 as Figures A2.5 and A2.6, respectively). The *meso* form is found to be 5.9 kcal mol^{-1} lower in energy ($\Delta G°$) than the *rac* form. The middle two trimethylsilyl groups in the *rac* form have a close Me···Me´ contact at 3.59 Å that may contribute to its higher energy.

2.1.3 Discussion

Extrapolation of the requirements for the effective synthesis of [MA´$_2$] complexes to other compounds cannot be made casually. Yet as the use of halide metathesis is widespread in organometallic synthesis,[13] there are certain features of the reactions that may be relevant to related systems. It is clear that dry grinding of [KA´] and [MCl$_2$] is not an effective route to the formation of [MA´$_2$] species, certainly not when compared to solution outcomes for M = Cr, Fe, and Co (Figures 2.2, 2.3). Using THF in LAG quantities notably increases the yield of the bis(allyl) complexes, although this is strongly metal dependent,

ranging from 59% isolated yield with M = Cr to ≤ 4% yield with M = Ni. The exact reasons for this difference are unclear, although the relative oxophilicities of the metals may be involved, with chromium the most likely to interact with an ethereal solvent and nickel the least.[69]

Compared to grinding the respective nickel halide dry or in the presence of the free solvent, solvated salts are slightly to greatly superior precursors for reaction with [KA′] under mechanochemical conditions. Although they differ marginally in efficacy, [Ni(dme)Br_2], [Ni(thf)$_{1.5}Cl_2$], and [Ni_3(thf)$_5Br_6$] all produced low yields of only 3–9%. However, the use of [Ni(pyr)$_4Cl_2$] as a dry precursor and **[**Ni(dme)Br_2**]** in the presence of THF as a LAG solvent both produced the nickel allyl complex as the major product in greater than 50% yield.

There are distinctive differences between the latter two solvate-supported reactions that deserve individual comment. In the case of the reaction of [Ni(dme)Br_2] with THF, it should be noted that [Ni_3(thf)$_5Br_6$] was originally reported as a by-product of the reaction of [$NiBr_2$] with 4 eq. of [{PhP(CH_2NHEt_2)$_2$}Br_2] in refluxing THF.[53] The authors of the study were unable to confirm that the THF adduct was obtainable from the reaction of [$NiBr_2$] alone in hot THF. The fact that we have found that crystals of [Ni_3(thf)$_5Br_6$] can be had by simply extracting [Ni(dme)Br_2] with THF at room temperature, and the solution evaporated, illustrates the effect that coordinated DME has on the reactivity of [$NiBr_2$]. In the [Ni(dme)Br_2]/THF LAG system, it is possible that the [Ni(dme)Br_2] is converted to a [$NiBr_2$(thf)$_x$] species and that the released DME then provides some synergic effect as an additional LAG solvent. However, given the minimal effects seen with the use of either THF or DME alone as LAG solvents or with their solvates, it is also possible that with only a limited amount of THF, the DME is not entirely displaced and instead a mixed-solvent adduct of the form [Ni(dme)$_x$(thf)$_y$$Br_2$] is present. We have yet to isolate such a species, although work on this is continuing.

The use of pyridine in the synthesis of [NiA′$_2$] deserves special mention. The [Ni(pyr)$_4Cl_2$] adduct appears to be an especially useful precursor to [NiA′$_2$], but it should be noted that nickel and pyridine actually form an extensive series of adducts with the formula [Ni(pyr)$_n$$Cl_2$] ($n$ = $^2/_3$, 1, 2, 4), and all of them have been structurally authenticated (Figure 2.6).[66,70,71] [Ni(pyr)$_4Cl_2$] comprises monomeric molecules (Figure 2.6a), but the rest are coordination polymers that display an inverse relationship between the number of Ni–Cl interactions and the number of bound pyridines. In this way, these adducts represent a spectrum from fully monomeric [Ni(pyr)$_4Cl_2$] to the complete 3-dimensional lattice of [$NiCl_2$]$_n$ with its edge-sharing $NiCl_6$ octahedra and μ_3-Cl atoms (Figure 2.6e).

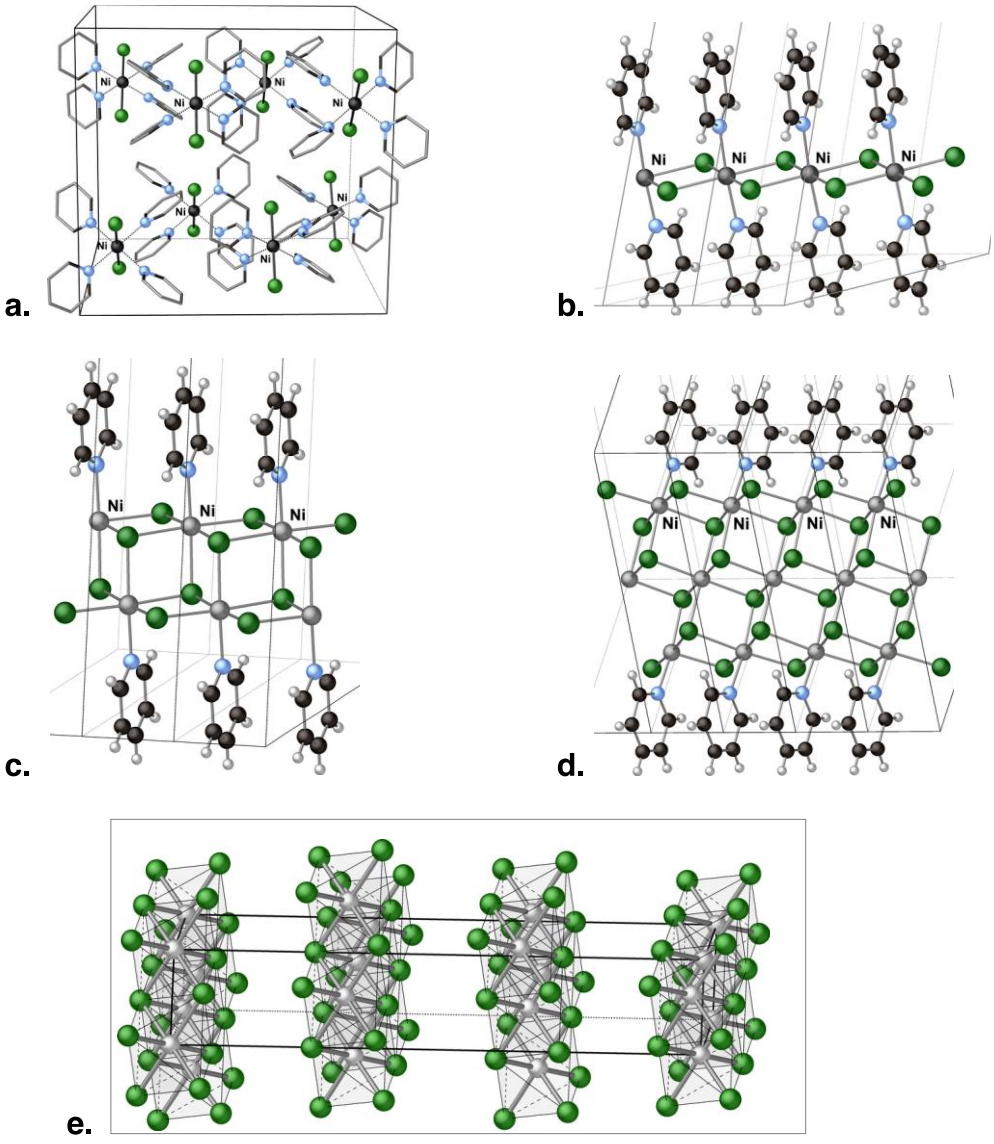

Figure 2.6: a. The unit cell of $[Ni(pyr)_4Cl_2]$, with hydrogens removed for clarity ($I4_1/acd$);[71] b. Portions of several unit cells of $[Ni(pyr)_2(\mu\text{-}Cl)_2]_n$ ($P2/c$);[67] c. Portions of several unit cells of $[Ni(pyr)(\mu\text{-}Cl)_2]_n$ ($P\bar{1}$);[70] d. Portions of several unit cells of $[Ni(pyr)_{2/3}Cl_2]_n$ ($P\bar{1}$);[70] e. the unit cell and environment of $[NiCl_2]$ ($R\bar{3}m$), illustrating the $CdCl_2$-layered structure (4.4 Å interlayer spacing); the same structure is shared with $FeCl_2$ and $CoCl_2$.[72]

The series provides an illustration of how adduct formation may be associated with increased reactivity. An extended review of organometallic synthesis, reactivity, and catalysis in the solid state[29] noted that general reactivity, including access to metal coordination sites, is assisted by increases in the porosity of the extended solid structures (such a structural difference aids in the formation of reaction cavities, and ultimately increases the ease with which a new ligand could incorporate itself into the coordination sphere of a metal ion). Not surprisingly, as n increases in the $[Ni(pyr)_nCl_2]$ adducts, the bulk density decreases (from 3.55 g cm^{-3} for $NiCl_2$ to 1.40 g cm^{-3} for $[Ni(pyr)_4Cl_2]$), with a corresponding increase in calculated porosity (see Figure A2.7 for plots of the data).

Apart from such structural changes, the relative lability of metal ligand bonds needs to be considered. Even by qualitative metrics, electroneutrality considerations[73] would lead to the expectation that the strong donation ability of pyridine would contribute to weakening of the nickel–chloride interactions, and thus assistance in the halide metathesis reaction pathway. However, quantitative, or even semi-quantitative comparisons of the metal-ligand bond strength in a discrete molecule (e.g., $[Ni(pyr)_4Cl_2]$) and coordination polymers/3D lattices in the other pyridine adducts and $[NiCl_2]$) are not as easily made. For a simple comparison, however, one could evaluate the energy change involved in the loss of a chloride ion from the monomeric molecular species $[NiCl_2]$[74] and from $[Ni(pyr)_4Cl_2]$ (i.e., the reactions represented by the processes $NiCl_2 \rightarrow [NiCl]^+ + Cl^-$ and $[Ni(pyr)_4Cl_2] \rightarrow [Ni(pyr)_4Cl]^+ + Cl^-$). At the B3PW91-D3BJ/def2TZVPD level, $\Delta G°$ for the two reactions are +202 kcal mol^{-1} and +99 kcal mol^{-1}, respectively. Of course, the Ni environment around monomeric $[NiCl_2]$ and the bulk $[NiCl_2]$ are substantially different, but even allowing for difficulties in the comparisons, replacement of the chloride appears to be more facile in $[Ni(pyr)_4Cl_2]$. It suggests that the activating effect that solvates offer in halide metathetical reactions in general is to weaken the metal–halide bond, and thus assist in the halide/ligand exchange pathway. It is also possible that the pyridines serve to open up an accessible coordination site on the metal center, allowing an allyl to substitute in place of a pyridine rather than the more difficult-to-displace chloride ligand.

2.2 Broader Precursor Investigation

2.2.1 Introduction:

Salt metathesis is among the most widely applicable methods in transition metal organometallic synthesis. Due to the availability and ease of use of simple salts of most metals, this technique is exceedingly broad and generally straightforward to employ. Perhaps due to this simplicity, little investigation into the particulars of the transformation has been performed. However, due to the broad implementation of metathesis processes, insight into the factors influencing the outcome of these reactions would be highly valuable.

By a large margin, the most common transition metal source for metathesis reactions are metal halide salts. These are accessible, inexpensive, and are expected to generally perform well in salt metathesis due to the formation of stable, insoluble MX_n as a byproduct. The investigation presented in Section 2.1 indicated that, in the formation of $[M(A')_2]$ (M = Cr, Fe, Co, Ni) complexes, solvated metal halide salts generally gave better metathesis performance than their unsolvated counterparts. Of particular note is the case of nickel chloride; replacement of unsolvated $[NiCl_2]$ with $[Ni(pyr)_4Cl_2]$ caused $[NiA'_2]$ to shift from a trace minor product to the exclusive product. Two broad implications of this result are that variation of the transition metal source can lead to dramatic changes in reaction outcome and that simple metal halide salts are not always ideal metathesis partners.

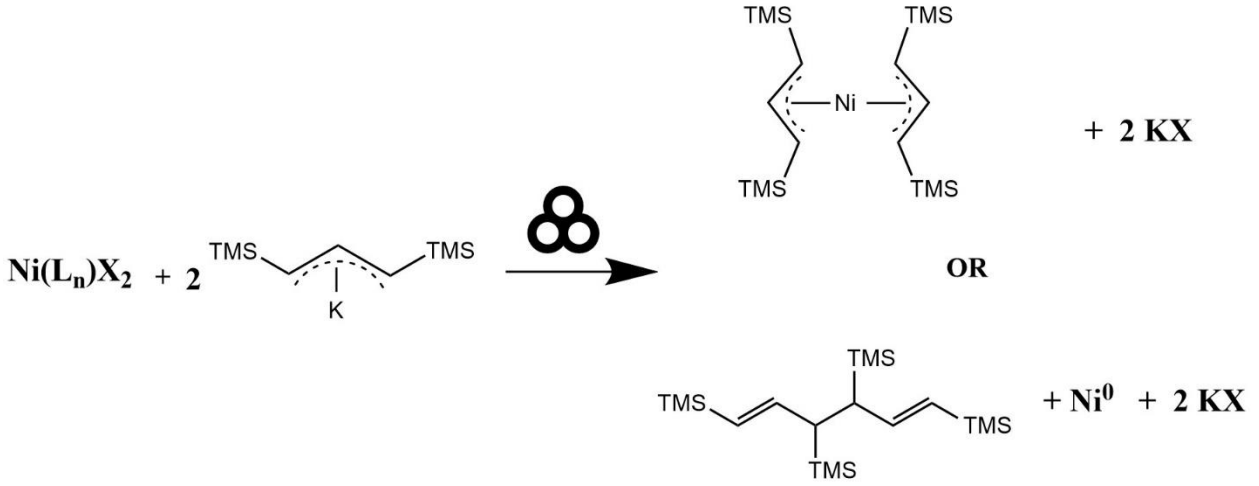

Figure 2.7: Competing pathways in the reaction of nickel(II) salts with [KA´]

It was found that introduction of Lewis basic solvents increased the preference for the desired halide metathesis pathway, and our investigation suggested that this effect was caused by the binding of solvent in the coordination sphere of the transition metal before reaction with the allyl salt. Leveraging these insights, the mechanochemical preparation of the difficult $[NiA'_2]$ in good yield and with perfect selectivity was acheived. However, our understanding was not complete, as it remained unclear how solvent binding produced this effect. Without such an understanding, the generality of our results is unclear, and there is no predictive ability for precursors other than halide salts. In search of such an understanding, we continued our study of the $[NiX_2]$/[KA´] system with a broader selection of precursors.

2.2.2 Mechanochemical Metathesis Reactions Results and Discussion

Our group's standard procedure for the solution phase synthesis of $[NiA'_2]$ uses $[Ni(dme)Br_2]$ as a precursor, but the above investigation showed that this reacts to yield primarily $\{A'_2\}$ under mechanochemical conditions. However, the original report for the synthesis of $[NiA'_2]$ used $[Ni(acac)_2]$ as

the nickel(II) source instead, so this seemed a natural starting point for a broader study of nickel precursors. Completely surpassing expectations, [Ni(acac)$_2$] reacted with [KA´] under solvent-free mechanochemical conditions to yield [NiA´$_2$] without even a spectroscopically detectable amount of {A´$_2$}. This matched the selectivity performance of the best precursor previously identified, [Ni(pyr)$_4$Cl$_2$]. However, the most interesting element of this result is that it dispels the notion that some solvent must be present for clean halide metathesis under mechanochemical conditions to occur. This prompted the questions: Are the halide salts were atypically poor precursors? Would such clean reactivity be commonly observed for other simple [NiX$_2$] salts?

Unfortunately, this desirable reactivity was not as widespread as initially hoped, as shown in Table 2.3. See Table A2.5 for experimental conditions and quantitative outcomes for all reactions. Cyanide is often referred to as a "*pseudo*-halide," so it is not entirely surprising that [Ni(CN)$_2$] also reacts to yield primarily dimer, although to a much lesser extent than any of the true halide salts. Contrastingly, the triflate (trifluoromethanesulfonate, -OS(O$_2$)CF$_3$, -OTf) anion is also referred to as a *pseudo*-halide, but [NiOTf$_2$] reacted to yield almost exclusively [NiA´$_2$] in high yield.

Table 2.3: Reaction outcomes of grinding [KA´] with various unsolvated nickel(II) salts

Entry	Nickel source	[NiA´$_2$] : {A´}$_2$
1	[Ni(acac)$_2$]	No {A´$_2$}
2	[Ni(OTf)$_2$]	31 : 1
3	[Ni(OAc)$_2$]	1 : 1.1
4	[Ni(CN)$_2$]	1 : 3.3
5	[NiSO$_4$]	1 : 33
6	[NiCl$_2$]	Trace [NiA´$_2$]
7	[NiBr$_2$]	Trace [NiA´$_2$]
8	[NiI$_2$]	Trace [NiA´$_2$]

Our previous study has shown that isolable solvent adducts react substantially differently than their unsolvated counterparts, and this data is reproduced here for analysis in this broader context. In addition, other adducts were synthesized and tested. [Ni(diglyme)Cl$_2$][75] can be compared to the similar ether adducts [Ni(thf)$_{1.5}$Cl$_2$][50] and [Ni(dme)Cl$_2$][76]; the diglyme adduct yielded the greatest proportion of [NiA´$_2$] in the product mixture, though still slightly less than {A'$_2$}. The cationic species [Ni(NCMe)$_6$(BF$_4$)$_2$][77] was also investigated, forming a moderate excess of complex relative to dimer, though in poor yield.

From these results, it is abundantly clear that dramatically differing reactivity can be observed depending on which nickel precursor is used. This prompts the question: why do some precursors undergo

clean salt metathesis while others give only coupled dimer? We therefore aimed to identify the factors that contribute to a given precursor's predilection towards one reactivity pathway or the other. Certain properties can be immediately dismissed by comparing certain entries from Table 2.3. While the identity of the anion that is being displaced would be the simplest determinant, the diversity of results seen by precursors of the form $[Ni(L)_nCl_2]$ (Table 2.2 above) quickly dispels this idea. Furthermore, comparison of $[Ni(acac)_2]$, and $[Ni(SO_4)]$ (Table 2.3, entries 1 and 5) shows that neither the identity of the coordinating atom nor the coordination number of nickel are important factors.

Before the study of this system under mechanochemical conditions, it was believed that precursor solubility dictated its preferred reaction pathway, with more soluble compounds yielding greater proportions of complex. Of course, solubility cannot be a direct cause under mechanochemical conditions, and furthermore, this proposition is disproven by the case of $[Ni(pyr)_4Cl_2]$, which produced only $[NiA'_2]$ despite having negligible solubility in any organic solvent. Nonetheless, these two variables do appear to be somewhat correlated: the most redox-favoring precursors are all rigorously insoluble, while two of the three metathesis-favoring precursors show moderate to high solubility in THF. Therefore, while causation can be dismissed, the observed correlation indicates that similar factors may give rise to both properties. Another promising candidate for a primary factor was aggregation state. In addition to being insoluble, the strongly redox-favoring precursors are all ionic salts. Contrastingly, the only two precursors that exclusively react via metathesis are both molecular in the solid state. Furthermore, the two $[Ni(dme)X_2]$ species, $[Ni(CN)_2]$, and $[Ni(thf)_{(5/3)}Br_2]$ are all best described as coordination polymers, and accordingly form a set of intermediate selectivity values. While the crystal structure of the dimethoxyethane adducts have not been solved, spectroscopic evidence[76] and the crystal structure of the analogous manganese-dimethoxyethane compound[75] support the assignment of a polymeric structure, which will be assumed for this discussion. A plot of reaction outcomes grouped by aggregation state of the various precursors tested is included below as Figure 2.8.

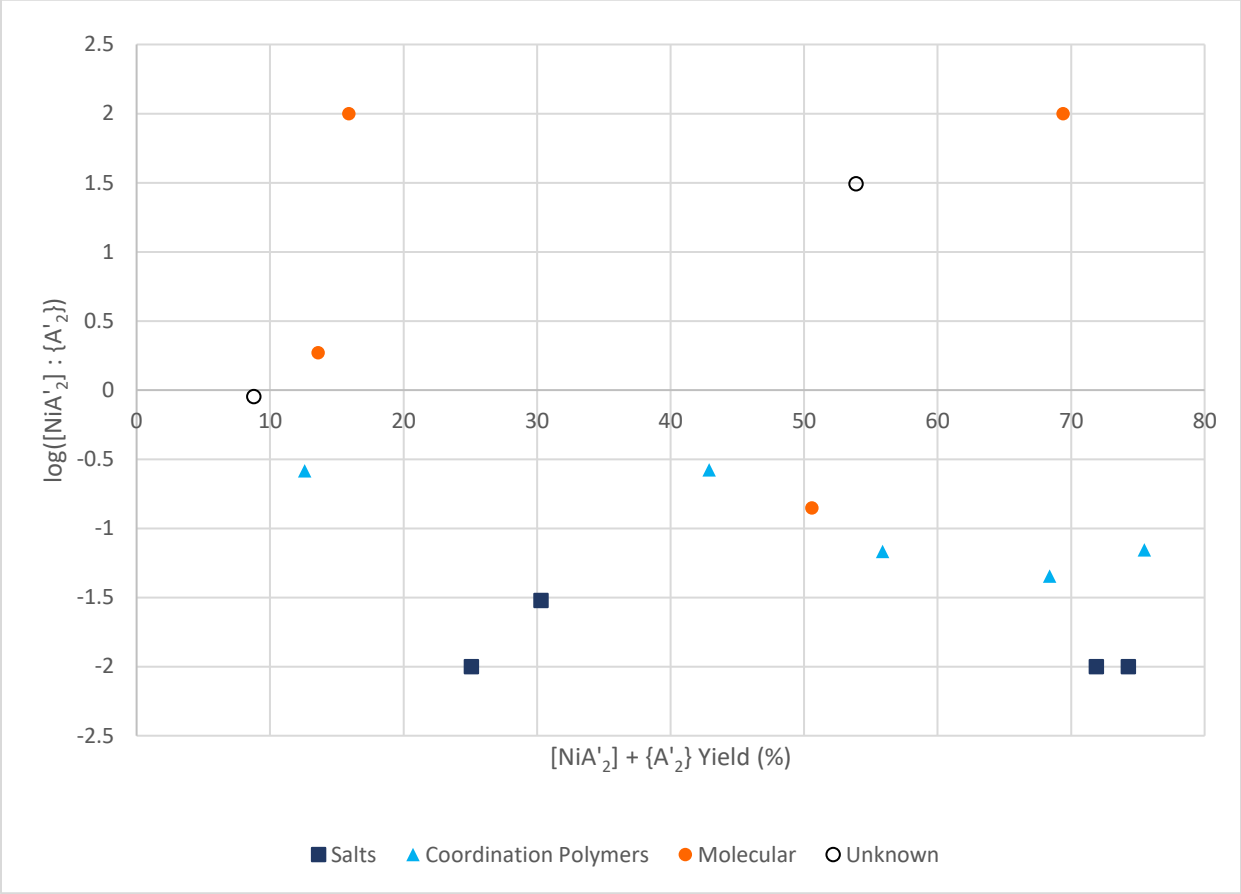

Figure 2.8: A plot of the outcomes of reactions between different nickel precursors and [KA´]. Selectivity is plotted on the y-axis, expressed as the base-10 logarithm of the ratio of [NiA´$_2$] to {A´$_2$} (defined as the number of moles of [NiA´$_2$] present for each mole of {A´$_2$}) observed by ^{1}H NMR; if no {A´$_2$} was observable, then [NiA´$_2$] : {A´$_2$} was arbitrarily assigned a value of 100. If only trace [NiA´$_2$] was observed, then [NiA´$_2$] : {A´$_2$} was arbitrarily assigned a value of 0.01. Total product yield (percent yield of [NiA´$_2$] + percent yield of {A´$_2$}) is plotted on the x-axis. Precursors are grouped by the aggregation state present in their solid-state structures, if known.

We were therefore disheartened to discover that the molecular [Ni(diglyme)Cl$_2$][75] reacted primarily via the redox pathway, albeit still in much less excess than observed for unsolvated nickel chloride. Comparing the diglyme adduct to other ether adducts, it is notable that diglyme is a tridentate ligand, and is thus subject to a strong chelate effect. As such, despite similar binding at each individual oxygen, diglyme is expected to bind much more strongly to nickel overall. This then leads to the conclusion that formation

of a molecular species is insufficient to ensure effective metathesis; some weak ligands must also be present, presumably to allow the incoming allyl to easily bind to nickel. Indeed, of the two, the nearly ideal reactivity of nickel triflate suggests that the presence of weakly binding ligands might be the more important of the two. Another interesting conclusion made from Figure 2.8 is that there is no apparent trend whatsoever between selectivity and yield of products. However, a thorough accounting of mass balance has not been undertaken, so the implications of this lack of correlation are not clear.

Some additional reactions were performed in the course of this investigation, namely grinding of some additional precursors in the presence of THF, and reactions of solids in the absence of mechanical activation. The results of these experiments are included in Appendix 2.

As a whole, this analysis suggests that the outcome of the reaction considered is directed by the availability of the nickel center, defined as the ease with which an incoming allyl ligand can enter the coordination sphere of a nickel ion and adopt its desired η^3-binding mode. The most important factor in determining the availability of the nickel center seems to be the presence of easily accessed coordination sites at the metal center. This can be due to coordinative unsaturation or the presence of weakly bound ligands that can be easily displaced by an incoming allyl ligand. This model provides a consistent rationalization for the solvate effect observed in Section 2.1 and provides predictive power for selecting a precursor for a metathesis reaction. In the long term, further study should focus on the generality of these conclusions in metathesis reactions with other ligand classes. Allyls show a strong preference for binding nickel in an η^3-fashion, and formation of [NiA′$_2$] requires a square planar geometry. It could be enlightening to learn if such a wide disparity in outcomes would be observed if a ligand without such strong binding preferences were employed.

In making these conclusions, though, it is important to note that the quality of this data is currently poor. Many precursors have only been tested once, so there is considerable uncertainty associated with each value. Additionally, the conditions were not uniform among the data set considered here, varying in grind time and scale. While grind time has been shown to have negligible impact on the outcome of fast halide metathesis reactions like these, the impact of scale has not been studied, and may further contribute to uncertainty. Therefore, at this point in the investigation, these results should be interpreted only to the extent of indicating qualitative trends, and even then, the indicated trends should be treated cautiously. Furthermore, the precursor [Ni(NCMe)$_6$(BF$_4$)$_2$] would appear to be ideal, based on the criteria presented above, having exclusively weak ligands and being fully molecular. Despite this, it gives only a slight excess of [NiA′$_2$] compared to {A′$_2$}, and in very poor yield. This suggests that our understanding remains incomplete, and that further relevant factors have yet to be identified. The immediate future of this project will involve improving the quality of the data on the current selection of precursors and further broadening the scope of precursors considered.

2.2.4 Novel diastereomer of bis(A′)nickel(II)

During the course of this investigation, [NiA′$_2$] was synthesized many times. In addition to the two known diastereomers, each containing equivalent allyls with *syn,anti* configured substituents, in some cases, two other allyl spin systems were identified whose features were strongly suggestive of a bis(η^3-allyl)nickel complex. One of the allyl systems clearly displayed a *syn,anti* configuration, called A while the second was *syn,syn,* called B. However, despite both substituents on allyl B unambiguously having the same configuration, the two *anti* protons are inequivalent. Both the central and *anti* protons of A nearly perfectly overlap with matching protons on staggered bis(*syn,anti*-A′)nickel, implying an extremely similar structure. Finally, it was observed that the two allyls were always found together, and with similar relative abundances. Based on the above reasoning, this new species is confidently identified as (*syn,syn*-A′)(*syn,anti*-A′)nickel(II), a new diastereomer of bis(A′)nickel containing two allyls with different substituent configurations. This was unexpected, given the dearth of mixed acyclic allyl complexes of nickel and the apparent preference of A′ ligands to bind in the *syn,anti* configuration in bis(allyl)nickel complexes (also see Section 4.2.2.2.)[49] However, it can be rationalized on the basis that incoming allyls will be in the *syn,syn* conformation. The crystal structure of unsolvated [KA′] has been determined;[78] the compound is a coordination polymer with each allyl η^3-bound to two potassium, and both TMS groups in a *syn* configuration. While this may be disrupted upon dissolution, this configuration is maintained in the solid state, and likely contributes to the sudden emergence of the new diastereomer in this purely mechanochemical investigation. Furthermore, it appears that the drive to adopt a *syn,anti* configuration is lessened in heteroleptic monoallyl complexes (also see Section 4.2.2.2.)[49] Therefore, it seems entirely possible that, in the solid state, the first allyl to bind to a nickel center might maintain its *syn,syn* configuration; if the second ligand exchange occurs fast enough, this configuration might become locked, as *syn/anti* interchange processes are much slower for allyls with bulky substituents.[49]

Excitingly, it was found that synthesizing [NiA′$_2$] from nickel triflate and [KA′] yielded this new species as the major product. Attempts to selectively crystallize this new diastereomer have thus far failed. It is not clear why nickel triflate reacts to yield this new product in such anomalously high abundance, though the weakly-coordinating nature of triflate ligands may be related. As stated above, it is hypothesized that this mixed allyl species is a kinetic product, and therefore having such a weakly bound anion may allow

for metathesis to proceed extremely quickly. This framework would also suggest that the abundance of this diastereomer might be further enriched by performing the reaction at low temperature. While relatively uncommon compared to low-temperature reactions in solution, cooling of milled reactions can be achieved via a simple adaptation to the standard mixer mill setup recently published by the Mack group.[79] It is therefore possible that the mixed species be produced in greater abundance, which may allow for its selective crystallization and structural determination.

2.3 Conclusions

It is clear that the presence of solvent has a profound effect on the reactivity of transition metal halide salts undergoing metathesis reactions to form allyl complexes. However, with the substituted bis(allyl) [MA´$_2$] complexes, there is no exact relationship between the volume of solvent and its effect on reactivity. This is especially true when the molar equivalents of solvents present under LAG, solvate, or solution conditions are considered. The maximum number of THF ligands that have been documented to bind to Fe or Co is 6. Therefore, LAG reactions run with 10 molar equivalents of THF ($\eta \approx 1.5$, Figure 3) have more than enough solvent molecules to coordinately saturate the metal center, yet the solution reactions generate a higher yield of product.

A dominant role of solvent in these systems appears to be direct chemical interaction with the metal center. It seems that metal solvates hold a great deal of potential as 'solvent reservoirs'; but it appears that, distinct from LAG, the concept of "solvate assisted grinding" (SAG) would be appropriate to introduce. These results support the concept that solvated metal salts can provide access to more active solid-state transition metal precursors than does just the addition of solvent alone. Furthermore, the origin of this effect seems to be the introduction of weakly bound ligands to the metal centers. This appears to be generalizable to unsolvated nickel precursors, suggesting that molecular species with easily displaced ligands, either in the form of weakly coordinating anions (acac$^-$, OTf$^-$) or mono-dentate donor ligands are ideal metal sources for smooth salt metathesis reactions. Future work in this direction will attempt to decouple kinetic and thermodynamic factors giving rise to this effect so that these conclusions can be properly generalized.

2.4 Synthetic procedure and characterization

2.4.1 Synthesis of novel [NiA´$_2$] diastereomer

In a nitrogen-filled glovebox, a stainless-steel grinding jar was charged with 25 g ball bearings, [NiOTf$_2$] (157.2 mg, 0.44 mmol), and [KA´] (199 mg, 0.89 mmol). The jar was then tightly sealed, removed from the glovebox, and placed in the planetary mill. The mixture was ground for 10 min at 600 rpm, at which point the jar was returned to the glovebox. The jar was opened, and products were taken up in hexane and filtered through a glass frit. Evaporation of solvent yielded the isolated product, which was weighed and

then analyzed with ^{1}H NMR. The *syn,syn* allyl is referred to as SS, while the *syn,anti* allyl is referred to as SA.

^{1}H NMR (400 MHz, C_6D_6): δ 5.65 (dd; 15.9, 9.8 Hz; 1H; SA center allyl C-H); δ 5.46 (dd; 15.3, 14.8 Hz; 1H; SS center allyl C-H); δ 4.03 (d, 9.8 Hz, 1H, SA *syn* terminal C-H); δ 2.07 (d, 15.9 Hz, 1H, SA *anti* terminal C-H); δ 1.79 (dd; 14.8, 1.2 Hz; 1H, SS *anti* terminal C-H); δ 1.40 (dd; 15.3, 1.2 Hz; 1H; SS *anti* terminal C-H); δ 0.31 (s, 9H, $Si(CH_3)_3$); δ 0.28 (s, 9H, $Si(CH_3)_3$); δ 0.25 (s, 9H, $Si(CH_3)_3$); δ 0.01 (s, 9H, $Si(CH_3)_3$).

2.5 References

(1) Reichardt, C.; Welton, T. *Solvents and Solvent Effects in Organic Chemistry*, 4th ed.; Wiley-VCH: Marburg, 2010. https://doi.org/10.1002/9783527632220.

(2) Hynes, J. T. Chemical Reaction Dynamics in Solution. *Annu. Rev. Phys. Chem.* **1985**, *36* (2), 573–597. https://doi.org/https://doi.org/10.1146/annurev.pc.36.100185.003041.

(3) Litwinienko, G.; Beckwith, A. L. J.; Ingold, K. U. The Frequently Overlooked Importance of Solvent in Free Radical Syntheses. *Chem. Soc. Rev.* **2011**, *40* (5), 2157–2163. https://doi.org/10.1039/c1cs15007c.

(4) Tan, D.; Loots, L.; Friščić, T. Towards Medicinal Mechanochemistry: Evolution of Milling from Pharmaceutical Solid Form Screening to the Synthesis of Active Pharmaceutical Ingredients (APIs). *Chem. Commun.* **2016**, *52* (50), 7760–7781. https://doi.org/10.1039/c6cc02015a.

(5) James, S. L.; Adams, C. J.; Bolm, C.; Braga, D.; Collier, P.; Frišcic, T.; Grepioni, F.; Harris, K. D. M.; Hyett, G.; Jones, W.; Krebs, A.; Mack, J.; Maini, L.; Orpen, A. G.; Parkin, I. P.; Shearouse, W. C.; Steed, J. W.; Waddell, D. C. Mechanochemistry: Opportunities for New and Cleaner Synthesis. *Chem. Soc. Rev.* **2012**, *41* (1), 413–447. https://doi.org/10.1039/c1cs15171a.

(6) Rightmire, N. R.; Hanusa, T. P.; Rheingold, A. L. Mechanochemical Synthesis of [1,3-$(SiMe_3)_2C_3H_3]_3$(Al,Sc), a Base-Free Tris(Allyl)Aluminum Complex and Its Scandium Analogue. *Organometallics* **2014**, *33* (21), 5952–5955. https://doi.org/10.1021/om5009204.

(7) Rightmire, N. R.; Hanusa, T. P. Advances in Organometallic Synthesis with Mechanochemical Methods. *Dalton Trans.* **2016**, *45* (6), 2352–2362. https://doi.org/10.1039/c5dt03866a.

(8) Shi, Y. X.; Xu, K.; Clegg, J. K.; Ganguly, R.; Hirao, H.; Friščić, T.; García, F. The First Synthesis of the Sterically Encumbered Adamantoid Phosphazane $P_4(NtBu)_6$: Enabled by Mechanochemistry. *Angew. Chem. - Int. Ed.* **2016**, *55* (41), 12736–12740. https://doi.org/10.1002/anie.201605936.

(9) Zhu, S. E.; Li, F.; Wang, G. W. Mechanochemistry of Fullerenes and Related Materials. *Chem. Soc. Rev.* **2013**, *42* (18), 7535–7570. https://doi.org/10.1039/c3cs35494f.

(10) Boyde, N. C.; Rightmire, N. R.; Hanusa, T. P.; Brennessel, W. W. Symmetric Assembly of a Sterically Encumbered Allyl Complex: Mechanochemical and Solution Synthesis of the Tris(Allyl)Beryllate, K[BeA′$_3$] (A′ = 1,3-$(SiMe_3)_2C_3H_3$). *Inorganics* **2017**, *5* (2), 1–11. https://doi.org/10.3390/inorganics5020036.

(11) Koby, R. F.; Hanusa, T. P.; Schley, N. D. Mechanochemically Driven Transformations in Organotin Chemistry: Stereochemical Rearrangement, Redox Behavior, and Dispersion-Stabilized Complexes. *J. Am. Chem. Soc.* **2018**, *140* (46), 15934–15942. https://doi.org/10.1021/jacs.8b09862.

(12) Koby, R. F.; Doerr, A. M.; Rightmire, N. R.; Schley, N. D.; Long, B. K.; Hanusa, T. P. An η^3-Bound Allyl Ligand on Magnesium in a Mechanochemically Generated Mg/K Allyl Complex. *Angew. Chemie* **2020**, *59* (24), 9542–9548. https://doi.org/https://doi.org/10.1002/anie.201916410.

(13) Elschenbroich, C. *Organometallics*, 3rd ed.; VCH Publishers: Weinheim, 2006.

(14) King, R. B. *Organometallic Syntheses*, 1st ed.; Academic: New York, 1965.

(15) Trask, A. V.; Shan, N.; Motherwell, W. D. S.; Jones, W.; Feng, S.; Tan, R. B. H.; Carpenter, K. J. Selective Polymorph Transformation via Solvent-Drop Grinding. *Chem. Commun.* **2005**, No. 7, 880–882. https://doi.org/10.1039/b416980h.
(16) Tan, D.; García, F. Main Group Mechanochemistry: From Curiosity to Established Protocols. *Chem. Soc. Rev.* **2019**, *48* (8), 2274–2292. https://doi.org/10.1039/c7cs00813a.
(17) Loots, L.; Wahl, H.; van der Westhuizen, L.; Haynes, D. A.; le Roex, T. Interconversion between Different Stoichiometric Forms of a Three-Component Crystal via Liquid-Assisted Grinding. *Chem. Commun.* **2012**, *48* (94), 11507–11509.
(18) Gracin, D.; Štrukil, V.; Friščič, T.; Halasz, I.; Užarevič, K. Laboratory Real-Time and in Situ Monitoring of Mechanochemical Milling Reactions by Raman Spectroscopy. *Angew. Chemie - Int. Ed.* **2014**, *53* (24), 6193–6197. https://doi.org/10.1002/anie.201402334.
(19) Howard, J. L.; Sagatov, Y.; Repusseau, L.; Schotten, C.; Browne, D. L. Controlling Reactivity through Liquid Assisted Grinding: The Curious Case of Mechanochemical Fluorination. *Green Chem.* **2017**, *19* (12), 2798–2802. https://doi.org/10.1039/c6gc03139k.
(20) Friščić, T.; Reid, D. G.; Halasz, I.; Stein, R. S.; Dinnebier, R. E.; Duer, M. J. Ion- and Liquid-Assisted Grinding: Improved Mechanochemical Synthesis of Metal-Organic Frameworks Reveals Salt Inclusion and Anion Templating. *Angew. Chem. - Int. Ed.* **2010**, *49* (4), 712–715. https://doi.org/10.1002/anie.200906583.
(21) Hasa, D.; Carlino, E.; Jones, W. Polymer-Assisted Grinding, a Versatile Method for Polymorph Control of Cocrystallization. *Cryst. Growth Des.* **2016**, *16* (3), 1772–1779. https://doi.org/10.1021/acs.cgd.6b00084.
(22) Braga, D.; Maini, L.; Grepioni, F. Mechanochemical Preparation of Co-Crystals. *Chem. Soc. Rev.* **2013**, *42* (18), 7638–7648. https://doi.org/10.1039/c3cs60014a.
(23) Do, J. L.; Friščić, T. Mechanochemistry: A Force of Synthesis. *ACS Cent. Sci.* **2017**, *3* (1), 13–19. https://doi.org/10.1021/acscentsci.6b00277.
(24) Friščić, T. Supramolecular Concepts and New Techniques in Mechanochemistry: Cocrystals, Cages, Rotaxanes, Open Metal–Organic Frameworks. *Chem. Soc. Rev.* **2012**, *41* (9), 3493–3510. https://doi.org/10.1039/c2cs15332g.
(25) Braga, D.; Giaffreda, S. L.; Grepioni, F.; Pettersen, A.; Maini, L.; Curzi, M.; Polito, M. Mechanochemical Preparation of Molecular and Supramolecular Organometallic Materials and Coordination Networks. *Dalton Trans.* **2006**, *6* (10), 1249–1263. https://doi.org/10.1039/b516165g.
(26) Friscic, T.; Childs, S. L.; Rizvi, S. A. A.; Jones, W. The Role of Solvent in Mechanochemical and Sonochemical Cocrystal Formation: A Solubility-Based Approach for Predicting Cocrystallisation Outcome. *Cryst. Eng. Comm.* **2009**, *11* (3), 418–426. https://doi.org/10.1039/b810822f.
(27) Do, J. L.; Mottillo, C.; Tan, D.; Štrukil, V.; Friščić, T. Mechanochemical Ruthenium-Catalyzed Olefin Metathesis. *J. Am. Chem. Soc.* **2015**, *137* (7), 2476–2479. https://doi.org/10.1021/jacs.5b00151.
(28) Strauss, S. H. The Search for Larger and More Weakly Coordinating Anions. *Chem. Rev.* **1993**, *93* (3), 927–942. https://doi.org/10.1021/cr00019a005.
(29) Sebastian, D. P.; Andrew, S. W. Organometallic Synthesis, Reactivity and Catalysis in the Solid State Using Well-Defined Single-Site Species. *Philos. Trans. R. Soc. A Math. Phys. Eng. Sci.* **2015**, *373* (2037). https://doi.org/10.1098/rsta.2014.0187.
(30) Verat, A. Y.; Pink, M.; Fan, H.; Tomaszewski, J.; Caulton, K. G. [($tBu_2PCH_2SiMe_2)_2$N]Rh(I)? Rapidly Reversible H-C(sp^2) Bond Cleavage by Rhodium(I). *Organometallics* **2008**, *27*, 166–168.
(31) Abo-Amer, A.; McCready, M. S.; Zhang, F.; Puddephatt, R. J. The Role of Solvent in Organometallic Chemistry - Oxidative Addition with Dichloromethane or Chloroform. *Can. J. Chem.* **2012**, *90* (1), 46–54. https://doi.org/10.1139/v11-096.
(32) Moustafa, M. E.; Boyle, P. D.; Puddephatt, R. J. Reactivity and Mechanism in Reactions of Methylene Halides with Cycloneophylplatinum(II) Complexes: Oxidative Addition and Methylene Insertion. *J. Organomet. Chem.* **2021**, *941*. https://doi.org/10.1016/j.jorganchem.2021.121803.
(33) Jiang, Z. J.; Li, Z. H.; Yu, J. B.; Su, W. K. Liquid-Assisted Grinding Accelerating: Suzuki-Miyaura

Reaction of Aryl Chlorides under High-Speed Ball-Milling Conditions. *J. Org. Chem.* **2016**, *81* (20), 10049–10055. https://doi.org/10.1021/acs.joc.6b01938.

(34) Seo, T.; Ishiyama, T.; Kubota, K.; Ito, H. Solid-State Suzuki-Miyaura Cross-Coupling Reactions: Olefin-Accelerated C-C Coupling Using Mechanochemistry. *Chem. Sci.* **2019**, *10* (35), 8202–8210. https://doi.org/10.1039/c9sc02185j.

(35) Yu, J.; Zhang, C.; Yang, X.; Su, W. Decarboxylative Acylation of: N-Free Indoles Enabled by a Catalytic Amount of Copper Catalyst and Liquid-Assisted Grinding. *Org. Biomol. Chem.* **2019**, *17* (18), 4446–4451. https://doi.org/10.1039/c9ob00622b.

(36) Pang, Y.; Ishiyama, T.; Kubota, K.; Ito, H. Iridium(I)-Catalyzed C-H Borylation in Air by Using Mechanochemistry. *Chem. Eur. J.* **2019**, *25*, 4654–4659. https://doi.org/10.1002/chem.201900685.

(37) Schumacher, C.; Crawford, D. E.; Raguž, B.; Glaum, R.; James, S. L.; Bolm, C.; Hernández, J. G. Mechanochemical Dehydrocoupling of Dimethylamine Borane and Hydrogenation Reactions Using Wilkinson's Catalyst. *Chem. Commun.* **2018**, *54* (60), 8355–8358. https://doi.org/10.1039/c8cc04487b.

(38) Kubota, K.; Takahashi, R.; Ito, H. Mechanochemistry Allows Carrying out Sensitive Organometallic Reactions in Air: Glove-Box-and-Schlenk-Line-Free Synthesis of Oxidative Addition Complexes from Aryl Halides and Palladium(0). *Chem. Sci.* **2019**, *10* (22), 5837–5842. https://doi.org/10.1039/c9sc01711a.

(39) Bjelopetrović, A.; Lukin, S.; Halasz, I.; Užarević, K.; Đilović, I.; Barišić, D.; Budimir, A.; Juribašić Kulcsár, M.; Ćurić, M. Mechanism of Mechanochemical C−H Bond Activation in an Azobenzene Substrate by PdII Catalysts. *Chem. Eur. J.* **2018**, *24* (42), 10672–10682. https://doi.org/10.1002/chem.201802403.

(40) Shan, N.; Toda, F.; Jones, W. Mechanochemistry and Co-Crystal Formation: Effect of Solvent on Reaction Kinetics. *Chem. Commun.* **2002**, *2* (20), 2372–2373. https://doi.org/10.1039/b207369m.

(41) Karki, S.; Friščić, T.; Jones, W.; Motherwell, W. D. S. Screening for Pharmaceutical Cocrystal Hydrates via Neat and Liquid-Assisted Grinding. *Mol. Pharm.* **2007**, *4* (3), 347–354. https://doi.org/10.1021/mp0700054.

(42) Cantat, T.; Scott, B. L.; Kiplinger, J. L. Convenient Access to the Anhydrous Thorium Tetrachloride Complexes $ThCl_4(DME)_2$, $ThCl_4(1,4\text{-Dioxane})_2$ and $ThCl_4(THF)_{3.5}$ Using Commercially Available and Inexpensive Starting Materials. *Chem. Commun.* **2010**, *46* (6), 919–921. https://doi.org/10.1039/b923558b.

(43) Lee, D. G.; Baek, J. W.; Lee, J. H.; Lee, H. J.; Seo, Y. H.; Lee, J.; Lee, C. G.; Lee, B. Y. Replacement of the Common Chromium Source $CrCl_3(Thf)_3$ with Well-Defined $[CrCl_2(\mu\text{-}Cl)(Thf)_2]_2$. *Molecules* **2021**, *26*, 1167–1178. https://doi.org/https://doi.org/10.3390/molecules26041167.

(44) Woodman, T. J.; Sarazin, Y.; Garratt, S.; Fink, G.; Bochmann, M. Chromium Allyl and Alkyl Catalysts for the Vinyl Polymerization of Norbornene and Ethylene-Norbornene Copolymerizations. *J. Mol. Catal. A Chem.* **2005**, *235* (1–2), 88–97. https://doi.org/10.1016/j.molcata.2005.03.017.

(45) Solomon, S. A.; Layfield, R. A. The Coordination Chemistry of Silyl-Substituted Allyl Ligands. *Dalton Trans.* **2010**, *39* (10), 2469–2483. https://doi.org/10.1039/b918619k.

(46) Chmely, S. C.; Hanusa, T. P. Complexes with Sterically Bulky Allyl Ligands: Insights into Structure and Bonding. *Eur. J. Inorg. Chem.* **2010**, No. 9, 1321–1337. https://doi.org/10.1002/ejic.200900813.

(47) Smith, J. D.; Hanusa, T. P.; Young, J. Steric Stabilization of Homoleptic Bis(π-Allyl) Complexes of Chromium(II) and Iron(II). *J. Am. Chem. Soc.* **2001**, *123* (26), 6455–6456. https://doi.org/10.1021/ja015626j.

(48) Smith, J. D.; Quisenberry, K. T.; Hanusa, T. P.; Brennessel, W. W. Bis[1,3-Bis(Trimethylsilyl)Allyl]-Cobalt(II), a Stable Electron-Deficient Allyl Complex. *Acta Crystallogr. Sect. C Cryst. Struct. Commun.* **2004**, *60* (10). https://doi.org/10.1107/S0108270104020293.

(49) Quisenberry, K. T.; Smith, J. D.; Voehler, M.; Stec, D. F.; Hanusa, T. P.; Brennessel, W. W. Trimethylsilylated Allyl Complexes of Nickel. The Stabilized Bis(π-Allyl)Nickel Complex $[\eta^3\text{-}1,3\text{-}(SiMe_3)_2C_3H_3]_2Ni$ and Its Mono(π-Allyl)NiX (X = Br, I) Derivatives. *J. Am. Chem. Soc.* **2005**, *127*

(12), 4376–4387. https://doi.org/10.1021/ja044308s.
(50) Eckert, N. A.; Bones, E. M.; Lachicotte, R. J.; Holland, P. L. Nickel Complexes of a Bulky B-Diketiminate Ligand. *Inorg. Chem.* **2003**, *42* (5), 1720–1725. https://doi.org/10.1021/ic025986n.
(51) Long, G. J.; Clarke, P. J. Crystal and Molecular Structures of Trans-Tetrakis (Pyridine)Dichloroiron (II), -Nickel (II), and -Cobalt (II) and Trans-Tetrakis (Pyridine)Dichloroiron (II) Monohydrate. *Inorg. Chem.* **1978**, *17* (6), 1394–1401. https://doi.org/10.1021/ic50184a002.
(52) Bard, A. J. *Standard Potentials in Aqueous Solution*, 1st ed.; Routledge: New York, 1985. https://doi.org/10.1201/9780203738764.
(53) Hitchcock, P. B.; Lee, T. H.; Leigh, G. J. The Synthesis and Properties of a New Linear NPN Proligand. *J. Chem. Soc. Dalt. Trans.* **2003**, *3* (11), 2276–2279. https://doi.org/10.1039/b300596h.
(54) Ward, L. G. L.; Pipal, J. R. Anhydrous Nickel(II) Halides and Their Tetrakis(Ethanol) and 1,2-Dimethoxyethane Complexes. In *Inorg. Synth.*; 1972; pp 154–164.
(55) Standley, E. A.; Smith, S. J.; Müller, P.; Jamison, T. F. A Broadly Applicable Strategy for Entry into Homogeneous Nickel(0) Catalysts from Air-Stable Nickel(II) Complexes. *Organometallics* **2014**, *33* (8), 2012–2018. https://doi.org/10.1021/om500156q.
(56) Aragoni, M. C.; Arca, M.; Demartin, F.; Devillanova, F. A.; Graiff, C.; Isaia, F.; Lippolis, V.; Tiripicchio, A.; Verani, G. Ring-Opening of Lawesson's Reagent: New Syntheses of Phosphono- and Amidophosphono-Dithioato Complexes - Structural and CP-MAS ^{31}P-NMR Characterization of [p-$CH_3OPh(X)PS_2$]M (X = MeO, IPrNH; M = Ni(II), Pd(II), and Pt(II). *Eur. J. Inorg. Chem.* **2000**, *2000* (10), 2239–2244.
(57) Feng, D.; Chung, W. C.; Wei, Z.; Gu, Z. Y.; Jiang, H. L.; Chen, Y. P.; Darensbourg, D. J.; Zhou, H. C. Construction of Ultrastable Porphyrin Zr Metal-Organic Frameworks through Linker Elimination. *J. Am. Chem. Soc.* **2013**, *135* (45), 17105–17110. https://doi.org/10.1021/ja408084j.
(58) Kwasny, M. T.; Zhu, L.; Hickner, M. A.; Tew, G. N. Thermodynamics of Counterion Release Is Critical for Anion Exchange Membrane Conductivity. *J. Am. Chem. Soc.* **2018**, *140* (25), 7961–7969. https://doi.org/10.1021/jacs.8b03979.
(59) Wöhlert, S.; Runčvski, T.; Dinnebier, R. E.; Ebbinghaus, S. G.; Näther, C. Synthesis, Structures, Polymorphism, and Magnetic Properties of Transition Metal Thiocyanato Coordination Compounds. *Cryst. Growth Des.* **2014**, *14* (4), 1902–1913. https://doi.org/10.1021/cg500037d.
(60) Zimmerman, J. R.; Smucker, B. W.; Dain, R. P.; Van Stipdonk, M. J.; Eichhorn, D. M. Tridentate N_2S Ligand from 2,2′-Dithiodibenzaldehyde and N,N-Dimethylethylenediamine: Synthesis, Structure, and Characterization of a Ni(II) Complex with Relevance to Ni Superoxide Dismutase. *Inorg. Chim. Acta* **2011**, *373* (1), 54–61. https://doi.org/10.1016/j.ica.2011.03.052.
(61) Joannou, M. V.; Sarjeant, A. A.; Wisniewski, S. R. Diboron-Promoted Reduction of Ni(II) Salts: Precatalyst Activation Studies Relevant to Ni-Catalyzed Borylation Reactions. *Organometallics* **2021**, No. Ii. https://doi.org/10.1021/acs.organomet.1c00325.
(62) Ni, Q. L.; Liao, Y. F.; Wang, X. J.; Bi, X. S.; Meng, X. G. N,N′-Bis[(Diphenylphosphinoyl)Methyl]-1,4-Phenylenediamine. *Acta Crystallogr. Sect. E Struct. Reports Online* **2006**, *62* (6), 2–7. https://doi.org/10.1107/S1600536806018861.
(63) Fukuda, T.; Ono, K.; Homma, S.; Kobayashi, N. A Phthalocyanine Producing Green, Ocher, and Red Colors Depending on the Central Metals. *Chem. Lett.* **2003**, *32* (8), 736–737. https://doi.org/10.1246/cl.2003.736.
(64) Kopylovich, M. N.; Pombeiro, A. J. L.; Fischer, A.; Kloo, L.; Kukushkin, V. Y. Facile Ni(II)/Ketoxime-Mediated Conversion of Organonitriles into Imidoylamidine Ligands. Synthesis of Imidoylamidines and Acetyl Amides. *Inorg. Chem.* **2003**, *42* (22), 7239–7248. https://doi.org/10.1021/ic0349813.
(65) Kopylovich, M. N.; Kukushkin, V. Y.; Haukka, M.; Luzyanin, K. V.; Pombeiro, A. J. L. An Efficient Synthesis of Phthalocyanines Based on an Unprecedented Double-Addition of Oximes to Phthalonitriles. *J. Am. Chem. Soc.* **2004**, *126* (46), 15040–15041. https://doi.org/10.1021/ja046759i.
(66) Alig, E.; Bernert, T.; Fink, L.; Külcü, N.; Yeilkaynak, T. Catena-Poly[[Dipyridine-Nickel(II)]-Trans-Di-μ-Chlorido] from Powder Data. *Acta Crystallogr. Sect. E Struct. Reports Online* **2010**, *66*

(2). https://doi.org/10.1107/S1600536810001820.
(67) Ton, T. M. U.; Tejo, C.; Tania, S.; Chang, J. W. W.; Chan, P. W. H. Iron(II)-Catalyzed Amidation of Aldehydes with Iminoiodinanes at Room Temperature and under Microwave-Assisted Conditions. *J. Org. Chem.* **2011**, *76* (12), 4894–4904. https://doi.org/10.1021/jo200284a.
(68) Ray, B.; Neyroud, T. G.; Kapon, M.; Eichen, Y.; Eisen, M. S. Synthesis, Characterization, and Catalytic Activities for the Polymerization of Olefins Promoted by Zirconium(III) and Titanium(III) Allyl Complexes. *Organometallics* **2001**, *20* (14), 3044–3055. https://doi.org/10.1021/om0009942.
(69) Kepp, K. P. A Quantitative Scale of Oxophilicity and Thiophilicity. *Inorg. Chem.* **2016**, *55* (18), 9461–9470. https://doi.org/10.1021/acs.inorgchem.6b01702.
(70) Krysiak, Y.; Fink, L.; Bernert, T.; Glinnemann, J.; Kapuscinski, M.; Zhao, H.; Alig, E.; Schmidt, M. U. Crystal Structures and Polymorphism of Nickel and Copper Coordination Polymers with Pyridine Ligands. *Z. Anorg. und Allg. Chem.* **2014**, *640* (15), 3190–3196. https://doi.org/10.1002/zaac.201400505.
(71) Mandal, S.; Bachman, R. E.; Whitmire, K. H.; Bharadwaj, P. K. Dichlorotetrakis(Pyridine)Nickel(II). *Acta Crystallogr. Sect. C* **1992**, *48* (10), 1836–1837. https://doi.org/10.1107/S0108270192001872.
(72) Wells, A. F. *Structural Inorganic Chemistry*; Oxford University Press: Oxford, 2012.
(73) Pauling, L. *The Nature of the Chemical Bond*, 3rd ed.; Cornell University Press: Ithaca, 1960.
(74) Hargittai, M. Molecular Structure of Metal Halides. *Chem. Rev.* **2000**, *100* (6), 2233–2301. https://doi.org/10.1021/cr970115u.
(75) Petriček, S.; Demšar, A. Syntheses and Crystal Structures of Manganese, Nickel and Zinc Chloride Complexes with Dimethoxyethane and Di(2-Methoxyethyl) Ether. *Polyhedron* **2010**, *29* (18), 3329–3334. https://doi.org/10.1016/j.poly.2010.09.014.
(76) Fowles, G. W. A.; Rice, D. A.; Walton, R. A. The Donor Properties of Simple Ethers-II[1]. Complexes of Manganese(II), Iron(II), Cobalt(II) and Nickel(II) Halides with Tetrahydrofuran and 1,2-Dimethoxyethane. *J. Inorg. Nucl. Chem.* **1969**, *31* (10), 3119–3131. https://doi.org/10.1016/0022-1902(69)80095-3.
(77) Heintz, R. A.; Smith, J. A.; Szalay, P. S.; Weisgerber, A.; Dunbar, K. R. HOMOLEPTIC TRANSITION METAL ACETONITRILE CATIONS WITH TETRAFLUOROBORATE OR TRIFLUOROMETHANESULFONATE ANIONS. In *Inorg. Synth., Volume 33*; 2002; pp 75–80.
(78) Gren, C. K.; Hanusa, T. P.; Rheingold, A. L. Solvent-Resistant Structures of Base-Free Lithium and Potassium Allyl Complexes M[(SiMe3)NC3H5-n] (M = Li, n = 3; M = K, n = 2). *Main Gr. Chem.* **2009**, *8* (4), 225–235.
(79) Andersen, J.; Mack, J. Insights into Mechanochemical Reactions at Targetable and Stable Sub-ambient Temperatures. *Angew. Chemie* **2018**, *130*, 13246–13249.

Chapter 3: Synthesis of Simple Nickel Complexes of the 1,3-bis(*t*-butyl)allyl Ligand

This chapter is adapted from "Distinction with a difference: t-Butyl and trimethylsilyl substituents in nickel allyl complexes" submitted to ACS Organic and Inorganic Gold and has been reproduced with permission from the publisher and my co-authors, Tim Hanusa and Isaiah Speight

Abstract

Metal complexes with *t*Bu-substituted allyl ligands are relatively rare, especially when compared to their conceptually similar trimethylsilyl-substituted analogues. The scarcity partially stems from there being few general synthetic entry points for the *t*Bu versions. This situation was studied through a modified synthesis for the allyl ligand itself and by the formation of several mono(allyl)nickel derivatives. A mixture of $Ni(COD)_2$ and 5-bromo-2,2,6,6-tetramethylhept-3-ene ($A^{2t}Br$) in the presence of a neutral donor ligand such as MeCN was found to produce the dark red dimeric $[\{A^{2t}NiBr\}_2]$. The latter will form adducts with neutral donors such as PPh_3 and IMes (IMes = 1,3-dimesitylimidazol-2-ylidene) but the resulting $[A^{2t}Ni(PPh_3)Br]$ complex is not as stable as its trimethylsilyl analogue. The $[A^{2t}Ni(IMes)Br]$ complex crystallizes from hexanes as a monomer, with an η^3-coordinated $[A^{2t}]$ ligand, and in contrast to the starting arrangement in $[\{A^{2t}NiBr\}_2]$, the *t*-Bu groups on the A^{2t} ligand are in a *syn*, *anti*-relationship. This structure is paralleled in the trimethylsilyl analog [A´Ni(IMes)Br]. DFT calculations were used to compare the structure and behavior of the *t*Bu- and related trimethylsilyl-substituted complexes.

3.1 Introduction

Transition metal allyl complexes are staple participants in many organic transformations, including cross coupling reactions and catalytic polymerizations.[1–8] As they provide useful steric bulk and kinetic stability, silyl-substituted allyl ligands,[9,10] and in particular those with trimethylsilyl (TMS) groups, are often valuable in these contexts.[11–15] Nevertheless, silyl groups are typically labile in acidic media or with fluoride-containing precursors, which can restrict their range of applications.[16–18] There may also be direct electronic effects of trimethylsilyl substituents that contribute to their unsuitability in specific cases. For example, TMS groups commonly function as electron donors,[19,20] but they can also exhibit the β-silicon effect, in which Si-C hyperconjugation serves to weaken metal-ligand bonds in delocalized systems such as allyls and indenyls.[21–24]

Although it is not a drop-in replacement for TMS, the *t*-butyl group is of course conceptually related,[25] and substituted allyl ligands such as $[1\text{-}(t\text{-Bu})C_3H_4]^-$ (= A^{1t}) and $[1,3\text{-}(t\text{-Bu})_2C_3H_3]^-$ (= A^{2t}) have been incorporated into metal complexes.[26–28] It should be noted that various cobalt and nickel complexes containing the open pentadienyl $2,4\text{-}(t\text{-Bu})_2C_5H_5$ ligand are known that display η^3-bonding to the metals, giving the appearance of 2-(*t*-Bu)-substituted allyl ligands, but are not considered here.[29] Compared to their silyl analogues, however, *t*-Bu-substituted allyl metal complexes remain a relatively rare and understudied class of compounds. Apart from difficulties synthesizing such complexes (see below), some display instability that has been ascribed to the steric bulk of the *t*-Bu substituents. For example, both $[TpMo(CO)_2A^{1t}]$ and $[TpMo(CO)_2A^{2t}]$ (Tp = trispyrazolylborate) decompose rapidly as solids or on standing in solution, whereas the analogous complexes with methyl or phenyl substituents on the allyl ligands are stable in solution and only slowly decompose on exposure to air.[27] Nevertheless, the successful application of, for example, the related 1-(*t*-Bu)-indenyl ligand to palladium catalysis suggests that an improved understanding of *t*-Bu-substituted allyls and their metal complexes could have useful consequences.[7]

The synthesis of *t*-Bu-substituted allyl complexes is typically different from the routes used for TMS analogues. For the latter, the alkali metal salts of the $[1\text{-}(TMS)C_3H_4]^-$ and $[1,3\text{-}(TMS)_2C_3H_3]^-$ (= A′) anions are readily prepared (Figure 3.1), and metathesis with main-group and transition metal halides is a broadly effective method.[9,10] Although NMR characterization of $[(tmeda)Li][A^{2t}]$ has been reported,[26] to our knowledge no salt metathesis reactions have been described using *t*-Bu-substituted allyl salts. However, a variety of other methods have been used in the synthesis of *t*-Bu-substituted allyl complexes, usually from a neutral substituted precursor or by assembling the ligand *in situ*. For example, $[\{(1\text{-}t\text{-Bu})(2\text{-Me})C_3H_3]Pd(\mu\text{-Cl})\}_2]$ was formed from $[PdCl_4]^{2-}$ and 2,4,4-trimethyl-2-pentene,[30] and the osmium-coordinated allyl ligand in the trinuclear cluster $[Os_3(CO)_8(\mu\text{-CO})(\mu\text{-}\gamma\text{-}C_5H_3O_2)A^{1t}]$ was generated during the photochemical reaction of $[Os_3(CO)_{10}(\mu\text{-H})(\mu\text{-}\gamma\text{-}C_5H_3O_2)]$ with *t*-BuC≡CMe.[28] The trispyrazolylborate

derivative [TpMo(CO)$_2$A^{1t}] noted above was synthesized from the reaction of 3-acetoxy-4,4-dimethyl-1-pentene, [(DMF)$_3$Mo(CO)$_3$], and [K(Tp)].[27]

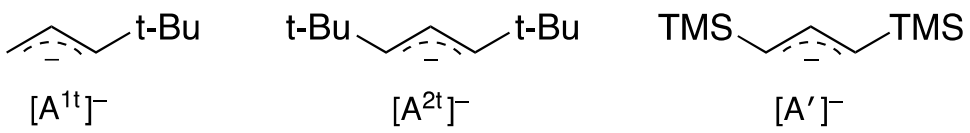

Figure 3.1: Abbreviations for substituted allyl ligands mentioned in the text.

Among the first allyl complexes synthesized were those containing nickel,[31] and nickel derivatives are still critical in the development of high-performance olefin polymerization catalysts.[32–35] To examine the effect of *t*-butyl substitution on the allyl ligand, several nickel allyl complexes containing the A^{2t} ligand were prepared from the bromo alkene, which allow direct comparisons with TMS-substituted derivatives.

3.2 Results

3.2.1 Formation of 5-hydroxy-2,2,6,6-tetramethylheptan-3-yl pivalate

The synthesis of organic molecules relating to the di-*t*Bu-propene scaffold has been previously described.[36,37] However, in the course of this investigation it was found that, when pivaldehyde is used in excess, 5-hydroxy-2,2,6,6-tetramethylheptan-3-yl pivalate (**19**) is frequently formed as a byproduct (Figure 3.2). To our knowledge, this compound has not been previously reported. It likely forms via deprotonation of the initial condensation product to form an enolate, followed by O-centered attack on another molecule of pivaldehyde. The observance of this product along with the complete absence of the product of C-centered attack likely implicates steric influence in directing reactivity. Only one set of peaks is observed in the proton NMR spectrum; taken in conjunction with the structure obtained from some isolated crystals of the compound (see Figure A3.2), this suggests that only the *anti*-enantiomer is formed. Preliminary evidence suggests that the use of sodium or potassium bis(trimethylsilyl)amide in the place of the lithium salt increases the proportion of **19** formed, but this has not been systematically studied.

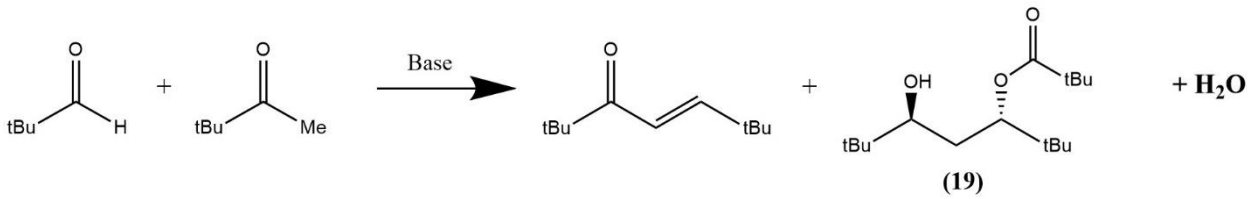

Figure 3.2: Aldol condensation of pivaldehyde and pinacolone to yield 2,2,6,6-tetramethyl-4-hepten-3-one. 5-hydroxy-2,2,6,6-tetramethylheptan-3-yl pivalate (19) is frequently observed as a byproduct of this reaction.

3.2.2 Synthesis of *t*-butyl-substituted (allyl)nickel bromides

(Allyl)nickel bromide compounds were prepared in order to allow comparisons between complexes of the parent allyl $[C_3H_5]^-$, the TMS-substituted $[A']^-$, and the *t*-Bu derivative $[A^{2t}]^-$ ligands. In general, (allyl)nickel bromides are red to red-purple, air- and moisture-sensitive compounds that can be prepared in several ways,[38,39] the most relevant of which involves oxidative addition between an allyl bromide and a source of Ni(0), such as bis(cyclooctadiene)nickel (e.g., Figure 3.3a).[38] The bromide complex with the parent allyl is a dimer in aromatic hydrocarbons (i.e., $[\{(C_3H_5)NiBr\}_2]$), but Schlenk equilibrium is established if the compound is dissolved in a coordinating donor solvent such as DMF or HMPA (Figure 3.3b).[40]

(a) $2\ C_3H_5Br + 2\ Ni(COD)_2 \longrightarrow [\{(C_3H_5)NiBr\}_2] + 4\ COD$

(b) $2\ [(C_3H_5)NiBr] \rightleftarrows [(C_3H_5)_2Ni] + NiBr_2$

(c) $2\ C_3(TMS)_2H_3Br + 2\ Ni(COD)_2 \longrightarrow [\{A'NiBr\}_2] + 4\ COD$

Figure 3.3: Reactions of (allyl)nickel bromides.

The oxidative addition method of (allyl)nickel halide preparation is also successful with TMS-substituted allyls; for example, the bis(trimethylsilyl)allyl bromide $[1,3\text{-}(TMS)_2C_3H_3Br]$ reacts with $[Ni(cod)_2]$ in toluene to generate the substituted (allyl)nickel bromide (Figure 3.3c).[13] In contrast to $[\{(C_3H_5)NiBr\}_2]$, $[\{A'NiBr\}_2]$ is stable to rearrangement in solution, i.e., there is no NMR evidence for the formation of $[NiA'_2]$ via Schlenk rearrangement in THF.

Given this precedent, it was somewhat surprising that the mixture of [BrA^{2t}] and [Ni(cod)$_2$] in THF did not react to form a nickel complex (Table 3.2, entry 1). The allyl halide instead initiated the decomposition of [Ni(cod)$_2$] to nickel metal, with a black solid visible within 5 min of addition. Workup of the remaining solution revealed the presence only of free COD and unreacted allyl halide. Modifying the reaction conditions, e.g., with UV-irradiation or by conducting the reaction at reflux (66 °C), did not affect the outcome of the reaction. As a test, the addition of two extra equivalents of COD to the reaction mixture did not substantially retard the decomposition, suggesting that the displacement of COD by [A^{2t}Br] was not a rate-limiting step. If the allyl chloride [ClA^{2t}] was used in place of the bromide, the rate of decomposition was slower, but nickel metal still deposited within 30 min.

Table 3.2: Comparative reaction conditions for the synthesis of **20** ([{A^{2t}NiBr}$_2$])

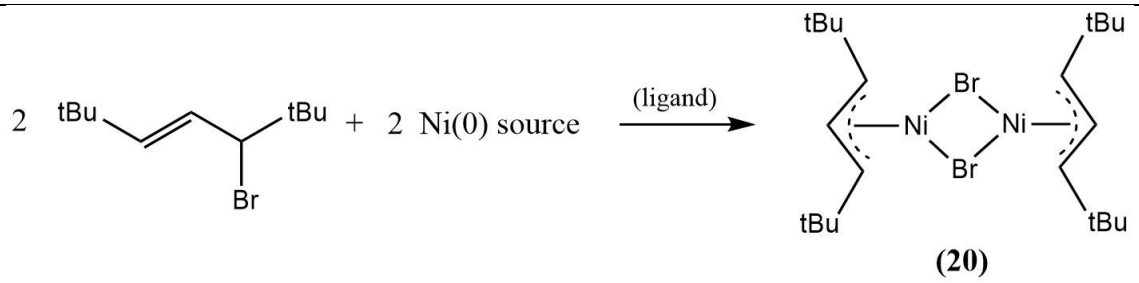

(20)

Entry	Nickel source	Base	Conditions	Yield %
1[a]	[Ni(cod)$_2$]	none	THF (RT or reflux), 5 min	0
2	[Ni(CO)$_4$]	none	THF	0
3	[Ni(CO)$_4$]	MeCN, 5 eq.	THF	0
4	[Ni(CO)$_2$(PPh$_3$)$_2$]	none	toluene (70 °C)	trace
5	[Ni(cod)$_2$]	PPh$_3$, 1 eq.	THF	40–60
6	[Ni(cod)$_2$]	IMes, 1 eq.	THF	40–60
7	[Ni(cod)$_2$]	MeCN, 1 eq.	THF	40–60
8	[Ni(cod)$_2$]	MeCN, 10 eq.	THF	70
9	[Ni(cod)$_2$]	MeCN	MeCN (neat)	37

[a])No product was observed under UV radiation.

Modifying the coordination environment of the nickel was eventually found to be critical to generating an allyl complex. Although reactions using [Ni(CO)$_4$] and [BrA^{2t}] were not successful (entries 2 and 3), a few crystals of the expected bromide-bridged nickel complex, [{A^{2t}NiBr}$_2$] (**20**), were obtained

when [Ni(cod)$_2$] was used as the Ni(0) source in toluene solution (entry 1). Only trace quantities could be obtained by this route, however, with most of the recovered material being unreacted [A^{2t}Br].

A series of optimization experiments was conducted that ultimately led to useful quantities of **20** (Table 3.2). A substantial improvement came through the discovery that the original mixture of [Ni(cod)$_2$] and [BrA^{2t}] in THF yielded **20** when one eq. of an additional neutral donor ligand (L = PPh$_3$, IMes, and MeCN) was added to the reaction (entries 5–7; Figure 3.4), which increased yields to 40–60%. Although encouraging, the still-moderate yields of **20** and the absence of the ancillary ligands in the product (which would be expected to form adducts; see below) suggested that some nickel was being prematurely captured, thereby being unavailable for oxidative addition. In all cases, hexane-insoluble material was present in the reaction mixtures, which may have been composed of ligand adducts of partially oxidized nickel. Evidence for this came from colorless crystals isolated as a by-product when PPh$_3$ was used as the auxiliary base. Their unit cell matched that for [Ni(PPh$_3$)$_3$Br],[41] confirming the presence of incompletely oxidized nickel. An analogous Ni(I) species is known with IMes (i.e., [Ni(IMes)$_2$Br]),[42] which could serve as a nickel trap. Incomplete oxidation is further evidenced by the consistent presence of unreacted [A^{2t}Br] and the coupled hexadiene {A^{2t}$_2$} in the crude product mixture. Use of a neutral donor ligand to accelerate allylic oxidative addition to nickel has been previously reported.[43]

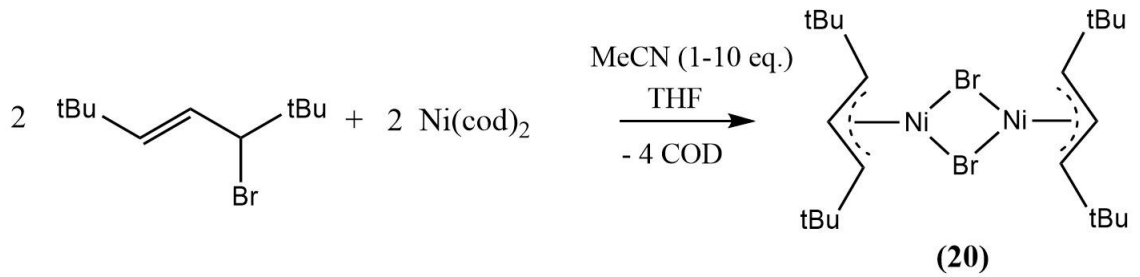

Figure 3.4: Formation of the (allyl)nickel bromide [{A^{2t}NiBr}$_2$]. Other neutral donors that can be used in place of MeCN include PPh$_3$ and IMes.

Not all neutral donor ligands are effective additives, however. The addition of pyridine to a mixture of [Ni(cod)$_2$] and [BrA^{2t}] in THF, for example, did not cause the swift color change associated with oxidative addition. Pyridine also seemed to suppress the decomposition of [Ni(cod)$_2$], as no metallic nickel was observed after 10 min of stirring. It has been observed that the inclusion of small amounts of butadiene in the synthesis of [Ni(cod)$_2$] completely prevents the formation of nickel metal, presumably due to facile

ligation of any unstable Ni(0) species that form;[44] pyridine may be serving the same function here. Subsequent addition of acetonitrile initiated the expected oxidative addition reaction, however.

Acetonitrile was eventually found to be the superior additive, as its lesser basicity allowed for an excess of ligand to be used without irreversible incorporation into the product. In fact, when 10 eq. of MeCN were used in the reaction, [{A^{2t}NiBr}$_2$] could be recovered in an average isolated yield of 70% (Table 3.2, entry 8). The use of MeCN as the sole reaction solvent led to a yield only half that from a MeCN/THF mixture (entry 9), however, indicating that a mixed-solvent system is critical to an optimal reaction outcome.

Isolated **20** is a chalky red solid that appears stable for months under nitrogen in the solid state or in hydrocarbon solution. It is slightly soluble in hexanes, soluble in aromatic hydrocarbons, and highly soluble in polar organic solvents. As with [{A´NiBr}$_2$], an NMR spectrum taken in a Lewis basic solvent (DMSO-d_6) shows no evidence for the operation of Schlenk equilibrium.

Even though both PPh_3 and IMes were suboptimal additives, their use did lead us to another example of distinctive reactivity of the A^{2t}Br/Ni(0) system. It is commonly found that oxidative addition of an allyl halide to nickel in the presence of one equivalent of phosphine or N-heterocyclic carbene (NHC) yields adduct complexes [(allyl)Ni(L)X],[45–50] but even when a full equivalent of either PPh_3 and IMes was added to the mixture of $Ni(COD)_2$ and BrA^{2t}, unligated **20** was the dominant product. In the case of IMes, a corresponding adduct was completely absent, while in the case of PPh_3, an adduct was inconsistently present as a minor product (10–25%) when 0.5–1.0 eq. was used. The extent to which this new complex resists additional ligand binding will be discussed in more detail below. Interestingly, the inclusion of a donor ligand did not lead to successful reaction when either [$Ni(CO)_2(PPh_3)_2$] or [$Ni(CO)_4$] was used in place of [$Ni(cod)_2$] as a nickel(0) source. These results suggest that the clean oxidative addition of [A^{2t}Br] to nickel requires specifically optimized conditions and reagents.

The allyl complex crystallizes from hexanes as a bromide-bridged dimer, joining a family of bridged π-allyl nickel species.[13,51–56] The molecule lies on a crystallographic inversion center, thus only one half of the molecule is unique (Figure 3.5).

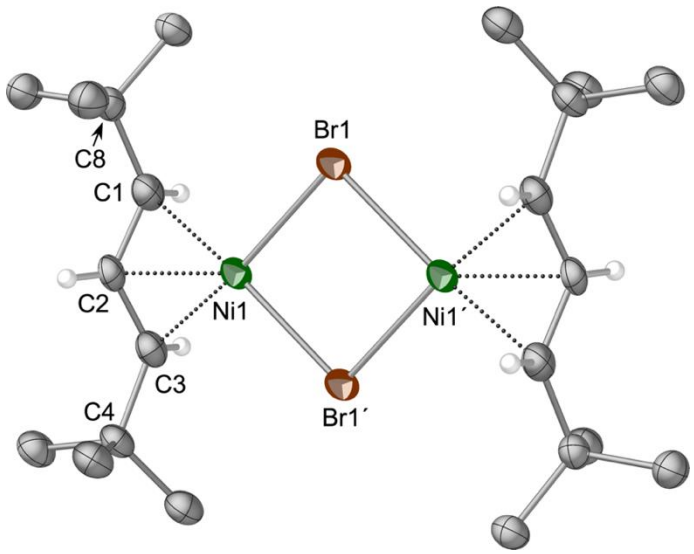

Figure 3.5: Thermal ellipsoid plot (50% level) of the structure of **20**; for clarity, hydrogen atoms have been removed from the *t*-Bu groups, and the rest have been given arbitrary radii. Selected bond distances (Å) and angles (°): Ni1–Br(1), 2.3690(14); Ni1–Br(1)´, 2.3636(15); Ni(1)–C(1), 2.041(8); Ni(1)–C(2), 1.975(7); Ni(1)–C(3), 2.053(8); C(1)–C(2), 1.396(11); C(2)–C(3), 1.407(11); C(3)–C(4), 1.518(10); C(1)–C(8), 1.527(11); C(1)–C(2)–C(3), 118.7(7); C(3)–C(2)–C(1)–C(8), 179.85; C(1)–C(2)–C(3)–C(4), -179.90.

The Ni–C bond lengths range from 1.975(7) to 2.053(8) Å, which are within 0.01 Å of those in [{A´NiBr}$_2$].[13] Although not required to be so by symmetry, the Ni(1)–Br(1) and Ni(1)–Br(1)´ bond lengths are identical within 2s (2.366(2) Å, ave.), and also track with the Ni–Br bonds in the TMS-substituted analogue (2.362, 2.365 Å). The Ni(1)···Ni(1)´ separation is 3.39(1) Å, too long to represent any significant interaction (cf. the 2.49 Å distance in nickel metal.[57] The allyl C-C bonds are nearly identical, indicative of nearly ideal η^3-binding. The angle between the C_3 plane and $(NiBr)_2$ plane is 116.5°. The carbon atoms C(4) and C(8) lie almost exactly in the C_3 plane (0.0005 Å and 0.004 Å displacements, respectively). This configuration has been observed before in other bridged allyl dimers of nickel, such as {(1,3-$Me_2C_3H_3$)Ni(μ-Me)}$_2$,[58] {[1-Me-3-($OSiMe_3$)C_3H_3]NiCl}$_2$,[53] and [{A´NiBr}$_2$].[13]

In the course of this investigation, the synthesis of [{A´NiBr}$_2$] was reexamined. One reported synthetic route is via the reaction of [NiA´$_2$] with elemental bromine.[13] However, the reported procedure was found to be inconsistent in both outcome and yield. Minor alterations were made to the procedure, allowing for high-quality [{A´NiBr}$_2$] to be consistently isolated, albeit in slightly less than previously

reported yields. Additionally, further analysis of the NMR spectra of this molecule led to substantial reinterpretation. The reaction of [NiA′$_2$] with elemental bromine was reported to yield two isomers of [{A′NiBr}$_2$], each with a *syn,anti* configuration. ^{1}H-^{1}H COSY NMR demonstrated that these signals were composited from peaks belonging to the known organic byproducts, [A′Br] and the meso form of {A′$_2$}. Removal of these impurities by MeCN/hexane extraction showed that the *syn,syn* conformer of [{A′NiBr}$_2$] was the predominant product. Therefore, the outcome of the reaction does not appear to depend on the synthetic method used, in contrast to the previous report. However, ^{1}H NMR analysis of the more pure compound led to the identification of two minor species consistent with *syn,anti* configurations of [{A′NiBr}$_2$].

As with the ^{1}H NMR spectrum of [{A′NiBr}$_2$],[13] the ^{1}H NMR spectrum of **20** indicates that the *t*-Bu groups are equivalent in the primary species, and hence in a *syn*,*syn* arrangement, which is also that found in the solid state (see below). Unlike its trimethylsilylated analogue, minor amounts of its *syn*,*anti*-isomers do not appear to be present. Although two stereoisomers (with eclipsed or staggered allyl ligands) of the bis(*syn syn*) complex are conceivable (Figure 3.6), only one set of signals is observed, indicating that either exclusively one form is present or that they interchange rapidly in solution. To probe this, computational investigation of the possible stereoisomers of [{A^{2t}NiBr}]$_2$ was undertaken. In accordance with the observed NMR features, complexes with *syn*,*anti*-configurations were consistently found to be higher energy than the corresponding *syn*,*syn* complex (see Appendix 3, Table A3.2). In addition, the eclipsed conformation was found to be consistently more stable than the staggered conformation. This finding was unexpected, as the solid-state structure of the molecule (see below) exclusively contains staggered allyls. The free energy difference between the most stable eclipsed and staggered isomers was found to be < 10 kJ mol^{-1}, however, which could be plausibly be the result of differences in crystal packing.[59]

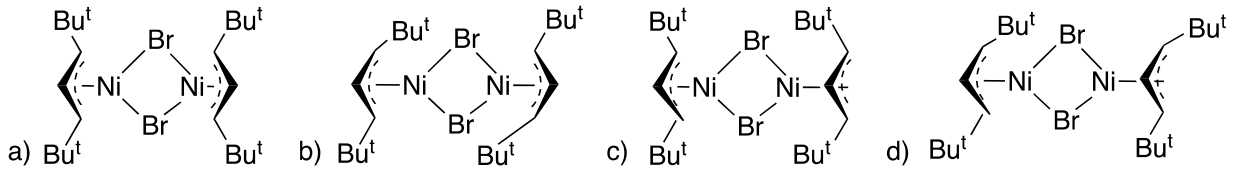

Figure 3.6: Possible stereoisomers of **20**: (a) staggered, with *syn*,*syn t*-Bu groups; (b) staggered, with *syn*,*anti t*-Bu groups; (c) eclipsed, with *syn*,*syn t*-Bu groups; (d) eclipsed, with *syn*,*anti t*-Bu groups.

3.2.3 Ligand adducts of [A^{2t}NiBr]

As noted above, the reaction of bridged allyl nickel halide compounds with monodentate neutral donor ligands is well documented,[46,47,49,50] generating monomeric adduct complexes. Accordingly, reaction

of **20** with 2 eq. of ligand (L = PPh_3, IMes; 1 eq. per metal center) generates new complexes consistent with such adducts, as evidenced with ^1H NMR spectra (Figure 3.7).

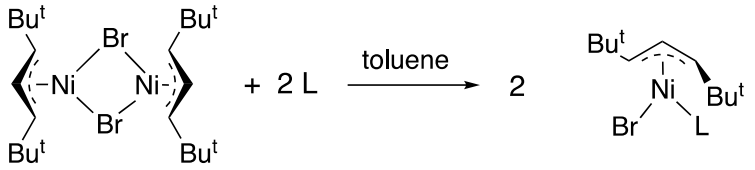

Figure 3.7: Formation of ligand adducts of [A^{2t}NiBr]; L = PPh_3, IMes.

In the case of triphenylphosphine, the reaction does not proceed to completion, forming an approximately 2:1 mixture of a monomeric adduct to unreacted dimeric complex. Although the ^1H NMR signal for the center allyl proton of the phosphine adduct is sharp, the terminal proton signals are substantially broadened; the peaks of both free and bound triphenylphosphine are also broadened. Additionally, only one peak is present in the ^{31}P NMR spectrum in C_6D_6 (δ 23.7), well downfield of free triphenylphosphine (δ -4.7),[60] suggesting that phosphine binding is reversible, and that exchange is slow on the ^1H NMR timescale but fast on the ^{31}P timescale. Variable temperature (VT) NMR experiments showed that the ratio of adducted to unadducted complex consistently increased as temperature decreased (see Appendix 3 for details). This process reversed upon warming back to room temperature, confirming a dynamic equilibrium between the two species. The chemical shifts and coupling constants of the allyl protons suggest a *syn*,*anti*-orientation. The mixture solidifies as a hard paste and all attempts to crystallize the phosphine adduct have been unsuccessful. The adduct degrades over time, slowly in solution and more quickly in the solid state; the rate of solid-state degradation was found to vary over a period of weeks to months. The degradation process was found to yield the coupled hexadiene $\{A^{2t}\}_2$ while the [$\{A^{2t}NiBr\}_2$] appears unaffected. This observation, along with the lack of visible metallic nickel, suggests that triphenylphosphine remains bound to nickel after it is reduced, and that there may be a complex mechanism for its decomposition.

The NMR ratio of [$A^{2t}Ni(PPh_3)Br$] to [$\{A^{2t}NiBr\}_2$] at various temperatures (298–253 K) was used to calculate the free energy change associated with adduct formation ([$\{A^{2t}NiBr\}_2$] + 2 PPh_3 → 2[$A^{2t}Ni(PPh_3)Br$]; see Appendix 3, Section A3.5.2). At 298 K, $\Delta G°$ is only -1.7 kJ mol^{-1}, which is consistent with the easily reversible binding of PPh_3 to the nickel allyl complex. This number should be taken as an approximation, as at low temperatures, a third species begins to be visible, likely an intermediate for PPh_3 exchange (see Figure A3.10). A probable candidate for this species is [$A^{2t}Ni(PPh_3)_2Br$], whose analogues are well documented,[61–63] but a monomeric unit of [A^{2t}NiBr] is also conceivable As this species has not

been identified, an exact equilibrium constant cannot be calculated. However, only small amounts of this compound are present; at the minimum temperature observed, considering the new species to be either of the above complexes resulted in a maximum of 25% difference in the calculated $\Delta G°$ value. Therefore, especially at higher temperatures, our calculated values are believed to be reasonably accurate.

For comparison, PPh_3 was also allowed to react with the trimethylsilyl analogue [{A´NiBr}$_2$]. This reaction also produced a dark red paste that, like the result with [{A^{2t}NiBr}$_2$], resisted crystallization, but ^{1}H NMR analysis revealed several differences from the reaction involving **20**. Most notable is the complete absence of unreacted bimetallic complex; instead, only one species consistent with [A´Ni(PPh_3)Br] is present in the spectrum. When a slight excess of free triphenylphosphine is present, it is observed in the ^{31}P spectrum as a distinct peak at its expected chemical shift.[64] Together, this suggests that the adduct formation reaction goes to completion and that any exchange processes are slow on the NMR timescale. A final difference from the *t*-Bu analogue is that the A´ adduct appears to be stable in the solid state under N_2, showing no apparent decomposition over a month. Analysis of the ^{1}H-^{1}H, ^{1}H-^{31}P, and ^{13}C-^{31}P coupling constants allowed unambiguous determination of the geometry of the molecule: the allyl is present in a *syn,anti*-configuration with the phosphine bound *trans* to the *syn*-$SiMe_3$ group, similar to that in [A^{2t}Ni(PPh_3)Br].

In the case of IMes, the new compound, [A^{2t}Ni(IMes)Br] (**21),** displays sharp A^{2t} allyl C-H resonances at room temperature, and there is no evidence for free IMes. The molecule is sparingly soluble in hexane, but highly soluble in aromatic solvents and polar organic solvents. The mixture shows very little degradation over months when stored in the solid state but appears to degrade in weeks when dissolved in hexanes. The compound has a *syn,anti*-configuration in solution, as evidenced by inequivalent *t*-butyl groups and a large difference between the two allylic coupling constants (J = 8.3, 14.6 Hz). The two imidazole methylene groups are equivalent, which implies that rotation around the carbene-Ni bond is fast on the NMR timescale. On the other hand, the *ortho* methyl groups and *meta* protons of the mesityl rings are both split into two separate signals, indicating that rotation about the N-Mes bond is slow. These NMR features are consistent with the reported NMR dynamics of an analogous complex featuring an unsubstituted allyl ligand, and suggest that IMes exchange does not occur.[65] A small amount of a second species is also consistently present whose NMR features are consistent with a *syn,syn* isomer of the complex, A computational investigation suggests that such a species is not entirely implausible ($\Delta G°$ = +21.5 kJ mol^{-1} relative to the *syn,anti*-isomer; see Appendix 3, Section 3.5.1). A potential reason for the observation of this higher energy isomer is kinetic trapping. It is possible that fast reaction with IMes could lead to retention of the *syn,syn* configuration of the [{A^{2t}NiBr}$_2$] starting material; given the apparently non-fluxional binding of IMes in this compound, this initial configuration may become trapped, lacking any accessible *syn*/*anti* exchange processes.

Complex **21** crystallizes from hexanes as a monomer, with an η^3-coordinated [A^{2t}] ligand and terminally bonded bromide and IMes ligands. The *t*-Bu groups on the A^{2t} ligand are in a *syn,anti*-relationship (Figure 3.8). The Ni–C bond lengths range from 1.9671(15) to 2.1132(15) Å, which are comparable to those in other [(allyl)NiX(NHC)] complexes.[50,65–73] In [(C_3H_5)NiBr(Me_4Im)] (Me_4Im = 1,3,4,5-tetramethylimidazol-2-ylidene), for example, the corresponding distances are 1.984(4) to 2.056(3) Å.[67] Similarly, the Ni–Br and Ni–NHC distances of 2.3461(3) and 1.9409(15) Å in **21** can be compared to the analogous lengths of 2.3856(7) and 1.907(2) Å, respectively, in [(C_3H_5)NiBr(Me_4Im)]. As is typical for similar configurations with $SiMe_3$ substituents,[13] the central carbon atom in the *syn t*-Bu group (C4) is close to the C_3 plane (0.09 Å), whereas the center of the *anti t*-Bu group (C8) is considerably displaced from the allyl plane (0.89 Å).

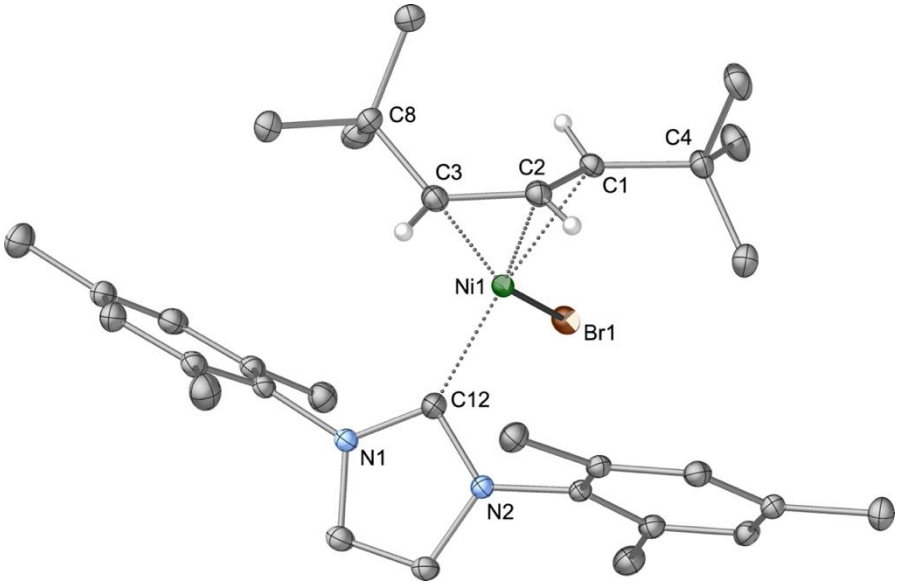

Figure 3.8: Thermal ellipsoid plot (50% level) of the structure of **21**. For clarity, all hydrogen atoms except those on the C_3 fragment of the allyl ligands are removed, and the others are given arbitrary radii. Selected bond distances (Å) and angles (°): Ni1–Br(1), 2.3461(3); Ni(1)–C(1), 2.1132(15); Ni(1)–C(2), 1.9671(15); Ni(1)–C(3), 2.0463(15); Ni(1)–C(12), 1.9409(15); C(1)–C(2), 1.399(2); C(2)–C(3), 1.419(2); C(1)–C(4), 1.524(2); C(3)–C(8), 1.545(2); C(12)–Ni(1)–Br(1), 95.37(4); C(1)–C(2)–C(3), 121.46(14); C(4)–C(1)–C(2)–C(3), 177.18(14); C(1)–C(2)–C(3)–C(8), -44.4(2).

As a point of comparison, the trimethylsilyl analogue of **21**, i.e., [A´Ni(IMes)Br] (**22**), was synthesized and characterized. The same synthetic protocol was used (i.e., [A´NiBr] + IMes in toluene) and it generated a brick-red solid with identical solubility and similar solid-state stability. Its NMR spectrum is also consistent with a *syn*,*anti*-configuration of the TMS substituents on the allyl ligand, and it displays the same fast/slow rotations. No minor products are formed in this reaction. This is not unreasonable, as a substantial amount of [{A´NiBr}$_2$] is expected to be present in its *syn,anti*-conformation at equilibrium, making it much less likely for a *syn,syn* adduct to form and become trapped.

The complex crystallizes from hexanes as a monomer, with an η^3-coordinated A´ ligand and terminally bonded bromide and IMes ligands. The TMS groups on the A´ ligand are in a *syn*,*anti*-relationship. As the compound is isostructural with the A^{2t} analogue **21**, it will be discussed only briefly (Figure 3.9). All the bond lengths to Ni are within ~0.02 Å of those found in **22**, but are generally shorter. Even the displacements of the TMS or *t*-Bu groups on the allyl ligands from the respective C_3 planes are almost the same, as reflected in the closely similar torsion angles, differing at most by 2°. The steric bulk

of the TMS group relative to *t*-Bu has not introduced any significant distortions into their respective complexes, consistent with their being effectively isosteric substituents (see below).

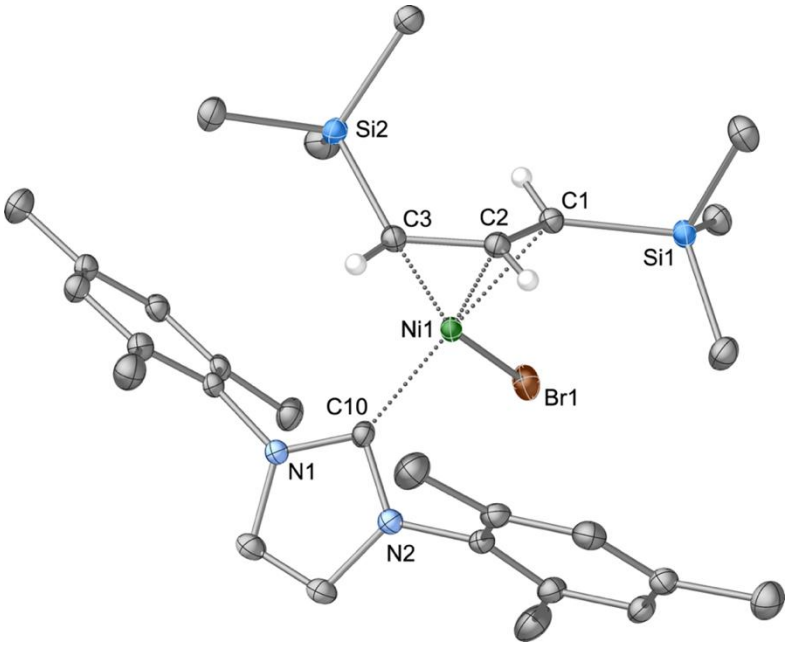

Figure 3.9: Thermal ellipsoid plot (50% level) of the structure of **22**. For clarity, all hydrogen atoms except those on the C_3 fragment of the allyl ligands are removed, and the others are given arbitrary radii. Selected bond distances (Å) and angles (°): Ni1–Br(1), 2.3333(3); Ni(1)–C(1), 2.095(2); Ni(1)–C(2), 1.976(2); Ni(1)–C(3), 2.025(2); Ni(1)–C(10), 1.923(2); C(1)–C(2), 1.404(2); C(2)–C(3), 1.425(2); C(1)–Si(1), 1.868(2); C(3)–Si(2), 1.888(2); C(12)–Ni(1)–Br(1), 93.99(5); C(1)–C(2)–C(3), 119.00(15); C(3)–C2)–C(1)–Si(1), -175.17(12); C(1)–C(2)–C(3)–Si(2), -44.3(2).

Previous study of the allyl coupling product $\{A'\}_2$ generated from solution reactions found that it was generated in two diastereomeric forms of C_i (*meso*) and C_2 (*rac*) symmetry.[13] A single crystal X-ray structure of the compound was severely disordered, rendering the exact conformation of the molecule uncertain. A higher quality structure of the *meso* form was obtained recently that displays approximate inversion symmetry.[74]

The related compound $\{A^{2t}\}_2$ (**23**) was produced during the present experiments, including some in highly crystalline form from hexanes. Compound **23** crystallizes in the triclinic space group $P\bar{1}$, and comprises a single diastereomer, the *meso* form (Figure 3.10). The molecule lies on a crystallographic inversion center, thus only one-half of the molecule is unique. The structure is largely as would be expected;

the central C1–C1′ bond, at 1.571(3) Å, exactly matches the comparable distance found in [(^{t}BuMe$_2$Si)CH(CH=CHSiMe$_2{}^t$Bu)]$_2$ (1.571(4) Å), for example, which was ascribed to steric crowding between the bulky alkylsilyl groups.[75] Even with their shorter C–C bonds compared to the C–Si bonds in the *t*-butyldimethylsilyl species, the *t*-Bu groups in **23** evidently exert similar steric pressure. DFT calculations at the B3PW91-D3BJ/def2-TZVP level indicate that the observed *meso* form of **23** (C_i) is 22 kJ kcal mol^{-1} lower in energy than a hypothetical *rac* (C_2) configuration.

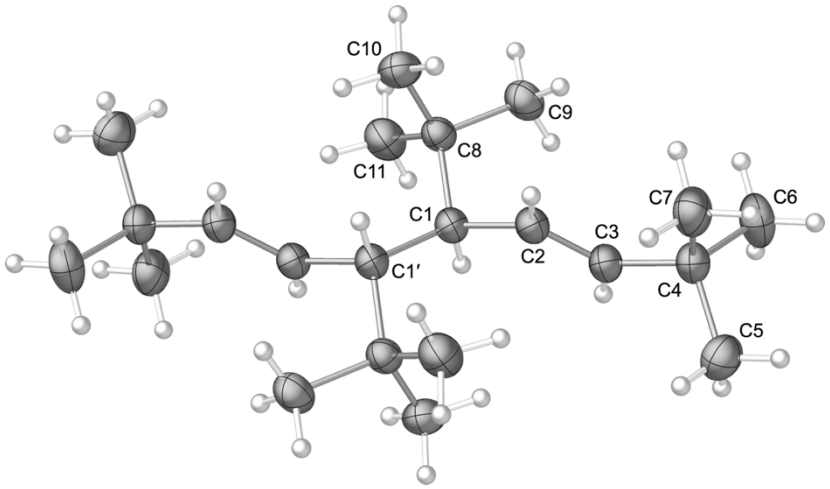

Figure 3.10: Thermal ellipsoid plot (30% level) of the structure of *meso*-{A^{2t}}$_2$ (**23**); hydrogen atoms are given arbitrary radii. Selected bond distances (Å) and angles (°): C1–C1′, 1.571(3); C1–C2, 1.506(2); C2–C3, 1.326(3); C3–C4, 1.507(2); C1–C8, 1.586(2); C1′–C1–C2, 111.37(16); C1–C2–C3, 125.21(16); C2–C3– C4, 128.52(17).

3.3 Discussion

The scarcity of complexes containing *t*-Bu substituted allyl ligands is related at least in part to the lack of efficient synthetic routes. Even so, it is worth comparing the properties of such ligands with the closely related TMS-substituted versions, which are currently more accessible.

Given the larger radius of silicon relative to carbon, it is not surprising that the calculated van der Waals volume of the $[A']^-$ anion is larger than $[A^{2t}]^-$. Relative to the unsubstituted $[C_3H_5]^-$ anion (57 Å^3), the $[A^{2t}]^-$ anion is approximately 3.4 times larger (195 Å^3), whereas $[A']^-$ (231 Å^3) is 4.1 times larger; equivalently, $[A']^-$ is about 18% larger than $[A^{2t}]^-$ (Figure 3.11).[76]

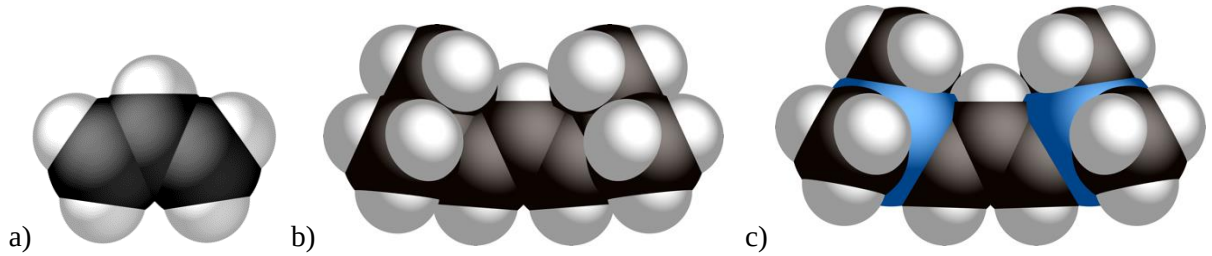

Figure 3.11: Relative van der Waals volumes of three allyl anions: (a) the parent $[C_3H_5]^-$ (57 Å^3); (b) $[A^{2t}]^-$ (195 Å^3); (c) $[A']^-$ (231 Å^3), the latter two calculated with *syn*,*syn* substituents.

The difference in vdW volumes does not translate into proportional changes of the metal coordination sphere shielding, however. As estimated with the program Solid-G,[77] and specifically by the value of G(L), the percentage of the metal coordination sphere shielded by the ligands, the numbers for $[A^{2t}]$ and $[A']$ ligands are actually quite similar. For example, in the isostructural $[\{(allyl')NiBr\}_2]$ dimers, G(L) = 41.6% and 42.2% for the A^{2t} and A′ ligands, respectively. The comparable G(L) values for the mono(allyl) complexes **21** and **22** ([(IMes)NiBr(allyl)]) are 44.0% and 44.2%, respectively. Crystallographically derived coordinates were used for input in these calculations, which are subject to some artifacts (e.g., the well-known shortening of C–H bond lengths).[78,79] In order to remove such effects and the influence of other ligands on the (allyl)–Ni bonding, DFT calculations were used to optimize the structures of $[Ni(C_3H_5)_2]$,[80] $[NiA'_2]$,[13] and (the yet unknown) $[Ni(A^{2t})_2]$, with the latter two calculated with *syn*,*anti*-substituents. For the three complexes, Solid-G's $G_{complex}$ value, which is the net coverage of the metal coordination sphere by all the ligands, is 70.4%, 90.8%, and 92.9%, respectively (Figure 3.12).

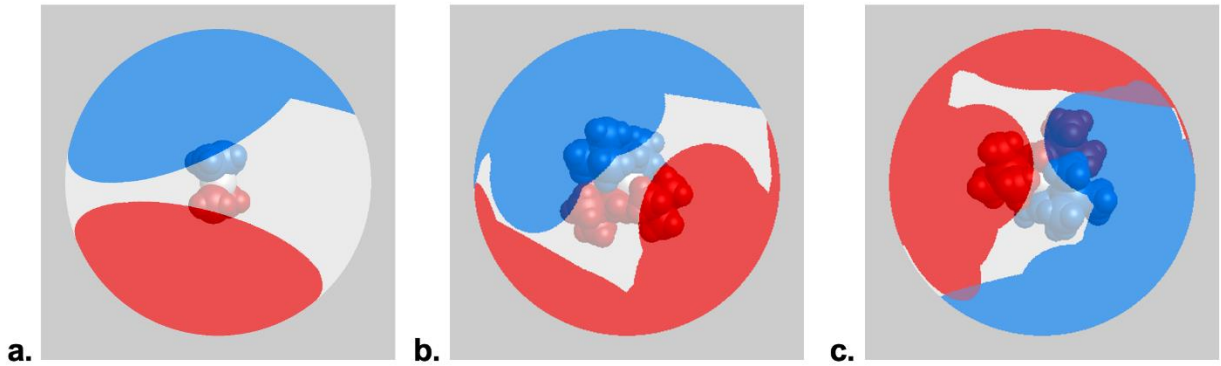

Figure 3.12: Visualization of the extent of coordination sphere coverage ($G_{complex}$) of: (a) [Ni(C_3H_5)$_2$], 70.4%; (b) [Ni(A^{2t})$_2$], 90.8%; (c) [Ni(A´)$_2$], 92.9%. Optimized coordinates (B3PW91-D3BJ/def2-TZVP on all atoms, C_2 symmetry) were used with the program Solid-G.[77] The $G_{complex}$ value represents the net coverage, so that regions of the coordination sphere where the projections of the ligands overlap are counted only once.

These results suggest that the two ligands [A´] and [A^{2t}] are nearly isosteric, a conclusion that comports with the similar structural parameters found in related compounds, e.g., **20** and [{A´NiBr}$_2$], and the IMes derivatives **21** and **22**. Differences in their coordination chemistry therefore must originate primarily from electronic effects, i.e., in the distinctions between purely hydrocarbyl and organosilyl-based compounds. For example, calculations at the B3PW91-D3BJ/def2TZVPD level of $\Delta H°$ for the reaction HA $\rightarrow$ $[A]^-$ + H^+, where HA is the relevant propene, demonstrate that HA´ is more easily deprotonated than HA^{2t}: $\Delta H° = +389$ kcal mol^{-1} and +367 kcal mol^{-1} for HA^{2t} and HA´, respectively. To establish the accuracy of our method, the enthalpy of the analogous reaction using propene, [C_3H_6], was performed. The obtained value of 391.4 kcal mol^{-1} compares favorably with the experimental value of 391.1 kcal mol^{-1}.[81]

These electronic effects were also examined in the context of molecular species. This was done by comparing analogous complexes of the parent allyl ligand [$C_3H_5^-$], A^{2t}, and A´. CO stretching frequencies were calculated for the geometry-optimized complexes of the form [A^xNi(CO)$_2$Br]. [(C_3H_5)Ni(CO)$_2$Br] has been studied as an intermediate in the carbonylation reaction of allyl bromide catalyzed by Ni(CO)$_4$,[82] and [(2-methylallyl)Ni(CO)$_2$Br] has been reported via the reaction of [{(2-methylallyl)NiBr}$_2$] with carbon monoxide, although the species could not be isolated.[83] The calculated stretching frequencies are included below in Table 3. Although the trimethylsilyl group is sometimes considered electronically analogous to a proton,[84] A´ was found to be substantially more electron donating than the parent allyl or 2-methylallyl. As expected, the A^{2t} complex was found to be the most electron donating of the ligands studied, but the

difference in the IR frequencies between it and A′ was approximately half the difference between the C_3H_5 derivative and A′. This suggests that their behaviors would be expected to be generally similar, except in particularly sensitive systems.

Table 3.3: Calculated CO stretching frequencies for a set of $[A^xNi(CO)_2Br]$ compounds.

Complex	**Calculated CO frequencies (cm^{-1})[a]**
$[(C_3H_5)Ni(CO)_2Br]$	2088, 2058
[(2-methylallyl)Ni(CO)$_2$Br]	2085, 2055 (exp. 2083, 2049)[83]
[A′Ni(CO)$_2$Br][b]	2068, 2037
[A^{2t}Ni(CO)$_2$Br][b]	2059, 2030

[a]) Geometries were optimized and frequencies calculated at the PW91PW91/def2TZVP level; [b]) The A′- and A^{2t}–ligated complexes were optimized with *syn*,*syn* geometries.

Although [{A^{2t}NiBr}$_2$] fits into the well-explored class of [{(allyl)NiX}$_2$] complexes, some details of its synthesis and reactivity were unexpected and deserve additional comment. For example, the reaction of [A^{2t}Br] with Ni(0) complexes is atypical, starting with the way that A^{2t}Br induces decomposition of [Ni(cod)$_2$]. In the recovered organic material from these reactions, only [A^{2t}Br] and COD are present in meaningful amounts, eliminating most sequential oxidation/reduction pathways from consideration. It is likely that A^{2t}Br acts as an olefin ligand, binding the nickel center in competition with COD, perhaps forming an unstable "[(cod)NiBr(A^{2t})]" complex that subsequently decomposes to the olefins and nickel metal. However, the rate of decomposition does not noticeably decrease upon addition of excess COD, which might be expected to retard the formation of such a mixed ligand species. The detailed mechanism of the decomposition therefore remains undetermined.

Even once isolated, the extent to which [{A^{2t}NiBr}$_2$] resists adduct formation is atypical. The formation of ligand adducts from [{(allyl)NiX}$_2$] complexes is well-precedented, and the [(allyl)NiLX] archetype has generally been found to be more stable than the bridged bimetallic species.[50,69,85] In the case of [{A^{2t}NiBr}$_2$], however, stable binding is only observed with the highly basic IMes ligand, and even this is accompanied by a decrease in solution-phase stability. The reactivity of [{A^{2t}NiBr}$_2$] with triphenylphosphine was distinct even from the very similar [{A′NiBr}$_2$], and so this reaction was studied computationally.

ETS-NOCV (Extended Transition State–Natural Orbitals for Chemical Valence) fragmentation analysis on both [A^{2t}Ni(PPh_3)Br] and [A′Ni(PPh_3)Br] was conducted in order to evaluate the relative

strength of the Ni-P interaction in each complex (Figure 3.13). The sum of all NOCV pairs (ΔE^{orb}) is -63.7 kcal mol^{-1} and -64.7 kcal mol^{-1} for [A^{2t}Ni(PPh$_3$)Br] and [A′Ni(PPh$_3$)Br], respectively, indicating that the orbital interaction stabilizes both complexes nearly equally. The Ph$_3$P→NiBr(allyl) donation is by far the most energetically significant interaction, equaling 39.0 kcal mol^{-1} for [A′Ni(PPh$_3$)Br] and 37.6 kcal mol^{-1} for [A^{2t}Ni(PPh$_3$)Br]. For comparison, the next most important interaction for either molecule is < 8 kcal mol^{-1}. The binding affinity of nickel for triphenylphosphine is essentially as high for the [A^{2t}NiBr] monomer as the [A´NiBr] monomer. This small difference is also captured in the Mayer bond orders of 0.84 and 0.80 for the Ni–P bonds in [A′Ni(PPh$_3$)Br] and [A^{2t}Ni(PPh$_3$)Br], respectively. This perhaps suggests that the difference might lie earlier in the adduct formation, i.e., in the rearrangement of the *syn*,*syn*-conformations found in the [{A^{x}NiBr}$_2$] dimers into the *syn,anti* arrangements in the PPh$_3$ adducts. Although the activation energies for these changes are currently unknown, the energies of *syn,anti* dimers relative to the *syn*,*syn*-versions are higher for the A^{2t} complex than the A´ counterpart (see Appendix 3, Section 3.5.1). Even though all the steric and electronic differences between the [A^{2t}Ni(PPh$_3$)Br] and [A′Ni(PPh$_3$)Br] complexes are relatively small, they all point in the same direction, and their cumulative effect may well be to inhibit PPh$_3$ binding in the [A^{2t}Ni(PPh$_3$)Br] complex then. The greater basicity of IMes overcomes these differences and ligand dissociation is not observed in solution. To verify the generality of this conclusion, an NMR reaction of [{A^{2t}NiBr}$_2$] with a more basic phosphine, tri-*n*-butylphosphine,[86] was performed. Only a single set of allyl peaks were present in the 1H NMR spectrum of the mixture (see Fig. A3.15). These signals very closely match the spectral features of [A^{2t}Ni(PPh$_3$)Br] and [A´Ni(PPh$_3$)Br], strongly suggesting the quantitative formation of an analogous adduct complex. Based on this result, it should be possible to leverage ligand basicity to tune the extent of binding, making [{A^{2t}NiBr}$_2$] a potentially versatile precatalyst.

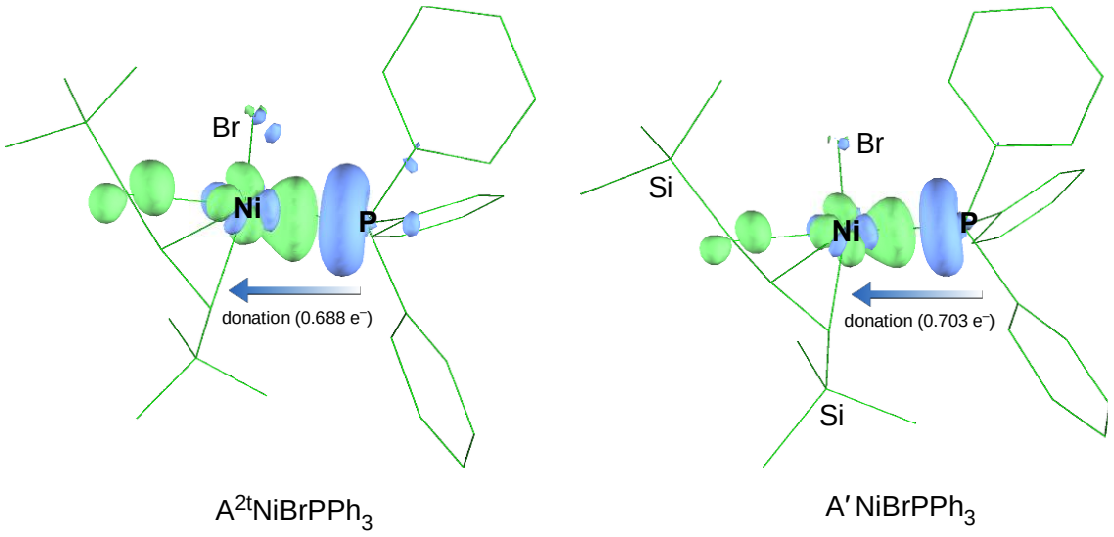

Figure 3.13: Blue and green isosurfaces display the region where electron density is decreased and increased, respectively, owing to the orbital interaction described by NOCV pair 1 ($\Delta \boldsymbol{E}_1^{orb}$).

3.4 Conclusions

Although the volumes of the $[1,3\text{-}(t\text{-Bu})_2C_3H_3]^-$ (= A^{2t}) and $[1,3\text{-}(TMS)_2C_3H_3]^-$ (= A′) anions are different, in metal complexes the ligands appear to be functionally isosteric. The dissimilarities in their coordination chemistry therefore must be primarily electronic in origin. With no readily available alkali metal salt for the A^{2t} ligand, synthesis of its metal complexes must currently rely on customized approaches. In the case of nickel, $[\{A^{2t}NiBr\}_2]$ proves to be a versatile starting material for substitution reactions. It shares similarities with its trimethylsilyl counterpart, particularly in the structures of its complexes, but their behavior is not exactly parallel. For example, $[\{A^{2t}NiBr\}_2]$ was found to be atypically resistant to interacting with PPh_3, forming only a weakly bound complex. This reluctance could, however, be useful for applications in which ligand dissociation is desirable, such as catalysis of addition-type olefin polymerization (e.g., a nickel complex with weakly binding $SbPh_3$ ligands was found to be uniquely effective in polymerizing silylnorbornenes).[87]

3.5 Synthetic Procedures and characterization data

5-hydroxy-2,2,6,6-tetramethylheptan-3-yl pivalate

Both reported methods for the synthesis of 2,2,6,6-tetramethylhept-4-en-3-one frequently generate double addition products as minor products in varying amounts. For example, 5-(*t*-Bu)-2,2,8,8-tetramethylnonane-3,7-dione is invariably found under conditions of excess pinacolone, and occasionally seen even when the ketone is the limiting reagent. When pivaldehyde is used in excess, 5-hydroxy-2,2,6,6-tetramethylheptan-3-yl pivalate is frequently formed, which readily forms X-ray quality crystals. Only one set of peaks is observed in the proton NMR spectrum; taken in conjunction with the crystal structure, this suggests that only the *anti*-enantiomers are formed.

^{1}H NMR (400 MHz, $CDCl_3$, 298 K): δ 0.86 (s, 9H, $C(CH_3)_3$); 0.91 (s, 9H, $C(CH_3)_3$); 1.21 (s, 9H, $C(CH_3)_3$); 1.52 (m, 2H, methylene CH_2); 2.81 (irreg d, 4.30 Hz, 1H, OH); 2.88 (m, 1H, OC(*H*)*t*-Bu); 4.84 (m, 1H, C(*H*)OH).

3-bromo-2,2,6,6-tetramethyl-4-heptene

The compound was prepared as described in the literature.[88] The proton NMR spectrum of this molecule in aromatic solvents differs substantially from its spectrum in $CDCl_3$, so these shifts are included here.

^{1}H NMR (400 MHz, C_6D_6, 298 K): δ 0.87 (s, 9H, $C(CH_3)_3$); 0.96 (s, 9H, $C(CH_3)_3$); 4.24 (d, 10.36 Hz, 1 H, sp^3 C-H); 5.38 (d, *J* = 15.5 Hz, 1 H, sp^2 C(*t*-Bu)-H); 5.68 (dd, *J* = 15.5, 10.4 Hz, 1 H, center sp^2 C-H). ^{13}C{^{1}H} NMR (151 MHz, C_6D_6, 298 K): δ 144.0 (s, center vinyl carbon); 124.4 (s, terminal vinyl C(H)*t*-Bu); δ 69.9 (s, BrC(H)*t*-Bu); 35.5 (s, *t*-Bu CMe_3); 32.4 (s, *t*-Bu CMe_3); 29.0 (s, *t*-Bu $(CH_3)_3$); 27.1 (s, *t*-Bu $(CH_3)_3$).

*[{A^{2t}NiBr}$_2$] (**20**)*

The synthesis was performed in a nitrogen-filled glovebox. [A^{2t}Br] (0.179 g, 0.767 mmol) and acetonitrile (0.303 g, 7.38 mmol) were combined in a glass vial, then dissolved in 3-5 mL THF. In a round bottom flask equipped with a magnetic stir bar, [Ni(cod)$_2$] (0.212 g, 0.771 mmol) was dissolved in 3-5 mL THF. The [A^{2t}Br] solution was then added dropwise to the [Ni(cod)$_2$] solution, during which the mixture gradually darkened to a deep red color. This solution was allowed to stir for 30 min, during which time a black solid was deposited at the bottom of the flask. The solution was then filtered through a fine glass frit, and the volatiles were removed by vacuum. The resulting red solid was then dissolved in 5 mL acetonitrile, followed by extraction with 3 × 3 mL portions of hexanes. The hexane washes were discarded, and the acetonitrile solution evaporated under vacuum, leaving spectroscopically pure [{A^{2t}NiBr}$_2$] (0.173 g, 77%; yields in

repeated reactions consistently ranged from 65–80%) as a chalky red, thin powder. The solid is sparingly soluble in nonpolar solvents and can be stored indefinitely in the glovebox.

^{1}H NMR (400 MHz, DMSO-d_6): δ 5.16 (t, *J* = 12.0 Hz, 1H, center allyl proton); 2.82 (d, *J* = 12.0 Hz, 2H, allyl *anti* C(H)*t*-Bu); 1.02 (s, 18 H, *t*-Bu $(CH_3)_3$). ^{1}H NMR (400MHz, C_6D_6): δ 4.94 (t, *J* = 12.3 Hz, 1H, center allyl proton); 2.46 (d, *J* = 12.3 Hz, 2H, allyl *anti* C(H)*t*-Bu); 1.11 (s, 18 H, *t*-Bu $(CH_3)_3$). ^{13}C{^{1}H} NMR (151 MHz, C_6D_6): δ 96.8 (s, center allyl carbon); 84.2 (s, allyl terminal C(H)*t*-Bu); 33.4 (s, *t*-Bu CMe_3) 29.4 (s, *t*-Bu $(CH_3)_3$). Despite repeated attempts, satisfactory elemental analysis could not be obtained for this compound.

[{A^{2t}NiCl}$_2$]

An identical procedure used for the synthesis of [{A^{2t}NiBr}$_2$] except using [A^{2t}Cl] as the allyl halide was used. The isolated product was a bright red solid that was indefinitely stable in the glovebox atmosphere. No deviations from the properties of [{A^{2t}NiBr}$_2$] were observed.

^{1}H NMR (400 MHz, C_6D_6): δ 4.98 (t, J = 12.0 Hz, 1H, center allyl C-H); δ 2.42 (d, J = 12.0 Hz, 2H, terminal allyl C-H); δ 1.09 (s, 18H, *t*Bu $(CH_3)_3$).

Improved synthesis of [{A´NiBr}$_2$] from [NiA´$_2$]

In a nitrogen-filled glovebox, a 10 mL Schlenk flask was charged with 10.0 mL dry hexane. This flask was placed on a Schlenk line, and [Br_2] (0.21 mL, 4.08 mmol) was added, and the flask is swirled until well-mixed. A separate 50 mL Schlenk flask was charged with a magnetic stir bar and [NiA´$_2$,] (0.637 g, 1.48 mmol) which was then dissolved in 25-30 mL hexane. This flask was placed on the Schlenk line and cooled to -78 °C. A plastic syringe was used to add the [Br_2]/hexane solution (3.60 mL, 1.44 mmol) dropwise to the [NiA´$_2$] solution. The reaction mixture slowly changed from dark orange to deep scarlet. The solution was then allowed to warm to room temperature overnight. The flask was brought into the glovebox, the mixture filtered through a glass frit, and the filtrate solution concentrated under vacuum. The concentrated hexane solution was extracted three times with acetonitrile, losing most of its color in the process. The combined acetonitrile extracts were then extracted twice with hexane, and the volatiles removed under vacuum. Spectroscopically pure [{A´NiBr}$_2$] was isolated in 62% yield (0.297 g). Higher yields have been reported using the previously published methods, but these are likely inflated by unrecognized impurities, and the present method has been found to be substantially more consistent.

Two previously unreported species are present in the product mixture, believed to be the eclipsed and staggered isomers of *syn*,*anti*-[{A´NiBr}$_2$]. New product **A** is always in excess compared to new product **B**, generally by a ratio of 2-4 : 1. One or both of these species have been identified as minor products in all known previously recorded spectra of [{A´NiBr}$_2$], in ratios from 0.5-1 (combined new products) : 1

syn,*syn*-[{A´NiBr}$_2$]. However, the new procedure outlined here initially produces these products in much larger amounts, as great as 2 : 1 compared to *syn*,*syn*-[{A´NiBr}$_2$]. It is thought that transient binding of trace acetonitrile leftover from the new extraction process promotes a *syn*,*anti* configuration; this is in line with all known [A´Ni(L)Br] complexes, which display *syn*,*anti* configurations. Interestingly, the relative amount of the new products decreases over time, eventually reaching as low as 0.30 : 1; this might be the result of evaporation of the leftover acetonitrile, followed by slow isomerization to the thermodynamically favored *syn*,*syn* form. Unfortunately, the TMS CH_3 protons appear to overlap with each other or with trace impurities, and therefore cannot be confidently assigned at this time.

New product **A** ^{1}H NMR (400 MHz, C_6D_6, 298 K): δ 5.58 (d, *J* = 14.8, 9.2 Hz, 1H, center allyl proton); 2.99 (d, *J* = 9.2 Hz, 1H, allyl *syn*-C(H)TMS); 2.06 (d, *J* = 14.78, 1 H, allyl *anti* C(H)TMS).

New product **B** ^{1}H NMR (C_6D_6): δ 5.56 (dd, *J* = 15.3, 9.4 Hz, 1H, center allyl proton); 2.91 (d, *J* = 9.4 Hz, 1H, allyl *syn*-C(H) TMS); 1.99 (d, *J* = 15.3 Hz, 1 H, allyl *anti*-C(H)TMS).

Synthesis of [A^{2t}Ni(PPh$_3$)Br]

In a nitrogen-filled glovebox, [{A^{2t}NiBr}$_2$] (0.016 g, 0.027 mmol) was placed in a glass vial and dissolved in 5 mL THF. Solid [PPh_3] (0.014 g, 0.053 mmol) was then added to the solution. The [PPh_3] quickly dissolved with no change in the color of the solution. The solution was then filtered through a celite-packed pipette filter, and the volatiles removed by vacuum to yield a hard, dark red paste. NMR analysis shows this material to be composed of a mixture of [A^{2t}Ni(PPh_3)Br], [{A^{2t}NiBr}$_2$], and free triphenylphosphine (see Table A3.4 for ratio details). Elemental Analysis: Found – 60.90% C, 6.23% H; Calculated (for $C_{29}H_{36}$ NiBrP) – 62.85% C, 6.55% H. The minor deviation from expectations is likely the result of the solid-state decomposition of the adduct.

^{1}H NMR (600 MHz, d_8-toluene, 298 K): δ 7.78 (bs, 6H, PPh_3 Ar-H); 7.03 (m, PPh_3 Ar-H); 4.86 (dd, *J* = 14.6, 8.7 Hz, 1 H, center allyl CH); 4.18 (bm, 1 H, allyl *anti* C(**H**) *t*-Bu); 3.14 (bm, 1 H, allyl *syn* C(H) *t*-Bu); 1.48 (s, 9 H, *t*-Bu (CH_3)$_3$); 0.93 (s, 9 H, *t*-Bu (CH_3)$_3$). ^{1}H NMR (600 MHz, d_8-toluene, 253 K): δ 7.78 (bm, 6H, PPh_3 Ar-H); 7.00 (bm, PPh_3 Ar-H); 4.82 (dd, *J* = 14.34, 8.75 Hz, 1 H, center allyl CH); 4.20 (dd, *J* = 14.3, 8.9 Hz, 1 H, allyl *anti* C(**H**)*t*-Bu); 3.12 (bm, 1 H, allyl *syn* C(H) *t*-Bu); 1.52 (s, 9 H, *t*-Bu (CH_3)$_3$; 0.92 (s, 9 H, *t*-Bu (CH_3)$_3$). ^{13}C{^{1}H} NMR (151 MHz, toluene-d_8, 298 K): δ 134.5 (bd, *J* = 8.4 Hz, PPh_3 C-H); 133.1 (bd, *J* = 34.8 Hz, PPh_3 ipso C); 129.7 (bs, PPh_3 para C-H); 128.1 (vb s, PPh_3 C-H); 98.3 (s, allyl center C-H); 96.9 (bd, *J* = 20.0 Hz, *anti* allyl C(H) *t*-Bu); 81.8 (s, *syn* allyl C(H) *t*-Bu); 35.6 (s, *t*-Bu CMe_3) 34.5 (s, *t*-Bu Cme_3); 31.1 (s, *t*-Bu (CH_3)$_3$); 30.6 (s, *t*-Bu (CH_3)$_3$). ^{31}P{^{1}H} NMR (162 MHz, C_6D_6, 298 K): δ 23.72.

Synthesis of [A´Ni(PPh$_3$)Br]

The same procedure detailed for [A^{2t}Ni(PPh$_3$)Br] was used here, substituting [{A´NiBr}$_2$] for [{A^{2t}NiBr}$_2$]. The isolated product is a dark red, hard paste that is indefinitely stable in the glovebox atmosphere. Elemental Analysis: Found – 55.74% C, 6.35% H; Calculated (for $C_{27}H_{36}Si_2NiBrP$) – 55.31% C, 6.19% H.

^{1}H NMR (600 MHz, d$_8$-toluene, 298 K): δ 7.76 (irregular t, *J* = 8.7 Hz, 6H, PPh$_3$ Ar-H); 7.03 (m, PPh$_3$ Ar-H); 5.69 (dd, *J* = 16.1, 9.1 Hz, 1 H, center allyl CH); 3.15 (dd, *J* = 16.1, 7.1 Hz, 1 H, allyl *anti* C(**H**) *t*-Bu); 2.76 (dd, *J* = 9.1, 5.7 Hz,1 H, allyl *syn* C(H) *t*-Bu); 0.50 (s, 9 H, TMS (CH$_3$)$_3$; 0.02 (s, 9 H, TMS (CH$_3$)$_3$). ^{13}C{^{1}H} NMR (151 MHz, toluene-d$_8$, 298 K): δ 134.9 (d, *J* = 11.0 Hz, PPh$_3$ C-H); 133.3 (d, *J* = 39.4 Hz, PPh$_3$ ipso C); 130.2 (s, PPh$_3$ *para* C-H); 128.4 (d, *J* = 9.5 Hz, PPh$_3$ C-H); 120.1 (s, allyl center C-H); 80.3 (d, *J* = 20.4 Hz, *anti* allyl C(H) *t*-Bu); 71.3 (d, *J* = 3.3 Hz, *syn* allyl C(H) *t*-Bu); 0.80 (s, TMS (CH$_3$)$_3$); 0.30 (s, TMS (CH$_3$)$_3$). ^{31}P{^{1}H} NMR (162 MHz, C$_6$D$_6$, 298 K): δ 23.60.

*Synthesis of [A^{2t}Ni(IMes)Br] (**21**)*

The same procedure detailed for [A^{2t}Ni(PPh$_3$)Br] was used here, substituting IMes for PPh$_3$. [{A^{2t}NiBr}$_2$] (0.053 g, 0.082 mmol) and IMes (0.055 g, 0.18 mmol) were allowed to react in THF (5 mL) to yield 0.097 g (90% yield) of **21**. The isolated product is a dark red, hard solid that is sparingly soluble in hexanes but soluble in aromatic hydrocarbons and polar organic solvents. The compound appears indefinitely stable in the solid state, but when stored in hexane solution, a white solid is slowly deposited. After removing the white solid, the NMR features of the compound were unchanged, making the mechanism of decomposition unclear. A small amount of a second product is consistently present in NMR spectra, and its spectral features are consistent with a *syn*,*syn* A^{2t} -nickel complex, but its exact nature is unknown. Due to its low concentration and broadened peaks, some of the signals belonging to this species cannot be found, but those that have are listed here. Elemental Analysis: Found – 63.84% C, 6.67% H, 4.70% N; Calculated (for $C_{32}H_{45}NiBrN_2$) – 64.34% C, 7.76% H, 4.69% N.

Major product: ^{1}H NMR (400 MHz, C_6D_6, 298 K): δ 6.83 (s, 2H, Mes Ar-H); 6.81 (s, Mes Ar-H); 6.10 (s, 2 H, NHC HC=CH); 4.20 (dd, *J* = 14.6, 8.3 Hz, 1 H, center allyl CH); 3.27 (m, 2 H, allyl *syn* and *anti*-C(H) *t*-Bu); 2.29 (bs, 6 H, Ar-CH_3); 2.25 (bs, 6 H, Ar-CH_3); 2.14 (bs, 6 H, Ar-CH_3); 1.24 (s, 9 H, *t*-Bu $(CH_3)_3$; 1.00 (s, 9 H, *t*-Bu $(CH_3)_3$). ^{13}C{^{1}H} NMR (101 MHz, C_6D_6, 298 K): δ 185.4 (s, NHC N-C-N); 138.9 (s, Mes *ipso* C); 137.0 (s, Mes *para* C-Me); 129.5 (s, Mes Ar-H); 129.5 (s, Mes Ar-H); 123.6 (s, NHC HC=CH); 98.8 (s, allyl center C-H); 91.6 (s, *anti* -allyl C(H)*t*-Bu); 68.9 (s, *syn*-allyl C(H)*t*-Bu); 34.5 (s, *t*-Bu Cme_3); 33.9 (s, *t*-Bu Cme_3); 32.0 (s, *t*-Bu $(CH_3)_3$); 30.3 (s, *t*-Bu $(CH_3)_3$). 21.2 (s, Ar-CH_3); 19.8 (s, Ar-CH_3).
Minor product: ^{1}H NMR (400 MHz, C_6D_6, 298 K): δ 6.79 (s, 4H, Mes Ar-H); 6.28 (bs, 2H, NHC HC=CH); 4.67 (t, *J* = 12.3 Hz, 1 H, center allyl CH); 2.36 (irregular bs, 14 H, Ar-CH_3 and terminal allyl C-H); 2.08 (s, 6 H, Ar-CH_3); 1.12 (s, 9 H, *t*-Bu $(CH_3)_3$. ^{13}C{^{1}H} NMR (101 MHz, C_6D_6, 298 K): 98.2 (s, allyl center C-H); 35.0 (s, *t*-Bu Cme_3); 34.5 (s, *t*-Bu Cme_3); 30.2 (s, *t*-Bu $(CH_3)_3$); 30.0 (s, *t*-Bu $(CH_3)_3$). 20.9 (s, Ar-CH_3); 19.5 (s, Ar-CH_3).

Synthesis of [A´Ni(IMes)Br] (22)

The same procedure detailed for [A^{2t}Ni(PPh_3)Br] was used here, substituting IMes for PPh_3 and [{A´NiBr}$_2$] for [{A^{2t}NiBr}$_2$]. [{A´NiBr}$_2$] (0.011 g, 0.019 mmol) and IMes (0.012 g, 0.039 mmol) were allowed to react in THF (5 mL) to yield 0.023 g (quantitative) of **22**. The isolated product is a dark scarlet, hard solid that is sparingly soluble in hexane and soluble in aromatic hydrocarbons and polar organic solvents. The compound appears indefinitely stable in the glovebox atmosphere. Elemental Analysis: Found – 57.48% C, 7.36% H, 4.28% N; Calculated (for $C_{30}H_{45}NiBrN_2Si_2$) – 57.33% C, 7.21% H, 4.46% N.

^{1}H NMR (400 MHz, C_6D_6, 298 K): δ 6.85 (s, 2H, Mes Ar-H); 6.81 (s, 2H, Mes Ar-H); 6.05 (s, 2 H, NHC HC=CH); 5.14 (dd, *J* = 15.9, 8.5 Hz, 1 H, center allyl CH); 2.95 (d, 1 H, allyl *syn*-C(H)TMS); 2.27 (bs, 6 H, Ar-CH_3); 2.17 (s, 6 H, Ar-CH_3); 2.17 (d, 15.9 Hz, 1 H, *anti*-allyl C(H)TMS); 2.16 (bs, 6 H, Ar-CH_3); 0.26 (s, 9 H, TMS $(CH_3)_3$; 0.05 (s, 9 H, TMS $(CH_3)_3$). ^{13}C{^{1}H} NMR (151 MHz, C_6D_6, 298 K): δ 182.6 (s, NHC N-C-N); 139.0 (s, Mes *ipso* C); 136.8 (s, Mes *para* C-Me); 136.2 (s, Mes *ortho* C-Me); 129.7 (s, Mes Ar-H); 129.5 (s, Mes Ar-H); 123.6 (s, NHC HC=CH); 118.2 (s, allyl center C-H); 73.1 (s, *anti*-allyl C(H)TMS); 59.7 (s, *syn*-allyl C(H)TMS); 21.0 (s, Ar-CH_3); 19.7 (s, Ar-CH_3); 19.2 (s, Ar-CH_3); 1.2 (s, TMS $(CH_3)_3$); 0.0 (s, TMS $(CH_3)_3$).

3.5 References:

(1) Trost, B. M.; Crawley, M. L. Asymmetric Transition-Metal-Catalyzed Allylic Alkylations: Applications in Total Synthesis. *Chem. Rev.* **2003**, *103* (8), 2921–2943. https://doi.org/10.1021/cr020027w.

(2) Chen, Q. A.; Chen, Z.; Dong, V. M. Rhodium-Catalyzed Enantioselective Hydroamination of Alkynes with Indolines. *J. Am. Chem. Soc.* **2015**, *137* (26), 8392–8395. https://doi.org/10.1021/jacs.5b05200.

(3) Cruz, F. A.; Zhu, Y.; Tercenio, Q. D.; Shen, Z.; Dong, V. M. Alkyne Hydroheteroarylation: Enantioselective Coupling of Indoles and Alkynes via Rh-Hydride Catalysis. *J. Am. Chem. Soc.* **2017**, *139* (31), 10641–10644. https://doi.org/10.1021/jacs.7b05893.

(4) Yang, X. H.; Dong, V. M. Rhodium-Catalyzed Hydrofunctionalization: Enantioselective Coupling of Indolines and 1,3-Dienes. *J. Am. Chem. Soc.* **2017**, *139* (5), 1774–1777. https://doi.org/10.1021/jacs.6b12307.

(5) Simpson, C. K.; White, R. E.; Carlson, C. N.; Wrobleski, D. A.; Kuehl, C. J.; Croce, T. A.; Steele, I. M.; Scott, B. L.; Young, V. G.; Hanusa, T. P.; Sattelberger, A. P.; John, K. D. The Role of Alkali Metal Cations in MMA Polymerization Initiated by Neutral and Anionic Allyl Lanthanide Complexes. *Organometallics* **2005**, *24* (15), 3685–3691. https://doi.org/10.1021/om050098w.

(6) Chalkley, M. J.; Guard, L. M.; Hazari, N.; Hofmann, P.; Hruszkewycz, D. P.; Schmeier, T. J.; Takase, M. K. Synthesis, Electronic Structure, and Reactivity of Palladium(I) Dimers with Bridging Allyl, Cyclopentadienyl, and Indenyl Ligands. *Organometallics* **2013**, *32* (18), 4223–4238. https://doi.org/10.1021/om400687m.

(7) Melvin, P. R.; Nova, A.; Balcells, D.; Dai, W.; Hazari, N.; Hruszkewycz, D. P.; Shah, H. P.; Tudge, M. T. Design of a Versatile and Improved Precatalyst Scaffold for Palladium-Catalyzed Cross-Coupling: (H3-1-TBu-Indenyl)2(μ-Cl)2Pd2. *ACS Catal.* **2015**, *5* (6), 3680–3688. https://doi.org/10.1021/acscatal.5b00878.

(8) Dardir, A. H.; Melvin, P. R.; Davis, R. M.; Hazari, N.; Mohadjer Beromi, M. Rapidly Activating Pd-Precatalyst for Suzuki-Miyaura and Buchwald-Hartwig Couplings of Aryl Esters. *J. Org. Chem.* **2018**, *83* (1), 469–477. https://doi.org/10.1021/acs.joc.7b02588.

(9) Sulway, S. A.; Girshfeld, R.; Solomon, S. A.; Muryn, C. A.; Poater, J.; Sola, M.; Bickelhaupt, F. M.; Layfield, R. A. Alkali Metal Complexes of Silyl-Substituted Ansa-(Tris)Allyl Ligands: Metal-, Co-Ligand-, and Substituent-Dependent Stereochemistry. *Eur. J. Inorg. Chem.* **2009**, *2009* (27), 4157–4167. https://doi.org/10.1002/ejic.200900618.

(10) Chmely, S. C.; Hanusa, T. P. Complexes with Sterically Bulky Allyl Ligands: Insights into Structure and Bonding. *Eur. J. Inorg. Chem.* **2010**, No. 9, 1321–1337. https://doi.org/10.1002/ejic.200900813.

(11) Harvey, M. J.; Hanusa, T. P.; Young, Jr., V. G. Synthesis and Crystal Structure of the Bis(Allyl)Calcium Complex $[Ca\{C_3(SiMe_3)_2H_3\}_2{\cdot}(Thf)_2]$. *Angew. Chem. Int. Ed.* **1999**, *38* (1–2), 217–219. https://doi.org/10.1002/(SICI)1521-3773(19990115)38:1/2<217::AID-ANIE217>3.0.CO;2-Q.

(12) Carlson, C. N.; Smith, J. D.; Hanusa, T. P.; Brennessel, W. W.; Young, V. G. Homoleptic Allyl Complexes of Chromium with Trimethylsilylated Ligands. *J. Organomet. Chem.* **2003**, *683* (1), 191–199. https://doi.org/10.1016/S0022-328X(03)00603-X.

(13) Quisenberry, K. T.; Smith, J. D.; Voehler, M.; Stec, D. F.; Hanusa, T. P.; Brennessel, W. W. Trimethylsilylated Allyl Complexes of Nickel. The Stabilized Bis(π-Allyl)Nickel Complex $[\eta^3\text{-}1,3\text{-}(SiMe_3)_2C_3H_3]_2Ni$ and Its Mono(π-Allyl)NiX (X = Br, I) Derivatives. *J. Am. Chem. Soc.* **2005**, *127* (12), 4376–4387. https://doi.org/10.1021/ja044308s.

(14) Rightmire, N. R.; Hanusa, T. P.; Rheingold, A. L. Mechanochemical Synthesis of $[1,3\text{-}(SiMe_3)_2C_3H_3]_3(Al,Sc)$, a Base-Free Tris(Allyl)Aluminum Complex and Its Scandium Analogue. *Organometallics* **2014**, *33* (21), 5952–5955. https://doi.org/10.1021/om5009204.

(15) Koby, R. F.; Doerr, A. M.; Rightmire, N. R.; Schley, N. D.; Brennessel, W. W.; Long, B. K.; Hanusa,

T. P. Mechanochemical Formation, Solution Rearrangements, and Catalytic Behavior of a Polymorphic Ca/K Allyl Complex. *Chem. Eur. J.* **2021**, *27* (31), 8195–8202. https://doi.org/10.1002/chem.202100589.

(16) Zhang, W.; Robins, M. J. Removal of Silyl Protecting Groups from Hydroxyl Functions with Ammonium Fluoride in Methanol. *Tetrahedron Lett.* **1992**, *33* (9), 1177–1180. https://doi.org/10.1016/S0040-4039(00)91889-6.

(17) Scheidt, K. A.; Chen, H.; Follows, B. C.; Chemler, S. R.; Coffey, D. S.; Roush, W. R. Tris(Dimethylamino)Sulfonium Difluorotrimethylsilicate, a Mild Reagent for the Removal of Silicon Protecting Groups. *J. Org. Chem.* **1998**, *63* (19), 6436–6437. https://doi.org/10.1021/jo981215i.

(18) Ferreira, F.; Vasseur, J. J.; Morvan, F. Lewis Acid Deprotection of Silyl-Protected Oligonucleotides and Base-Sensitive Oligonucleotide Analogues. *Tetrahedron Lett.* **2004**, *45* (33), 6287–6290. https://doi.org/10.1016/j.tetlet.2004.06.081.

(19) Walton, D. R. M. The Relative Electron-Releasing Power of Trimethylsilyl and Tert-Butyl Groups. *J. Organomet. Chem.* **1965**, *3* (6), 438–441. https://doi.org/10.1016/S0022-328X(00)83572-X.

(20) Weiss, T.; Böhme, U.; Walfort, B.; Rheinwald, G.; Lang, H. Trimethylsilyl-Substituted Indenyl-TiCl3 Half-Sandwich Complexes: Synthesis, Solid-State Structure, and Analysis of Substituent Effects. *Organometallics* **2005**, *24* (11), 2577–2581. https://doi.org/10.1021/om0400898.

(21) Kawakami, K.; Kuivila, H. G. Preparation and Spectral Characteristics of Some Allyltins. Nature of Allyltin Interactions. *J. Org. Chem.* **1969**, *34* (5), 1502–1504. https://doi.org/10.1021/jo01257a083.

(22) Weidner, U.; Schweig, A. Nature of the "Silicon Beta-Effect" in Allyltrimethylsilane. *Angew. Chem. - Int. Ed.* **1972**, *11* (2), 146–147. https://doi.org/10.1002/anie.197201461.

(23) Burshtein, K. Y.; Isaev, A. N.; Shorygin, P. P. Sigma-Pi Interaction in Some Sigma-Bonded Allyl Compounds. A MNDO Study. *J. Organomet. Chem.* **1989**, *361* (1), 21–25. https://doi.org/10.1016/0022-328X(89)87347-4.

(24) Koby, R. F.; Schley, N. D.; Hanusa, T. P. Di(Indenyl)Beryllium. *Angew. Chem. - Int. Ed.* **2021**, *60* (39), 21174–21178. https://doi.org/10.1002/anie.202107980.

(25) Hardy, J. P.; Cumming, W. D. The Conformational Preferences of the N-Trimethylsilyl and O-Trimethylsilyl Groups. *J. Am. Chem. Soc.* **1971**, *93* (4), 928–932. https://doi.org/https://doi.org/10.1021/ja00733a024.

(26) Fraenkel, G.; Cabral, J.; Lanter, C.; Wang, J. Reorientation Dynamics within Ion-Paired Allylic Lithium Compounds: Isolation of Inversion Processes. *J. Org. Chem.* **1999**, *64* (4), 1302–1310. https://doi.org/10.1021/jo982196f.

(27) Ward, Y. D.; Villanueva, L. A.; Allred, G. D.; Payne, S. C.; Semones, M. A.; Liebeskind, L. S. Synthesis, Characterization, and Configurational Lability of (η^3-Allyl)Dicarbonyl[Hydrotris(1-Pyrazolyl)Borato]Molybdenum Complexes Bearing Substituents at the Termini: Thermodynamic Preference for the Anti Stereoisomer. *Organometallics* **1995**, *14* (9), 4132–4156. https://doi.org/10.1021/om00009a017.

(28) Lin, Q.; Leong, W. K.; Gao, L. The Photochemical and Thermal Reactions of a Triosmium Cluster Carrying a γ-Pyrone Ligand with Alkynes. *J. Organomet. Chem.* **2004**, *689* (1), 25–34. https://doi.org/10.1016/j.jorganchem.2003.09.022.

(29) Reiners, M.; Fecker, A. C.; Baabe, D.; Freytag, M.; Jones, P. G.; Walter, M. D. Cobalt and Nickel Compounds with Pentadienyl and Edge-Bridged Pentadienyl Ligands: Revisited. *Organometallics* **2019**. https://doi.org/10.1021/acs.organomet.9b00592.

(30) Volger, H. C. Synthesis of Beta-alkyl and Beta-aryl Pi-allylic Palladium Halide Complexes and Its Mechanistic Aspects. *Recl. des Trav. Chim. des Pays-Bas* **1968**, *87*, 225–240.

(31) Wilke, G.; Bogdanovic, B. Bis-Pi-Allyl-Nickel. *Angew. Chemie* **1961**, *73* (23), 756. https://doi.org/https://doi.org/10.1002/ange.19610732306.

(32) Chen, M.; Chen, C. A Versatile Ligand Platform for Palladium- and Nickel-Catalyzed Ethylene Copolymerization with Polar Monomers. *Angew. Chem. - Int. Ed.* **2018**, *57* (12), 3094–3098. https://doi.org/10.1002/anie.201711753.

(33) Xu, M.; Yu, F.; Li, P.; Xu, G.; Zhang, S.; Wang, F. Enhancing Chain Initiation Efficiency in the Cationic Allyl-Nickel Catalyzed (Co)Polymerization of Ethylene and Methyl Acrylate. *Inorg. Chem.* **2020**, *59* (7), 4475–4482. https://doi.org/10.1021/acs.inorgchem.9b03647.
(34) Liang, T.; Goudari, S. B.; Chen, C. A Simple and Versatile Nickel Platform for the Generation of Branched High Molecular Weight Polyolefins. *Nat. Commun.* **2020**, *11* (1), 1–8. https://doi.org/10.1038/s41467-019-14211-0.
(35) Zhang, R.; Gao, R.; Gou, Q.; Lai, J.; Li, X. Recent Advances in the Copolymerization of Ethylene with Polar Comonomers by Nickel Catalysts. *Polymers (Basel).* **2022**, *14* (18). https://doi.org/10.3390/polym14183809.
(36) Speight, I. R. OPTIMIZED SYNTHESIS OF MECHANOCHEMICALLY GENERATED METAL COMPLEXES, Ph. D. Thesis, Vanderbilt University, 2021.
(37) Degroot, H. P.; Speight, I. R.; Brennessel, W. W.; Hanusa, T. P. Distinction with a Difference: T -Butyl and Trimethylsilyl Substituents in Nickel Allyl Complexes. *Submitted - ACS Org. Inorg. Au* **2024**.
(38) Stransky, N.; Herzschuh, R.; Gehrke, J.-P.; Taube, R. Komplexkatalyse XXII. Elektronenstoss-Induzierter Zerfall Der Dimeren η^3-Allylnickel(II)-Halogenide $(C_3H_5NiX)_2$ (X=Cl, Br, I). *J. Organomet. Chem.* **1984**, *270*, 353–356.
(39) Wilke, G.; Bogdanović, B.; Hardt, P.; Heimbach, P.; Keim, W.; Kröner, M.; Oberkirch, W.; Tanaka, K.; Steinrücke, E.; Walter, D.; Zimmermann, H. Allyl-Transition Metal Systems. *Angew. Chem. Int. Ed.* **1966**, *5* (2), 151–164. https://doi.org/10.1002/anie.196601511.
(40) Hegedus, L. S.; Thompson, D. H. P. Reactions of Organic Halides with (π-Allyl)Nickel Halide Complexes: A Mechanistic Study. *J. Am. Chem. Soc.* **1985**, *107* (20), 5663–5669. https://doi.org/10.1021/ja00306a012.
(41) Mealli, C.; Dapporto, P.; Sriyunyongwat, V.; Albright, T. A. The Structure of Bromotris (Triphenylphosphine) Nickel(I), $C_{54}H_{45}BrNiP_3$. *Acta Crystallogr. Sect. C* **1983**, *39*, 995–996. https://doi.org/https://doi.org/10.1107/S0108270183007131.
(42) Zhang, K.; Conda-Sheridan, M.; R. Cooke, S.; Louie, J. N-Heterocyclic Carbene Bound Nickel(I) Complexes and Their Roles in Catalysis. *Organometallics* **2011**, *30* (9), 2546–2552. https://doi.org/10.1021/om200090d.
(43) Eisch, J. J.; Im, K. R. Electron Transfer in the Cleavage of Ethers and Epoxides by Nickel(0) Complexes. *J. Organometa* **1977**, *139*, C45–C50.
(44) Bogdanovic, B.; Kroner, M.; Wilke, G. Ubergangsmetallkomplexe, I Olefin-Komplexe Des Nickels(0). *Justus Liebigs Ann. Chem.* **1966**, *699* (1), 1–23. https://doi.org/https://doi.org/10.1002/jlac.19666990102.
(45) Brandes, H.; Goddard, R.; Jolly, P. W.; Krüger, C.; Mynott, R.; Wilke, G. Transition Metal Allyls, V The Preparation and Structure of [NiX(PmenthylR1R2)(η^3-Allyl)] Complexes. *Z. Naturforsch. - Sect. B* **1984**, *39* (8), 1139–1150. https://doi.org/10.1515/znb-1984-0827.
(46) Andrews, P.; Corker, J. M.; Evans, J.; Webster, M. Highly Active Homogeneous Nickel Catalysts for Alkene Dimerisation: Crystal Structure of [Ni(H3-C3H5)(PPh3)Br] and in Situ Characterisation of AlEt3-Activated [Ni(H3-C3H5)(PPh3)Br] by Nuclear Magnetic Resonance and Extended X-Ray Absorption Fine Structure. *J. Chem. Soc. Dalt. Trans.* **1994**, No. 9, 1337–1347. https://doi.org/10.1039/DT9940001337.
(47) Hyder, I.; Jiménez-Tenorio, M.; Puerta, M. C.; Valerga, P. Oligomerization and Regioselective Hydrosilylation of Styrenes Catalyzed by Cationic Allyl Nickel Complexes Bearing Allylphosphine Ligands. *Dalt. Trans.* **2007**, No. 28, 3000–3009. https://doi.org/10.1039/b705579j.
(48) Broomfield, L. M.; Boschert, D.; Wright, J. A.; Hughes, D. L.; Bochmann, M. Synthesis of Neutral and Zwitterionic Phosphinomethylpyrrolato Complexes of Nickel. *J. Organomet. Chem.* **2009**, *694* (25), 4084–4089. https://doi.org/10.1016/j.jorganchem.2009.08.033.
(49) Martín, M. T.; Marín, M.; Maya, C.; Prieto, A.; Nicasio, M. C. Ni(II) Precatalysts Enable Thioetherification of (Hetero)Aryl Halides and Tosylates and Tandem C−S/C−N Couplings. *Chem. - A Eur. J.* **2021**, *27* (48), 12320–12326. https://doi.org/10.1002/chem.202101906.

(50) Berthel, J. H. J.; Krahfuß, M. J.; Radius, U. Nickel Tetracarbonyl as Starting Material for the Synthesis of NHC-Stabilized Nickel(II) Allyl Complexes. *Z. Anorg. und Allg. Chem.* **2020**, *646* (13), 692–704. https://doi.org/10.1002/zaac.201900326.
(51) Churchill, M. R.; O'Brien, T. A. The Crystal and Molecular Structure of Dimeric 2-Carboxyethyl-Π-Allylnickel Bromide. *Inorg. Chem.* **1967**, *6* (7), 1386–1390. https://doi.org/10.1021/ic50053a022.
(52) Massa, W.; Faza, N.; Kang, H.-C.; Focke, C.; Heitz, W. Combining Oxidative Addition and Polymerization: A Study towards the Synthesis of Macromonomers. *Acta Polym.* **1997**, *48* (10), 432–437. https://doi.org/https://doi.org/10.1002/actp.1997.010481003.
(53) Johnson, J. R.; Tully, P. S.; Mackenzie, P. B.; Sabat, M. A Practical Reversed-Polarity Alternative to Organocuprate Conjugate Addition Chemistry. Halocarbon Coupling Reactions of Enal- and Enone-Derived Allylnickel Reagents. *J. Am. Chem. Soc.* **1991**, *113* (16), 6172–6177. https://doi.org/10.1021/ja00016a037.
(54) McMullen, A. K.; Tilley, T. D.; Rheingold, A. L.; Geib, S. J. Trialkoxysiloxy Complexes of Nickel. Molecular Structures of $Na_3(\mu_3\text{-}I)\{Ni[\mu_3\text{-}OSi(OtBu)_3]_3I\}\cdot 0.5THF\cdot 0.5C_5H_{12}$ and $\{(\eta^3\text{-}C_3H_5)Ni[\mu_2\text{-}OSi(OtBu)_3]\}_2$. *Inorg. Chem.* **1990**, *29* (12), 2228–2232. https://doi.org/10.1021/ic00337a010.
(55) Lee, B. Y.; Kim, Y. H.; Shin, H. J.; Lee, C. H. Synthesis, Molecular Structures, and Norbornene Polymerization of Methallyl Nickel (II) Complexes of 2-(Diphenylamino)Benzoate. *Organometallics* **2002**, *21* (16), 3481–3484. https://doi.org/10.1021/om020134g.
(56) Yamashita, K. ichiro; Takeda, H.; Kashiwabara, T.; Hua, R.; Shimada, S.; Tanaka, M. Ni-Catalyzed Addition Reaction of Allylic Selenides to Alkynes. *Tetrahedron Lett.* **2007**, *48* (38), 6655–6659. https://doi.org/10.1016/j.tetlet.2007.07.112.
(57) Wells, A. F. *Structural Inorganic Chemistry*; Oxford University Press: Oxford, 2012.
(58) Kruger, C.; Sekutowski, J. C.; Berke, H.; Hoffman, R. Bis [-Mu-Methyl-1,3-Dimethyl-H3-Allyl-Nickel] The Bonding in an Alkyl-Bridged Ni-Ni System. *Z. Naturforsch.* **1978**, *33b*, 1110–1115.
(59) Buntine, M. A.; Hall, V. J.; Kosovel, F. J.; Tiekink, E. R. T. Influence of Crystal Packing on Molecular Geometry: A Crystallographic and Theoretical Investigation of Selected Diorganotin Systems. *J. Phys. Chem. A* **1998**, *102* (14), 2472–2482. https://doi.org/10.1021/jp9728722.
(60) Schraml, J.; Čapka, M.; Blechta, V. 31P and 13C NMR Spectra of Cyclohexylphenylphosphines, Tricyclohexylphosphine and Triphenylphosphine. *Magn. Reson. Chem.* **1992**, *30* (6), 544–547. https://doi.org/10.1002/mrc.1260300615.
(61) Walter, D.; Wilke, G. Pi-Allylnickel Bromide under the Influence of Phosphines and Phosphites. *Angew. Chem. - Int. Ed.* **1966**, *5* (10), 897–898.
(62) Carmona, E.; Palma, P.; Poveda, M. L. Eta-3-2-Methylallyl Phosphine Complexes of Nickel(II). *Polyhedron* **1990**, *9* (5), 757–761.
(63) Brunkan, N. M.; Jones, W. D. Preparation, Structure, and Dynamics of a Nickel π-Allyl Cyanide Complex. *J. Organomet. Chem.* **2003**, *683* (1), 77–82. https://doi.org/10.1016/S0022-328X(03)00431-5.
(64) Maryasin, B.; Zipse, H. Theoretical Studies of 31P NMR Spectral Properties of Phosphanes and Related Compounds in Solution. *Phys. Chem. Chem. Phys.* **2011**, *13* (11), 5150–5158. https://doi.org/10.1039/c0cp02653k.
(65) Dible, B. R.; Sigman, M. S. Steric Effects in the Aerobic Oxidation of π-Allylnickel(II) Complexes with N-Heterocyclic Carbenes. *Inorg. Chem.* **2006**, *45* (20), 8430–8441. https://doi.org/10.1021/ic0612451.
(66) Dible, B. R.; Sigman, M. S. Unusual Reactivity of Molecular Oxygen with π-Allylnickel(N-Heterocyclic Carbene) Chloride Complexes. *J. Am. Chem. Soc.* **2003**, *125* (4), 872–873. https://doi.org/https://doi.org/10.1021/ja0286876.
(67) Silva, L. C.; Gomes, P. T.; Veiros, L. F.; Pascu, S. I.; Teresa Duarte, M.; Namorado, S.; Ascenso, J. R.; Dias, A. R. Synthesis, Structure, and Solution Dynamics of Neutral Allylnickel Complexes of N-Heterocyclic Carbenes. *Organometallics* **2006**, *25* (18), 4391–4403. https://doi.org/10.1021/om060444p.
(68) Tamaki, T.; Ohashi, M.; Ogoshi, S. [3+2] Cycloaddition Reaction of Cyclopropyl Ketones With

Alkynes Catalyzed By Nickel/Dimethylaluminum Chloride. *Angew. Chem. - Int. Ed.* **2011**, *50* (50), 12067–12070. https://doi.org/10.1002/anie.201106174.

(69) Martin, A. R.; Nelson, D. J.; Meiries, S.; Slawin, A. M. Z.; Nolan, S. P. Efficient C-N and C-S Bond Formation Using the Highly Active [Ni(Allyl)Cl(IPr*OMe)] Precatalyst. *European J. Org. Chem.* **2014**, *2014* (15), 3127–3131. https://doi.org/10.1002/ejoc.201402022.

(70) Fernandez-Salas, J. A.; Marelli, E.; Cordes, D. B.; Slawin, A. M. Z.; Nolan, S. P. General and Mild Ni0-Catalyzed Alpha-Arylation of Ketones Using Aryl Chlorides. *Chem. Eur. J.* **2015**, *21* (10), 3906–3909. https://doi.org/https://doi.org/10.1002/chem.201406457.

(71) Hazlehurst, R. J.; Hendriks, S. W. E.; Boyle, P. D.; Blacquiere, J. M. Ligand Dynamics and Aerobic Allylic Oxidation with Bifunctional Ni(NHC) Complexes. *ChemistrySelect* **2017**, *2* (23), 6732–6737. https://doi.org/10.1002/slct.201701609.

(72) Nazari, S. H.; Bourdeau, J. E.; Talley, M. R.; Valdivia-Berroeta, G. A.; Smith, S. J.; Michaelis, D. J. Nickel-Catalyzed Suzuki Cross Couplings with Unprotected Allylic Alcohols Enabled by Bidentate N-Heterocyclic Carbene (NHC)/Phosphine Ligands. *ACS Catal.* **2018**, *8* (1), 86–89. https://doi.org/10.1021/acscatal.7b03079.

(73) Frosch, J.; Freytag, M.; Jones, P. G.; Tamm, M. Nickel(II) Allyl Complexes with Anionic N-Heterocyclic Carbene-Borate Ligands. *J. Organomet. Chem.* **2020**, *918*, 121311. https://doi.org/10.1016/j.jorganchem.2020.121311.

(74) Degroot, H. P.; Hanusa, T. P. Solvate-Assisted Grinding: Metal Solvates as Solvent Sources in Mechanochemically Driven Organometallic Reactions. *Organometallics* **2021**, *40* (21), 3516–3525. https://doi.org/10.1021/acs.organomet.1c00316.

(75) Ray, B.; Neyroud, T. G.; Kapon, M.; Eichen, Y.; Eisen, M. S. Synthesis, Characterization, and Catalytic Activities for the Polymerization of Olefins Promoted by Zirconium(III) and Titanium(III) Allyl Complexes. *Organometallics* **2001**, *20* (14), 3044–3055. https://doi.org/10.1021/om0009942.

(76) Zhao, Y. H.; Abraham, M. H.; Zissimos, A. M. Fast Calculation of van Der Waals Volume as a Sum of Atomic and Bond Contributions and Its Application to Drug Compounds. *J. Org. Chem.* **2003**, *68* (19), 7368–7373. https://doi.org/10.1021/jo034808o.

(77) Guzei, I. A.; Wendt, M. An Improved Method for the Computation of Ligand Steric Effects Based on Solid Angles. *J. Chem. Soc. Dalton Trans.* **2006**, No. 33, 3991–3999. https://doi.org/10.1039/b605102b.

(78) Stewart, R. F.; Davidson, E. R.; Simpson, W. T. Coherent X-Ray Scattering for the Hydrogen Atom in the Hydrogen Molecule. *J. Chem. Phys.* **1965**, *42* (9), 3175–3187. https://doi.org/10.1063/1.1696397.

(79) Cooper, R. I.; Thompson, A. L.; Watkin, D. J. CRYSTALS Enhancements: Dealing with Hydrogen Atoms in Refinement. *J. Appl. Crystallogr.* **2010**, *43* (5 PART 1), 1100–1107. https://doi.org/10.1107/S0021889810025598.

(80) Goddard, R.; Krüger, C.; Mark, F.; Stansfield, R.; Zhang, X. The Effect upon the Hydrogen Atoms of Bonding an Allyl Group to a Transition Metal. A Theoretical Investigation and an Experimental Determination Using Neutron Diffraction of the Structure of Bis(η^3-Allyl) Nickel. *Organometallics* **1985**, *4* (2), 285–290. https://doi.org/10.1021/om00121a014.

(81) Ellison, G. B.; Davico, G. E.; Bierbaum, V. M.; DePuy, C. H. Thermochemistry of the Benzyl and Allyl Radicals and Ions. *Int. J. Mass Spectrom. Ion Process.* **1996**, *156* (1–2), 109–131. https://doi.org/10.1016/s0168-1176(96)04383-2.

(82) Bottoni, A.; Miscione, G. Pietro; Novoa, J. J.; Prat-Resina, X. DFT Computational Study of the Mechanism of Allyl Halides Carbonylation Catalyzed by Nickel Tetracarbonyl. *J. Am. Chem. Soc.* **2003**, *125* (34), 10412–10419. https://doi.org/https://doi.org/10.1021/ja030100f.

(83) Corey, E. J.; Semmelhack, M. F.; Hegedus, L. S. The Course of Allylic Coupling Reactions Involving Allylnickel Complexes. *J. Am. Chem. Soc.* **1968**, *90* (9), 2416–2417. https://doi.org/https://doi.org/10.1021/ja01011a035.

(84) Langmaier, J.; Samec, Z.; Varga, V.; Horacek, M.; Coukroun, R.; Mach, K. Cyclic Voltammetry of Methyl- and Trimethylsilyl-Substituted Zirconocene Dichlorides. *J. Organomet. Chem.* **1999**, *584*

(2), 323–328. https://doi.org/https://doi.org/10.1016/S0022-328X(99)00170-9.
(85) Bogdanović, B.; Bonnemann, H.; Wilke, G. Pi-Allylmethylnickel. *Angew. Chem. internat. Ed.* **1966**, *5* (6), 582–583.
(86) Tolman, C. A. Steric Effects of Phosphorus Ligands in Organometallic Chemistry and Homogeneous Catalysis. *Chem. Rev.* **1977**, *77* (3), 313–348. https://doi.org/10.1021/cr60307a002.
(87) Gmernicki, K. R.; Hong, E.; Maroon, C. R.; Mahurin, S. M.; Sokolov, A. P.; Saito, T.; Long, B. K. Accessing Siloxane Functionalized Polynorbornenes via Vinyl-Addition Polymerization for CO2Separation Membranes. *ACS Macro Lett.* **2016**, *5* (7), 879–883. https://doi.org/10.1021/acsmacrolett.6b00435.
(88) Herberg, C.; Verevkin, S. P.; Nolke, M.; Beckhaus, H.-D.; Ruchardt, C. Kinetics of the Generation of 1,3-Di-Tert-Butylallyl Radicals by Thermal CC Bond Cleavage Reactions. *Liebigs Ann.* **1995**, *1995* (3), 515–522.

Chapter 4: Leveraging the Steric Stabilization of the 1,3-bis(*tert*-butyl)allyl Ligand to Access Novel Species and Isolate Elusive Compounds

Abstract:

The steric stability conferred upon metal complexes by bulky, 1,3-disubstituted allyl ligands has been noted. However, complexes featuring these ligands have thus far been restricted to common, well-studied archetypes, where this additional stability is of limited consequence. Here, the bromide-bridged bimetallic complex [{A^{2t}NiBr}$_2$], featuring the bulky 1,3-bis(*tert*-butyl)allyl (A^{2t}) ligand, is used as a convenient synthon for a variety of heteroleptic allylnickel complexes. These include putative catalytic intermediates that have not been previously isolated, such as [{A^{2t}NiOH}$_2$], as well a rare fluorenylnickel complex. The impact of the bulky allyl substituents on the structure and reactivity of these complexes is discussed, and a preliminary analysis of the complex stereochemistry is included.

4.1 Introduction:

As discussed in previous chapters, transition metal allyl complexes are a broadly important class of molecules. Isolated allylmetal compounds have been used as precatalysts for polymerization[1–4] and cross-coupling reactions,[5–10] and allyl metal species are commonly invoked as reaction intermediates. Given the broad relevance of these compounds, understanding their dynamics and reactivity is highly desirable. The application of sterically bulky groups has been shown to substantially stabilize nickel complexes compared to the unsubstituted parent allyl ($C_3H_5^-$ = A).[11,12] However, the only bulky allyl complexes that have been studied previously fall within the extremely well-studied [M(allyl)$_2$] and [{(allyl)NiX}$_2$] motifs. Given their known ability to impart kinetic stability, bulky allyls might appear to be useful tools in isolating compounds outside the most stable motifs. A particularly interesting case is that of allylnickel complexes with mixed organic ligands. While certain classes of such heteroleptic compounds are stable,[13,14] many undergo rapid disproportionation to a mixture of the corresponding homoleptic complexes.[15–17] Given that the installation of bulky groups to the 1 and 3 carbons of the allyl backbone is known to dramatically slow mechanisms of allyl interconversion,[11] this represents a difficulty that bulky allyls are well-suited to address.

The extra stability provided by the bulky allyl ligands might also be useful in isolating elusive catalytic intermediates. One class of particularly elusive species are compounds of the form [{(allyl)MER_n}$_2$] (M = Ni, Pd, Pt; E = N, O, S). The dearth of isolated and structurally characterized of group 10 allylmetal complexes with heteroatom ligands is partially due to the difficulty in handling these compounds. While early ideas of the inherent weakness of M-ER_n bonds have been shown to be incorrect, they are nonetheless highly polarized, and as such tend to be highly basic.[18] Therefore, in the absence of steric stabilization, such [{A^{2t}NiER_n}$_2$] complexes are expected to be highly reactive. This is unfortunate, as such species are often invoked as intermediate in important organic transformations.

The case of nickel oxo compounds demonstrates this well. Nickel is one of the premier metals for use in catalytic cycles that begin with allylic C-O activation. In particular, it has been notably successful at utilizing allyl alcohol as an alternative allyl source to toxic allyl halides.[19–24] Activation of allyl ethers is also notable.[19] These reactions often proceed through allylnickel intermediates containing both allyl and alkoxide/hydroxide ligands. Furthermore, bridged hydroxo species have been implicated in nickel-catalyzed Suzuki-Miyaura reactions,[25] including those proceeding through an η^3-allylnickel intermediate,[26,27] as well as in certain allylation reactions.[28] Finally, isolated allylnickel alkoxide species themselves have been shown to be effective catalysts for the polymerization of dienes[29] and the dimerization of short-chain olefins.[30] Despite this broad importance, no hydroxo- nor aryloxo-nickel allyl complexes have ever been structurally characterized, leaving an important gap in the understanding of structure-reactivity relationships. A similar situation is seen in the case of amido ligands;[6,8] while the relevant

landscape for heavier chalcogenide-bound ligands is better explored, there are still significant gaps in understanding.

It has been established that [{(allyl)NiX}$_2$] compounds can undergo salt metathesis reactions, replacing the bridging halides with other anions.[17,30,31] We recently reported on the preparation of [{A^{2t}NiBr}$_2$] and found that it was more stable and much easier to work with than complexes of the unsubstituted parent allyl ligand. It was expected that, by virtue of the steric stabilization of the [A^{2t}]$^-$ ligand and the presence of a labile bromide ligand, a variety of different anionic ligands could be installed, expanding the range of allylnickel complexes amenable to full characterization. It should be noted that a handful of published papers[17,30,32–34] make reference to similar work done in the Wilke group, in which anionic ligands are reacted with the parent allylnickel bromide dimer to successfully yield complexes of the form [{ANiER$_n$}$_2$] (E = O, S, N). However, to our knowledge, these secondhand references are the only presence of this metathetical work in peer-reviewed literature; publication of the investigations themselves is limited to dissertations that are not electronically available,[35–39] if published at all. Given the poor availability of this knowledge, along with the advancements in spectroscopic and crystallographic methods in the ensuing 50 years, the following studies provide valuable insight.

4.2 Results and Discussion:

4.2.1 Initial efforts towards alkyl or hydride bridged complexes

Our initial efforts focused on organic or organic-adjacent ligand types. The first target was the nickel hydride complex [{A^{2t}NiH}$_2$]. The generation of the analogous complex of the parent allyl ([$C_3H_5^-$], A) was inferred in a previous report, but was found to be unstable even at -178 °C; its presence was diagnosed from analysis of decomposition products.[16] It was hypothesized that the kinetic stabilization provided by the bulky A^{2t} ligand might be useful here. Disappointingly, though, treatment of [{A^{2t}NiBr}$_2$] with sodium triethylborohydride at room temperature induced immediate deposition of nickel, clear evidence of decomposition.

Attention was therefore turned to the methyl-bridged species. This compound was also reported in the 1960s, and was sufficiently stable to be isolated, though only at -78 °C. The compound was reported to be violet and had its proton NMR spectrum described, but no other characterization was given.[14] Interestingly, when the original synthetic method was attempted using [{A^{2t}NiBr}$_2$] and a Grignard reagent, no reaction was observed, and unchanged [{A^{2t}NiBr}$_2$] was recovered. The same thing was observed when using methyllithium in a purely ethereal solvent system. The cause of this is unclear, as the MeLi is expected to be a potent nucleophile. However, when a mixture of hexanes and diethyl ether were used as the solvent system, an immediate color change to black was observed, and solid began to collect at the bottom of the vial. The parent compound discussed above was reported to decompose cleanly via disproportionation,

yielding bis(allyl)nickel and nickel black, with the production of ethane inferred. However, a ^{1}H NMR of the material collected from this reaction showed no evidence of the allyl moiety at all, merely an extremely complex set of upfield peaks. This suggests that the *t*Bu groups of the allyl were sufficient to prevent some, but not all accessible, decomposition pathways. The loss of all allylic NMR signals suggests that the allyl groups are involved in this decomposition; this could proceed via direct reductive elimination of A^{2t}-Me, which would perhaps be sufficiently volatile to be lost under vacuum, or perhaps via a γ C-H activation of the *t*Bu group. In an attempt to avoid this by further increasing the steric bulk of both ligands in the desired product, we attempted the same reaction with trimethylsilylmethyllithium. This caused immediate decomposition, even in ethereal solvent.

4.2.2 Delocalized organic anions.

4.2.2.1 Synthesis and Characterization

As reaction with localized organic anions roundly failed to yield compounds stable at room temperature, we moved to consider delocalized organic anions. The simplest and by far the most well precedented examples of the [A^xNiR] archetype are those where R = an allyl group - that is to say, bis(allyl)nickel complexes, [A^xNiA^y]. Of course, nearly all examples of these are homoleptic, such that A^x = A^y. This is due to the apparent ease of disproportionation, with reactions of allylic Grignard reagents A^yMgBr with [{A^xNiBr}$_2$] yielding mixtures of [NiA^x_2] and [NiA^y_2] in almost all cases.[17,40] Previous study of the homoleptic nickel complex of the related A´ ligand showed that common allylic rotation processes are not accessible at room temperature; this suggests that bulky groups can be placed at the terminal allyl carbons in order to prevent most, if not all, mechanisms for allyl interconversion at room temperature.[11] We hypothesized that the mechanisms for intramolecular and intermolecular allyl exchange might be related, and that added bulk might also suppress disproportionation. We endeavored to test this by reacting [{A^{2t}NiBr}$_2$] with KA´. While [NiA^{2t}_2] is not a known species, [NiA´$_2$] is known to be highly stable and has been well characterized by NMR, and therefore can serve as an effective spectroscopic tag for identifying disproportionation.

Gratifyingly, ^{1}H NMR analysis of the product mixture from [{A^{2t}NiBr}$_2$] and KA´ showed six new sets of allyl peaks, three corresponding to A^{2t} ligands and three corresponding to A´ ligands, all being consistent with η^3 binding. The contents of the product mixture did not meaningfully differ when the reaction was performed at -78 °C or at room temperature. Each set of A^{2t} peaks in the ^{1}H NMR spectrum had a set of A´ peaks of matching intensity. Notably, no more than trace [NiA´$_2$] was observed, and more [NiA´$_2$] did not form upon sitting for weeks. Together, this NMR analysis strongly suggests the formation of mixed A^{2t}-A´ bis(allyl) complexes of the form [A^{2t}NiA´]. Furthermore, the ratio of the three presumed

isomers does not change over weeks, and no additional [NiA´$_2$] is formed, suggesting that redistribution is completely suppressed at room temperature.

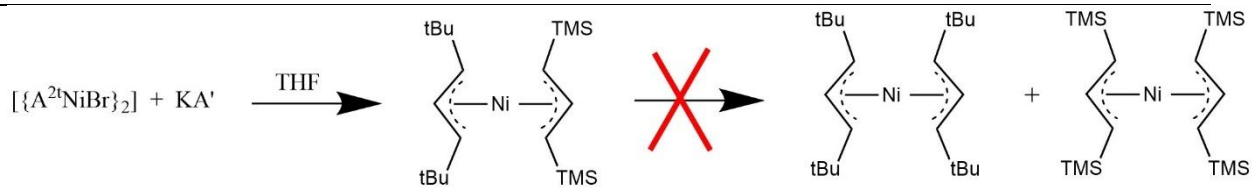

Figure 4.1: Formation of mixed allyl species [A^{2t}NiA´], which is stable to ligand redistribution.

Despite this, the initial orange-yellow oil becomes slightly opaque over time. Furthermore, on two occasions, crystals obtained from long crystallizations of [A^{2t}NiA´] were instead found to be [{A^{2t}Ni(OH)}$_2$]. The most obvious explanation would be via exposure to water, but there are two factors that make this result unexpected. First, [A^{2t}NiA´] might be expected to display similar hydrolytic stability to the related [NiA´$_2$], whose solution in hexane could be layered above water and allowed to sit for hours before visible decomposition was evident,[11] and even the parent bis(A) complex of nickel is reported to be resistant to degradation by water.[3] Second, based on the computationally derived relative basicities of the two ligands,[12] protonation of [A^{2t}]$^-$ would be expected to occur preferentially. A plausible explanation for this discrepancy cannot be supplied at this time, and further work is required to crystallographically characterize this compound and fully elucidate its reactivity. Stereochemical considerations are discussed below in section 4.2.2.2.

But is it required for both allyls to be bulky to achieve this effect? Reaction of [{A^{2t}NiBr}$_2$] with allyl magnesium bromide produced a light-yellow oil. ^{1}H NMR analysis of this mixture showed two equal intensity pairs of A and A^{2t} peaks. However, the unsubstituted allyl peaks closely matched those reported for [NiA$_2$],[17] suggesting complete redistribution. Furthermore, the eclipsed and staggered isomers of [NiA$_2$] are reported to equilibrate at room temperature;[41] therefore, the ratio of the two isomers should be constant when measured at room temperature. Indeed, the ratio of the two parent allyl peaks is similar to that reported for isolated [NiA$_2$] (2.1 : 1 *st*:*ec* compared to 2.6 : 1). However, these peaks did not disappear after exposure to vacuum nor after sitting for weeks; this was unexpected, as [NiA$_2$] is reported to decompose below room temperature and be volatile. Given the expected similarity between [NiA$_2$] and [A^{2t}NiA], it is conceivable that there is not a meaningful difference in NMR shifts between the two. Future experiments will conclusively establish the identity of these compounds by applying heat, which may either cause the loss of [NiA$_2$] by evaporation or by causing shifts in the isomer ratios observed, allowing for conclusive determination of which allyls, if any, are bound to the same metal center.

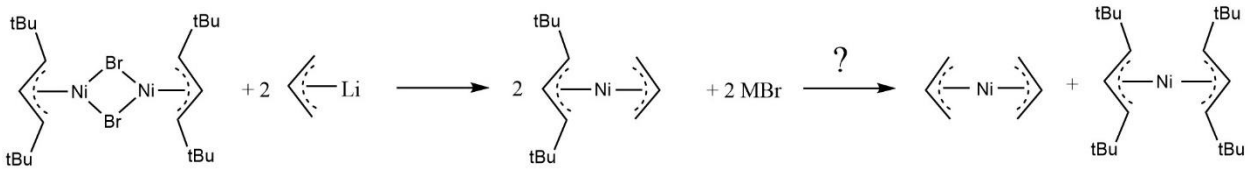

Figure 4.2: Proposed formation of [A^{2t}NiA], which likely undergoes ligand redistribution to form [NiA^{2t}_2] and [NiA_2].

While the benzyl ligands are a distinct class from allyls, they are related by frequently binding through delocalized π electrons with η^3 hapticity. Indeed, benzylnickel complexes have been reported that mimic common structural motifs seen in allylnickel compounds.[42,43] Therefore, we were curious if a mixed allyl/benzyl compound of nickel would be stabilized by the bulky A^{2t}. Reaction of [{A^{2t}NiBr}$_2$] with benzylpotassium yielded a dark orange material. ^{1}H NMR analysis of the isolated material showed a highly complex mixture with both sharp and highly broadened peaks. Further study was hampered as the material darkened completely to a black paste after sitting overnight. It is possible that substituted benzyls would be less prone to decomposition, but this has not yet been pursued.

Perhaps the most ubiquitous ligand in organometallic chemistry is the cyclopentadienyl ligand. It is therefore not surprising that Cp complexes are among the most well studied allylnickel derivatives.[13,31,44] Preparation of an A^{2t}-Ni-Cp complex was therefore a natural place to begin this investigation. Reaction of NaCp with [{A^{2t}NiBr}$_2$] at room temperature caused an immediate color change to a translucent charcoal color. Workup isolates a reddish-gray residue that NMR and single-crystal X-ray crystallography confirm as [A^{2t}NiCp] (**26**).

In contrast to its unsubstituted analogue, [A^{2t}NiCp] degrades only slowly in air, and appears indefinitely stable in the glovebox atmosphere. The compound is exceedingly soluble in organic solvents, even dissolving in crystal mounting oil within seconds at room temperature. While the compound is a solid, it does appear to be somewhat volatile; if stored in a plastic capped glass vial, material is gradually lost from the bottom of the vial while the vial cap becomes increasingly black. Some material dissolves upon washing the vial, but the black coloration remains, implying that some degree of degradation is occurring, although the cause of this is unclear. The parent [ANiCp] is a volatile liquid at room temperature, so this behavior is not unexpected.[31]

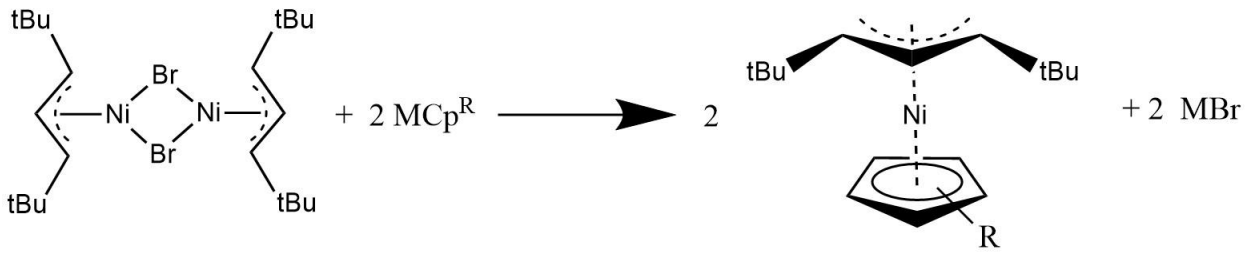

Figure 4.3: Formation of A^{2t}-Ni complexes with Cp type ligands.

NMR analysis suggests that only one isomer is present, with the *t*Bu groups in a *syn,syn* orientation. This contrasts with reported results of the formation of 1- or 1,3-substituted allylnickel-Cp compounds via the reaction of nickelocene with dienes in the presence of Grignard reagents. In these reactions, mixtures of *syn* and *anti* isomers were always observed; indeed, in three cases, the *anti* isomer was the dominant product.[13] *Syn* substituents were generally more stable, though, as evidenced by enrichment of the *syn* isomers upon overcoming the thermal barrier to interconversion. The one exception to this was [(1-isopropyl-2-methylallyl)NiCp], which displayed a 5 : 95 *syn* to *anti* isomer ratio that did not change with heating. This isopropyl substituent is the most like the *t*Bu groups considered in this work, making this discrepancy particularly noteworthy. This discrepancy was investigated computationally. Both the syn,syn and *syn,anti* isomers of [A^{2t}NiCp] were geometrically optimized (See Appendix 1 for computational methods) to a minimum, and their relative energies compared. The *syn,syn* isomer was found to be more stable by 17.4 kJ/mol; this energy difference corresponds to a greater than 99 : 1 isomer ratio for the compound at equilibrium. On this basis, it is proposed that the observed anti preference for [(1-isopropyl-2-methylallyl)NiCp] is a result of kinetic trapping that could not be overcome at 90 °C, rather than an expression of thermodynamic preference. It has been shown that bulky substituents indeed do increase the temperature required to access *syn/anti* interconversion.[11]

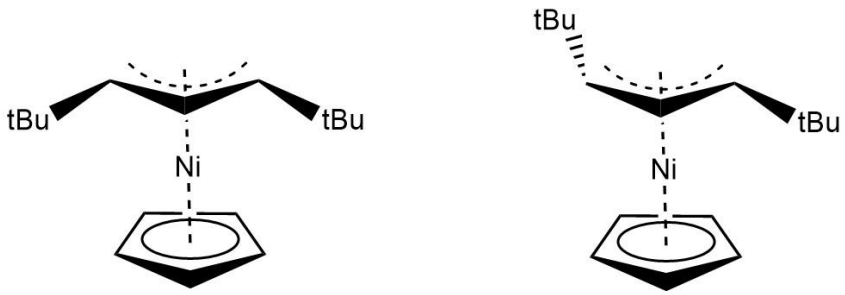

[*syn,syn*-A^{2t}NiCp] [*syn,anti*-A^{2t}NiCp]

0 kJ/mol 17.4 kJ/mol

Figure 4.4: Structures of the *syn,syn* and *syn,anti* isomers of 26, including computed relative energies.

As the volatility of [A^{2t}NiCp] decreased its ability to be easily stored for long periods, a homologous compound featuring the pentamethylcyclopendienyl ligand (Cp*) was sought. A Cp*-nickel complex of the parent allyl has been reported, though not structurally characterized.[45] The reaction of [{A^{2t}NiBr}$_2$] with KCp* produced a dark green, highly crystalline solid identified as [A^{2t}NiCp*] (**27**). Like **26**, only the *syn,syn* configuration is observed by NMR. This material undergoes the same sublimation as **26** when stored in a sealed vial, but dramatically slower, with only a slight green tint to the vial cap after sitting for months. We had concerns that increasing the electron donating ability of both ligands might decrease the compound's stability compared to the parent analogue, but [A^{2t}NiCp*] seems indefinitely stable in a glovebox atmosphere, and indeed a solution of the compound in a capped NMR tube took weeks to fully degrade after removal from the glovebox.

At first glance, the indenyl ligand might appear as simply a 1,2-disubstituted derivative of Cp. However, since observations in the late 1960s showed that indenyl-transition metal complexes underwent CO substitution reactions orders of magnitude faster than homologous Cp complexes,[46,47] indenyl complexes have been an area of distinct interest. This has been termed the "indenyl effect," and is most commonly attributed to the tendency of indenyl ligands to slip from η^5 to η^3. This slip is more favorable than expected for a Cp type ligand as it restores full local aromaticity to the attached benzenoid ring.[48] This is demonstrated by the archetypal bis(indenyl)nickel,[49] where the observation of substantial slippage is rationalized by the drive to decrease the formal 20e$^-$ count of a nickelocene-type structure.[50] In this way, indenide can be considered an intermediate ligand, whose bonding generally falls somewhere between the

extremes of allyl-type η^3 binding[51] and Cp-type η^5 binding.[50] However, despite their conceptual connections and the relative prominence of each ligand, only one mixed allyl/indenyl complex of nickel has been reported, and this was not structurally characterized.[45]

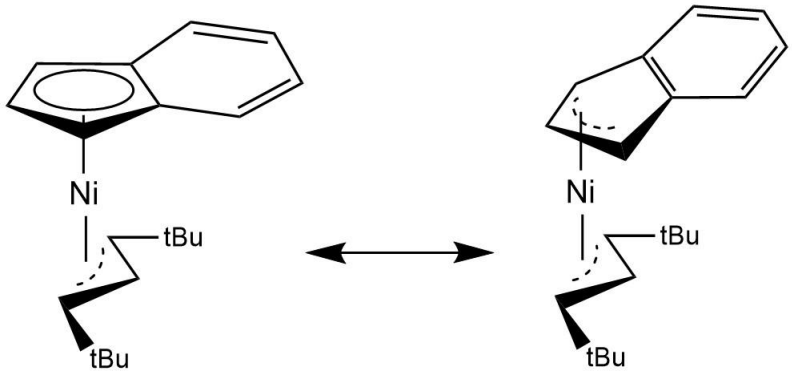

Figure 4.5: Diagram of the ring-slippage process in [A^{2t}NiInd], showing resonance between η^5 and η^3 binding modes.

Reaction of with potassium indenide produced a yellow orange oil whose ^{1}H NMR was suggestive of [A^{2t}NiInd]. In an effort to attain a simple NMR spectrum and a more crystalline product, the same reaction was performed using potassium 4,7-dimethylindenide. This reaction proceeded identically and yielded a highly crystalline orange product confirmed to be [A^{2t}NiInd^{2Me}] (**28**). A more detailed discussion of the crystal structure of this compound is included below, but the allyl is bound in the expected η^3, *syn,syn* manner, while the indenyl ligand is bound in an intermediate fashion between η^3 and η^5. However, unlike in the allyl complexes, no isomerism appears to be present in either of the indenyl complexes synthesized as determined by ^{1}H NMR. This is more consistent with the Cp complexes than the bis(allyl) complexes, suggesting that η^5 coordination is predominant in solution. While the five-membered ring structure of indene prevents any *syn*/*anti* isomerism, staggered/eclipsed isomerism would still be possible. In the crystal structure, the ligands are in a pseudo-staggered arrangement, and only one species is ever observed by NMR. Based on the lack of rotations observed for the more compact allyl ligands, it seems unlikely that eclipsed and staggered forms are in rapid equilibrium. Therefore, only the pseudo-staggered isomer appears to be formed. This is consistent with previous observations of bis(allyl) complexes with cyclic allyls, which were atypical in their lack of apparent eclipsed/staggered isomerism.[41]

One can consider the indenyl ligand as a cyclopentadienide with a fused benzene ring. If a second benzene ring is attached to the same 5-membered center cycle, one arrives at the fluorenyl ligand. In both indenide and fluorenide, the fused benzenoid rings concentrate negative charge in the non-bridging carbons

of the center five-membered ring. In the case of fluorenyl, this is only carbon 9; accordingly, Mulliken negative charge[52] and the HOMO[53] are calculated to be concentrated on this carbon. Despite this, the majority of transition metal fluorenyl complexes display η^5-binding, most notably those of the early transition metals that have a prominent place in stereospecific olefin polymerization.[54,55] Fluorenyl complexes of late transition metals, on the other hand, are very poorly studied, especially compared to the related ligands discussed above. In fact, to our knowledge, there exists only a single documented nickel-fluorenyl archetype reported in the literature, a pair of homoleptic trisfluorenyl nickelates.[56] It is possible that this is related to the observed lower stability of fluorenyl- compared to cyclopentadienyl complexes;[53] Therefore, the stabilizing [A^{2t}Ni-] fragment seemed an appropriate tool for the isolation of a rare fluorenylnickel compound.

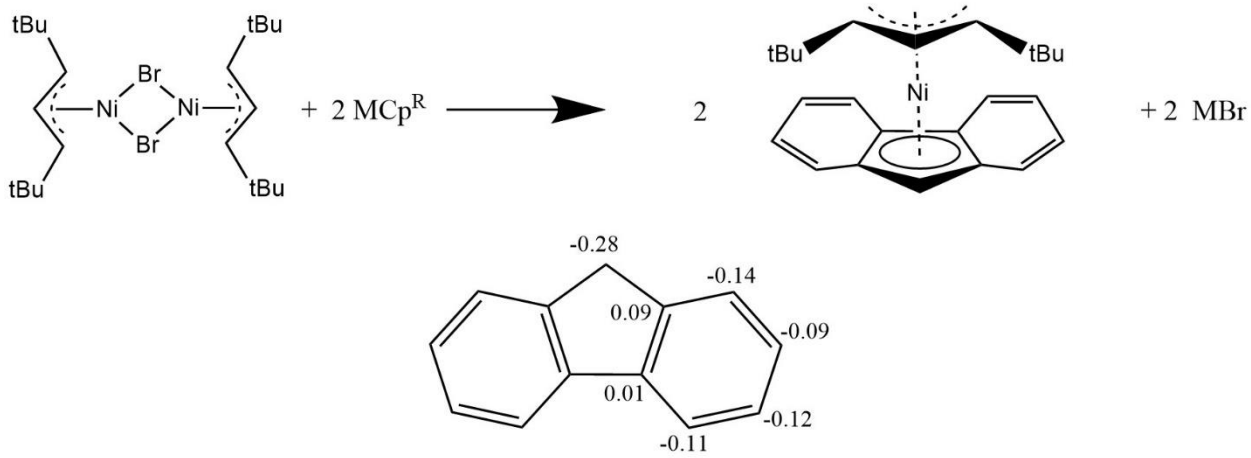

Figure 4.6: Reaction scheme of the formation of [A^{2t}NiFluor] (top) and calculated Mulliken charges of the fluorenyl anion[52] (bottom.)

The reaction of [{A^{2t}NiBr}$_2$] with potassium fluorenide was attempted in THF. Addition of KFluor induced an immediate color change to dark brick red; after sitting overnight, this color had changed to light orange. Indeed, upon work up, only decomposition products were observed; these products were later identified as [{A^{2t}NiOH}$_2$] and the protonated ligand HFluor. When attempted in toluene, no initial color change was observed after stirring for days, and ^{1}H NMR of the isolated material showed primarily HFluor, as well as a small amount of a new compound; no [{A^{2t}NiOH}$_2$] was observed. However, by running the reaction in THF and immediately working up the reaction, a red solid could be isolated in 65-85% yield. The ^{1}H NMR features of the red solid matched those of the new compound seen in previous reactions. Even isolated, the ^{1}H spectrum is very poorly resolved, with only the central allyl and fluorenyl protons appearing as highly sharp signals. The aryl and *t*Bu protons are highly broadened, and it is not clear that the terminal

allyl proton resonance is observable at all. This indicates a dynamic process on the timescale of the NMR experiment, presumably via some ring-slipped fluorenyl intermediate, but the nature of this process is not yet known. The aryl and *tert*-butyl peaks become slightly sharper when the spectrum is taken in THF, though the terminal allyl C-H peaks are still not observed; this could imply that interactions with a Lewis basic solvent inhibit the molecular motion causing the broadened features. However, even rapidly analyzed samples in THF show substantial decomposition, complicating analysis. An attempt to record the ^{1}H NMR spectrum of the molecule in d_6-DMSO showed only decomposition products.

Crystals grown from slow evaporation of a hexane solution allowed for the molecular structure of the compound to be determined, confirming its identity as [A^{2t}NiFluor] (**29**); the structure of the compound will be discussed in more detail below. This represents the first neutral nickel fluorenyl compound reported in the literature. Unlike the previously mentioned complexes of Cp-derived ligands, the fluorenyl complex is not indefinitely stable, substantially decomposing within 1-5 days at room temperature, even when stored in the solid state in a glovebox atmosphere. As basicity does increase in the sequence Cp^-, Ind^-, $Fluor^-$, the observed trend in stability was expected; however the extent to which [A^{2t}NiFluor] is less stable was surprising.[57–59] Decomposition is most clearly indicated by the deposition of colorless plates around and above the red solid, which also darkens to a dull brown. In every case, HFluor was observed as a decomposition product, and in most cases, [{A^{2t}NiOH}$_2$] (discussed below in Section 4.2.3.) As was observed for [A^{2t}NiA´], this suggests a simple explanation of the infiltration of adventitious water but again, one would expect for the A^{2t} to be the more basic ligand; the pK_a of fluorene is 22.6[59] compared to 44 for propene,[60] which is likely an underestimation of the true value for [HA^{2t}]. This would suggest unexpectedly high stability for the A^{2t}-Ni fragment, but other potential explanations are discussed in Section 4.2.4. It is worth noting that a related fluorenylcobalt compound is apparently stable at room temperature, and indeed survives for minutes after air exposure in the solid state,[61] making the apparent sensitivity of **29** somewhat surprising.

Given the apparent stability of the [A^{2t}Ni-η^5-R] motif, we also considered the possibility of similar bonding by heterocyclopentadienides, namely pyrrolide and imidazolate. While η^1 N-coordination is most common, η^5-binding to transition metals has been reported.[62–64] However, reactions with both anions gave results more consistent with amido nucleophiles (See Section 4.2.4.) The case of pyrollide will be discussed in Section 4.2.4, but the reaction with lithium imidazolate yielded a poorly soluble yellow material. The ^{1}H NMR of this material shows a complex mixture of many different allyl signals; these properties are consistent with the formation of multiple N,N'-μ^2-imidazolate bridged allyl nickel species. All attempts to grow crystals from this mixture have failed, so this identification remains unsubstantiated.

4.2.2.2 Structural and Bonding Considerations

Investigation of [A^{2t}NiA′] Stereochemistry

As [A^{2t}NiA′] has yet to be crystallographically characterized, other methods were employed to obtain insight into the stereochemistry of the three isomers observed. As the trimethylsilylated allyl complexes of nickel have been spectroscopically well-characterized (See Chapters 3 and 5), it was possible to use established trends to gain insight into the structure of the novel compound. From the ^{1}H-^{1}H coupling constants, it was found that all three A′ ligands displayed *syn,anti* configurations; both reported isomers of [NiA′$_2$] also display this configuration.[11] In [NiA′$_2$], the allylic proton signals of the staggered isomer display a larger spread of chemical shift values compared to the eclipsed isomer. Fortunately, the three new species also displayed two clearly distinct ranges of allylic ^{1}H shifts, allowing for each species to be assigned as staggered or eclipsed. Assigning the *syn/anti* configuration of the A^{2t} ligands was less trivial, as in general both the chemical shifts and coupling constants of *syn* and *anti* protons are less distinct for A^{2t} than A′. Both the most and least prominent product could be assigned with reasonable confidence, but the third product was ambiguous. Furthermore, no trends have yet been noted that allow *cis* and *trans* isomers to be distinguished spectroscopically.

Therefore, computational methods were employed to evaluate the plausibility of these assignments and to determine the most likely configuration of the final isomer. The ground state energies of a selection of plausible isomers of [A^{2t}NiA′] were computed, identifying the five configurations shown below as the most likely candidates for the observed isomers; computational methods and the full list of computed energies can be found in Appendix 4.

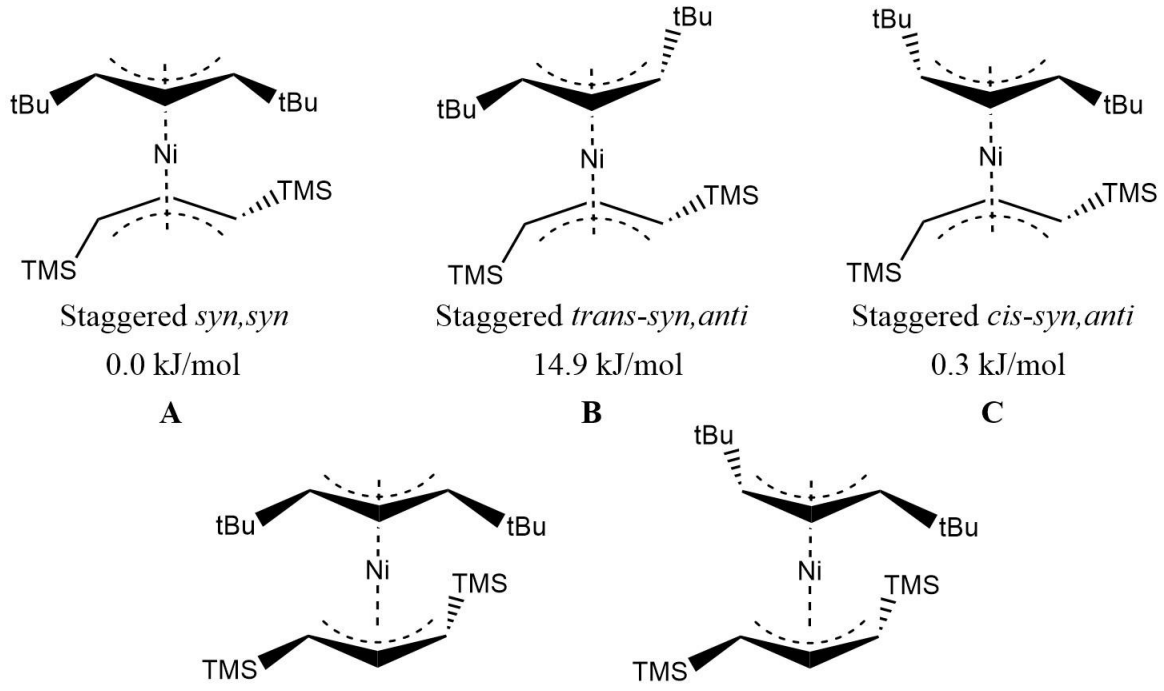

Figure 4.7: Five configurations of [A^{2t}NiA´] that are plausible identities for the three isomers observed spectroscopically. Each isomer is labelled with its stereochemical specifications, the computed energy relative to isomer A, and a letter label. In all cases, the substituents on the A´ ligand are in the *syn,anti* configuration, so this specification is omitted.

This analysis supported the assignment of the major product as isomer A. From the NMR data, D and E were the likely structures of the secondary product, while B and C were possible for the tertiary product. These computational results suggest that isomer B can be disregarded; this is sensible, as the staggered *trans syn,anti* arrangement places two pairs of -EMe_3 groups directly across from each other, maximizing steric interactions. The tertiary product is therefore assigned as isomer C. For the secondary product, both structures D and E remain plausible. However, the computed energies would suggest that C should be favored over both D and E; however, based on the experimental ^{1}H NMR spectrum, the secondary product (D or E) is approximately twice as abundant as C. Assigning the secondary product as isomer D allows this discrepancy to be rationalized, as the relative enrichment could be attributed to retention of the *syn,syn* configuration of the [{A^{2t}NiBr}$_2$] starting material.

Structures of [A^{2t}NiCp]-type Complexes

The structures of **26** and **27** are both broadly as expected. The Ni-C(allyl) distances are similar between **26** and **27** (ca. 2.112 and 1.942 Å compared to 2.042 and 1.951 Å, respectively), suggesting that the additional methyl groups are not sufficiently bulky to induce strain in the nickel-allyl interaction. These Ni-C(allyl) distances also do not substantially differ from those in [{A^{2t}NiBr}$_2$] (ca. 1.978 – 2.062 Å), indicating that the change from 4- to 5-coordinate nickel does not have a meaningful effect on the metal-ligand orbital overlap. Finally, the Ni-Cp distance is similar between **26** and [$CpNiC_6H_8NiCp$] (ca. 2.079 – 2.167 Å), indicating that the additional *t*-butyl groups do not substantially impact complex geometry.

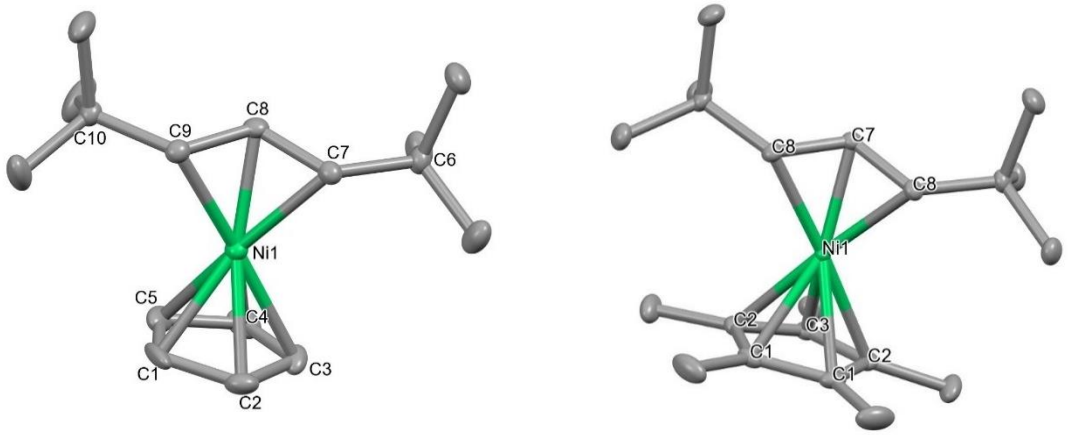

Figure 4.8: Thermal ellipsoid plot of the molecular structure of a) [A^{2t}NiCp] 26 and b) [A^{2t}NiCp*] 27 (50% probability). Hydrogen atoms are omitted for clarity. Selected bond distances (Å): a) Ni-C7, 2.205(2); Ni-C8, 1.942(2); Ni-C9, 2.018(2); Ni-C1, 2.054(6); Ni-C2, 2.098(9); Ni-C3, 2.116(6); Ni-C4, 2.178(10); Ni-C5, 2.117(10); C7-C8, 1.414(2); C8-C9, 1.416(2). b) Ni-C7, 1.951(2); Ni-C8, 2.042(1); Ni-C1, 2.110(1); Ni-C2, 2.145(1); Ni-C3, 2.208(2); C7-C8, 1.411(2).

Table 4.1: Structural data for allylnickel cyclopentadienyl complexes and related compounds

Compound	Ni-C(allyl terminal) (Å, avg.)	Ni-C (allyl center) (Å)	Ni-C(Cp) (avg.) (Å)	$\Delta C\text{-}C_{allyl}$[a]	$\Delta C\text{-}C_{Cp}$[a]	Ref.
[A^{2t}NiCp] (**26**)	2.112(2)	1.942(2)	2.113(10)	0.002(2)	0.047(2)	[b]
[A^{2t}NiCp*] (**27**)	2.042(1)	1.951(2)	2.154(2)	0	0.032(2)	[b]
[$CpNiC_6H_8NiCp$]	1.9556(4)	1.965(4)	2.107(4)	0.003(6)	0.09(6)	[65]
[{A^{2t}NiBr}$_2$]	2.05(1)	1.98(1)	NA	0.01(1)	NA	[b]
[$NiCp_2$]	NA	NA	2.178 (4)	NA	0.01	[66]

[a]) Defined as the difference between the longest and shortest C-C bonds in the core of the ligand, where core is the set of carbon atoms directly bound to nickel. [b]) This work.

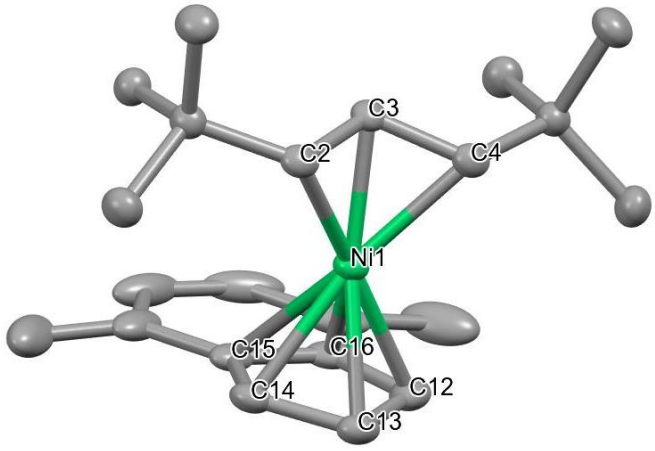

Figure 4.9: Thermal ellipsoid plot of the molecular structure of [A^{2t}NiInd^{2Me}] (50% probability). Hydrogen atoms are omitted for clarity. Selected bond distances (Å): Ni-C2, 2.025(7); Ni-C3, 1.957(2); Ni-C4, 2.030(4); Ni-C12, 2.088(7); Ni-C13, 2.061(3); Ni-C14, 2.089(5); Ni-C15, 2.316(3); Ni-C16, 2.310(3); C2-C3, 1.408(3); C3-C4, 1.412(6); C12-C13, 1.413(4); C13-C14, 1.410(6); C14-C15, 1.449(4); C15-C16, 1.418(6); C16-C12, 1.445(4).

The structure of [A^{2t}NiInd^{2Me}] is largely as expected. The Ni-C(allyl) bond lengths are similar to those in **26** and **27,** suggesting similar bonding interactions. The benzenoid ring on the allyl ligand therefore does not contribute substantial steric strain. The two ligands are in a pseudo-staggered arrangement, the same arrangement seen in structurally characterized bis(indenyl)nickel complexes.[50,67]

Table 4.2: Quantitative metrics of indenyl hapticity for [$A^{2t}NiInd^{2Me}$] and related compounds

Compound	$\delta\,^{13}C_{3a,\,7a}$	$\Delta^{13}C$[a]	M-$C_{1,3}$[b] (Å, avg)	M-$C_{3a,7a}$[b] (Å, avg.)	$\Delta_{M\text{-}C}$ (Å)[c]	HA (°)[d]	FA (°)[e]	Ref.
[$A^{2t}NiInd$]	119.8	-9.9	NA	NA	NA	NA	NA	[f]
[$A^{2t}NiInd^{2Me}$]	122.0	-7.7	2.089(6)	2.313(3)	0.224	8.7	9.1	[f]
[ANiInd]	120.1	-9.6	NA	NA	NA	NA	NA	[45]
[$NiInd_2$]	134.3	+3.6	2.062(3)	2.482(3)	0.418	13.9	13.1	[50]
[$NiInd^{tBu}{}_2$]	NA	NA	2.086(2)	2.483(2)	0.396	9.9	14.1	[67]
[IndNi(PPh_3)Cl]	125.9	-4.8	2.068(2)	2.311(2)	0.263	10.9	11.7	[68]
[$FeInd_2$][g]	87.0	-43.7	2.049(4)	2.090(4)	0.043	2.2	0.8	[50]
[IndIr($PMe_2Ph)_3$]	156.4	+25.7	2.235(14)	3.025(8)	0.790	NA	28	[51]

[a]) Calculated as the difference between the chemical shift of the 3a carbon in the complex and the 3a carbon in sodium indenide (δ 130.7 ppm.) [b]) The numbering system referenced here is that shown below in Figure 4.10, not that used above in Figure 4.9. [c])Defined as the difference of the average M-$C_{3a,7a}$ and M-$C_{1,3}$ bond lengths. [d]) HA = Hinge Angle; defined as the angle between the [C1, C2, C3] plane and the [C1, C3, C3a, C7a] plane. [e]) FA = Fold Angle; defined as the angle between the [C1, C2, C3] plane and the plane of the benzenoid ring. [f]) This work.

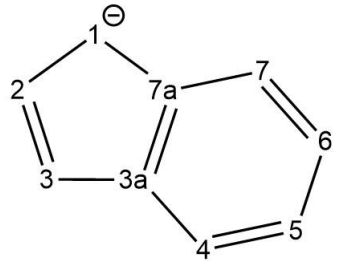

Figure 4.10: Numbering system used in discussions of indenyl complexes.

Table 4.2 shows several common metrics for quantifying the degree of $\eta^5 \rightarrow \eta^3$ slippage displayed by a metal-bound indenyl ligand. The two extremes are represented by [$FeInd_2$], displaying essentially pure η^5-binding, and [IndIr($PMe_2Ph)_3$], in which there is no meaningful interaction between the iridium center and carbons 3a and 7a. As expected for a nickel complex, all the metrics considered here fall well between these two extremes, confirming a partially slipped indenyl. Compared to known bis(indenyl)nickel species, the degree of slippage is slightly less ($\Delta_{M\text{-}C}$ of 0.396 vs. 0.224 for **28**); this is reasonable, as in the case of **28**, the η^5-binding mode leads to a 18e$^-$ configuration that is known to be stable, rather than the 20e$^-$

configuration in the bis(indenyl) complexes. While [ANiInd] has not been characterized, the similar diagnostic ^{13}C NMR shifts suggests that the additional *t*Bu groups did not meaningfully change the geometry of the molecule; the same can be said of the additional methyl groups of **28** compared to [A^{2t}NiInd].

29 crystallizes in the P_n space group with four distinct molecules in the unit cell; while distinct, the four molecules do not substantially differ, so all parameters discussed below will use values averaged over the four molecules. The allyl backbone is essentially perpendicular to the C21-C20-C24 section of the fluorenide; this is similar to the arrangement in **29**. The *t*Bu groups are both in the *syn* configuration. The fluorenyl ligand retains nearly ideal planarity, with an average angle of 3.7° between the central five-membered ring and the flanking benzenoid rings; there is no consistent difference in this fold angle between the two flanking rings. However, the bonds from nickel to carbons 23 and 24, opposite the allyl tip, are slightly shorter than those to carbons 21 and 22 (2.179 vs. 2.217 Å), adjacent to the allyl tip. This slight deformation is most probably attributable to steric interactions with the *tert*-butyl groups; that this displacement occurs rather than bending of the benzenoid ring demonstrates the rigidity of the fluorenyl ligand in comparison to indenyl.

Of particular note is the Ni-Fluor(centroid) distance in **29**, which is substantially shorter than that in the previously reported nickel fluorenyl compounds (1.793 vs. 1.858 and 1.834 Å for the lithium and sodium salts, respectively),[56] and is more similar to the value of 1.775 Å displayed by an isoelectronic cobalt complex.[61] It is unclear if this is indicative of a stronger Ni-Fluor interaction in **29** or merely a consequence of the net negative charge of the nickelate complexes.

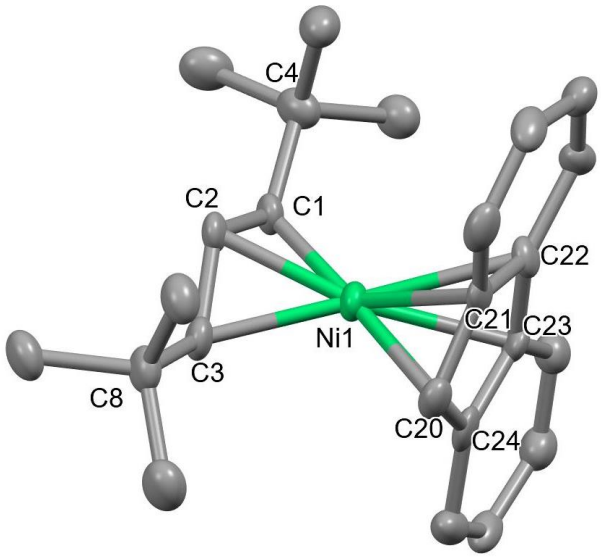

Figure 4.11: Thermal ellipsoid plot of the molecular structure of [A^{2t}NiFluor] (50% probability). Hydrogen atoms are omitted for clarity. For simplicity, only the carbons of the central fluorenyl five-membered ring are labelled. Selected bond distances (average, Å): Ni-C1, 2.049(7); Ni-C2, 1.953(5); Ni-C3, 2.016(6); Ni-C20, 2.062(5); Ni-C21, 2.191(6); Ni-C22, 2.242(7); Ni-C23, 2.210(6); Ni-C24, 2.147(6); C1-C2, 1.395(8); C2-C3, 1.409(10); C20-C21, 1.425(11); C21-C22, 1.423(8); C22-C23, 1.485(11); C23-C24, 1.427(9); C24-C20, 1.441(10).

Table 4.3: Collected quantitative hapticity parameters for L_nM-fluorenyl complexes.

Compound	M-$C_{10,13}$[a] (Å, avg)	M-$C_{11,12}$[a] (Å, avg.)	Δ_{M-C} (Å)[b]	δ_{C-C} (Å)[c]	ΔC-C_{benz} (Å)	Ref.
[A^{2t}NiFluor]	2.169(6)	2.226(7)	0.057	0.014	0.078	[d]
[Li(thf)$_4$][Ni(**η^5-Fluor**)(η^1-Fluor)$_2$]	2.204(2)	2.328(2)	0.124	0.006	0.061	56
[Li(thf)$_4$][Ni(η^5-Fluor)(**η^1-Fluor**)$_2$]	2.825(8)	3.689(8)	0.864	0.051	0.033	56
[(η^1-Fluor)Re(CO)$_5$]	3.209(7)	4.143(7)	0.934	0.095	0.041	69
Tetrahydrobenzo[b]-η^3-fluorenyl-adamantylamidotitanium	2.389(6)	2.585(7)	0.196	0.038	0.069	70
[*ansa*-Me_2C(Cp)(η^5-Fluor)Zr]	2.515(8)	2.658(7)	0.143	0	0.09	71

[a]) The numbering system referenced here is that shown below in Figure 4.12, not that used above in Figure 4.11. [b])Defined as the difference of the average M-$C_{3a,7a}$ and M-$C_{1,3}$ bond lengths. [c]) Defined as δ = (C9-C10 + C9-C13 – C13-C12 – C10-C11)/2 [d]) This work

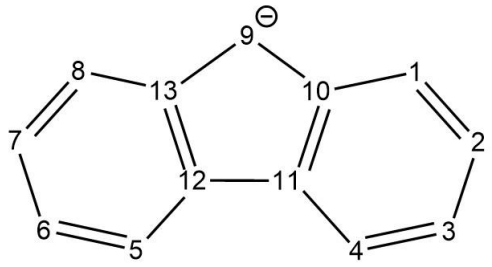

Figure 4.12: Numbering system used in discussions of fluorenyl complexes.

While the nickel-fluorenyl bonding is best described as η^5, there are deviations from ideality. As expected, the Ni-C20 (C9 in Figure 4.12) bond is the shortest of the Ni-C(fluorenyl) bonds; the Ni-C1 bond is also slightly longer than Ni-C3, likely due to the increased *trans* influence of carbon 20. The longest Ni-C bonds are those to C22 and C23, the two carbons distal to C20. This implies some degree of ring slippage. While fluorenyl slippage has not been addressed in the literature to the same extent as indenyl slippage, there are some parameters used to quantify fluorenyl hapticity. In addition to Δ_{M-C} used with indenyls,[56] a parameter δ has been defined, relating to the variance in the C-C bonds of the five-membered ring; a decrease in δ is associated with an increase in η^5 character.[72] Similarly, the variance in the C-C bonds of the benzenoid rings has been used as an indicator of the distribution of aromaticity in the fragment.[56] This is

quantified here with $\Delta C\text{-}C_{benz}$, defined as the difference in the longest and shortest C-C bonds in a given benzenoid ring, averaged across all benzenoid rings; this parameter is positively correlated with η^5 character.

These values of these parameters for **29** and some relevant complexes from the literature are compiled in Table 4.2. The parameters are, with one exception, consistent among themselves and in agreement with the assigned hapticity, suggesting that they are an appropriate collection of metrics to evaluate the hapticity of **29**. Despite the deformations mentioned above, all the collected metrics suggest an unambiguous η^5-binding mode to be the most appropriate description of the fluorenyl nickel interaction in **29**. This was unexpected, given the apparent fluxionality observed in solution. This near-ideal behavior further underscores the particular favorability of the 18e$^-$, *pseudo*-pentacoordinate [(η^3-allyl)Ni(η^5-Cp)] structural motif.

Table 4.4: Structural parameters of 26, 27, 28, and 29

	Ni-Cp(centroid) (Å)	Ni-A^{2t}(centroid) (Å)	$\Delta C\text{-}C_{allyl}$[a] (Å)	Angle between ligand planes (°)
[A^{2t}NiCp]	1.739(10)	1.702(2)	0.002(2)	21.0
[A^{2t}NiCp*]	1.768(2)	1.721(2)	0.000(2)	27.3
[A^{2t}NiInd^{2Me}]	1.806(6)	1.711(7)	0.004(6)	28.0
[A^{2t}NiFluor][b]	1.793(7)	1.715(8)	0.018(10)	26.9

[a]) Defined as the difference between the longest and shortest C-C bonds in the core of the ligand, where core is the set of carbon atoms directly bound to nickel. [b]) Values averaged across the four independent molecules

Comparing general structural parameters among the four A^{2t}Ni-Cp type complexes, few meaningful differences can be found. The increase in Ni-Cp(centroid) distance in the purely η^5-sequence [**26, 27, 29**] is as expected from a purely steric argument, and in spite of the bulky allyl substituents, only a modest increase in this distance is seen across the series. The identity of the Cp-type ligand seems to have very little impact on the nickel-allyl interaction, as the Ni-A^{2t} distance is essentially indistinguishable between **27, 28,** and **29**, while being just slightly lower in **26**. Furthermore, the angle between the allyl and five-membered ring planes does not meaningfully change among the set. The allyls in **26, 27,** and **28** display ideal 1.5-order C-C bonding, and the allyls in **29** deviate from ideal behavior only slightly.

4.2.3 η^1-Heteroatom Anions

4.2.3.1 Synthesis and Characterization

The utility of the above synthetic method in accessing compounds containing heteroatom-bound ligands was also investigated. In Section 4.2.2, formation of A^{2t}-nickel complexes with polyhaptic organic anions led to monomeric $[L^1NiL^2]$ compounds. In contrast, complexes with monodentate anions, such as those considered here, as a rule maintain the anion-bridged dimer motif of the $[\{A^{2t}NiBr\}_2]$ starting material.

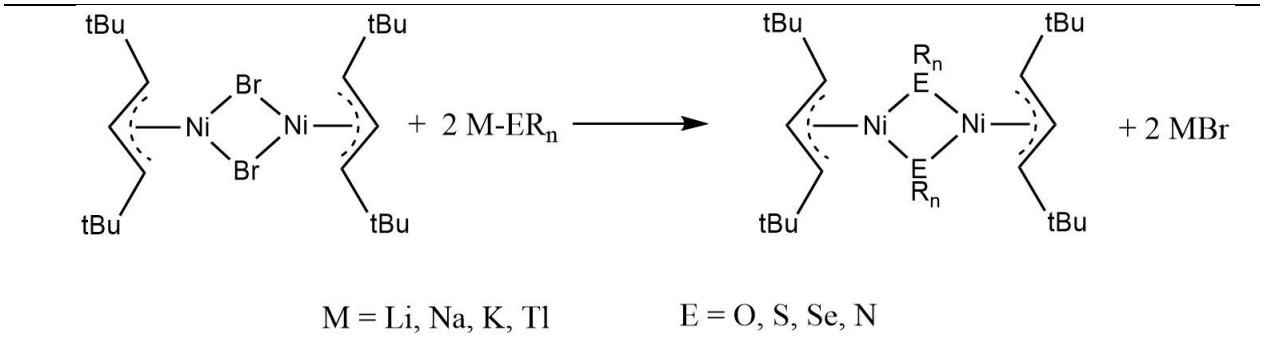

Figure 4.13: Formation of various anion-bridged dimeric A^{2t}-nickel complexes via salt metathesis.

A simple variation on the $[\{A^{2t}NiX\}_2]$ motif reported is allyl nickel acetate. In 1981, it was reported that oxidative addition of allyl acetate to Ni^0 generated $[NiA_2]$ and $Ni(OAc)_2$, presumably via initial formation of $[\{ANi(OAc)\}_2]$ followed by ligand redistribution.[15] The palladium analogue, on the other hand, could be isolated and crystallographically characterized,[73] as have 2-methallylnickel complexes of halogenated acetates.[74] Generation of an A^{2t}-nickel acetate, therefore, seemed a natural starting point for this investigation. Reaction of $[\{A^{2t}NiBr\}_2]$ with sodium acetate led to formation of a new species, identified by ^1H NMR. The product mixture contained 84% of the new species and 16% $[\{A^{2t}NiBr\}_2]$. Attempts to push the reaction to full conversion by numerous methods were unsuccessful. Finally, thallous acetate was used as an acetate source; reaction at room temperature in THF over nine days allowed for isolation of the spectroscopically pure new species in 76% yield. Single crystals were grown by slow evaporation of a hexane solution, allowing the solid-state structure to be determined. The compound appears indefinitely stable under nitrogen atmosphere, in contrast to the parent allyl analogue.

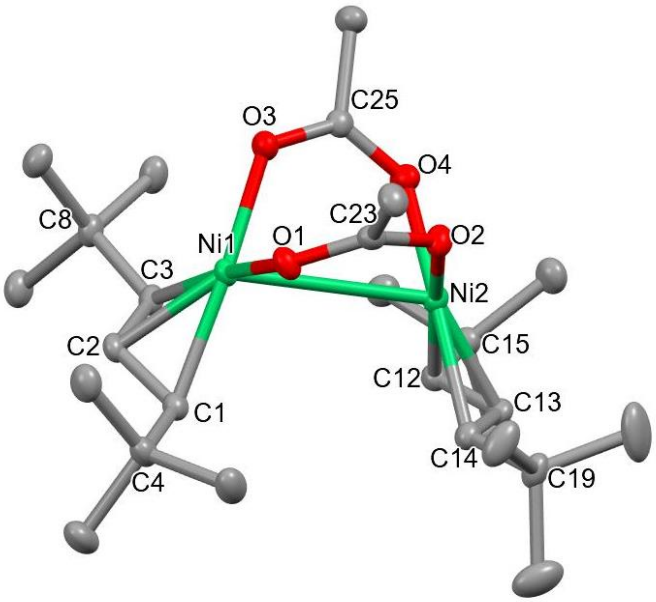

Figure 4.14: Thermal ellipsoid plot of the molecular structure of [{A^{2t}Ni(OAc)}$_2$] (50% Probability). Hydrogen atoms are omitted for clarity. Selected bond distances (Å): Ni1-O1, 1.921(2); Ni1-O3, 1.925(2); Ni2-O2, 1.926(3); Ni2-O4, 1.927(2); Ni1-C1, 2.028(3); Ni1-C2, 1.969(2); Ni1-C3, 2.027(3); Ni2-C12, 2.024(3); Ni2-C13, 1.971(2); Ni2-C14, 2.053(2); C23-O1, 1.263(2); C23-O2, 1.259(2); C25-O3, 1.261(2); C25-O4, 1.258(2); C1-C2, 1.404(3); C2-C3, 1.406(2); C12-C13, 1.408(2); C13-C14, 1.403(3).

As expected, the structure of [{A^{2t}Ni(OAc)}$_2$] closely matches those reported for [{APd(OAc)}$_2$][73] and [{(allyl)Ni(O$_2$CCF$_3$)}$_2$],[74] reproducing the κ^2-acetato bridge and highly bent Ni-allyl planes. The two allyls are in a *pseudo*-eclipsed conformation, in that, if the molecule was to be "unbent" such that the {NiOO}$_2$ core was planar, the two allyls would be eclipsed. The core is also slightly twisted; this induces an 18.5° angle between the planes of the two allyl ligands. All four *t*Bu groups are in the *syn* configuration; the *syn* configuration was also seen in bis[(η^3-3-phenylallyl)(trifluoroacetato)nickel].[74] The C-C bonds of the allyl backbone are identical within error, suggesting ideal delocalization; this is supported by the consistent Ni-C(allyl terminal) distances. Similarly, the charge on the acetate ligand appears fully delocalized, as evidenced by the nearly identical C-O bond distances. The Ni-C(allyl) distances are very slightly longer compared to [{(2-trimethylsilylallyl)Ni(O$_2$CCF$_3$)}$_2$] (<0.05 Å,) while the Ni-O distances are essentially equivalent.[75] The structure of [{A^{2t}Ni(OAc)}$_2$] can also be compared to a five-coordinated

allylnickel species featuring a 1,1'-bis(diphenylphosphino)ferrocene ligand and a monodentate acetate ligand.[76] Despite the increased bulk of the allyl ligand, the Ni-C(allyl) bonds are slightly shorter in [{A^{2t}Ni(OAc)}$_2$] (1.969-2.053 Å compared to 1.982-2.072 Å), as are the Ni-O bonds (1.921-1.927 Å compared to 1.947 Å). As in the structure of [{APdOAc}$_2$],[73] each nickel center exists in a local square planar coordination environment, and the two square planes are highly askew relative to each other. The two allyls are in a *pseudo*-eclipsed conformation, while all four *t*Bu groups are in the *syn* configuration.

The first dinuclear hydroxo-bridged organonickel species was reported in 1973,[77] and crystallographic characterization of a related benzylnickel compound was reported in 1989.[78] Furthermore, bridged hydroxo species have been implicated in nickel catalyzed Suzuki-Miyaura reactions,[25] including those proceeding through an η^3-allylnickel intermediate.[26,27] Despite this significance, no [{(allyl)Ni(OH)}$_2$] complex has been structurally authenticated. Light-orange crystals of [{A^{2t}Ni(OH)}$_2$] were repeatedly obtained as a decomposition product from other reactions (decomposition of A^{2t}-nickel complexes is discussed in more detail in Section 4.2.3.2), allowing for the molecular structure to be determined. To better characterize this complex, its direct synthesis was attempted. Reactions with alkali metal-hydroxide salts gave inconsistent results, but reaction with thallous hydroxide over 11-21 days led to isolation of a yellow-orange solid; the material is slightly soluble in hexane and DMSO, but highly soluble in THF. The ^{1}H NMR spectrum of this substance was consistent with spectral features observed in samples that produced [{A^{2t}NiOH}$_2$] crystals, implying the successful isolation of the compound. Two isomers are evident in the ^{1}H NMR, both of which display highly broadened and irregularly shaped resonances. This is in stark contrast to the NMR features of all other isolated [A^{2t}NiX}$_2$] compounds and implies a dynamic process occurring on the timescale of the NMR experiment. The two species are likely to be eclipsed and staggered isomers of the compound, but the consistent ratio between them could indicate interconversion; it is possible that the observed isomerism is instead due to the geometry of the {NiO}$_2$ core or the O-H orientation. The nature of this process is unclear at this point. The compound is indefinitely stable in the glovebox atmosphere.

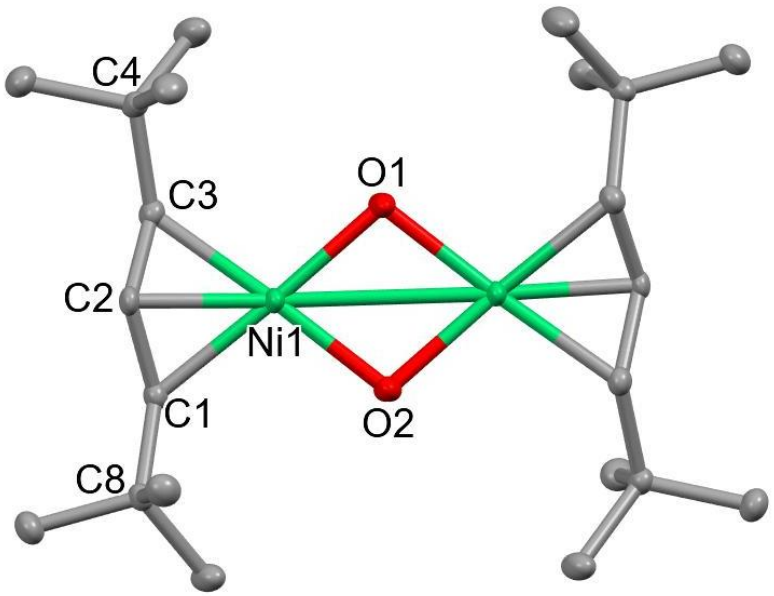

Figure 4.15: Thermal ellipsoid plot of the molecular structure of [{A^{2t}Ni(OH)}$_2$] (50%). Hydrogen atoms are omitted for clarity. Selected bond distances (Å): Ni1-O1, 1.915(5); Ni1-O2, 1.911(7); Ni1-C1, 2.011(1); Ni1-C2, 1.949(2); Ni1-C3, 2.012(1); C1-C2, 1.411(2); C2-C3, 1.408(2); Ni1-Ni1´, 2.929.

[{A^{2t}NiOH}$_2$] crystallizes in the *I*2/a space group; the two-fold axis runs through the center of the molecule, and the hydroxide ligands are evenly disordered above and below the axis. The {NiOH}$_2$ center is slightly bent, with the bending angle between the local square plane of each nickel found to be 171°. This is substantially less than the bending reported in the benzylnickel complex referred to above (134° reported.)[78] The allyl ligands are in a mutually staggered arrangement, and all four *t*Bu groups are in the *syn* configuration. The Ni-O bonds are substantially shorter than those reported for a previously reported bimetallic complex featuring a {Ni(OH}$_2$ core,[79] but indistinguishable from those in another[78] (1.913 vs. 2.002 and 1.919 Å on average, respectively.) However, they remain longer than the Ni-O bonds in some monomeric nickel complexes with terminal hydroxo ligands (≈1.87 Å.)[80,81] This compound is the direct analogue of the product of oxidative addition of allyl alcohol to a generic nickel(0) source, an exceedingly common entry point for nickel catalyzed allylation reactions.[21,22] Therefore this stable and easily accessible compound represents a particularly convenient model for mechanistic study of such reactions.

The power of thallous salts to drive difficult metatheses was clearly established by the above reactions. Reaction of [{A^{2t}NiBr}$_2$] with thallous nitrate was therefore performed in pursuit of a nitrate-bridged allylnickel species. However, even after a week, only [{A^{2t}NiBr}$_2$] was recovered, demonstrating the limits of thallium-driven metathesis.

Allylnickel complexes with alkoxide ligands have also been reported.[29,30,82,83] These include both alkyl- and aryl-oxide species; however, structural characterization is limited to a single instance, in which a secondhand interpretation of the structure of [{(2-methallyl)NiOMe}$_2$] was published.[33] Also of note is the reported reaction of [{ANiCl}$_2$] with sodium 2,6-di-tert-butyl-4-methylphenolate, in which the phenolate ligand was unexpectedly bound as an η^5 π-aromatic ligand rather than through the oxygen atom, presumably due to the steric bulk contributed by the two *t*Bu groups;[82] similar π-bonding is displayed in the homoleptic [Ni(2,6-di-*t*Bu-phenolate].[84] Reaction of [{A^{2t}NiBr}$_2$] with potassium phenolate yielded a red solid, indefinitely stable in the glovebox. ^{1}H NMR shows the presence of two isomers, both in the *syn,syn* configuration. The identity of the isomers cannot be conclusively determined at this time (See Section 4.2.3.2 for more details on the stereochemistry of this class of compounds). However, the simple NMR features of each isomer indicate molecules of high symmetry, ruling out the η^5-coordination mode. This demonstrates that, despite the apparent stability provided by the allylic *t*Bu groups, they exert less steric strain on the coordination environment of the nickel center than similarly bulky groups on the bridging ligands. The stability of this compound is of note, as alkoxo compounds of the parent allyl are reported to undergo full disproportionation at or slightly above room temperature.[17]

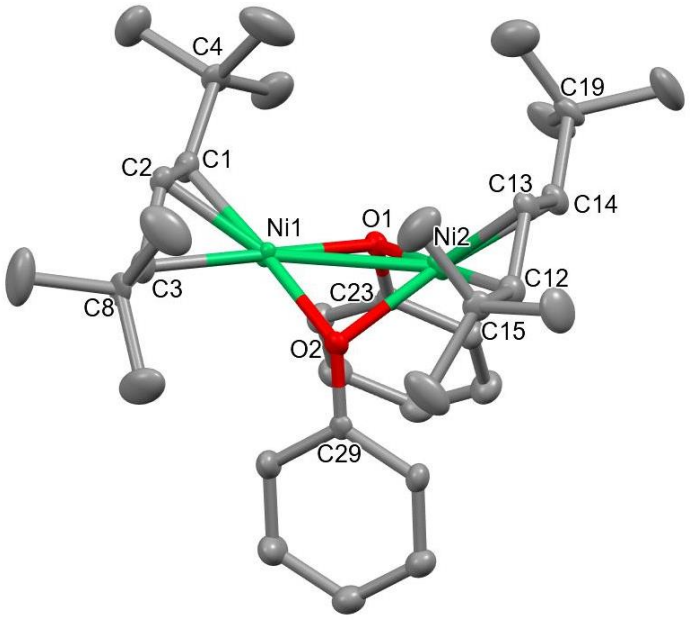

Figure 4.16: Thermal ellipsoid plot of the molecular structure of [{A^{2t}Ni(OPh)}$_2$] (50% probability). Hydrogen atoms are omitted for clarity. Selected bond distances (Å): Ni1-O1, 1.954(3); Ni1-O2, 1.958(3); Ni2-O1, 1.955(3); Ni2-O2, 1.957(3); Ni1-C1, 2.039(5); Ni1-C2, 1.971(4); Ni1-C3, 2.041(4); Ni2-C12, 2.027(5); Ni2-C13, 1.969(4); Ni2-C14, 2.055(4); C1-C2, 1.417(7); C2-C3, 1.403(7); C12-C13, 1.403(7); C13-C14, 1.419(7).

Repeated crystallization by evaporation of a hexane solution yielded scarlet needle-like crystals. Indeed, X-ray crystallography showed a molecular structure matching the expected [{A^{2t}NiOPh}$_2$] formula. The molecule is disordered over two positions in the unit cell, but discussion will be limited to the position with 93% occupancy. Interestingly, the {NiO}$_2$ core was found to be diamondoid, deviating from the planar core seen in the halide complexes. Each nickel center has a *pseudo*-square planar coordination environment, and these planes intersect at a 135.6° angle. The causes of this deformation and its implications for the stereochemical properties of its complexes will be discussed in detail below. The Ni-O bond distances in [{A^{2t}Ni(OPh)}$_2$] (1.956 Å on average) are slightly shorter than those found in two molecular nickel species containing bridging phenolate ligands (2.016-2.060 Å;[85] and 2.010-2.043 Å[86].) Both display planar {NiO}$_2$ cores, though this geometry may be influenced by phenoxide-tethered chelating groups. As one would expect, the bonds are notably longer than that in the terminal phenolate complex [(PNP)Ni(OPh)], which

was found to be 1.863 Å (PNP = $[N(o\text{-}C_6H_4P^iPr_2)_2]^-$),[87] and slightly longer than those in $[\{A^{2t}NiOH\}_2]$ (1.913 Å). Bond distances are comparable to a tris(*t*-butoxy)siloxy-bridged allylnickel compound (≈ 1.92 Å), which also displayed a very similar angle between the nickel square planes (135.3°.)[88] $[\{A^{2t}NiOPh\}_2]$ displays the shortest Ni-Ni distance of any reported in this work at 2.718 Å, but this is likely still too large to represent any nickel-nickel bonding (compare to 2.49 Å interatomic distances in bulk nickel metal.)[89]

Similar reactivity has been reported between the parent allyl complex and alkyl oxides, although characterization was minimal.[30] However, the reaction of $[\{A^{2t}NiBr\}_2]$ with sodium methoxide failed, yielding only decomposition products. The nature of these decomposition products will be discussed in more detail in Section 4.2.4. However, it should be noted that sodium methoxide is poorly soluble in THF. Throughout the course of this investigation, a general correlation between poorly soluble nucleophiles and poor reaction outcome was observed. Therefore, it is possible that the use of a more soluble alkoxide salt, such as $[LiO^nBu]$ might allow for the isolation of an $[\{A^{2t}NiOAlkyl\}_2]$ species. On the other hand, potassium phenolate is also very poorly soluble in THF, so the conclusion that aryloxide complexes are more stable than alkoxide complexes remains unaffected by these solubility considerations.

Compared to its lighter congener discussed above, allylmetal complexes with sulfide-bound ligands are well characterized.[90–93] This applies to nickel as well. The bridge-split, monomeric phenylthiolate complex $[ANi(PMe_3)SPh]$ has been fully characterized,[94] while a reported dimeric allylnickel-arylthiolate complex has been spectroscopically but not structurally characterized.[29] Like the methoxide structure discussed above, a secondhand interpretation of the structure of $[\{ANiSMe\}_2]$ has also been reported.[33] While this is a much smaller gap in the literature than was present for oxide ligands, it is still noteworthy given the growing importance of nickel thiolate complexes due to their relevance to C-S bond forming reactions. Nickel catalyzed C-S coupling reactions are an area of active development,[95,96] and an allylnickel-based catalyst system has shown promise in activating difficult aryl chlorides and triflates for such reactions.[9]

Within a minute of addition of lithium phenylthiolate to a solution of $[\{A^{2t}NiBr\}_2]$, the color of the reaction mixture had changed to a deep scarlet. Solutions of the isolated product show similar coloration, though a dull brown solid is collected upon evaporation of solvent; this drastic color change implies a meaningful change in the molecular structure of the compound upon removal of solvent, but any such changes must be entirely reversible upon re-dissolution. ^{1}H NMR shows a major product with exclusively *syn* substituents consistent with the desired product, along with two other allylic spin systems. These two minor systems are found in equal abundance in every case, suggesting that both lie on the same compound. The terminal allyl protons of the minor products show broadened resonances, implying dynamic interconversion on the NMR timescale. The stereoisomerism of this compound will be discussed in more detail in Section 4.2.3.2. Through rapid evaporation of a hexane solution of the product to near-dryness,

deep red crystals were obtained; analysis revealed a molecular structure analogous to the alkoxide analogue, including a diamondoid $\{NiS\}_2$ core. This compound was highly stable, showing no apparent decomposition over a year of glovebox storage; a very small increase in the relative abundance of the predominant product was observed, indicating that other species observed are likely kinetic products. In two reactions where conversion of $[\{A^{2t}NiBr\}_2]$ was incomplete, an additional species was observed; if the collected material was further treated with LiSPh, this species vanished. It is hypothesized that this species is the partial substitution product $[\{A^{2t}Ni\}_2(SPh)(Br)]$, but further work is required to isolate this species and confirm this identification.

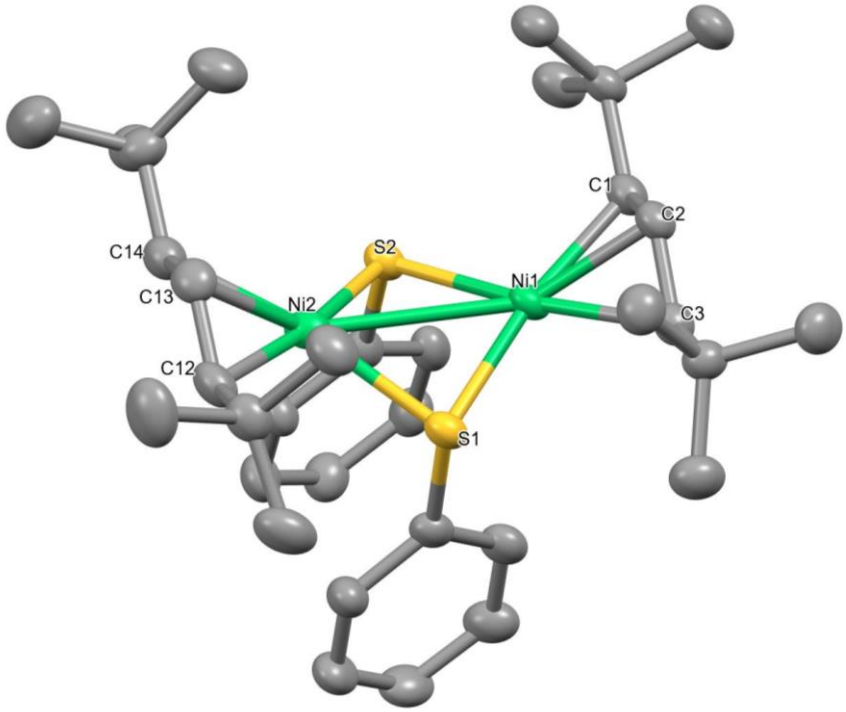

Figure 4.17: Thermal ellipsoid plot of the molecular structure of $[\{A^{2t}Ni(SPh)\}_2]$ (50% probability). Hydrogen atoms are omitted for clarity. Selected bond distances (Å): Ni1-S1, 2.231(2); Ni1-S2, 2.238(8); Ni2-S1, 2.244(6); Ni2-S2, 2.237(3); Ni1-C1, 2.063(5); Ni1-C2, 2.004(5); Ni1-C3, 2.063(7); Ni2-C12, 2.074(5); Ni2-C13, 1.995(5); Ni2-C14, 2.076(6); C1-C2, 1.410(6); C2-C3, 1.401(6); C12-C13, 1.417(6); C13-C14, 1.406(6).

The molecular structure largely matches that observed for $[\{A^{2t}NiOPh\}_2]$, with eclipsed allyls featuring exclusively *syn* *t*Bu groups. While crystallographically distinct, there is no significant difference in the bond distances between the two halves of the molecule, suggesting approximate C_{2v} symmetry. The $\{NiS\}_2$ core is less bent (134° interplanar angle) than its phenolate analogue (126°), a fluorophenylthiolate-bridged allylpalladium dimer (127°),[90] and the mixed metal compound $[(C_6F_5)_2Ni\{SPh\}_2Pd(dppe)]$

(120°).[97] The methylthiolate bridged complex [{ANiSMe}$_2$] was also reported to display a greater degree of bending, with a 117° angle between coordination planes.[32] It should also be noted, though, that a dinickel species bridged by fluorinated thiophenolates has been shown to contain a planar {NiS}$_2$ core.[98] The geometry about the bridging atoms is more pyramidalized than in [{A^{2t}NiOPh}$_2$], its bond angles summing to slightly less than 300°. As such, the phenyl rings are further displaced from the core, and lie nearly parallel to each other. This is consistent with previous theoretical work.[99] The Ni-S bond distances in [{A^{2t}NiSPh}$_2$] (2.238 Å on average) are indistinguishable from the those in the nickel-thiophenolate complexes discussed above, shorter than in the homoleptic dianion [Ni(SPh)$_4$]$^{2-}$ (2.288 Å on average),[100] but significantly longer than those in an allylnickel complex with a terminal SPh ligand (2.160 Å).[94]

Unlike the reaction outcomes seen with alkoxide ligands, sodium ethanethiolate reacted similarly to lithium phenylthiolate upon stirring for 6 days, yielding a dark red solid, though this product did appear to decompose slowly over weeks. The stereoselectivity of this reaction appears to be complex. Three primary products are formed in all reactions, but their relative abundance varied dramatically among the three syntheses. Two of these display fully symmetric allyls with *syn,syn* configurations, while the third was asymmetric, though its substituent configuration was ambiguous. Additionally, a number of minor species are formed in trace amounts; some of these could plausibly be other isomers of the expected product, but their low intensity makes assignment impossible. For all species, a mixture of sharp and broad signals is observed. This peak broadening implies dynamic processes occurring on the NMR timescale, but the varying ratios of the three consistent products implies that these dynamic processes strictly do not interconvert the observed isomers. This is consistent with isomerism based on statically coordinated allyl groups with dynamic SEt groups; the potential dynamic processes of bridging groups are discussed in more detail below. The material is a solid, but only extremely small crystals could be collected after multiple crystallization attempts, prohibiting the determination of its crystal structure. However, based on the physical and spectroscopic similarities to [{A^{2t}NiSPh}$_2$], the material almost certainly has a molecular formula [{A^{2t}NiSEt}$_2$].

To extend the series of allylnickel-chalcogenide complexes, reaction was also attempted with potassium selenophenolate. A dark red product was obtained and ^{1}H NMR analysis identified four new allyl spin systems in more than trace abundance. Three of these were consistent with [{A^{2t}NiSePh}$_2$], while the final species displayed features implying a C_3 core with localized single and double bonds. An η^1-allylnickel complex is possible, but as its ^{1}H NMR features are very similar to those of A^{2t}Br, the species is hypothesized to be the product of ligand cross-coupling, A^{2t}SePh. Future experiments will attempt to isolate this unknown species by vacuum distillation to confirm its identity. Attempts to obtain crystals of sufficient quality for structural determination have been thus far unsuccessful. Unlike the -OPh and -SPh complexes, the parent allyl analogue of [{A^{2t}NiSePh}$_2$] has been synthesized and structurally characterized.[101] This

compound also displays {NiSe}$_2$ bending, with a 107.5° angle between the local square plane of each nickel center. Interestingly, the phenyl groups are oriented towards the nickel atoms, contrasting with the *exo* orientation of the phenyl groups in [{A^{2t}NiOPh}$_2$] and [{A^{2t}NiSPh}$_2$]; this is also seen in thiophenolate-bridged allyl palladium dimers.[90,102] Both eclipsed and staggered isomers are observed, both in solution and in the crystal structure, implying similar energy for the two. Of particular note is the stability of the two products; [{ANiSePh}$_2$] was reported to entirely degrade in 30 minutes to form the C-Se bond formation product, while [{A^{2t}NiSePh}$_2$] appears stable for at least a week under the glovebox atmosphere.

In comparison to the complexes containing chalcogenide-bound ligands discussed above, molecular organometallic species featuring amido ligands bound to group 10 metals are less common. However, while the isolation of such compounds is rare, they are nonetheless important. C-N bond forming reactions are among the most prominent carbon-heteroatom coupling reactions due to the outsized prevalence of amine moieties in applications ranging from pharmaceuticals to organic materials to catalysts.[103–105] These transformations have traditionally been dominated by palladium catalysis, but recent years have seen increased performance under nickel catalysis.[106,107] Considering the context of the earlier mentioned general importance of allylic substitution reactions, this makes the poor characterization of simple allylnickel amido complexes a notable gap in the literature. The use of steric bulk to combat the frequent instability of nickel amido complexes is precedented,[108,109] making this a promising application of the A^{2t} ligand.

Reaction of [{A^{2t}NiBr}$_2$] with several amido nucleophiles failed to give isolable products of the expected [{A^{2t}NiNR$_2$}$_2$] form (See reactions with pyrrolide and imidazolate in Section 4.2.2.1 above and reactions with diphenylamide and bis(trimethylsilyl)amide discussed in Section 4.2.4 below. Reactions with potassium diisopropylamide also failed under multiple conditions.) However, the reaction with lithium anilide gave a smooth, rapid color change to deep red. As seen in the synthesis of [A^{2t}NiFluor], allowing the reaction mixture to sit overnight in THF leads to full decomposition, so the reaction times must be kept very short. This allows for the isolation of a red-orange crystalline solid. While crystals suitable for diffraction analysis have not yet been obtained, spectral features and reactivity suggest the formation of the partial substitution product, [{A^{2t}Ni}$_2$(μ^2-NHPh)(μ^2-Br)]. Also notable is the consistent presence of small amounts of [{A^{2t}NiBr}$_2$] in the product mixture (about 1 : 10 [{A^{2t}NiBr}$_2$] : [{A^{2t}Ni}$_2$(μ^2-NHPh)(μ^2-Br)].) The conversion of most starting material to the partially substituted product suggests that the first bromide-to-anilide substitution is fast relative to a potential second substitution. However, the presence of some unconverted [{A^{2t}NiBr}$_2$] could suggest that reaction did not proceed to completion; this is plausible given the time restraints forced by its instability in THF solution. Therefore, it may be possible to induce the second metathesis process using more forcing conditions. Additional reaction time might be possible if the reaction is performed in a mixture of THF and toluene (see *tert*-butoxide reactions below,) or the second

metathesis could be sped up using a large excess of [LiNHPh]. It should be noted that [{ANiN_R}$_2$] complexes (N_R = diphenylamide, aziridide, potentially others) can reportedly be formed by salt metathesis from the parent allylnickel bromide, but synthetic, structural,[17,35] and reactivity details of such compounds are not readily available.

^{1}H NMR analysis of the isolated product shows a mixture of many η^3-A^{2t}-nickel species. Two allyl spin systems predominate the mixture, though, in exactly equal abundance. One well-defined set of aryl proton signals is observed for the pair of allyl systems. Additionally, one allyl seems to display a *syn,syn* *t*Bu configuration, yet still sees distinct peaks for the two *anti* protons. This combination of features can only be attributed to a mono-anilide bridged dimer with two inequivalent allyl ligands. The distinct allyls can most easily be explained by one allyl having a *syn,anti* *t*Bu configuration. This differs from the exclusively *syn,syn* configurations seen in the primary products of all other heteroatom-bridged species isolated in this study. This could be due to the more strongly σ-donating nature of the amido ligand; it has been noted that terminal allyl substituents *trans* to good σ-donor ligands show an increased tendency to adopt the *anti* configuration.[6,12,110]

4.2.3.2 Structural and bonding considerations

Table 4.5: Collected structural parameters for [{A^{2t}NiER}$_2$] complexes. All parameters are averaged over all unique instances.

Compound	Ni-E (Å, avg.)	Ni-A^{2t}(centroid) (Å, avg.)	ΔC-C_{allyl}[a] (Å)	Interplane angle (°)[b]	Ni-E-Ni (°)	E-Ni-E (°)	C(allyl)-Ni-E (°)
[{A^{2t}NiOAc}$_2$]	1.925(3)	1.722(3)	0.004(3)	47	NA	90.9(3)	97.8(3)
[{A^{2t}NiOH}$_2$]	1.913(7)	1.697(2)	0.003(2)	171	99.9(7)	78.5(7)	103.2(7)
[{A^{2t}NiOPh}$_2$]	1.956(3)	1.724(5)	0.015(7)	126	88.0(3)	80.0(3)	103.4(5)
[{A^{2t}NiSPh}$_2$]	2.238(8)	1.758(7)	0.010(6)	134	83.57(3)	89.54(3)	99.2(1)

[a]) Defined as the difference between the C-C bonds in the allyl backbone, averaged across all allyls [b])Defined as the angle between the planes defined by atoms directly bound to each nickel atom.

For the three compounds with appropriate square planar organonickel complexes to compare to, no meaningful deviations were noted in the Ni-E bond distances. This suggests that the A^{2t} ligand, and allyl ligands in general, do not induce any unique structural effects compared to other organic ligands. Unlike the sequence of complexes discussed in Section 4.2.2, there is a meaningful difference in the Ni-allyl bond distances among the bridged complexes. The cause of this is not entirely clear. While the hydroxo ligands are certainly the smallest, there is no difference in the sterics of -OPh and -SPh. This suggests an electronic effect is responsible. The strong trans influence of thiophenolate ligands has been noted,[111] but relative influence of S- and O- bound ligands has not been well studied; study of tungsten complexes with oxido and sulfido ligands gave inconclusive results.[112] In all cases, though, nearly ideal delocalization of the allylic π-system is achieved. The observed metal-ligand bond angles seem to be primarily governed by the preferences of the bridging atoms rather than any property of the A^{2t}Ni- fragment.[99]

The observation of bending in {MER_n}$_m$ cores is not a novel development. Indeed, this phenomenon is well-established and much theoretical and experimental work has been done to explain and predict the presence of bending in dimeric d^8 species.[99,113–118] These have identified a complex blend of steric and electronic effects that are involved in the ideal conformation for a given molecule. The most commonly invoked cause of the bending in the absence of ligand-enforced geometry is the formation of weak metal-metal interactions, although triplet state character and metal-ligand antibonding interactions have also been invoked.[116,119] Bending is consistent across almost all structurally characterized group 10 allylmetal alkoxo- and thiolato- bridged species,[88,90,102] and our compounds generally agree with appropriate

points of comparison in this respect. [{A^{2t}NiSPh}$_2$], the most well-precedented of the structures considered here, seems to be slightly less bent than its peers, but only slightly so; the cause of this is not clear. The only exception is [{(2-methallyl)NiOMe}$_2$], which was reported to be planar;[32] the details of this compound are not available, however, making analysis of discrepancy difficult. Interestingly, this is not the case for related [{CpNiSR}$_2$], which are uniformly planar in the absence of conformationally rigid dithiolates.[116,120] This discrepancy between consistent bending for allylic species and strict planarity for Cp species suggests that differences in the organic moiety are an influential factor. A traditional explanation for this would be the presence of nickel-nickel bonding interactions, which would be expected to be stronger for the 16e$^-$ allylnickel centers than the 18e$^-$ cyclopentadienylnickel centers. However, the nickel-nickel distances in these compounds are quite long for this sort of interaction to have such a substantial effect on the equilibrium geometry. It is possible that the nature of this interaction, if any is present, could be probed using QTAIM computational methods.

Broadly speaking, the successfully isolated complexes described above fit the expected mold of the bridged allylnickel-anion dimer. However, this apparent consistency obscures a surprisingly complex stereochemical picture. This complexity is largely due to the introduction of the possibility of bending of the {NiER$_n$}$_2$ core; returning to the stereochemical diagram presented in the Introduction, three additional stereochemical relationships have been introduced, requiring additional definitions. The first of these is whether the core is flat or bent. One must then consider the stereochemistry of any substituent groups attached to the bridging atoms. The geometry about a bridging atom is not subject to any inherent restrictions. However, as our investigation only covered chalcogens and pnictogens with bent geometries, we can simplify the situation to two general cases. In the case of a bent core, these are categorized as *endo* or *exo*. A formal definition is included in Appendix 4, but a simple definition is as follows: if the E→R bond is in the same direction as the nickel atoms, the substituent is termed *endo*, whereas if the bond extends in the opposite direction, it is considered *exo*. In cases with a planar core, the substituents are defined relative to each other as *cis* or *trans*. In the case that the two allyls are eclipsed, and the substituents are *cis*, the substituents are considered "aligned" (*al*) if they point in the same direction as the allyl triangles or "opposed" (*opp*) if they point in the opposite direction as the allyls. For each substituent, this configuration is completely independent of all other relationships.

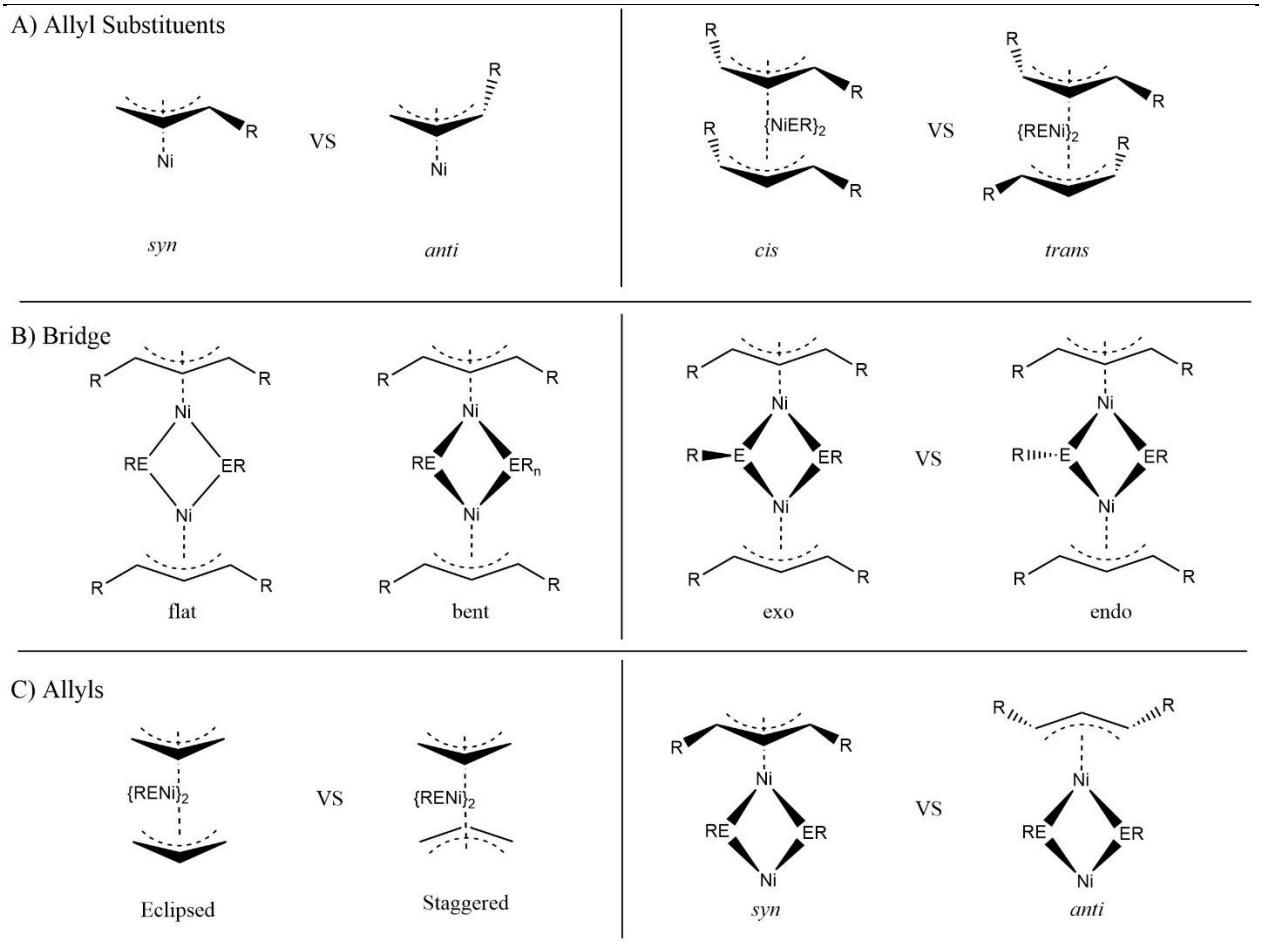

Figure 4.18: Stereochemical modes of allylnickel complexes bridged by atoms with bent local geometries.

Finally, the triangular arrangement of the carbon atoms of the allyl is asymmetric with respect to the square plane around the attached nickel center; the allyl triangle can "point" either above or below this plane. In a bent $\{NiE\}_2$ core, the E-Ni-E atoms also form a triangle pointing in one of two opposite directions. Therefore, each allyl can either point in the same direction as the E-Ni-E bonds, referred to as a *Syn* allyl, or in the opposite direction, referred to as *Anti* allyl. Despite the labelling overlap, this is entirely independent from the *syn* and *anti* configurations of the substituents of the terminal carbons of the allyl backbone. Note that, by definition, any bent complex with staggered allyls will have one *syn* and one *anti* allyl; as such, this relationship need only be specified for eclipsed isomers.

Considering all these degrees of freedom and eliminating degenerate isomers, it is found that each $[\{A^{2t}NiER\}_2]$ complex with a single substituent R has 147 distinct isomers. Some of these can be dismissed *a posteriori*, such as those displaying the never-observed *anti,anti* configuration of *t*Bu groups; however, even if all such isomers are removed, 81 possible isomers remain for each compound. Restricting

consideration to compounds bridged by a single atom, all the complexes in this section were isolated as mixtures of isomers, in contrast to the [{A^{2t}NiBr}$_2$] starting material. To our knowledge, the factors impacting the stereochemistry of bent bridged allyl-nickel dimers have not previously been meaningfully investigated; given its complexity, the current investigation represents a very preliminary mapping of this stereochemical space. Substantial future work, both computational and experimental, is needed to better understand these systems.

The primary stereochemical result of the use of the allyl ligands is direction dependence, due to the inherently directional nature of the allyl group. As such, the substituents on the bent bridging atoms and the potentially bent {NiER$_n$}$_2$ must have their directionality defined not just relative to each other, but also relative to the terminal allyl groups. This is the cause of the explosion in the number of possible isomers for these compounds compared to many of those previously studied.[99,113,115,121] However, while different isomers can be constructed, it is not clear that all directional relationships are important to consider. This is due to the potential for Ni-E bond rotation and E-centered pyramidal inversion, inverting the core Ni-E-Ni or E-R direction respectively; this is a simplified view, and true inversion mechanisms are likely more complex and may differ between different sub-classes of isomers. If a certain mode of interconversion has low energy barriers, then distinguishing the isomers becomes superfluous outside of crystal structure analysis. Unfortunately, the dynamics of bridged allylmetal systems are not yet well-understood, and the impact of allyl substituents is entirely unstudied. Therefore, analysis of the ^{1}H NMR features of the compounds reported here will be used to gain some insight into the nature of relevant room temperature dynamic processes.

First, a notable observation from previous results is that, to our knowledge, no previously reported [{(allyl)NiER$_n$}$_2$] compound has displayed more than two distinct isomers by proton NMR when measured at room temperature.[29,88,90,93,102] While this is a limited dataset, it suggests that eclipsed/staggered interchange has a greater energy barrier to interconversion than either ring or bridge inversion processes. Study of other dimeric ER$_n$-bridged species has suggested that as one moves down both group 10 and group 16, ring inversion processes become slower moving.[99,113] Based on this, the fact that none of the wide variety of allylpalladium thiolates and selenolates surveyed in a 1995 study displayed any evidence of *endo*/*exo* or *Syn* allyl/*Anti* allyl isomerism even at -45 °C is particularly notable. These conditions were nearly ideal bridge-centered isomer speciation, so its absence suggests that the inversion barriers between such isomers are very low. Therefore, we cautiously propose that eclipsed/staggered and substituent syn/anti substituent diastereomers are the only species that are distinguished in the room temperature spectra reported here. However, there is a notable increase in line broadness moving from OPh to SPh to SePh. This could suggest that the *t*Bu groups increase the activation energy for at least one of the bridge-centered inversion processes, such that the use of a heavier chalcogenide is sufficient to approach the point of coalescence at room

temperature. This could be further probed by low temperature NMR experiments on the thio-and seleno-phenolate complexes, or alternatively by the synthesis of the tellurolate-bridged analogue.

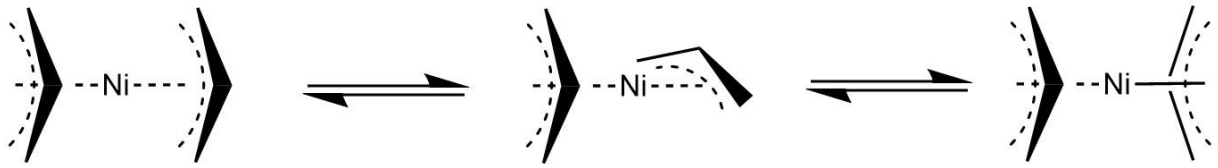

Figure 4.19: A proposed allyl rotation process producing staggered/eclipsed interconversion, a possible explanation for the observed trends in ^{1}H NMR spectral features of [{A^{2t}NiBr}$_2$] and [{A^{2t}Ni}$_2$(μ^2-NHPh)(μ^2-Br)] compounds. For clarity, the mechanism is shown on a bis(allyl)nickel complex.

It is also noteworthy that all three species identified as likely mono-substitution products, [{A^{2t}Ni}$_2$(μ^2-NHPh)(μ^2-Br)], [{A^{2t}Ni}$_2$(μ^2-OH)(μ^2-Br)], and [{A^{2t}Ni}$_2$(μ^2-SPh)(μ^2-Br)] show sharp, symmetric peaks despite the lateral asymmetry of the (Br)/(ER$_n$) bridges, and also appear to lack isomeric speciation like that seen in the [{A^{2t}NiER$_n$}$_2$] complexes. This is interesting, as it matches the behavior of the purely halide-bridged species (See Chapter 3). This was originally attributed to a lack of accessible modes to interconversion. However, the stark contrast between the species that have at least one substituent-lacking halide bridge and those that do not prompts a reevaluation of this idea. Furthermore, the observation that the small hydroxo-bridged dimer displays substantial peak broadening while the large phenolate-bridged species displays perfectly sharp peaks further supports the possibility that rapid eclipsed/staggered interconversion occurs in [{A^{2t}Ni}$_2$(ER$_n$)$_y$(X)$_{2-y}$] (y = 0-2) type species in the absence of steric hindrance from the bridging ligands. A 1994 paper proposed that such staggered/eclipsed interconversion in aryloxide-bridged allylnickel species most likely occurred via either a bridge fission-reformation or an allyl rotation (See Figure 4.19) mechanism.[29] The bulkier allyls of the complexes presented here would be expected to increase the rate of dissociative processes, yet no eclipsed/staggered interconversion appears to be operative in any [{A^{2t}NiER$_n$}$_2$] complex. Furthermore, the apparent requirement of only a single unhindered bridge is consistent with a one-directional rotation process like that depicted above; as such, we propose that this mechanism is operative in bridged dimeric allylnickel species across multiple bridge types, and indeed likely also operative in analogous palladium complexes. This mechanism appears to be distinct to the bimetallic [{A^{2t}NiX}$_2$] archetype, as no evidence for its occurrence in bis(allyl)nickel complexes has been observed. However, it must be stressed that these observations are suggestive, not definitive, and much

work remains to be done to determine an accurate and complete mechanism and to disentangle this process from related bridge-centered inversion processes.

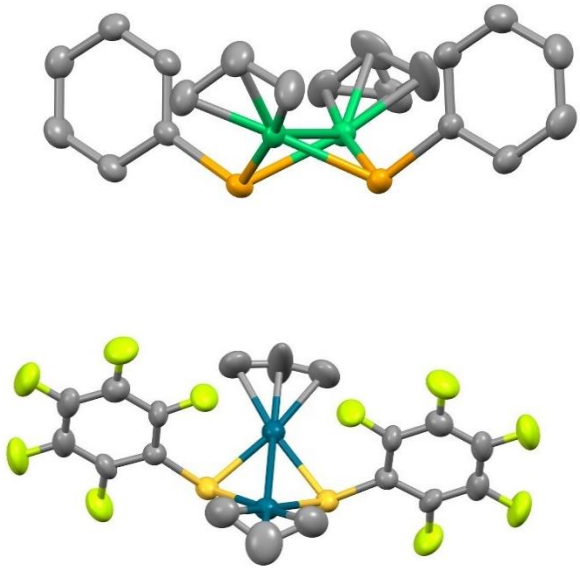

Figure 4.20: Thermal ellipsoid plot of the molecular structures of [{ANiSePh}$_2$][101] (top) and [{APd(SC_6F_5)}$_2$][90] (bottom) (50% probability). Hydrogen atoms are omitted for clarity.

Further information can be obtained by comparing the more diverse chemistry seen in the solid state. In [{APd(SC_6F_4H)}$_2$] and [{APd(SC_6F_5)}$_2$],[90] the allyls are disordered between eclipsed-*anti* and staggered, while in [{ANiSePh}$_2$][101] the allyls are disordered between eclipsed-*syn* and staggered, while in [{APd(p-C_6H_4F)}$_2$],[102] the relative orientation of the allyls is fully disordered (See Figure 4.20 above). This contrasts with analogous A^{2t} complexes, which show no disorder and are exclusively found in the eclipsed-*syn* orientation. It is also notable that in the parent allylnickel selenophenolate and in all three structurally characterized allylpalladium thiophenolates, the phenyl rings are exclusively *endo*, while in [{A^{2t}NiOPh}$_2$] and [{A^{2t}NiSPh}$_2$], exclusively *exo* substituents are observed. Together, these comparisons suggest that the *t*Bu groups create a meaningful energy difference between the eclipsed and staggered forms. The specific preference for the eclipsed-*syn* with *exo* E-Ph substituents is likely a purely steric effect. As *exo* substituents bend further from the {NiER}$_2$ core, this specific arrangement maximizes the distance between the phenyl rings and the bulky *tert*-butyl groups. The apparent dominance of steric effects observed suggests a shallow potential energy surface for deformation of the stereochemistry of the {NiER$_n$}$_2$ core. Considering the set

of previously reported sulfur- and selenium-bridged complexes, it is notable that their structures vary little despite large variations in the nature of the bridge-substituent phenyl rings. This suggests that the electron donating strength of the bridging ligand, at least within a series with the same bridging atom, does not have a meaningful effect on the optimal geometry of the complex.

The exclusive observation of allyls with *syn,syn* configurations is notable in the context of the apparently asymmetric allylic spin systems seen in the ^{1}H NMR spectra of certain [{A^{2t}NiER$_n$}$_2$] compounds. This was investigated computationally using the -SPh bridged species as the model compound. As mentioned above, complete mapping of this space is not feasible due to its complexity, and our attempts were hampered by inconsistent retention of the initial stereochemical relations. However, a few tentative conclusions can be drawn from the collected computational data (See Appendix 4 for full table of computed isomers.) First, the highest energy structure of all 13 compiled is the only one that optimized to a flat geometry. This underscores that the observed bending is not a crystal packing effect or even the result of minor energy differences, but instead the most significant conformational preference in the molecule. The data also suggests that the *syn,syn* configuration of allylic substituents is meaningfully preferred over the *syn,anti* configuration, as all three isomers within 10 kJ/mol of the most stable isomer display exclusively *syn t*Bu groups. However, the data compiled so far is not sufficient to rule out *syn,anti* allylic substituents as the cause of the asymmetry observed by NMR in some cases.

4.2.4 Bulky Heteroatom Anions and Decomposition Discussion

As briefly mentioned above, the reaction of [{A^{2t}NiBr}$_2$] with certain nucleophiles yielded apparent decomposition products as the only collectable material. However, certain nucleophiles reacted in a consistent, yet unexpected manner, deserving special comment. Specifically, potassium *tert*-butoxide and potassium hexamethyldisilazide (HMDS$^-$) both react immediately with [{A^{2t}NiBr}$_2$] in THF to yield solutions of identical appearance. These solutions have a peculiar appearance, displaying a dark purple coloration yet remaining quite translucent; this is notably distinct from the red-orange-yellow spectrum of colors seen for the heteroatom-bridged species discussed here. The most notable feature of these complexes is their pronounced instability in THF solution -- within seconds of addition, both mixtures undergo color changes to reddish-orange colors. They are more stable in less polar solvent systems; the solubility of [KHMDS] is sufficient for the reaction to proceed in toluene, while an equivolume mixture of THF and toluene was sufficient to stabilize the [KO*t*Bu] mixture until the solvent could be removed. This allowed for the isolation of deep purple solids from each reaction. Even after removal of solvent, the resulting purple solids were unstable towards storage in the THF-containing glovebox. The [KO*t*Bu] product fully degraded upon sitting overnight, while the [KHMDS] product took multiple days to fully degrade. Isolation of the purple solids allowed them to be characterized by ^{1}H NMR. In both cases, a single predominant species,

with very similar features, was observed. Each species consisted of a single *syn,syn* A^{2t} ligand in a 1:1 ratio with peaks consistent with -O*t*Bu and -HMDS ligands.

Reactions with potassium diphenylamide proceeded very similarly to the butoxide and silazide reactions, yielding a peculiarly translucent solution that was reddish brown rather than dark purple. This species demonstrated stability between that of the -O*t*Bu and -HMDS species. Additionally, this species appeared to be a single product that is consistent with an empirical formula of $[A^{2t}NiNPh_2]$. However, this species was never completely isolated from decomposition products that may have formed contemporaneously with metathesis. The compound $[\{ANi(NPh_2)\}_2]$ has been reported, but no details of the compounds synthesis or properties are readily available.[17,35]

Based on these NMR features, it might seem reasonable to conclude that the purple solids were the expected $[\{A^{2t}NiER\}_2]$ complexes. However, there are some notable deviations from the behavior expected for such compounds that make this assignment less obvious. First is the coloration, which was purple rather than red or orange. Secondly, no isomerism was seen in the proton NMR spectra. In both of these regards, these features are unique compared to every other bridged allyl nickel species isolated. The reaction with anilide is a useful foil in this respect. It also features an N-donor nucleophile and yields an unstable product that is made more unstable by exposure to THF. It, however, displays the same orange-red coloration and complex product mixture as the other heteroatom-bridged compounds. As such, alternative possibilities for the identities of these distinct products should be considered.

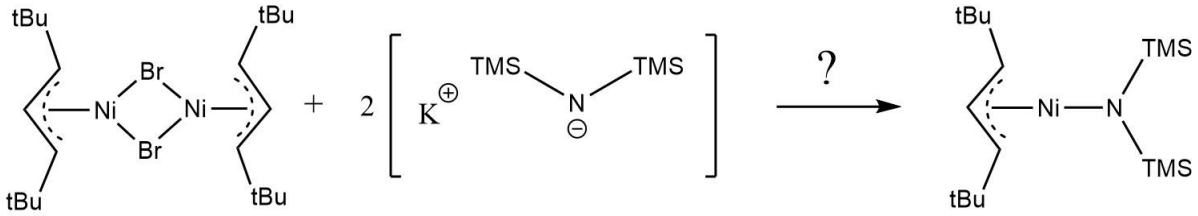

Figure 4.21: Reaction scheme showing the possible formation of three-coordinate species from sterically bulky, strongly basic nucleophiles, in this case $[HMDS]^-$.

The question therefore arises: what about these three anions leads to this divergent reactivity? A first notable feature of this group is their high basicity. Indeed, all three anions are more basic than any of the heteroatom-centered anions that gave stable products, as measured by the pK_a values of their conjugate acids.[60,122] Such a metric is likely appropriate, as a previous study on nickel(II) complexes on heteroatoms found anion conjugate acid pK_a to be a good predictor of complex basicity.[87] However, basicity alone cannot

explain the observed reactivity, as aniline is a weaker acid than diphenylamine; therefore at least one other factor must be involved. A second notable commonality between the three atypical anions is their size. These three are the most sterically bulky nucleophiles considered here; given the existing bulkiness of the allyl, atypical reactivity with such bulky anions seems plausible. One possibility is that these ligands are too bulky to accommodate the bridged motif, instead being limited to *pseudo*-three coordinate geometries (See Figure 4.21 above). The ability of bulky amido- ligands to support such low coordinate nickel centers is well established;[108,123,124] indeed, homoleptic nickel complexes of the diphenylamide ligand show trigonal planar geometries.[125] An alternative, more radical possibility is that, like the infamously elusive [Ni(HMDS)$_2$],[126] these complexes are spontaneously reduced to some manner of Ni(I) complex featuring a mixed A^{2t}/ER_n ligand set. Each of the last two possibilities would provide some stronger rationalization for the extreme sensitivity of the compounds. It is possible that some insight could be gained by studying the reaction with a source of the *tert*-butylthiolate anion. This would display the same steric bulk as *tert*-butoxide, but the apparent greater stability of alkylthiolates compared to their oxygen analogues might allow for the resulting species to be fully characterized. A S*t*Bu-bridged dipalladium species has been previously reported, demonstrating that such a species is plausible. [127]

The decomposition of these complexes deserves comment and relates to the decomposition of all A^{2t} species discussed above. The decomposition of reactions with alkoxides and amides were inconsistent and often complex, but certain species were observed repeatedly from disparate reactions. Indeed, crystals identified as [{A^{2t}NiOH}$_2$] were obtained from the products of reactions with [KA′], [KHMDS], [KPyrrolide], and [KNPh$_2$]. Consistent decomposition outcomes are substantiated by ^{1}H NMR, in which three spin systems were commonly seen. These three species are the two isomers identified as [{A^{2t}NiOH}$_2$] and a species that was once observed in the incomplete reaction of [{A^{2t}NiBr}$_2$] with [TlOH]; this suggests a partial substitution product [A^{2t}Ni(Br)(OH)NiA^{2t}], or perhaps some more complex hydroxo compound. One or both of these dominate the observed the post-decomposition mixtures of reactions with [KOtBu], [LiOtBu], and [LiNHPh] in addition to those listed above. Also of note are the atypical crystals obtained from one particular reaction with [KOtBu]; these were of poor quality, but are consistent with a tris(A^{2t})trinickel-bis(μ^3-hydroxo) species. The assignment as hydroxo rather than oxo is arbitrary, and the protonation state of the oxygens and oxidation state of the nickel are ambiguous. Such a structure is consistent with a hydroxo-bridged compound published in 1985.[128] The NMR of the mixture from which these crystals was grown did not show either of the common decomposition products mentioned above, suggesting that this trimetallic species is distinct.

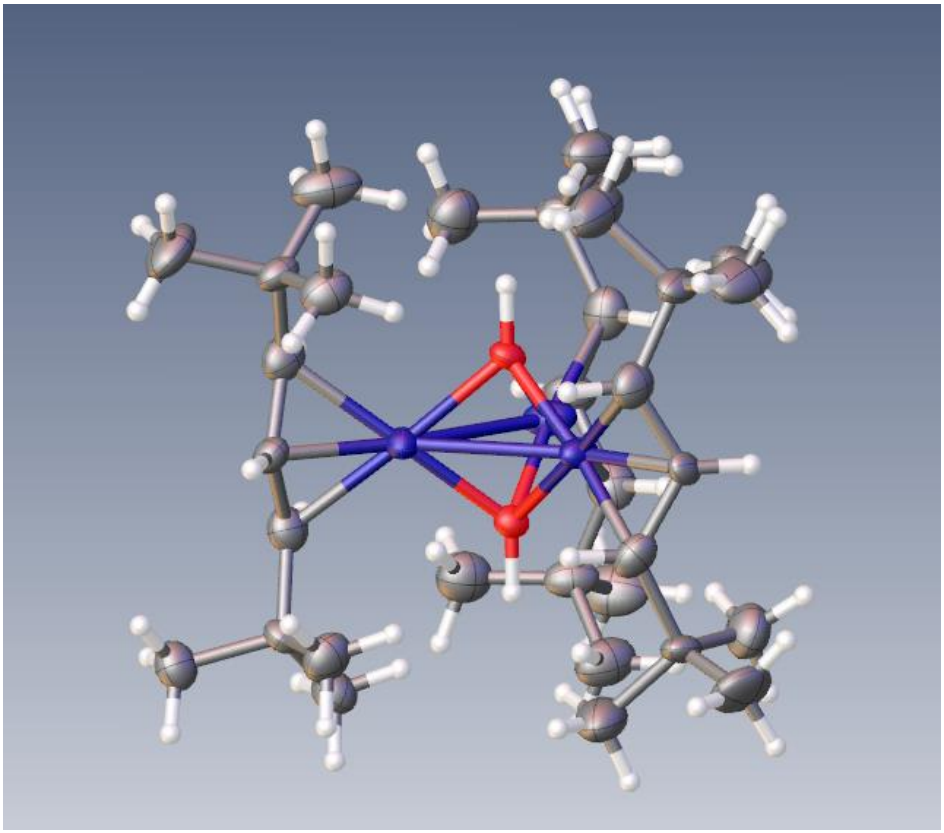

Figure 4.22: Structure of $[(\mu^3\text{-OH})_2(A^{2t}Ni)_3]$, a potential solution for crystals obtained as decomposition products in the reaction of $[\{A^{2t}NiBr\}_2]$ with KO*t*Bu. The bridging groups have been arbitrarily assigned as hydroxo, but their protonation state is ambiguous.

As in the fluorenyl and A′ complexes discussed above, the most obvious explanation for the decomposition pathways seen here is the intrusion of adventitious water. Indeed, the formation of two distinct hydroxo-bridged nickel(II) species via decomposition of related η^3-benzylnickel compounds upon reaction with pyrrolide salts has been noted.[42] These results were attributed to water infiltration; formation of $[\{Ni(CH_2C_6H_4\text{-o-Me})(PMe_3)(\mu\text{-OH})\}_2]$ was depressed when rigorously anhydrous conditions were used and reproducible formation of $[Ni_3(CH_2C_6H_4\text{-o-Me})_4(PMe_3)_2(\mu^3\text{-OH})_2]$ involved addition of a drop of water to the reaction mixture. While water is a convenient explanation for the observed reaction outcomes, some factors warrant additional discussion. After the first observation of the $[\{A^{2t}NiOH\}_2]$ complex, measures were taken to combat the apparent water contamination. The glovebox catalyst was regenerated, all glass

surfaces and many chemicals particularly sensitive to hydrolysis were removed, and all solvents were removed and replaced with freshly dried batches. However, these extensive measures did not have a noticeable impact on reaction outcome. During this investigation, anhydrous THF was obtained by three different methods: distillation from sodium/benzophenone; passage through a commercial SPS-alumina column; and passage of commercially obtained anhydrous THF through a homemade column of freshly activated alumina. In all methods, the dried THF was then allowed to sit over freshly dried 3Å molecular sieves for 12 hours before use. Despite these attempts to obtain rigorously anhydrous THF, no noticeable change in decomposition rate or outcome was ever observed.

It should be noted that no desiccation method is perfect, and after extensive drying, THF has been shown to have more than four times the residual water content than the nonpolar solvent toluene.[129] Therefore, a plausible explanation is that the compounds generated here are sufficiently reactive that even rigorously dried THF contains sufficient water content to induce complete degradation. However, it is worth noting that the putative [A^{2t}NiHMDS], due to the high solubility of [$HMDS^-$] salts, can be generated without exposure to THF. And indeed, if this material is made and then stored in a glovebox free from ethers, its longevity was substantially increased, showing slow decomposition over the course of approximately two or more weeks. If the water content of dry THF is solely responsible for the observed decomposition, then to account for this observation, the water content of the glovebox atmosphere must be directly tied to the water content of its wettest solvent. It is not clear that this must be true, especially in the low water concentration limits relevant here, and so the cause of the decomposition remains unclear. However, it is clear that decomposition most often involves obtaining one or more exogenous oxygen atoms, so other oxygen sources should be considered.

One possibility is that molecular oxygen, rather than water, is inducing this decomposition. The reaction of allylnickel complexes with molecular oxygen to produce hydroxide dimers is indeed precedented,[130,131] though the oxidized allyl byproducts have never been observed in our systems. This does not seem to account for the solvent dependent decomposition rate, though. Considering the role of ethereal solvents in inducing decomposition, it does become notable that these also contain oxygen atoms. Reaction of transition metal centers with THF is well-precedented,[132] and indeed has been observed for nickel(II) complexes.[133] Ring opening of THF to form an anionic O-bound ligand is also known for organometallic complexes.[134] This would represent a particularly convenient explanation consistent with the observed data. However, it is not clear that the ring opening is plausible at a nickel(II) center, there is no clear mechanism by which an initial activation product could be converted to an isolated hydroxo ligands, and no clear reason why any such process should be spontaneous. Therefore, this remains entirely speculative. Future investigation of these systems could include performing the reactions in non-polar solvents with

systematically varied amounts of water present and comparing the reaction outcomes to those performed in THF.

We also considered the possibility that decomposition is not induced by reaction with an external species but by direct nucleophilic attack of heteroatomic anion on the terminal allyl carbons. This is a common mechanism for activation of allylpalladium-based precatalysts. The formation of an olefin complex of the form (XA^{2t})Ni(0) might then be a plausible identity for the highly reactive purple species identified from reaction with [KHMDS] and [KO*t*Bu]. However, we consider this mechanism unlikely for two reasons. First of these is the decreased electrophilicity of nickel-bound allyls compared to palladium-bound. Second, it is expected that the final olefin decomposition product XA^{2t} would be observed in the product mixtures for these reactions, but no evidence of such a species has ever been seen by ^{1}H NMR.

4.4 Conclusions

From this investigation, it was found that, as predicted, complexes with the bulky A^{2t} ligand were substantially more stable than their analogues with unsubstituted allyl ligands. This is most apparent in the example of the bridged [{A^{2t}NiSePh}$_2$], which was stable for a week or longer, while its parent compound degraded entirely within 30 minutes. This stability can be leveraged to obtain novel compounds such as [A^{2t}NiA´], [A^{2t}NiFluor], and [{A^{2t}Ni}$_2$(Br)(NHPh)]. The increase in stability and ease of handling also allows for the isolation and structural characterization of putative catalytic intermediates, such as [{A^{2t}NiOH}$_2$] and [{A^{2t}NiOPh}$_2$], that have otherwise been elusive. Furthermore, this structural characterization has suggested that these A^{2t}-nickel complexes do not substantially differ from the structures of their unsubstituted analogues. This confirms that A^{2t} complexes are indeed appropriate model complexes for more common, less substituted catalytic intermediates.

4.5 Directions for further study

As mentioned above, the stereochemistry of the bent bridged allyl nickel species remains poorly understood. This will be partially remedied by general development of this class of molecules; as more species are crystallographically characterized, structural trends will become more apparent. However, some more targeted study could also be warranted. In particular, more information on the dynamic processes undergone by the {NiE}$_2$ core would be valuable. This can be pursued via a combination of new synthetic targets (tellurium and phosphorus analogues of phenolate and anilide complexes, [{A^{2t}NiNHPh}$_2$]), variable temperature NMR experiments, and broader computational modelling. Additionally, the effects of substitution of the bridge substituents should also be investigated. The phenyl ring of the stable thiophenolate complex offers a convenient avenue to systematically study the impact of bridge sterics and electronics on the observed structure.

In Chapter 3, it was noted that [{A^{2t}NiBr}$_2$] resists the binding of triphenylphosphine. The extent to which this property is shared by the novel bridged complexes described here would be of interest. Such a study would shed greater light on the factors giving rise to the observed resistance to ligand binding, and the potential benefits of tunable ligand binding in a catalytic context is discussed in Chapter 5. Furthermore, this study should be extended to a broader set of neutral ligands in order to more precisely determine the basicity required to induce full monomerization for each compound.

Despite the range of anionic ligands studied here, there are still a great many others that could also be investigated. A few of particular interest are discussed here. Complexes of heavier pnictogenides and chalcogenides are rarer than their lighter counterparts. The series of non-radioactive chalcogenides could be completed by pursuing phenyltellurolate-bridged species.[135] As an anilide bridge was accessible and that S-bridged species were generally more stable than the O-bridged species, it seems plausible that phosphide-bridged complexes are likely accessible. Indeed, a preliminary reaction with an impure sample of $LiPPh_2$ yielded a complex mixture that notably did not include the decomposition products seen in the reaction with $KNPh_2$. If phosphide bridges are possible, then perhaps arsenide-bridged complexes could be targeted.

A possibly interesting extension of the Cp-type ligand series would be the use of the open-face carborane [*nido*-7,8-$C_2B_9H_{11}$]$^{2-}$, also known as the dicarbollide anion. Dicarbollide ligands are well known for their ability to stabilize higher oxidation states, so it is possible that oxidation to a stable [A^{2t}Ni $C_2B_9H_{11}$] species could be isolated. As studied allyl nickel complexes have almost exclusively been in the Ni(II) state (one suite of exceptions are some palladium(I) dimers featuring bridging allyls[136]), it could be interesting to observe which, if any, properties are affected by a change in d-electron count. A dicarbollide complex of the parent allyl has been reported, but its electrochemistry was not investigated.[137]

4.6 Experimental:

4.6.1 General procedure for salt metathesis reactions with [{A^{2t}NiBr}$_2$]

Unless otherwise noted, reactions were performed using the following general procedure. Approximately 0.0050 g [{A^{2t}NiBr}$_2$] was measured into a 15 mL glass vial, and dissolved in 2.5 mL THF. A mass corresponding to two molar equivalents of a nucleophilic anion source M-An is dispersed in 2.5 mL THF, and the mixture added slowly to the [{A^{2t}NiBr}$_2$] solution. The mixture was swirled to ensure full mixing, the vial was capped, and the mixture allowed to stand overnight. At this point, the volatiles were removed from the reaction mixture. The resulting residue was extracted with hexane; this extract was filtered through a celite-packed pipette. The volatiles were removed from the filtrate, yielding the isolated product mixture.

Reaction of [{A^{2t}NiBr}$_2$] with sodium triethylborohydride:

The reaction of [{A^{2t}NiBr}$_2$] with [Na(HBEt$_3$)] in diethyl ether at -100 °C induced a color change to a reddish brown. This color persisted until warmed to about -50 °C, at which point the reaction mixture began to darken. By the time the reaction warmed to -30 °C, the solution had become colorless and a black solid had precipitated out. This clearly indicated decomposition via reduction of the metal center at temperatures above -50 °C. It is unclear if the brown compound formed initially was the desired hydrido bridged species.

Reaction of [{A^{2t}NiBr}$_2$] with methyllithium:

Standard procedure was followed with the exception that methyllithium was added dropwise from a stock solution prepared immediately before reaction. If the stock solution used only THF as a solvent, then no change was observed upon addition and spectroscopically pure [{A^{2t}NiBr}$_2$] could be recovered. If the stock solution used primarily hexane as solvent, including only enough THF to ensure the solubility of the methyllithium, then addition caused an immediate color change to black. ^{1}H NMR analysis of the product of this process showed only complex signals in the upfield region.

Reaction of [{A^{2t}NiBr}$_2$] with trimethylsilylmethyllithium:

The procedure described above for the reactions with methyllithium was recreated here. In this case, the immediate change to black was observed regardless of the solvent used in creating the stock solution, and ^{1}H NMR analysis of products was not performed.

*[(1,3-di-*tert*-butylallyl)(1,3-bis(trimethylsilylallyl)nickel(II)] "[A^{2t}NiA´]":*

Standard procedure produced a yellow-orange oil in quantitative (103% average) yield. The reaction was also performed at -78 °C, but no difference in yield or isomer ratios was observed. This transformation was also attempted under mechanochemical conditions (Mixer mill, 15 mL stainless steel jar, two 9.5 mm stainless steel balls, 15 min., 30 Hz) but this yielded only a dry black powder, indicative of reduction to nickel black. See Section 4.2.2.2 for discussion of stereochemical assignments.

Staggered [*syn,syn*-A^{2t}Ni-*syn,anti*-A´] (1 eq.): ^{1}H NMR (600 MHz, C_6D_6): δ 5.60 (dd, *J* = 16.4, 9.9 Hz, 1H, center A´ allyl proton); δ 5.15 (dd, J = 13.6, 12.1 Hz, 1H, center A^{2t} allyl proton); δ 3.85 (d, J = 9.9, 1H, *syn* allyl C(TMS)-H); δ 2.60 (dd, *J* = 12.1, 1.0 Hz, 1H, allyl *anti* C(H)*t*-Bu); δ 2.37 (dd, *J* = 13.6, 1.0 Hz, 1H, allyl *anti* C(H)*t*-Bu); δ 1.88 (d, 16.4 Hz, 1H, *anti* allyl C(TMS)-H); δ 1.27 (s, 9H, *t*-Bu (CH_3)$_3$); δ 1.20 (s, 9H, *t*-Bu (CH_3)$_3$); δ 0.34 (s, 9H, TMS (CH_3)$_3$); δ 0.05 (s, 9H, TMS (CH_3)$_3$). ^{13}C{^{1}H} NMR (151 MHz, C_6D_6): δ 124.8 (s, A´ center allyl carbon); δ 101.6 (s, central A^{2t} carbon); δ 92.4 (s, C(H)*t*-Bu);); δ 79.5 (s, C(H)*t*-Bu); δ 62.5 (s, C(H)TMS); δ 59.0 (s, C(H)TMS); δ 33.7 (s, *t*-Bu CMe_3); δ 33.3 (s, *t*-Bu (CH_3)$_3$); δ 32.9 (s, *t*-Bu CMe_3); δ 31.9 (s, *t*-Bu (CH_3)$_3$); δ 1.5 (s, TMS (CH_3)$_3$); 1.4 (s, TMS (CH_3)$_3$).

Eclipsed [*syn,syn*-A^{2t}Ni-*syn,anti*-A′] (0.76 eq.): ^{1}H NMR (600 MHz, C_6D_6): δ 5.13 (dd, *J* = 16.4, 10.0 Hz, 1H, center A′ allyl proton); δ 4.54 (dd, J = 14.2, 11.6 Hz, 1H, center A^{2t} allyl proton); δ 3.58 (d, J = 10.1, 1H, *syn* allyl C(TMS)-H); δ 3.30 (d, *J* = 12.1 Hz, 1H, allyl *anti* C(H)*t*-Bu); δ 2.93 (d, *J* = 13.6, 1H, allyl *anti* C(H)*t*-Bu); δ 2.34 (d, 16.4 Hz, 1H, *anti* allyl C(TMS)-H); δ 1.25 (s, 9H, *t*-Bu $(CH_3)_3$); δ 1.07 (s, 9H, *t*-Bu $(CH_3)_3$); δ 0.29 (s, 9H, TMS $(CH_3)_3$); δ 0.07 (s, 9H, TMS $(CH_3)_3$). ^{13}C{^{1}H} NMR (151 MHz, C_6D_6): δ 124.0 (s, A′ center allyl carbon); δ 101.6 (s, central A^{2t} carbon); δ 99.9 (s, C(H)*t*-Bu);); δ 74.8 (s, C(H)*t*-Bu); δ 63.9 (s, C(H)TMS); δ 58.9 (s, C(H)TMS); δ 33.2 (s, *t*-Bu CMe_3); δ 33.1 (s, *t*-Bu CMe_3); δ 32.2 (s, *t*-Bu $(CH_3)_3$); δ 32.1 (s, *t*-Bu $(CH_3)_3$); δ 1.5 (s, TMS $(CH_3)_3$); 1.1 (s, TMS $(CH_3)_3$).

Staggered *cis*-[*syn,anti*-A^{2t}Ni-*syn,anti*-A′] (0.36 eq.): ^{1}H NMR (600 MHz, C_6D_6): δ 5.541 (dd, *J* = 16.5, 10.1 Hz, 1H, center A′ allyl C-H); δ 4.58 (dd, J = 15.1, 9.3 Hz, 1H, center A^{2t} allyl C-H); δ 4.26 (dd, J = 9.39, 0.8 Hz, 1H, *syn* allyl C(H)*t*-Bu); δ 3.76 (d, *J* = 10.1 Hz, 1H, *syn* allyl C(H)TMS); δ 3.51 (dd, *J* = 15.0, 0.9 Hz, 1H, allyl *anti* C(H)*t*-Bu); δ 1.89, (d, J = 16.5 Hz, 1H, *anti* allyl C(H)TMS); δ 1.26 (s, 9H, *t*-Bu $(CH_3)_3$); δ 0.82 (s, 9H, *t*-Bu $(CH_3)_3$); δ 0.33 (s, 9H, TMS $(CH_3)_3$); δ -0.03 (s, 9H, TMS $(CH_3)_3$). ^{13}C{^{1}H}) NMR (151 MHz, C_6D_6): δ 123.6 (s, A′ center allyl carbon); δ 101.7 (s, A^{2t} central allyl carbon); δ 90.8 (s, A^{2t} terminal allyl carbon);); δ 77.1 (s, A^{2t} terminal allyl carbon); δ 62.6 (s, A′ terminal allyl carbon); δ 61.3 (s, A′ terminal allyl carbon); δ 35.6 (s, *t*-Bu CMe_3); δ 34.9 (s, *t*-Bu CMe_3); δ 32.9 (s, *t*-Bu $(CH_3)_3$); δ 32.3 (s, *t*-Bu $(CH_3)_3$); δ 1.2 (s, TMS $(CH_3)_3$); δ 1.1 (s, TMS $(CH_3)_3$).

Reaction of [{A^{2t}NiBr}$_2$] with allylmagnesium chloride:

The standard procedure allowed a thin yellow oil to be isolated. ^{1}H NMR analysis shows two equally intense A^{2t}/A pairs. The spectrum appeared identical after the sample was stored in the glovebox for seven days. As the identity of the molecule giving rise to each allyl spin system cannot be conclusively determined, each is presented separately.

A^{2t} system 1 (1 eq): ^{1}H NMR (600 MHz, C_6D_6): δ 5.07 (t, *J* = 13.0 Hz, 1H, allyl center C-H); δ 2.56 (d, *J* = 13.0 Hz, 2H, allyl terminal C-H); δ 1.20 (s, 18H, *t*Bu $(CH_3)_3$).

A system 1 (1 eq) ^{1}H NMR (600 MHz, C_6D_6): δ 4.85 (tt, *J* = 14.0, 7.4 Hz, 1H, allyl central C-H); 3.73 δ (d, *J* = 7.5 Hz, 2H, *syn* terminal allyl C-H); δ 1.74 (d, *J* = 14.1 Hz, 2H, *anti* terminal allyl C-H);

A^{2t} system 2 (0.48 eq) ^{1}H NMR (600 MHz, C_6D_6): δ 4.57 (t, *J* = 13.0 Hz, 1H, central allyl C-H); δ 2.93 (d, *J* = 12.9 Hz, 2H, terminal allyl C-H); δ 1.17 (s, 18H, *t*Bu $(CH_3)_3$);

A system 2 (0.48 eq) ^{1}H NMR (600 MHz, C_6D_6): δ 4.49 (tt, 1H, central allyl C-H); δ 3.48 (d, *J* = 7.7, 1.1 Hz, 2H, *syn* terminal allyl C-H); δ 2.16 (d, *J* = 14.2 Hz, 2H, *anti* terminal allyl C-H);

*[(1,3-di-*tert*-butylallyl)(cyclopentadienyl)nickel(II)] "[A^{2t}NiCp]":*

Standard procedure allowed for the isolation of a reddish-gray solid residue in 86.7% average yield. Small crystals were grown by slow evaporation of a hexane solution. The compound is exceedingly soluble in all nonpolar liquids.

^{1}H NMR (600 MHz, C_6D_6): δ 5.46 (s, 5H, Cp-?Me); δ 4.93 (t, *J* = 10.2 Hz, 1H, terminal allyl C-H); δ 2.21 (d, *J* = 10.3 Hz, 2H, terminal allyl C-H); δ 1.08 (s, 18H, *t*-Bu $(CH_3)_3$). ^{13}C{^{1}H}) NMR (151 MHz, C_6D_6): δ 88.7 (s, Cp C-Me); δ 83.1 (s, central allyl CH); δ 75.2 (terminal allyl C(H)*t*-Bu); δ 32.5 (s, center tBu CMe_3); δ 30.4 (s, $(CH_3)_3$).

*[(1,3-di-*tert*-butylallyl)(pentamethylcyclopentadienyl)nickel(II)] "[A^{2t}NiCp*]":*

Standard procedure allowed for the isolation of a dark green, highly crystalline solid in quantitative (107% average) yield. Material was highly soluble in non-polar liquids. Anal. Calcd for $C_{21}H_{36}Ni$: C, 72.64; H, 10.45. Found: C, 69.81; H, 9.93.

^{1}H NMR (600 MHz, C_6D_6): δ 4.88 (t, *J* = 10.3 Hz, 1H, center allyl C-H); δ 1.89 (s, 15H, Cp-Me); δ 1.71 (d, *J* = 10.32 Hz, 2H, terminal allyl C-H); δ 1.07 (s, 18H, *t*-Bu $(CH_3)_3$). ^{13}C{^{1}H}). NMR (151 MHz, C_6D_6): δ 98.4 (s, Cp C-Me); δ 86.3 (s, center allyl CH); δ 74.8 (s, terminal allyl C(H)*t*-Bu); δ 33.1 (s, center tBu CMe_3); δ 30.3 (s, $(CH_3)_3$); δ 11.3 (s, (Cp-CH_3).

*[(1,3-di-*tert*-butylallyl)(indenyl)nickel(II)] "[A^{2t}NiInd]":*

Standard procedure allowed for the isolation of an oily orange solid that appears indefinitely stable in the glovebox atmosphere.

^{1}H NMR (600 MHz, C_6D_6): δ 7.14 (m, 2H, phenyl); δ 6.91 (m, 2H, phenyl); δ 6.20 (t, *J* = 2.9 Hz, 1H, center indenyl); δ 5.60 (d, *J* = 2.92 Hz, 2H, terminal indenyl); δ 4.52 (t, *J* = 11.4 Hz, 1H, allyl center); δ 2.00 (d, *J* = 11.4 Hz, 2H, allyl terminal); δ 0.98 (s, 19H, tBu methyl). NMR (151 MHz, C_6D_6): δ 121.6 (s, phenyl CH); δ 119.8 (s, ring bridge C(H)*t*-Bu); δ 118.9 (s, phenyl CH); δ 100.1 (s, center indenyl CH); δ 90.3 (s, center allyl CH); δ 78.5 (s, terminal allyl C(H)*t*-Bu); δ 73.3 (s, terminal indenyl CH); δ 33.2 (s, tBu center *t*-Bu CMe_3); δ 30.4 (s, tBu methyl *t*-Bu $(CH_3)_3$).

*[(1,3-di-*tert*-butylallyl)(4,7-dimethylindenyl)nickel(II)] "[A^{2t}NiInd^{2Me}]":*

Standard procedure allowed for the isolation of an orange solid in quantitative (101.4%) yield. This material is highly soluble in organic solvents and appears indefinitely stable in the glovebox atmosphere. Anal. Calcd for $C_{22}H_{32}Ni$: C, 74.39; H, 9.08. Found: C, 73.61; H, 9.25.

^{1}H NMR (600 MHz, C_6D_6): δ 6.71 (s, 2H, aryl C-H); δ 6.33 (t, *J* = 3.0 Hz, 1H, center indenyl C-H); δ 5.69 (d, *J* = 3.0 Hz, 2H, terminal indenyl C-H); δ 4.55 (t, *J* = 11.4 Hz, 1H, center allyl C-H); δ 2.34 (s, 6H, Ar-CH_3); δ 2.11 (d, *J* = 11.5 Hz, 2H, terminal allyl C-H); δ 1.01 (s, 18H, *t*-Bu $(CH_3)_3$). ^{13}C{^{1}H} NMR (101 MHz, C_6D_6): δ 124.2 (s, aryl C-Me); δ 123.0 (s, aryl CH); δ 122.0 (s, ring bridge carbons); δ 99.9 (s center indenyl CH); δ 90.3 (s, center allyl CH); δ 77.9 (s, terminal allyl C(H)*t*-Bu); δ 71.8 (s, terminal indenyl CH); δ 33.0 (s, *t*-Bu CMe_3); δ 30.8 (s, *t*-Bu $(CH_3)_3$); δ 19.0 (s, Ar-CH_3).

*[(1,3-di-*tert*-butylallyl)(fluorenyl)nickel(II)] "[A^{2t}NiFluor]":*

Standard procedure was followed with the exception that the reaction mixture was allowed to stir for no more than two minutes after the addition of [KFluor]. At that point, the volatiles were removed, and workup proceeded as normal. This procedure allowed for the isolation of a brick-red, highly crystalline solid in 75% average yield. Anal. Calcd for $C_{24}H_{30}Ni$: C, 76.43; H, 8.02. Found: C, 74.18; H, 8.03.

The compound demonstrates substantial peak broadening in the ^{1}H NMR spectrum at room temperature. As such, many features cannot be observed. Only peaks that can be confidently assigned are included below. ^{1}H NMR (600 MHz, C_6D_6): δ 7.80 (bm); δ 7.04 (bm); δ 7.04 (bm); δ 5.53 (s, 1H, fluorenyl C9-H); δ 4.33 (t, J = 11.6 Hz, 1H, allyl center C-H); δ 0.91 (bs, 18H, *t*-Bu $(CH_3)_3$). ^{13}C{^{1}H} NMR (151 MHz, C_6D_6): δ 121.0 (s); δ 120.3 (s); δ 90.3 (s, center allyl C-H); δ 56.5 (s, fluorenyl C9-H); δ 27.7 (s, *t*-Bu $(CH_3)_3$).
^{1}H NMR (600 MHz, C_6D_6): δ 7.79 (bd, J = 7.5 Hz); δ 7.00 (bm); δ 7.04 (bm); δ 5.66 (s, 1H, fluorenyl C9-H); δ 4.40 (t, J = 11.3 Hz, 1H, allyl center C-H). ^{13}C{^{1}H} NMR (151 MHz, C_6D_6): δ 121.4 (s); δ 119.0 (s); δ 118.5.0 (s); δ 117.5.0 (s); δ 90.2 (s, center allyl C-H); δ 57.0 (s, fluorenyl C9-H).

Reaction of [{A^{2t}NiBr}$_2$] with potassium pyrrolide: Standard procedure yielded an orange residue. ^{1}H NMR analysis of this mixture showed a mixture of unknown decomposition product **U** (See below) and [{A^{2t}NiOH}$_2$]. This reaction was also attempted under mechanochemical conditions in the absence of solvent (Planetary mill, 50 mL ZrO_2 grinding jar, 25 grams of 4.8 mm stainless steel ball bearings, 15 min, 600 rpm,) but hexane extract of the resulting orange solid showed only {A^{2t}}$_2$ and [{A^{2t}NiOH}$_2$].

Reaction of [{A^{2t}NiBr}$_2$] with lithium imidazolate:

Standard procedure allowed for the isolation of a light yellow-orange residue in 47% yield that appears indefinitely stable in the glovebox atmosphere. Despite multiple attempts, no crystallites of any size have ever been observed. This could be due to the presence of multiple species at similar concentrations or it could be that the presumed (A^{2t}Ni-μ^2-Imid) units form an irregular structure in the solid state.

Analysis of the ^{1}H NMR of the recovered material is difficult due to substantial peak overlap and seemingly inconsistent integration values. As such, the signals cannot be confidently separated into separate spin systems. Therefore, all signals of strong intensity that cannot be assigned to solvent molecules are reported together below.

^{1}H NMR (600 MHz, C_6D_6): δ 5.09 (t, J = 12.3); δ 2.76 (d, J = 12.5); δ 2.67 (d, J = 12.3); δ 2.63 (d, J = 12.3); δ 2.58 (d, J = 12.1)

*[bis{(1,3-di-*tert*-butylallyl)(acetato)nickel(II)}] "[{A^{2t}NiOAc}$_2$]":*

The standard procedure was followed except that an excess of [TlOAc] was used (3-5 eq.) and the reaction was allowed to sit for at least one week before workup. At that point, workup proceeded as normal, yielding a dry-looking yellow-orange residue in 76% yield. This material appears indefinitely stable in a glovebox atmosphere. Anal. Calcd for $C_{13}H_{24}O_2Ni$: C, 57.61; H, 8.93. Found: C, 56.96; H, 9.10.

^{1}H NMR (600 MHz, C_6D_6): δ 5.66 (t, *J* = 12.1 Hz, 1H, center allyl C-H); δ 2.93 (d, *J* = 12.1 Hz, 2H, terminal allyl C-H); δ 1.74 (s, 3H, acetate CH_3); δ 1.20 (s, 18H, *t*-Bu $(CH_3)_3$). ^{13}C{^{1}H} NMR (151 MHz, C_6D_6): δ 181.9 (s, acetate C(O)O); δ 99.8 (s, center allyl CH); δ 73.4 (s, terminal allyl CH); δ 32.6 (s, *t*-Bu CMe_3); δ 28.3 (s, *t*-Bu $(CH_3)_3$); δ 23.5 (s, acetate CH_3).

*[bis{(1,3-di-*tert*-butylallyl)(hydroxo)nickel(II)}] "[{A^{2t}NiOH}$_2$]":*

The standard procedure was followed except that an excess of [TlOH] is used (3-5 eq.) and the reaction was allowed to sit for at least one week before workup. At that point, workup proceeded as normal, yielding a dry-looking yellow-orange residue. This material appears indefinitely stable in a glovebox atmosphere but degrades upon exposure to air.

NMR characterization of this compound is complex, as its peaks are often broadened and oddly shaped. The hypothesis that this may be caused by interconversion between eclipsed and staggered isomers on the order of the NMR timescale is discussed in Section 4.2.3.2. Additionally, the compound appears to show good solubility when a component of a decomposition mixture, but substantially lower solubility when pure; as such, carbon shifts were obtained from decomposition mixtures. Furthermore, the two apparent isomers show substantial overlap, even in the ^{13}C NMR, and peak broadening has prevented confident assignment of the central *t*Bu carbon.

Major isomer (1 eq); ^{1}H NMR (600 MHz, C_6D_6): δ 4.83 (bt, 1H, center allyl C-H); δ 1.96 (bd, 2H, terminal allyl C-H); δ 1.02 (s, 18H, *t*-Bu $(CH_3)_3$). ^{13}C{^{1}H} NMR (151 MHz, C_6D_6): δ 93.7 (s, center allyl CH); δ 71.0 (s, terminal allyl CH); δ 27.1 (s, *t*-Bu $(CH_3)_3$);

Minor isomer (0.73 eq): ^{1}H NMR (600 MHz, C_6D_6): δ 4.97 (bt, 1H, center allyl C-H); δ 1.79 (m, 2H, terminal allyl C-H); δ 1.02 (s, 18H, *t*-Bu $(CH_3)_3$). $^{13}C\{^{1}H\}$ NMR (151 MHz, C_6D_6): δ 93.7 (s, center allyl CH); δ 71.0 (s, terminal allyl CH); δ 27.1 (s, *t*-Bu $(CH_3)_3$);

*[bis{(1,3-di-*tert*-butylallyl)(phenyloxo)nickel(II)}] "[{A^{2t}NiOPh}$_2$]":*

Standard procedure allowed for the collection of a red solid in 50% average yield. This product is stable for months in the glovebox atmosphere. Slow evaporation of a hexane solution of this material yielded red crystalline needles.

The peak broadening displayed by the minor product makes complete identification of all peaks impossible. One of the aryl C-H peaks appears to be missing, and only two carbon peaks could be directly observed. Some additional carbon assignments have been made using HSQC couplings. Only those peaks that can be confidently assigned are included here.

Major product (1 eq.): ^{1}H NMR (400 MHz, C_6D_6): δ 7.56 (d, J = 7.7 Hz, 2H, Ar-H); δ 7.18 (t, J = 7.8 Hz, 2H, Ar-H); δ 6.76 (t, J = 7.3 Hz, 1H, *para* Ar-H); δ 5.31 (t, *J* = 12.1 Hz, 1H, center allyl C-H); δ 2.23 (d, *J* = 12.1 Hz, 2H, allyl *anti* C(H)*t*-Bu); δ 1.11 (s, 18 H, *t*-Bu $(CH_3)_3$). $^{13}C\{^{1}H\}$ NMR (151 MHz, C_6D_6): δ 164.8 (s, C-O); δ 128.8 (s, aryl C-H); δ 124.9 (s, aryl C-H); δ 117.1 (s, *para* aryl C-H); δ 98.2 (s, center allyl C-H); δ 76.0 (s, allyl terminal C(H)*t*-Bu); δ 33.7 (s, *t*-Bu CMe_3) δ 29.7 (s, *t*-Bu $(CH_3)_3$).

Minor Product (0.25 eq.): ^{1}H NMR (400 MHz, C_6D_6): δ 8.06 (d, J = 7.9 Hz, 1H, Ar-H); δ 7.38 (t, J = 7.7 Hz, 1H, Ar-H); δ 7.05 (m, 1H, Ar-H); δ 6.90 (t, J = 7.2 Hz, 1H, Ar-H); δ 5.07 (t, *J* = 11.8 Hz, 1H, center allyl C-H); δ 2.12 (bd, *J* = 11.8 Hz, 2H, allyl terminal C(H)*t*-Bu); δ 1.06 (s, 18 H, *t*-Bu $(CH_3)_3$). $^{13}C\{^{1}H\}$ NMR (151 MHz, C_6D_6): δ 128.9 (s, aryl C-H); δ 123.6 (s, aryl C-H); δ 117.8 (s, aryl C-H); δ 96.2 (s, center allyl C-H); δ 29.3 (s, *t*-Bu $(CH_3)_3$).

*[bis{(1,3-di-*tert*-butylallyl)(phenylthiolato)nickel(II)}] "[{A^{2t}NiSPh}$_2$]":*

Standard procedure allowed dark red solid that quickly turned brown upon full solvent loss in 44% average yield. This product was stable for months in the glovebox atmosphere. Slow evaporation of a hexane solution of this material to near dryness yielded dark red crystalline needles. Anal. Calcd for $C_{17}H_{26}SNi$: C, 63.58; H, 8.16. Found: C, 63.13; H, 8.29.

Major product (1 eq.): ^{1}H NMR (400 MHz, C_6D_6): δ 8.18 (d, J = 7.54 Hz, 2H, Ar-H); δ 6.95 (m, 3H, Ar-H); δ 4.97 (t, *J* = 12.6 Hz, 1H, center allyl C-H); δ 2.90 (d, *J* = 12.6 Hz, 2H, allyl *anti* C(H)*t*-Bu); δ 1.16 (s, 18 H, *t*-Bu $(CH_3)_3$). $^{13}C\{^{1}H\}$ NMR (151 MHz, C_6D_6): δ 141.1 (s, C-S); δ 135.8 (s, aryl C-H); δ 127.5 (s, aryl C-H); δ 100.0 (s, center allyl C-H); δ 84.1 (s, allyl terminal C(H)*t*-Bu); δ 33.5 (s, *t*-Bu CMe_3) δ 30.1 (s, *t*-Bu $(CH_3)_3$).

There are two spin systems that are formed as minor products. Due to their equal intensities, it is hypothesized that these are two inequivalent allyl groups on the same molecule; however, as this is unconfirmed, they are presented separately. Their *t*Bu proton peaks cannot be confidently identified at this time. Minor product aryl proton and carbon shifts cannot be assigned to one spin system or the other, and so are presented separately. The intensity of the allylic carbon peaks of the minor products were very weak, so shift assignments were done on the basis of HSQC couplings in some cases.

Minor allyl product A (0.37 eq.): ^{1}H NMR (400 MHz, C_6D_6): δ 5.00 (m, 1H, center allyl C-H); δ 3.50 (d, J = 13.5, 1H, terminal allyl C-H); δ 2.38 (d, *J* = 11.8 Hz, 1H, terminal allyl C-H). ^{13}C{^{1}H} NMR (151 MHz, C_6D_6): δ 100.1 (s, center allyl C-H); δ 91.1 (s, allyl terminal C(H)*t*-Bu); δ 75.8 (s, allyl terminal C(H)*t*-Bu); δ 30.5 (s, *t*-Bu CMe_3) δ 29.8 (s, *t*-Bu $(CH_3)_3$).

Minor allyl product B (0.37 eq.): ^{1}H NMR (400 MHz, C_6D_6): δ 4.90 (m, 1H, center allyl proton); δ 3.41 (d, J = 14.1, 1H, terminal allyl C-H); δ 2.81 (d, *J* = 8.5 Hz, 1H, allyl *anti* C(H)*t*-Bu). ^{13}C{^{1}H} NMR (151 MHz, C_6D_6): δ 97.5 (s, center allyl C-H); δ 86.9 (s, allyl terminal C(H)*t*-Bu); δ 86.6 (s, allyl terminal C(H)*t*-Bu); δ 30.1 (s, *t*-Bu CMe_3) δ 29.9 (s, *t*-Bu $(CH_3)_3$).

Minor product aromatic signals: ^{1}H NMR (400 MHz, C_6D_6): δ 8.29 (bd, 6.4 Hz, 2H); δ 7.90 (d, 7.6 Hz, 2H); δ 7.11 (bt, 7.6 Hz, 2H); δ 6.93 (m, 4H). ^{13}C{^{1}H} NMR (151 MHz, C_6D_6): 135.2, 134.4, 128.0, 124.5, 124.4.

*[bis{(1,3-di-*tert*-butylallyl)(ethylthiolato)nickel(II)}] "[{A^{2t}NiSEt}$_2$]":*

The standard procedure allowed a dark red, microcrystalline solid to be collected in quantitative (113%) yield.

Two diastereomers are clearly evident in the ^{1}H NMR spectrum; the dominant product, which appears to be *syn,syn*, and a second, apparently *syn,anti* product. A number of other -Et peaks are evident though; indeed, from the ^{1}H-^{1}H COSY spectrum, a second, seemingly *syn,syn* allyl can be seen overlapping with the down field peak of the primary product (δ 4.77 coupled to δ 3.35.) However, as the rest of the peaks associated with this compound cannot be identified, it is not further reported. The terminal ethylthiolate CH_3 and the *t*Bu protons of the *syn,anti* minor product cannot be identified at this time, likely due to peak overlap.

Major Product (1eq.): ^{1}H NMR (600 MHz, C_6D_6): δ 4.79 (bt, *J* = 12.5 Hz, 1H, center allyl C-H); δ 2.74 (bs, 2H, Et CH_2); δ 2.71 (d, *J* = 12.5 Hz, 2H, allyl terminal C-H); δ 1.76 (bs, 3H, Et CH_3); δ 1.24 (s, 18 H, *t*-Bu $(CH_3)_3$). ^{13}C{^{1}H} NMR (151 MHz, C_6D_6): δ 98.1 (s, center allyl C-H); δ 81.4 (s, allyl terminal C(H)*t*-Bu); δ 32.6 (s, *t*-Bu CMe_3); δ 29.5 (s, *t*-Bu $(CH_3)_3$); δ 24.6 (s, Et CH_2); δ 20.4 (s, Et CH_3).

Minor Product (0.11 eq.): ^{1}H NMR (600 MHz, C_6D_6): δ 4.60 (dd, *J* = 14.4, 9.0 Hz, 1H, center allyl C-H); δ 3.38 (bs, 2H, Et CH_2); δ 3.36 (d, *J* = 14.4 Hz, 1H, allyl terminal C(H)*t*-Bu); δ 3.30 (d, J = 9.0 Hz, 1H, allyl terminal C(H)*t*-Bu). ^{13}C{^{1}H} NMR (151 MHz, C_6D_6): δ 97.5 (s, center allyl C-H); δ 79.2 (s, allyl terminal C(H)*t*-Bu); δ 78.0 (s, allyl terminal C(H)*t*-Bu); δ 31.1 (s, *t*-Bu CMe_3); δ 30.8 (s, *t*-Bu CMe_3); δ 29.9 (s, *t*-Bu $(CH_3)_3$); δ 29.8 (s, *t*-Bu $(CH_3)_3$); δ 21.9 (s, Et CH_2); δ 19.7 (s, Et CH_3).

*[bis{(1,3-di-*tert*-butylallyl)(phenylselenolato)nickel(II)}] "[{A^{2t}NiSePh}$_2$]":*

Standard procedure allowed a dark red solid to be isolated in 21% yield. The cause of this low yield is unclear.

The *t*Bu peaks of the two minor products cannot be assigned at this time, likely due to substantial peak overlap. There is an additional signal (δ 5.10, bt, J ≈ 12.3 Hz) that is plausibly consistent with an additional diastereomer of [{A^{2t}NiSePh}$_2$], but due to low intensity and peak broadening, it is not reported here. Peak broadening also causes low intensity carbon resonances and as such, many expected carbon resonances are not observed. Carbon shift assignments, therefore, have been made using HSQC couplings when possible. The purely organic byproduct is hypothesized to be [PhSe-A^{2t}], but this has not been confirmed.

Major Product (1 eq.) – ^{1}H NMR (600 MHz, C_6D_6): δ 8.34 (d, J = 6.7 Hz, 2H, Ar-H); δ 6.97 (m, Ar-H); δ 4.93 (bt, *J* = 12.3 Hz, 1H, center allyl C-H); δ 2.99 (d, *J* = 12.4 Hz, 2H, terminal allyl C(H)*t*-Bu); δ 1.16 (s, 18H, *t*Bu $(CH_3)_3$); ^{13}C{^{1}H} NMR (151 MHz, C_6D_6): δ 142.6 (s, C-SePh) δ 137.0 (s, aryl C-H); δ 127.6 (s, aryl C-H); δ 126.3 (s, aryl C-H); δ 98.4 (s, center allyl C-H); δ 83.6 (s, terminal allyl C(H)*t*-Bu); δ 34.1 (s, *t*Bu CMe_3); δ 29.7 (s, *t*Bu $(CH_3)_3$).

Minor Product 1 (0.41 eq.) – ^{1}H NMR (600 MHz, C_6D_6): δ 8.31 (m, 2H, Ar-H); δ 7.02 (m, Ar-H); δ 5.00 (bt, *J* = 12.7 Hz, 1H, center allyl C-H); δ 3.43 (d, *J* = 13.6 Hz, 1H, terminal allyl C-H); δ 2.44 (d, *J* = 11.8 Hz, 1H, terminal allyl C(H)*t*-Bu). ^{13}C{^{1}H} NMR (151 MHz, C_6D_6): δ 136.6 (s, aryl C-H); δ 126.4 (s, aryl C-H); δ 99.1 (s, center allyl C-H); δ 91.4 (s, terminal allyl C(H)*t*-Bu); δ 75.6 (s, terminal allyl C(H)*t*-Bu).

Minor Product 2 (0.34 eq.) – ^{1}H NMR (600 MHz, C_6D_6): δ 7.92 (m, 2H, Ar-H); δ 6.96 (m, Ar-H); δ 4.78 (bdd, *J* = 13.4, 9.9 Hz, 1H, center allyl C-H); δ 3.60 (m, 1H, terminal allyl C(H)*t*-Bu); δ 2.95 (m, 1H, terminal allyl C(H)*t*-Bu). ^{13}C{^{1}H} NMR (151 MHz, C_6D_6): δ 134.8 (s, aryl C-H); δ 126.0 (s, aryl C-H); δ 95.2 (s, center allyl C-H); δ 87.6 (s, terminal allyl C(H)*t*-Bu); δ 85.4 (s, terminal allyl C(H)*t*-Bu).

Organic byproduct (0.20 eq.) - ^{1}H NMR (600 MHz, C_6D_6): δ 5.50 (dd, *J* = 15.6, 10.7 Hz, 1H, center vinyl C-H); δ 4.84 (d, J = 15.6 Hz, 1H, vinyl C(H)*t*Bu); δ 3.50 (d, J = 10.7 Hz, 1H, sp^3 C(H)*t*Bu). ^{13}C{^{1}H} NMR (151 MHz, C_6D_6): δ 142.6 (s, vinyl C(H)*t*Bu); δ 122.7 (s, center vinyl C-H); δ 64.0 (s, sp^3 C(H)*t*Bu).

*[(μ^2-anilido)(μ^2-bromido) bis{1,3-di-*tert*-butylallylnickel(II)}] "[{A^{2t}Ni}$_2$(NHPh)(Br)]":*

Standard procedure was followed with the exception that the reaction mixture was allowed to stir for no more than 15 minutes after the addition of [LiNHPh]. At that point, the volatiles were removed, and workup proceeded as normal. This procedure allowed for the isolation of a dark red-orange, microcrystalline solid in 80% yield. This species is unstable, with visual decomposition apparent within one day of storage in a glovebox, though full decomposition takes multiple days. A sample allowed to sit in THF solution overnight yielded a light orange material; ^{1}H NMR analysis showed this to be primarily composed of unknown decomposition product **U**, hypothesized to be a mixed A^{2t}-nickel hydroxo species.

NMR analysis shows a single predominant species. While other minor products are also observed, their low intensity prevents determination of the ratio of allyl peaks to aromatic peaks; therefore, it cannot be determined if they are diastereomers of [{A^{2t}Ni}$_2$(NHPh)(Br)], full substitution products, or some other species. As such, their shifts will not be reported here. The major product is composed of two inequivalent allyl spin systems; these are referred to as SS A^{2t} (likely *syn,syn* configuration) and SA A^{2t} (likely *syn,anti* configuration).

^{1}H NMR (600 MHz, C_6D_6): δ 7.68 (d, J = 7.9 Hz, 2H, *ortho* Ar-H); δ 7.27 (t, J = 7.7 Hz, 2H, *meta* Ar-H); δ 6.88 (t, J = 7.3 Hz, 1H, *para* Ar-H); δ 4.90 (dd, J = 13.2, 9.0 Hz, 1H, SA A^{2t} center C-H); δ 4.76 (t, J = 12.5, 1H, SS A^{2t} center C-H); δ 2.87 (dd, J = 13.0, 0.5 Hz, 1H, SS A^{2t} terminal C(H)*t*-Bu); δ 2.34 (dd, J = 9.0, 0.6 Hz, 1H, SA A^{2t} terminal *syn* C-H); δ 2.08 (dd, J = 13.2, 0.7 Hz, 1H, SA A^{2t} terminal *anti* C-H); δ 1.93 (dd, J = 12.0, 0.8 Hz, 1H, SS A^{2t} terminal C(H)*t*-Bu); δ 1.67 (s, 1H, N(H)Ph); δ 1.38 (s, 9H, *t*Bu $(CH_3)_3$); δ 0.93 (s, 9H, *t*Bu $(CH_3)_3$); δ 0.86 (s, 9H, *t*Bu $(CH_3)_3$); δ 0.81 (s, 9H, *t*Bu $(CH_3)_3$).

^{13}C{^{1}H} NMR (151 MHz, C_6D_6): δ 162.8 (s, C-NHPh); δ 129.7 (s, *meta* aryl C-H); δ 122.8 (s, *ortho* aryl C-H); δ 119.5 (s, *para* aryl C-H); δ 100.6 (s, SS A^{2t} center C-H); δ 96.2 (s, SA A^{2t} center C-H); δ 89.7 (s, SA A^{2t} terminal CH-*anti*-*t*Bu); δ 80.0 (s, SS A^{2t} terminal C(H)*t*-Bu); δ 71.8 (s, SS A^{2t} terminal C(H)*t*-Bu); δ 70.9 (s, SA A^{2t} terminal CH-*syn*-*t*Bu); δ 35.0 (s, *t*Bu CMe_3); δ 33.6 (s, *t*Bu CMe_3); δ 33.5 (s, *t*Bu CMe_3); δ 32.3 (s, *t*Bu CMe_3); δ 31.4 (s, *t*Bu $(CH_3)_3$); δ 31.1 (s, *t*Bu $(CH_3)_3$); δ 30.3 (s, *t*Bu $(CH_3)_3$); δ 29.9 (s, *t*Bu $(CH_3)_3$).

Decomposition product **U**, hypothesized to be [{A^{2t}Ni}$_2$(OH)(Br)]: This species was obtained as a decomposition product from reactions of [{A^{2t}NiBr}$_2$] with lithium *tert*-butoxide, potassium diphenylamide, potassium pyrrolide, and lithium anilide. It was also observed as the primary product of a reaction between [{A^{2t}NiBr}$_2$] and thallium hydroxide that did not proceed to completion, suggesting the proposed identification.

^{1}H NMR (400 MHz, C_6D_6): δ 4.91 (t, J = 11.8 Hz, 1H, center allyl C-H); δ 2.13 (d, 11.8 Hz, 2H, allyl terminal C-H); δ 1.04 (s, 18H, *t*Bu (CH_3)$_3$). ^{13}C{^{1}H} NMR (101 MHz, C_6D_6): δ 95.1 (s, center allyl C-H); δ 75.7 (s, terminal allyl C-H); δ 29.4 (s, *t*Bu (CH_3)$_3$).

Reaction of [{A^{2t}NiBr}$_2$] with potassium *tert*-butoxide:

Standard procedure was followed with the exception that the reaction was performed in a 50/50 mixture of THF and toluene, and the reaction was allowed to stir for no more than five minutes before volatiles were removed. This allowed for the isolation of a dark purple solid. This species is unstable, with complete decomposition apparent within two days of storage within a glovebox

^{1}H NMR of the isolated material shows a primary product with signals corresponding to an empirical formula of [A^{2t}NiO*t*Bu], though its true identity is not known. The peaks occur at expected chemical shifts and are slightly broadened. The spectrum also displays three broadened resonances of unknown origin. The resonances at δ 3.48 and δ 1.37 are weakly coupled on the ^{1}H-^{1}H COSY spectrum, and their chemical shifts are slightly offset from the standard chemical shifts of THF. This could suggest the presence of a bound THF molecule in the product, although the relative amount of THF apparent is insufficient for a 1 : 1 adduct. The identity of the resonance at 5.56 is unknown. The central allyl carbon resonance could not be identified in the ^{13}C{^{1}H} spectrum, likely due to peak broadening, so it has been assigned on the basis of HSQC coupling. Neither carbon signals nor HSQC couplings were observed for any of the unidentified broad resonances.

^{1}H NMR (400 MHz, C_6D_6): δ 4.78 (t, *J* = 11.5 Hz, 1H); δ 1.97 (d, *J* = 11.5 Hz, 2H); δ 1.75 (s, 9H); δ 1.00 (s, 18H); ^{13}C{^{1}H} NMR (101 MHz, C_6D_6) (all peaks are singlets): δ 87.8; δ 78.4; δ 36.5; δ 33.0; δ 28.8.

Reaction of [{A^{2t}NiBr}$_2$] with potassium bis(trimethylsilyl)amide (KHMDS):

Standard procedure was followed with the exception that the reaction was performed in toluene. This procedure allowed for the isolation of a dark purple residue in 49% yield. This species is unstable, with visual decomposition apparent within one day of storage in a glovebox, though this decomposition appeared to proceed more slowly when stored in the absence of ethereal solvents.

An attempt to remedy this solvent sensitivity by performing the reaction in the absence of solvent failed. Reaction of [A^{2t}NiBr}$_2$] with KHMDS under solvent-free mechanochemical conditions (Planetary mill, 50

mL ZrO_2 grinding jar, 25 grams of 4.8 mm stainless steel ball bearings, 15 min, 600 rpm,) generated a homogenous dark purple paste, appearing very much like the isolated [A^{2t}NiHMDS] species, but was entirely insoluble in organic solvents. The identity of this material remains unknown.

^{1}H NMR of the isolated material shows a primary product with signals corresponding to an empirical formula of [A^{2t}NiHMDS], though its true identity is not known. A small number of upfield peaks are observed as trace products; the identities of these species is unknown. The triplets at δ 5.31 and δ 5.32 represent decomposition products; these peaks grow as the material becomes discolored. The identity of these species is unknown, as they undergo further decomposition to a complex mixture with highly broadened NMR signals.

^{1}H NMR (400 MHz, C_6D_6): δ 4.76 (t, *J* = 12.0 Hz, 1H); δ 2.18 (d, *J* = 12.0 Hz, 2H); δ 1.00 (s, 18H); δ 0.65 (s, 9H); δ 0.28 (s, 9H).

Reaction of [{A^{2t}NiBr}$_2$] with potassium diphenylamide:

Standard procedure was followed with the exception that the reaction mixture was allowed to stir for no more than 15 minutes after the addition of [$KNPh_2$]. At that point, the volatiles were removed, and workup proceeded as normal. This allowed for a yellow brown solid to be isolated; the ^{1}H NMR spectrum of this organic product is given below; the spectrum shows a primary product with signals corresponding to an empirical formula of [$A^{2t}NiNPh_2$], though its true identity is not known. This material degrades entirely within two days of storage in the glovebox to a mixture of **U** and [{A^{2t}NiOH}$_2$], though it is possible that this degradation is slower when ethereal solvents are excluded. The residual, hexane-insoluble solid produced in this reaction was found to be THF soluble. The resulting solution was a deep blue color, very similar to the color observed in reactions of [{A^{2t}NiBr}$_2$] with [KO*t*Bu] and [KHMDS]. Upon sitting in THF solution overnight, this material fully degraded to an orange material that has not yet been characterized.

^{1}H NMR (400 MHz, C_6D_6): δ 7.51 (d, J = 7.9 Hz, 8H); δ 7.21 (t, J = 7.8 Hz, 8H); δ 6.93 (t, J = 7.3 Hz, 4H); δ 4.83 (t, *J* = 12.2 Hz, 1H); δ 2.23 (d, *J* = 12.2 Hz, 2H); δ 0.96 (s, 18H).

4.6 References:

(1) Gmernicki, K. R.; Hong, E.; Maroon, C. R.; Mahurin, S. M.; Sokolov, A. P.; Saito, T.; Long, B. K. Accessing Siloxane Functionalized Polynorbornenes via Vinyl-Addition Polymerization for CO2Separation Membranes. *ACS Macro Lett.* **2016**, *5* (7), 879–883. https://doi.org/10.1021/acsmacrolett.6b00435.

(2) Walter, M. D.; Moorhouse, R. A.; White, P. S.; Brookhart, M. Vinyl Addition Polymerization of Norbornene with Cationic (Allyl)Ni Catalysts: Mechanistic Insights and Characterization of First Insertion Products. *J. Polym. Sci. Part A Polym. Chem.* **2009**, *47* (10), 2560–2573. https://doi.org/10.1002/pola.

(3) Wilke, G.; Bogdanović, B.; Hardt, P.; Heimbach, P.; Keim, W.; Kröner, M.; Oberkirch, W.; Tanaka,

K.; Steinrücke, E.; Walter, D.; Zimmermann, H. Allyl-Transition Metal Systems. *Angew. Chem. - Int. Ed.* **1966**, *5* (2), 151–164. https://doi.org/10.1002/anie.196601511.

(4) Xu, M.; Yu, F.; Li, P.; Xu, G.; Zhang, S.; Wang, F. Enhancing Chain Initiation Efficiency in the Cationic Allyl-Nickel Catalyzed (Co)Polymerization of Ethylene and Methyl Acrylate. *Inorg. Chem.* **2020**, *59* (7), 4475–4482. https://doi.org/10.1021/acs.inorgchem.9b03647.

(5) Johnson, J. R.; Tully, P. S.; Mackenzie, P. B.; Sabat, M. A Practical Reversed-Polarity Alternative to Organocuprate Conjugate Addition Chemistry. Halocarbon Coupling Reactions of Enal- and Enone-Derived Allylnickel Reagents. *J. Am. Chem. Soc.* **1991**, *113* (16), 6172–6177. https://doi.org/10.1021/ja00016a037.

(6) Iglesias, M. J.; Prieto, A.; Nicasio, M. C. Well-Defined Allylnickel Chloride/N-Heterocyclic Carbene [(NHC)Ni(Allyl)Cl] Complexes as Highly Active Precatalysts for C-N and C-S Cross-Coupling Reactions. *Adv. Synth. Catal.* **2010**, *352* (11–12), 1949–1954. https://doi.org/10.1002/adsc.201000223.

(7) Espinosa, M. R.; Doppiu, A.; Hazari, N. Differences in the Performance of Allyl Based Palladium Precatalysts for Suzuki-Miyaura Reactions. *Adv. Synth. Catal.* **2020**, *362* (22), 5062–5078. https://doi.org/10.1002/adsc.202000987.

(8) Martin, A. R.; Nelson, D. J.; Meiries, S.; Slawin, A. M. Z.; Nolan, S. P. Efficient C-N and C-S Bond Formation Using the Highly Active [Ni(Allyl)Cl(IPr*OMe)] Precatalyst. *Eur. J. Org. Chem.* **2014**, *2014* (15), 3127–3131. https://doi.org/10.1002/ejoc.201402022.

(9) Martín, M. T.; Marín, M.; Maya, C.; Prieto, A.; Nicasio, M. C. Ni(II) Precatalysts Enable Thioetherification of (Hetero)Aryl Halides and Tosylates and Tandem C−S/C−N Couplings. *Chem. Eur. J.* **2021**, *27* (48), 12320–12326. https://doi.org/10.1002/chem.202101906.

(10) Asensio, J. M.; Andrés, R.; Gómez-Sal, P.; De Jesús, E. Aqueous-Phase Chemistry of η^3-Allylpalladium(II) Complexes with Sulfonated N-Heterocyclic Carbene Ligands: Solvent Effects in the Protolysis of Pd-C Bonds and Suzuki-Miyaura Reactions. *Organometallics* **2017**, *36* (21), 4191–4201. https://doi.org/10.1021/acs.organomet.7b00635.

(11) Quisenberry, K. T.; Smith, J. D.; Voehler, M.; Stec, D. F.; Hanusa, T. P.; Brennessel, W. W. Trimethylsilylated Allyl Complexes of Nickel. The Stabilized Bis(π-Allyl)Nickel Complex $[\eta^3\text{-}1,3\text{-}(SiMe_3)_2C_3H_3]_2Ni$ and Its Mono(π-Allyl)NiX (X = Br, I) Derivatives. *J. Am. Chem. Soc.* **2005**, *127* (12), 4376–4387. https://doi.org/10.1021/ja044308s.

(12) Degroot, H. P.; Speight, I. R.; Brennessel, W. W.; Hanusa, T. P. Distinction with a Difference: T -Butyl and Trimethylsilyl Substituents in Nickel Allyl Complexes. *Submitted - ACS Org. Inorg. Au* **2024**.

(13) Lehmkuhl, H.; Rufihka, A.; Mehler, K.; Benn, R.; Schroth, G. Reaktionen von Nickelocen Mit Organomagnesiumverbindungen Und Bildung von η^3-Allyl-η^5-Cyclopentadienylnickel-Komplexen. *Liebigs Ann. der Chemie* **1980**, *1980* (5), 744–753. https://doi.org/10.1002/jlac.198019800514.

(14) Bogdanović, B.; Bonnemann, H.; Wilke, G. Pi-Allylmethylnickel. *Angew. Chem. Int. Ed.* **1966**, *5* (6), 582–583.

(15) Yamamoto, T.; Ishizu, J.; Yamamoto, A. Interaction of Nickel(0) Complexes with Allyl Carboxylates, Allyl Ethers, Allylic Alcohols, and Vinyl Acetate. π-Complex Formation and Oxidative Addition to Nickel Involving Cleavage of the Alkenyl-Oxygen Bond. *J. Am. Chem. Soc.* **1981**, *103* (23), 6863–6869. https://doi.org/10.1021/ja00413a014.

(16) Chemie, A. π-Allylhydridonickel Compounds. *Angew. Chemie Int. Ed.* **1970**, *9*, 736–737.

(17) Jolly, P. W.; Wilke, G. π-Allyl Nickel Complexes. In *The Organic Chemistry of Nickel*; Academic, 1974; pp 329–401. https://doi.org/10.1016/b978-0-12-388401-5.50012-9.

(18) Fulton, R. R.; Holland, A. W.; Fox, D. J.; Bergman, R. G. Formation, Reactivity, and Properties of Nondative Late Transition Metal-Oxygen and -Nitrogen Bonds. *Acc. Chem. Res.* **2002**, *35* (1), 44–56. https://doi.org/10.1021/ar000132x.

(19) Mouhsine, B.; Karim, A.; Dumont, C.; Sauthier, M. The Salt-Free Nickel-Catalysed α-Allylation Reaction of Ketones with Allyl Alcohol and Diallylether. *Green Chem.* **2020**, *22* (3), 950–955.

https://doi.org/10.1039/c9gc03619a.
(20) Bernhard, Y.; Thomson, B.; Ferey, V.; Sauthier, M. Nickel-Catalyzed Alpha-Allylation of Aldehydes and Tandem Aldol Condensation/Allylation Reaction with Allylic Alcohols. *Angew. Chem. - Int. Ed.* **2017**, *56*, 7460–7464.
(21) Sweeney, J. B.; Ball, A. K.; Lawrence, P. A.; Sinclair, M. C.; Smith, L. J. A Simple, Broad-Scope Nickel(0) Precatalyst System for the Direct Amination of Allyl Alcohols. *Angew. Chem. - Int. Ed.* **2018**, *57* (32), 10202–10206. https://doi.org/10.1002/anie.201805611.
(22) Vaidya, G. N.; Choudhary, R. H.; Nagpure, M.; Lokhande, S. K.; Rana, P.; Kumar, D. 'In-Water', Nickel-Catalyzed Mild Preparation of Allylic Amines Employing Alcohols: Application to 'All-Water' Synthesis of Pharmaceuticals. *Green Chem.* **2022**, 3977–3984. https://doi.org/10.1039/d2gc00308b.
(23) Liu, D. G.; Xu, Z. Y.; Yu, H.; Fu, Y. Mechanistic Insights into the Nickel-Catalyzed Regioselective Carboxylation of Allylic Alcohols. *Organometallics* **2021**, *40* (7), 869–879. https://doi.org/10.1021/acs.organomet.0c00789.
(24) Yang, B.; Wang, Z. X. Nickel-Catalyzed Alkylation or Reduction of Allylic Alcohols with Alkyl Grignard Reagents. *J. Org. Chem.* **2020**, *85* (7), 4772–4784. https://doi.org/10.1021/acs.joc.0c00008.
(25) Payard, P. A.; Perego, L. A.; Ciofini, I.; Grimaud, L. Taming Nickel-Catalyzed Suzuki-Miyaura Coupling: A Mechanistic Focus on Boron-to-Nickel Transmetalation. *ACS Catal.* **2018**, *8* (6), 4812–4823. https://doi.org/10.1021/acscatal.8b00933.
(26) Akkarasamiyo, S.; Ruchirawat, S.; Ploypradith, P.; Samec, J. S. M. Transition-Metal-Catalyzed Suzuki-Miyaura-Type Cross-Coupling Reactions of π-Activated Alcohols. *Synth.* **2020**, *52* (5), 645–659. https://doi.org/10.1055/s-0039-1690740.
(27) Wang, G.; Gan, Y.; Liu, Y. Nickel-Catalyzed Direct Coupling of Allylic Alcohols with Organoboron Reagents. *Chinese J. Chem.* **2018**, *36* (10), 916–920. https://doi.org/10.1002/cjoc.201800237.
(28) Sekiguchi, Y.; Lee, Y. Y.; Yoshikai, N. Nickel-Catalyzed Ring-Opening Allylation of Cyclopropanols via Homoenolate. *Org. Lett.* **2021**, *23* (15), 5993–5997. https://doi.org/10.1021/acs.orglett.1c02072.
(29) Hampton, P. D.; Wu, S.; Alam, T. M.; Claverie, J. P. Synthesis of Allylnickel Aryloxides and Arenethiolates: Study of Their Dynamic Isomerization and 1,3-Diene Polymerization Activity. *Organometallics* **1994**, *13* (5), 2066–2074. https://doi.org/10.1021/om00017a073.
(30) Bonnemann, H.; Jentsch, J.-D. η^3-Allylnickel Alkoxides and Their Use as Homogeneous and Heterogeneous Catalysts for the Dimerization of Olefins. *Appl. Organomet. Chem.* **1993**, *7*, 553–565.
(31) Fischer, E. O.; Burger, G. Uber Ein Dimeres π-Allyl-Nickeliodid Und π-Allyl-Nickel-Cyclopentadienyl. *Chem. Ber.* **1961**, *94* (9), 2409–2412. https://doi.org/https://doi.org/10.1002/cber.19610940909.
(32) Goddard, R. Theoretical Considerations on the Puckered and Planar Forms of [(π-Allyl)-Nickel-X]2. *Fresenius' Z. Anal. Chemie* **1980**, *304* (4), 259. https://doi.org/10.1007/BF00488799.
(33) Krüger, C. Deformationsdichte-Bestimmungen in Dimeren π-Allyl-Nickel-Komplexen. *Fresenius' Z. Anal. Chemie* **1980**, *304* (4), 260–261. https://doi.org/10.1007/BF00488800.
(34) Bogdanovic, B. Catalyzed Olefin Oligomerization. *Adv. Organomet. Chem.* **1979**, *17* (2), 105–140.
(35) Birkenstock, U. No Title, Ph. D. Thesis, Technische Hochschule Aachen, 1966.
(36) Bönnemann, H. Neue π[Pi]-Allylnickelderivate Geringer Thermischer Stabilität, Ph. D. Thesis, Technische Hochschule Aachen, 1967.
(37) Walter, D. Ph. D. Thesis, Technische Hochschule Aachen, 1965.
(38) Keim, W. Ph. D. Thesis, Technische Hochschule Aachen, 1963.
(39) Fleck, W. Darstellung von Offenkettigen Oligomeren Aus 1,3-Dienen [Dienen] an Aminmodifizierten Nickel-Ligand-Katalysatoren, Ph. D. Thesis, Bochum, 1971.
(40) Carmona, E.; Palma, P.; Poveda, M. L. η^3-2-Methylallyl Phosphine Complexes of Nickel(II).

Polyhedron **1990**, *9* (5), 757–761.
(41) Henc, B.; Jolly, P. W.; Salz, R.; Stobbe, S.; Wilke, G.; Benn, R.; Mynott, R.; Seevogel, K.; Goddard, R.; Krüger, C. Transition Metal Allyls III The $(\eta^3\text{-Allyl})_2$M Complexes of Nickel, Palladium and Platinum: Structural Considerations. *J. Organomet. Chem.* **1980**, *191* (2), 449–475. https://doi.org/10.1016/s0022-328x(00)81073-6.
(42) Carmona, E.; Marin, J. M.; Paneque, M.; Poveda, M. L. New Nickel O-Methylbenzyl Complexes: Crystal and Molecular Structures of $Ni(\eta^3\text{-}CH_2C_6H_4$ -o-Me)Cl(PMe_3) and $Ni_3(\eta^1\text{-}CH_2C_6H_4\text{-o-Me})_4(PMe_3)_2(\mu_3\text{-}OH)_2$. *Organometallics* **1987**, *6* (8), 1757–1765. https://doi.org/10.1021/om00151a023.
(43) Trost, B. M.; Czabaniuk, L. C. Structure and Reactivity of Late Transition Metal η^3-Benzyl Complexes. *Angew. Chem. - Int. Ed.* **2014**, *53* (11), 2826–2851. https://doi.org/10.1002/anie.201305972.
(44) Fischer, E. O.; Warner, H. Übergangsmetall-Komplexe Mit π-Allyl- und π-Enyl-Liganden. *Z. Chem.* **1962**, *2* (6–7), 174–185.
(45) Lehmkuhl, H.; Naser, J.; Mehler, G.; Keil, T.; Danowski, F.; Benn, R.; Mynott, R.; Schroth, G.; Gabor, B.; Kruger, C.; Betz, P. Verschiedenartige Koordinationen Bei (2-Alken)- (η^5-cyclopentadienyl)Organylnickel(II)-Komplexen. *Chem. Ber.* **1991**, *124*, 441–452.
(46) Schuster-Woldan, H. G.; Basolo, F. Kinetics and Mechanism of Substitution Reactions of π-Cyclopentadienyldicarbonylrhodium. *J. Am. Chem. Soc.* **1966**, *88* (8), 1657–1663.
(47) Hart-Davis, A. J.; Mawby, R. J. Reactions of π-Indenyl Complexes of Transition Metals. Part I. Kinetics and Mechanisms of Reactions of Tricarbonyl-π-Indenylmethylmolybdenum with Phosphorus(III) Ligands. *J. Chem. Soc. A Inorganic, Phys. Theor. Chem.* **1969**, No. 0, 2403–2407. https://doi.org/10.1039/J19690002403.
(48) Zargarian, D. Group 10 Metal Indenyl Complexes. *Coord. Chem. Rev.* **2002**, *233–234*, 157–176. https://doi.org/10.1016/S0010-8545(02)00201-1.
(49) Fritz, H. P.; Köhler, F. H.; Schwarzhans, K. E. Spektroskopische Untersuchungen an Organometallischen Verbindungen. LIV. Di-π-Indenylnickel(II). *J. Organomet. Chem.* **1969**, *19* (2), 449–452. https://doi.org/10.1016/S0022-328X(00)85322-X.
(50) Westcott, S. A.; Kakkar, A. K.; Stringer, G.; Taylor, N. J. Flexible Coordination of Indenyl Ligands in Sandwich Complexes of Transition Metals. Molecular Structures of $[(\eta\text{-}C_9R_7)_2M]$ (M = Fe, R = H, Me; M = Co, Ni, R = H): Direct Measurement of the Degree of Slipfold Distortion as a Function of d-Electron Count. *J. Organomet. Chem.* **1990**, *394*, 777–794.
(51) Merola, J. S.; Kacmarcik, R. T.; Van Engen, D. η^5 to η^3 Conversion in Indenyliridium Complexes. *J. Am. Chem. Soc.* **1986**, *108* (2), 329–331.
(52) Yoshizawa, K.; Yahara, K.; Taniguchi, A.; Yamabe, T.; Kinoshita, T.; Takeuchi, K. Orbital Interactions and Solvent Effects Determining the Stability of Condensed Cyclopentadienides in Solution. *J. Org. Chem.* **1999**, *64* (8), 2821–2829. https://doi.org/10.1021/jo982286k.
(53) Kirillov, E.; Saillard, J. Y.; Carpentier, J. F. Groups 2 and 3 Metal Complexes Incorporating Fluorenyl Ligands. *Coord. Chem. Rev.* **2005**, *249* (11–12), 1221–1248. https://doi.org/10.1016/j.ccr.2005.01.011.
(54) Alt, H. G.; Samuel, E. Fluorenyl Complexes of Zirconium and Hafnium as Catalysts for Olefin Polymerization. *Chem. Soc. Rev.* **1998**, *27* (5), 323–329. https://doi.org/10.1039/a827323z.
(55) Shiono, T. Living Polymerization of Olefins with Ansa-Dimethylsilylene(Fluorenyl) (Amido)Dimethyltitanium-Based Catalysts. *Polym. J.* **2011**, *43* (4), 331–351. https://doi.org/10.1038/pj.2011.13.
(56) Kozioł, A.; Jerzykiewicz, L. B.; Justyniak, I.; Lis, T.; Pasynkiewicz, S.; Pietrzykowski, A. New Ionic Fluorenylnickel Complexes: Synthesis and Solid State Structure. *J. Organomet. Chem.* **2014**, *767*, 22–26. https://doi.org/10.1016/j.jorganchem.2014.05.026.
(57) Bordwell, F. G.; Drucker, G. E.; Fried, H. E. Acidities of Carbon and Nitrogen Acids: The Aromaticity of the Cyclopentadienyl Anion. *J. Org. Chem.* **1981**, *46* (3), 632–635.
(58) Bordwell, F. G.; Drucker, G. E. Acidities of Indene and Phenyl-, Diphenyl-, and Triphenylindenes.

J. Org. Chem. **1980**, *45* (16), 3325–3328.
(59) Matthews, W. S.; Bares, J. E.; Bartmess, J. E.; Cornforth, F. J.; Drucker, G. E.; McCallum, R. J.; McCollum, G. J.; Vanier, N. R.; Bordwell, F. G.; Margolin, Z. Equilibrium Acidities of Carbon Acids. VI. Establishment of an Absolute Scale of Acidities in Dimethyl Sulfoxide Solution. *J. Am. Chem. Soc.* **1975**, *97* (24), 7006–7014. https://doi.org/10.1021/ja00857a010.
(60) Bordwell, F. G. Equilibrium Acidities in Dimethyl Sulfoxide Solution. *Acc. Chem. Res.* **1988**, *21* (12), 456–463. https://doi.org/10.1021/ar00156a004.
(61) Gutnov, A.; Drexler, H. J.; Spannenberg, A.; Oehme, G.; Heller, B. Syntheses of Chiral Nonracemic Half-Sandwich Cobalt Complexes with Menthyl-Derived Cyclopentadienyl, Indenyl, and Fluorenyl Ligands. *Organometallics* **2004**, *23* (5), 1002–1009. https://doi.org/10.1021/om030357m.
(62) Kreye, M.; Daniliuc, C. G.; Freytag, M.; Jones, P. G.; Walter, M. D. Coordination Chemistry of Sterically Encumbered Pyrrolyl Ligands to Chromium(II): Mono(Pyrrolyl)Chromium and Diazachromocene Formation. *Dalt. Trans.* **2014**, *43* (24), 9052–9060. https://doi.org/10.1039/c4dt00533c.
(63) Kershner, D. L.; Basolo, F. Syntheses of η^5-Heterocyclic Manganese Tricarbonyls. Effect of the Heteroatom and Heterocycle Ring Substituents on CO Substitution Reactions. *J. Am. Chem. Soc.* **1987**, *109*, 7396–7402.
(64) Perera, J. R.; Heeg, M. J.; Winter, C. H. η^5-Imidazolato Complexes of Ruthenium. *Organometallics* **2000**, *19*, 5263–5265.
(65) Smith, A. E. The Crystal and Molecular Structure of Bis(Cyclopentadienyl)-2,2'-bi-π-allyl-bis(nickel) ($C_5H_5NiC_3H_4$-$C_3H_4NiC_5H_5$). *Inorg. Chem.* **1972**, *11* (1), 165–170.
(66) Seiler, P.; Dunitz, J. D. The Structure of Nickelocene at Room Temperature and at 101 K. *Acta Crystallogr. Sect. B Struct. Crystallogr. Cryst. Chem.* **1980**, *36* (10), 2255–2260. https://doi.org/10.1107/s0567740880008539.
(67) Bauer, H.; Sun, Y.; Sitzmann, H. Bis(η^5-1-*tert*-butylindenyl)Nickel(II). *Acta Crystallogr. Sect. E Struct. Reports Online* **2011**, *67* (9). https://doi.org/10.1107/S1600536811028510.
(68) Huber, T. A.; Bélanger-Gariépy, F.; Zargarian, D. Preparation and Characterization of [(Eta-Indenyl)Ni(PPh3)Cl]. *Organometallics* **1995**, *14* (11), 4997–4999.
(69) Mejdrich, A. L.; Hanks, T. W. Structures of (η^1-Fluorenyl)$Re(CO)_5$ and (η^5-Fluorenyl)$Re(CO)_3$ and Their Thermal Interconversion in Solid Matrices. *Synth. React. Inorg. Met. Chem.* **1998**, *28* (6), 953–973. https://doi.org/10.1080/00945719809351681.
(70) Tanaka, R.; Yanase, C.; Cai, Z.; Nakayama, Y.; Shiono, T. Structure-Stereospecificity Relationships of Propylene Polymerization Using Substituted Ansa-Silylene(Fluorenyl)(Amido) Titanium Complexes. *J. Organomet. Chem.* **2016**, *804*, 95–100. https://doi.org/10.1016/j.jorganchem.2015.12.028.
(71) Razavi, A.; Ferrara, J. Preparation and Crystal Structures of the Complexes (η^5-$C_5H_4CMe_2$-η5-$C_{13}H_8$)MCl_2 (M = Zr, Hf) and Their Role in the Catalytic Formation of Syndiotactic Polypropylene. *J. Organomet. Chem.* **1992**, *435* (3), 299–310. https://doi.org/10.1016/0022-328X(92)83400-C.
(72) Irwin, L. J.; Reibenspies, J. H.; Miller, S. A. Synthesis and Characterization of Sterically Expanded ansa- η^1-Fluorenyl-Amido Complexes. *Polyhedron* **2005**, *24* (11), 1314–1324. https://doi.org/10.1016/j.poly.2005.03.011.
(73) Churchill, M. R.; Mason, R. Molecular Structure of π-Allyl-Palladium Acetate. *Nature* **1964**, *101* (49), 1964.
(74) Massa, W.; Faza, N.; Kang, H.-C.; Focke, C.; Heitz, W. Combining Oxidative Addition and Polymerization: A Study towards the Synthesis of Macromonomers. *Acta Polym.* **1997**, *48* (10), 432–437. https://doi.org/https://doi.org/10.1002/actp.1997.010481003.
(75) Massa, W.; Faza, N.; Kang, H.-C.; Focke, C.; Heitz, W. Combining Oxidative Addition and Polymerization: A Study towards the Synthesis of Macromonomers. *Acta Polym.* **1997**, *48*, 432–437.
(76) Kita, Y.; Sakaguchi, H.; Hoshimoto, Y.; Nakauchi, D.; Nakahara, Y.; Carpentier, J.-F.; Ogoshi, S.; Mashima, K. Pentacoordinated Carboxylate π-Allyl Nickel Complexes as Key Intermediates for the

Ni-Catalyzed Direct Amination of Allylic Alcohols. *Chem. - A Eur. J.* **2015**, *21*, 14571–14578. https://doi.org/10.1002/chem.201502329.

(77) Klein, H.-F.; Karsch, H. H. Stabile Methylnickelverbindungen, II Methyl(Trimethylphosphin)Nickel-hydroxid und Verwandte Verbindungen. *Chem. Ber.* **1973**, *106*, 1433–1452. https://doi.org/10.1002/cber.19731060509.

(78) Carmona, E.; Marín, J. M.; Palma, P.; Paneque, M.; Poveda, M. L. Pyrrolyl, Hydroxo, and Carbonate Organometallic Derivatives of Nickel(II). Crystal and Molecular Structure of $[Ni(CH_2C_6H_4\text{-}o\text{-}Me)(PMe_3)(M\text{-}OH)]_2$-2,5-$HNC_4H_2Me_2$. *Inorg. Chem.* **1989**, *28* (10), 1895–1900. https://doi.org/10.1021/ic00309a025.

(79) Kitajima, N.; Tanaka, M.; Moro-oka, Y.; Hikichi, S. Fixation of Atmospheric CO_2 by a Series of Hydroxo Complexes of Divalent Metal Ions and the Implication for the Catalyic Role of Metal Ion in Carbonic Anhydrase. Synthesis, Characterisation, and Molecular Structure of $[LM(OH)]_n$ (n = 1 or 2) and $LM(\mu\text{-}CO_3)$. *J. Am. Chem. Soc.* **1993**, *115* (13), 5496–5508.

(80) Cámpora, J.; Palma, P.; Del Río, D.; Álvarez, E. CO Insertion Reactions into the M-OH Bonds of Monomeric Nickel and Palladium Hydroxides. Reversible Decarbonylation of a Hydroxycarbonyl Palladium Complex. *Organometallics* **2004**, *23* (8), 1652–1655. https://doi.org/10.1021/om040002i.

(81) Cámpora, J.; Matas, I.; Palma, P.; Graiff, C.; Tiripicchio, A. Fluoride Displacement by Lithium Reagents. An Improved Method for the Synthesis of Nickel Hydroxo, Alkoxo, and Amido Complexes. *Organometallics* **2005**, *24* (12), 2827–2830. https://doi.org/10.1021/om0489709.

(82) Campora, J.; Reyes, M. L.; Hackl, T.; Monge, A.; Ruiz, C. Synthesis of π-Aryloxide Complexes of Nickel and Palladium. *Organometallics* **2000**, *19*, 2950–2952. https://doi.org/10.1021/om0001772.

(83) Yamamoto, T.; Ishizu, J.; Yamamoto, A. REACTIONS OF ALLYL PHENYL AND DIALLYL ETHERS WITH Ni(cod)2 IN THE PRESENCE OF PHOSPHINE LIGANDS WITH AND WITHOUT C–O BOND CLEAVAGE. PREPARATION OF $Ni(\eta^3\text{-}C_3H_5)(OC_6H_5)(PPh_3)$ BY THE OXIDATIVE ADDITION OF ALLYL PHENYL ETHER TO NICKEL AND PREPARATION OF Ni(π-DIALLYL ETHER)(PR_3). *Chem. Lett.* **1979**, *8* (11), 1385–1386. https://doi.org/10.1246/cl.1979.1385.

(84) Cámpora, J.; Reyes, M. L.; Mereiter, K. Synthesis and Structure of Three Unusual Homoleptic Aryloxides of Nickel and Palladium. *Organometallics* **2002**, *21* (6), 1014–1016. https://doi.org/10.1021/om010918e.

(85) Prushan, M. J.; Tomezsko, D. M.; Lofland, S.; Zeller, M.; Hunter, A. D. A Nickel(II) Di-μ_2-Phenolato Bridged Dinuclear Complex: Weak Antiferromagnetic Interactions in Nickel(II) Dimers. *Inorganica Chim. Acta* **2007**, *360* (7), 2245–2254. https://doi.org/10.1016/j.ica.2006.11.008.

(86) Deb, T.; Rohde, G. T.; Young, V. G.; Jensen, M. P. Aerobic and Hydrolytic Decomposition of Pseudotetrahedral Nickel Phenolate Complexes. *Inorg. Chem.* **2012**, *51* (13), 7257–7270. https://doi.org/10.1021/ic300551z.

(87) Liang, L. C.; Chien, P. S.; Lee, P. Y.; Lin, J. M.; Huang, Y. L. Terminal Nickel(II) Amide, Alkoxide, and Thiolate Complexes Containing Amido Diphosphine Ligands of the Type $[N(o\text{-}C_6H_4PR_2)_2]$- (R = Ph, IPr, Cy). *Dalt. Trans.* **2008**, No. 25, 3320–3327. https://doi.org/10.1039/b719894a.

(88) McMullen, A. K.; Tilley, T. D.; Rheingold, A. L.; Geib, S. J. Trialkoxysiloxy Complexes of Nickel. Molecular Structures of $Na_3(\mu_3\text{-}I)\{Ni[\mu_3\text{-}OSi(OtBu)_3]_3I\}\cdot 0.5THF\cdot 0.5C_5H_{12}$ and $\{(\eta^3\text{-}C_3H_5)Ni[\mu_2\text{-}OSi(OtBu)_3]\}_2$. *Inorg. Chem.* **1990**, *29* (12), 2228–2232. https://doi.org/10.1021/ic00337a010.

(89) Wells, A. F. *Structural Inorganic Chemistry*; Oxford University Press: Oxford, 2012.

(90) Redón, R.; Torrens, H.; Hahn, F. E.; Lügger, T.; Hernández-Ortega, S.; Toscano, R. A.; Morales-Morales, D. X-Ray Structural and Dynamic Behaviour Study of Allyl Palladium Compounds with Fluorinated Benzenethiolate Bridges. *J. Mol. Struct.* **2003**, *655* (3), 423–433. https://doi.org/10.1016/S0022-2860(03)00291-6.

(91) Osakada, K.; Ozawa, Y.; Yamamoto, A. Preparation of $(Me_3P)_2Pd_2(\mu\text{-}\eta^3\text{-}C_3H_5(\mu\text{-}SPH)$ by Reaction of Pd(0) Complex with Allyl Phenyl Sulfide. *J. Organomet. Chem.* **1990**, *399* (3), 341–348. https://doi.org/10.1016/0022-328X(90)85498-N.

(92) Miyauchi, Y.; Watanabe, S.; Kuniyasu, H.; Kurosawa, H. Ligand-Dependent Relative Stability Order in Allyl Sulfide/Palladium(0) Species *vs* (η^3-Allyl)Palladium(II) Thiolate Species. *Organometallics* **1995**, *14* (11), 5450–5453. https://doi.org/10.1021/om00011a074.
(93) Singhal, A.; Jain, V. K. Synthesis and Characterization of Dimeric Organochalcogenido-Bridged Methylpalladium and Allylpalladium Complexes. *J. Organomet. Chem.* **1995**, *494* (1–2), 75–80. https://doi.org/10.1016/0022-328X(95)05388-6.
(94) Hua, R.; Takeda, H.; Onozawa, S. Y.; Abe, Y.; Tanaka, M. Nickel-Catalyzed Thioallylation of Alkynes with Allyl Phenyl Sulfides. *Org. Lett.* **2007**, *9* (2), 263–266. https://doi.org/10.1021/ol062686r.
(95) Huang, S.; Wang, M.; Jiang, X. Ni-Catalyzed C-S Bond Construction and Cleavage. *Chem. Soc. Rev.* **2022**, *51* (19), 8351–8377. https://doi.org/10.1039/d2cs00553k.
(96) Kanchana, U. S.; Diana, E. J.; Mathew, T. V. Recent Trends in Nickel-Catalyzed C-S Bond Formation. *Asian J. Org. Chem.* **2022**, *11* (6), e202200038.
(97) Sanchez, G.; Momblona, F.; Sanchez, M.; Perez, J.; Lopez, G.; Asabo, J.; Molins, E.; Miravitlles, C. Synthesis of Homo- and Hetero-Bimetallic Complexes Containing the $Ni(C_6F_5)_2$ Moiety - Crystal Structure of $[(C_6F_5)_2Ni(\mu\text{-}SPh)_2Pd(Dppe)]$. *Eur. J. Inorg. Chem.* **1998**, *1998* (8), 1199–1204.
(98) Sánchez, G.; Ruiz, F.; Serrano, J. L.; Carmen Ramirez De Arellano, M.; López, G. Organometallic Nickel(II) Complexes Containing Thiolate and Dithiocarbamate Ligands. *Eur. J. Inorg. Chem.* **2000**, No. 10, 2185–2191. https://doi.org/10.1002/1099-0682(200010)2000:10<2185::AID-EJIC2185>3.0.CO;2-K.
(99) Aullon, G.; Ujaque, G.; Lledos, A.; Alvarez, S. Edge-Sharing Binuclear d^8 Complexes with XR Bridges: Theoretical and Structural Database Study of Ther Molecular Conformation. *Chem. - A Eur. J.* **1999**, *5* (5), 1391–1410.
(100) Swenson, D.; Baenziger, N. C.; Coucouvanis, D. Tetrahedral Mercaptide Complexes. Crystal and Molecular Structures of $[(C_6H_5)_4P]_2M(SC_6H_5)_4$ Complexes (M = Cd(II), Zn(II), Ni(II), Co(II), and Mn(II)) Recently. *J. Am. Chem. Soc.* **1978**, *100* (6), 1932–1934.
(101) Yamashita, K.; Takeda, H.; Kashiwabara, T.; Hua, R.; Shimada, S.; Tanaka, M. Ni-Catalyzed Addition Reaction of Allylic Selenides to Alkynes. *Tetrahedron Lett.* **2007**, *48* (38), 6655–6659. https://doi.org/10.1016/j.tetlet.2007.07.112.
(102) Morales, D.; Torrens, H. Allyl–Palladium Compounds with Fluorinated Benzenethiolate Ligands. X-Ray Crystal Structure of $[(\eta^3\text{-}C_3H_5)Pd(\mu\text{-}SC_6H_4F\text{-}4)_2Pd(\eta^3\text{-}C_3H_5)]$. *Polyhedron* **2001**, *20*, 3119–3125.
(103) Trowbridge, A.; Walton, S. M.; Gaunt, M. J. New Strategies for the Transition-Metal Catalyzed Synthesis of Aliphatic Amines. *Chem. Rev.* **2020**, *120* (5), 2613–2692. https://doi.org/10.1021/acs.chemrev.9b00462.
(104) Heravi, M. M.; Kheilkordi, Z.; Zadsirjan, V.; Heydari, M.; Malmir, M. Buchwald-Hartwig Reaction: An Overview. *J. Organomet. Chem.* **2018**, *861*, 17–104. https://doi.org/10.1016/j.jorganchem.2018.02.023.
(105) Ruiz-Castillo, P.; Buchwald, S. L. Applications of Palladium-Catalyzed C-N Cross-Coupling Reactions. *Chem. Rev.* **2016**, *116* (19), 12564–12649. https://doi.org/10.1021/acs.chemrev.6b00512.
(106) Philip, R. M.; Saranya, P. V.; Anilkumar, G. Nickel-Catalysed Amination of Arenes and Heteroarenes. *European J. Org. Chem.* **2022**, *2022* (25). https://doi.org/10.1002/ejoc.202200184 www.eurjoc.org.
(107) Kuai, M.; Jia, Z.; Chen, L.; Gao, S.; Fang, W. Nickel Metallaphotoredox Buchwald–Hartwig Amination Reactions: A Perspective on Irradiation Light Wavelength. *European J. Org. Chem.* **2024**, *27* (2). https://doi.org/10.1002/ejoc.202300933.
(108) Li, J.; Song, H.; Cui, C.; Cheng, J. P. Synthesis and Characterization of Linear and Square-Planar Nickel Complexes with Primary Amido Ligands. *Inorg. Chem.* **2008**, *47* (9), 3468–3470. https://doi.org/10.1021/ic800288x.
(109) Mindiola, D. J.; Hillhouse, G. L. Terminal Amido and Imido Complexes of Three-Coordinate

Nickel. *J. Am. Chem. Soc.* **2001**, *123* (19), 4623–4624. https://doi.org/10.1021/ja010358a.
(110) Berthel, J. H. J.; Krahfuß, M. J.; Radius, U. Nickel Tetracarbonyl as Starting Material for the Synthesis of NHC-Stabilized Nickel(II) Allyl Complexes. *Z. Anorg. Allg. Chemie* **2020**, *646* (13), 692–704. https://doi.org/10.1002/zaac.201900326.
(111) Hunt, A. P.; Lehnert, N. The Thiolate Trans Effect in Heme $\{FeNO\}_6$ Complexes and Beyond: Insight into the Nature of the Push Effect. *Inorg. Chem.* **2019**, *58* (17), 11317–11332. https://doi.org/10.1021/acs.inorgchem.9b00091.
(112) Coe, B. J.; Glenwright, S. J. Trans-Effects in Octahedral Transition Metal Complexes. *Coord. Chem. Rev.* **2000**, *203* (1), 5–80. https://doi.org/10.1016/S0010-8545(99)00184-8.
(113) Aullón, G.; Ujaque, G.; Lledós, A.; Alvarez, S.; Alemany, P. To Bend or Not to Bend: Dilemma of the Edge-Sharing Binuclear Square Planar Complexes of d^8 Transition Metal Ions. *Inorg. Chem.* **1998**, *37* (4), 804–813. https://doi.org/10.1021/ic9713386.
(114) Stephan, D. W. Early-Late Heterobimetallics. *Coord. Chem. Rev.* **1989**, *95* (1), 41–107. https://doi.org/10.1016/0010-8545(89)80002-5.
(115) Fong, S.-W. A.; Hor, T. S. A. The $\{Pt_2S_2\}$ Core—a Butterfly That Stings. *J. Chem. Soc. Dalt. Trans* **1999**, 639–651.
(116) Chambers, G. M.; Rauchfuss, T. B.; Arrigoni, F.; Zampella, G. Effect of Pyramidalization of the $M_2(SR)_2$ Center: The Case of $(C_5H_5)_2Ni_2(SR)_2$. *Organometallics* **2016**, *35* (5), 836–846. https://doi.org/10.1021/acs.organomet.6b00068.
(117) Aullón, G.; Lledós, A.; Alvarez, S. Structural Correlations and Conformational Preference in Edge-Sharing Binuclear d^8 Complexes with XR_2 Bridges. A Theoretical Study. *Inorg. Chem.* **2000**, *39* (5), 906–916. https://doi.org/10.1021/ic991268y.
(118) Blower, P. J.; Dilworth, J. R. Thiolato-Complexes of the Transition Metals. *Coord. Chem. Rev.* **1987**, *76* (C), 121–185. https://doi.org/10.1016/0010-8545(87)85003-8.
(119) Burdett, J. K. A Molecular-Orbital Study of Some Di-μ-Phosphido-Bis(Tricarbonyliron) Complexes. The Importance of Metal–Bridging Ligand Interactions in Determining Molecular Geometry. *J. Chem. Soc. Dalton Trans.* **1977**, No. 5, 423–428.
(120) Ho, N.; Mak, T. C. W.; Luh, T. Reductive Cleavage of the C-S Bond in $[Ni_2(Cp)_2(\mu\text{-}SR)_2]$ (Cp = η-C_5H_5) by $LiAlH_4$. Crystal Structures of $[Ni_2(Cp)_2(\mu\text{-}SPh)_2]$ and $[Ni_2(Cp)_2\{\mu\text{-}o\text{-}(SCH_2)_2\text{-}C_6H_4\}]$. *J. Chem. Soc. Dalton Trans.* **1990**, No. 12, 3591–3595.
(121) Hay, P. J.; Thibeault, J. C.; Hoffmann, R. Orbital Interactions in Metal Dimer Complexes. *J. Am. Chem. Soc.* **1975**, *97* (17), 4884–4899. https://doi.org/10.1021/ja00850a018.
(122) Fraser, R. R.; Mansour, T. S.; Savard, S. Acidity Measurements of Pyridines in Tetrahydrofuran Using Lithiated Silylamines. *J. Org. Chem.* **1985**, *50* (17), 3232–3234.
(123) Mindiola, D. J.; Hillhouse, G. L. Terminal Amido and Imido Complexes of Three-Coordinate Nickel. *J. Am. Chem. Soc.* **2001**, *123* (19), 4623–4624. https://doi.org/10.1021/ja010358a.
(124) Lin, C. Y.; Fettinger, J. C.; Power, P. P. Reversible Complexation of Lewis Bases to Low-Coordinate Fe(II), Co(II), and Ni(II) Amides: Influence of the Metal, Donor Ligand, and Amide Substituent on Binding Constants. *Inorg. Chem.* **2017**, *56* (16), 9892–9902. https://doi.org/10.1021/acs.inorgchem.7b01387.
(125) Hope, H.; Olmstead, M. M.; Murray, B. D.; Power, P. P. Syntheses and X-Ray Structures of $[Li(THF)_4][Ni(NPh_2)_3]\cdot 0.5C_7H_8$, $[\{Ni(NPh_2)_2\}_2]$, and $[\{Co(NPh_2)_2\}_2]$: Structural Characterization of Three Coordinate First-Row d^7 and d^8 Complexes. *J. Am. Chem. Soc.* **1985**, *107* (3), 712–713. https://doi.org/10.1021/ja00289a038.
(126) Faust, M.; Bryan, A. M.; Mansikkamäki, A.; Vasko, P.; Olmstead, M. M.; Tuononen, H. M.; Grandjean, F.; Long, G. J.; Power, P. P. The Instability of $Ni\{N(SiMe_3)_2\}_2$: A Fifty Year Old Transition Metal Silylamide Mystery. *Angew. Chem. - Int. Ed.* **2015**, *54* (44), 12914–12917. https://doi.org/10.1002/anie.201505518.
(127) Fackler, J. P.; Zegarski, W. M. Bridged Mercaptide Complexes of Nickel(II) and Palladium(II) with Metal-Metal Interactions. *J. Am. Chem. Soc.* **1973**, *95* (26), 8566–8574. https://doi.org/10.1021/ja00807a012.

(128) Carmona, E.; Marín, J. M.; Palma, P.; Peneque, M.; Poveda, M. L. New Nickel O-Xylyl Complexes. Crystal and Molecular Structure of $Ni_3(CH_2C_6H_4Me\text{-}o)_4(PMe_3)_2(\mu_3\text{-}OH)_2$. *Organometallics* **1985**, *4* (11), 2053–2055. https://doi.org/10.1021/om00130a021.
(129) Williams, D. B. G.; Lawton, M. Drying of Organic Solvents: Quantitative Evaluation of the Efficiency of Several Desiccants. *J. Org. Chem.* **2010**, *75* (24), 8351–8354. https://doi.org/10.1021/jo101589h.
(130) Dible, B. R.; Sigman, M. S. Unusual Reactivity of Molecular Oxygen with π-Allylnickel(N-Heterocyclic Carbene) Chloride Complexes. *J. Am. Chem. Soc.* **2003**, *125* (4), 872–873. https://doi.org/https://doi.org/10.1021/ja0286876.
(131) Dible, B. R.; Sigman, M. S. Steric Effects in the Aerobic Oxidation of π-Allylnickel(II) Complexes with N-Heterocyclic Carbenes. *Inorg. Chem.* **2006**, *45* (20), 8430–8441. https://doi.org/10.1021/ic0612451.
(132) Meiners, J.; Friedrich, A.; Herdtweck, E.; Schneider, S. Facile Double C-H Activation of Tetrahydrofuran by an Iridium PNP Pincer Complex. *Organometallics* **2009**, *28* (21), 6331–6338. https://doi.org/10.1021/om9006906.
(133) Wang, S.; Ma, P.; Shaik, S.; Chen, H. Valence-Inverted States of Nickel(II) Complexes Perform Facile C-H Bond Activation. *J. Am. Chem. Soc.* **2022**, *144* (32), 14607–14613. https://doi.org/10.1021/jacs.2c03835.
(134) Zhang, Z. F.; Su, M. Der. Insights into the Reactivity of the Ring-Opening Reaction of Tetrahydrofuran by Intramolecular Group-13/P- and Al/Group-15-Based Frustrated Lewis Pairs. *ACS Omega* **2023**, *8* (6), 5316–5331. https://doi.org/10.1021/acsomega.2c06194.
(135) Pasynskii, A. A.; Shapovalov, S. S.; Skabitskii, I. V.; Tikhonova, O. G. Syntheses and Structures of Nickel–Tungsten μ-Tellurophenyl Complexes $CpNi(PPh_3)(\mu\text{-}TePh)W(CO)_5$ and $[CpNi(PPh_3)(\mu\text{-}TePh)]_2W(CO)_4$. *Russ. J. Coord. Chem. Khim.* **2017**, *43* (12), 837–842. https://doi.org/10.1134/S1070328417120065.
(136) Chalkley, M. J.; Guard, L. M.; Hazari, N.; Hofmann, P.; Hruszkewycz, D. P.; Schmeier, T. J.; Takase, M. K. Synthesis, Electronic Structure, and Reactivity of Palladium(I) Dimers with Bridging Allyl, Cyclopentadienyl, and Indenyl Ligands. *Organometallics* **2013**, *32* (18), 4223–4238. https://doi.org/10.1021/om400687m.
(137) Carr, N.; Mullica, D. F.; Sappenfield, E. L.; Stone, F. G. A. Carborane Complexes of Nickel and Platinum: Synthesis and Protonation Reactions of Anionic Allyl(Carborane) Species. *Inorg. Chem.* **1994**, *33* (8), 1666–1673. https://doi.org/10.1021/ic00086a017.

Chapter 5: Preliminary Steps Towards Catalytic Application and Future Directions

5.1 Introduction

As mentioned in the Introduction, group 10 metals, particularly palladium and nickel, are widely used in catalytic materials. Furthermore, allylmetal complexes have displayed catalytic utility in various transformations.[1–5] Therefore, opportunities to leverage the unique properties of the types of bulky allyl complexes discussed in this work to achieve desirable catalytic properties are of natural interest. Two broad categories are considered here: initial steps in the development of highly-effective catalysts for the synthesis of vinyl-addition type polynorbornenes and consideration of the potential utility of bulky allyl complexes in catalyzing small molecule organic transformations.

5.2 Polymerization of norbornenes by allylnickel complexes

5.2.1 Background and motivations

Transition metal-catalyzed olefin polymerization was a crucial technological advance that allowed for the proliferation of cheap plastic materials that are now ubiquitous in society. The most common polyolefins are generated from simple acyclic monomers, but use of cyclic substrates can generate polymers with desirable properties. One commonly studied cyclic olefin is norbornene, as the rigidity imposed by its saturated bicyclic structure leads to polymers with high stability, transparency, fractional free volume, and glass transition temperatures.[6,7] Norbornene is prone to polymerization via a ring-opening metathesis (ROMP) mechanism,[8,9] which eliminates the bicyclic structure and maintains unsaturated C-C bonds, so the development of catalysts specific for vinyl-addition type polymerization (VAP) were required to achieve the above properties.[10] These have most commonly been organometallic complexes of nickel or palladium, often including allyl ligands.[11]

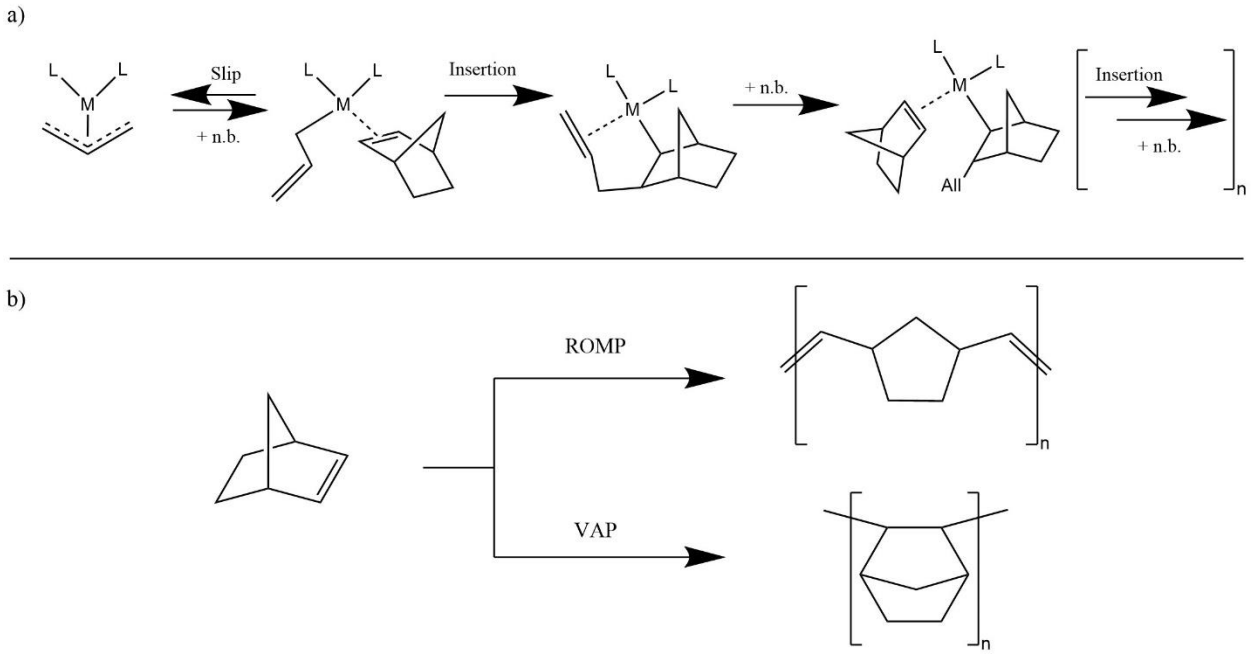

Figure 5.1: a) Idealized mechanism for Vinyl-Addition polymerization by a generic allylmetal complex, showing chain initiation and monomer coordination. n.b. = norbornene; All = allyl; L = generic supporting ligands b) Divergent polymerization outcomes for norbornene undergoing ring-opening metathesis polymerization (ROMP) or vinyl-addition polymerization (VAP), including the polymer backbone structure that results from each mechanism.

The properties of the synthesized polynorbornene can be altered by the presence of substituents, even at positions distal to the olefin moiety. One class of substituted polynorbornenes of particular interest are those containing trialkylsilyl or trialkoxysilyl groups at the five position, as these have shown great promise as materials for membranes with selective CO_2 permeability.[7,12,13] The corresponding silylated monomers, though, have proven difficult substrates for polymerization, generating a need for more efficient catalytic systems. Recently, a highly efficient cationic allylpalladium complex was reported that was able to convert silylated norbornenes to the corresponding polymer in high yield and with high molecular weight.[11] However, this requires elevated temperatures and an expensive palladium catalyst, limiting the efficiency of the system for process-scale synthesis. Obtaining similar levels of reactivity under milder conditions or using a nickel-based catalyst is therefore desirable.

More substituted allyl ligands were associated with lower activity in a cationic allylpalladium species used for norbornene polymerization, in line with the general inverse relationship between stability and catalytic activity. However, the more substituted allyl was also found to give substantially higher

molecular weight polymers.[11] This suggested that complexes of the [A´] ligand, particularly those of nickel, might have a useful niche in this reaction.

5.2.2 Early polymerization results with [MA´$_2$] complexes

*Note: Polymerization reactions and polymer characterization in this section were performed by Alicia Doerr of the Long group at the University of Tennessee – Knoxville.

The previously described bis(A´) complexes of the first row transition metals (M = Cr,[14] Fe,[14] Co,[15] Ni[15,16]) were synthesized and tested for their effectiveness in polymerizing variously substituted norbornenes. While multiple species were capable of polymerizing unsubstituted norbornene, only [NiA´$_2$] was generally effective across multiple monomers. The full compilation of polymerization outcomes and the methodology used to conduct reactions and characterize polymers can be found in Appendix 5.

Table 5.1: Outcomes of the polymerization of various 5-substituted norbornenes under [NiA´$_2$] catalysis.[a]

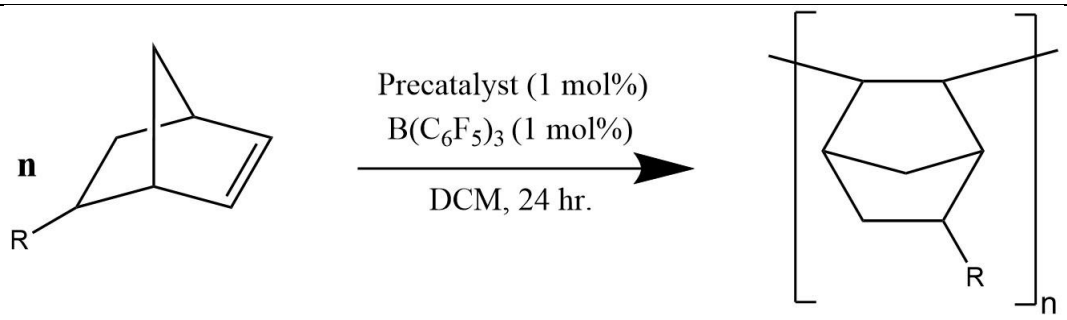

Entry	Monomer R Group	Yield (%)	M_n (kg/mol)	M_w/M_n
1	H	100	insoluble	----------
2	$Si(OEt)_3$	41	111,000	2.653
3	CH_2OH	No polymer	----------	----------
4	$C(O)OCH_2C_6H_5$	Trace	----------	----------
5	$CH_2OCH_2C_6H_5$	64	60,000	3.1
6	$Si(OMe)_3$	65.7	244,000	2.812
7	CH_2Br	24	60,000	1.98
8	TMS	39	29,000	2.462

[a]) Polymerizations were conducted using 0.15 g monomer, 1 mol % precatalyst, 1 mL DCM, activated using 1 equiv. $B(C_6F_5)_3$, and run for 24 hours.

Of particular note was the ability of [NiA´$_2$] to polymerize silyl-substituted norbornene monomers. Especially in the case of the alkoxysilyl-norbornenes, high molecular weights were obtained from moderate overall polymer yields. Furthermore, while performance with the bromo-substituted monomer was poor,

the production of polymer from a polar-functionalized norbornene at all was notable; the general difficulty of this class of substrate has been noted.[11,17] There were limits to this tolerance, though, as the hydroxylated monomer could not be polymerized. This was an overall promising result, but [NiA´$_2$] still underperformed a well-known norbornene polymerization catalyst, [Ni($SbPh_3$)$_2$(C_6F_5)$_2$] (compare entry 5 with reported 71% yield, M_n = 150 kg/mol, M_w/M_n = 1.47 for Si(OEt)$_3$-substituted norbornene).[7,18]

5.2.3 Early polymerization results with [{A´NiBr}$_2$] and related complexes

*Note: Polymerization reactions and polymer characterization reported in this section were performed by Xinyi Wang of the Long group at the University of Tennesssee – Knoxville.

Given the broad use of allylmetal halide complexes in catalysis, [{A^{2t}NiBr}$_2$] was also evaluated for its catalytic competency in this polymerization reaction. The use of the halide-bridged archetype also allowed for testing of bridge-split complexes featuring neutral donor ligands. The results of polymerizations using these compounds as precatalysts are shown below in Table 5.2.

Table 5.2: Polymerization of norbornenes catalyzed by [{A^{2t}NiBr}$_2$] and two bridge-split derivatives.[a]

Monomer R Group	Precatalyst	Yield (%)	Entry
Trimethylsilyl	[{A^{2t}NiBr}$_2$]	11.7	1
	[A^{2t}Ni(PPh_3)Br]	22.4	2
	[A^{2t}Ni(IMes)Br]	9.3	3
Trimethoxysilyl	[{A^{2t}NiBr}$_2$]	80.7	4
	[A^{2t}Ni(PPh_3)Br]	44.2	5
	[A^{2t}Ni(IMes)Br]	98.2	6
n-hexyl	[{A^{2t}NiBr}$_2$]	94.8	7
	[A^{2t}Ni(PPh_3)Br]	96.0	8
	[A^{2t}Ni(IMes)Br]	93.5	9

[a]) Polymerizations were conducted using 0.15 g monomer, 1 mol % precatalyst, 1 mL DCM, activated using 1 equiv. B(C_6F_5)$_3$, and ran for 24 hours.

There is no clear, consistent difference in the reactivities of the three complexes, suggesting that the propagating species is similar in all three cases. It should be noted that, for all three complexes, polymerization could also be initiated by halide abstraction with the silver salt [$AgSbF_6$]; unfortunately, the complexes used under these conditions were later found to contain substantial impurities, perhaps as high as 50 mol%, so quantitative evaluation of catalytic performance under these conditions is not productive. One qualitative observation, though, is the weaker performance of the carbene adduct [A´Ni(IMes)Br] when activated with [$AgSbF_6$] instead of [B(C_6F_5)$_3$]; only unsubstituted and hexyl substituted norbornenes could

be polymerized in meaningful quantities (48.8% for *n*-hexyl-norbornene; compare to entry 9. All other monomers reacted to yield only trace amounts of polymer). The reason for this is not clear at this time. The Brookhart group reported that [$B(C_6F_5)_3$] activated a cationic allylnickel species towards norbornene polymerization by displacement of other neutral ligands with an Ar^F ring to form a highly reactive cationic species.[19] It is clear that this mechanism cannot be operative in the activation of [NiA´$_2$], though, and more likely is a full or partial deallylation as reported by Bochmann.[20] In the case of [A´Ni(L)Br] complexes, though, both of those mechanisms are possible, in addition to halide abstraction, analogous to the mechanism reported by the Chen group.[21] It is therefore difficult to diagnose the cause of differential reactivity; characterizing the product of activation with various different activators is therefore an important step in the future development of this class of catalysts.

As these results still fell short of the benchmark Espinet catalyst mentioned above, further development of the catalytic system was necessary. To identify productive directions for this development, a number of derivatives of [NiA´$_2$] with systematically varied features were sought. As the most broadly accessible class of allyl nickel complexes are those based on the [{(allyl)NiX}$_2$] motif, these were chosen as the primary targets of derivatization.

5.2.4 Synthesis of derivatives of [NiA´$_2$]

5.2.4.1 Synthesis of mono-trimethylsilylated allyl complexes

The first factor to be investigated was steric bulk. While the steric stability provided by the TMS groups of A´ were obviously desirable, we considered the possibility that a more optimal ratio of stability to activity might be achieved with slightly less steric bulk. Therefore, the synthesis of nickel complexes of the analogous mono-silylated allyl ligand ($Me_3SiC_3H_4$ = A^{1Si}) was pursued. Reaction of potassium 1-trimethylsilylallyl with nickel acetylacetonate yielded a thin yellow oil, albeit in 35% yield. ^{1}H NMR analysis of the material showed an extremely complex mixture of species, with 11 distinct allyl spin systems present in greater than trace amounts, all of which were consistent with a bis(allyl) species. On this basis and the reactivity discussed below, this compound was identified as [NiA^{1Si}_2], and preliminary assignments of each species are given in Appendix 5. The observed stereochemical complexity is in stark contrast to that observed for bis(crotyl)nickel,[22] which likely reflects the increased propensity for silyl substituents to be found in an *anti* configuration. The observed isomer ratios were not changed by performing the reaction at low temperature, not by increasing the grinding time to 45 minutes. The abundance of the lowest abundance product increased slightly upon sitting for one week. Based on these observations, it seems likely that the isomers are able to interconvert at room temperature, and that the isomers are at equilibrium. Experiments to confirm this and quantify the barriers associated with interconversion of these isomers by VT-NMR have not yet been attempted.

Despite repeated efforts, the compound did not solidify from the yellow oil, and lowering the temperature to 5 °C caused the mixture to solidify as a large mass, preventing the determination of its crystal structure. It was hypothesized that the single TMS group might be sufficient to confer most of the stability seen in [NiA´$_2$]. This was not the case, however. The isolated yellow oil degraded over the course of one month, making its direct applications limited. This degradation is presumed to proceed via reductive elimination of the two allyl groups but has not been studied.

According to the reasoning given above, complexes displaying the bridged bromide dimer motif were desired for polymerization testing. Therefore, [NiA$^{1Si}_2$] was converted to [{A^{1Si}NiBr}$_2$] by reaction with elemental bromine. It was also expected that [{A^{1Si}NiBr}$_2$] might be more stable than the bis(allyl) complex, as is often observed for allylnickel complexes.[23] Using the improved methodology for bromination described in Appendix 3, [{A^{1Si}NiBr}$_2$] was successfully synthesized. Analysis of the allyl C-H peaks by 1D and 2D NMR suggests that only two isomers are present, but the more complex mixture of anomalously small TMS peaks suggests a more complex mixture with extensive peak overlap.

After repeated attempts, slow evaporation of a hexane solution of [{A^{1Si}NiBr}$_2$] yielded small crystal of sufficient quality for structural determination. The compound crystallizes in the P_{21}/c space group, with an inversion center lying directly in the center of the molecule. The allyls are staggered relative to each other, as seen in [{A´NiBr}$_2$].[16] The bond distances are also similar between the two complexes. The nickel-terminal allyl carbon bonds are slightly shorter in [{A^{1Si}NiBr}$_2$], while the C-C bonds in the allyl backbone differ less. Together, these two differences imply slightly greater delocalization in the less bulky compound. Interestingly, the TMS group is in the *anti* configuration. Substituents that are stable in the *anti* configuration are rare,[16,22,24] and the increased tendency for silyl substituents to adopt the *anti* configuration compared to alkyl substituents is an area of active investigation.

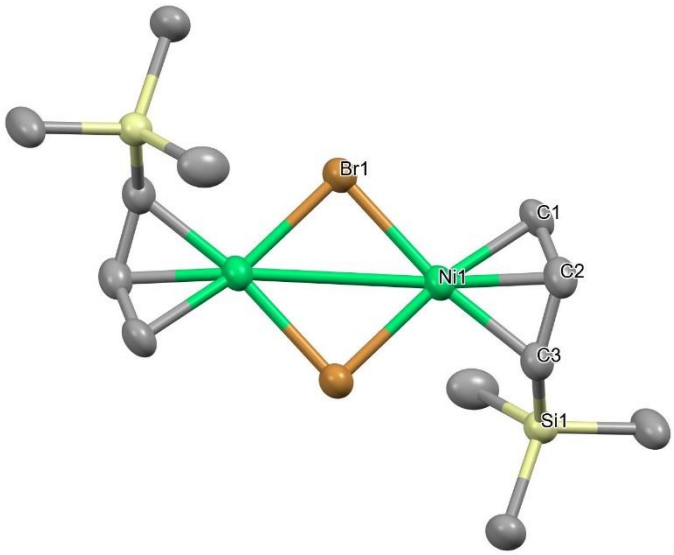

Figure 5.3: Thermal ellipsoid plot of the molecular structure of [{A^{1Si}NiBr}$_2$] (50% probability). Hydrogen atoms are omitted for clarity. Selected Bond distances (Å): Ni-C1, 2.004(8); Ni-C2, 1.973(8); Ni-C3, 2.024(8); Ni-Br, 2.356(4); C1-C2, 1.39(1); C2-C3, 1.41(1).

5.2.4.2 Synthesis of [{A´NiCl$_2$}$_2$]

To study the effect of halide identity, [NiA´$_2$] was allowed to react with HCl in dioxane to yield a red solid, determined to be [{A´NiCl}$_2$]. The material was lighter and redder in color compared to [{A´NiBr}$_2$], but no other distinguishing features were observed. Slow evaporation of a hexane solution of the compound yielded red needles, allowing its crystal structure to be determined. The resulting structure is of imperfect quality - the best model for the obtained diffraction data displays disorder of unclear origin in both an allyl backbone and in a chloride bridge. As such, a detailed discussion of structural parameters is not productive. However, the structure appears to be overall consistent with previously studied allylnickel halide complexes.

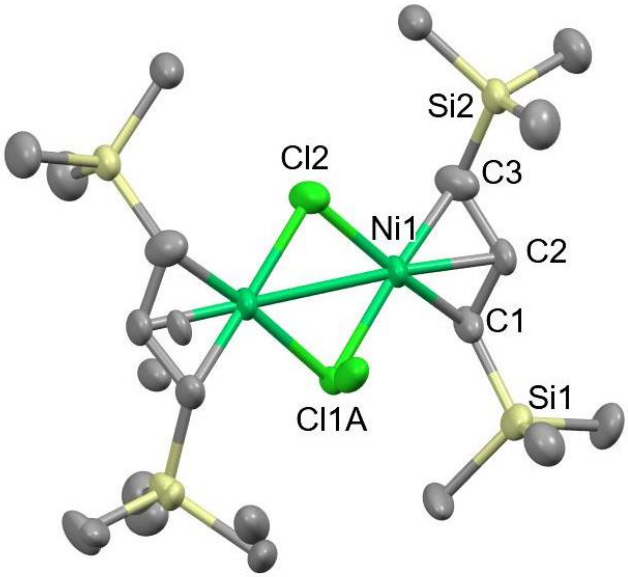

Figure 5.4: Thermal ellipsoid plot of the molecular structure of [{A´NiCl}$_2$] (50% probability). Disordered atoms can be seen near the left-side allyl backbone and in front of Cl1A. Hydrogen atoms are omitted for clarity. Selected Bond distances (Å): Ni-Cl1A, 2.251(5); Ni-Cl2, 2.218(2); Ni-C1, 2.086(4); Ni-C2, 1.990(4); Ni-C3, 2.019(3); C1-C2, 1.439(6); C2-C3, 1.474(5).

5.2.4.3 Attempted synthesis of A´ complexes of heavy group 10 metals

*Note: Attempts to synthesize silylallyl-palladium complexes by C-H activation were done with the assistance of undergraduate researcher Chang Kyu Jung.

Work by the Hanusa group and others has extensively investigated the chemistry of the A´ ligand, and seen its successful application across the periodic table.[25,26] The most notable exception to this broad success is the second and third row transition metals. Outside of the most electropositive of these metals (Groups 3-5), no A´ such complexes of these metals have ever been reported. This is despite the generally greater stability and ease of access of noble metal allyl complexes compared to allyl complexes of other metals. Previous unpublished efforts in the Hanusa group attempting to adapt the conditions used in the synthesis of [FeA´$_2$] and [NiA´$_2$][14,16] to palladium and ruthenium produced coupled hexadiene as the only organic product. This can be rationalized, as compared to first row transition metals, reductive elimination from heavier TM centers tends to be more favorable. Non-metathesis routes to noble metal allyls are commonplace, most prominently activation of allylic C-H or C-X (X = halogen, carboxylate). However, in the case of A´, these methods encounter an extra difficulty in the lability of the allylic C-Si bond. Even

weak nucleophiles such as chloride are able to rapidly cleave this bond to yield a desilylated allyl complex.[27] The Murai group reported conditions allowing for C-H activation of allyl silanes without desilylation, but attempts to replicate this result failed, as did all attempts to adapt the reported conditions.[27] Reactions typically yielded complex mixtures of species; the only exception to this outcome was when desilylation proceeded cleanly. In the course of this investigation, [{A^{1Si}PdCl}$_2$] generated from an attempted synthesis of [{A´PdCl}$_2$] was allowed to react with triphenylphosphine, forming the expected adduct [A^{1Si}Pd(PPh_3)Cl], which was subsequently crystallographically characterized. The allyl group is disordered over two positions, differing in the direction of the C1-C2-C3 triangle of the allyl backbone and in the configuration of the TMS group, being found in both *syn* and *anti* positions; the structure containing the *anti* TMS is predominant, being 67% occupied. The TMS-bound carbon is trans to the phosphine and accordingly, the Ni-C3 bond is longer than the other Ni-C bonds. This could plausibly be favored on steric grounds, as it positions the bulky TMS substituent farther from the rest of the molecule. However, as the molecule does not appear to be sterically crowded, it is not clear that this is relevant. This is a second example of an allyl complex where having exclusively *anti* substituents seems to be the most favorable arrangement, though the ancillary ligand *trans* to the substituted carbon may play a role in this preference.[28]

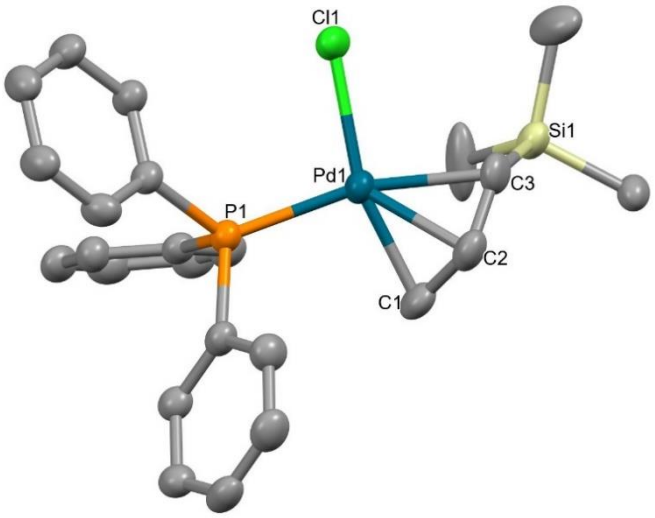

Figure 5.5: Thermal ellipsoid plot of the molecular structure of the predominant isomer of [A^{1Si}Pd(PPh_3)Cl] (50% probability). Hydrogen atoms are omitted for clarity. Selected Bond distances (Å): Pd-C1, 2.09(1); Pd-C2, 2.124(8); Pd-C3, 2.21(1); Pd-Cl, 2.362(4); Pd-P, 2.314(7); C1-C2, 1.41(1); C2-C3, 1.40(1).

Due to the difficulty in finding appropriate synthetic methods using C-H activation, the improved methodology for the synthesis of [MA´$_2$] by halide metathesis was adapted to fill this gap. This gives the further advantage of directly generating [MA´$_2$] complexes; these can be trivially converted to [{A´MX}$_2$]

type complexes,[16,29] while the reverse reaction is less precedented. Palladium was the first focus due to its prominent place in catalysis of organic transformations. Therefore, the solvated precursor $[Pd(NCMe)_2Cl_2]$ was used in the place of $[PdCl_2]$. Additionally, a softer source of the A′ anion, potassium tris(A′)stannate,[30] was employed; the use of organotin compounds as allyl transfer agents to a palladium center is exceedingly well-established as a part of the ubiquitous Stille coupling reaction.[31,32] Reaction of $[K\{SnA'_3\}]$ with $[Pd(NCMe)_2Cl_2]$ yielded a complex mixture of species, among which were found two spin systems closely matching the features of $[NiA'_2]$. On this basis, these have been identified and the staggered and eclipsed isomers of $[PdA'_2]$. Finally, the use of $[Pd(OAc)_2]$ as the palladium source yielded 80% total yield with a 3 : 1 $[PdA'_2]$: $\{A'_2\}$ ratio, giving a noble metal-A′ complex as the primary product of a reaction for the first time. The product mixture remains somewhat complex, with an additional localized byproduct, as well as a *syn,syn* η^3-bound allyl spin system hypothesized to belong to $[\{A'PdOAc\}_2]$. It is possible that the reaction outcome could be further improved by the use of palladium acetylacetonate, as suggested by results with nickel (See Chapter 2), or by the use of an even softer allyl source, such as $[GeA'_4]$.[33]

Attempts to crystallize $[PdA'_2]$ have been thus far unsuccessful. However, an NMR tube sample of the isolated $[PdA'_2]/\{A'_2\}$ mixture, synthesized from $[Pd(NCMe)_2Cl_2]$ and $[K\{SnA'_3\}]$, yielded thin, pale yellow crystals upon sitting in air for approximately 14 months. Single crystal X-ray diffractometry revealed this compound to have the molecular formula $[\{A'PdCl\}_2]$, thereby representing the first structurally characterized palladium-A′ complex. The two allyl groups are staggered relative to each other and all four TMS groups are in the *syn* configuration, matching the conformation seen in $[\{A'NiBr\}_2]$.[16] The molecule lies on a crystallographic twofold axis, thus only half of the molecule is unique.

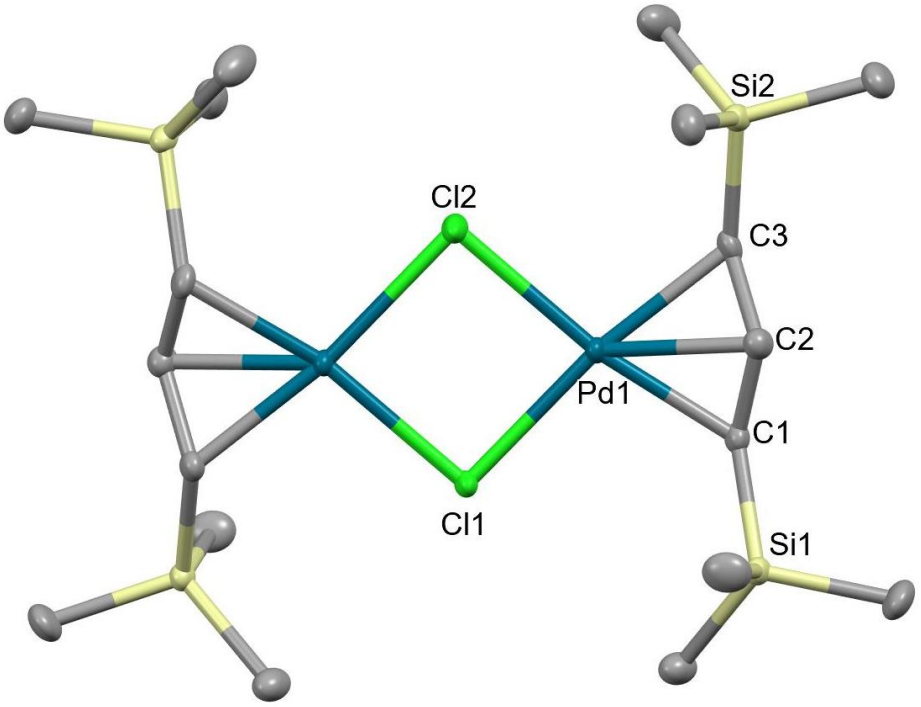

Figure 5.6: Thermal ellipsoid plot (50%) of the molecular structure of [{A´PdCl}$_2$]. Hydrogen atoms are omitted for clarity. Selected bond distances (Å): Pd1-Cl1, 2.407(1); Pd-Cl2, 2.412(1); Pd-C1, 2.149(4); Pd-C2, 2.109(4); Pd-C3, 2.164(4); C1-C2, 1.431(6); C2-C3, 1.415(6).

The parent allyl analogue, [{APdCl}], displays slightly greater crystallographic symmetry (space group = $P2_1/n$,) but the structures are otherwise very similar. [{APdCl}] shares the planar {PdCl}$_2$ core and mutually staggered allyls.[34] The average palladium-chloride distances are 0.008 Å longer, the Pd-C(allyl terminal) distances 0.034 Å longer, and the Pd-C(allyl center) distances equidistant in [{A´PdCl}$_2$] compared to its parent compound. There is no meaningful difference in the bond angles around the palladium center. This confirms that bulky allyl complexes display limited structural deformation when compared to their unsubstituted counterparts.

5.2.5 Future directions for improved norbornene polymerization catalysts

Of course, the first step in progressing this investigation is to test the synthesized derivatives for their performance in catalyzing the polymerization of silylated norbornenes. While [{A´PdCl}$_2$] has not previously been intentionally synthesized, it is expected that it can easily be obtained from even impure samples of [PdA´$_2$] by the same method used to synthesize [{A´NiCl}$_2$]. Therefore, samples of the three

new [{A´MX}$_2$] compounds described above could be provided to collaborators in the Long group, and the impact that each modification has on catalytic performance can be evaluated. Additionally, [{A^{2t}NiBr}$_2$] and some of its derivatives described in Chapter 4, perhaps [{A^{2t}NiOH}$_2$], [{A^{2t}NiOPh}$_2$], [A^{2t}NiInd], or [A^{2t}NiFluor], would also be complexes of interest. The utility of weakly binding ancillary ligands in this polymerization has been well-established,[11,18] but only bridge-split complexes featuring strongly binding ancillary ligands (PPh_3 and IMes) have been studied thus far. The relative reactivity of [A´Ni($SbPh_3$)Br] should also be investigated. The information gained from this precatalyst survey could then be used for second-generation catalyst development.

There are also some other derivatives of interest that should be targeted for synthesis. A general trend amongst recently reported high-performance norbornene polymerization catalysts is the presence of highly electrophilic metal centers.[11,35] This follows from the basic mechanism of vinyl addition polymerization, in which metal centers must bind free olefin to both initiate and propagate chain growth. One way that electrophilicity can be achieved is via weakly coordinating anions, generating a metal center with a formal positive charge. This is a commonly employed strategy across olefin polymerization catalysis.[36–39] The formation of cationic complexes from allylnickel compounds is well precedented.[29,40,41] It has therefore been surprising that all attempts to synthesize such a complex by halide abstraction from either [{A´NiBr}$_2$] or [{A^{2t}NiBr}$_2$] have failed. Several mono- and bi-dentate ancillary ligand systems have been employed to attempt to stabilize a cationic nickel center, but in all cases only complex decomposition products could be observed. The reason for this is unclear, but the unexpected apparent lower stability of the bulky allyl complexes compared to their unsubstituted analogues might suggest the involvement of the bulky substituents in the decomposition process, perhaps via a *pseudo* γ-elimination type reaction.

A second way that electrophilic metal centers can be achieved is via weakly electron-donating ligands. Most recent norbornene polymerization catalysts not based on an allyl-metal motif have achieved this via the use of fluorinated aryl groups.[11,42,43] However, this strategy has not been applied to the allyl-based catalysts. Therefore, [{(allyl)NiX}$_2$] species featuring a fluorinated allyl ligand would be an interesting synthetic target. Of particular note, a direct analogue of HA^{2t} featuring perfluorinated *tert*-butyl groups has been reported.[44] This would make an appealing synthetic target, though the published synthesis using octafluoroisobutylene would need to be altered.

Finally, as mentioned above, the initiation mechanism for the various classes of allyl complexes discussed here should be investigated. This study is of particular importance to complexes that have access to multiple activation modes, including the [{(allyl)Ni(L)X}$_2$] complexes discussed above and any of the novel [{A^{2t}NiER$_n$}$_2$] complexes that are tested. Additionally, study of the activation of the hetero-diorganonickel species ([A^{2t}NiA´], [A^{2t}NiCp], [A^{2t}NiInd], and [A^{2t}NiFluor]) could be of interest. While the mechanism of activation would be limited to alkyl-abstraction type processes, the preference for which

alkyl group is abstracted could be of interest. This would also allow for differential activity of the remaining organonickel fragments to be studied. It is also possible that, given the apparent fluxionality implied by the NMR spectrum of [A^{2t}NiFluor], catalysis in the absence of an external initiator could be achieved.

5.3 Potential utility of bulky allyl complexes in catalysis of organic coupling or functionalization reactions

5.3.1 Studies using A^{2t}-nickel complexes

One potentially interesting area of study is the stoichiometric activity of [{A^{2t}NiOH}$_2$] and [{A^{2t}NiOPh}$_2$] compared to [{A^{2t}NiBr}$_2$] in boron-to-nickel transmetallation reactions. These represent rare examples of isolated and easily handled nickel oxo species, and their activity in such reactions is relevant due to debate over the importance of bridged oxo species in nickel catalyzed Suzuki-Miyaura reactions. The potential for oxo-ligands to modulate the rate of the transformation has been recognized.[45,46] A computational investigation proposed that dimeric hydroxide species represent a resting state for the catalyst and that the effective concentration of this resting state has a large impact on reaction outcome.[46] However, this study was limited to aryl-bis(phosphine)nickel bromide complexes. Study of pre-formed hydroxide complexes would allow this finding to be experimentally validated and the conclusions extended to broader ligand sets. If [{A^{2t}NiOH}$_2$] displays the same resistance to ancillary ligand binding observed for [{A^{2t}NiBr}$_2$], then the importance of such ligands in the transmetallation step could also be easily established.

[{A^{2t}NiBr}$_2$] and other related compounds could also be evaluated for catalytic competency; some recently reported C-N and C-S coupling systems mediated by allylnickel precatalysts would seem promising candidates. However, in these systems, and indeed in general, allylnickel precatalysts are believed to lose the allyl ligand upon activation. As such, alterations to the allyl are not expected to have a substantial impact on reaction outcome. For example, one result that inspired the initial investigation into *tert*-butyl allyls was the 2015 publication detailing the effectiveness of catalysts based on 1-*t*Bu-indenylpalladium complexes. These complexes were found to be much more reactive than their standard cinnamyl-based counterparts. This established the value of *tert*-butyl ligands on the terminal carbons of an η^3-bound ligand: would using the less coordinatively demanding allyl ligand in place of indenyl lead to further increases in activity? However, the cause of the increased activity was found to be that the bulky groups prevented the formation of inactive palladium(I) dimers.[47] Nickel is generally not believed to form such species under typical conditions; in fact, it is more common that catalyst deactivation rin nickel-based systems results from the instability of its more reduced forms,[48] not their spontaneous formation. Indeed, the increased stability of A^{2t}-nickel complexes towards reductive elimination would likely negatively

impact catalyst activation and consistency. Therefore, it is expected that useful catalytic improvements will require the synthesis of the palladium complex, [{A^{2t}PdBr}$_2$]

5.3.2 Attempted synthesis of [{A^{2t}PdBr}$_2$]

Reaction of bis(dibenzylideneacetone)palladium(0) with [BrA^{2t}] led to darkening of the solution and eventual deposition of black solid, similar to the reactions with [Ni(cod)$_2$] discussed in Chapter 3. Workup isolated a bright yellow solution from a black solid. ^{1}H NMR of the isolated organic product showed primarily free DBA as well as [BrA^{2t}] and a new *syn,syn* species in a 2 : 1 ratio. This species could be isolated from [BrA^{2t}] by MeCN/hexane extraction, allowing a clean ^{1}H NMR spectrum to be obtained; based on these spectral features, this compound is believed to be [{A^{2t}PdBr}$_2$]. However, overall yield of this material was scarcely above trace (approximately 10% by NMR,) and could not be easily isolated from residual DBA.

As oxidative addition to nickel was improved by the introduction of an ancillary ligand, the reaction was reattempted in the presence of 0.5 eq. triphenylphosphine. Indeed, the deposition of palladium metal was not observed under these conditions. However, oxidative addition products remained trace species; a mixture of the presumed [{A^{2t}PdBr}$_2$] and a new species, likely the monomeric phosphine adduct, were observed. For Pd(dba)$_2$, therefore, the addition of triphenylphosphine suppresses the decomposition reaction producing elemental palladium but does not substantially boost the extent of oxidative addition. This demonstrates that the atypical behavior of [BrA^{2t}] towards oxidative addition extends to metals other than nickel, and that modifying conditions to promote oxidative addition to different metal centers is non-trivial.

While successful synthesis of [{A^{2t}PdBr}$_2$] has not yet been achieved, the better reactivity seen for [Pd(dba)$_2$] compared to [Ni(cod)$_2$] in the absence of ligand suggests that appropriate tuning of conditions will allow for the desired compound to be isolated in reasonable yield. The use of Pd-olefin complexes as starting materials, mimicking the conditions effective for nickel, could improve reaction outcome, and would have the added benefit of addressing the difficulty in isolating [{A^{2t}PdBr}$_2$] from side-products. Attempted oxidative addition of [BrA^{2t}] to [Pt(PPh$_3$)$_4$] produced no product whatsoever, though, so it is possible that there are limits to which metals can easily form A^{2t} complexes via oxidative addition.

5.3.3 Long term outlook

The early progress in accessing both A´ and A^{2t} complexes of palladium are promising, suggesting the viability of bulky allyl complexes of the noble metals. Long term study should be dedicated to

determining the range of metals and ligand sets amenable to allylmetal complex synthesis via the methodologies described in this thesis, or adaptations thereof. This will inform the potential catalytic applications that can be pursued.

Generally speaking, the bulky allyls discussed here display two properties that could be exploited to give exciting catalytic materials. The first of these is the kinetic stability that they provide. In general, transition metal centers are more active catalysts when they have easily accessible coordination sites; precatalysts frequently contain weak ligands that are easily displaced, thereby "masking" open coordination sites. A downside of decreased coordinative saturation, though, is increased instability, which can contribute to shorter catalyst lifetimes. The use of bulky allyl ligands may allow for such highly active metal centers to be used in harsher transformations or at higher temperatures.

The second is their less fluxional stereochemical features. As mentioned throughout this work, the common mechanisms for allyl-centered exchange processed are substantially slowed when bulky groups are present on the 1 and 3 carbons of the allyl backbone, and can be entirely ignored below approximately 55 °C in bis(allyl) complexes. As such, the stereochemistry of the allyl group is essentially set upon synthesis of the compound. This opens the possibility of asymmetric catalysis. The most obvious implementation of this idea would be stereospecific polymerization. For example, the presence of *syn,syn* -*t*Bu groups on one face of a metal center might reasonably expect to favor chain growth extending towards the opposite face, yielding syndiotactic polymer. Additionally, it is possible that the improved understanding of the preferred configurations of different bulky allyl complexes might be valuable in the development of convenient late stage allylic functionalization processes. If the geometry of a large organic molecule upon allylic activation can be confidently predicted, then stereodivergent functionalization may be easily realized. The installation of chiral bulky substituents might even allow for enantioselective catalysis to be achieved.

5.4 Synthetic procedures and characterization data

[Bis(1-trimethylsilylallyl)nickel(II)] "[NiA$^{1Si}_2$]":

In a nitrogen filled glovebox, 0.12 g (0.46 mmol) g of [Ni(acac)$_2$] and 0.13 g (0.87 mmol) of potassium trimethylsilylallyl were measured and placed into a 50 mL stainless steel grinding jar along with 25 g 4.8 mm stainless steel ball bearings (approximately 57 ball bearings). The jar was clamped to be airtight and transferred to a Retsch PM100 planetary mill. The mixture was milled at 600 rpm for 15 minutes, after which it was transferred to the glovebox. The residual solid was extracted three times with 10 mL hexane, and the extracts filtered through a fine porosity fritted funnel. The filtrate was then placed under vacuum, eventually yielding 0.058 g (47% yield) of a thin yellow oil identified as [NiA$^{1Si}_2$]. Gravimetric analysis of nickel content was performed by precipitation with a dimethylglyoxime solution, followed by repeated

drying in a 120 °C oven until mass loss was no longer observed. Anal. Calcd for $C_{12}H_{26}Si_2Ni$: Ni, 20.58. Found: Ni, 20.16. The compound can also be synthesized in solution, but the mechanochemical route was found to give the most reproducible results.

The ^{1}H NMR spectrum shows an extremely complex mixture of allylic spin systems. Each peak is sharp, allowing distinct spin systems to be fully identified. The combination of coupling constants, chemical shift ranges, and, when possible, integration ratios allowed for the likely conformations of each isomer to be assigned. No spectral features relating to *cis/trans* isomerism have been identified; it is assumed on steric grounds that *trans* conformations will be generally more stable, so where relevant, the *trans* isomer is always assumed to be the more predominant species. In the case of the eclipsed *syn,anti* conformation, one species is initially predominant, but after sitting for about one week, the two show nearly identical abundances; the initially dominant species has been assigned as *trans*, but this assignment is speculative. Due to the extent of peak overlap, carbons have not been assigned, and only one TMS proton signal for the likely eclipsed *syn,anti trans* isomer was resolved. An additional staggered *syn* allyl can be identified via ^{1}H-^{1}H COSY couplings but is of sufficiently low abundance that its peaks cannot be made out; it is not reported here.

Staggered *syn,syn trans* (11 eq.): ^{1}H NMR (400 MHz, C_6D_6): δ 5.03 (ddd, J = 15.5, 13.3, 7.0 Hz, 1H, center allyl C-H); δ 3.89 (m, 1H, terminal allyl *syn* C-H); δ 1.82 (dt, J = 13.8, 1.4 Hz, 1H, terminal allyl *anti* C-H); δ 1.46 (m, 1H, terminal allyl *anti* C(TMS)-H); δ 0.20 (s, 9H, $Si(CH_3)_3$).

Staggered *syn,anti trans* (10 eq.): ^{1}H NMR (400 MHz, C_6D_6): δ 5.32 (m, 1H, center allyl with *anti* TMS C-H); δ 5.01 (ddd, J = 15.5, 13.5, 7.1 Hz, 1H, center allyl with *syn* TMS C-H); δ 3.90 (m, 1H, terminal allyl with *syn* TMS *syn* C-H); δ 3.84 (m, 1H, terminal allyl with *anti* TMS *syn* C-H); δ 3.49 (m, 1H, terminal allyl with *anti* TMS *syn* C-H); δ 1.97 (ddd, J = 14.7, 1.9, 0.5 Hz, 1H, terminal allyl *anti* C-H); δ 1.85 (dt, J = 13.5, 1.2 Hz, 1H, terminal allyl with *syn* TMS *anti* C-H); δ 1.46 (m, 1H, terminal allyl with *syn* TMS *anti* C(TMS)-H); δ 0.19 (s, 9H, *syn* $Si(CH_3)_3$); δ -0.08 (s, 9H, *anti* $Si(CH_3)_3$). kek

Staggered *anti,anti trans* (8.3 eq.): ^{1}H NMR (400 MHz, C_6D_6): δ 5.40 (m, center allyl C-H); δ 3.83 (m, terminal allyl *syn* C-H); δ 3.49 (dd, J = 10.6, 2.2 Hz, terminal allyl *syn* C-H); δ 1.97 (ddd, J = 14.6, 2.0, 0.5 Hz, terminal allyl *anti* C-H); -0.07 (s, 9H, $Si(CH_3)_3$).

Staggered *anti,anti cis* (5.8 eq.): ^{1}H NMR (400 MHz, C_6D_6): δ 5.41 (ddd, J = 14.4, 10.5, 7.7 Hz, 1H center allyl C-H); δ 3.84 (m, 1H, terminal allyl *syn* C-H); δ 3.56 (m, 1H, terminal allyl *syn* C-H); δ 2.02 (ddd, J = 14.7, 1.9, 0.5 Hz, 1H, terminal allyl *anti* C-H); -0.08 (s, 9H, $Si(CH_3)_3$).

Eclipsed *syn,syn trans* (4.5 eq.): ^{1}H NMR (400 MHz, C_6D_6): δ 4.54 (m, 1H, center allyl C-H); δ 3.66 (m, 1H, terminal allyl *syn* C-H); δ 2.34 (bd, J = 13.7 Hz, 1H, terminal allyl *anti* C-H); δ 2.06 (d, J = 15.4 Hz, 1H, terminal allyl *anti* C-H); 0.14 (s, 9H, $Si(CH_3)_3$).

Eclipsed *syn,anti trans* (2 eq.): ^{1}H NMR (400 MHz, C_6D_6): δ 4.87 (m, 1H, center allyl with *anti* TMS C-H); δ 4.51 (ddd, J = 15.7, 13.4, 7.1 Hz, 1H, center allyl with *syn* TMS C-H); δ 3.66 (m, 1H, terminal allyl with *syn* TMS *syn* C-H); δ 3.60 (dt, J = 8.0, 2.2 Hz, 1H, terminal allyl with *anti* TMS *syn* C-H); δ 3.21 (dd, J = 10.7, 2.3 Hz, 1H, terminal allyl with *anti* TMS *syn* C-H); δ 2.59 (dd, J = 14.6, 2.0 Hz, 1H terminal allyl with *anti* TMS *anti* C-H); δ 2.40 (bd, J = 13.5 Hz, 1H, terminal allyl with *syn* TMS *anti* C-H); δ 2.20 (d, J = 15.6 Hz, 1H, terminal allyl with *syn* TMS *anti* C-H); δ 0.02 (s, 9H, *anti* $Si(CH_3)_3$).

Eclipsed *syn,anti cis* (1 eq.): ^{1}H NMR (400 MHz, C_6D_6): δ 4.83 (m, 1H, center allyl with *anti* TMS C-H); δ 4.52 (m, 1H, center allyl with *syn* TMS C-H); δ 3.90 (m, 1H, terminal allyl with *syn* TMS *syn* C-H); δ 3.47 (m, 1H, terminal allyl with *anti* TMS *syn* C-H); δ 3.42 (m, 1H, terminal allyl with *anti* TMS *syn* C-H); δ 2.51 (dd, J = 14.5, 2.3 Hz, 1H terminal allyl with *anti* TMS *anti* C-H); δ 2.41 (bdd, J = 13.7, 4.6 Hz, 1H, terminal allyl with *syn* TMS *anti* C-H); δ 2.26 (d, J = 15.2 Hz, 1H, terminal allyl with *syn* TMS *anti* C-H); δ 0.16 (s, 9H, *syn* $Si(CH_3)_3$); δ 0.02 (s, 9H, *anti* $Si(CH_3)_3$).

[Di{(1-trimethylsilylallyl)-bromonickel(II)}] "[{A^{1Si}NiBr}$_2$]" :

This was synthesized from [NiA^{1Si}_2] in the same manner as [{A´NiBr}$_2$].[28] 0.148 g (0.519 mmol) of [NiA^{1Si}_2] reacted with 1.4 mL of a 0.408 M solution of [Br_2] (0.571 mmol) to yield a 0.031 g (23%) of the named compound as a bright red residue. It was noted that during the course of acetonitrile/hexane extraction, if the layered solvents were shaken vigorously, a small amount of green solid was precipitated. This is believed to be [$NiBr_2$], indicative of Schlenk equilibrium in acetonitrile solution, but this has not been confirmed spectroscopically. The precise speciation of this compound cannot be confidently determined at this time. Two clear, distinct allylic systems can be identified via 2D NMR experiments; these are presented as allyl 1 and 2, though it is likely that these are in fact composite peaks formed by the overlap of multiple similar species.

^{1}H NMR (400 MHz, C_6D_6): δ 5.34 (m, A^{1Si} 1 center allyl C-H); δ 4.92 (m, A^{1Si} 2 center allyl C-H); δ 2.92 (m, A^{1Si} 2 terminal allyl *syn* C-H); δ 2.79 (m, A^{1Si} 1 terminal allyl *syn* C-H); δ 2.00 (m, A^{1Si} 1 terminal allyl *anti* C-H); δ 1.89 (m, A^{1Si} 2 terminal allyl *anti* C-H); δ 1.57 (m, A^{1Si} 2.00 terminal allyl *anti* C-H); δ 0.31 (s, TMS $(CH_3)_3$); δ 0.31 (s, TMS $(CH_3)_3$); δ 0.29 (s, TMS $(CH_3)_3$); δ 0.18 (s, TMS $(CH_3)_3$); δ 0.16 (s, TMS $(CH_3)_3$); δ 0.11 (s, TMS $(CH_3)_3$). ^{13}C{^{1}H} NMR (101 MHz, C_6D_6): δ 111.7 (s, A^{1Si} 1 center allyl CH); δ 109.9 (s, A^{1Si} 2 center allyl CH); δ 67.7 (s, A^{1Si} 1 terminal allyl C(H)TMS); δ 65.6 (s, A^{1Si} 2 terminal allyl C(H)TMS); δ 58.4 (s, A^{1Si} 2 terminal allyl CH_2); δ 56.6 (s, A^{1Si} 1 terminal allyl CH_2); δ 1.1 (bs, TMS $(CH_3)_3$); δ 1.1 (bs, TMS $(CH_3)_3$); δ 1.1 (bs, TMS $(CH_3)_3$); δ -0.9 (bs, TMS $(CH_3)_3$); δ -0.9 (bs, TMS $(CH_3)_3$); δ -1.0 (s, TMS $(CH_3)_3$).

[Bis{(1,3-bis(trimethylsilyl)allyl)-chloronickel(II)}] "[{A´NiCl}$_2$]" :

In a nitrogen filled glovebox, 0.078 g (0.18 mmol) [NiA´$_2$] was measured into a 50 mL Schlenk flask along with a Teflon stir bar, then dissolved in 7.5 mL THF. The flask was transferred to a Schlenk line under nitrogen and cooled to -78 °C. After purging the bottle's atmosphere for 2 minutes with nitrogen, 0.10 mL of HCl solution was measured, then transferred to the nickel solution by syringe. No initial change was noted. After 30 minutes of stirring, the dry ice bath was removed; within ten minutes, the color had darkened to a rosy red. Allowed to stir at room temperature overnight. The flask was then transferred to the glovebox, the volatiles removed, and the residue extracted with two portions of diethyl ether. The extract was filtered and the volatiles removed to yield a red paste. Slow evaporation of a diethyl ether solution of the product yielded dark red crystals.

Unfortunately, attempts to characterize this species by NMR were ineffective due to extensive line broadening. Such broadening is often also seen in [{A´NiBr}$_2$] when it has been freshly synthesized; the cause of this is unclear. It could also be due to the presence of impurities; while it was not performed in this case, compounds of this type can be easily purified by dissolution in acetonitrile, extraction with three portions of hexanes, and then removal of the acetonitrile by vacuum.

[Triphenylphosphine(1-trimethylsilylallyl)-chloropalladium(II)] "[A^{1Si}Pd(PPh$_3$)Cl]":

0.010 g (0.37 mmol) of [{A^{1Si}PdCl}$_2$] was dissolved in 2.5 mL benzene in a glass vial with a Teflon-coated stir bar. 0.010 g (0.37 mmol) triphenylphosphine was dissolved in 2.5 mL benzene and the solution added dropwise. The mixture was allowed to stir overnight, after which the volatiles were removed. Hexane extraction of the resulting residue, followed by filtration and removal of volatiles, yielded an oily yellow solid. After sitting for one month within a glovebox, crystals were observed, with which the solid-state structure of the compound was determined.

NMR analysis shows a single primary product in addition to two or more other new species, likely other isomers of the compound. However, due to substantial peak broadening, the peaks of these minor products cannot be assigned. Due to the likely similar structures of the species, substantial peak overlap is present, so shift assignments are done primarily based on the ^{1}H-^{1}H COSY spectrum.

^{1}H NMR (400 MHz, C_6D_6): δ 7.75 (m, Ar-H); δ 7.01 (m, Ar-H); δ 5.12 (m, *J* = 15.5, 9.0, 9.0 Hz, 1H, center A´ allyl proton); δ 3.63 (m, 1H, allyl C-H); δ 2.72 (m, 1H, allyl C-H); δ 2.49 (m, 1H, allyl C-H); δ 0.26 (s, 9H, TMS $(CH_3)_3$); δ -0.03 (s, 9H, TMS $(CH_3)_3$).

Reaction of palldium(II) acetate with [K{SnA´$_3$}] -- formation of [bis{1,3-bis-(trimethylsilyl)allyl}palladium(II)] "[PdA´$_2$]":

0.054 g (0.24 mmol) [PdOAc$_2$] was dissolved in 2.5 mL THF inside a glass vial within a glovebox. 0.021 g (0.14 mmol) [K{SnA´$_3$}] was dissolved in 2.5 mL THF and the resulting solution was added dropwise

with stirring at room temperature. An immediate color change to dark orange was observed; the mixture was allowed to stir overnight. Removal of volatiles deposited a dark brown residue. Hexane extraction, followed by filtration and removal of volatiles yielded 0.092 g (80% yield) of a dense, pale yellow oil. ^{1}H NMR analysis showed a complex mixture of species was formed. These include both isomers of $\{A'\}_2$ and two species identified as the eclipsed and staggered isomers of [PdA′$_2$] based on their similarity to the same two isomers of [NiA′$_2$].

Staggered [PdA′$_2$] (1.34 eq.): ^{1}H NMR (400 MHz, C_6D_6): δ 5.35 (dd, *J* = 15.5, 9.8 Hz, 1H, center A′ allyl proton); δ 4.05 (d, J = 9.8, 1H, *syn* allyl C(TMS)-H); δ 2.90 (d, 15.5 Hz, 1H, *anti* allyl C(TMS)-H); δ 0.26 (s, 9H, TMS $(CH_3)_3$); δ -0.03 (s, 9H, TMS $(CH_3)_3$). ^{13}C $\{^{1}H\}$ NMR (101 MHz, d_8-toluene): δ 124.8 (s, allyl center carbon); δ 68.6 (s, *syn*-TMS-**C**); δ 67.8 (s, *anti*-TMS-**C**); δ 1.2 (TMS-$(CH_3)_3$); δ 1.2 (TMS-$(CH_3)_3$).

Eclipsed [PdA′$_2$] (1 eq.): ^{1}H NMR (400 MHz, C_6D_6): δ 5.18 (dd, *J* = 15.1, 10.1 Hz, 1H, center A′ allyl proton); δ 3.92 (d, J = 10.1, 1H, *syn* allyl C(TMS)-H); δ 2.96 (d, 15.1 Hz, 1H, *anti* allyl C(TMS)-H); δ 0.24 (s, 9H, TMS $(CH_3)_3$); δ 0.14 (s, 9H, TMS $(CH_3)_3$). ^{13}C $\{^{1}H\}$ NMR (101 MHz, d_8-toluene): δ 125.7 (s, allyl center carbon); δ 69.6 (s, *anti*-TMS-**C**); δ 66.1 (s, *syn*-TMS-**C**); δ 1.8 (TMS-$(CH_3)_3$); δ 0.4 (TMS-$(CH_3)_3$).

Attempted synthesis of $[\{A^{2t}PdBr\}_2]$:

In a nitrogen-filled glovebox, 0.098 g (0.170 mmol) [Pd(dba)$_2$] was placed in a 50 mL Schlenk flask along with a Teflon stir bar and 12.5 mL toluene. 0.043 g (0.185 mmol) [BrA^{2t}] was dissolved in 6.3 mL toluene, then this solution was added to a pressure equalizing addition funnel. The apparatus was then placed on a nitrogen-filled Schlenk line, heated to 45 °C, and excluded from ambient light by wrapping in aluminum foil. Addition proceeded dropwise over 45 minutes. After about 30 minutes, the solution had almost entirely lost its initial yellow color, and copious black powder had been deposited on the bottom of the flask. After the addition was completed, the flask was transferred to the glovebox, the mixture filtered, and the volatiles removed from the filtrate, yielding a dark yellow solid. This was then dissolved in acetonitrile, extracted three times with hexane, then the volatiles removed to yield the final product. ^{1}H NMR analysis found the product to be primarily composed of free dibenzylideneacetone, but a single η^3 allylic spin system was present as a minor product, and tentatively identified as $[\{A^{2t}PdBr\}_2]$ due to similarities with $[\{A^{2t}NiBr\}_2]$. ^{1}H NMR (400 MHz, C_6D_6): δ 4.99 (t, J = 11.4 Hz, 1H, center allyl C-H); δ 3.46 (d, J = 11.4 Hz, 2H, terminal allyl C-H); δ 1.26 (s, 18H, *t*Bu $(CH_3)_3$).

5.5 References

(1) Bricout, H.; Carpentier, J. F.; Mortreux, A. Nickel vs. Palladium Catalysts for Coupling Reactions of Allyl Alcohol with Soft Nucleophiles: Activities and Deactivation Processes. *J. Mol. Catal. A Chem.* **1998**, *136* (3), 243–251. https://doi.org/10.1016/S1381-1169(98)00067-3.

(2) Szabó, K. J. Palladium-Catalyzed Electrophilic Allylation Reactions via Bis(Allyl)Palladium Complexes and Related Intermediates. *Chem. Eur. J.* **2004**, *10* (21), 5268–5275. https://doi.org/10.1002/chem.200400261.

(3) Martin, A. R.; Nelson, D. J.; Meiries, S.; Slawin, A. M. Z.; Nolan, S. P. Efficient C-N and C-S Bond Formation Using the Highly Active [Ni(Allyl)Cl(IPr*OMe)] Precatalyst. *Eur. J. Org. Chem.* **2014**, *2014* (15), 3127–3131. https://doi.org/10.1002/ejoc.201402022.

(4) Marion, N.; Navarro, O.; Mei, J.; Stevens, E. D.; Scott, N. M.; Nolan, S. P. Modified (NHC)Pd(Allyl)Cl (NHC = N-Heterocyclic Carbene) Complexes for Room-Temperature Suzuki - Miyaura and Buchwald - Hartwig Reactions. *J. Am. Chem. Soc.* **2006**, *128* (11), 4101–4111.

(5) Connor, A. R. O. Reactions of Cationic (Allyl)Ni(II) Complexes with 1,3-Dienes and Olefins : Polymerization and Mechanistic Studies, University of North Carolina at Chapel Hill, 2008.

(6) Woodman, T. J.; Sarazin, Y.; Garratt, S.; Fink, G.; Bochmann, M. Chromium Allyl and Alkyl Catalysts for the Vinyl Polymerization of Norbornene and Ethylene-Norbornene Copolymerizations. *J. Mol. Catal. A Chem.* **2005**, *235* (1–2), 88–97. https://doi.org/10.1016/j.molcata.2005.03.017.

(7) Gmernicki, K. R.; Hong, E.; Maroon, C. R.; Mahurin, S. M.; Sokolov, A. P.; Saito, T.; Long, B. K. Accessing Siloxane Functionalized Polynorbornenes via Vinyl-Addition Polymerization for CO_2 Separation Membranes. *ACS Macro Lett.* **2016**, *5* (7), 879–883. https://doi.org/10.1021/acsmacrolett.6b00435.

(8) Sun, H.; Liang, Y.; Thompson, M. P.; Gianneschi, N. C. Degradable Polymers via Olefin Metathesis Polymerization. *Prog. Polym. Sci.* **2021**, *120*, 101427. https://doi.org/10.1016/j.progpolymsci.2021.101427.

(9) Feist, J. D.; Lee, D. C.; Xia, Y. A Versatile Approach for the Synthesis of Degradable Polymers via Controlled Ring-Opening Metathesis Copolymerization. *Nat. Chem.* **2022**, *14* (1), 53–58. https://doi.org/10.1038/s41557-021-00810-2.

(10) Mehler, C.; Risse, W. The Pd^{2+} -catalyzed Polymerization of Norbornene. *Makromol. Che.e, Rapid Commun.* **1991**, *12* (5), 255–259.

(11) Bermesheva, E. V.; Medentseva, E. I.; Khrychikova, A. P.; Wozniak, A. I.; Guseva, M. A.; Nazarov, I. V.; Morontsev, A. A.; Karpov, G. O.; Topchiy, M. A.; Asachenko, A. F.; Danshina, A. A.; Nelyubina, Y. V.; Bermeshev, M. V. Air-Stable Single-Component Pd-Catalysts for Vinyl-Addition Polymerization of Functionalized Norbornenes. *ACS Catal.* **2022**, *12* (24), 15076–15090. https://doi.org/10.1021/acscatal.2c04345.

(12) Hong, E. K. Siloxane and Silane-Functionalized Polynorbornenes as Membranes for Passive Carbon Dioxide Separation, 2015.

(13) Finkelshtein, E. S.; Bermeshev, M. V; Gringolts, M. L.; Starannikova, L. E.; Yampolskii, Y. P. Substituted Polynorbornenes as Promising Materials for Gas Separation Membranes. *Russ. Chem. Rev.* **2011**, *80* (4), 341–361. https://doi.org/10.1070/RC2011v080n04ABEH004203.

(14) Smith, J. D.; Hanusa, T. P.; Young, J. Steric Stabilization of Homoleptic Bis(π-Allyl) Complexes of Chromium(II) and Iron(II). *J. Am. Chem. Soc.* **2001**, *123* (26), 6455–6456. https://doi.org/10.1021/ja015626j.

(15) Schormann, M.; Garratt, S.; Bochmann, M. Reactivity of Silyl-Substituted Allyl Compounds with Group 4, 5, 9, and 10 Metals: Routes to η^3-Allyls, Alkylidenes, and Sec-Alkyl Carbocations. *Organometallics* **2005**, *24* (7), 1718–1724. https://doi.org/10.1021/om0491692.

(16) Quisenberry, K. T.; Smith, J. D.; Voehler, M.; Stec, D. F.; Hanusa, T. P.; Brennessel, W. W. Trimethylsilylated Allyl Complexes of Nickel. The Stabilized Bis(π-Allyl)Nickel Complex $[\eta^3$-1,3-$(SiMe_3)_2C_3H_3]_2$Ni and Its Mono(π-Allyl)NiX (X = Br, I) Derivatives. *J. Am. Chem. Soc.* **2005**, *127* (12), 4376–4387. https://doi.org/10.1021/ja044308s.

(17) Martínez-Arranz, S.; Albéniz, A. C.; Espinet, P. Versatile Route to Functionalized Vinylic Addition Polynorbornenes. *Macromolecules* **2010**, *43* (18), 7482–7487. https://doi.org/10.1021/ma101137z.

(18) Casares, J. A.; Espinet, P.; Martín-Alvarez, J. M.; Martínez-Ilarduya, J. M.; Salas, G. Stable Nickel Catalysts for Fast Norbornene Polymerization: Tuning Reactivity. *Eur. J. Inorg. Chem.* **2005**, *2* (19), 3825–3831. https://doi.org/10.1002/ejic.200500121.

(19) Walter, M. D.; Moorhouse, R. A.; White, P. S.; Brookhart, M. Vinyl Addition Polymerization of Norbornene with Cationic (Allyl)Ni Catalysts: Mechanistic Insights and Characterization of First Insertion Products. *J. Polym. Sci. Part A Polym. Chem.* **2009**, *47*, 2560–2573. https://doi.org/10.1002/pola.

(20) Bochmann, M.; Lancaster, S. J.; Hannant, M. D.; Rodriguez, A.; Schormann, M.; Walker, D. A.; Woodman, T. J. Role of $B(C_6F_5)_3$ in Catalyst Activation, Anion Formation, and as C_6F_5 Transfer Agent. *Pure Appl. Chem.* **2003**, *75* (9), 1183–1195.

(21) Chen, M.; Zou, W.; Cai, Z.; Chen, C. Norbornene Homopolymerization and Copolymerization with Ethylene by Phosphine-Sulfonate Nickel Catalysts. *Polym. Chem.* **2015**, *6* (14), 2669–2676. https://doi.org/10.1039/c5py00010f.

(22) Henc, B.; Jolly, P. W.; Salz, R.; Stobbe, S.; Wilke, G.; Benn, R.; Mynott, R.; Seevogel, K.; Goddard, R.; Krüger, C. Transition Metal Allyls III The $(\eta^3$-Allyl$)_2$M Complexes of Nickel, Palladium and Platinum: Structural Considerations. *J. Organomet. Chem.* **1980**, *191* (2), 449–475. https://doi.org/10.1016/s0022-328x(00)81073-6.

(23) Wilke, G.; Bogdanović, B.; Hardt, P.; Heimbach, P.; Keim, W.; Kröner, M.; Oberkirch, W.; Tanaka, K.; Steinrücke, E.; Walter, D.; Zimmermann, H. Allyl-Transition Metal Systems. *Angew. Chem. Int.*

Ed. **1966**, *5* (2), 151–164. https://doi.org/10.1002/anie.196601511.

(24) Lehmkuhl, H.; Rufihka, A.; Mehler, K.; Benn, R.; Schroth, G. Reaktionen von Nickelocen Mit Organomagnesiumverbindungen und Bildung von η^3-Allyl-η^5-Cyclopentadienylnickel-Komplexen. *Liebigs Ann. Chem.* **1980**, *1980* (5), 744–753. https://doi.org/10.1002/jlac.198019800514.

(25) Chmely, S. C.; Hanusa, T. P. Complexes with Sterically Bulky Allyl Ligands: Insights into Structure and Bonding. *Eur. J. Inorg. Chem.* **2010**, No. 9, 1321–1337. https://doi.org/10.1002/ejic.200900813.

(26) Solomon, S. A.; Layfield, R. A. The Coordination Chemistry of Silyl-Substituted Allyl Ligands. *Dalt. Trans.* **2010**, *39* (10), 2469–2483. https://doi.org/10.1039/b918619k.

(27) Ogoshi, S.; Yoshida, W.; Ohe, K.; Murai, S. Reaction of Palladium(II) Complexes with Allylsilanes: Convenient Synthesis of [η^3-1-(Silyl)Allyl]Palladium Complexes. *Organometallics* **1993**, *12* (2), 578–579. https://doi.org/10.1021/om00026a049.

(28) Degroot, H. P.; Speight, I. R.; Brennessel, W. W.; Hanusa, T. P. Distinction with a Difference: T - Butyl and Trimethylsilyl Substituents in Nickel Allyl Complexes. *Submitted - ACS Org. Inorg. Au* **2024**.

(29) Jolly, P. W.; Wilke, G. π-Allyl Nickel Complexes. In *The Organic Chemistry of Nickel*; Academic, 1974; pp 329–401. https://doi.org/10.1016/b978-0-12-388401-5.50012-9.

(30) Layfield, R. A.; García, F.; Hannauer, J.; Humphrey, S. M. Ansa-Tris(Allyl) Complexes of Alkali Metals: Tripodal Analogues of Cyclopentadienyl and Ansa-Metallocene Ligands. *Chem. Commun.* **2007**, *43* (47), 5081–5083. https://doi.org/10.1039/b712285c.

(31) Kosugi, M.; Shimizu, Y.; Migita, T. Reaction of Allyltin Compounds III) Allylation of Aromatic Halides with Allyltributyltin in the Presence of Tetrakis(Triphenylphosphine)Palladium(0). *Chem. Lett.* **1977**, *6* (3), 301–302. https://doi.org/10.1246/cl.1977.301.

(32) Cordovilla, C.; Bartolomé, C.; Martínez-Ilarduya, J. M.; Espinet, P. The Stille Reaction, 38 Years Later. *ACS Catal.* **2015**, *5* (5), 3040–3053. https://doi.org/10.1021/acscatal.5b00448.

(33) Wenger, L. E. Mechanochemical Exploration of the P-Block, Ph. D. Thesis, Vanderbilt University, 2024.

(34) Oberhansli, W. E.; Dahl, L. F. Structure of and Bonding in $[(C_3H_5)PdCl]_2$. *J. Organomet. Chem.* **1965**, *3*, 43–54.

(35) Walter, M. D.; Moorhouse, R. A.; Urbin, S. A.; White, P. S.; Brookhart, M. γ-Agostic Species as Key Intermediates in the Vinyl Addition Polymerization of Norbornene with Cationic (Allyl)Pd Catalysts: Synthesis and Mechanistic Insights. *J. Am. Chem. Soc.* **2009**, *131*, 9055–9069.

(36) Wang, B.; Daugulis, O.; Brookhart, M. Ethylene Polymerization with Ni(II) Diimine Complexes Generated from 8 - Halo-1-Naphthylamines: The Role of Equilibrating Syn / Anti Diastereomers in Determining Polymer Properties. *Organometallics* **2019**, *38* (24), 4658–4668.

https://doi.org/10.1021/acs.organomet.9b00649.

(37) Shamiri, A.; Chakrabarti, M. H.; Jahan, S.; Hussain, M. A.; Kaminsky, W.; Aravind, P. V.; Yehye, W. A. The Influence of Ziegler-Natta and Metallocene Catalysts on Polyolefin Structure, Properties, and Processing Ability. *Materials (Basel).* **2014**, *7* (7), 5069–5108. https://doi.org/10.3390/ma7075069.

(38) Zhang, R.; Gao, R.; Gou, Q.; Lai, J.; Li, X. Recent Advances in the Copolymerization of Ethylene with Polar Comonomers by Nickel Catalysts. *Polymers (Basel).* **2022**, *14* (18). https://doi.org/10.3390/polym14183809.

(39) Langford, D.; Göttker-schnetmann, I.; Wimmer, F. P.; Casper, L. A. Tetrakis[3,5-Bis(Pentafluorosulfanyl)Phenyl]Borate: A Weakly Coordinating Anion Probed in Polymerization Catalysis. *Organometallics* **2019**, *38*, 2710–2713. https://doi.org/10.1021/acs.organomet.9b00332.

(40) Hyder, I.; Jiménez-Tenorio, M.; Puerta, M. C.; Valerga, P. Oligomerization and Regioselective Hydrosilylation of Styrenes Catalyzed by Cationic Allyl Nickel Complexes Bearing Allylphosphine Ligands. *Dalton Trans.* **2007**, No. 28, 3000–3009. https://doi.org/10.1039/b705579j.

(41) Jiménez-Tenorio, M.; Puerta, M. C.; Salcedo, I.; Valerga, P.; Costa, S. I.; Silva, L. C.; Gomes, P. T. Cationic Nickel Complexes Containing Bulky Phosphine Ligands: Catalyst Precursors for Styrene Polymerization. *Organometallics* **2004**, *23* (13), 3139–3146. https://doi.org/10.1021/om049883j.

(42) Pérez-Ortega, I.; Albéniz, A. C. Vinylic Addition Poly(Norbornene-Co-Alkenylnorbornenes) Synthesized with Benzylic Palladium Catalysts: Materials for Manifold Functionalization. *Polym. Chem.* **2022**, *13* (28), 4154–4161. https://doi.org/10.1039/d2py00643j.

(43) Casares, J. A.; Espinet, P.; Salas, G. Palladium Catalysts for Norbornene Polymerization. A Study by NMR and Calorimetric Methods. *Organometallics* **2008**, *27* (15), 3761–3769. https://doi.org/10.1021/om800264a.

(44) Gervits, L. L.; Makarov, K. N.; Cheburkov, Y. A.; Knunyants, I. L. The New Reaction of Octafluoroisobutene with Alpha-Oxides. Synthesis of Olefins with Perfluorotertiary Butyl Substituent. *J. Fluor. Chem.* **1977**, *9*, 45–52.

(45) Christian, A. H.; Müller, P.; Monfette, S. Nickel Hydroxo Complexes as Intermediates in Nickel-Catalyzed Suzuki-Miyaura Cross-Coupling. *Organometallics* **2014**, *33* (9), 2134–2137. https://doi.org/10.1021/om5001327.

(46) Payard, P. A.; Perego, L. A.; Ciofini, I.; Grimaud, L. Taming Nickel-Catalyzed Suzuki-Miyaura Coupling: A Mechanistic Focus on Boron-to-Nickel Transmetalation. *ACS Catal.* **2018**, *8* (6), 4812–4823. https://doi.org/10.1021/acscatal.8b00933.

(47) Melvin, P. R.; Nova, A.; Balcells, D.; Dai, W.; Hazari, N.; Hruszkewycz, D. P.; Shah, H. P.; Tudge, M. T. Design of a Versatile and Improved Precatalyst Scaffold for Palladium-Catalyzed Cross-

Coupling: (η^3-1-tBu-Indenyl)$_2$(μ-Cl)$_2$Pd$_2$. *ACS Catal.* **2015**, *5* (6), 3680–3688. https://doi.org/10.1021/acscatal.5b00878.

(48) Nazari, S. H.; Bourdeau, J. E.; Talley, M. R.; Valdivia-Berroeta, G. A.; Smith, S. J.; Michaelis, D. J. Nickel-Catalyzed Suzuki Cross Couplings with Unprotected Allylic Alcohols Enabled by Bidentate N-Heterocyclic Carbene (NHC)/Phosphine Ligands. *ACS Catal.* **2018**, *8* (1), 86–89. https://doi.org/10.1021/acscatal.7b03079.

Appendix 1: General Supplemental Information for All Chapters

A1.1 General Considerations:

All syntheses were conducted under rigorous exclusion of air and moisture using Schlenk line and glovebox techniques under nitrogen atmosphere unless noted otherwise. Proton (^{1}H), carbon (^{13}C), and phosphorus (^{31}P) NMR spectra were obtained at ambient temperature on a Bruker AV-400 MHz or Bruker AV-II 600 MHz spectrometer. Proton and carbon spectra were referenced to the residual resonances of the NMR solvent. Phosphorus spectra were referenced to 85% solution of phosphoric acid in water. Structural assignments were made with additional information from gCOSY and gHSQC experiments where noted. Unless otherwise noted, all spectra were obtained at room temperature.

A1.2 Materials:

Hexanes were refluxed over Na/benzophenone, distilled, and allowed to sit over 3Å molecular sieves for at least one day prior to use. Anhydrous pyridine, benzene, acetonitrile, and dimethoxyethane were received from Sigma and stored over 3Å molecular sieves. Diethyl ether and toluene were purified over a solvent purification column. Anhydrous, inhibitor-free THF was purchased from Fischer, passed through a column of activated alumina, then placed over 3Å molecular sieves for at least day day prior to use. All solvents were stored in the glovebox over 4Å molecular sieves. Benzene-d_6, toluene-d_8, dimethylsulfoxide-d_6, and tetrahydrofuran-d_8 were obtained from Cambridge Isotopes and stored over 4Å molecular sieves in a nitrogen-filled glovebox.

A1.3 Crystallographic Methodology:

A suitable crystal of each sample was selected for analysis and mounted in a polyimide loop. Unless otherwise noted, all measurements were made on a Rigaku Oxford Diffraction Supernova Eos CCD with Cu-Kα radiation at a temperature of 100 K. Using Olex2,[1] the structures were solved with the ShelXT[2] structure solution program using Direct Methods and refined with the ShelXL[3] refinement package using least squares minimization.

A1.4 General Computational Methodology

All calculations were performed with the Gaussian 16W.[4] The B3PW91 functional, which incorporates Becke's three-parameter exchange functional with the 1991 gradient-corrected correlation functional of Perdew and Wang, was used.[5] To add dispersion corrections, Grimme's D3 correction[6] with additional Becke-Johnson damping[7] was used (Gaussian keyword: empiricaldispersion=GD3BJ). Unless otherwise noted, geometrical optimization was performed in three steps: initial optimization using the PM6 semi-empirical method,[8] subsequent optimization using full DFT methods with the BPV86 functional and a STO-3G basis set, then optimization and frequency calculation at the final level of theory. Only the final optimized structures were used for the calculation of any values presented in this work.

A1.5 Elemental Analysis procedure:

C, H, and N analyses were performed by Dr. William Brennessel at the University of Rochester Center for Enabling New Technologies Through Catalysis. Microanalyses were determined on a PerkinElmer 2400 Series II Analyzer. Sample weights were measured on a PerkinElmer Model AD6000 Autobalance. Air-sensitive materials were prepared in a dedicated VAC Atmospheres glovebox loaded with Ar (argon) gas, and then crimp-sealed in special tin capsules with a designated die apparatus.

A1.5 References

(1) Dolomanov, O. V.; Bourhis, L. J.; Gildea, R. J.; Howard, J. A. K.; Puschmann, H. OLEX2: A Complete Structure Solution, Refinement and Analysis Program. *J. Appl. Crystallogr.* **2009**, *42* (2), 339–341. https://doi.org/10.1107/S0021889808042726.

(2) Sheldrick, G. M. SHELXT - Integrated Space-Group and Crystal-Structure Determination. *Acta Crystallogr. Sect. A Found. Crystallogr.* **2015**, *71* (1), 3–8. https://doi.org/10.1107/S2053273314026370.

(3) Sheldrick, G. M. Crystal Structure Refinement with SHELXL. *Acta Crystallogr. Sect. C Struct. Chem.* **2015**, *71* (Md), 3–8. https://doi.org/10.1107/S2053229614024218.

(4) Frisch, M. J.; Trucks, G. W.; Schlegel, H. B.; Scuseria, G. E.; Robb, M. a.; Cheeseman, J. R.; Scalmani, G.; Barone, V.; Petersson, G. a.; Nakatsuji, H.; Li, X.; Caricato, M.; Marenich, a. V.; Bloino, J.; Janesko, B. G.; Gomperts, R.; Mennucci, B.; Hratchian, H. P.; Ortiz, J. V.; Izmaylov, a. F.; Sonnenberg, J. L.; Williams; Ding, F.; Lipparini, F.; Egidi, F.; Goings, J.; Peng, B.; Petrone, A.; Henderson, T.; Ranasinghe, D.; Zakrzewski, V. G.; Gao, J.; Rega, N.; Zheng, G.; Liang, W.; Hada, M.; Ehara, M.; Toyota, K.; Fukuda, R.; Hasegawa, J.; Ishida, M.; Nakajima, T.; Honda, Y.; Kitao, O.; Nakai, H.; Vreven, T.; Throssell, K.; Montgomery Jr., J. a.; Peralta, J. E.; Ogliaro, F.; Bearpark, M. J.; Heyd, J. J.; Brothers, E. N.; Kudin, K. N.; Staroverov, V. N.; Keith, T. a.; Kobayashi, R.; Normand, J.; Raghavachari, K.; Rendell, a. P.; Burant, J. C.; Iyengar, S. S.; Tomasi, J.; Cossi, M.; Millam, J. M.; Klene, M.; Adamo, C.; Cammi, R.; Ochterski, J. W.; Martin, R. L.; Morokuma, K.; Farkas, O.; Foresman, J. B.; Fox, D. J. Gaussian 16 Rev. C.01. Wallingford, CT 2016, Gaussian, Inc.

(5) Becke, A. D. Thermochemistry. III. The Role of Exact Exchange. *J. Chem. Phys.* **1993**, *98*, 5648–5652.

(6) Grimme, S.; Antony, J.; Ehrlich, S.; Krieg, H. A Consistent and Accurate Ab Initio Parametrization of Density Functional Dispersion Correction (DFT-D) for the 94 Elements H-Pu. *J. Chem. Phys.* **2010**, *132* (15). https://doi.org/10.1063/1.3382344.

(7) Grimme, S.; Ehrlich, S.; Goerigk, L. Effect of the Damping Function in Dispersion Corrected Density Functional Theory. *J. Comput. Chem.* **2011**, *32* (7), 1456–1465. https://doi.org/10.1002/jcc.

(8) Stewart, J. J. P. Optimization of Parameters for Semiempirical Methods V: Modification of NDDO Approximations and Application to 70 Elements. *J. Mol. Model.* **2007**, *13* (12), 1173–1213. https://doi.org/10.1007/s00894-007-0233-4.

Appendix 2: Supplementary Information for Chapter 2

A2.1 Materials

Anhydrous metal halides, [Ni(dme)Br_2], [Ni(AcAc)$_2$], [Ni(OAc)$_2$], [Ni(OH)$_2$] and [$NiCl_2$•$6H_2O$] were purchased from Aldrich; the hydrate was heated to 80 °C for 24 h under vacuum to remove water and form the dihydrate [$NiCl_2$•$2H_2O$].[1] [Ni(thf)$_{1.5}Cl_2$],[2] [$NiCl_2$(py)$_4$],[3] [Fe(py)$_4Cl_2$],[4] [Ni(dme)Cl_2],[5]

[Ni(diglyme)Cl_2],[6] [Ni(dmgH)$_2$],[7] [Ni(CN)$_2$],[8] and both [1,3-$(SiMe_3)_2C_3H_4$] and [LiA′][9] were synthesized according to literature procedures. [$Ni(NCMe)_6$][BF_4] was prepared by an adaptation of Driessen and Reedijk's procedure,[10] as described in the literature.[11] [KA′] was prepared by transmetallation of [LiA′] with potassium tert-butoxide in hexanes solution.

A2.2 Experimental protocols

A2.2.1 General procedures for mechanochemical reactions

Ball milling reactions used stainless steel (440 grade) ball bearings (3/16 in (5 mm), 0.44 g) that were thoroughly cleaned with detergent and water, then washed with acetone, and dried in a 125 °C oven prior to use. Planetary milling was performed with a Retsch PM100 mill, 50 mL stainless steel grinding jar type C, and a safety clamp for air-sensitive grinding. A typical mechanochemical reaction was performed as follows.

A2.2.2 Specific experimental conditions for mechanochemical reactions

In the course of this investigation, four different sets of reaction conditions were used. These are defined here, and labelled A-E.

Condition A: In a nitrogen-filled glovebox, a stainless steel grinding jar is charged with 25 g ball bearings, nickel(II) source (0.43 mmol), [KA′] (200 mg, 0.89 mmol), then an appropriate volume of LAG solvent. The jar is then tightly sealed, removed from the glovebox, and placed in the planetary mill. The mixture is ground for 10 min at 600 rpm, at which point the jar is returned to the glovebox. The jar is opened, and products are taken up in hexane and filtered through a glass frit. Evaporation of solvent yields the isolated product, which is weighed and then analyzed with ^{1}H NMR.

Condition B: The same protocol as Condition A is followed, with the exception that no LAG solvent is added.

Condition C: The same protocol as Condition B is followed, with the exception that the scale is increased such that approximately 300 mg [KA′] is used, and the mixture is milled for 20 minutes.

Condition D: The same protocol as Condition C is followed, with the exception that the scale is increased such that approximately 400 mg [KA′] is used.

Condition E: The same protocol as Condition A is followed, with the exception that grinding is done for 15 minutes.

For all reactions reported in Section 2.1, either Condition A or B is used as specified in the Tables of Section 2.1.

For syntheses of the paramagnetic complexes (M = Cr, Fe, Co), an additional protonolysis procedure was performed. The isolated product mixture was taken up in benzene-d_6 in a glass vial. To this was added pyridinium chloride[12] (0.125 g, 1.1 mmol) and the contents well mixed. After standing overnight, the solution was filtered and analyzed by ^{1}H NMR. This spectrum was then compared to the original spectrum

of the isolated product; the proportion of the complex in the isolated product was taken to be one-half the difference in the relative abundance of the protonated ligand.

A2.2.3 Protocols for solution reactions

A typical solution phase reaction was performed as follows. In a nitrogen-filled glovebox, a 125 mL Schlenk flask was charged with $NiCl_2$ (56.0 mg, 0.43 mmol), approximately 20 mL of THF, and a magnetic stir bar. A pressure-equalizing addition funnel was attached to the neck of the flask and charged with K[A´] (200 mg, 0.89 mmol) and approx. 15 mL THF. The homogenous K[A´] solution was added dropwise over 20 minutes, during which time the stirred reaction mixture adopted a dark orange-brown color. After stirring overnight, THF was removed via vacuum, the residue was extracted with hexanes and filtered, and the hexane was then removed. A sample of the isolated product was analyzed with ^1H NMR. For the syntheses of paramagnetic complexes, an identical protonolysis procedure to that described above was performed.

A2.2.4 Protocols for aging reactions

In a nitrogen-filled glovebox whose atmosphere has been freshly purged, a nickel(II) source (0.43 mmol) and [KA´] (200 mg, 0.89 mmol) are placed in a ceramic mortar and pestle, then ground together extremely gently. The combined powder is then transferred to a glass vial. The vial is then tightly capped and monitored periodically for 3 months, or until reaction is apparent. Qualitative reaction outcomes are determined visually. For aging reactions in THF enriched atmospheres, after the powders have been transferred to a vial, a second, smaller vial is then charged with 5 drops of THF. This smaller vial is placed uncapped inside the reaction vial, and the reaction vial is tightly sealed.

A2.3 Collected experimental results

A2.3.1 Compiled outcomes of metathesis reactions

Table A2.1: Reaction outcomes from solution phase reactions of [KA´] and $[Ni(L)_nCl_2]$

No.	**Solvent**	**Metal Halide**	**[NiA´$_2$] Yield (%)**	**[NiA´$_2$] : {A´}$_2$**
1	THF	$NiCl_2$	2	1 : 15
2		$[Ni(thf)_{1.5}Cl_2]$	10	1 : 7
3	Et_2O	$[Ni(thf)_{1.5}Cl_2]$	2	1 : 40
4		$[Ni(pyr)_4Cl_2]$	91	No {A´}$_2$

Table A2.2: Reaction outcomes from mixing [KA´], [NiX_2], and THF

No.	Condition	Metal halide	Time (min)	Equiv. THF	η (or equiv.)	[$NiA´_2$] yield (%)	[$NiA´_2$] : {A´}$_2$
1	Dry grind	$NiCl_2$	10	0	0	1	1 : 43
2		$NiBr_2$	10	0	0	< 1	< 1: 100
3		NiI_2	10	0	0	< 1	< 1: 100
4	LAG	$NiCl_2$	10	5	0.73	4	1 : 13
5		$NiBr_2$	10	7.5	0.90	1	1 : 44
6		NiI_2	10	5	0.54	< 1	< 1 : 100
7	Solvate grind	$[Ni(thf)_{1.5}Cl_2]$	10	1.5	0.20	5	1 : 14
8		$[Ni_3(thf)_5Br_6]$	10	1.7	0.19	9	1 : 4

Table A2.3: Reaction outcomes from mixing [KA´], [Ni(L)$_n$X$_2$], and DME

No.	Conditions	Nickel Reagent	Time (min)	Equiv. DME	η (or equiv.)	[NiA´$_2$] yield (%)	[NiA´$_2$] : {A´}$_2$
1	LAG	$Ni(H_2O)_2Cl_2$	10	5	0.92	1	1 : 42
2		$NiBr_2$	10	5	0.74	< 1	1 : 89
3	Solvate grind	$[Ni(dme)Cl_2]$	10	1	0.18	4	1 : 15
4		$[Ni(dme)Br_2]$	10	1	0.16	3	1 : 22
5	Solution	$NiBr_2$	10	>>10	>100	1	1 : 40

Table A2.4: Reaction outcomes of [KA´], $[Ni(H_2O)_2Cl_2]$, and various solvents

No.	Solvent	Time (min)	Equiv. Solvent	η (mL/g)	[NiA´$_2$] yield (%)	[NiA´$_2$] : {A´$_2$}
1	none	10	0	0	< 1	1 : 93
2	benzene	10	5	0.78	< 1	1 : 85
3	Et_2O	10	5	0.90	< 1	1 : 95
4	THF	10	5	0.74	1	1 : 34
5	DME	10	5	0.92	1	1 : 42
6	pyridine	10	5	0.70	46	No {A´}$_2$

Table A2.5: Compiled parameters for all reactions presented in Figure 2.8 and discussed in Section 2.2

No.	Precursor	Condition	Total Product Yield (%)[a]	[NiA´$_2$] : {A´$_2$}
1	[$NiCl_2$]	B	25.1	≈ 0.0
2	[$NiBr_2$]	B	71.9	≈ 0.0
3	[NiI_2]	B	74.3	≈ 0.0
4	[$NiSO_4$]	D	30.3	≈ 0.0
5	[$NiCN_2$]	C	12.6	0.3
6	[Ni(dme)Br_2]	B	68.4	0.1
7	[Ni(dme)Cl_2]	B	42.9	0.3
8	[Ni(thf)$_{5/3}Br_2$]	B	55.9	0.1
9	[Ni(thf)$_{1.5}Cl_2$]	B	75.5	0.1
10	[Ni(diglyme)Cl_2]	D	50.6	0.1
11	[Ni(acac)$_2$]	D	15.9	No {A´$_2$}
12	[Ni(pyr)$_4Cl_2$]	B	69.4	No {A´$_2$}
13	[Ni(NCMe)$_6$][(BF_4)$_2$]	B	13.6	1.9
14	[Ni(OAc)$_2$]	D	8.8	0.9
15	[Ni(OTf)$_2$]	B	53.9	31.0

[a]) Defined as the sum of the percent yield of [NiA´$_2$] and the percent yield of {A´$_2$}.

Some other precursors were tested that did not yield useful results. No reaction was observed between [KA´] and [Ni(OH)$_2$]. [Ni(dmgH)$_2$] reacted to yield pure [HA´], presumably due to deprotonation of the dimethylglyoximinato ligand. This was somewhat surprising, as we previously noted that deprotonation was not a problem when using nickel chloride dihydrate; it is possible that even the dimethylglyoximinate anion is a stronger acid than water, but it is also possible that its greater affinity for nickel[75,76] causes it to remain in the coordination sphere of nickel long enough to transfer a proton to an incoming [A´$^-$] ligand. Nickel *tert*-butoxide was synthesized according to multiple published procedures; however, different batches demonstrated substantially different reactivity. Due to the difficulty of precise

characterization, these results have been omitted. [Ni(dppe)Cl_2] (dppe = bis(1,2-diphenylphosphino)ethane) reacted to yield an unknown compound that appeared to degrade upon sitting.

Table A2.6: Reaction outcomes for the mechanochemical reaction of different precursors with [KA´] with and without LAG quantities of THF

No.	Precursor	[NiA´$_2$] : {A´$_2$} (Dry Grind)	Eq. THF	[NiA´$_2$] : {A´$_2$}	Complex Yield (%)	Condition
1	[$NiCl_2$]	≈ 0.0	5	0.1	4.1	A
2			10	0.1	4.2	A
3	[Ni(dme)Br_2]	0.1	1	1.7	NA	E
4			2	1.5	NA	E
5			5	2.1	51.6	E
6			8	1.1	NA	E
7			16	1.5	NA	E
8	[Ni(H_2O)$_2Cl_2$]	≈ 0.0	5	≈ 0.0	1.8	A
9			10	0.1	2.7	A
10	[$NiSO_4$]	≈ 0.0	5	≈ 0.0	NA	E
11	[$NiCN_2$]	0.3	2	4.3	NA	E
12			10	No {A´$_2$}	NA	E
13	[NiI_2]	≈ 0.0	5	≈ 0.0	0.4	A
14	[Ni(thf)$_{1.5}Cl_2$]	0.1	10	0.2	NA	E
15	[Ni(diglyme)Cl_2]	0.1	10	15.2	84.5	E
16	[Ni(acac)$_2$]	No {A´$_2$}	5	No {A´$_2$}	9.8	E
17	[Ni(OAc)$_2$]	0.9	5	No {A´$_2$}	NA	E

Table A2.7: Reaction outcomes for the mechanochemical reaction of different precursors with [KA´] with and without LAG quantities of THF

	[KA^{1Si}]		[KA´]	
Ni(II) Source	**[NiA^{1Si}_2] : {A^{1Si}_2}**	**[NiA^{1Si}_2] + {A^{1Si}_2} Yield (%)**	**[$NiA´_2$] : {$A´_2$}**	**[$NiA´_2$] + {$A´_2$} Yield (%)**
[$NiCl_2$]	0.2	NA	≈ 0.0	57
[Ni(dme)Br_2]	1.4	NA	≈ 0.0	68
[Ni(acac)$_2$]	No {A^{1Si}_2}	35	No {$A´_2$}	19

Figure A2.1: ^{1}H NMR (400 MHz) of material collected from reaction of [$NiCl_2$] with [KA^{1Si}], taken in C_6D_6. Peaks used in the calculation of [NiA^{1Si}_2] to {A^{1Si}_2} ratios are integrated; those integration values marked with an asterisk represent only half of the relevant peak and are therefore doubled for the purposes of ratio calculation.

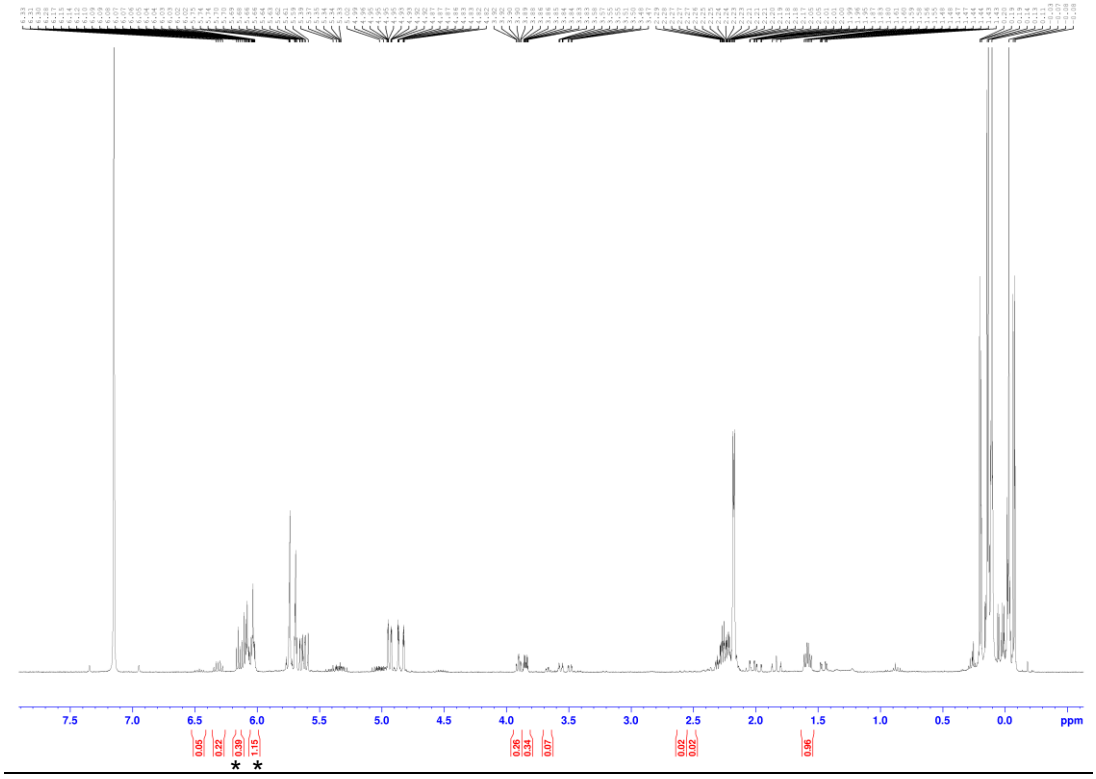

A2.3.2 Results of Aging Reactions

Aging reactions refer to reactions in which solid-state reagents are intimately mixed then allowed to react without the input of external energy. Such conditions can be considered complimentary to mechanochemical methodologies, as they allow solid-state reactions isolated from the input of mechanical energy. A small selection of nickel(II) precursors were allowed to react with [KA´] under aging conditions. These reactions were periodically monitored over the course of 3 months or until reaction outcome was apparent. Qualitative evaluation of reaction outcomes was done visually; formation of a bright orange residue was taken to indicate primarily metathesis reactivity, forming [NiA´$_2$], while generation of black solid was taken to indicate primarily redox reactivity, forming Ni^0. If neither of these outcomes was apparent after 3 months, the system was considered to have not reacted. From the results compiled below in Table A2.8, it is apparent that, in the complete absence of solvent, both possible reactivity modes are difficult to access. Only solvent adducts [Ni(dme)Br_2], [Ni(thf)$_{1.5}Cl_2$], and [Ni(pyr)Cl_2] display reactivity under dry-aging conditions, and even these require long reaction times. All of these reactions yielded the same primary product observed under mechanochemical conditions. As noted in the main text, that [Ni(diglyme)Cl_2] does not react under these conditions in contrast to the other solvent adducts is evidence that the change in ligand binding strength is relevant in the context of the Ni(II)/[KA´] system.

Table A2.8: Primary product of the reaction of various Ni(II) sources with [KA´] under aging conditions. Approximate reaction time is given in parentheses where appropriate.

Condition	**[Ni(acac)$_2$]**	**[$NiCl_2$]**	**[$NiSO_4$]**	**[Ni(dme)Br_2]**	**[Ni(diglyme)Cl_2]**	**[Ni(pyr)$_4Cl_2$]**
Dry	No rxn	No rxn	No rxn	{A´$_2$} (5 days)	No rxn	[NiA´$_2$] (7 days)
THF-enriched	[NiA´$_2$] (1 day)	NA	{A´$_2$} (1 day)	{A´$_2$} (30 minutes)	{A´$_2$} (<10 minutes)	NA

Aging reactions were also performed in the presence of THF enriched atmospheres. Comparing these results to those under dry-aging conditions, it is apparent that the presence of trace atmospheric solvent substantially decreases the barrier for reaction, as all precursors investigated reacted within minutes in the THF enriched atmospheres. Also, in all cases, the primary product of the accelerated aging reactions matches that of the analogous dry mechanochemical reaction. This can be rationalized by trace atmospheric solvent interacting primarily with [KA´], breaking down the coordination polymer structure, and generating a more reactive nucleophile.

2.3.2 Pyridine solution reaction analysis

Figure A2.1: ^{1}H NMR spectrum of the product mixture of [$NiCl_2$] allowed to react with [KA´] in pyridine solution (Table 2.2, entry 4). Magnification shows the frequency range at which the center proton of the [A´] group resonates.

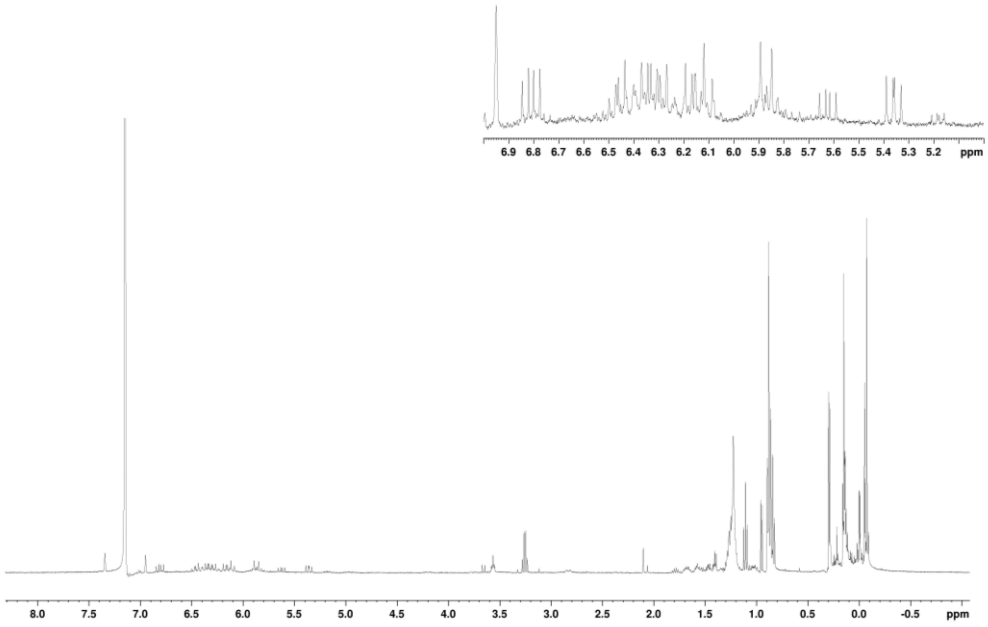

A2.3.3 Powder X-ray diffraction (PXRD) experiments

A2.3.3.1 Procedure for PXRD

Note: PXRD measurements were obtained by Chris Sharp and Jeremy Espano.

Reaction mixtures were ground in the planetary mill for 15 min at 600 rpm using a 50 mL stainless steel jar and in the presence of 25 g of small ball bearings. The jar was returned to the glovebox and the walls of the jar were scraped with a spatula to collect powdered material. This was dry transferred onto a low-background silicon XRD wafer, sealed, and taken to the instrument. Powder X-ray diffraction (XRD) spectra were obtained using a Rigaku SmartLab® X-ray Diffractometer with a CuKα source and a D/TeX Ultra 250 detector. The operating voltage and current were 40 kV and 44 mA, respectively. The step size was 0.1 degree at a rate of 10 degrees per minute.

A2.3.3.2 PXRD results

Figure A2.2: PXRD of the mixture formed from grinding $NiCl_2$ with pyridine; the two major components are $[Ni(py)_4Cl_2]$ and $[Ni(py)_2Cl_2]$ (see main text for details).

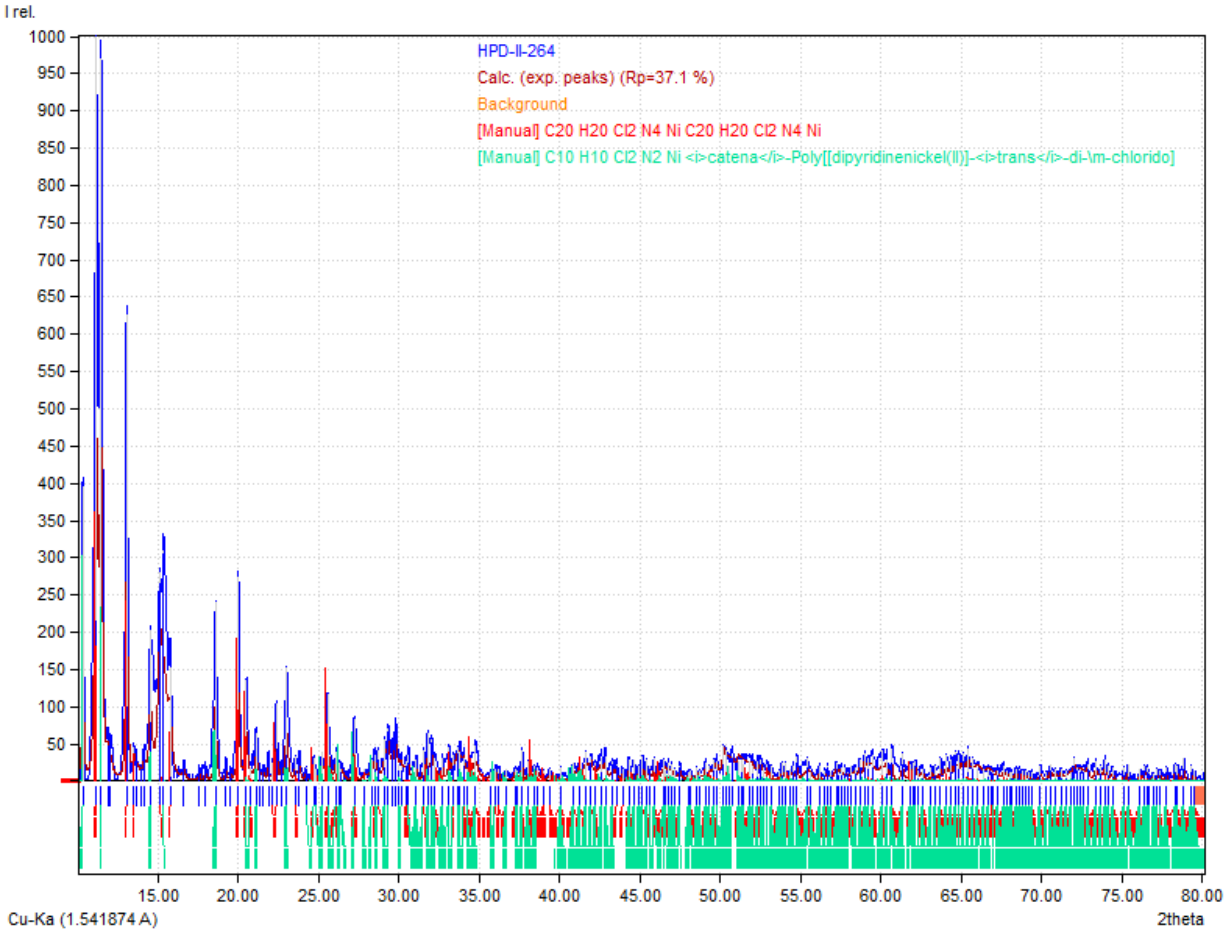

Figure A2.3: PXRD of $[Ni(py)_4Cl_2]$, formed from grinding $Ni(H_2O)_2Cl_2$ with pyridine (see Chapter 2 for details).

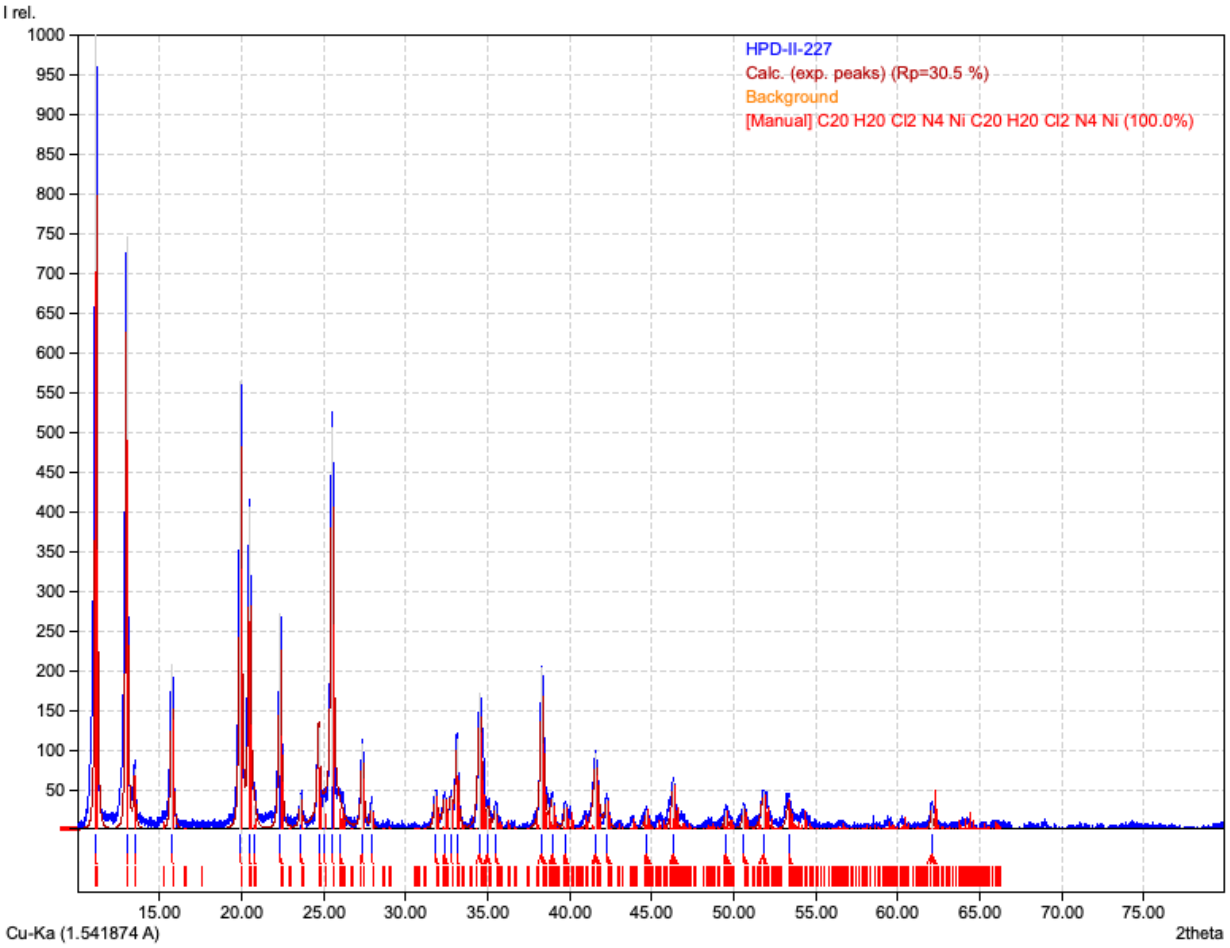

A2.3.4 Demonstration of the breakdown of the commonly used definition of the LAG region at high scales

Figure A2.4: (a) A mixture of [$FeCl_2$] (1.00 g, 7.9 mmol) and [NaCp] (1.39 g, 15.8 mmol); (b) after addition of 2.4 mL of THF (h = 1). Substantial reaction (and reduction of volume) has occurred without grinding. If there is a LAG region for this reaction, it exists at η values << 1.

a.  b. 

A2.3.5 Crystallographic details

A2.3.5.1 Specific procedural details for X-Ray crystallography

The crystal of meso-$\{A'\}_2$ was kept at 105 K during data collection. All non-hydrogen atoms were refined with anisotropic displacement parameters.

Table A2.7: Crystal Data and Summary of X–ray Data Collection

Compound	*meso*-1,3,4,6-tetrakis(trimethylsilyl)hexa-1,5-diene
Empirical formula	$C_{18}H_{42}Si_4$
Formula weight	370.87
Color of compound	colorless
Crystal size/mm^3	0.137 × 0.101 × 0.025
Radiation	CuKα (λ = 1.54184)
Temperature/K	105
Crystal system	monoclinic
Space group	$P2_1/c$
a/Å	14.9821(4)
b/Å	6.4776(2)
c/Å	26.2520(8)
α/°	90
β/°	99.379(3)
γ/°	90
Volume/Å^3	2513.64(13)
Z	4
ρ_{calc} g/cm^3	0.980
μ/mm^{-1}	2.152
F(000)	824.0
2Θ range for data collect/°	2.990 to 73.204
Index ranges	$-18 \leq h \leq 18$, $-5 \leq k \leq 7$, $-31 \leq l \leq 32$
Reflections collected	10 388
Independent reflections	4933 [R_{int} = 0.0329]
Data/restraints/parameters	4933/0/211
Goodness-of-fit on F^2	1.104
Final *R* indexes [$I > 2\sigma(I)$]	R_1 = 0.0716, wR_2 = 0.1805
Final *R* indexes [all data]	R_1 = 0.0814, wR_2 = 0.1904
Largest diff. peak/hole/e Å^{-3}	1.80/-0.48

A2.4 Computational details

A2.4.1 General Procedures for Calculations

Either the def2TZVP or def2TZVPD (with diffuse functions) basis sets were used on all atoms.[13] Porosity calculations were made with CrystalMaker® software (CrystalMaker Software Ltd, Oxford, England).

A2.4.2 Compiled computational results

Figure A2.5: Calculated geometry (B3PW91-D3BJ/def2TZVP) of *meso*-{A´}$_2$. Selected bond distances (Å) and angles (°): C1–C2, 1.335; C2–C3, 1.486; C3–C4, 1.548; C4–C5, 1.486; C5–C6, 1.335; C1–C2–C3, 126.78, C2–C3–C4, 112.19, C3–C4–C5, 112.19, C4–C5–C6, 127.77.

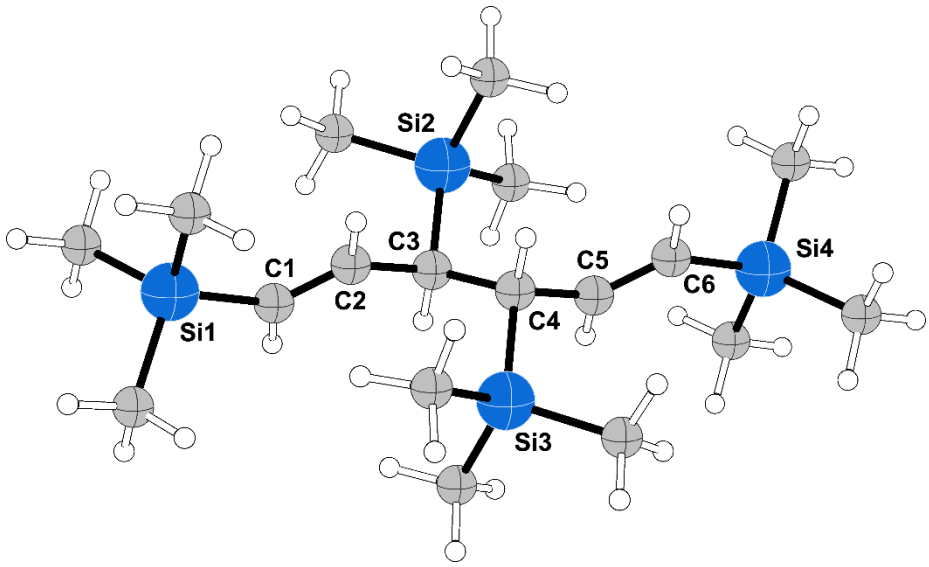

Figure A2.6: Calculated geometry (B3PW91-D3BJ/def2TZVP) of *rac*-{A´}$_2$ (*R*,*R* form). Selected bond distances (Å) and angles (°): C1–C2, 1.334; C2–C3, 1.488; C3–C4, 1.554; C4–C5, 1.488; C5–C6, 1.334; C1–C2–C3, 127.15, C2–C3–C4, 113.83, C3–C4–C5, 113.83, C4–C5–C6, 127.15.

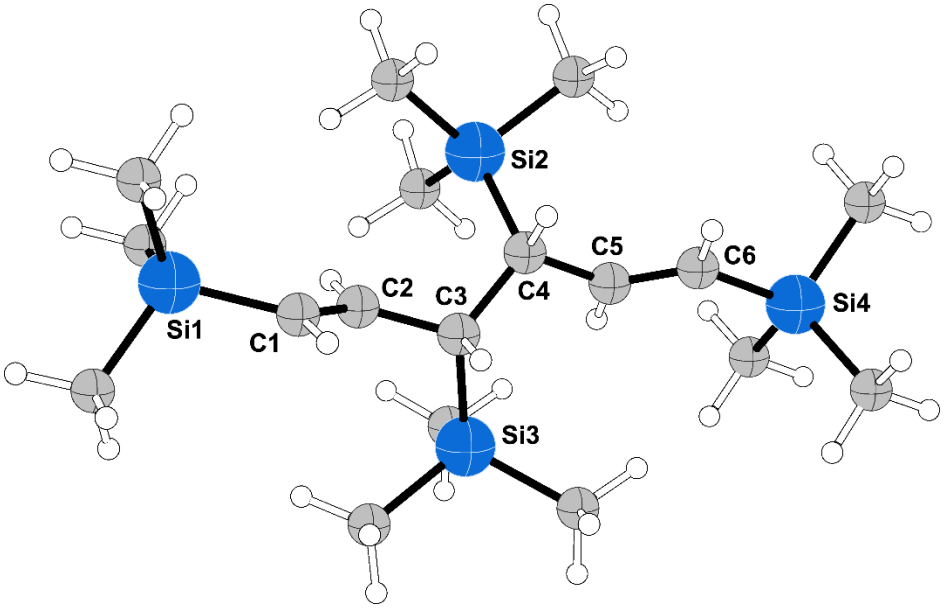

Figure A2.7: Density and corresponding porosities (void volume) of the pyridine adducts of $NiCl_2$, $[Ni(py)_nCl_2]$, as a function of the number of pyridine molecules. Densities and porosities calculated from the crystallographically determined structures ($[NiCl_2]$[14]; $[Ni(py)_{2/3}Cl_2]_n$, $Ni(py)(\mu\text{-}Cl)_2]_n$[15]; $[Ni(py)_2(\mu\text{-}Cl)_2]_n$[16]; $[Ni(py)_4Cl_2]$[17] using CrystalMaker® (CrystalMaker Software Ltd, Oxford, England (www.crystalmaker.com)). Increasing amounts of pyridine leads to less dense structures.

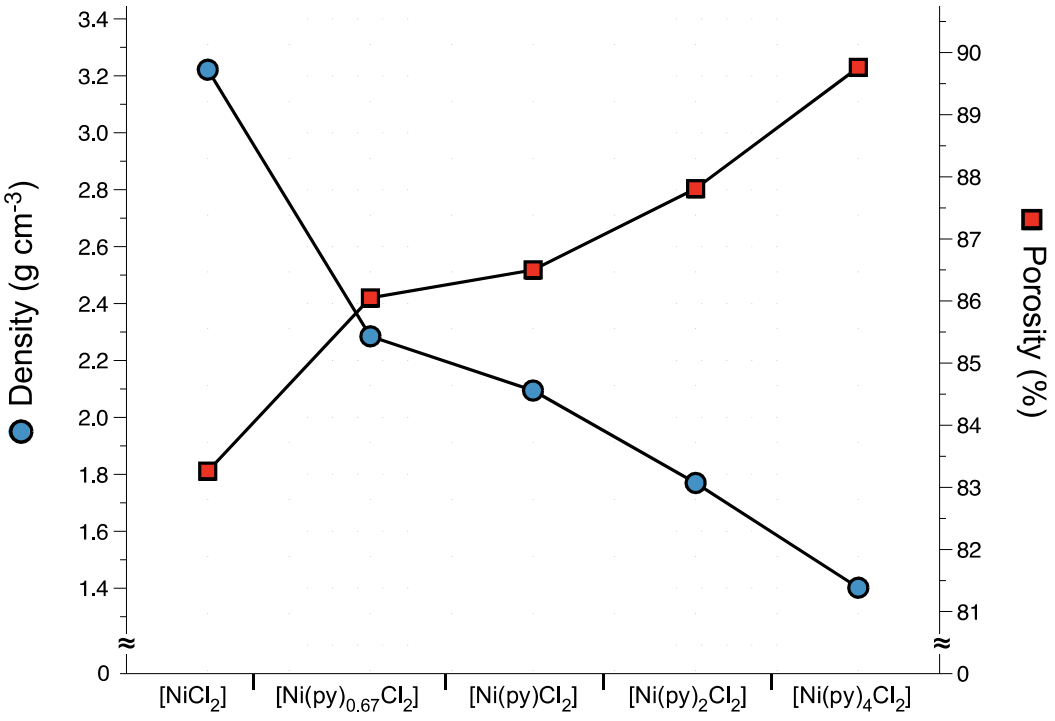

A2.6: References

(1) Ward, L. G. L.; Pipal, J. R. Anhydrous Nickel(II) Halides and Their Tetrakis(Ethanol) and 1,2-Dimethoxyethane Complexes. In *Inorg. Synth.*; 1972; pp 154–164.

(2) Eckert, N. A.; Bones, E. M.; Lachicotte, R. J.; Holland, P. L. Nickel Complexes of a Bulky B-Diketiminate Ligand. *Inorg. Chem.* **2003**, *42* (5), 1720–1725. https://doi.org/10.1021/ic025986n.

(3) Long, G. J.; Clarke, P. J. Crystal and Molecular Structures of Trans-Tetrakis (Pyridine)Dichloroiron (II), -Nickel (II), and -Cobalt (II) and Trans-Tetrakis (Pyridine)Dichloroiron (II) Monohydrate. *Inorg. Chem.* **1978**, *17* (6), 1394–1401. https://doi.org/10.1021/ic50184a002.

(4) Ton, T. M. U.; Tejo, C.; Tania, S.; Chang, J. W. W.; Chan, P. W. H. Iron(II)-Catalyzed Amidation of Aldehydes with Iminoiodinanes at Room Temperature and under Microwave-Assisted

Conditions. *J. Org. Chem.* **2011**, *76* (12), 4894–4904. https://doi.org/10.1021/jo200284a.

(5) Fowles, G. W. A.; Rice, D. A.; Walton, R. A. The Donor Properties of Simple Ethers-II[1]. Complexes of Manganese(II), Iron(II), Cobalt(II) and Nickel(II) Halides with Tetrahydrofuran and 1,2-Dimethoxyethane. *J. Inorg. Nucl. Chem.* **1969**, *31* (10), 3119–3131. https://doi.org/10.1016/0022-1902(69)80095-3.

(6) Petriček, S.; Demšar, A. Syntheses and Crystal Structures of Manganese, Nickel and Zinc Chloride Complexes with Dimethoxyethane and Di(2-Methoxyethyl) Ether. *Polyhedron* **2010**, *29* (18), 3329–3334. https://doi.org/10.1016/j.poly.2010.09.014.

(7) Tschugaeff, L. Ueber Ein Neues, Empfindliches Reagens Auf Nickel. *Ber. Dtsch. Chem. Gesell.* **1905**, *38* (3), 2520–2522.

(8) Gail, E.; Gos, S.; Kulzer, R.; Lorösch, J.; Rubo, A.; Sauer, M.; Kellens, R.; Reddy, J.; Steier, N.; Hasenpusch, W. Cyano Compounds, Inorganic. In *Ullman's Encyclopedia of Industrial Chemistry*; Wiley-VCH, 2011.

(9) Fraenkel, G.; Chow, A.; Winchester, W. R. Dynamics of Solvated Li^+ within Exo, Exo-[1,3-Bis(Trimethylsilyl)Allyl]Lithium N, N, N', N'-Tetramethylethylenediamine Complex. *J. Am. Chem. Soc.* **1990**, *112* (4), 1382–1386. https://doi.org/10.1021/ja00160a014.

(10) Driessen, W.; Reedijk, J. Solid Solvates: The Use of Weak Ligands in Coordination Chemistry. In *Inorg. Synth. Volume 29*; Grimes, R. N., Ed.; 1992; pp 111–118.

(11) Heintz, R. A.; Smith, J. A.; Szalay, P. S.; Weisgerber, A.; Dunbar, K. R. HOMOLEPTIC TRANSITION METAL ACETONITRILE CATIONS WITH TETRAFLUOROBORATE OR TRIFLUOROMETHANESULFONATE ANIONS. In *Inorg. Synth., Volume 33*; 2002; pp 75–80.

(12) Taylor, M. D.; Grant, L. R. Preparation of Anhydrous Pyridine Hydrochloride. *J. Chem. Educ.* **1955**, *32* (1), 39. https://doi.org/10.1021/ed032p39.

(13) Rappoport, D.; Furche, F. Property-Optimized Gaussian Basis Sets for Molecular Response Calculations. *J. Chem. Phys.* **2010**, *133* (13). https://doi.org/10.1063/1.3484283.

(14) Wells, A. F. *Structural Inorganic Chemistry*; Oxford University Press: Oxford, 2012.

(15) Krysiak, Y.; Fink, L.; Bernert, T.; Glinnemann, J.; Kapuscinski, M.; Zhao, H.; Alig, E.; Schmidt, M. U. Crystal Structures and Polymorphism of Nickel and Copper Coordination Polymers with Pyridine Ligands. *Z. Anorg. Allg. Chemie* **2014**, *640* (15), 3190–3196. https://doi.org/10.1002/zaac.201400505.

(16) Alig, E.; Bernert, T.; Fink, L.; Külcü, N.; Yeilkaynak, T. Catena-Poly[[Dipyridine-Nickel(II)]-Trans-Di-μ-Chlorido] from Powder Data. *Acta Crystallogr. Sect. E Struct. Reports Online* **2010**, *66* (2). https://doi.org/10.1107/S1600536810001820.

(17) Mandal, S.; Bachman, R. E.; Whitmire, K. H.; Bharadwaj, P. K.

Dichlorotetrakis(Pyridine)Nickel(II). *Acta Crystallogr. Sect. C* **1992**, *48* (10), 1836–1837. https://doi.org/10.1107/S0108270192001872.

Appendix 3: Supplemental Information for Chapter 3

A3.1 Materials

Pivaldehyde, pinacolone, neopentyl iodide, triphenylphosphine, lithium hexamethyldisilazane in THF, and sodium borohydride were purchased from Oakwood Products. Thionyl bromide, thionyl chloride, and potassium metal were purchased from Sigma Aldrich. Bis(cyclooctadiene)nickel(0) was purchased from Strem and used as received. The literature method was used to prepare [A^{2t}Cl].[1]

A3.2 Crystallographic details

A3.2.1 Crystallographic determinations

Prof. Nathan Schley (Vanderbilt Univ.) performed the data collection and structure solution for (**19**), (**20**), and (**21**); Prof. William Brennessel (Univ. of Rochester) did the same for (**22**), (**23**), and (**24**). The structure of **24** was solved at 294 K.

A3.2.2 Collected crystallographic data

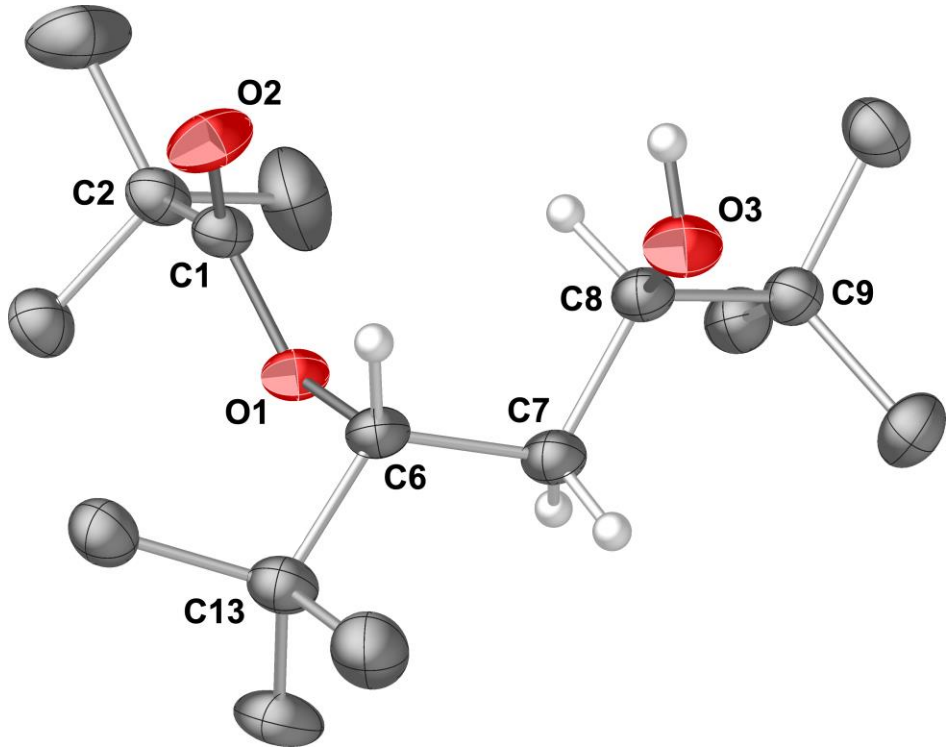

Figure A3.1. Thermal ellipsoid plot (50% level) of 5-hydroxy-2,2,6,6-tetramethylheptan-3-yl pivalate (19); for clarity, hydrogen atoms have been removed from the *t*-Bu groups, and the rest have been given arbitrary radii. Selected bond distances (Å) and angles (°): O1–C1, 1.3378(16); O1–C6, 1.4680(15); O2–C1,

1.2097(17); O3–C8, 1.4303(16); C1–C2, 1.5222(19); C6–C7, 1.5188(18); C6–C13, 1.5403(18); C7–C8, 1.5259(18); C8–C9, 1.5420(18); C1–O1–C6, 119.92(10); O1–C1–C2, 111.45(11); O2–C1–O1, 123.99(13); O2 C1 C2, 124.55(12); O1–C6–C7, 104.70(10); O1–C6–C13, 108.11(10); C7–C6–C13, 117.55(11); C6–C7–C8, 110.68(10); O3–C8–C7, 105.78(11); O3–C8–C9, 111.85(11); C7–C8–C9, 115.21(11).

Table A3.1: Crystal Data and Summary of X–ray Data Collection

	5-hydroxy-2,2,6,6-tetramethyl-heptan-3-yl pivalate (19)	**[{A^{2t}NiBr}$_2$] (20)**
Empirical formula	$C_{16}H_{32}O_3$	$C_{22}H_{42}Br_2Ni_2$
Formula weight	272.41	583.79
Temperature	99.99(10) K	100.00(10) K
Wavelength	1.54184 Å	1.54184 Å
Crystal system	Triclinic	Triclinic
Space group	P-1	P-1
Unit cell dimensions	a = 9.2256(2) Å	a = 6.2987(6) Å
	b = 9 5320(2) Å	b = 10.0280(9) Å
	c = 22.5042 (5) Å	c = 11.3301(12) Å
	α = 95.965(2)°	α = 72.341(9)°
	β = 96.641(2)°	β = 78.427(8)°
	γ = 114.486(2)°	γ = 72.315(8)°
Volume	1763.49(8) Å^3	645.04(12) Å^3
Z	4	1
Density (calculated)	1.026 g/cm^3	1.503 g/cm^3
Absorption coefficient	0.538 mm^{-1}	5.445 mm^{-1}
F(000)	608	300
Crystal size (mm^3)	0.4 x 0.27 x 0.2	0.112 x 0.037 x 0.023
Crystal color, habit	colorless block	orange, block
Theta range for data collection	4.012 to 71.657 °	4.124 to 63.610°
Index ranges	-11 ≤ h ≤ 11, -11 ≤ k ≤ 11, -27 ≤ l ≤ 27	-7 ≤ h ≤ 7, -11 ≤ k ≤ 11, -13 ≤ l ≤ 13
Reflections collected	24 293	3848
Independent reflections	6780 [R(int) = 0.0236]	3848
Absorption correction	Gaussian	Gaussian
Max. and min. transmission	1.000 and 0.581	0.924 to 0.651
Refinement method	Full-matrix least-squares on F^2	Full-matrix least-squares on F^2
Data / restraints / parameters	6780 / 0 / 363	3848 / 0 / 134
Goodness-of-fit on F^2	1.044	1.009
Final R indices [I>2sigma(I)]	R_1 = 0.0451, wR_2 = 0.1174	R_1 = 0.0787, wR_2 = 0.2034
R indices (all data)	R_1 = 0.0499, wR_2 = 0.1213	R_1 = 0.0866, wR_2 = 0.2093
Largest diff. peak and hole	0.352 and -0.192 e/ Å^{-3}	1.93 and -1.29 e Å^{-3}

Table A3.1: Crystal Data and Summary of X–ray Data Collection (cont.)

	[A^{2t}Ni(IMes)Br] (21)	**[A´Ni(IMes)Br] (22)**	**meso-{A^{2t}}$_2$ (23)**
Empirical formula	$C_{32}H_{45}BrN_2Ni$	$C_{30}H_{45}BrN_2NiSi_2$	$C_{22}H_{42}$
Formula weight	596.32	628.48	306.58
Temperature	100.00(10) K	100.00(10) K	294.0(2) K
Wavelength	1.54184 Å	0.71073 Å	1.54184 Å
Crystal system	Triclinic	Monoclinic	Triclinic
Space group	P-1	$P2_1/c$	P-1
Unit cell dimensions	a = 9.7948(1) Å	a = 9.5897(3)Å	a = 6.1994(4) Å
	b = 10.0560(1) Å	b = 30.6431(8) Å	b = 9.0864(5) Å
	c = 16.5671(1) Å	c = 11.1601(3)Å	c = 9.6578(4) Å
	α = 82.023(1)°	α = 90°	α = 91.363(4)°
	β = 77.240(1)°	β = 101.287(2)°	β = 90.556(4)°
	γ = 74.474(1)°	γ = 90°	γ = 94.247(5)°
Volume	1527.91(3) $Å^3$	3216.06(16) $Å^3$	542.34(5) $Å^3$
Z	2	4	1
Density (calculated)	1.296 g/cm^3	1.298 g/cm^3	0.939 g/cm^3
Absorption coefficient	2.593 mm^{-1}	1.941 mm^{-1}	0.370 mm^{-1}
F(000)	628	1320	174
Crystal size (mm^3)	0.221 x 0.185 x 0.122	0.203 x 0.08 x 0.054	0.186 x 0.144 x 0.035
Crystal color, habit	red, block	red, needle	colorless, plate
Theta range for data collection	4.580 to 80.339°	2.265 to 33.096°	4.591 to 75.643°
Index ranges	$-12 \leq h \leq 12$, $-10 \leq k \leq 12$, $-21 \leq l \leq 20$	$-13 \leq h \leq 14$, $-46 \leq k \leq 12$, $-16 \leq l \leq 17$	$-7 \leq h \leq 7$, $-11 \leq k \leq 11$, $-12 \leq l \leq 10$
Reflections collected	39 331	79257	2126
Independent reflections	6567 [R(int) = 0.0373]	10969 [R(int) = 0.0509]	5356 [R(int) = 0.0382]
Absorption correction	Multi-scan	Multi-scan	Multi-scan
Max. and min. transmission	1.000 and 0.897	1.000 and 0.688	1.000 and 0.853
Refinement method	Full-matrix least-squares on F^2	Full-matrix least-squares on F^2	Full-matrix least-squares on F^2
Data / restraints / parameters	6567 / 0 / 349	10969 / 0 / 349	2126 / 0 / 106
Goodness-of-fit on F^2	1.038	1.015	1.068
Final R indices [I>2sigma(I)]	R_1 = 0.0276, wR_2 = 0.0681	R_1 = 0.0381, wR_2 = 0.0756	R_1 = 0.0621, wR_2 = 0.1876
R indices (all data)	R_1 = 0.0282, wR_2 = 0.0685	R_1 = 0.0581, wR_2 = 0.0807	R_1 = 0.0806, wR_2 = 0.2043
Largest diff. peak and hole	0.337 and -0.572 e $Å^{-3}$	0.849 and -0.492 e $Å^{-3}$	0.250 and -0.161 e $Å^{-3}$

A3.3 General Procedures for Calculations

(Gaussian keyword: empiricaldispersion=GD3BJ). For the energy of deprotonation ($HA \rightarrow [A]^- + H^+$), all steps of the fragmentation analysis of phosphine complexes, and all calculations on carbonyl complexes,

the def2-TZVPD basis set was used on all atoms.[2] For all other calculations, the def2-SVP basis set was used on first and second row elements, while def2-TZVP was used for all other atoms. For all calculated CO stretching frequencies, a scaling factor was applied to account for systematic overestimation of frequencies by DFT methods. While, to our knowledge, there is no previously computed scaling factor for the specific functional/basis set combination used here, a scaling factor has been provided for the B3PW91 functional with the related TZP basis set. To verify that this was appropriate to use, carbon monoxide was optimized under our methods. When the suggested scaling factor was applied to our calculated stretching frequency, the resulting value was 2145.2 cm^{-1}, closely matching the experimental value for free CO (2143 cm^{-1}).

A3.4 NMR Spectra for New Compounds

Figure A3.2: ^{1}H NMR (400 MHz) of *anti*-5-hydroxy-2,2,6,6-tetramethylheptan-3-yl pivalate at 298 K in $CDCl_3$. Peaks belonging to 2,2,6,6-tetramethylhept-4-en-3-one are marked with an asterisk.

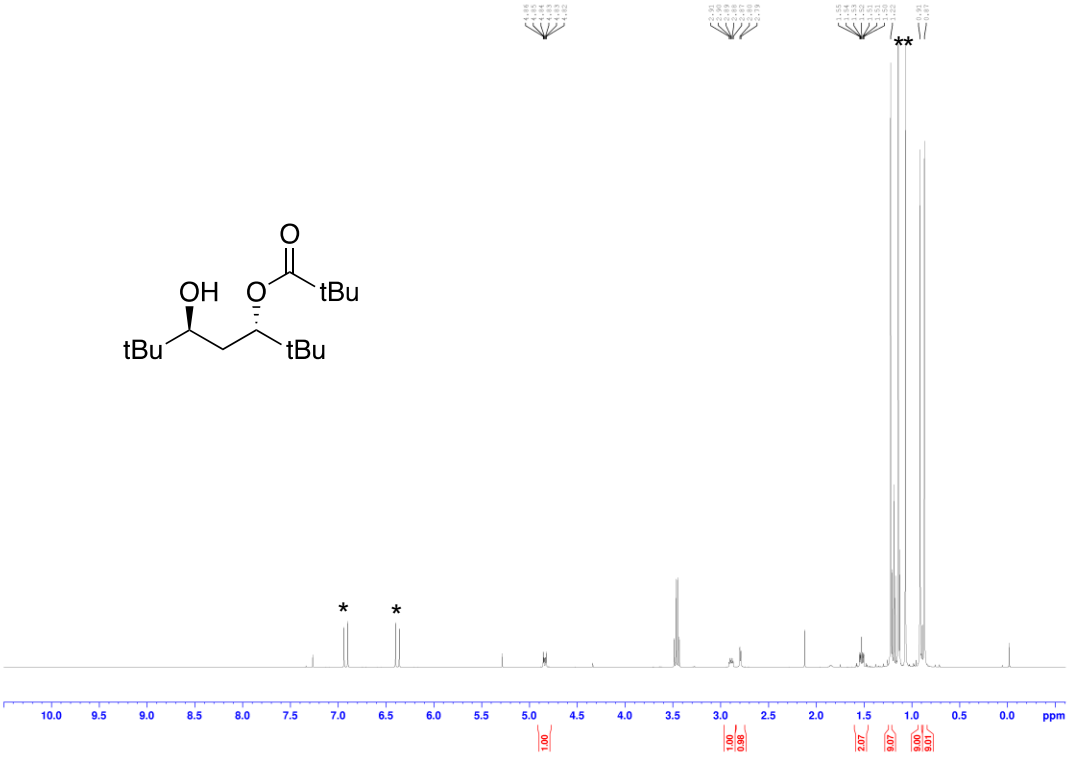

Figure A3.3: ^{1}H NMR (400 MHz) of [{A^{2t}NiBr}$_2$] at 298 K in C_6D_6.

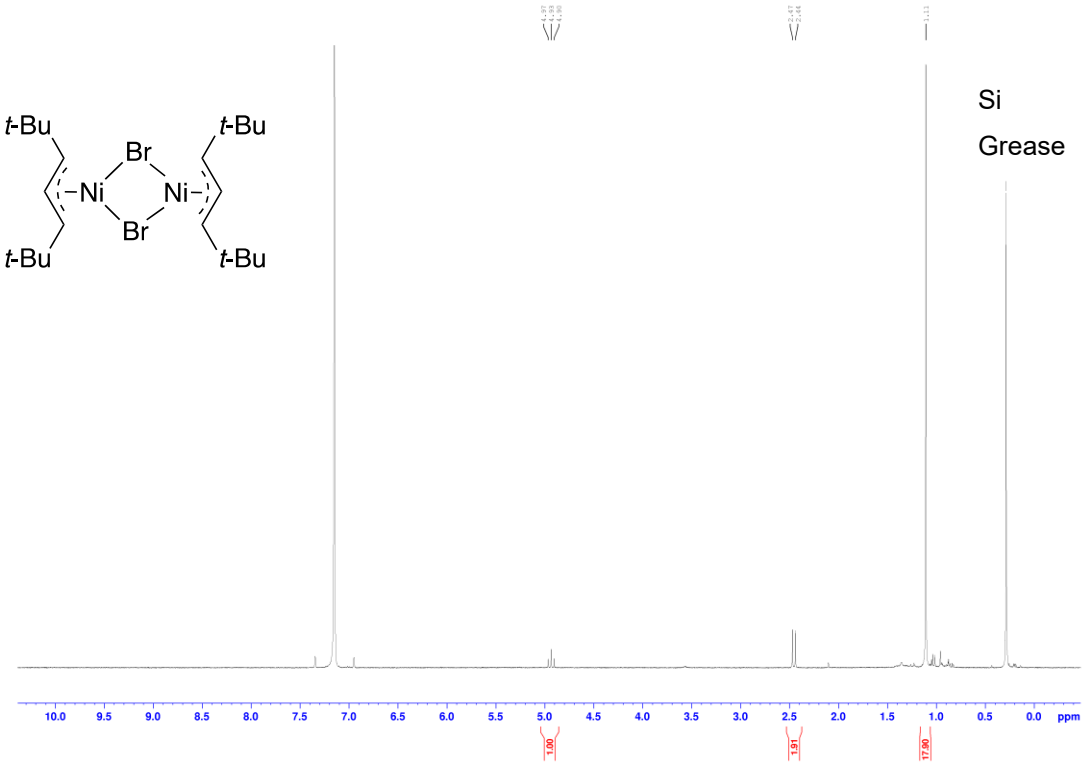

Figure A3.4: ^{1}H NMR (400 MHz) of [{$A^{2t}NiBr$}$_2$] in DMSO-d_6

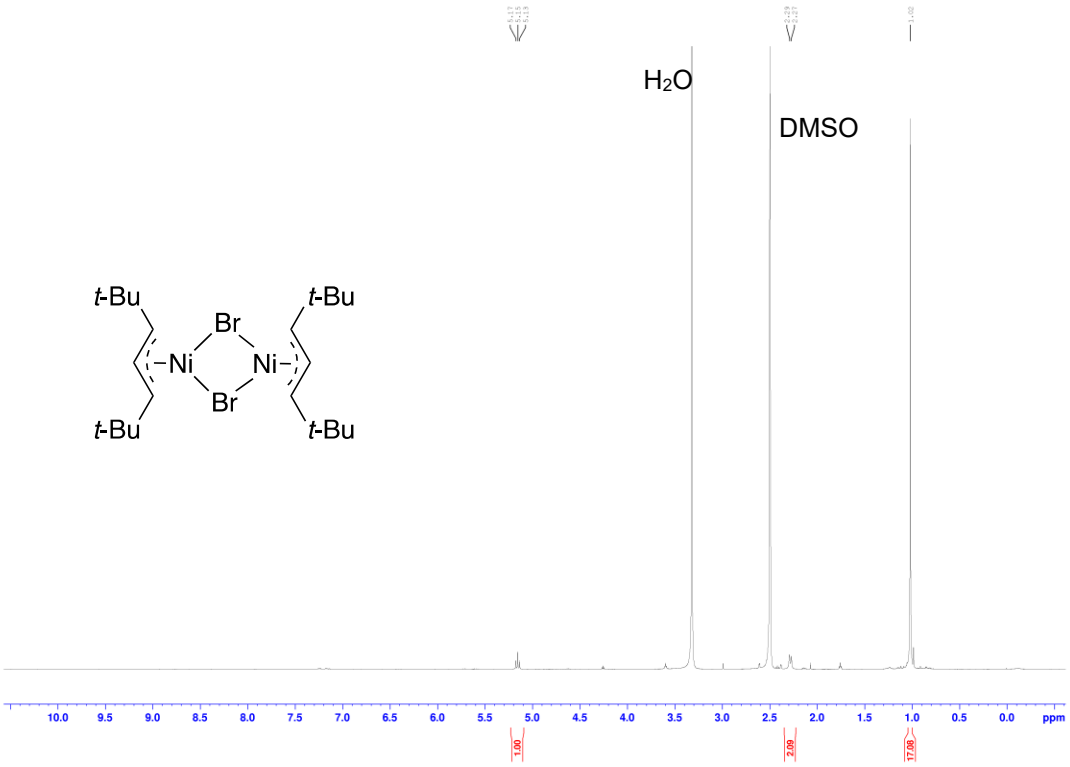

Figure A3.5: $^{13}C\{^{1}H\}$ NMR (151 MHz) of $[\{A^{2t}NiBr\}_2]$ in C_6D_6

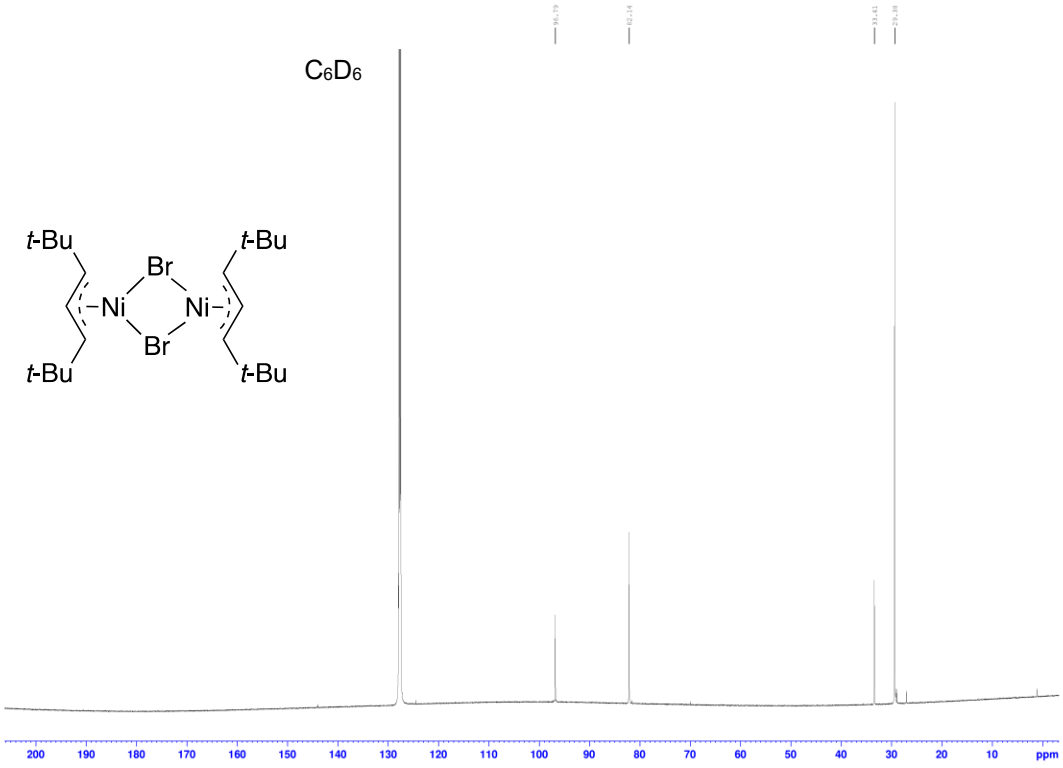

Figure A3.6: ^{1}H NMR (400 MHz) of [{A´NiBr}$_2$] in C_6D_6, including an enlargement of the TMS region. Peaks belonging to the previously known *syn*, *syn* product are marked with S/S.

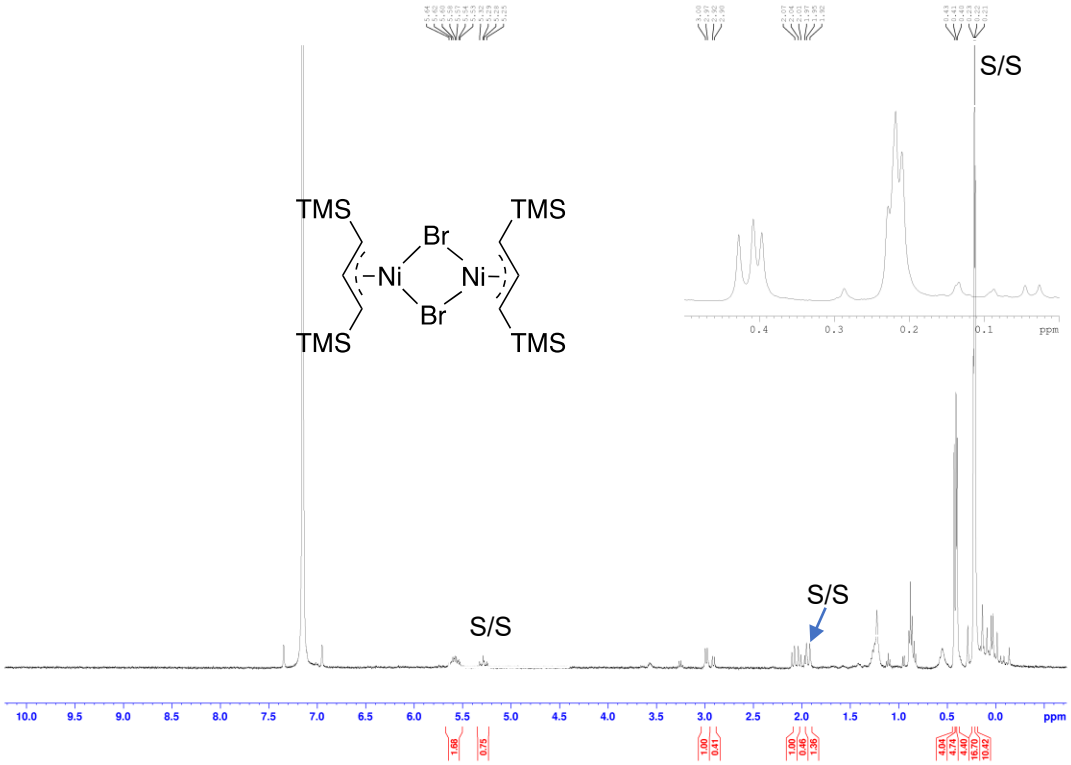

Figure A3.7: ^{1}H NMR (400 MHz) of $[\{A^{2t}NiCl\}_2]$ at 298 K in C_6D_6.

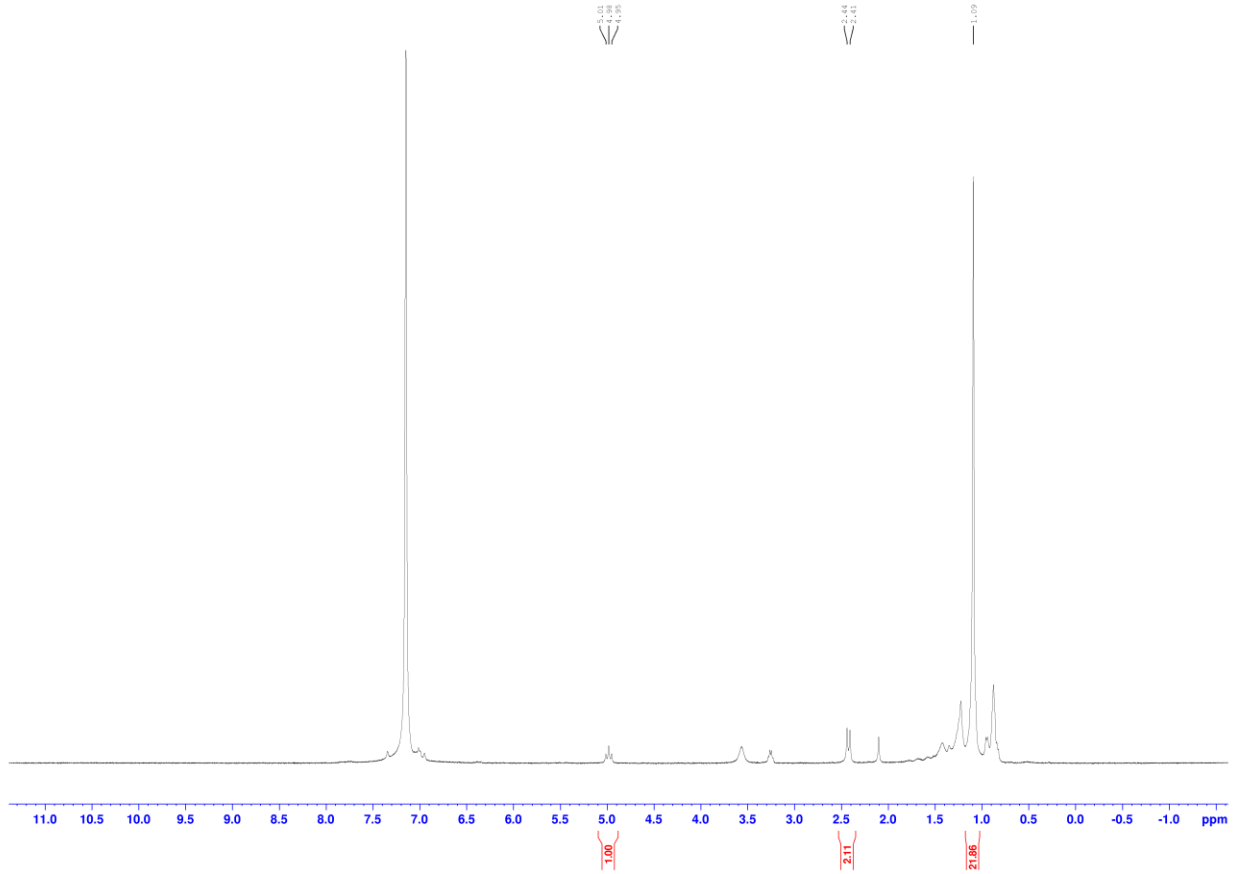

Figure A3.8: ^{1}H NMR (600 MHz) of [A^{2t}Ni(PPh_3)Br] in toluene-d_8 at room temperature; peaks belonging to [{A^{2t}NiBr}$_2$], free PPh_3, or toluene are marked with an asterisk, while peaks where [A^{2t}Ni(PPh_3)Br] overlaps with another species are marked with an O. The peak marked I represents an impurity in the toluene-d_8.

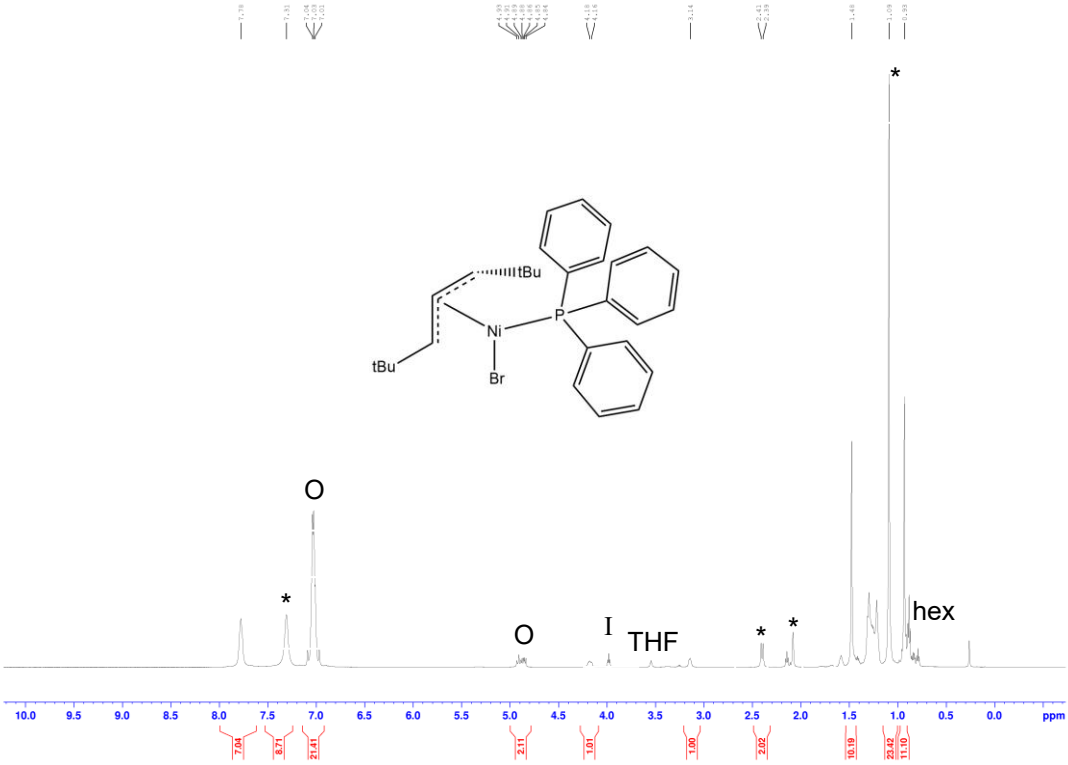

Figure A3.9: ^{1}H-^{1}H COSY NMR (400 MHz) of [A^{2t}Ni(PPh$_3$)Br] in C_6D_6 at 298 K. Allylic proton couplings are marked with an A.

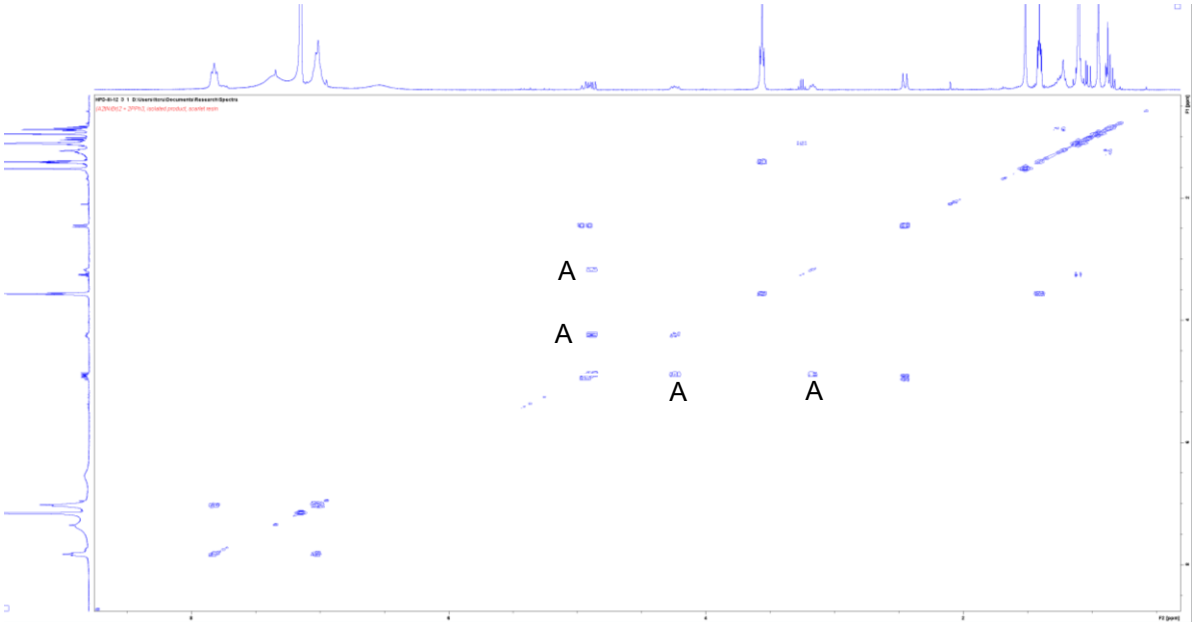

Figure A3.10: ^{1}H NMR (600 MHz) of [A^{2t}Ni(PPh_3)Br] in toluene-d_8 at varying temperatures; peaks belonging to [{A^{2t}NiBr}$_2$] are marked with an asterisk, while peaks belonging to [A^{2t}Ni(PPh_3)Br] are marked with an P. The peak marked I represents a consistent impurity in the d_8-toluene. The unmarked signal at δ 3.4 ppm is hypothesized to be an intermediate in phosphine exchange.

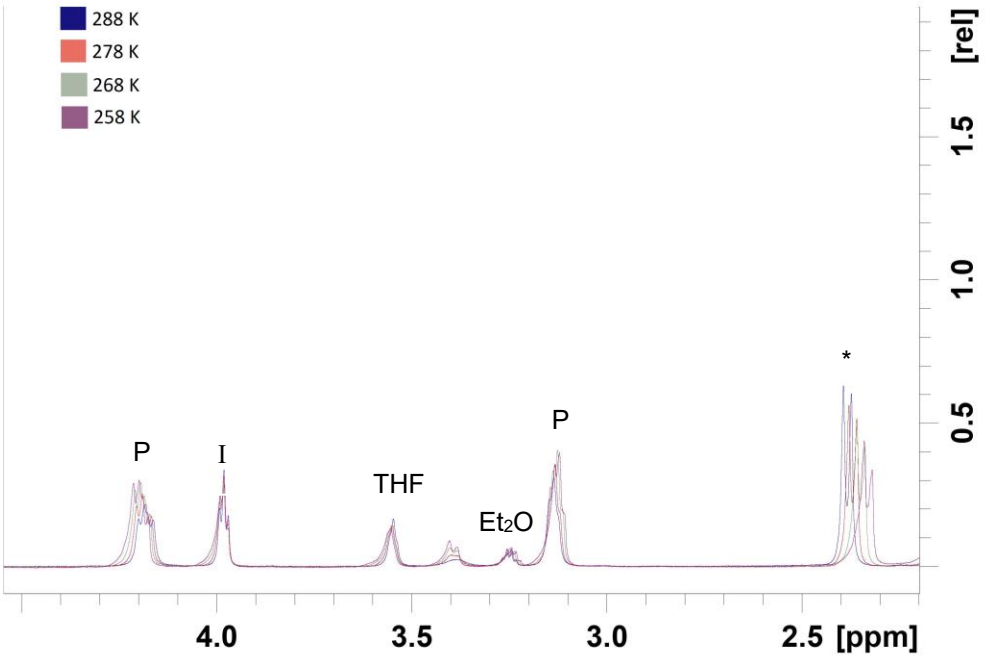

Figure A3.11: ^{1}H NMR (600 MHz) of [A^{2t}Ni(PPh_3)Br] in toluene-d_8 at 253 K; peaks belonging to [{A^{2t}NiBr}$_2$], free PPh_3, or toluene are marked with an asterisk, while peaks where [A^{2t}Ni(PPh_3)Br] overlaps with another species are marked with an O. Phasing was done to optimize a consistent baseline for the purposes of integration; with other phasing parameters, evenly distributed peaks can be achieved. The peak marked I represents a consistent impurity in the d_8-toluene

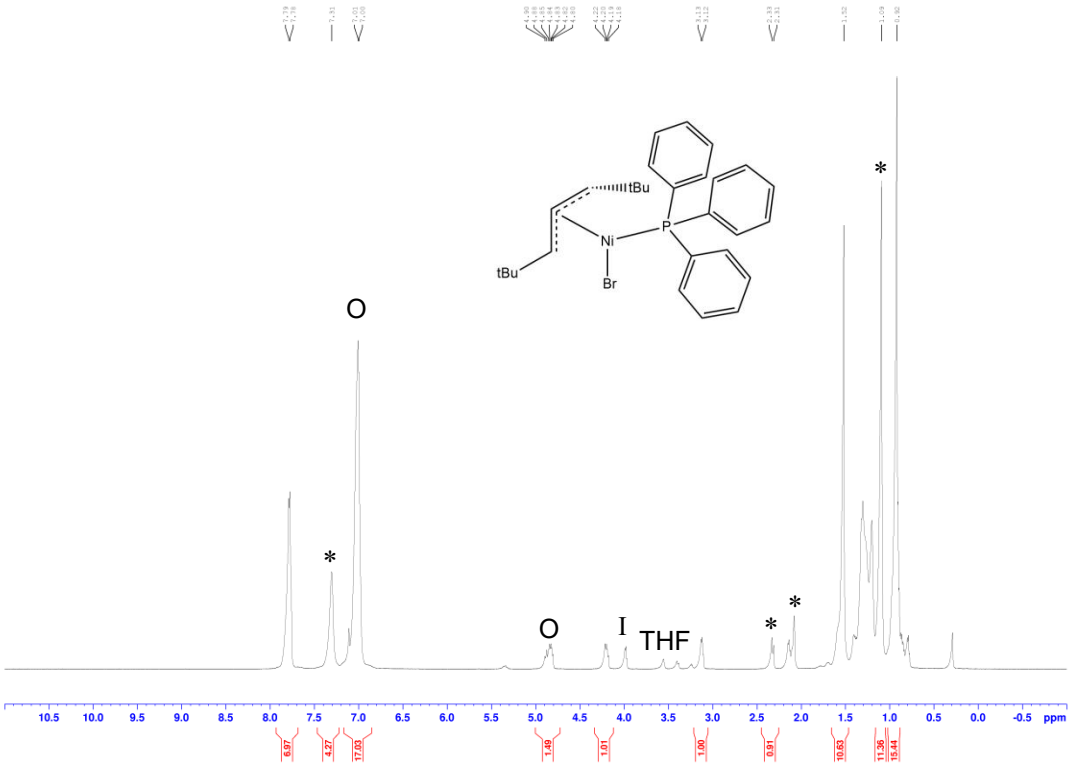

Figure A3.12: $^{13}C\{^{1}H\}$ NMR (151 MHz) of $[A^{2t}Ni(PPh_3)Br]$ in toluene-d_8 at room temperature; peaks belonging to $[\{NiBr(A^{2t})\}_2]$ or are marked with an asterisk, while peaks where $[A^{2t}Ni(PPh_3)Br]$ overlaps with another species are marked with an O.

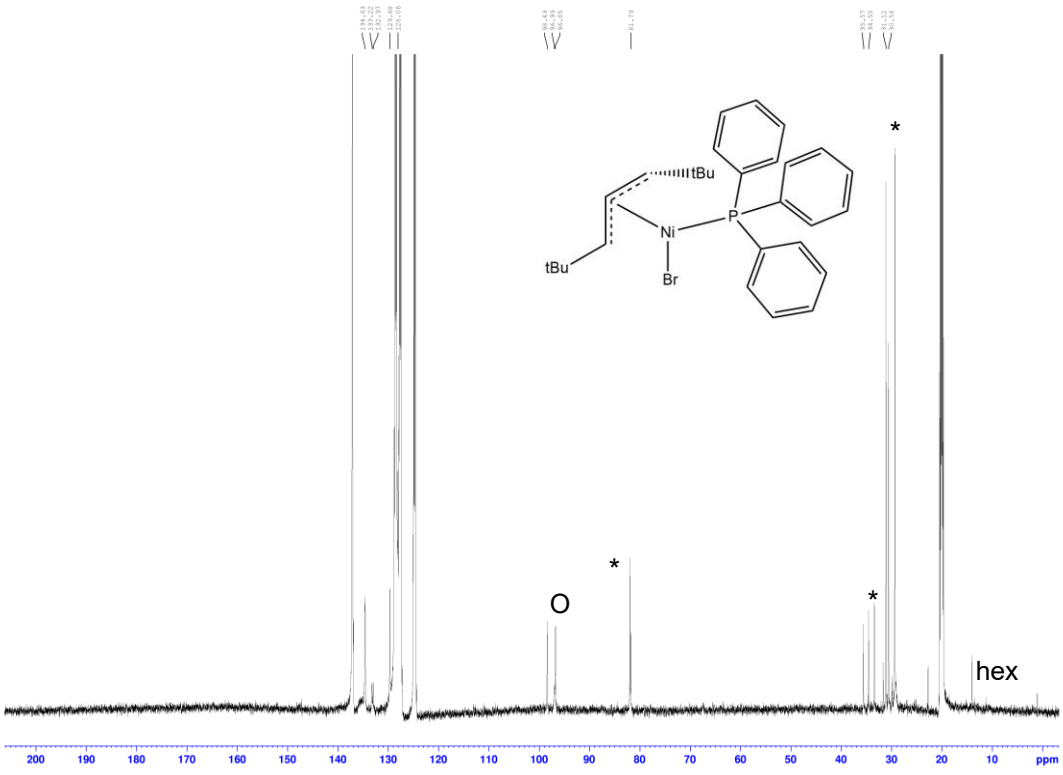

Figure A3.13: ^{1}H-^{13}C HSQC NMR (600-151 MHz) of [$A^{2t}Ni(PPh_3)Br$] in toluene-d_8 at room temperature. Allylic proton-carbon couplings are marked with an A.

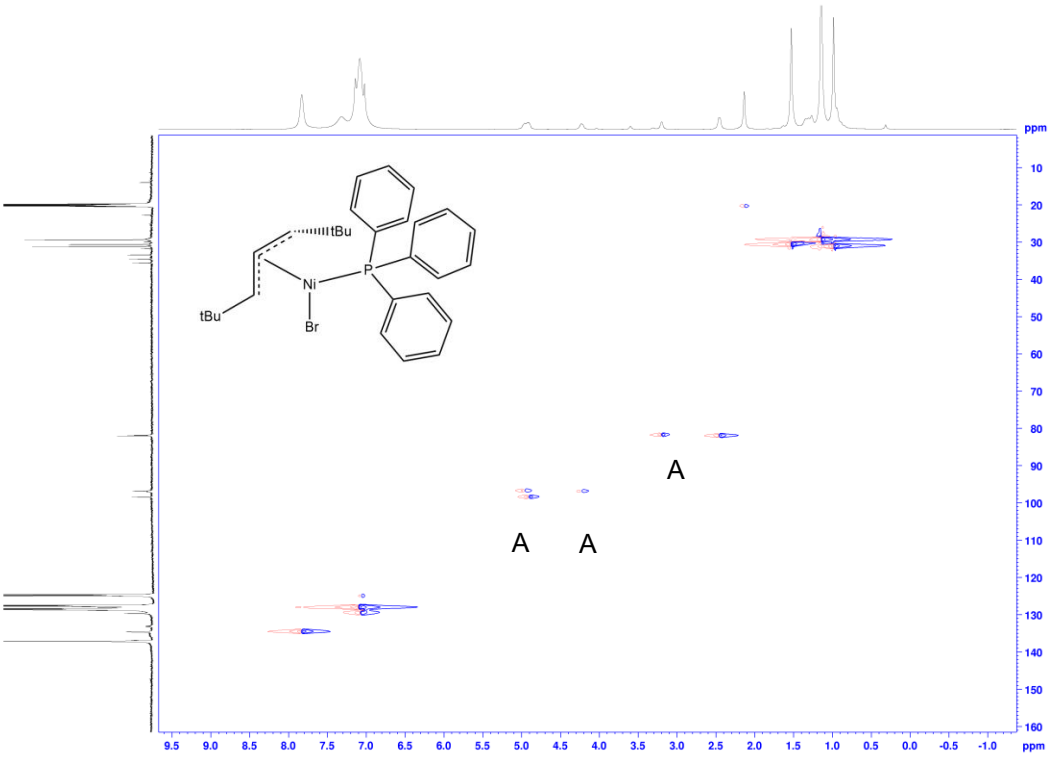

Figure A3.14: $^{31}P\{^{1}H\}$ NMR (162 MHz) of [A^{2t}Ni(PPh_3)Br] in C_6D_6 at room temperature.

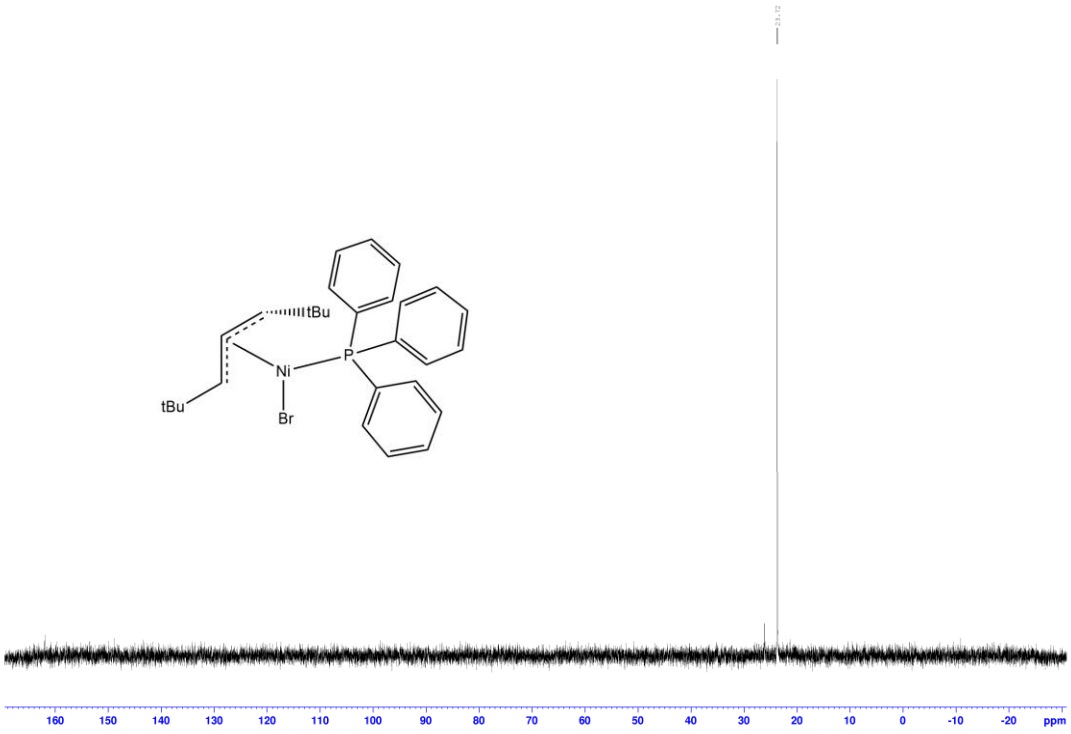

Figure A3.15: ^{1}H NMR (400 MHz) of reaction mixture of [{A^{2t}NiBr}$_2$] with 2 equivalents of tri-*n*-butylphosphine in C_6D_6 at room temperature. The presence of only one species, whose spectral features are similar to [A^{2t}Ni(PPh$_3$)Br], strongly suggests quantitative formation of an adduct of the form [A^{2t}Ni(P*n*Bu$_3$)Br].

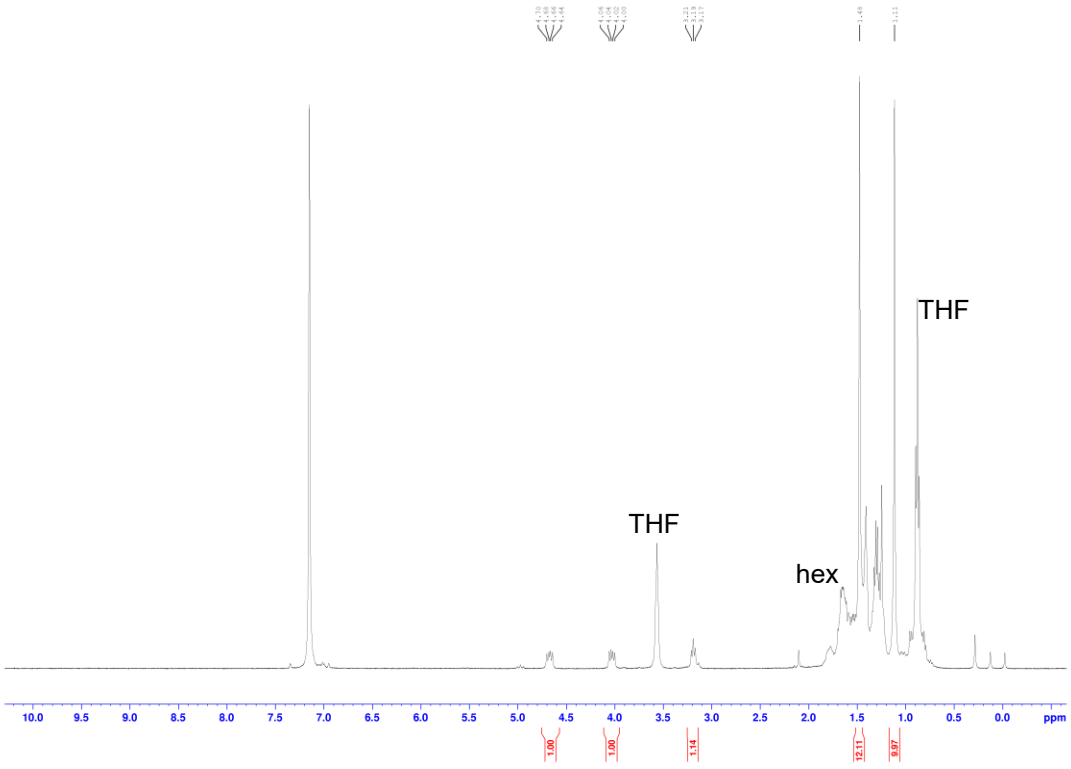

Figure A3.16: ^{1}H NMR (600 MHz) of [A´Ni(PPh_3)Br] in toluene-d_8 at room temperature. The peak marked I represents a consistent impurity in the toluene-d_8

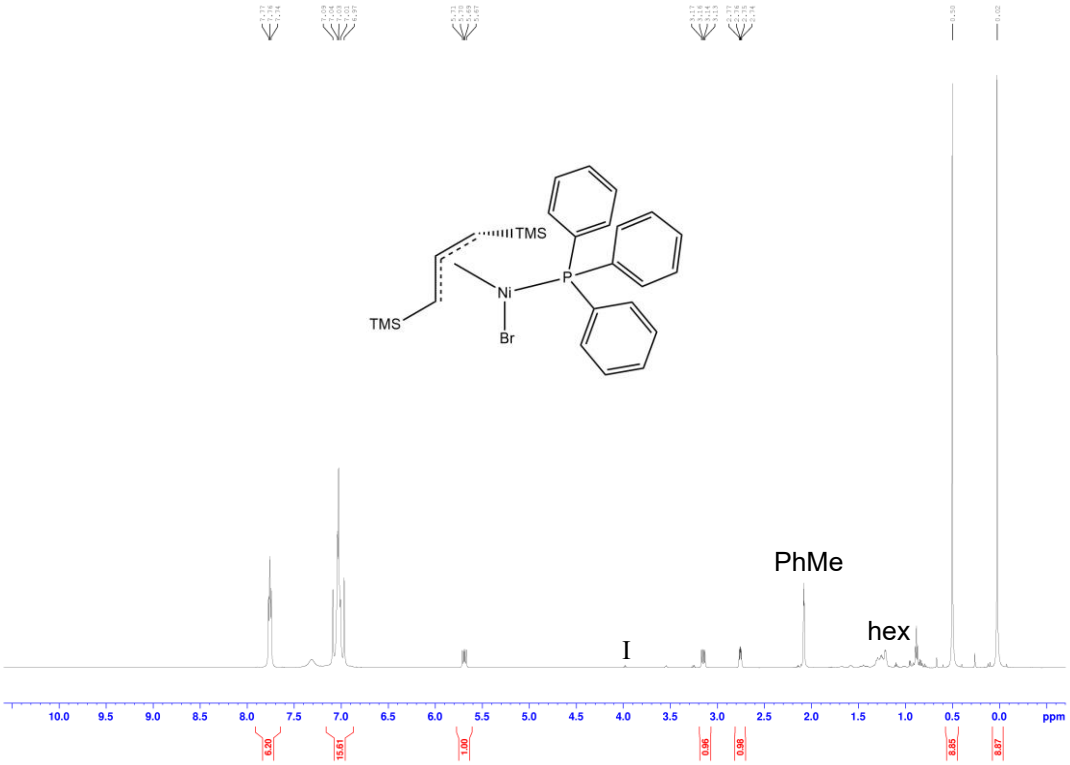

Figure A3.17: $^{13}C\{^{1}H\}$ NMR (151 MHz) of [A´Ni(PPh_3)Br] in toluene-d_8 at room temperature.

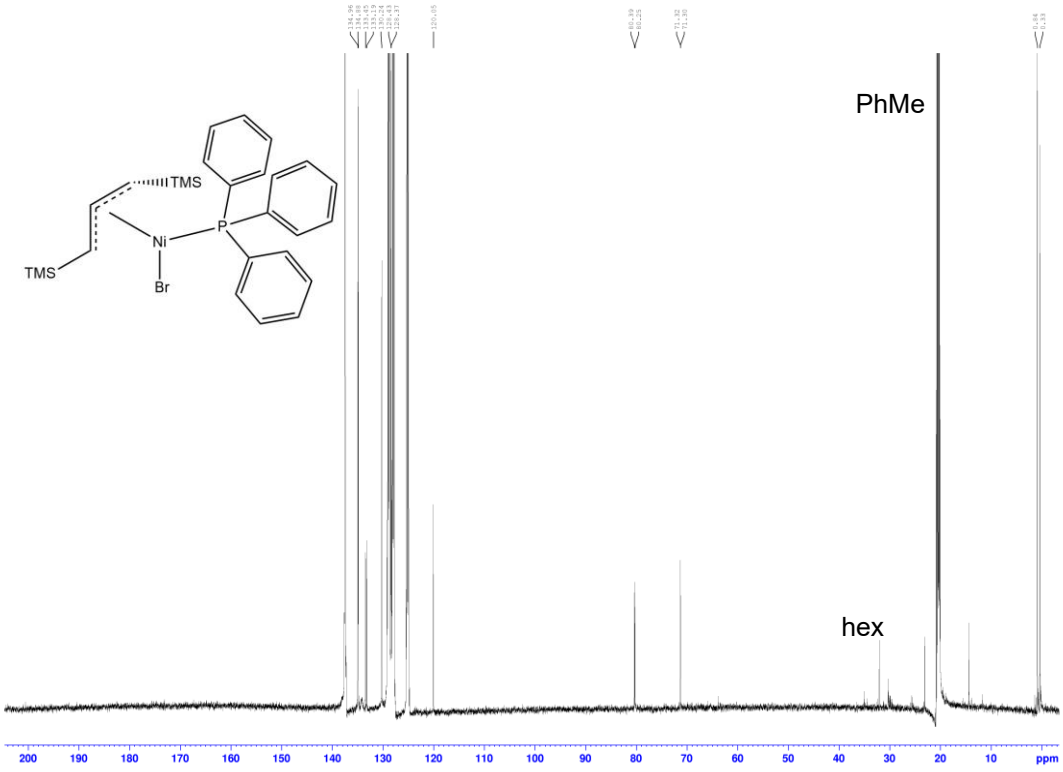

Figure A3.18: ^{1}H-^{13}C HSQC NMR (600-151 MHz) of [A´Ni(PPh_3)Br] in toluene-d_8 at room temperature.

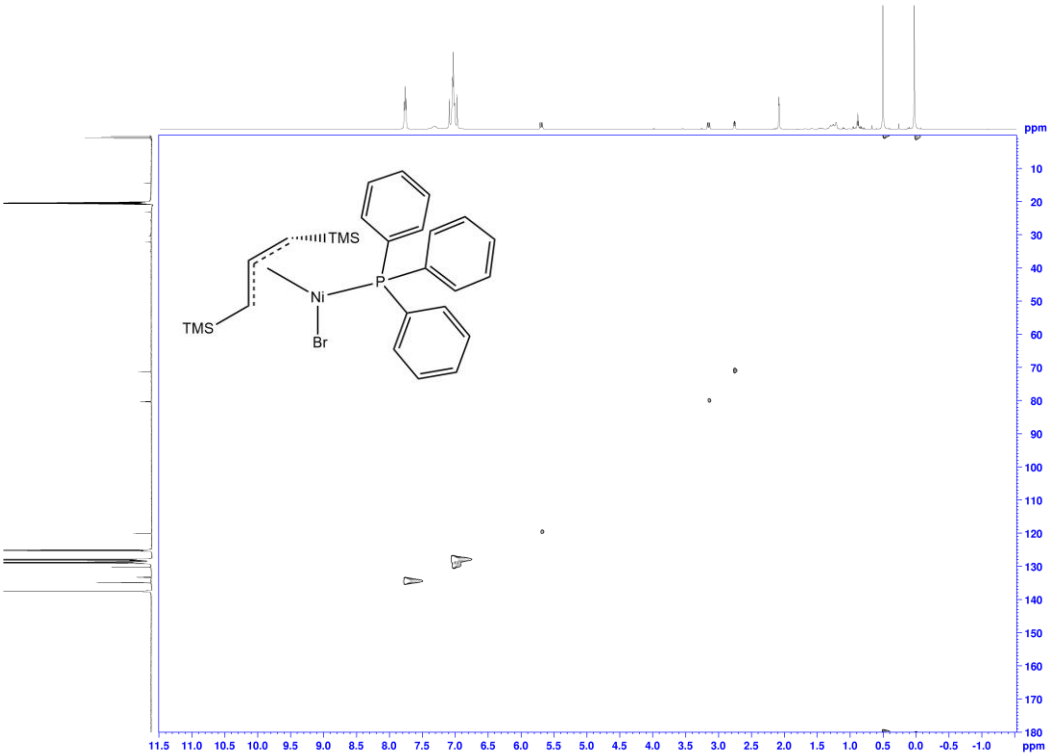

Figure A3.19: $^{31}P\{^{1}H\}$ NMR (162 MHz) of [A´Ni(PPh_3)Br] in C_6D_6 at room temperature.

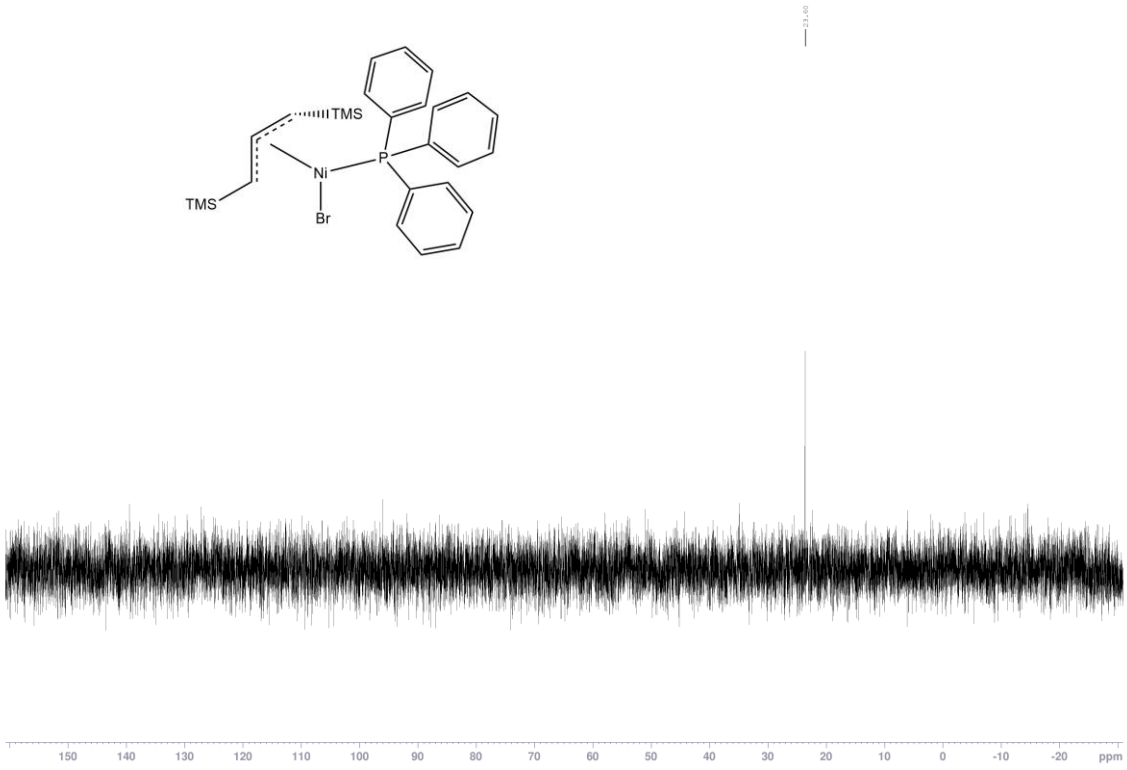

Figure A3.20: ^{1}H NMR (400 MHz) of [A^{2t}Ni(IMes)Br] in C_6D_6 at room temperature. Peaks belonging to the minor product are marked with an M

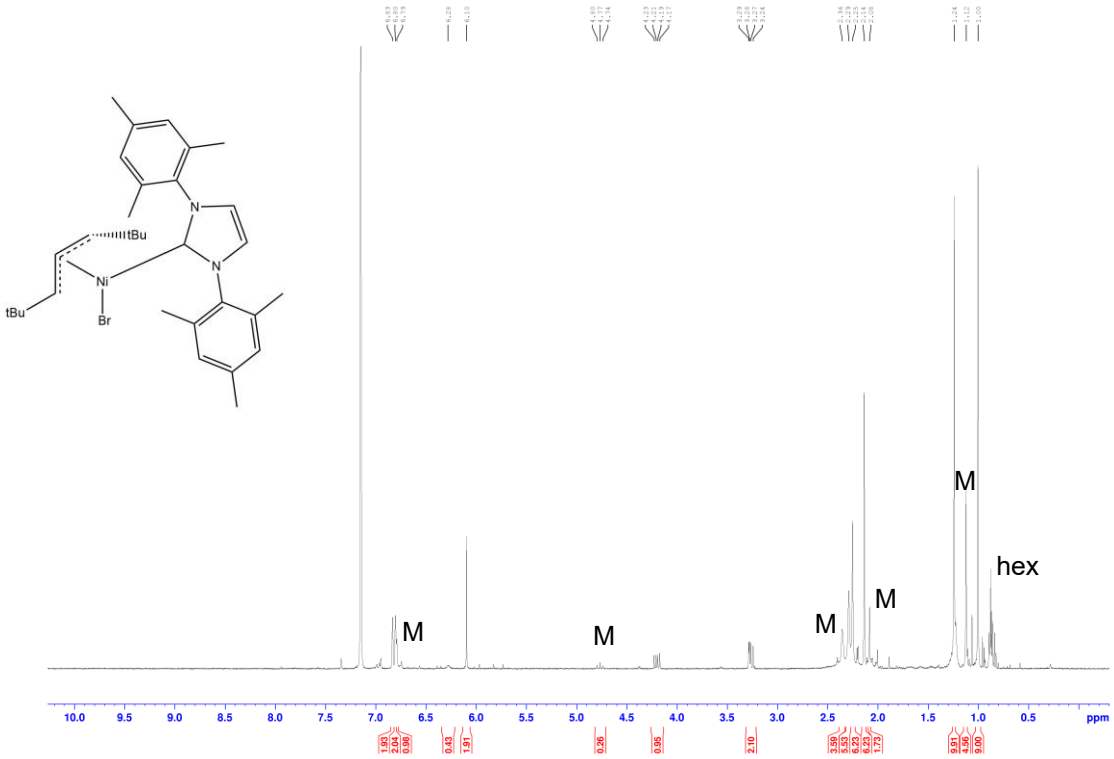

Figure A3.21: $^{13}C\{^{1}H\}$ NMR (101 MHz) of [A^{2t}Ni(IMes)Br] in C_6D_6 at room temperature. Peaks belonging to the minor product are marked with an M.

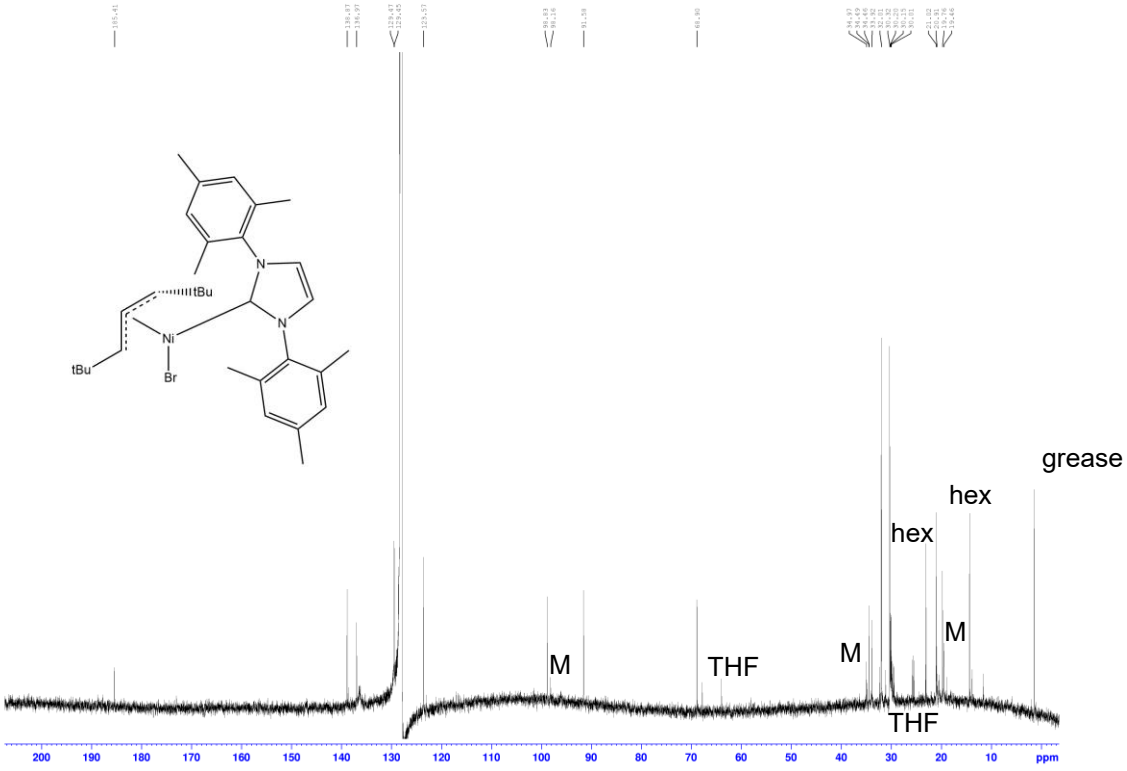

Figure A3.22: ^{1}H-^{13}C HSQC NMR (400-101 MHz) of [A^{2t}Ni(IMes)Br] in C_6D_6 at 298 K. Allylic proton-carbon couplings are marked with an A.

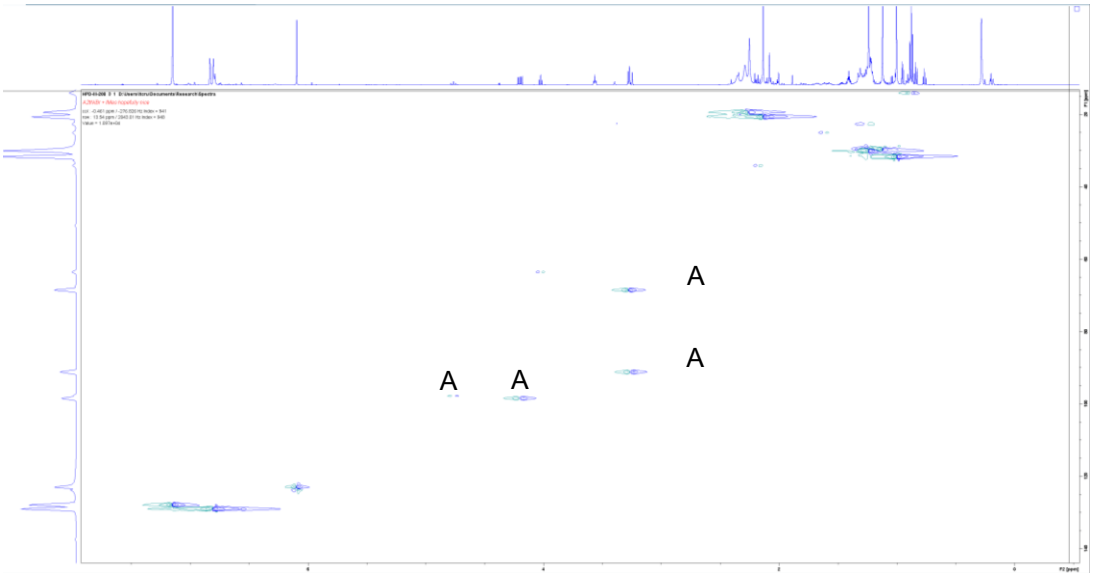

Figure A3.23: ^{1}H NMR (400 MHz) of [A´Ni(IMes)Br] in C_6D_6 at room temperature.

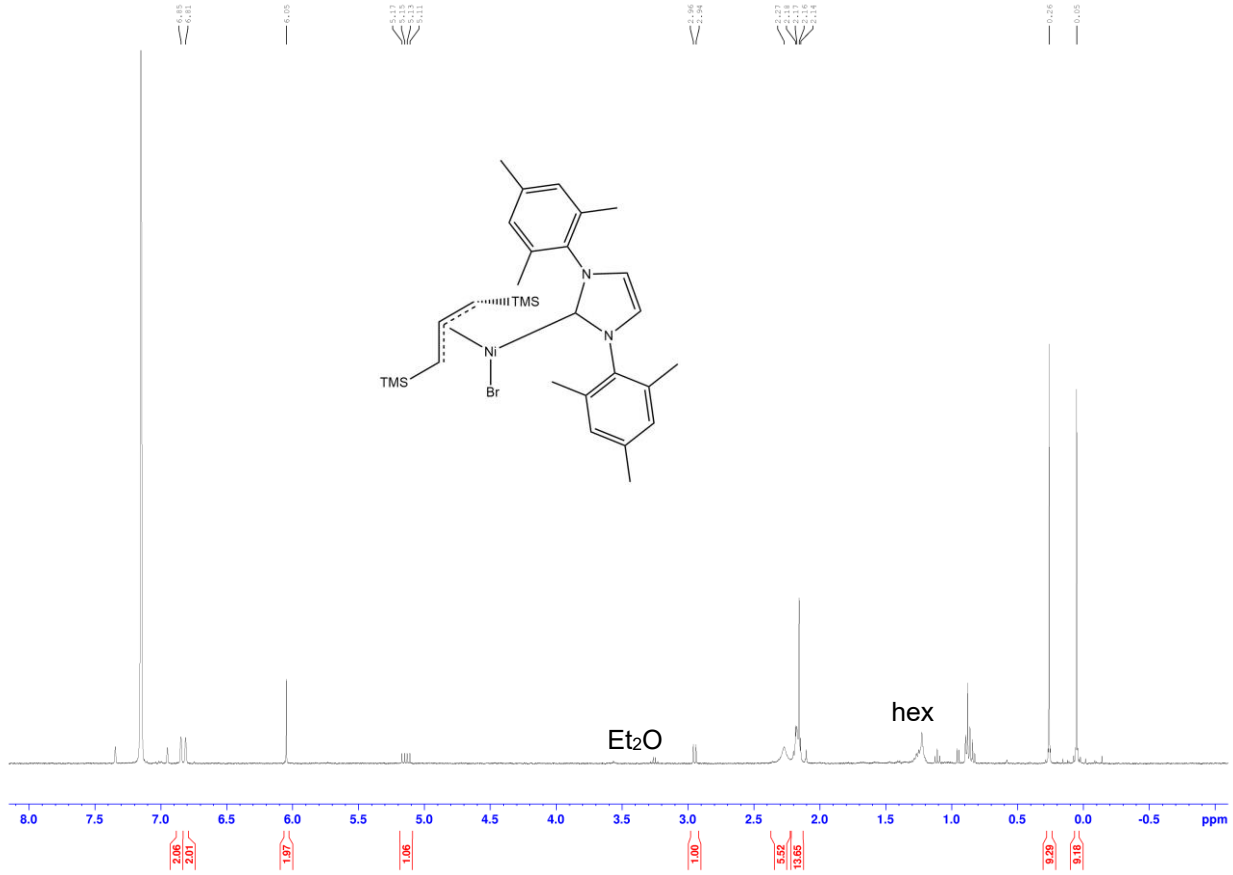

Figure A3.24: $^{13}C\{^{1}H\}$ NMR (151 MHz) of [A´Ni(IMes)Br] in C_6D_6 at room temperature.

Figure A3.25: ^{1}H-^{13}C HSQC NMR (600-151 MHz) of [A´Ni(IMes)Br] in C_6D_6 at 298 K. Allylic proton-carbon couplings are marked with an A.

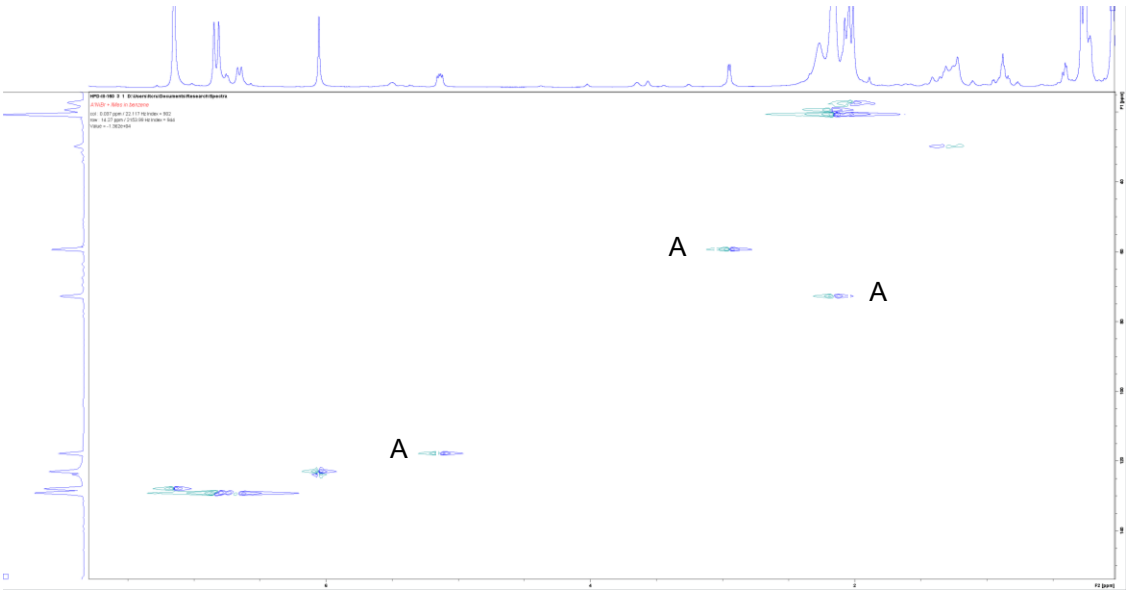

A3.5 Collected computational and experimental VT-NMR data

A3.5.1 Compiled computational data on relative energies and charge distributions of A^{2t}-nickel complexes

Table A3.2: Calculated relative energies of configurations of selected A^{2t}-nickel complexes

[{A^{2t}NiBr}$_2$]

Isomer	**Energy (ΔG°, Hartrees)**	**Rel. Energy (ΔG°, kJ mol^{-1})**
Eclipsed *syn,syn*/*syn,syn*	-9028.454539	0.00
Eclipsed *syn,syn*/*syn,anti*	-9028.449938	12.08
Eclipsed *syn,anti* /*syn,anti* (trans)	-9028.446737	20.48
Eclipsed *syn,anti* /*syn,anti* (cis)	-9028.444546	26.24
Eclipsed *anti,anti* /*anti,anti*	-9028.395249	155.67
Staggered *syn,syn*/*syn,syn*	-9028.450845	9.70
Staggered *syn,syn*/*syn,anti*	-9028.449938	12.08
Staggered *syn,anti* /*syn,anti* (cis)	-9028.442375	31.94

[A^{2t}Ni(PPh$_3$)Br]

Isomer	**Energy (ΔG°, Hartrees)**	**Rel. Energy (ΔG°, kJ mol^{-1})**
syn,syn	-5550.345462	5.99
syn,anti (P trans to *syn t*-Bu)	-5550.347744	0.00
syn,anti (P trans to *anti t*-Bu)	-5550.341071	17.52

[A^{2t}Ni(IMes)Br]

Isomer	**Energy (ΔG°, Hartrees)**	**Rel. Energy (ΔG°, kJ mol^{-1})**
syn,syn	-5436.738861	21.54
syn,anti (carbene trans to syn t-Bu)	-5436.747064	0.00

Table A3.3: Calculated NPA charges for selected atoms in allyl nickel complexes (A^x = unspecified allyl; A = parent allyl, $C_3H_5^-$)

[{A^xNiBr}]

Complex	Ni Charge(avg.)	Br Charge(avg.)	Net Allyl Charge (avg.)
[{ANiBr}]	0.12	- 0.17	0.05
[{A^{2t}NiBr}]	0.15	- 0.20	0.05
[{A´NiBr}]	0.12	- 0.16	- 0.04

[A^xNi(PPh_3)Br]

Complex	Ni	Br	P	Net Allyl
Free PPh_3	NA	NA	0.82	NA
[ANi(PPh_3)Br]	- 0.08	- 0.40	1.17	0.03
[A^{2t}Ni(PPh_3)Br]	- 0.31	- 0.46	1.04	0.05
[A´Ni(PPh_3)Br]	- 0.07	- 0.40	1.18	0.02

[A^xNi(IMes)Br]

Complex	Ni	Br	C(carbene)	Net Allyl
Free Imes	NA	NA	0.14	NA
[ANi(Imes)Br]	0.07	- 0.43	0.34	0.02
[A^{2t}Ni(Imes)Br]	0.10	- 0.44	0.32	- 0.03
[A´Ni(IMesBr]	0.13	- 0.43	0.33	- 0.07

A3.5.2 Computational and experimental data regarding the reaction of [{A^{2t}NiBr}$_2$] with triphenylphosphine

Formation of [A^{2t}Ni(PPh_3)Br]

The ratio of the monomeric adduct and bromide bridged dimer at various temperatures was observed by variable temperature NMR in d_8-toluene solution. The apparent equilibrium constant for this reaction was then calculated at each temperature. For these purposes, the reaction has been formally written according to the following equation:

$$1\ [\{A^{2t}NiBr\}_2]\ +\ 2\ PPh_3 \rightarrow 2\ [A^{2t}Ni(PPh_3)Br]$$

This equation has an equilibrium constant with the following expression:

$$K = \frac{[[A^{2t}Ni(PPh_3)Br]]^2}{\left[[\{A^{2t}NiBr\}_2]\right] \times [PPh_3]^2}$$

Given that the ratio of [{NiBr(A^{2t})}$_2$] to free PPh_3 should remain at a constant value of 1 : 2 at all times, the equilibrium constant can then be written purely in terms of the two nickel complexes, yielding the following expression:

$$K = \frac{[[A^{2t}Ni(PPh_3)Br]]^2}{4 \times \left[[\{A^{2t}NiBr\}_2]\right]^3}$$

The NMR spectra have been calibrated to [A^{2t}Ni(PPh_3)Br] so that its concentration is always set to unity. Under this system, a single-term expression for the equilibrium constant is achieved, into which the apparent integration value for [{NiBr(A^{2t})}$_2$] in each expression can be inserted. The upfield doublet of [{NiBr(A^{2t})}$_2$] divided by four was used as its integration value in all cases. The calculated value of the equilibrium constant was then used to calculate the associated Gibbs free energy at each temperature.

Table A3.4: NMR ratio of [$A^{2t}Ni(PPh_3)Br$] to [$\{A^{2t}NiBr\}_2$]

Temp (K)	[$A^{2t}Ni(PPh_3)Br$] : [$\{A^{2t}NiBr\}_2$]	Calc. *K*	Calc. Δ*G* (kJ mol^{-1})
298	2.00	2.00	-1.72
288	2.38	3.37	-2.91
278	2.86	5.83	-4.08
268	3.44	10.3	-5.19
258	4.17	18.1	-6.21
253	4.35	20.5	-6.36

From the relationship ln K = $^{-\Delta H^\circ}/_{RT} + {}^{\Delta S^\circ}/_{R}$, a plot of $1/T$ vs ln K (at right) allows extraction of ΔH° = -33.25 kJ mol^{-1} and ΔS° = -105.3 J mol^{-1}

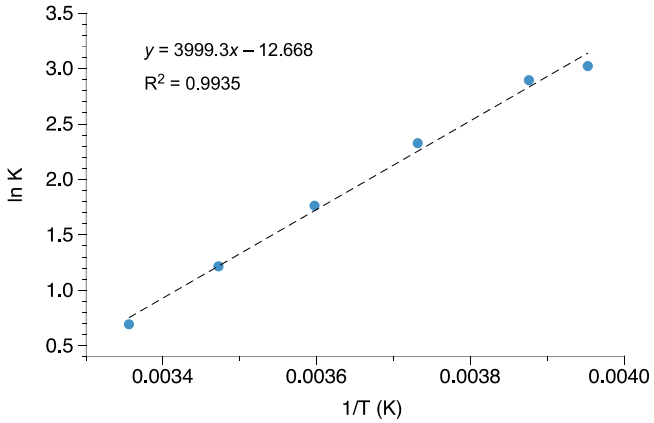

A3.6 References:

(1) Fraenkel, G.; Cabral, J.; Lanter, C.; Wang, J. Reorientation Dynamics within Ion-Paired Allylic Lithium Compounds: Isolation of Inversion Processes. *J. Org. Chem.* **1999**, *64* (4), 1302–1310. https://doi.org/10.1021/jo982196f.

(2) Rappoport, D.; Furche, F. Property-Optimized Gaussian Basis Sets for Molecular Response Calculations. *J. Chem. Phys.* **2010**, *133* (13). https://doi.org/10.1063/1.3484283.

Appendix 4: Supplemental Information for Chapter 4

A4.1 Materials

Methylmagnesium bromide (3.0 M solution in diethyl ether), Trimethylsilylmethyl lithium (1.0 M solution in pentane), sodium triethylborohydride (1.0 M solution in toluene), potassium t-butoxide, sodium methoxide, phenol, sodium ethanethiolate, diphenyl disulfide, allylmagnesium bromide (1.0 M solution in diethyl ether), pyrrole, imidazole, diphenylamine, potassium hexamethyldisilazide, aniline, thallium acetate, and bromine were purchased from Sigma-Aldrich and used as received. Nickel bis(cyclooctadiene), nickel acetylacetonate, and palladium bis(dibenzylideneacetone) were purchased from Strem and used as received. Potassium 1,3-bis(trimethylsilyl)allyl (K[A´]),[1] sodium cyclopentadienide,[2] potassium pentamethylcyclopentadienide,[3] potassium indenide,[4] potassium 4,7-dimethylindenide,[4] potassium fluorenide,[4] 1-bromo-1,3-di-*t*Bu-propene (BrA^{2t}),[5] and thallium hydroxide[6] were synthesized according to published procedures. Potassium diphenylamide and potassium pyrrolide were prepared by the reaction of the appropriate protonated molecule with KH in THF. Lithium thiophenolate was prepared by the reaction of diphenyl disulfide with lithium metal in THF. Potassium selenophenolate was prepared by the reaction of diphenyl diselenide with potassium metal in THF. Lithium imidazolate and lithium anilide were prepared by the reaction of the appropriate protonated molecule with *n*BuLi in THF. Potassium phenolate was prepared by the reaction of phenol with potassium *t*-butoxide in a mixture of THF and diethylether, followed by prolonged vacuum drying at 75° C, followed by repeated washing of the precipitate with toluene.

A4.2 Crystallographic details

A4.2.1 Crystallographic determinations

Prof. William Brennessel (Univ. of Rochester) performed the data collection and structure solution for [A^{2t}NiFluor]; Prof. Nathan Schley (Vanderbilt Univ.) did the same for all other compounds.

A4.2.2 Collected crystallographic data

Table A4.1 Experimental X-ray diffraction parameters and crystal data for [A^{2t}NiCp], [A^{2t}NiInd^{2Me}], and [A^{2t}NiFluor]

	[A^{2t}NiCp] (26)	**[A^{2t}NiCp*] (27)**	**[A^{2t}NiInd^{2Me}] (28)**	**[A^{2t}NiFluor] (29)**
Empirical formula	C16 H26 Ni	C21 H36 Ni	C22 H32 Ni	C24 H30 Ni
Formula weight	277.08	347.21	355.18	377.19
Temperature (K)	100	100	100	100
Wavelength	1.54184	1.54184	1.54184	1.54184
Crystal system	Monoclinic	Orthorhombic	Monoclinic	Monoclinic
Space group	P 1 21/n 1	P n m a	P 1 21/c 1	P 1 n 1
Unit cell dimensions	5.85970(10)	10.92980(10)	10.6039(6)	12.15207(14)
	14.2819(2)	17.3104(2)	17.9193(4)	17.06092(13)
	18.0836(3)	10.48770(10)	11.2921(4)	19.99914(19)
	90	90	90	90
	98.230(2)	90	113.730(6)	107.4267(11)
	90	90	90	90
Volume	1497.79(4)	1984.26(3)	1964.25(16)	3956.02(7)
Z	4	4	4	8
Density (calculated) (g/cm^3)	1.229	1.162	1.201	1.267
Absorption coefficient	1.660	1.345	1.376	1.403
$F(000)$	600	760	768	1616
Crystal size (mm)	0.18 x 0.05 x 0.02	0.21 x 0.16 x 0.07	0.215 x 0.127 x 0.018	0.283 x 0.135 x 0.037
Crystal color, habit	Violet block	Green plate	Yellow plate	Orange-red needle
Theta range for data collection	4.9370 to 71.3190°	4.9110 to 71.5710°	4.5540 to 71.5850°	3.4760 to 78.7760°
Index ranges	$-6 \le h \le 7$, $-17 \le k \le 16$, $-22 \le l \le 21$	$-13 \le h \le 13$, $-16 \le k \le 21$, $-12 \le l \le 12$	$-13 \le h \le 12$, $-21 \le k \le 21$, $-13 \le l \le 13$	$-13 \le h \le 15$, $-21 \le k \le 21$, $-25 \le l \le 25$
Reflections collected	2883	1992	6349	16344
Independent reflections	8521	10140	6349	132760
Absorption correction	Gaussian	Gaussian	Gaussian	Multi-scan
Max. and min. transmission	0.968 and 0.754	1.000 and 0.701	10000000.000 and -0.010	0.950 and 0.692
Refinement method	Full-matrix least-squares on F^2	Full-matrix least-squares on F^2	Full-matrix least-squares on F^2	Full-matrix least-squares on F^2
Data / restraints / parameters	2883 /	1992 / 0 / 119	6349 / 0 / 217	16344 / 2 / 928
Goodness-of-fit on F^2	1.051	1.041	0.905	1.060
Final R indices [I>2sigma(I)]	R_1 = 0.0285 wR_2 = 0.0680	R_1 = 0.0269 wR_2 = 0.0705	R_1 = 0.0406 wR_2 = 0.0970	R_1 = 0.0493 wR_2 = 0.1243
R indices (all data)	R_1 = 0.0360 wR_2 = 0.0720	R_1 = 0.0283 wR_2 = 0.0716	R_1 = 0.0565 wR_2 = 0.1012	R_1 = 0.0505 wR_2 = 0.1261
Largest diff. peak and hole	0.363 and -0.238 e $Å^{-3}$	0.318 and -0.280 e $Å^{-3}$	0.846 and -0.384 e $Å^{-3}$	1.323 and -0.749 e $Å^{-3}$

Refinement notes: *[A^{2t}NiCp]:* Disorder in the Cp ring was modeled over two positions without restraint. The three allyl hydrogen atoms were located in the difference map and refined without restraint.

[A^{2t}NiCp]:* The allylic hydrogen atoms were located in the difference map and refined without restraint.

Table A4.2: Experimental X-ray diffraction parameters and crystal data for [{A^{2t}NiOAc}$_2$], [{A^{2t}NiOH}$_2$], [{A^{2t}NiOPh}$_2$], and [{A^{2t}NiSPh}$_2$]

	[{A^{2t}NiOAc}$_2$]	**[{A^{2t}NiOH}$_2$]**	**[{A^{2t}NiOPh}$_2$]**	**[{A^{2t}NiSPh}$_2$]**
Empirical formula	C26 H48 Ni2 O4	C22 H44 Ni2 O2	C34 H52 Ni2 O2	C34 H52 Ni2 S2
Formula weight	542.06	457.99	610.17	642.29
Temperature (K)	100	100	100	100
Wavelength (Å)	1.54184	1.54184	1.54184	1.54184
Crystal system	Triclinic	Monoclinic	Monoclinic	Triclinic
Space group	P -1	I2/a	P 1 21/n 1	P -1
Unit cell dimensions	9.4075(2)	10.4436(1)	12.2954(4)	10.1083(4)
	11.3455(2)	21.7024(3)	18.7734(7)	11.8930(4)
	14.6821(3)	10.7031(1)	14.0912(4)	16.6010(5)
	74.575(2)	90	90	106.731(3)
	82.977(2)	102.098(1)	92.726(3)	94.443(3)
	69.286(2)	90	90	114.443(3)
Volume	1412.27(5)	2371.99(5)	3248.95(19)	1695.14(11)
Z	2	4	4	2
Density (calculated)	1.275	1.282	1.247	1.258
Absorption coefficient	1.856	2.046	1.627	2.661
F(000)	584	992.0	1312	688
Crystal size (mm^3)	0.22 x 0.20 x 0.12	0.35 x 0.12 x 0.05	0.11 x 0.07 x 0.05	0.25 x 0.16 x 0.03
Crystal color, habit	Orange block	Orange block	Orange block	Orange Plate
Theta range for data collection	3.1110 to 71.6600°	4.0630 to 71.5960°	3.8910 to 71.5000°	2.853 to 71.680°
Index ranges	$-11 \le h \le 11$, $-13 \le k \le 12$, $-17 \le l \le 18$	$-12 \le h \le 12$, $-26 \le k \le 25$, $-13 \le l \le 13$	$-14 \le h \le 14$, $-23 \le k \le 17$, $-15 \le l \le 17$	$-12 \le h \le 12$, $-14 \le k \le 14$, $-20 \le l \le 16$
Reflections collected	5445	2306	6204	6563
Independent reflections	21156	10286	17350	5612
Absorption correction	Gaussian	Gaussian	Gaussian	Gaussian
Max. and min. transmission	1.000 and 0.642	1.000 and 0.418	1.000 and 0.845	1.000 and 0.521
Refinement method	Full-matrix least-squares on F^2	Full-matrix least-squares on F^2	Full-matrix least-squares on F^2	Full-matrix least-squares on F^2
Data / restraints / parameters	5445 / 0 / 327	2306 / 2 / 153	6204 / 1884 / 699	6563 / 15 / 379
Goodness-of-fit on F^2	1.058	1.036	1.083	1.035
Final R indices [*I*>2sigma(I)]	R_1 = 0.0237 wR_2 = 0.0617	R_1 = 0.0214 wR_2 = 0.0596	R_1 = 0.0790 wR_2 = 0.2018	R_1 = 0.0532 wR_2 = 0.1396
R indices (all data)	R_1 = 0.0247 wR_2 = 0.0623	R_1 = 0.0222 wR_2 = 0.0602	R_1 = 0.0970 wR_2 = 0.2157	R_1 = 0.0622 wR_2 = 0.1486
Largest diff. peak and hole	0.306 and -0.246 e Å^{-3}	0.282 and -0.205 e Å^{-3}	1.808 and -0.601 e Å^{-3}	0.974 and -0.778 e Å^{-3}

Refinement notes:

[{A^{2t}NiSPh}$_2$]: The allyl hydrogen atoms were located in the difference map and refined with similarity restraints placed on their C-H bond distances. Their atomic thermal parameters were refined freely.

[{A^{2t}NiOH}$_2$]: Disorder in the hydroxyl groups was modeled over two positions. Vinylic hydrogen atoms bound to the allyl moiety were located in the difference map and refined with isotropic thermal parameters without restraint. Hydrogen atoms on the hydroxyl group were refined with isotropic thermal parameters and a weak distance restraint on the O-H bond length.

[{A^{2t}NiOAc}$_2$]: Vinylic hydrogen atoms were located in the difference map and refined without restraint.

[{A^{2t}NiOPh}$_2$]: Whole molecule disorder was identified by the observation of difference density matching the same shame and dimensions of the Ni_2O_2 butterfly core in a second position. The final refined model fit was modeled over two positions with the major site being 92.7(2)% occupied. Similarity restraints were applied to relevant atom pairs to aid refinement of the minor component. Hydrogen atoms were added at idealized positions.

A4.3 Collected Computational Results

A4.3.1 Computational method details

For calculations on [A^{2t}NiCp], the def2-TZVPD basis set was used on all atoms. For all other calculations, the def2-SVP basis set was used on first and second row elements, while def2-TZVP was used for all other atoms.

A4.3.2 Collected computational results

Table A4.3: Computed energies of different isomers of bis(allyl)nickel complexes

Entry Number	Relative Allyl Direction	A^{2t} Substituents	A´ Substituents	*Cis/trans*	Relative Energy (kJ/mol)
1	Staggered	*Syn,Syn*	*Syn,Syn*	NR	19.39
2			*Syn,Anti*	NR	0.00
3			*Anti,Anti*	NR	35.35
4		*Syn,Anti*	*Syn,Syn*	NR	17.18
5			*Syn,Anti*	*cis*	0.29
6				*trans*	14.92
7	Eclipsed	*Syn,Syn*	*Syn,Syn*	NR	30.08
8			*Syn,Anti*	NR	2.83
9		*Syn,Anti*	*Syn,Anti*	*trans*	8.01

Table A4.4: Computed energies of different isomers of [{A^{2t}NiSPh}$_2$]. Some isomers were converted to other isomers in the process of geometry optimization. In these cases, the resulting isomer is referred to by a bracketed entry number in the relative energy column; the relative energy of the resultant isomer is assumed to be a lower bound of the energy of the original isomer.

Entry Number	Allyl 1 relative to S-Ni-S angle	Allyl 2 relative to allyl 1	Allyl 1 left *t*Bu[a]	Allyl 1 right *t*Bu	Allyl 2 left *t*Bu	Allyl 2 right *t*Bu	Left S-Phenyl orientation	Right S-Phenyl orientation	Relative Energy (kJ/mol)
1	*Syn*	Eclipsed	*syn*	*syn*	*syn*	*syn*	*exo*	*exo*	0
2							*exo*	*endo*	[12]
3			*syn*	*anti*	*syn*	*anti*	*exo*	*exo*	31.52
4							*exo*	*endo*	14.30
5					*anti*	*syn*	*exo*	*exo*	[14][b]
6							*endo*	*exo*	[13]
7							*endo*	*endo*	[14]
8		Staggered	*syn*	*syn*	*syn*	*syn*	*endo*	*endo*	8.39
9							*endo*	*exo*	17.87
10				*anti*	*syn*	*anti*	*exo*	*endo*	38.59
11					*anti*	*syn*	*exo*	*endo*	22.38
12	*Anti*	Eclipsed	*syn*	*syn*	*syn*	*syn*	*exo*	*endo*	9.72
13			*syn*	*anti*	*anti*	*syn*	*endo*	*exo*	37.02
14	Flat	Eclipsed	*syn*	*anti*	*anti*	*syn*	[c]	[c]	42.58

[a]) The initial choice of "left" is arbitrary and merely serves as a convenient way to specify the position of different substituents relative to a bisector of the {NiS}$_2$ core that passes through both nickel atoms. [b]) This calculation was re-attempted from the same initial coordinates without initial geometry optimization at the semi-empirical/PM6 level of theory, which tended to output planar structures. The resulting computation did optimize to a local minimum with a relative energy of 740.21 kJ/mol. The impact of this difference in procedure is not known, though, so this result was omitted from the above compilation. [c]) The phenyl rings in this complex were found to be *cis-opp*.

A4.4 Formal definition of *endo and exo* substituents in bridged allylnickel complexes.

Let E-R be a vector beginning at a bridging atom E and ending at the *ipso* atom of a given substituent R that is bonded to E. Let E-Ni_n be the sum of the two vectors beginning at E and ending at each of the two directly bonded nickel atoms. Further, let M be the plane defined by E and the two nickel atoms to which it is directly bound. Further, let L be the line lying within M, passing through E, and bisecting the Ni-E-Ni

angle. Further, let P_R and P_{Ni} be the projections of E-R and E-Ni_n, respectively, onto L. Finally, let θ be the angle between P_R and P_{Ni}. For each R, if θ is 0°, then R is *endo*, while if θ is 180°, then R is *exo*.

A4.5 NMR spectra

Figure A4.1: ^{1}H NMR (400 MHz) of material collected from reaction of [{A^{2t}NiBr}$_2$] with MeLi in THF taken in C_6D_6. Picked and integrated peaks belong to [{A^{2t}NiBr}$_2$].

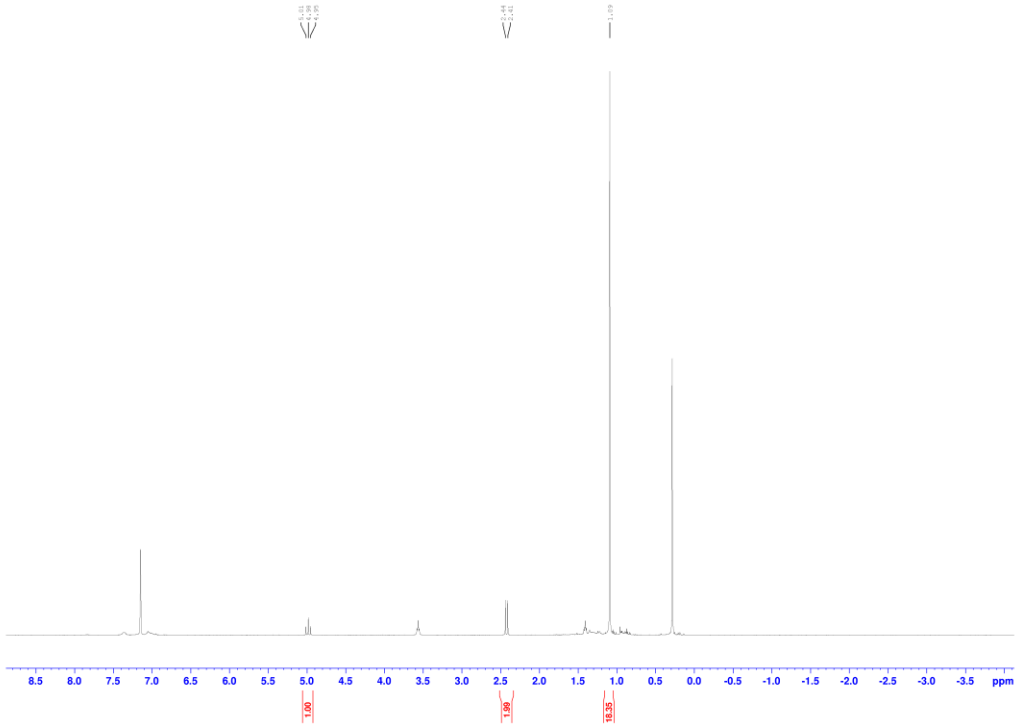

Figure A4.2: ^{1}H NMR (400 MHz) of material collected from reaction of [{A^{2t}NiBr}$_2$] with MeLi in hexane/THF taken in C_6D_6.

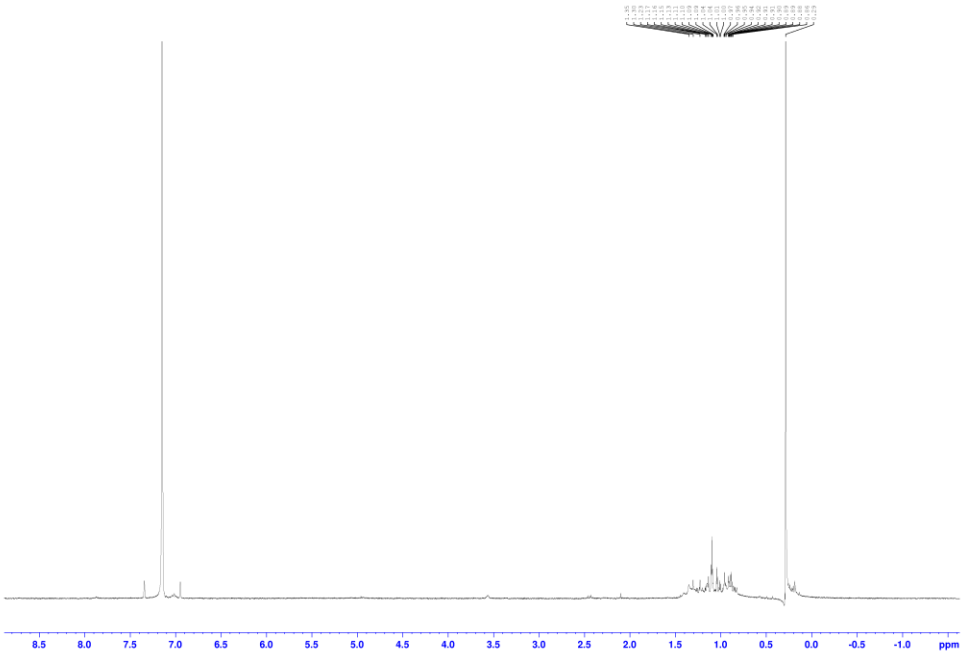

Figure A4.3: ^{1}H NMR (600 MHz) of [A^{2t}NiA´] in C_6D_6

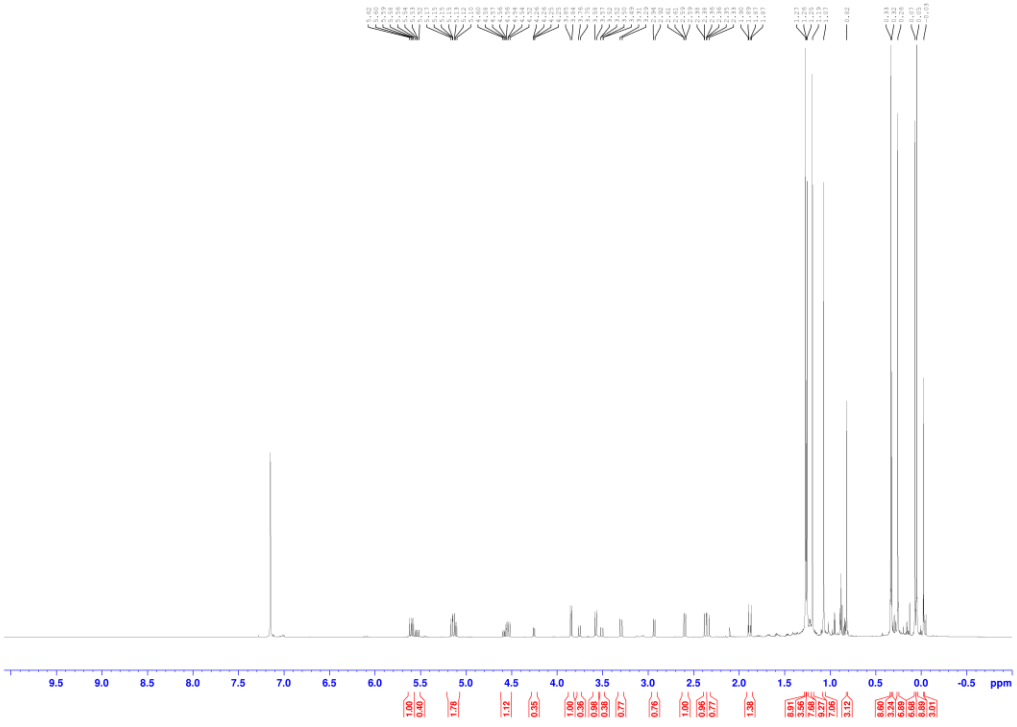

Figure A4.4: $^{13}C\{^{1}H\}$ NMR (151 MHz) of $[A^{2t}NiA']$ in C_6D_6

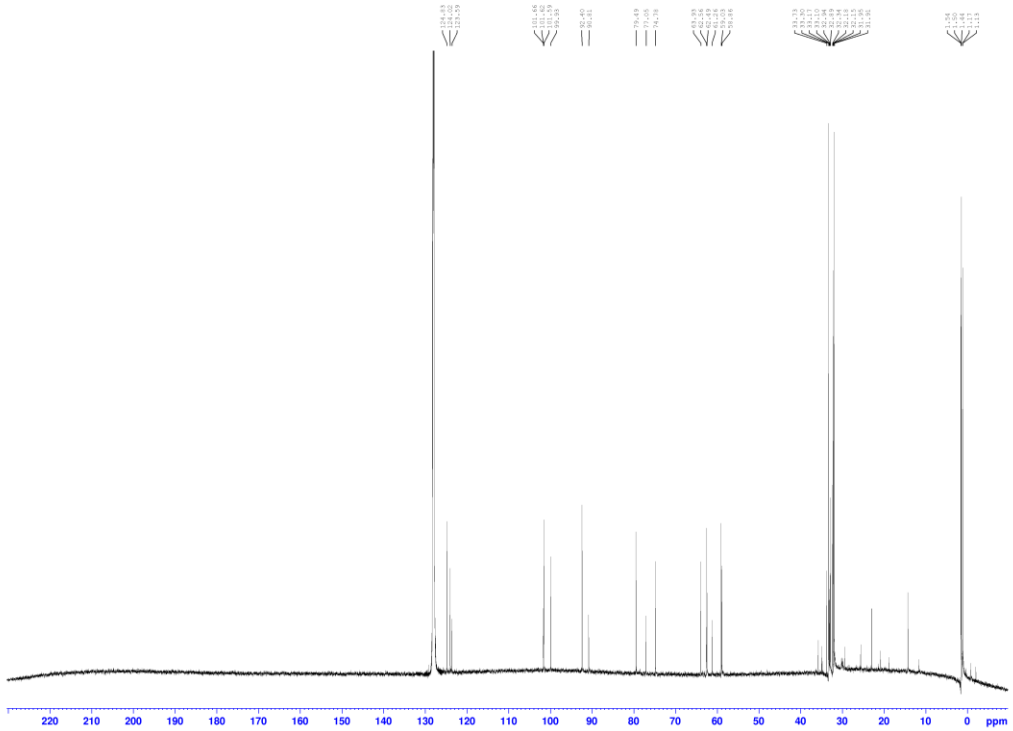

Figure A4.5: ^{1}H-^{13}C HSQC NMR (600-151 MHz) of $[A^{2t}NiA']$ in C_6D_6.

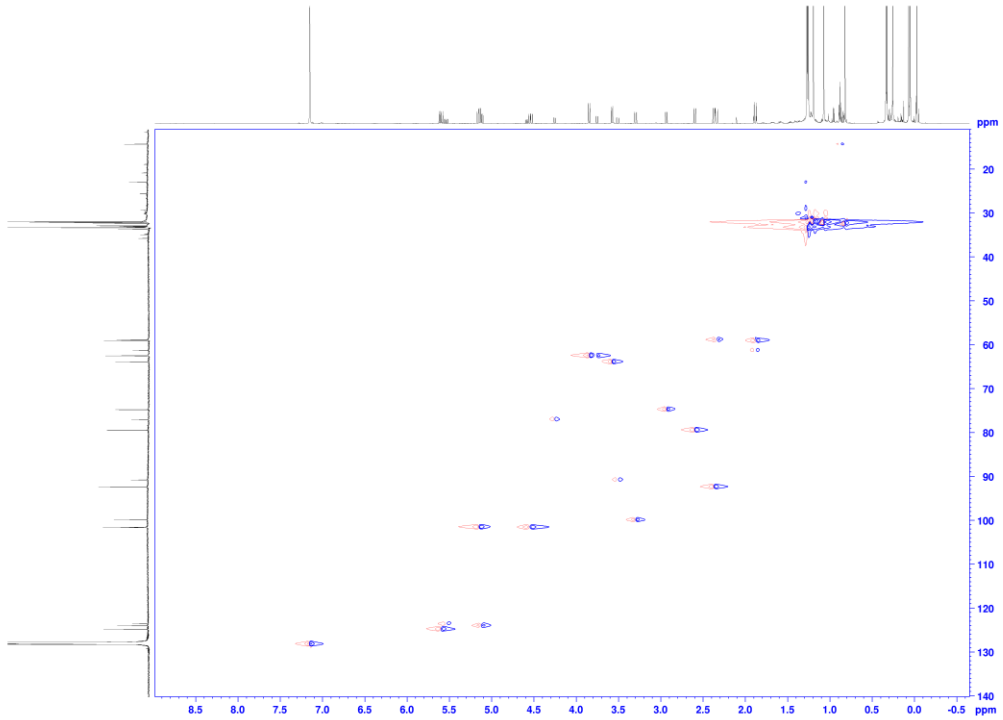

Figure A4.6: ^{1}H NMR (400 MHz) of material collected from reaction of [{$A^{2t}NiBr$}$_2$] with Allylmagnesium bromide, taken in C_6D_6

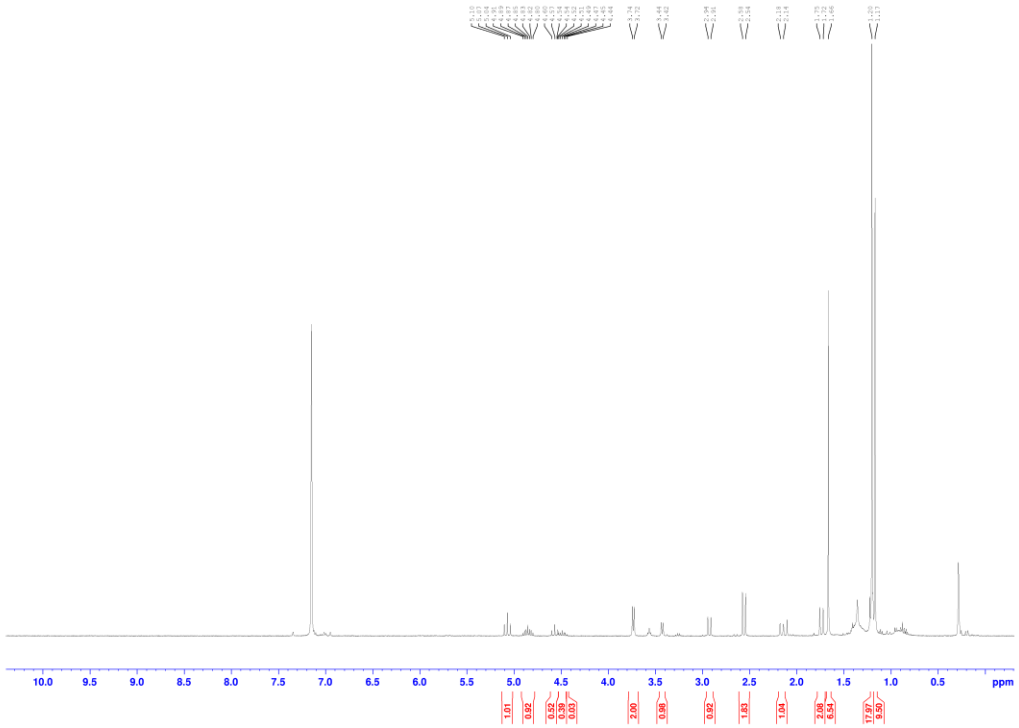

Figure A4.7: ^{1}H-^{1}H COSY NMR (400 MHz) of material collected from reaction of [{$A^{2t}NiBr$}$_2$] with Allylmagnesium bromide, taken in C_6D_6

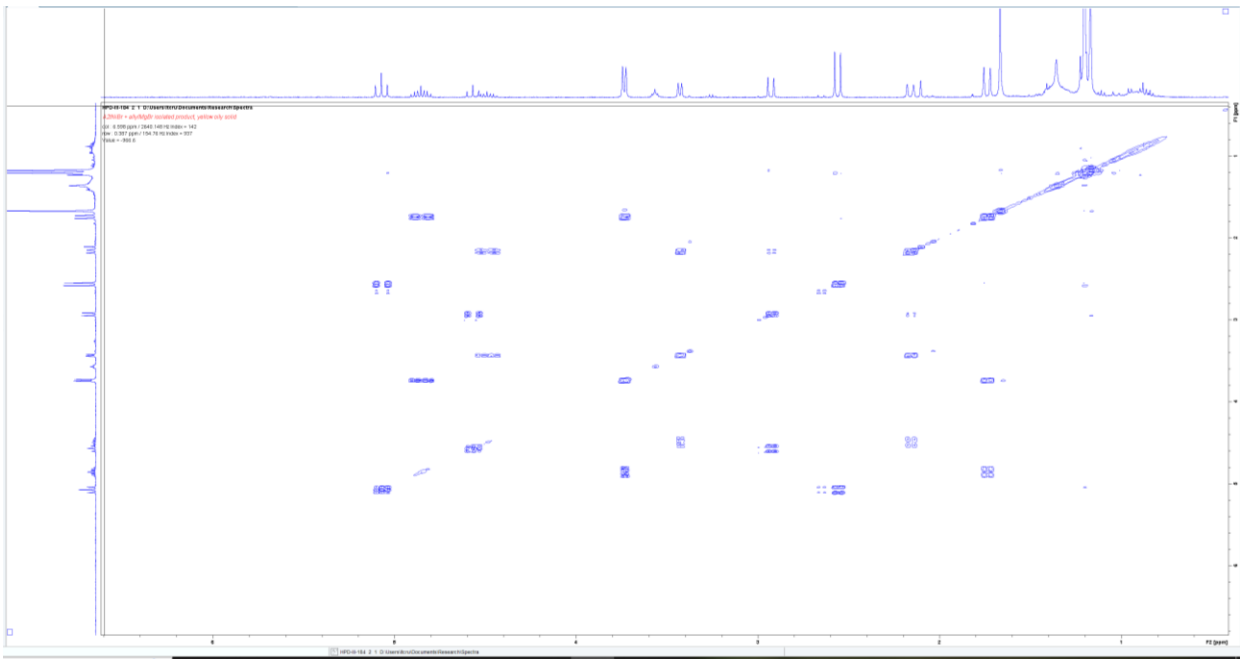

Figure A4.8: ^{1}H NMR (600 MHz) of material collected from reaction of [{A^{2t}NiBr}$_2$] with [K(CH$_2$C$_6$H$_5$)] in C_6D_6

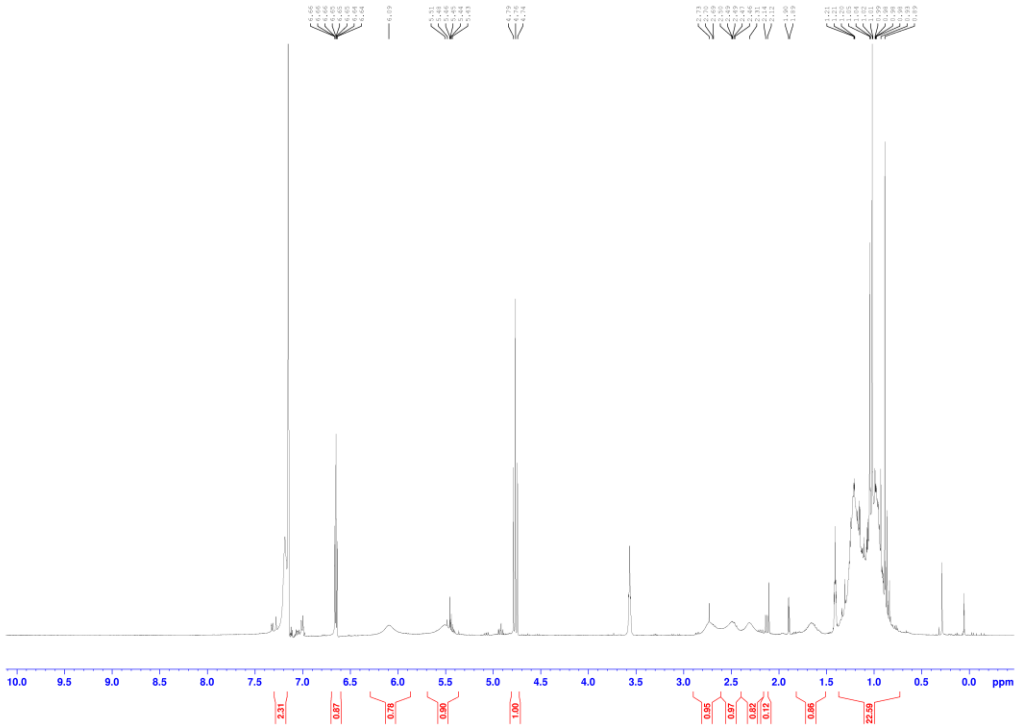

Figure A4.9: ^{1}H NMR (400 MHz) of [A^{2t}NiCp] in C_6D_6

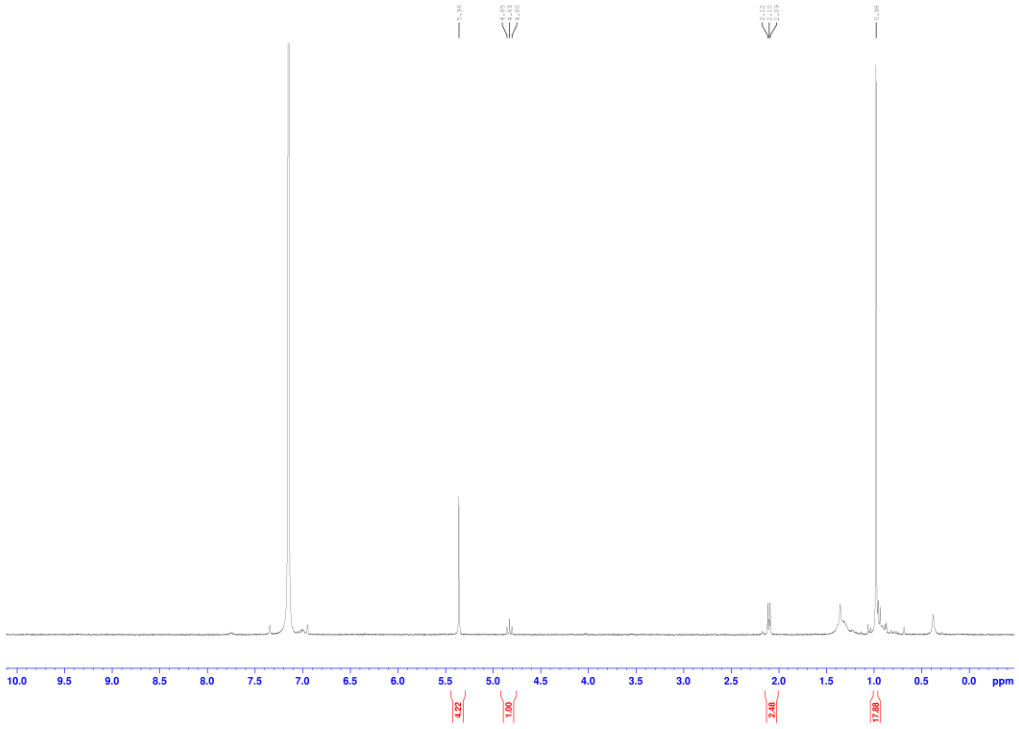

Figure A4.10: $^{13}C\{^{1}H\}$ NMR (101 MHz) of [A^{2t}NiCp] in C_6D_6

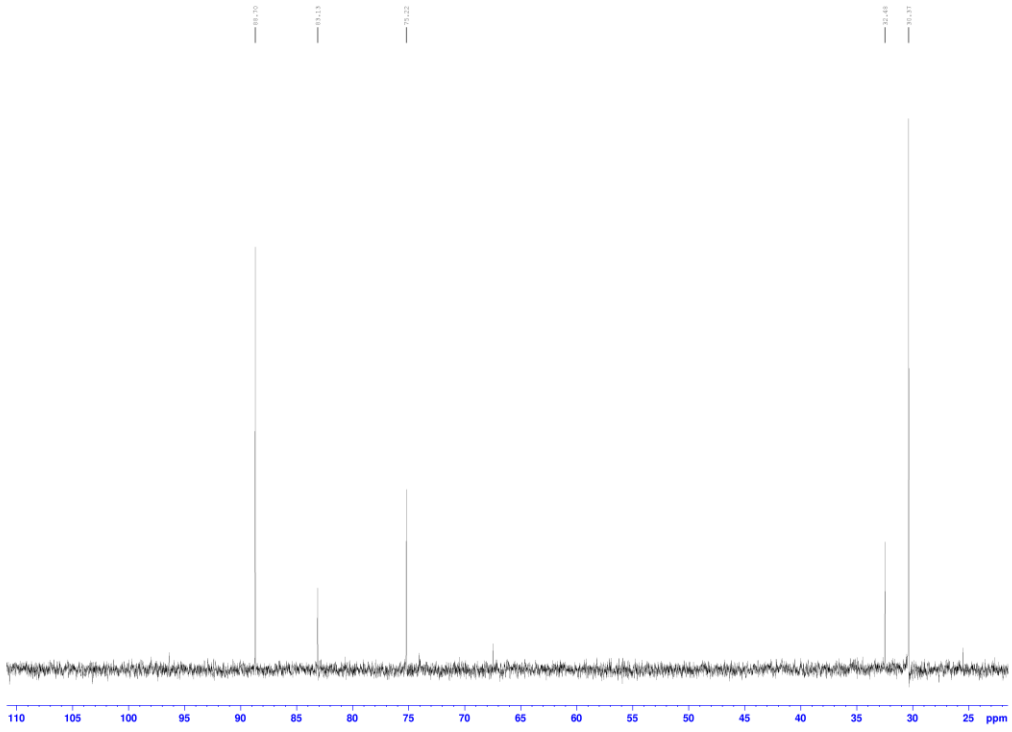

Figure A4.11: ^{1}H NMR (400 MHz) of [A^{2t}NiCp*] in C_6D_6

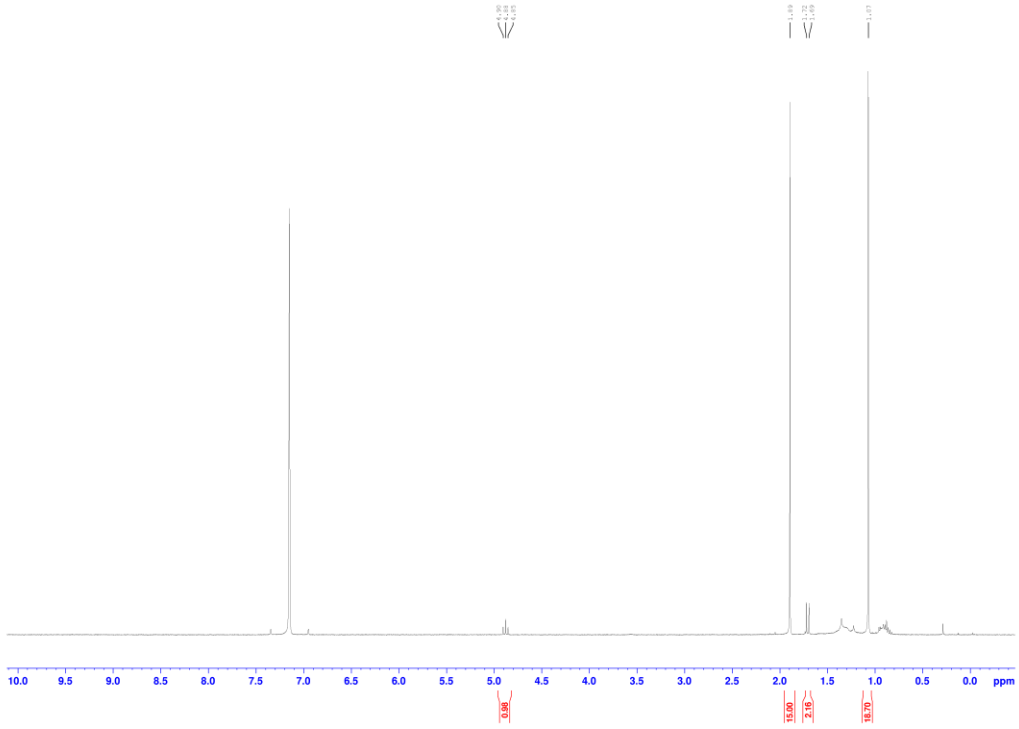

Figure A4.12: $^{13}C\{^{1}H\}$ NMR (101 MHz) of [A^{2t}NiCp*] in C_6D_6

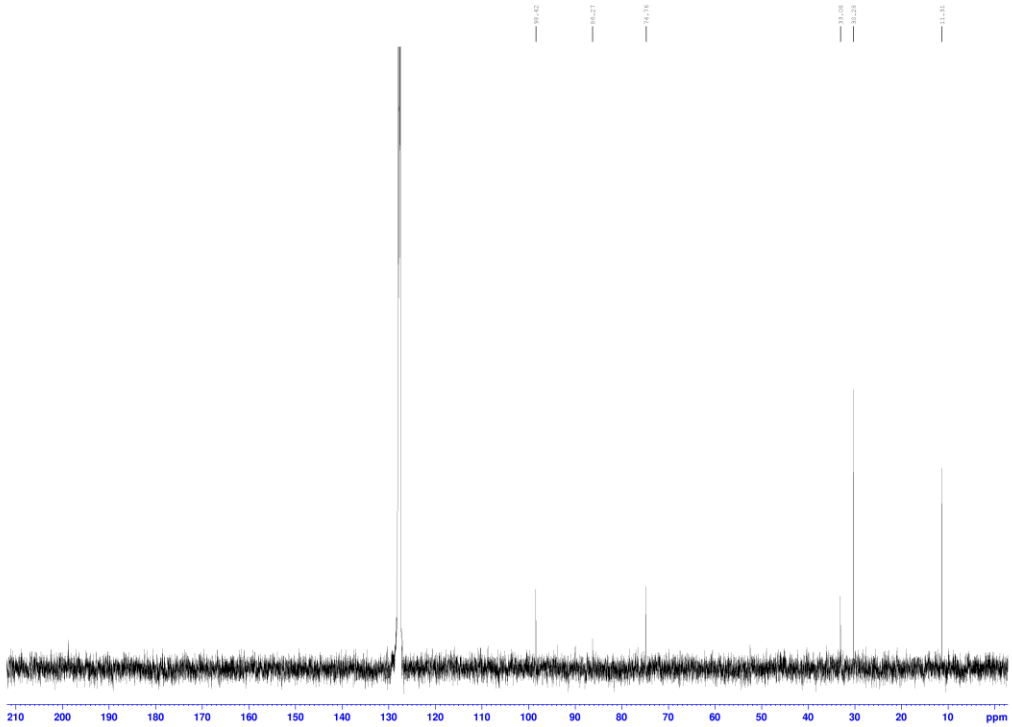

Figure A4.13: ^{1}H NMR (400 MHz) of [A^{2t}NiInd] in C_6D_6

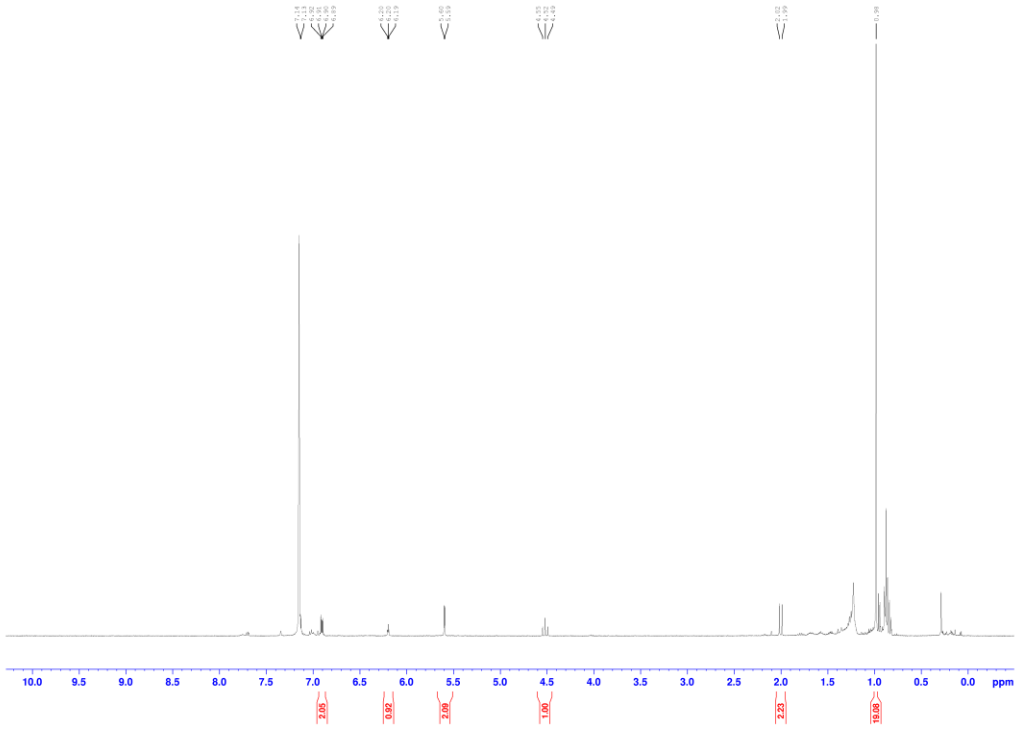

Figure A4.14: $^{13}C\{^{1}H\}$ NMR (151 MHz) of [A^{2t}NiInd] in C_6D_6

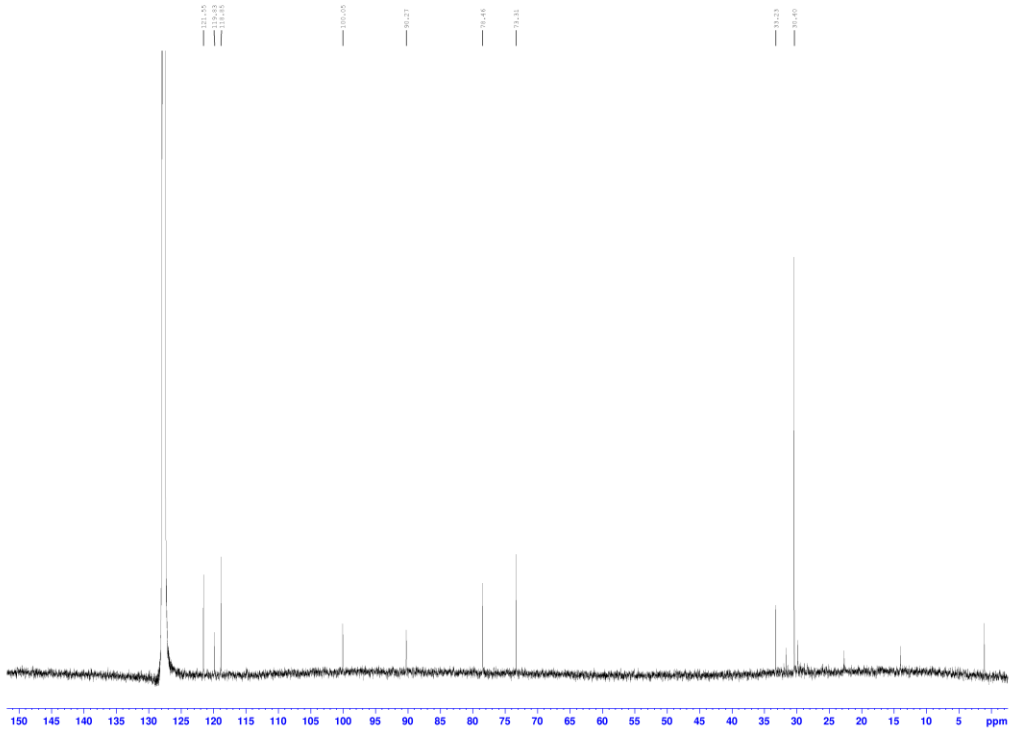

Figure A4.15: ^{1}H-^{13}C HSQC NMR (600-151 MHz) of [A^{2t}NiInd] in C_6D_6.

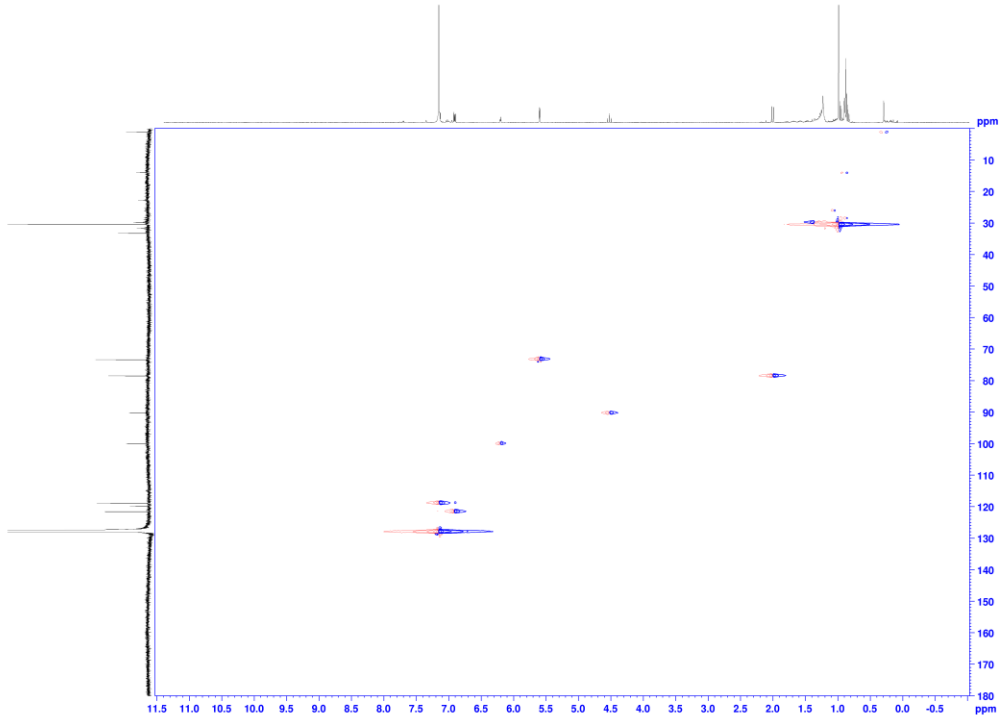

Figure A4.16: ^{1}H NMR (400 MHz) of [$A^{2t}NiInd^{2Me}$] in C_6D_6

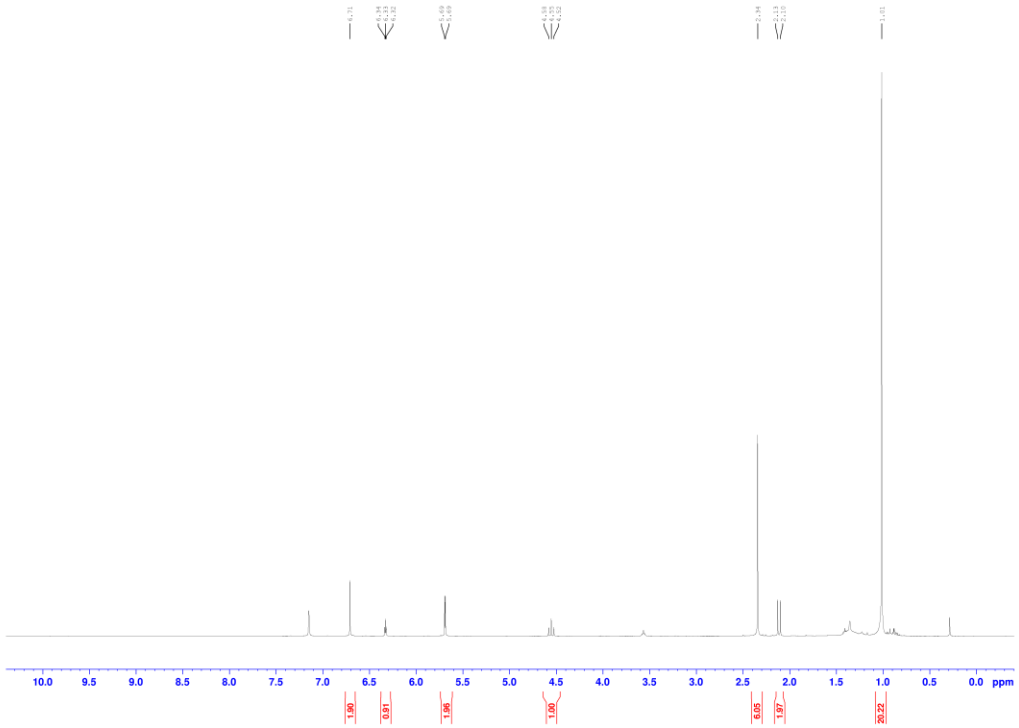

Figure A4.17: $^{13}C\{^{1}H\}$ NMR (101 MHz) of [$A^{2t}NiInd^{2Me}$] in C_6D_6

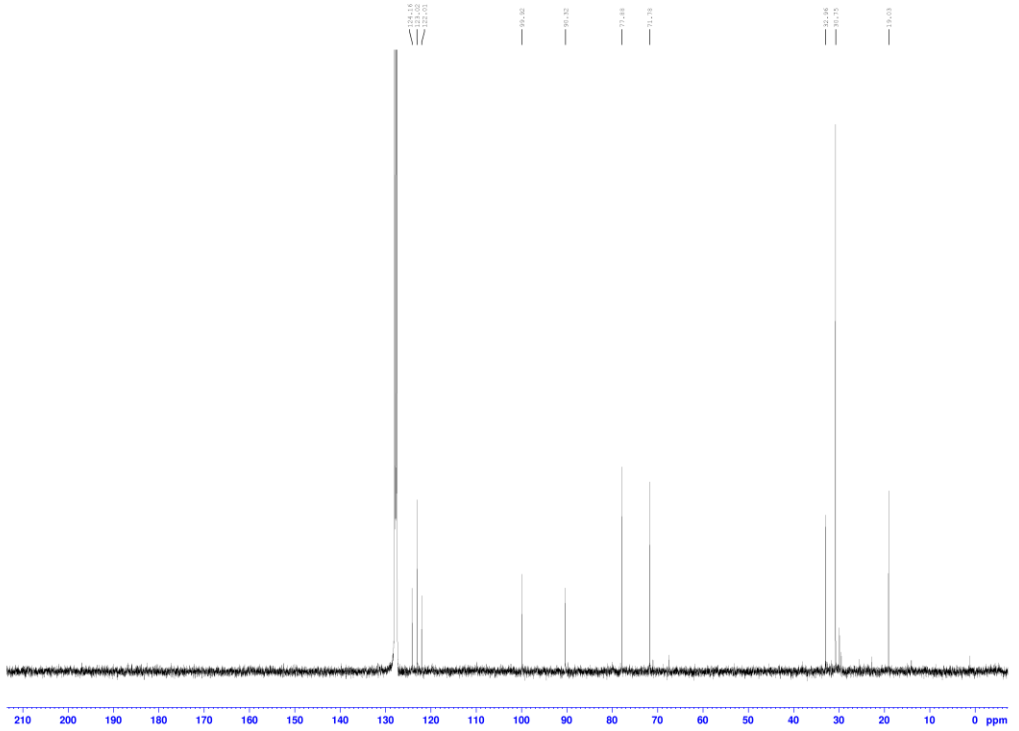

Figure A4.18: ^{1}H NMR (400 MHz) of [A^{2t}NiFluor] taken in C_6D_6

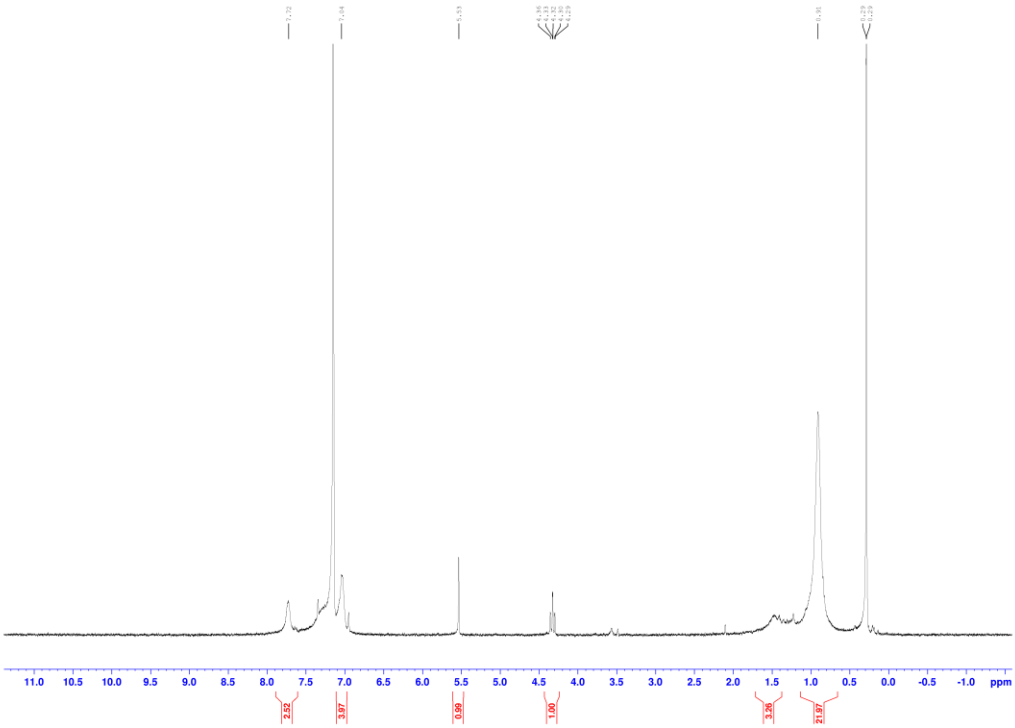

Figure A4.19: ^{1}H NMR (400 MHz) of [A^{2t}NiFluor] taken in d_4-THF

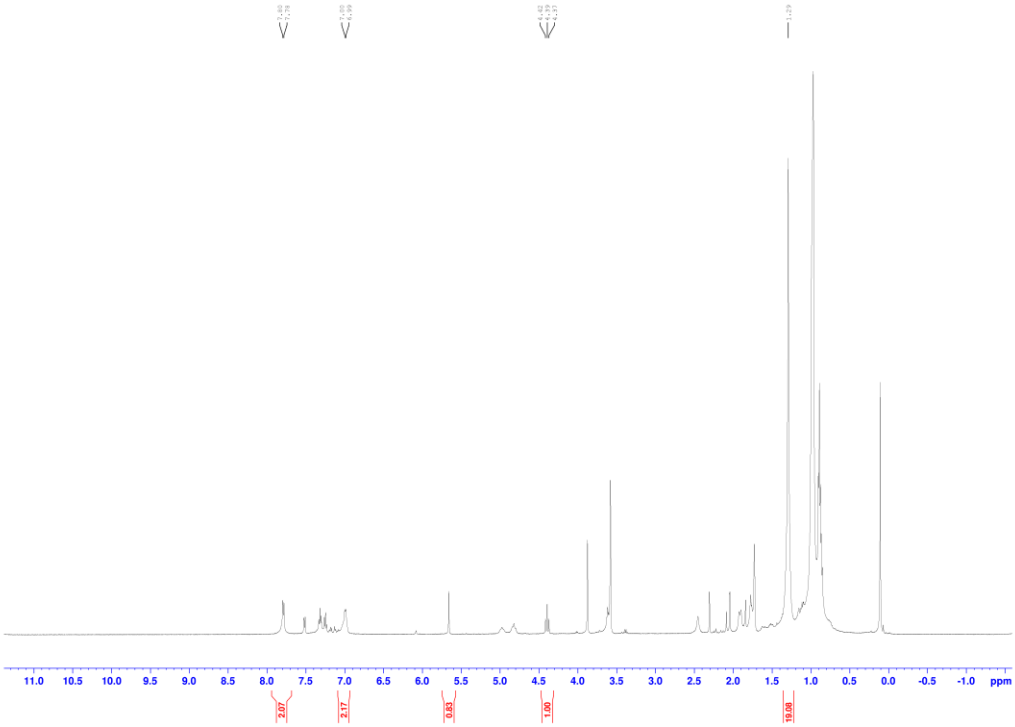

Figure A4.20: ^{1}H NMR (600 MHz) of [A^{2t}NiFluor] after four days of storage in the glovebox, taken in C_6D_6. The center allyl C-H of [A^{2t}NiFluor] is marked F. Peaks due to [{A^{2t}NiOH}$_2$] are marked H. The C9 peak of HFluor is marked P.

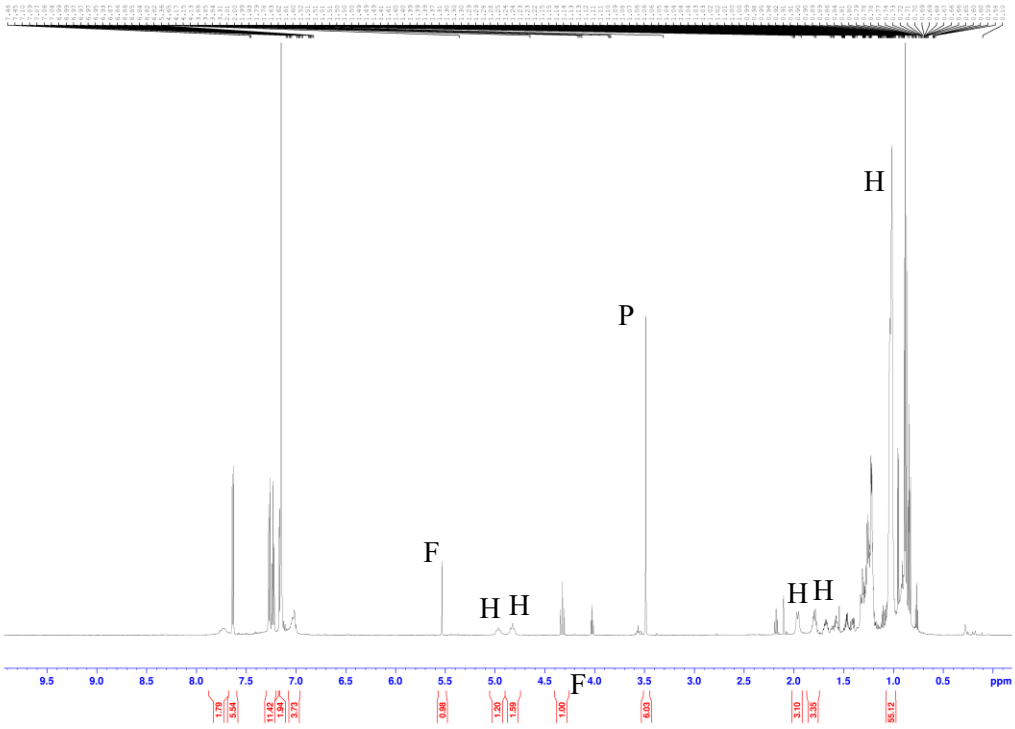

Figure A4.21: ^{1}H-^{13}C HSQC NMR (600-151 MHz) of [A^{2t}NiFluor] after four days of storage in the glovebox, taken in C_6D_6. Crosspeaks attributable to [A^{2t}NiFluor] are marked F. Crosspeaks due to [{A^{2t}NiOH}$_2$] are marked H.

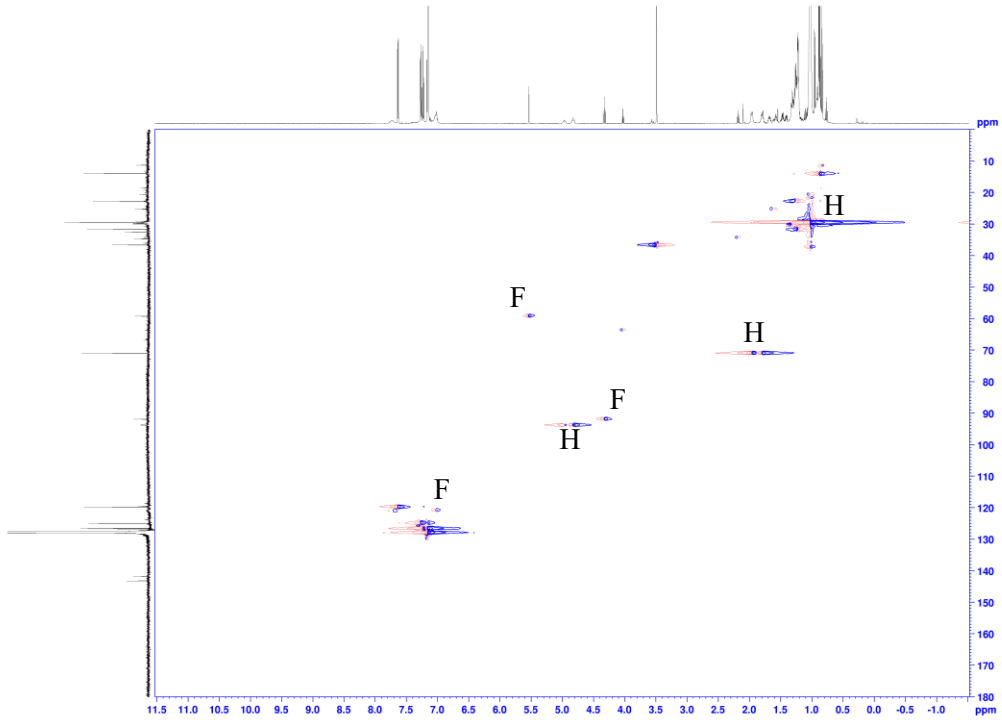

Figure A4.22: ^{1}H NMR (600 MHz) of material collected from reaction of [{A^{2t}NiBr}$_2$] with [LiIm] taken in C_6D_6

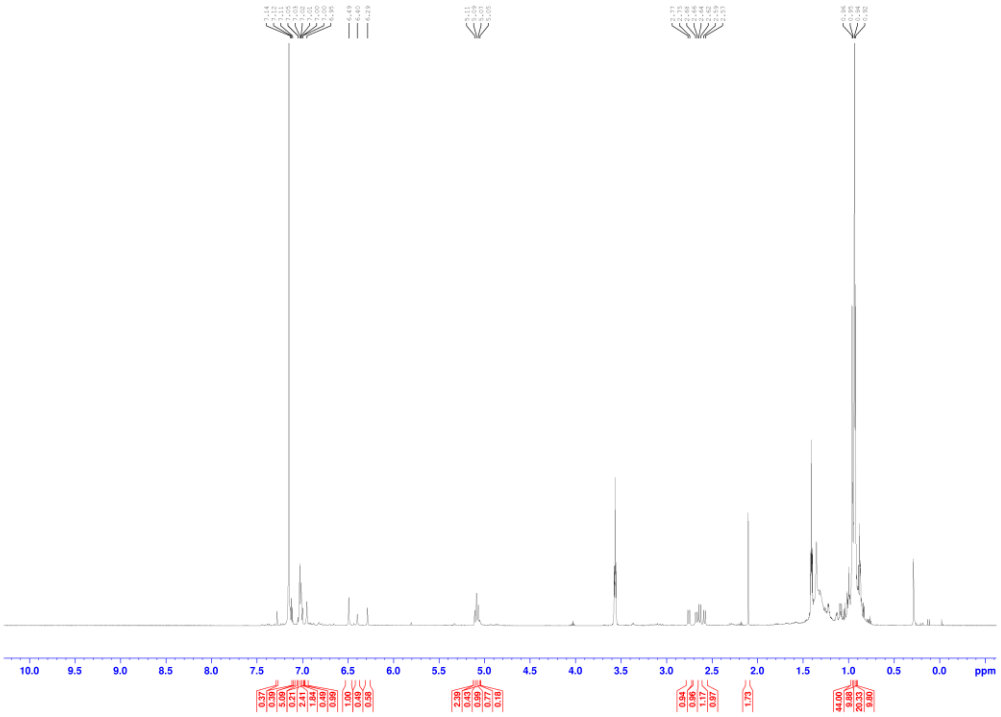

Figure A4.23: ^{1}H-^{1}H COSY NMR (600 MHz) of material collected from reaction of [{A^{2t}NiBr}$_2$] with [LiIm] in C_6D_6

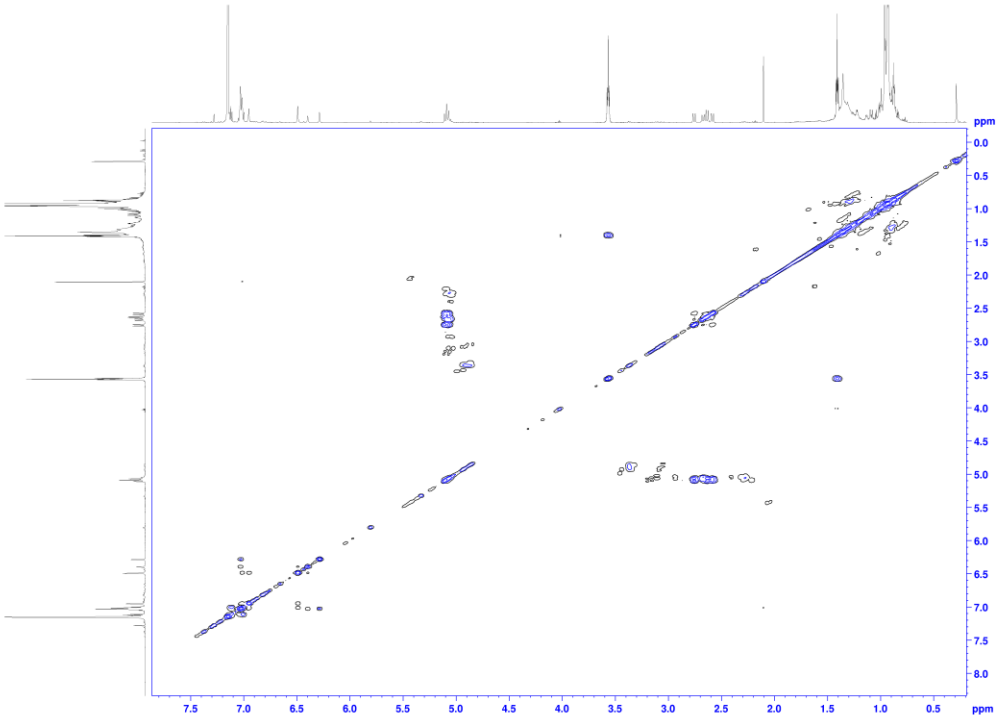

Figure A4.24: $^{13}C\{^{1}H\}$ NMR (151 MHz) of material collected from reaction of $[\{A^{2t}NiBr\}_2]$ with [LiIm] taken in C_6D_6

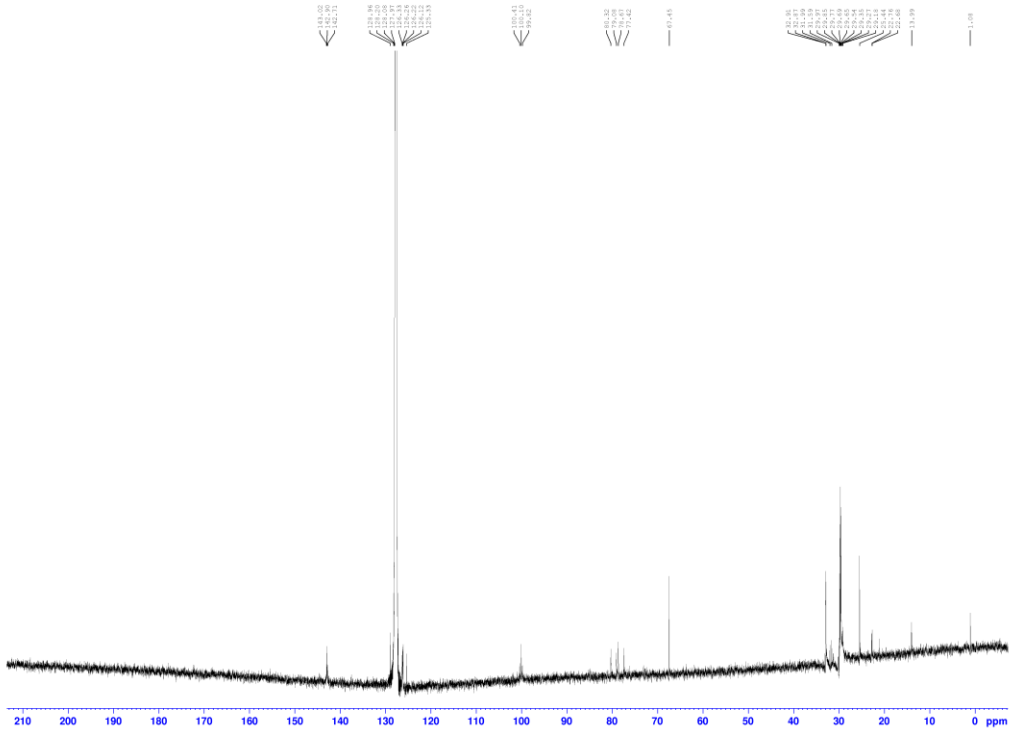

Figure A4.25: ^{1}H-^{13}C HSQC NMR (600-151 MHz) of material collected from reaction of $[\{A^{2t}NiBr\}_2]$ with [LiIm] taken in C_6D_6.

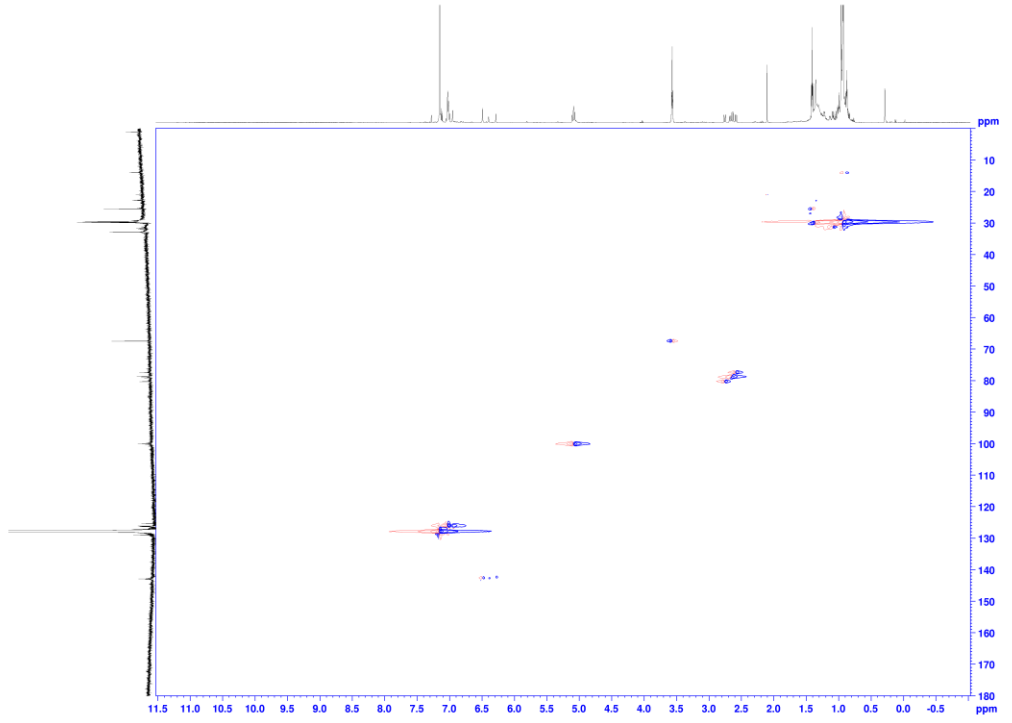

Figure A4.26: ^{1}H NMR (600 MHz) of $[\{A^{2t}NiOAc\}_2]$ taken in C_6D_6

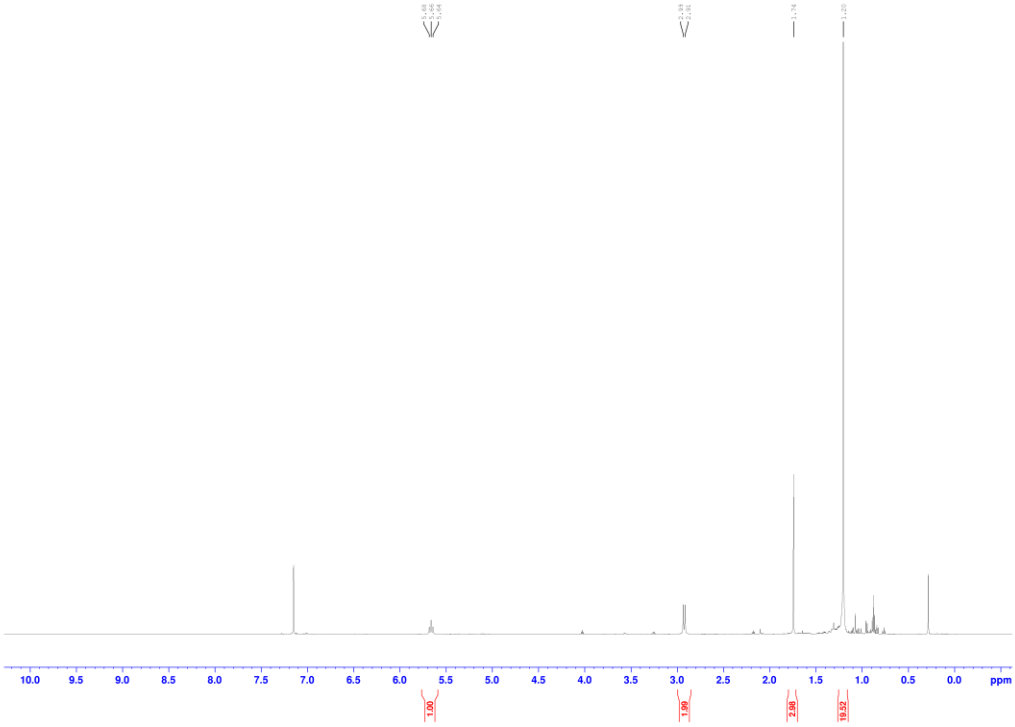

Figure A4.27: $^{13}C\{^{1}H\}$ NMR (151 MHz) of $[\{A^{2t}NiOAc\}_2]$ taken in C_6D_6

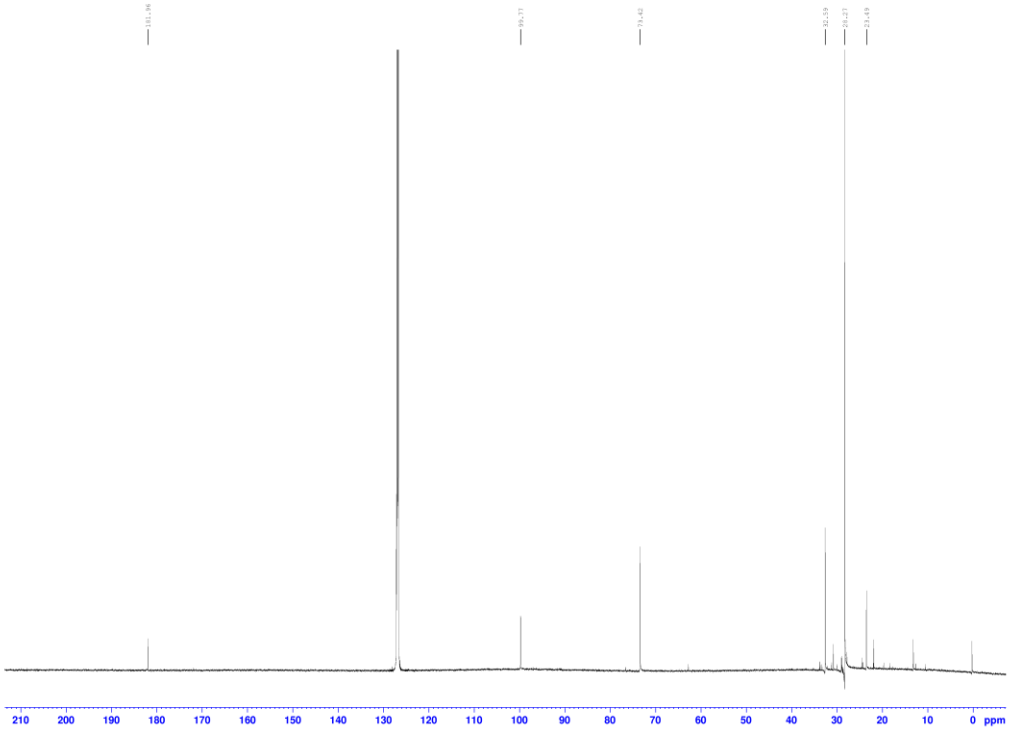

Figure A4.28: ^{1}H-^{13}C HSQC NMR (600-151 MHz) of [{$A^{2t}NiOAc$}$_2$] taken in C_6D_6

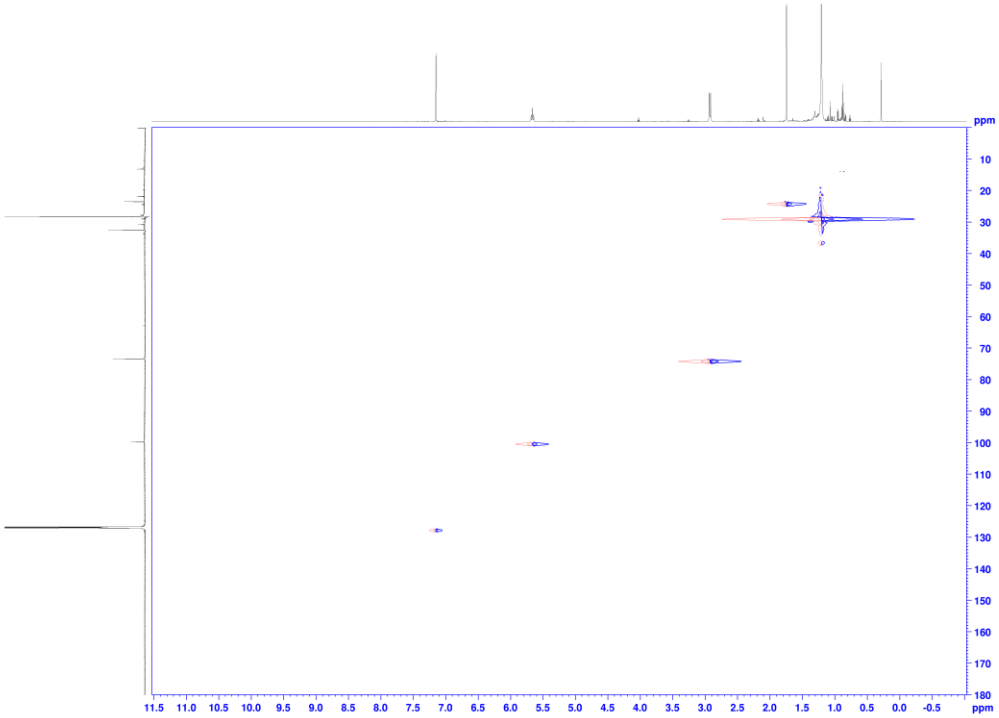

Figure A4.29: ^{1}H NMR (400 MHz) of [{$A^{2t}NiOH$}$_2$] taken in C_6D_6

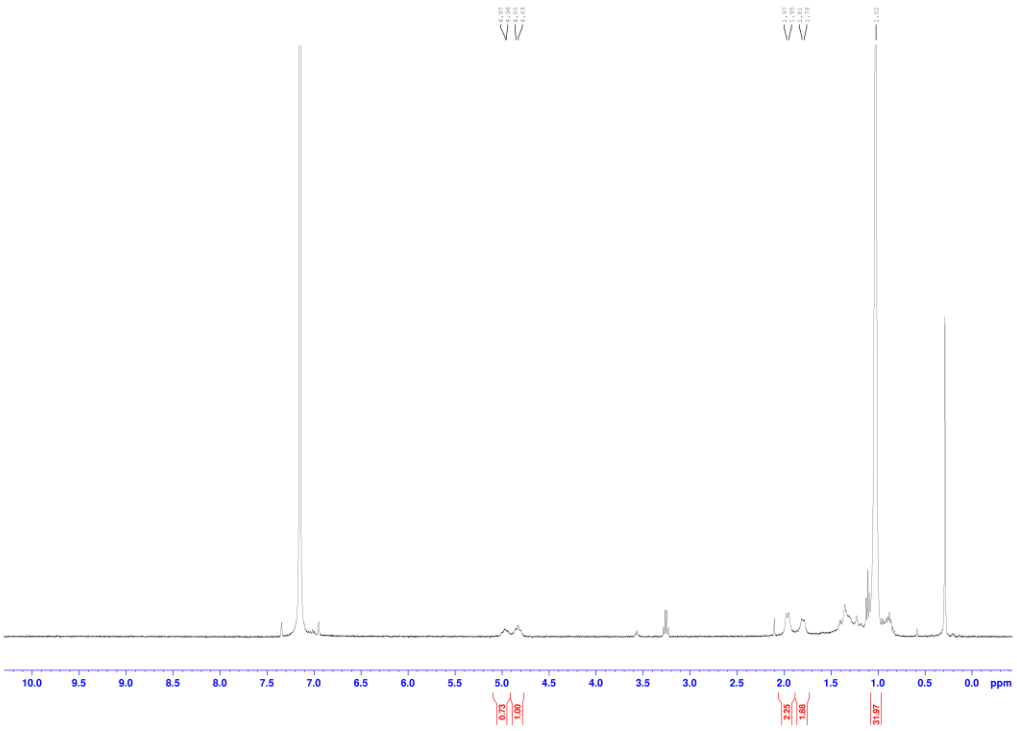

Figure A4.30: ^{1}H NMR (600 MHz) of [{A^{2t}NiOPh}$_2$] taken in C_6D_6

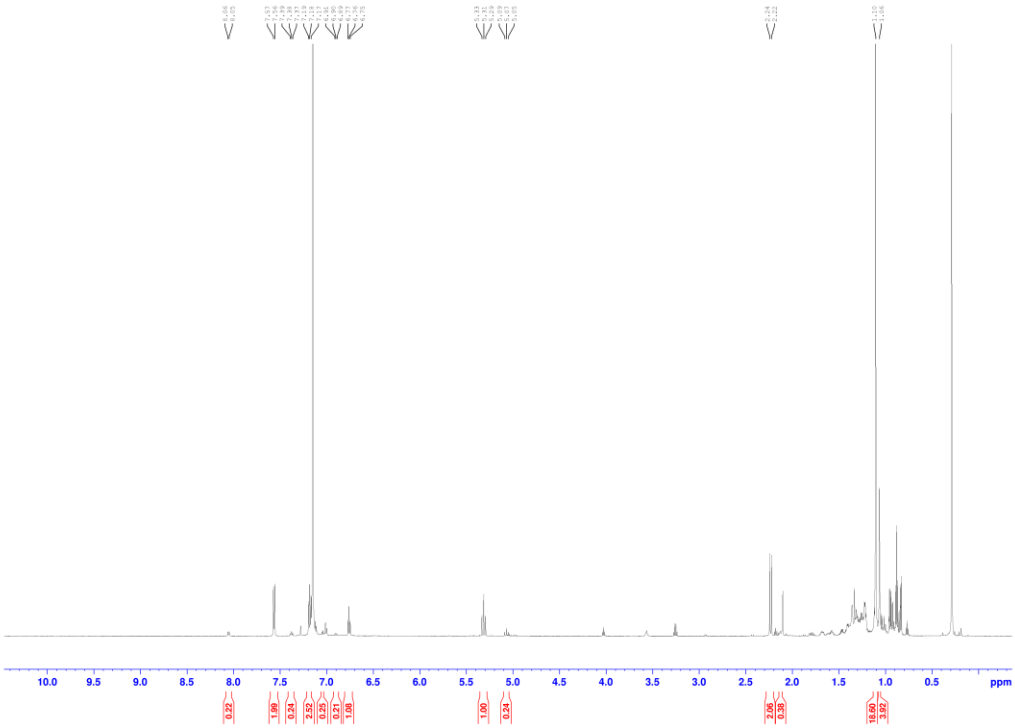

Figure A4.31: $^{13}C\{^{1}H\}$ NMR (151 MHz) of [{A^{2t}NiOPh}$_2$] taken in C_6D_6

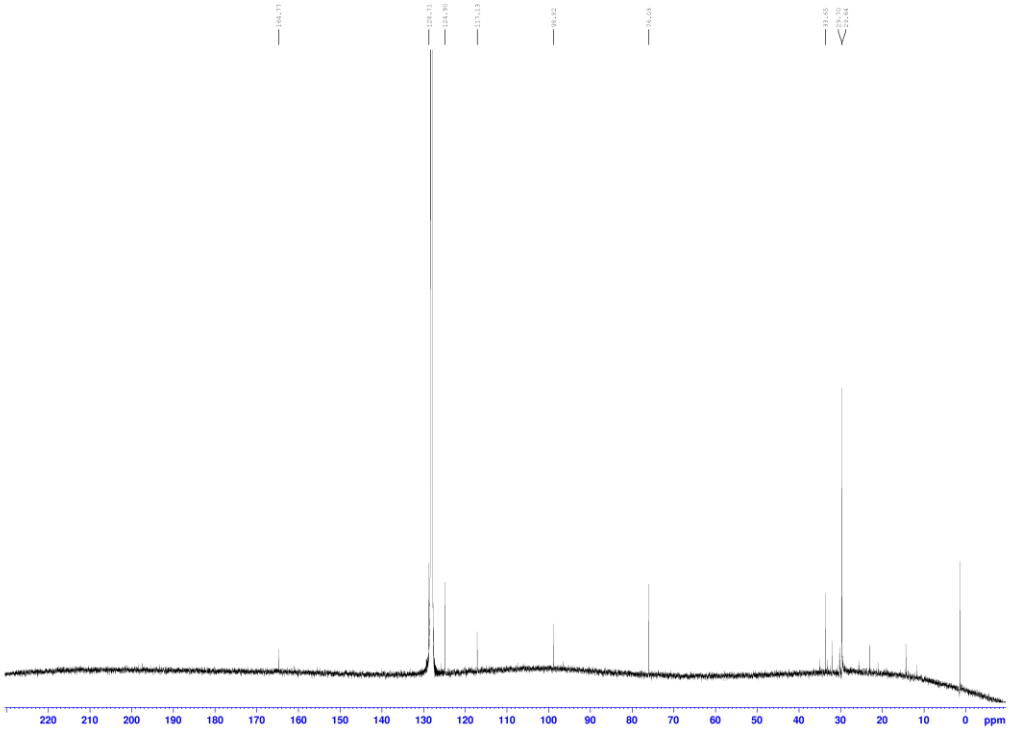

Figure A4.32: ^{1}H-^{13}C HSQC NMR (600-151 MHz) of [{$A^{2t}NiOPh$}$_2$] in C_6D_6

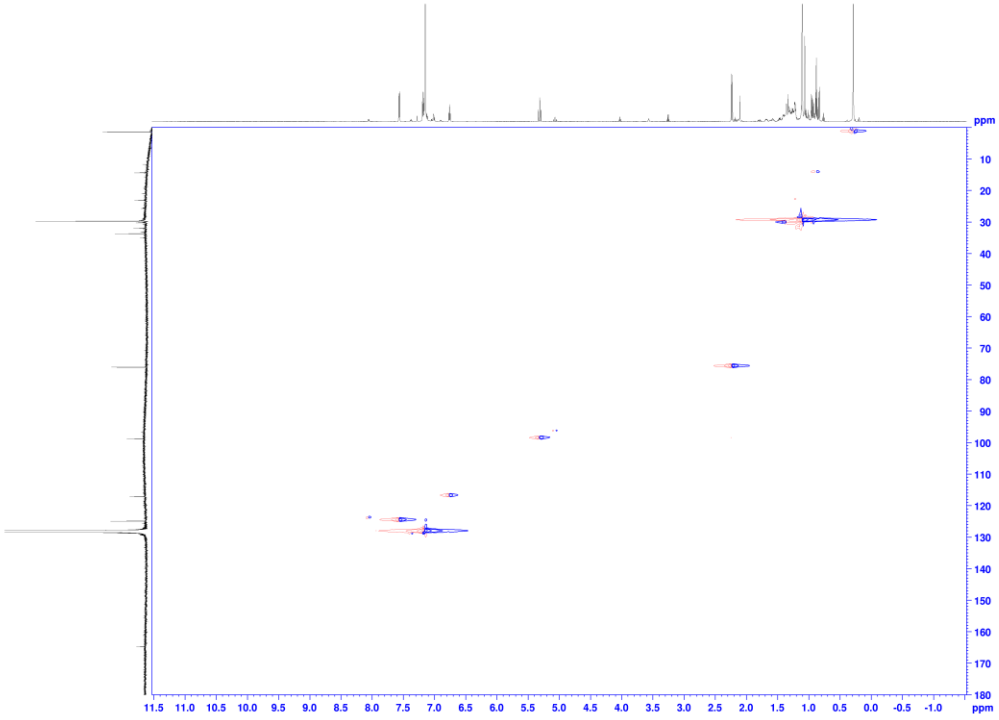

Figure A4.33: ^{1}H NMR (600 MHz) of reaction of [{$A^{2t}NiBr$}$_2$] with LiSPh, worked up prior ro full conversion of starting material taken in C_6D_6. Only peaks belonging to the potential partial substitution product are picked and integrated. [{$A^{2t}NiSPh$}$_2$] and [{$A^{2t}NiBr$}$_2$] peaks are marked with an asterisk,

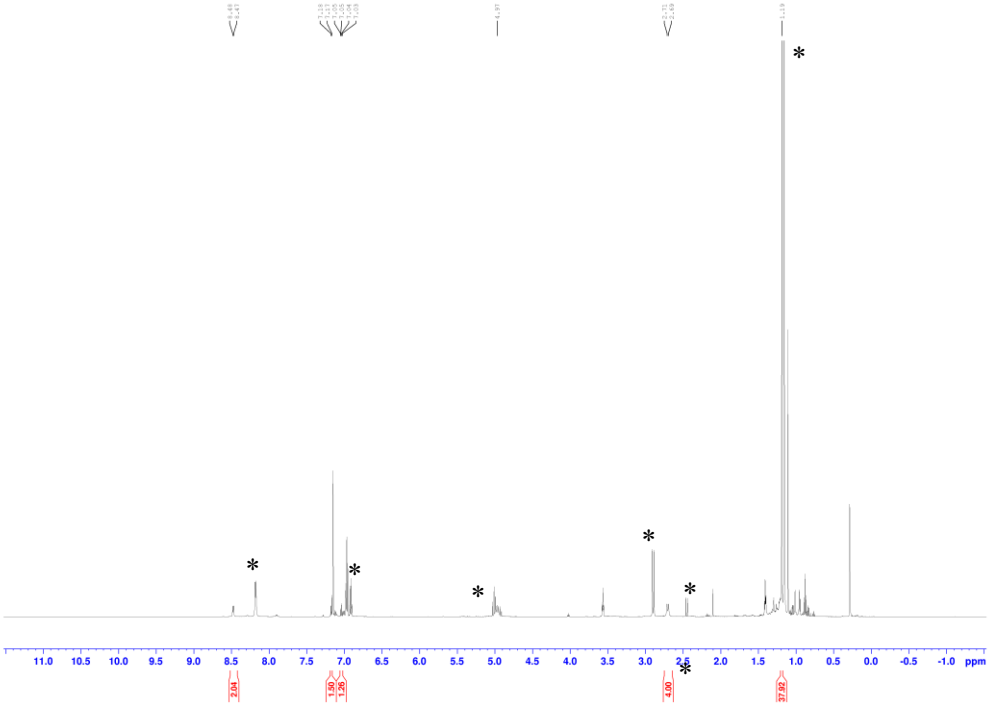

Figure A4.34: ^{1}H NMR (400 MHz) of [{A^{2t}NiSPh}$_2$] in C_6D_6. Peaks belonging to hexane are marked.

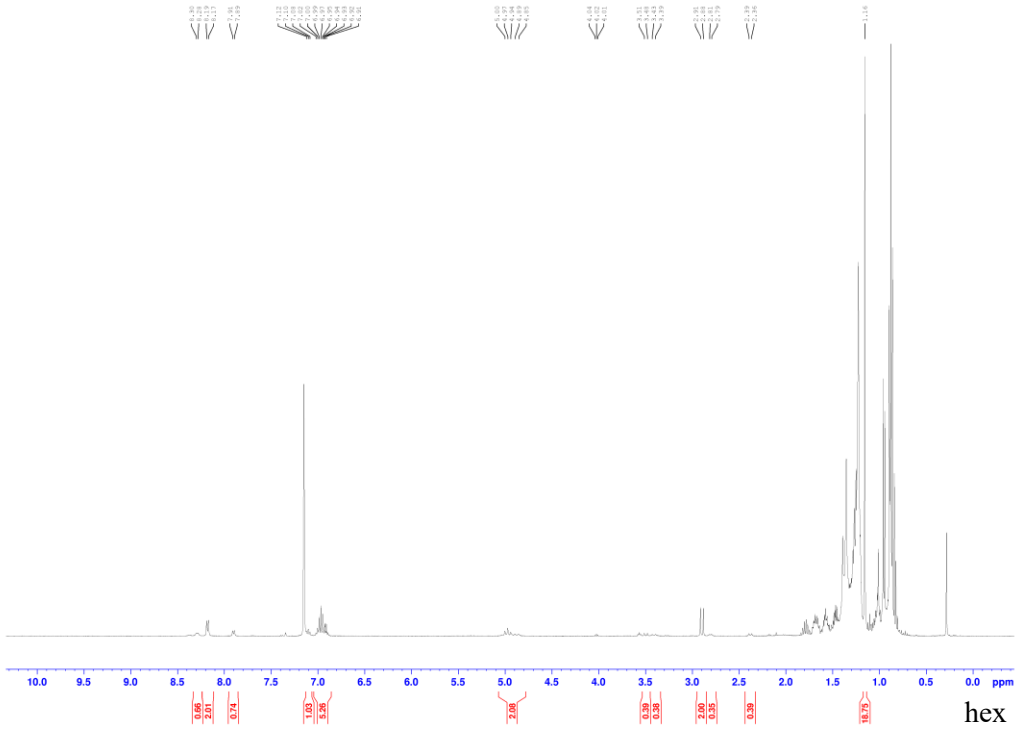

Figure A4.35: $^{13}C\{^{1}H\}$ NMR (151 MHz) of [{A^{2t}NiSPh}$_2$] in C_6D_6. Peaks belonging to hexane are marked.

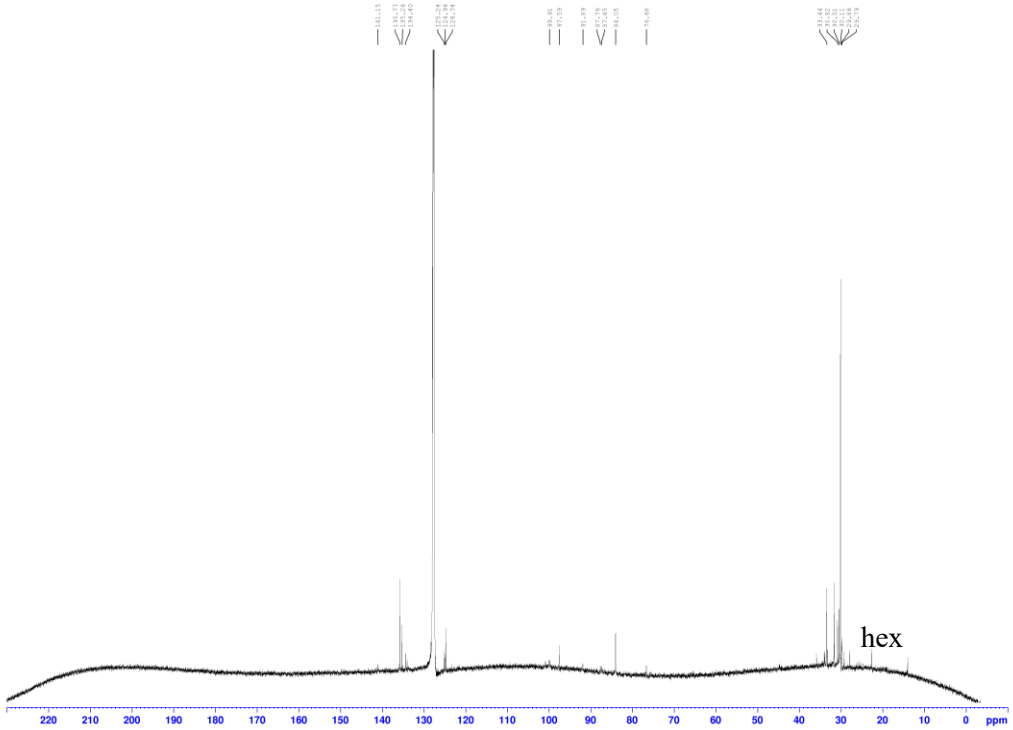

Figure A4.36: ^{1}H-^{13}C HSQC NMR (600-151 MHz) of [{$A^{2t}NiSPh$}$_2$] in C_6D_6

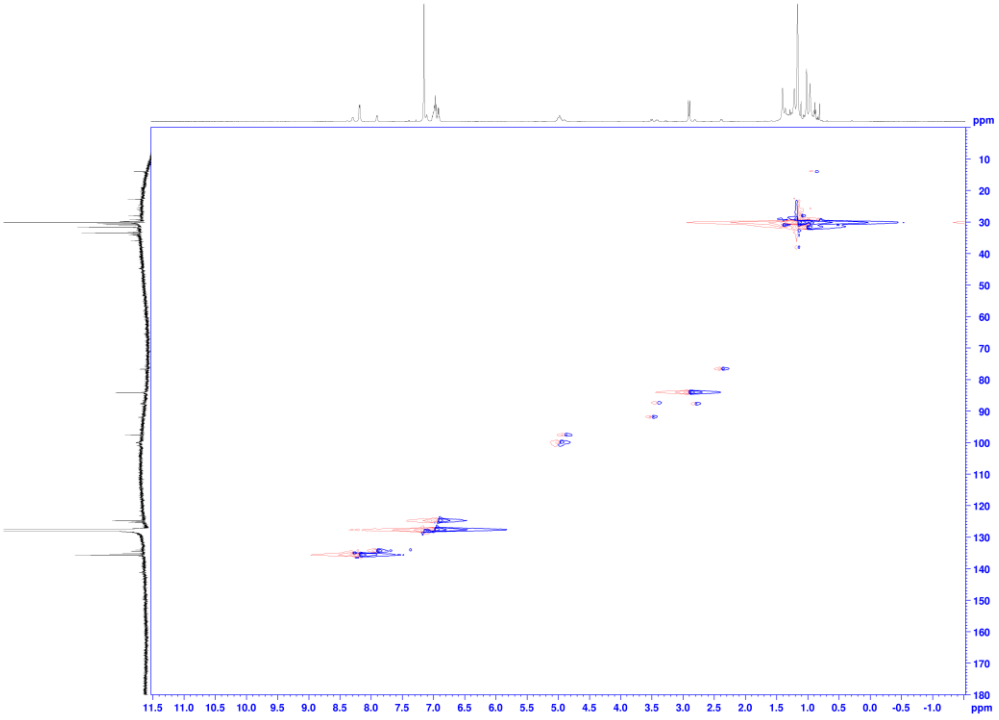

Figure A4.37: ^{1}H NMR (600 MHz) of [{$A^{2t}NiSEt$}$_2$] in C_6D_6. Peaks belonging to THF have been marked.

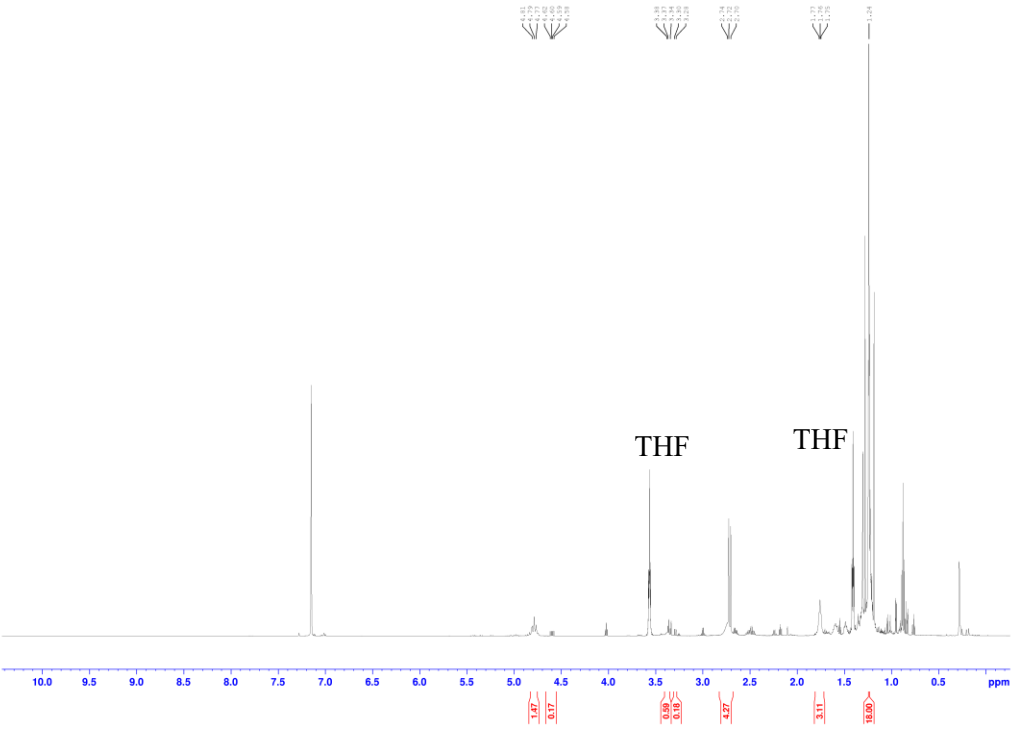

Figure A4.38: ^{1}H-^{1}H COSY NMR spectrum (600 MHz) of [{$A^{2t}NiSEt$}$_2$] taken in C_6D_6.

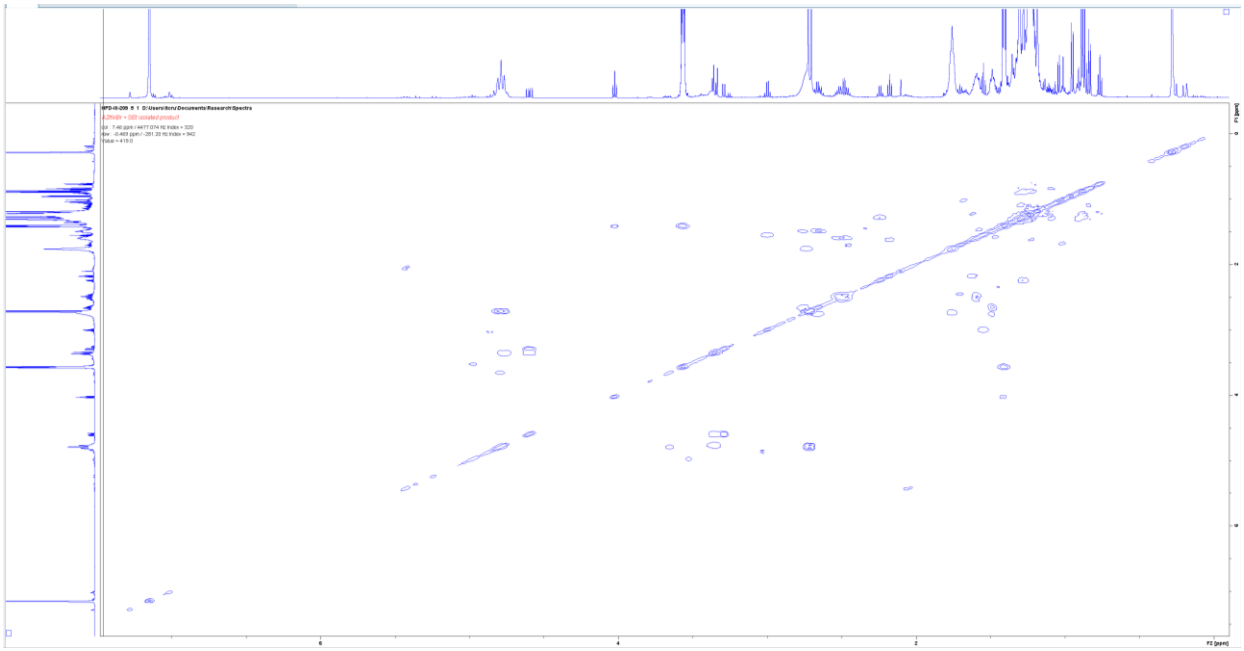

Figure A4.39: $^{13}C\{^{1}H\}$ NMR (151 MHz) of [{$A^{2t}NiSEt$}$_2$] in C_6D_6. Peaks belonging to THF have been marked.

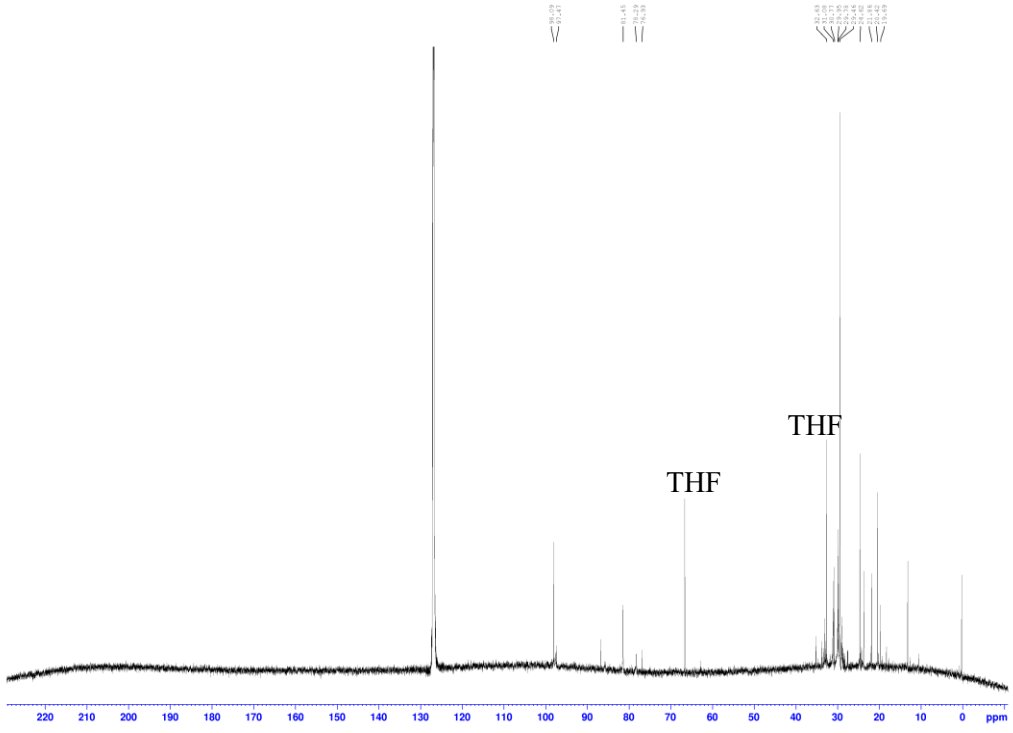

Figure A4.40: ^{1}H-^{13}C HSQC NMR (600-151 MHz) of [{$A^{2t}NiSEt$}$_2$] taken in C_6D_6

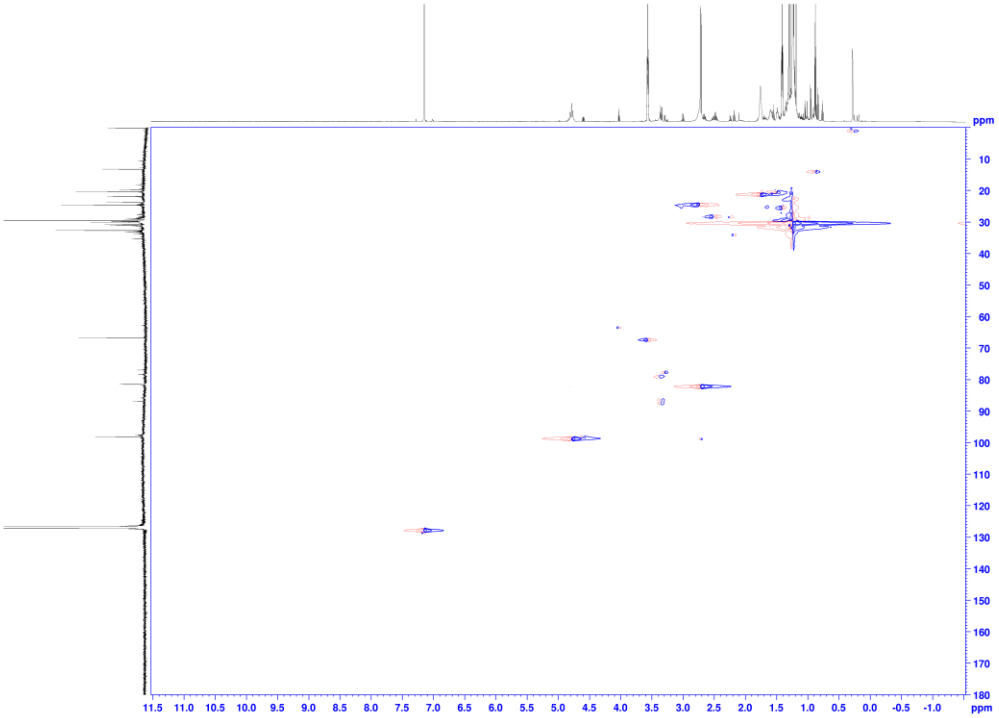

Figure A4.41: ^{1}H NMR (600 MHz) of [{$A^{2t}NiSePh$}$_2$] taken in C_6D_6. Peaks belonging to THF have been marked.

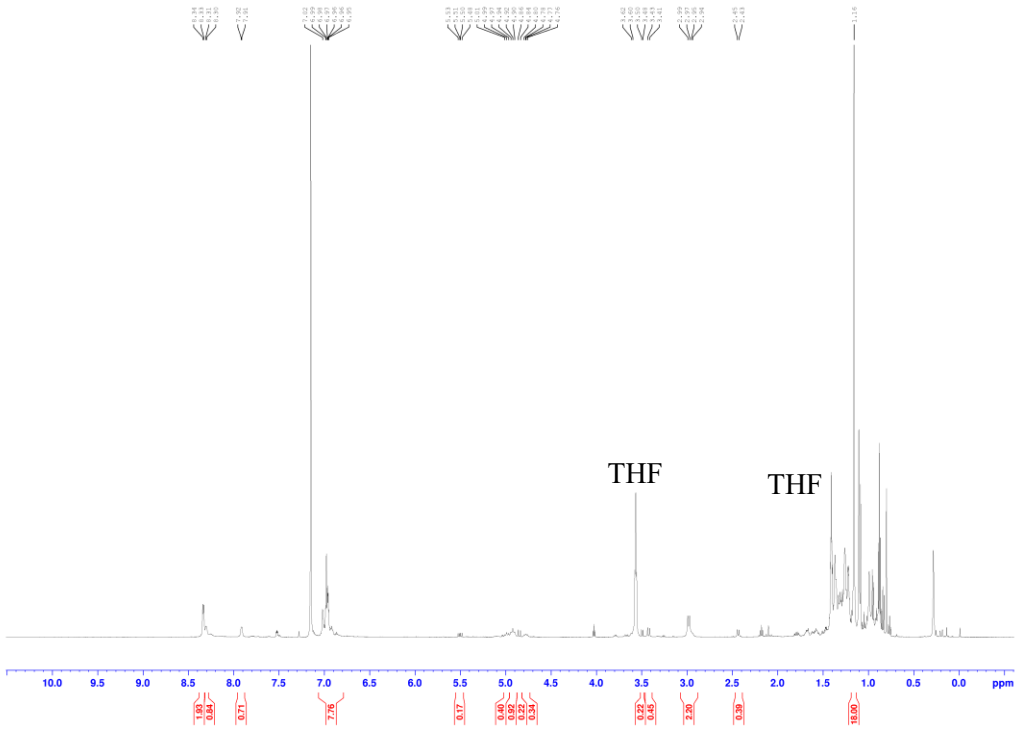

Figure A4.42: ^{1}H-^{1}H COSY NMR spectrum (600 MHz) of [{$A^{2t}NiSePh$}$_2$] taken in C_6D_6.

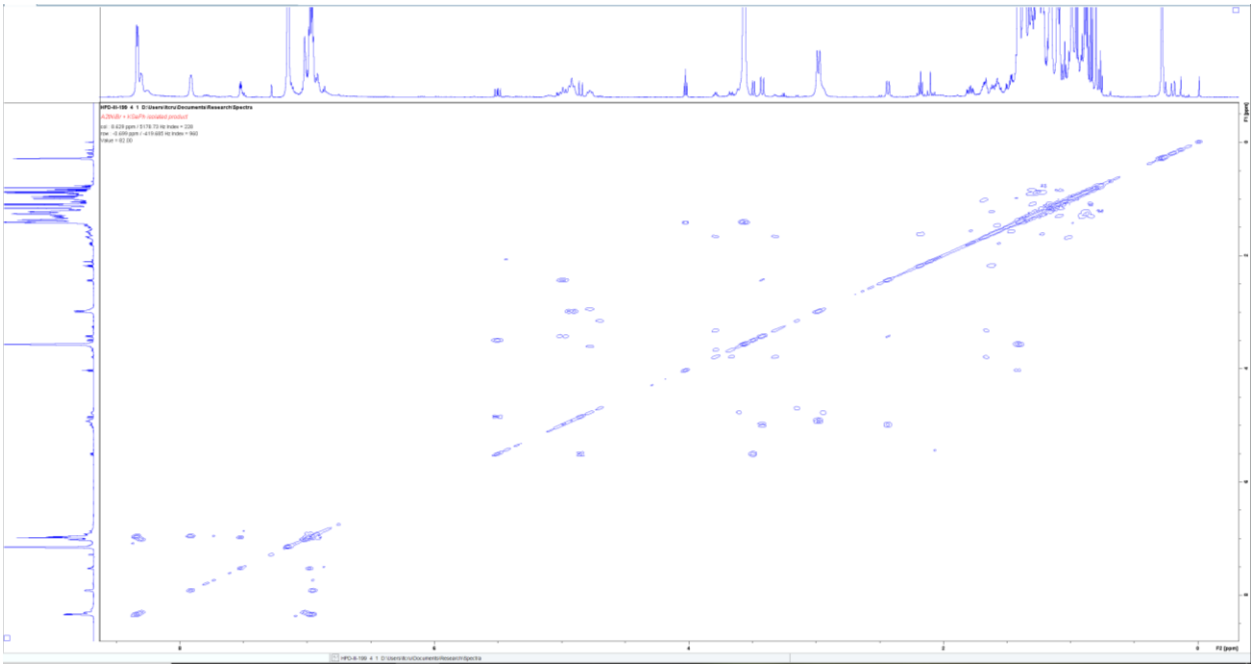

Figure A4.43: $^{13}C\{^{1}H\}$ NMR (151 MHz) of [{$A^{2t}NiSePh$}$_2$] taken in C_6D_6. Peaks belonging to THF have been marked.

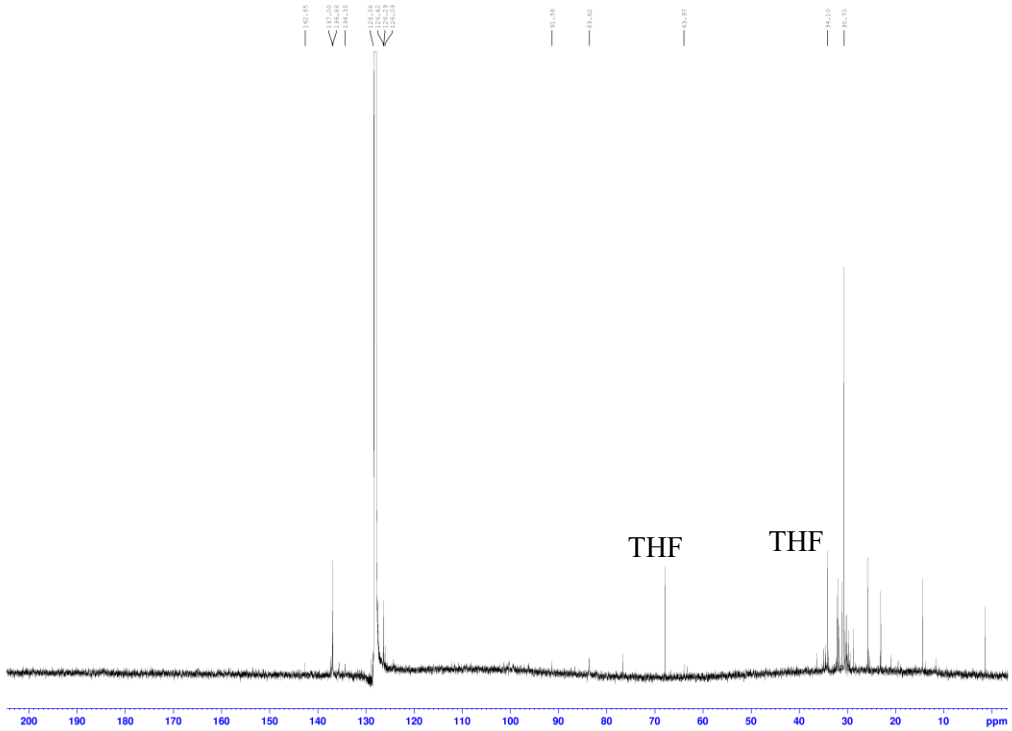

Figure A4.44: ^{1}H-^{13}C HSQC NMR (600-151 MHz) of [{$A^{2t}NiSePh$}$_2$] taken in C_6D_6

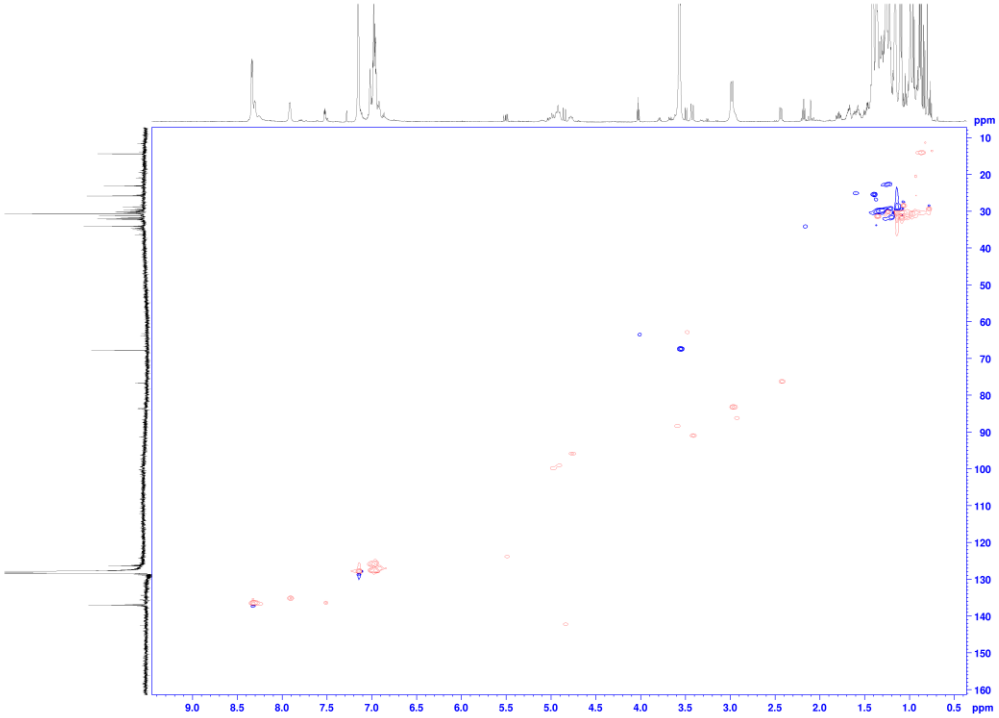

Figure A4.45: ^{1}H NMR (600 MHz) of [{$A^{2t}Ni$}$_2$(NHPh)(Br)] taken in C_6D_6

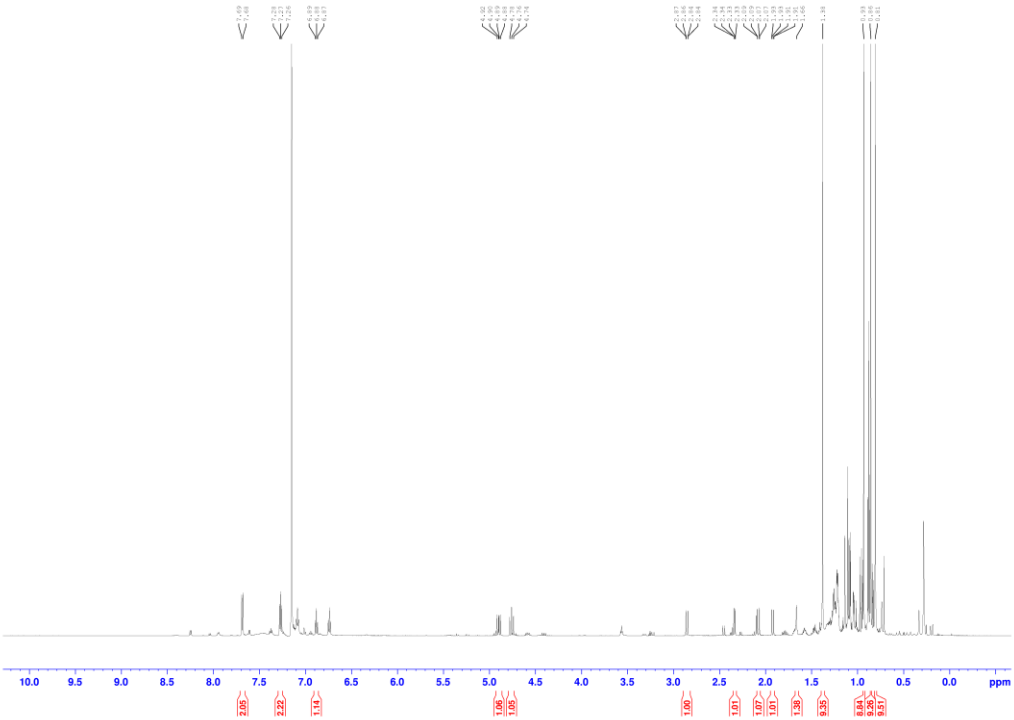

Figure A4.46: ^{1}H-^{1}H COSY NMR (600 MHz) of [{A^{2t}Ni}$_2$(NHPh)(Br)] taken in C_6D_6

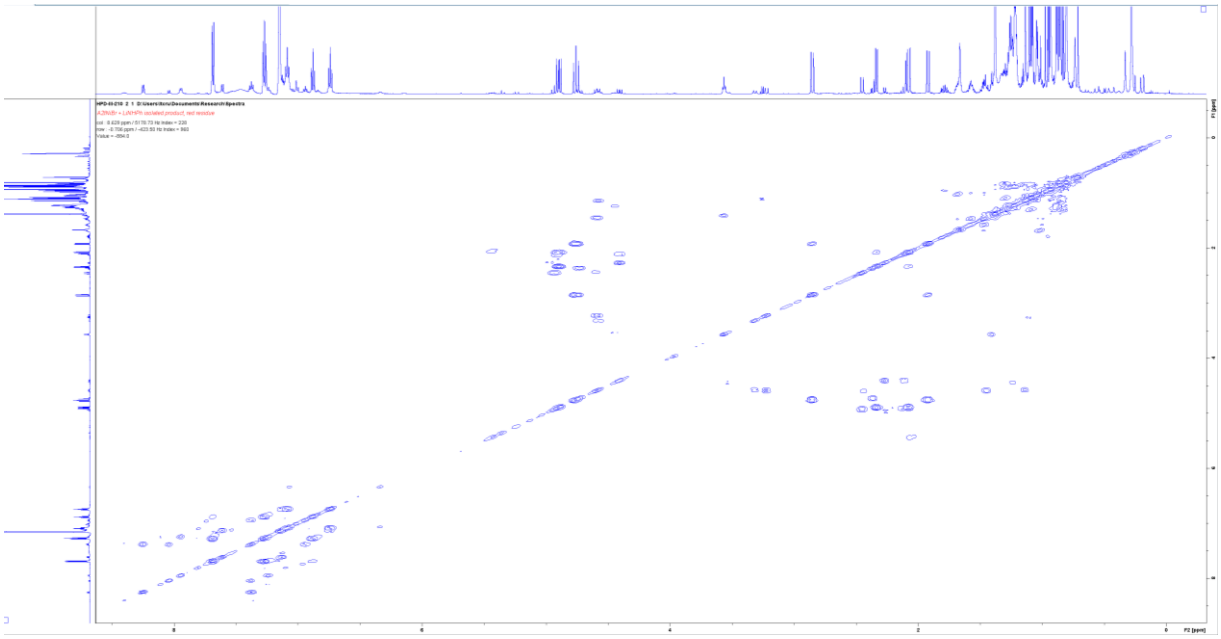

Figure A4.47: ^{13}C{^{1}H} NMR (151 MHz) of [{A^{2t}Ni}$_2$(NHPh)(Br)] taken in C_6D_6

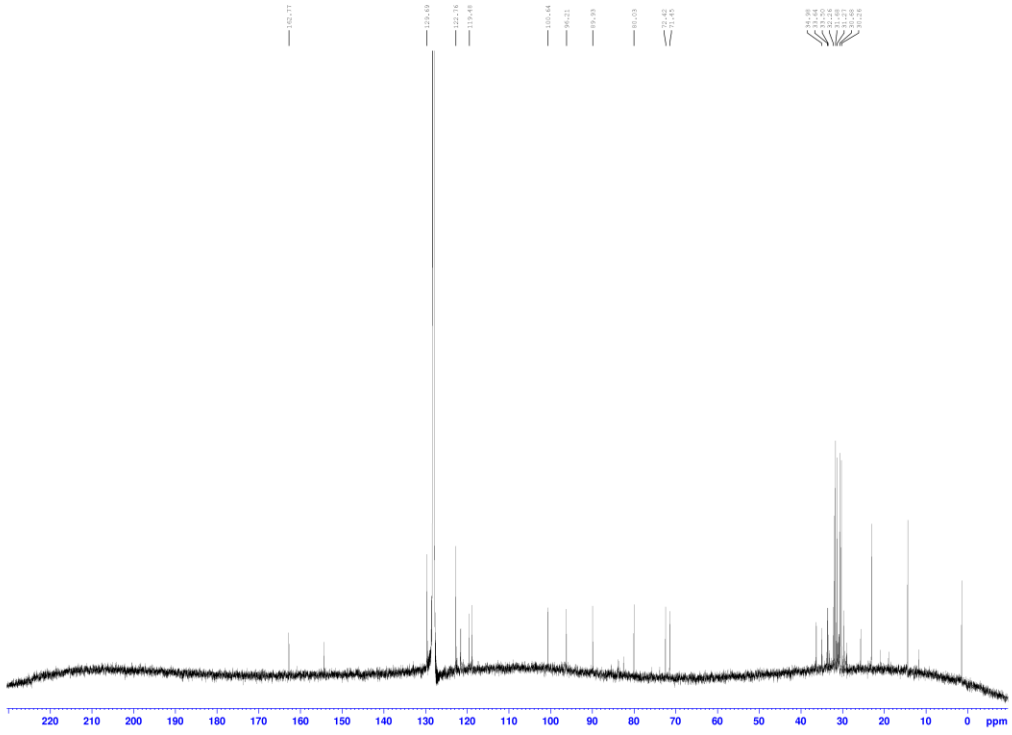

Figure A4.48: ^{1}H-^{13}C HSQC NMR (600-151 MHz) of [{$A^{2t}Ni$}$_2$(NHPh)(Br)] taken in C_6D_6

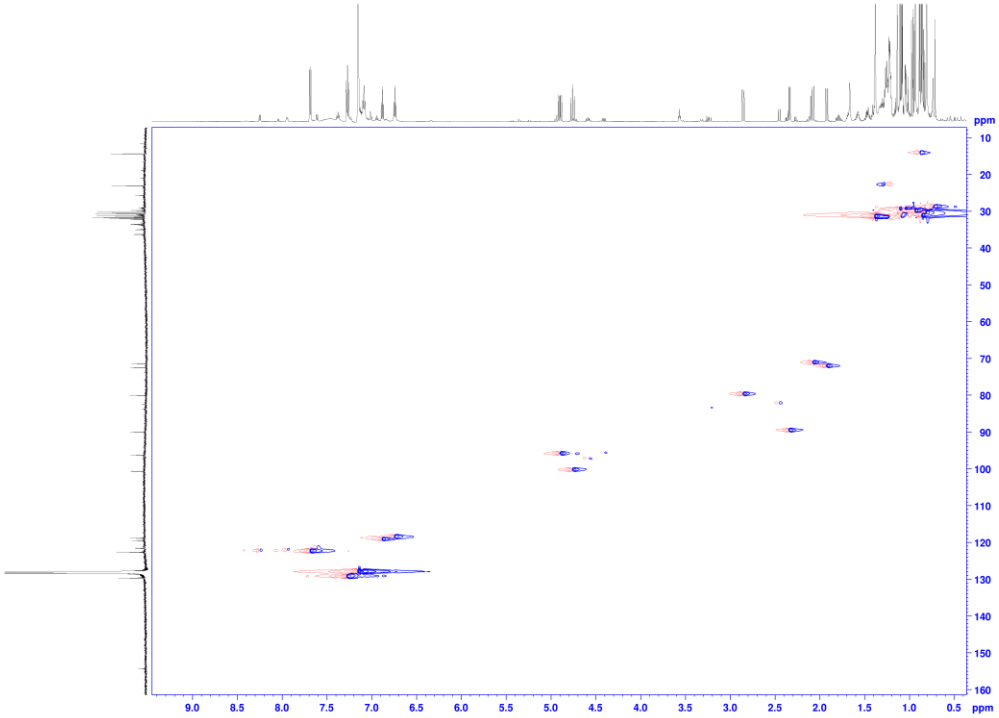

Figure A4.49: ^{1}H NMR (400 MHz) of material collected from reaction of [{$A^{2t}NiBr$}$_2$] with [KO*t*Bu] taken in C_6D_6. The origin of the broadened resonance at 5.56 ppm is not known.

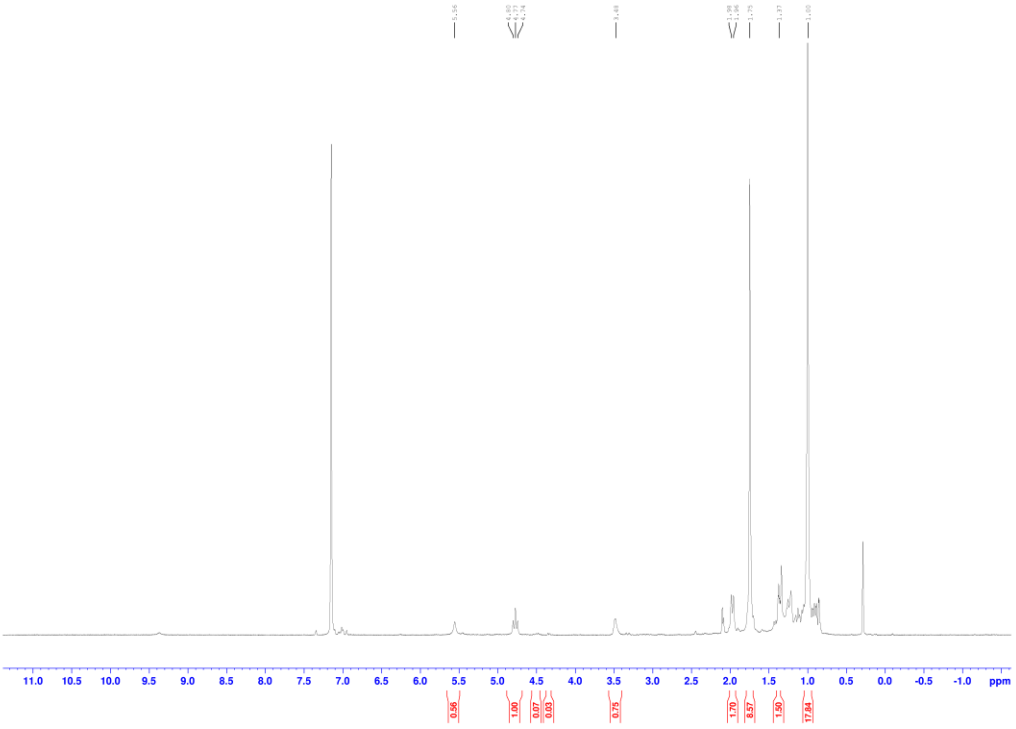

Figure A4.50: ^{1}H-^{1}H COSY NMR (400 MHz) of material collected from reaction of [{A^{2t}NiBr}$_2$] with [KO*t*Bu] taken in C_6D_6.

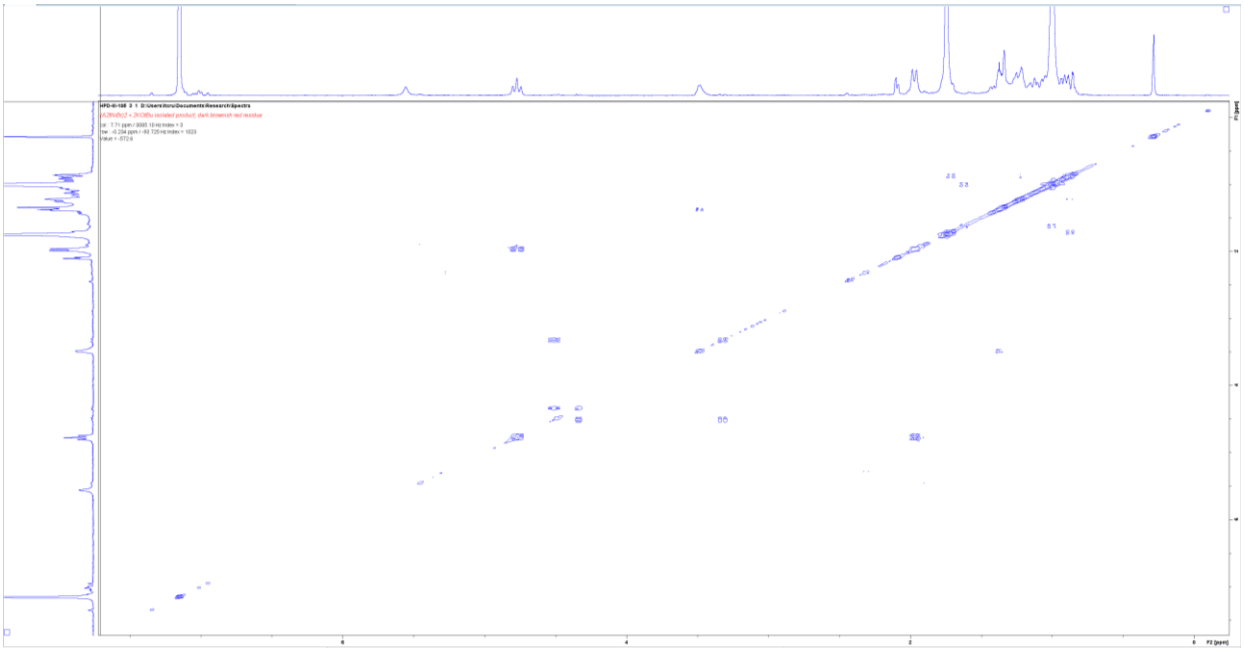

Figure A4.51: ^{13}C{^{1}H} NMR (101 MHz) of material collected from reaction of [{A^{2t}NiBr}$_2$] with [KO*t*Bu] taken in C_6D_6.

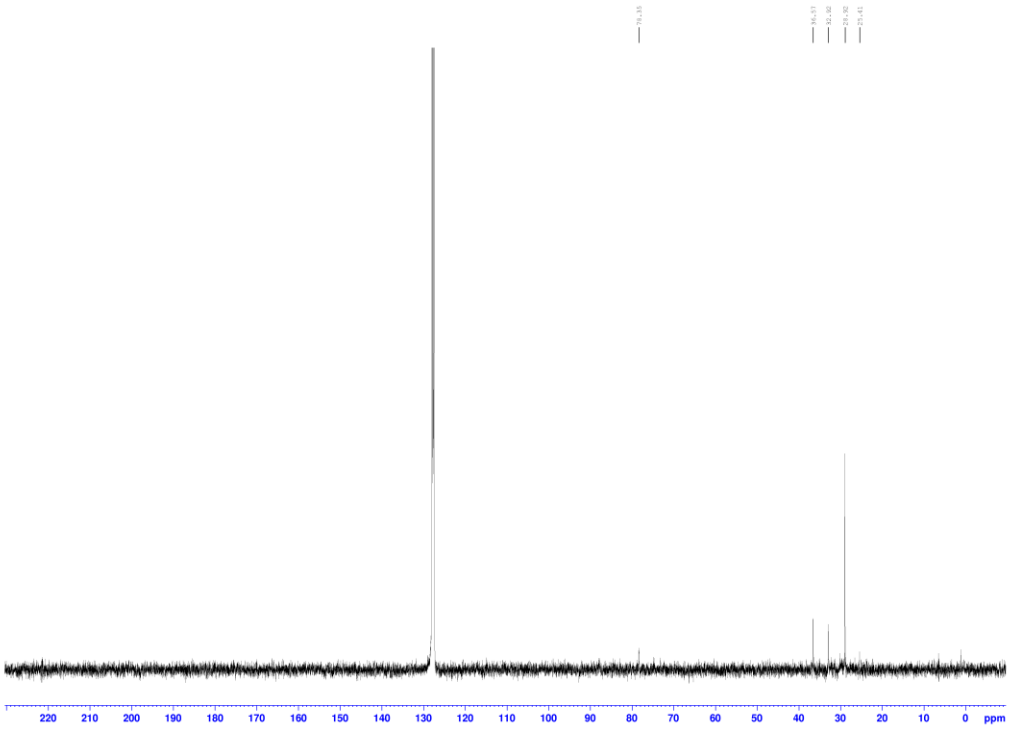

Figure A4.52: ^{1}H-^{13}C HSQC NMR (400-101 MHz) of material collected from reaction of [{A^{2t}NiBr}$_2$] with [KO*t*Bu] taken in C_6D_6.

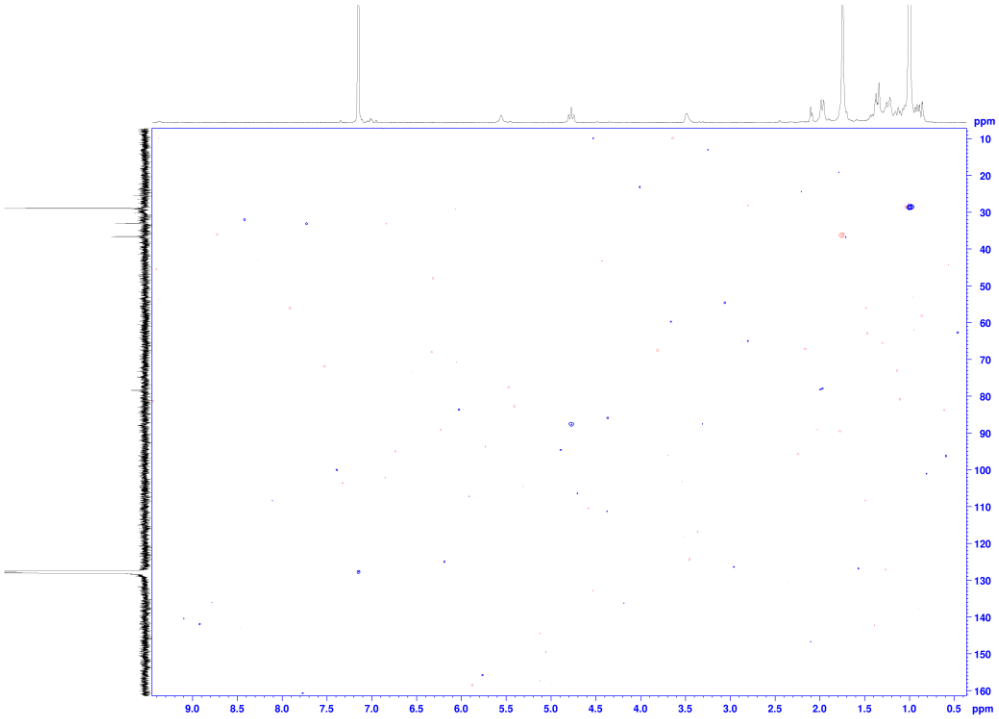

Figure A4.53: ^{1}H NMR (400 MHz) of material collected from reaction of [{A^{2t}NiBr}$_2$] with [KHMDS] taken in C_6D_6.

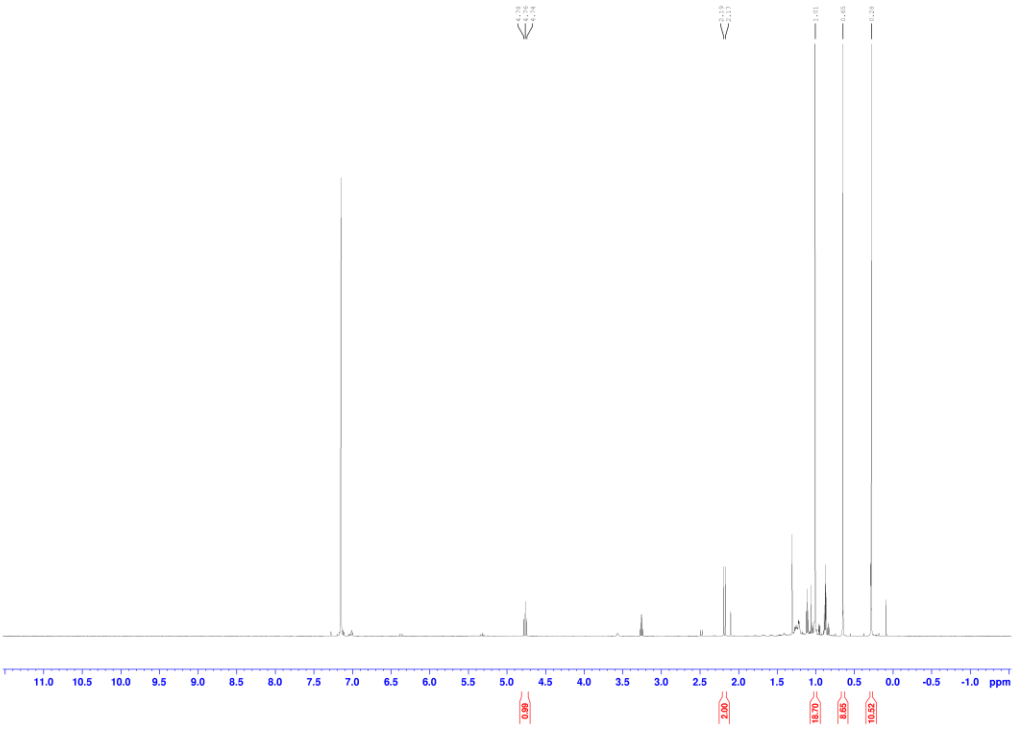

Figure A4.54: ^{1}H NMR (400 MHz) of material collected from reaction of [{A^{2t}NiBr}$_2$] with [KNPh$_2$] taken in C_6D_6. Unrelated aryl proton signals from an unidentified source are marked with an asterisk.

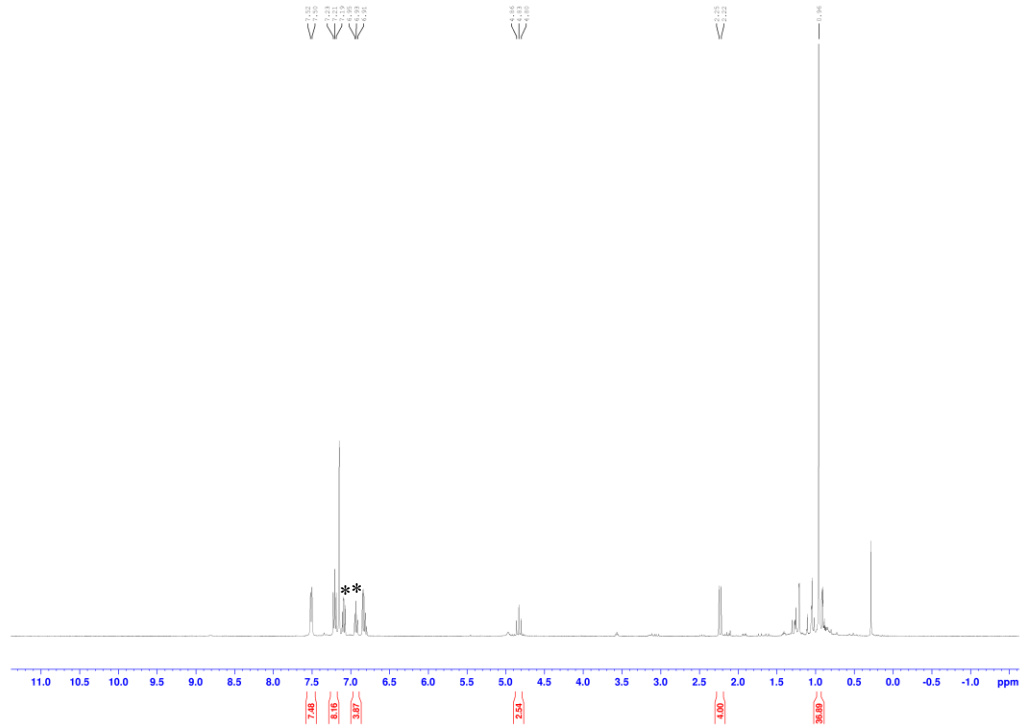

A4.7 References

(1) Quisenberry, K. T.; Smith, J. D.; Voehler, M.; Stec, D. F.; Hanusa, T. P.; Brennessel, W. W. Trimethylsilylated Allyl Complexes of Nickel. The Stabilized Bis(π-Allyl)Nickel Complex [η^3-1,3-(SiMe$_3$)$_2$C$_3$H$_3$]$_2$Ni and Its Mono(π-Allyl)NiX (X = Br, I) Derivatives. *J. Am. Chem. Soc.* **2005**, *127* (12), 4376–4387. https://doi.org/10.1021/ja044308s.

(2) Panda, T. K.; Gamer, M. T.; Roesky, P. W. An Improved Synthesis of Sodium and Potassium Cyclopentadienide. *Organometallics* **2003**, *22* (4), 877–878. https://doi.org/10.1021/om0207865.

(3) Avens, L. R.; Burns, C. J.; Butcher, R. J.; Clark, D. L.; Gordon, J. C.; Schake, A. R.; Scott, B. L.; Watkin, J. G.; Zwick, B. D. Mono(Pentamethylcyclopentadienyl)Uranium(III) Complexes : Synthesis , Properties , and X-Ray Structures of (η-C$_5$Me$_5$)UI$_2$(THF)$_3$, (η-C$_5$Me$_5$)UI$_2$(Py)$_3$, and (η-C$_5$Me$_5$)U[N(SiMe$_3$)$_2$]$_2$. *Organometallics* **2000**, *19*, 451–457.

(4) Evans, W. J.; Gummersheimer, T. S.; Boyle, T. J.; Ziller, J. W. Synthesis and Structure of New Soluble Organosamarium(II) Reagents: (Indenyl)$_2$Sm(THF) and (Fluorenyl)$_2$Sm(THF)$_2$. *Organometallics* **1994**, *13* (4), 1281–1284. https://doi.org/10.1021/om00016a034.

(5) Degroot, H. P.; Speight, I. R.; Brennessel, W. W.; Hanusa, T. P. Distinction with a Difference: T -Butyl and Trimethylsilyl Substituents in Nickel Allyl Complexes. *Submitted - ACS Org. Inorg. Au* **2024**.

(6) Lamy, M. A. De l'Existence d'un Nouveau Metal, Le Thallium. *Ann. Chim. Phys.* **1863**, *67* (3), 385–417.

Appendix 5: Supplemental Information for Chapter 5

A5.1 Materials

Triphenylphosphine, anhydrous nickel chloride, anhydrous nickel acetylacetonate, elemental bromine, hydrogen chloride (4 M solution in dioxane), triethylamine, and palladium chloride were purchased from Sigma and used as received. Allyltrimethylsilane was purchased from Gelest and used as received. Chromium,[1] iron,[1] cobalt,[2] and nickel[3] bis(A′) complexes, dichloro bis(acetonitrile) palladium,[4] potassium 1-trimethylsilylallyl,[5] 1,3-Bis(2,4,6-trimethylphenyl)-1,3-dihydro-2H-imidazol-2-ylidene (IMes),[6] and potassium tris(A′)stannate[7] were synthesized according to published procedures. Potassium 1-trimethylsilylallyl was prepared by deprotonation of allyltrimethylsilane with *n*BuLi, followed by transmetallation with potassium *tert*-butoxide.

A5.2 Crystallographic Details

A5.2.1 Crystallographic methods

Prof. Nathan Schley (Vanderbilt Univ.) performed the data collection and structure solution for [{A′NiCl}$_2$] and [{A′PdCl}$_2$]; Prof. William Brennessel (Univ. of Rochester) did the same for [{A^{1Si}NiBr}$_2$] and [A^{1}SiPd(PPh$_3$)Cl]. The structure of [A^{1Si}Pd(PPh$_3$)Cl] was determined with Mo-Kα radiation.

A5.2.2 Collected diffraction parameters and crystal information

Table A5.1 Experimental X-ray diffraction parameters and crystal data for [{A^{1Si}NiBr}$_2$], [{A´NiCl}$_2$], [{A´PdCl}$_2$], and [{A^{1Si}Pd(PPh_3)Cl}$_2$].

	[{A^{1Si}NiBr}$_2$]	**[{A´NiCl}$_2$]**	**[{A´PdCl}$_2$]**	**[A^{1Si}Pd(PPh_3)Cl]**
Empirical formula	C12 H26 Br2 Ni2 Si2	C9 H21 Cl Ni Si2	C18 H42 Cl2 Pd2 Si4	C24 H28 Cl P Pd Si
Formula weight	503.75	279.60	654.57	517.37
Temperature (K)	100	100	100	100
Wavelength	1.54184	1.54184	1.54184	0.71073
Crystal system	Monoclinic	Monoclinic	Monoclinic	Triclinic
Space group	P 1 21/c 1	I 1 2/a 1	I 1 2/a 1	P -1
Unit cell dimensions	13.2288(8)	11.2117(3)	11.07710(10)	10.2886(5)
	6.7119(3)	23.0985(4)	23.1812(3)	11.1637(6)
	10.8558(6)	11.3080(2)	11.31090(10)	11.8411(5)
	90	90	90	80.139(4)
	90.872(5)	100.568(2)	96.7800(10)	65.136(4)
	90	90	90	78.368(4)
Volume	963.77(9)	2878.80(11)	2884.11(5)	1202.90(10)
Z	2	8	4	2
Density (calculated)	1.736	1.290	1.507	1.428
Absorption coefficient	8.333	4.936	13.371	1.006
F(000)	504	1184	1328	528
Crystal size (mm^3)	0.085 x 0.056 x 0.012	0.199 x 0.17 x 0.083	0.13 x 0.03 x 0.03	0.166 x 0.15 x 0.055
Crystal color, habit	Dark red block	Red block	Yellow needle	Light yellow block
Theta range for data collection	3.3720 to 77.4450°	3.7940 to 71.5970°	3.8050 to 71.5310°	2.2700 to 31.7410°
Index ranges	$-16 \le h \le 16$, $-8 \le k \le 7$, $-13 \le l \le 13$	$-13 \le h \le 9$, $-28 \le k \le 28$, $-13 \le l \le 13$	$-13 \le h \le 11$, $-28 \le k \le 27$, $-13 \le l \le 11$	$-14 \le h \le 15$, $-14 \le k \le 16$, $-17 \le l \le 17$
Reflections collected	2023	2794	2795	6883
Independent reflections	15451	13670	10736	35153
Absorption correction	Multi-scan	Gaussian	Gaussian	Multi-scan
Max. and min. transmission	0.907 and 0.538	0.685 and 0.440	0.690 and 0.275	1.00000 and 0.40593
Refinement method	Full-matrix least-squares on F^2	Full-matrix least-squares on F^2	Full-matrix least-squares on F^2	Full-matrix least-squares on F^2
Data / restraints / parameters	2023 / 0 / 101	2794 / 0 / 193	2795 / 0 / 134	6883 / 136 / 323
Goodness-of-fit on F^2	1.053	1.094	1.102	1.092
Final R indices [*I*>2sigma(I)]	R_1 = 0.0664 wR_2 = 0.1901	R_1 = 0.0353 wR_2 = 0.0919	R_1 = 0.0404 wR_2 = 0.1087	R_1 = 0.0574 wR_2 = 0.1363
R indices (all data)	R_1 = 0.0714 wR_2 = 0.1960	R_1 = 0.0399 wR_2 = 0.0960	R_1 = 0.0425 wR_2 = 0.1102	R_1 = 0.0749 wR_2 = 0.1504
Largest diff. peak and hole	1.647 and -1.303 e $Å^{-3}$	0.424 and -0.370 e $Å^{-3}$	1.188 and -0.785 e $Å^{-3}$	2.511 and -1.918 e $Å^{-3}$

Refinement notes:

[{A´NiCl}$_2$]: Disorder in one of the bridging chloride ligands and the allyl are modeled over two positions without restraint.

[{A´PdCl}$_2$]: The allyl hydrogens were located in the difference map and their positions refined without restraint. Their atomic thermal parameters were fixed to ride on the parent carbon atom.

[A^{1Si}Pd(PPh$_3$)Cl]: The allyl ligand is modeled as disordered over two positions (0.672(9):0.328(9)). Analogous bond lengths and angles between the two positions were restrained to be similar. Anisotropic displacement parameters for proximal atoms were restrained to be similar and restrained toward the expected motion relative to bond direction.

A5.3 Polymerization studies

A5.3.1 Methods

Polymer molecular weight (Mn and Mw) and dispersity (Đ) were determined using a Tosoh EcoSEC GPC equipped with a refractive index (RI) detector operating at 40 °C and referenced to polystyrene standards. THF was the eluent, and samples were prepared at 1.5 mg/mL. Polymerization studies were conducted by Drs. Alicia Doerr and Xinyi Wang in the laboratory of Prof. Brian Long at the University of Tennessee, Knoxville, TN.

A5.3.2 Polymerization of norbornenes catalyzed by [MA´$_2$] complexes

Figure A5.1: Polymerization of 5-substituted norbornenes mediated by bis(A´) complexes

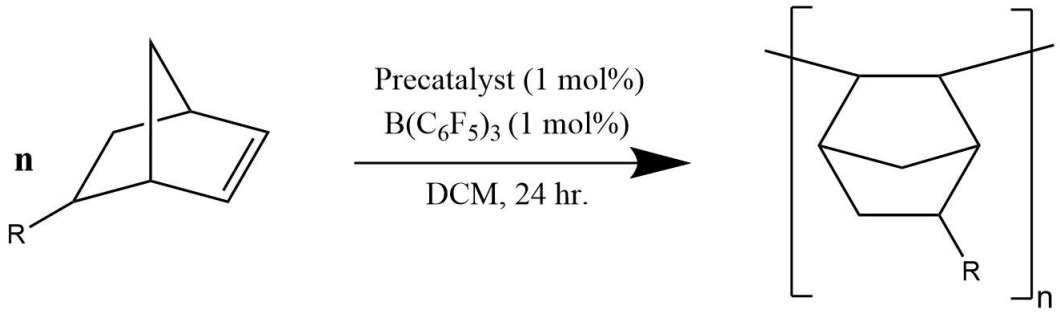

Table A5.2: Results of poly(R-norbornene) synthesis using various [MA´$_2$] compounds as precatalysts. Reactions run and data collected by Alicia Doerr of the Long group at the University of Tennessee – Knoxville.

Monomer R group	Precatalyst	Yield (%)
H	[CrA´$_2$]	89.4
	[FeA´$_2$]	4.6
	[CoA´$_2$]	74.0
	[NiA´$_2$]	Quant
$SiMe_3$	[CrA´$_2$]	Trace
	[FeA´$_2$]	None
	[CoA´$_2$]	11.0
	[NiA´$_2$]	39.0
$Si(OMe)_3$	[CrA´$_2$]	Trace
	[FeA´$_2$]	None
	[CoA´$_2$]	2.5
	[NiA´$_2$]	65.7
$Si(OEt)_3$	[CrA´$_2$]	Trace
	[FeA´$_2$]	None
	[CoA´$_2$]	5.7
	[NiA´$_2$]	41
CH_2Br	[CrA´$_2$]	Trace
	[FeA´$_2$]	None
	[CoA´$_2$]	None
	[NiA´$_2$]	24
CH_2OH	[CrA´$_2$]	None
	[FeA´$_2$]	None
	[CoA´$_2$]	Trace
	[NiA´$_2$]	None
$C(O)OCH_2C_6H_5$	[CrA´$_2$]	None
	[FeA´$_2$]	None
	[CoA´$_2$]	None
	[NiA´$_2$]	Trace
$CH_2OCH_2C_6H_5$	[CrA´$_2$]	None
	[FeA´$_2$]	None
	[CoA´$_2$]	Trace
	[NiA´$_2$]	64

[a]) Polymerizations were conducted using 0.15 g monomer, 1 mol % precatalyst, 1 mL DCM, activated using 1 equiv. $B(C_6F_5)_3$, and run for 24 hours.

A5.4 NMR spectra of new compounds

Figure A5.2: ^{1}H NMR (400 MHz) of [NiA$^{1Si}_{2}$] taken in C_6D_6.

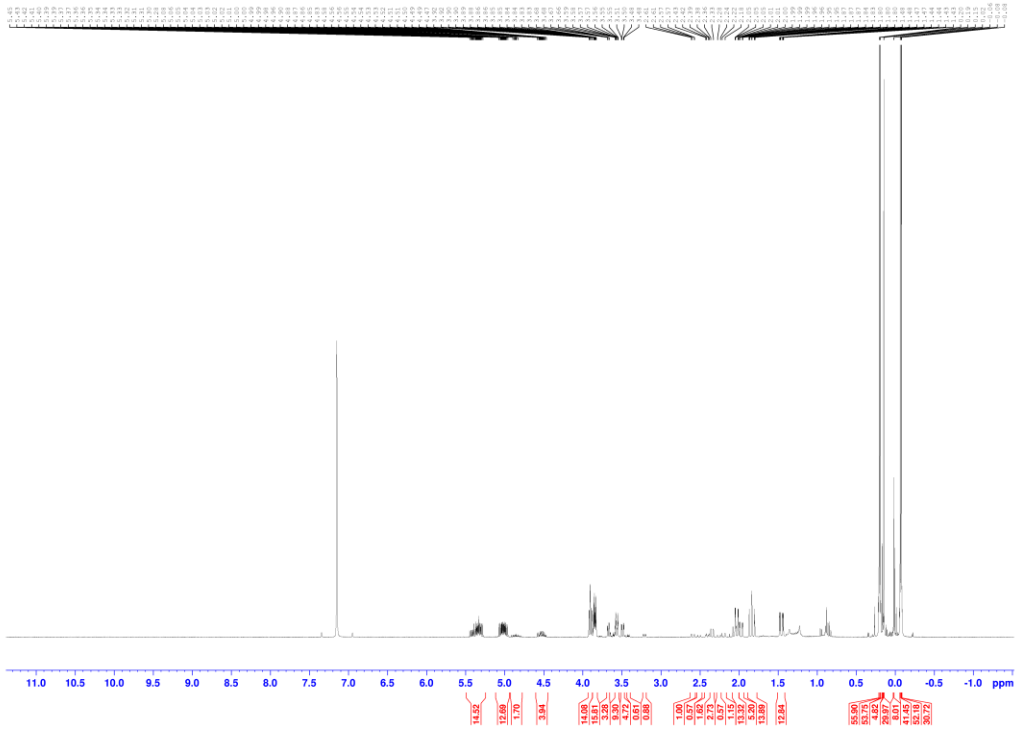

Figure A5.3: ^{1}H-^{1}H COSY NMR (400 MHz) of [NiA$^{1Si}_{2}$] taken in C_6D_6

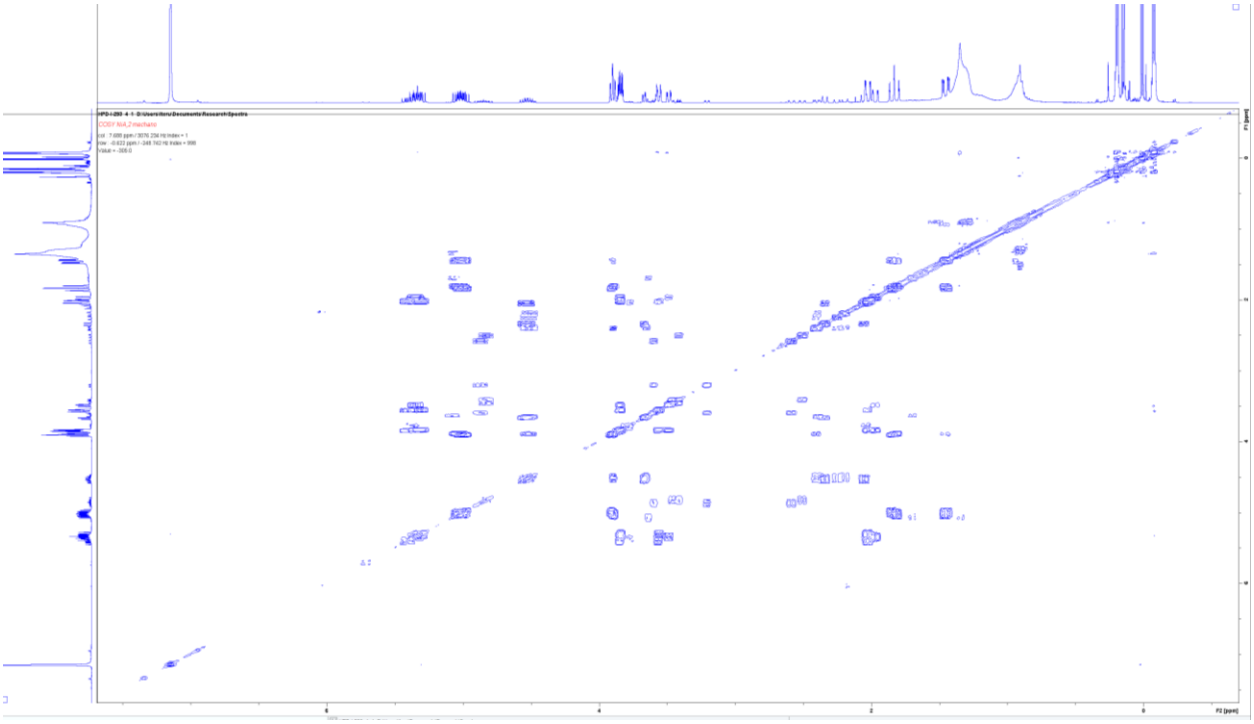

Figure A5.4: ^{1}H-^{13}C HSQC NMR (400-101 MHz) of [NiA^{1Si}_2] taken in C_6D_6

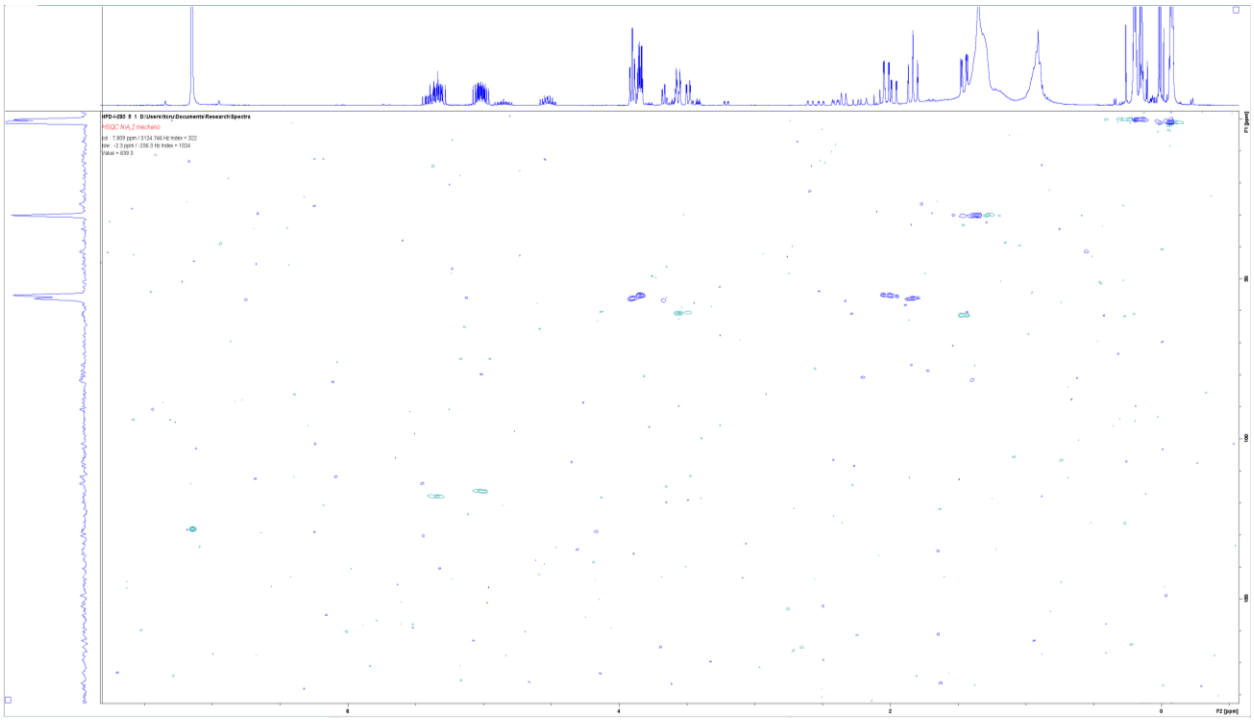

Figure A5.5: ^{1}H NMR (400 MHz) of [{$A^{1Si}NiBr$}$_2$] taken in C_6D_6.

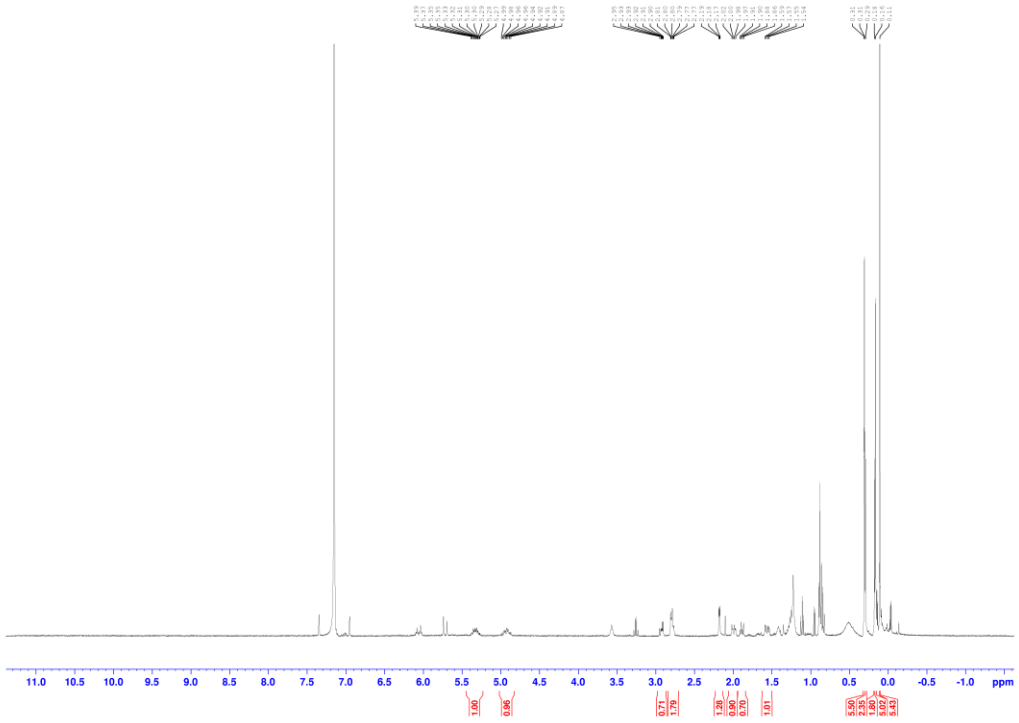

Figure A5.6: ^{1}H-^{1}H COSY NMR (400 MHz) of [{A^{1Si}NiBr}$_2$] taken in C_6D_6. Substantial unreacted [NiA^{1Si}_2] is present as an impurity. Crosspeaks that can definitively be attributed to [{A^{1Si}NiBr}$_2$] are marked, one allyl system is marked * while the other is marked °.

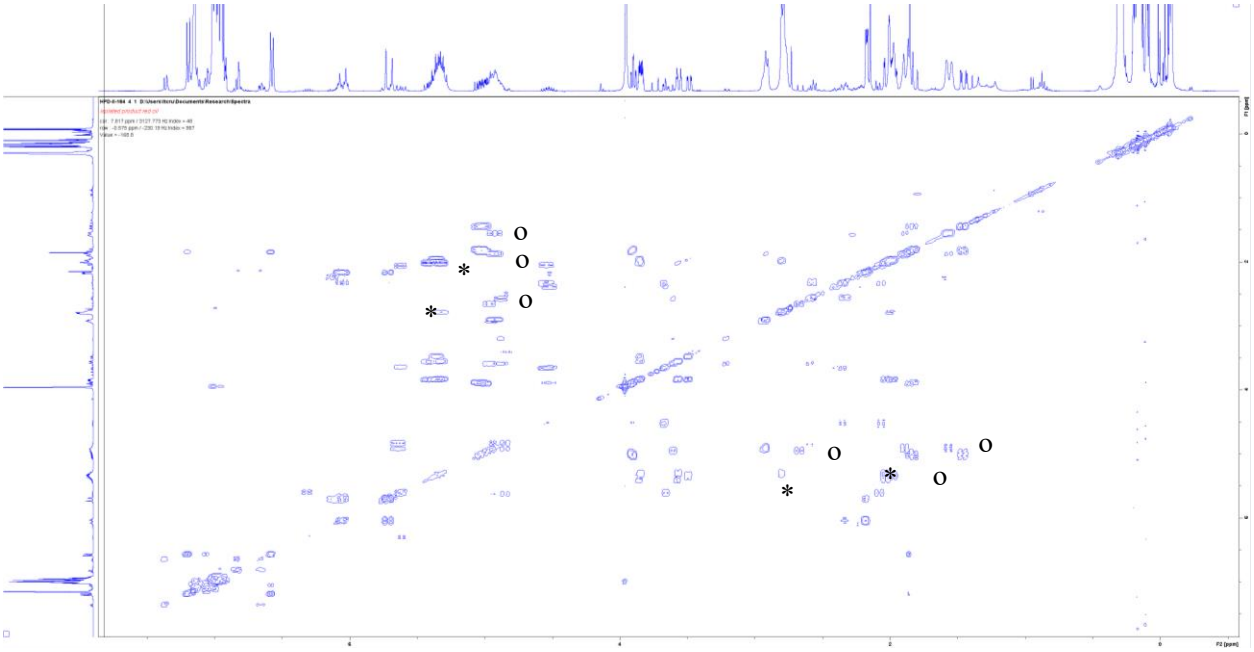

Figure A5.7: ^{1}H-^{13}C HSQC NMR (400 MHz) of [{A^{1Si}NiBr}$_2$] taken in C_6D_6. While [NiA$^{1Si}_2$] is present in the sample, its C-H couplings are not sufficiently intense to be observed. The peaks marked with an asterisk represent an aromatic impurity, hypothesized to be benzyl bromide, formed as a byproduct of the bromination reaction performed in toluene.

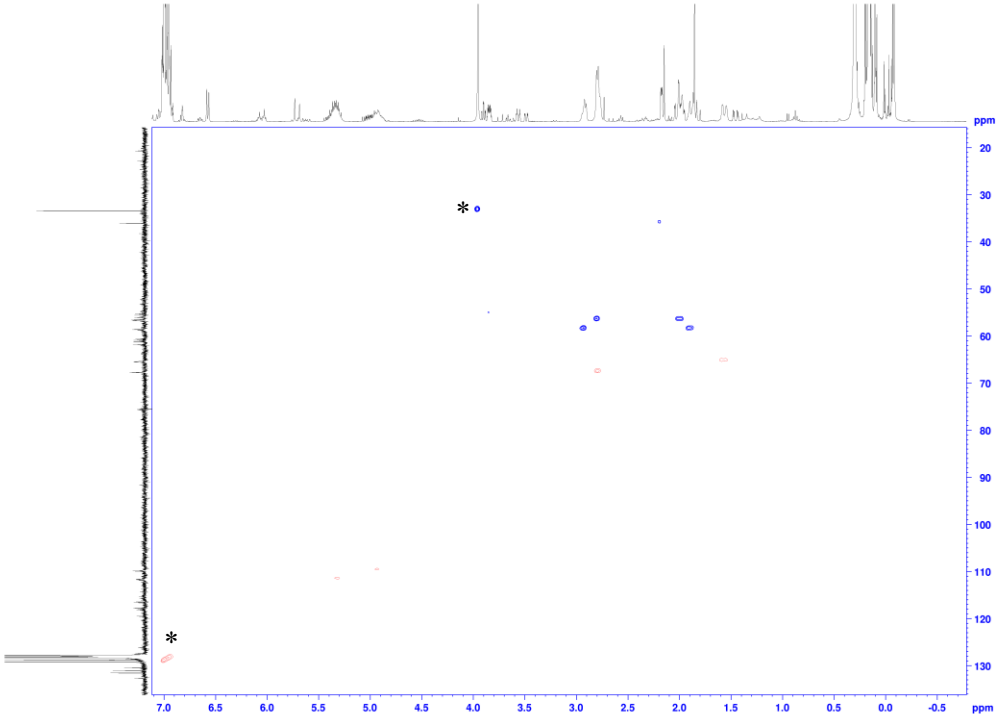

Figure A5.8: ^{1}H NMR (400 MHz) of [{A´NiCl}$_2$] taken in C_6D_6.

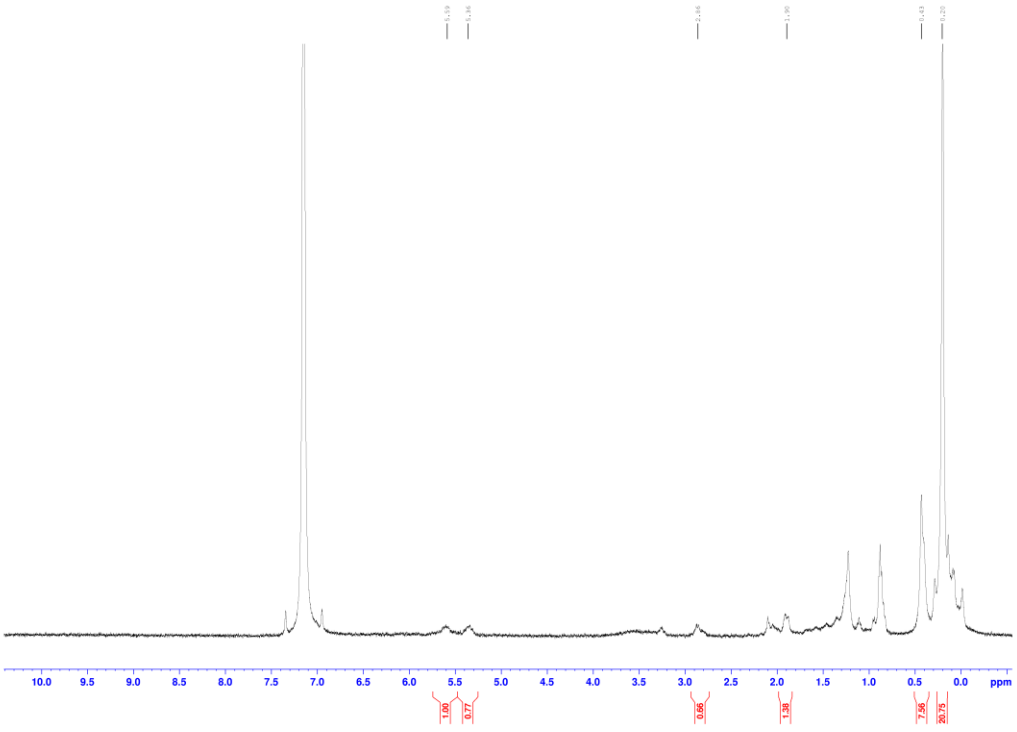

Figure A5.9: ^{1}H NMR (400 MHz) of material collected from reaction of [{$A^{1Si}PdCl$}$_2$] with triphenylphosphine taken in C_6D_6.

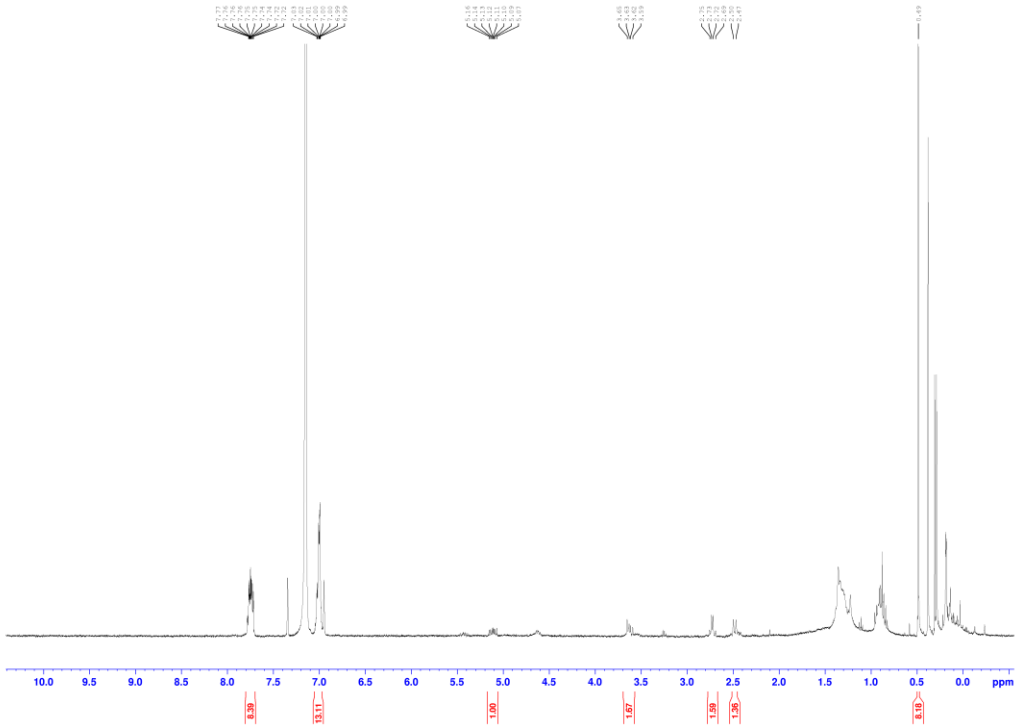

Figure A5.10: ^{1}H-^{1}H COSY NMR (400 MHz) of material collected from reaction of [{$A^{1Si}PdCl$}$_2$] with triphenylphosphine taken in C_6D_6.

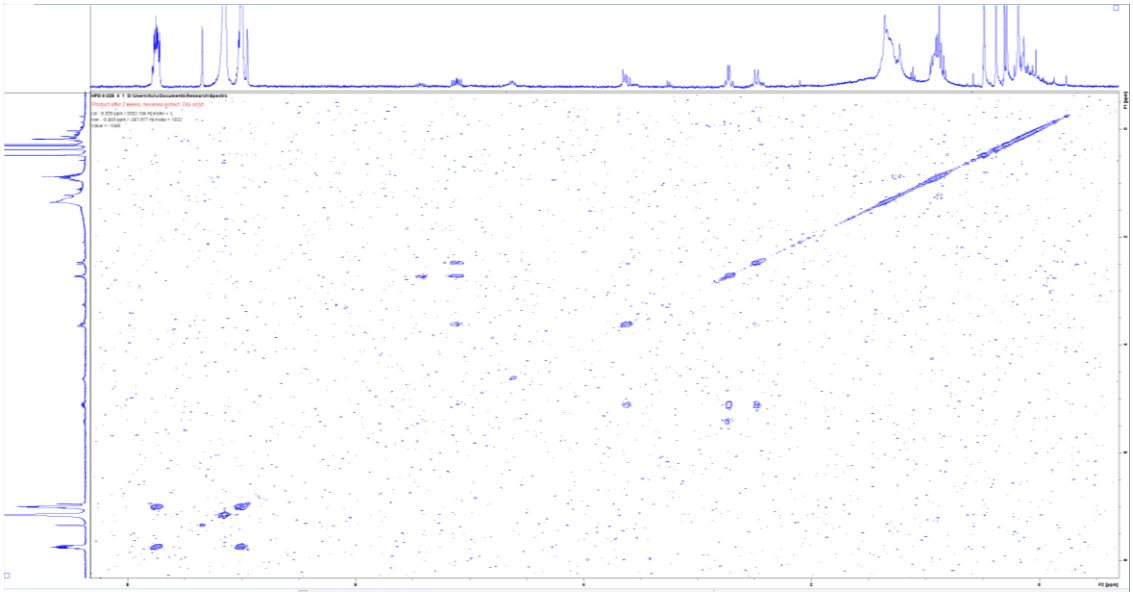

Figure A5.11: $^{31}P\{^{1}H\}$ NMR (161 MHz) of material collected from reaction of $[\{A^{1Si}PdCl\}_2]$ with triphenylphosphine taken in C_6D_6.

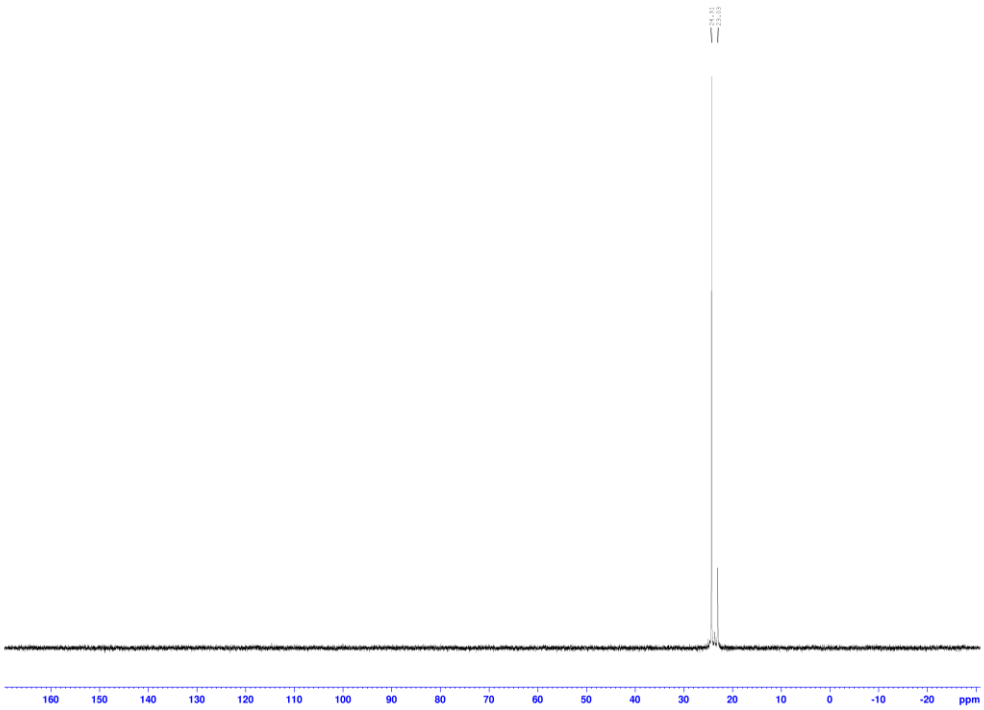

Figure A5.12: ^{1}H NMR (400 MHz) of material collected from reaction of $[Pd(NCMe)_2Cl_2]$ with $[K\{SnA'_3\}]$ taken in C_6D_6.

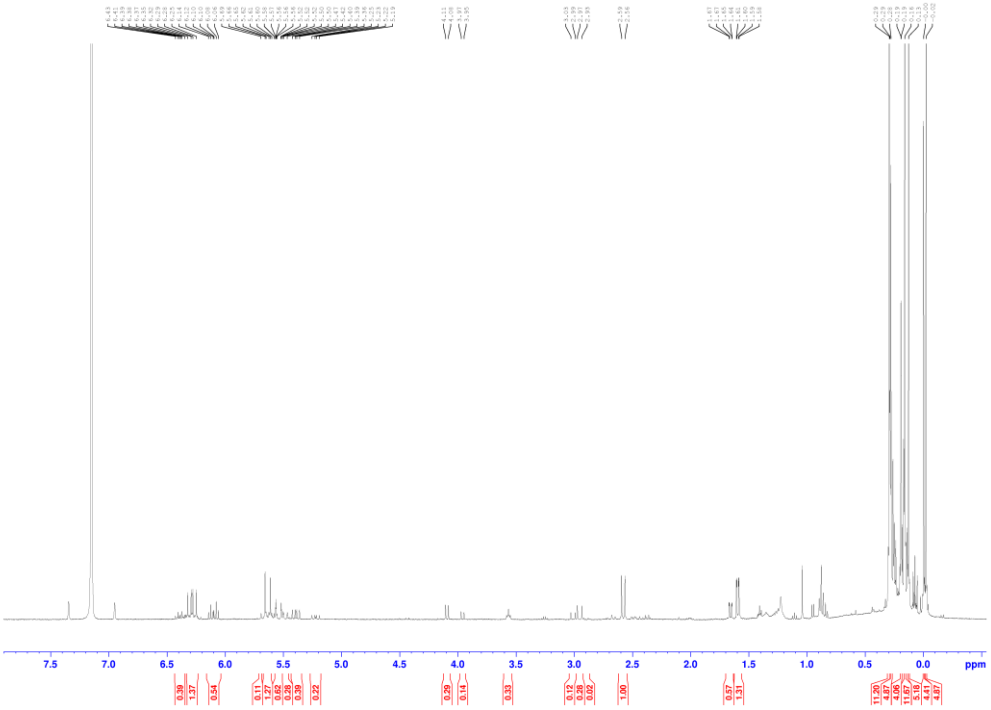

Figure A5.13: ^{1}H NMR (400 MHz) of material collected from reaction of [$PdOAc_2$] with [K{SnA'_3}] taken in d_8-toluene.

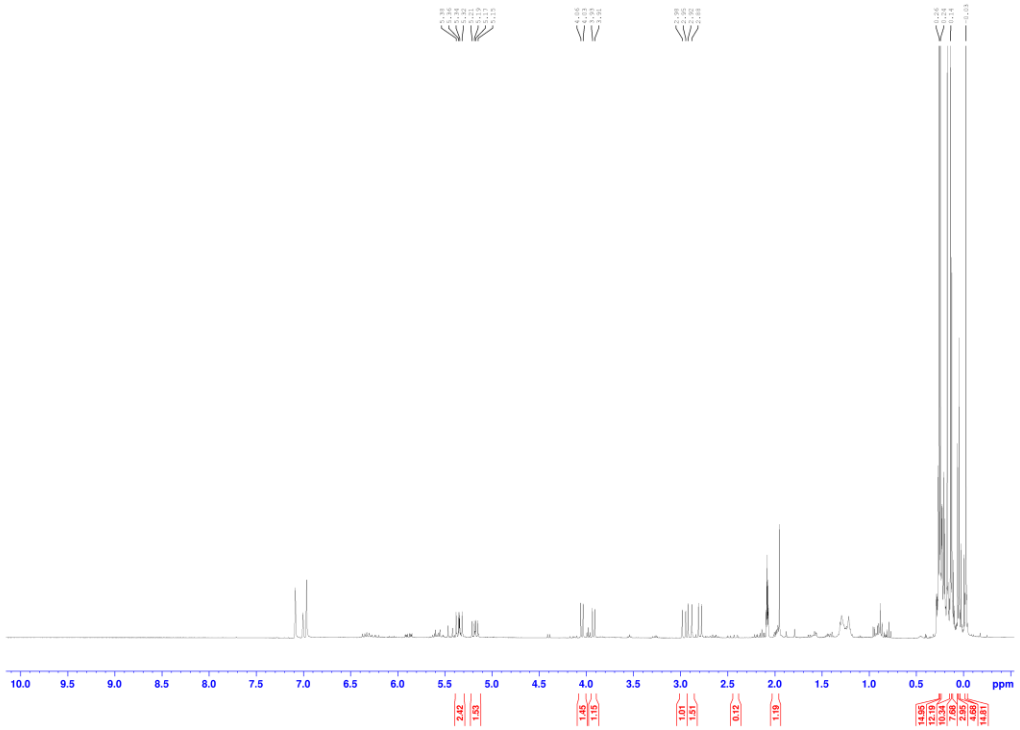

Figure A5.14: $^{13}C\{^{1}H\}$ NMR (101 MHz) of material collected from reaction of [$PdOAc_2$] with [K{SnA'_3}] taken in d_8-toluene.

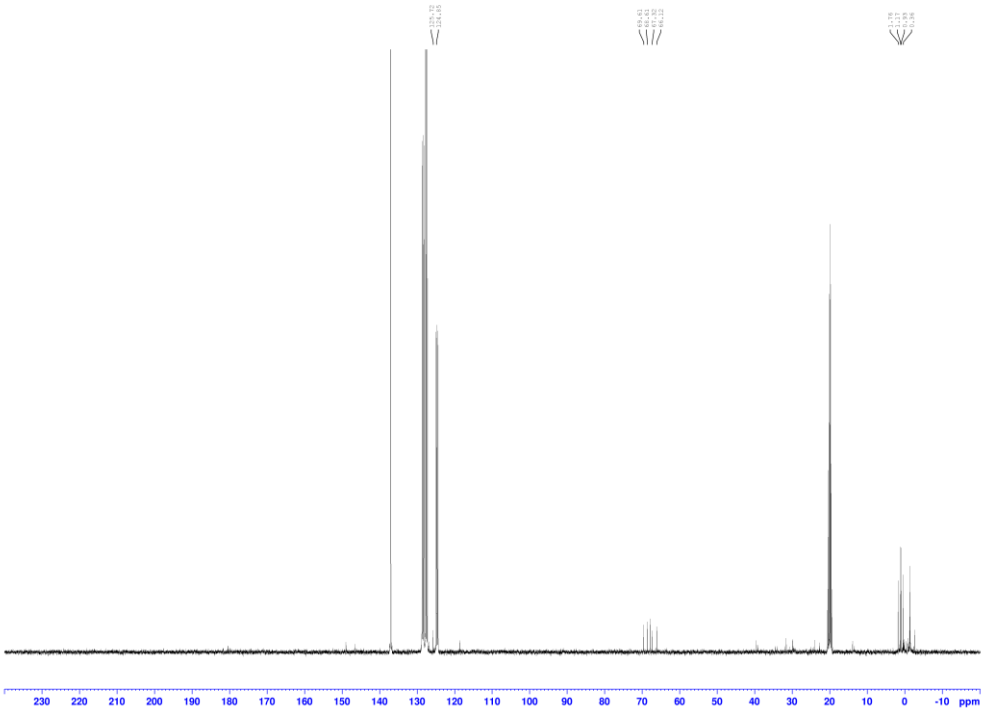

Figure A5.15: ^{1}H-^{13}C HSQC NMR (400-101 MHz) of material collected from reaction of [$PdOAc_2$] with [K{SnA'_3}] taken in d_8-toluene.

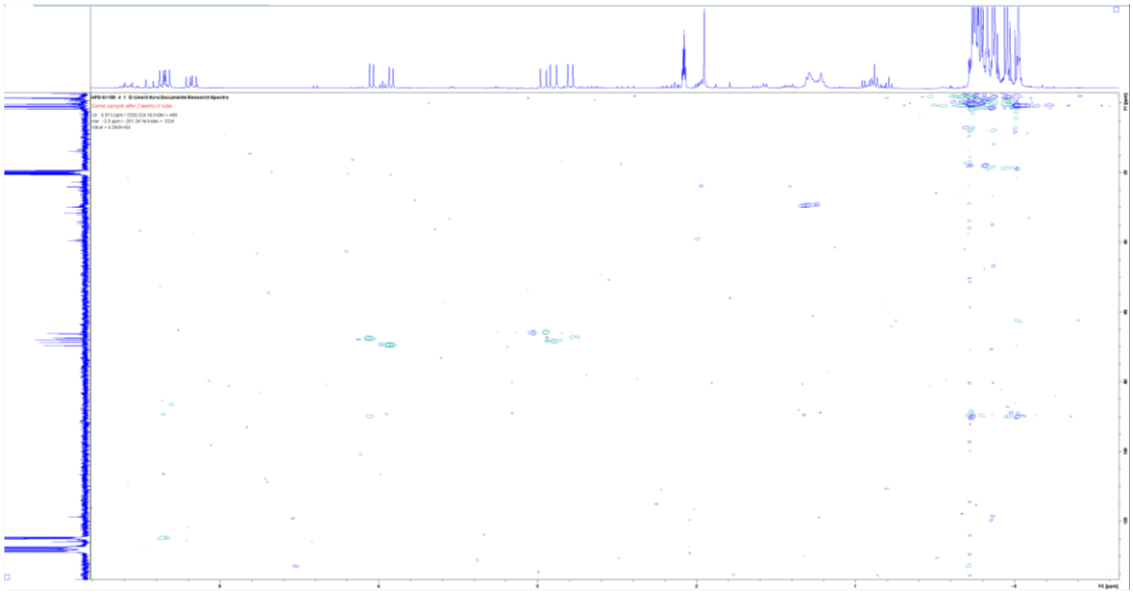

Figure A5.16: ^{1}H NMR (400 MHz) of material collected from reaction of [$Pd(dba)_2$] with [BrA^{2t}] taken in C_6D_6. Downfield aromatic peaks are attributed to free dibenzylideneacetone.

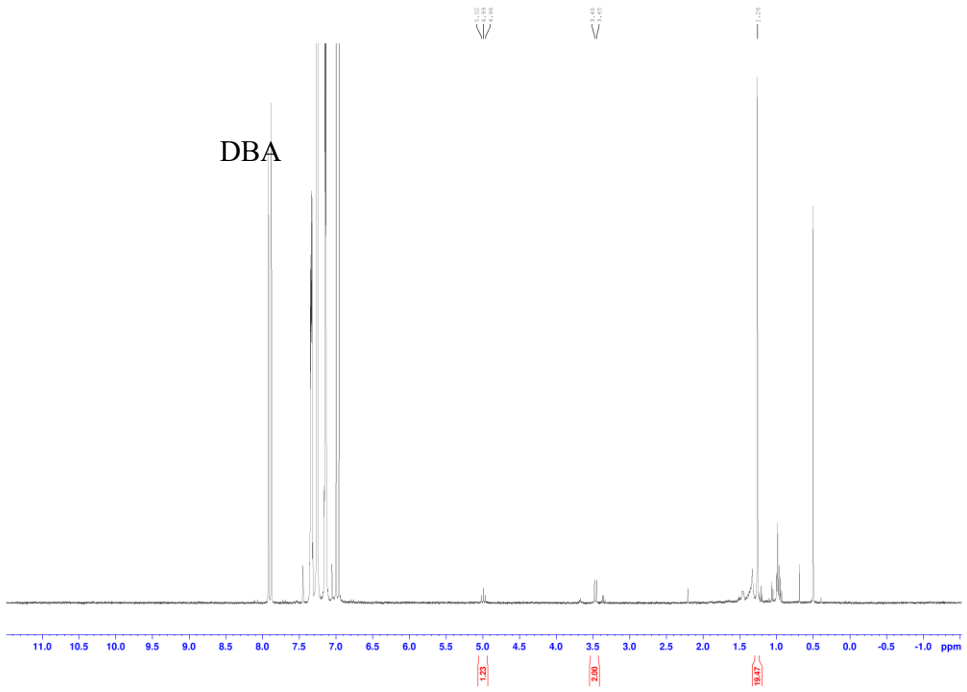

A5.5 References

(1) Smith, J. D.; Hanusa, T. P.; Young, J. Steric Stabilization of Homoleptic Bis(π-Allyl) Complexes of Chromium(II) and Iron(II). *J. Am. Chem. Soc.* **2001**, *123* (26), 6455–6456. https://doi.org/10.1021/ja015626j.

(2) Smith, J. D.; Quisenberry, K. T.; Hanusa, T. P.; Brennessel, W. W. Bis[1,3-Bis(Trimethylsilyl)Allyl]-Cobalt(II), a Stable Electron-Deficient Allyl Complex. *Acta Crystallogr. Sect. C Cryst. Struct. Commun.* **2004**, *60* (10). https://doi.org/10.1107/S0108270104020293.

(3) Quisenberry, K. T.; Smith, J. D.; Voehler, M.; Stec, D. F.; Hanusa, T. P.; Brennessel, W. W. Trimethylsilylated Allyl Complexes of Nickel. The Stabilized Bis(π-Allyl)Nickel Complex $[\eta^3\text{-}1,3\text{-}(SiMe_3)_2C_3H_3]_2Ni$ and Its Mono(π-Allyl)NiX (X = Br, I) Derivatives. *J. Am. Chem. Soc.* **2005**, *127* (12), 4376–4387. https://doi.org/10.1021/ja044308s.

(4) Carretero, J. C.; Arrayas, R. G. Dichloro Bis(Acetonitrile) Palladium. In *Encyclopedia of Reagents for Organic Synthesis (EROS)*; Wiley-VCH, 2008.

(5) Fraenkel, G.; Chow, A.; Winchester, W. R. Dynamics of Solvated Li^+ within Exo, Exo-[1,3-Bis(Trimethylsilyl)Allyl]Lithium N, N, N', N'-Tetramethylethylenediamine Complex. *J. Am. Chem. Soc.* **1990**, *112* (4), 1382–1386. https://doi.org/10.1021/ja00160a014.

(6) Arduengo, A. J.; Rasika Dias, H. V.; Harlow, R. L.; Kline, M. Electronic Stabilization of Nucleophillic Carbenes. *J. Am. Chem. Soc.* **1992**, *114* (14), 5530–5534.

(7) Koby, R. F.; Hanusa, T. P.; Schley, N. D. Mechanochemically Driven Transformations in Organotin Chemistry: Stereochemical Rearrangement, Redox Behavior, and Dispersion-Stabilized Complexes. *J. Am. Chem. Soc.* **2018**, *140* (46), 15934–15942. https://doi.org/10.1021/jacs.8b09862.